Design, synthesis and use of chiral pheromone-based probes to study pheromone enantiomer discrimination in the pheromone binding proteins from the gypsy moth, *Lymantria dispar*

by

Govardhana Reddy Pinnelli

M.Sc., Andhra University, 2008

Thesis Submitted in Partial Fulfillment of the
Requirements for the Degree of
Doctor of Philosophy

in the
Department of Chemistry
Faculty of Science

SIMON FRASER UNIVERSITY
Summer 2021

Declaration of Committee

Name:	**Govardhana Reddy Pinnelli**
Degree:	**Doctor of Philosophy (Chemistry)**
Title:	**Design, synthesis and use of chiral pheromone-based probes to study pheromone enantiomer discrimination in the pheromone binding proteins from the gypsy moth, *Lymantria dispar***
Committee:	**Chair:** **Hua-Zhong Yu** Professor, Chemistry
	Erika Plettner Supervisor Professor, Chemisty
	Bingyun Sun Committee Member Associate Professor, Chemisty
	Peter D. Wilson Committee Member Associate Professor, Chemisty
	Robert A. Britton Committee Member Professor, Chemisty
	David Vocadlo Examiner Professor, Molecular Biology and Biochemistry
	Jan Heinrich Bergmann External Examiner Principal Investigator Institute of Chemistry University of Valparaiso

Abstract

The gypsy moth is a widespread and harmful pest causing extensive damage to the Canada's forest and orchard ecosystems. It uses (+)-disparlure as a sex pheromone. Discovery of the pheromone, including its absolute configuration, has enabled monitoring of gypsy moth populations. Disparlure of low enantiopurity is not attractive to the moths and, for this reason, enantiopure (+)-disparlure has been a synthetic target for many years. To access (+)-disparlure of high enantiopurity we have used a diastereoselective nucleophilic addition reaction with the enantiopure α-chloroaldehyde (2-chlorododecanal) that yields a stereocontrolled access to the 1,2-*anti* chlorohydrin core. The (+)-disparlure was prepared through a series of transformations that include a Mitsunobu inversion. We have successfully completed the synthesis of (+)-disparlure in 5 steps as compared to Iwaki's first synthesis in 12 steps and Sharpless's widely used synthesis in 6 steps. The same approach was used to produce 18-hydroxydisparlure enantiomers, which were coupled to a linker with an alkyne moiety at the end. The alkyne was then coupled to azide-based commercial fluorescent probes, to furnish fluorescent disparlure-based probes for physical studies.

The gypsy moth has two different pheromone binding proteins, *Ldis*PBP1 and *Ldis*PBP2. Previously, our group has addressed the enantiomer selectivity of these two PBPs and found that PBP1 binds (-)-disparlure more strongly than (+)-disparlure, while PBP2 binds (+)-disparlure more strongly. Despite several binding assays, the interaction and discrimination of gypsy moth PBPs towards disparlure enantiomers are not fully understood due to lack of binding interaction and kinetic studies, which are technically demanding, due to the hydrophobicity of the pheromone. In this thesis, we have studied the binding interaction of deuterium-labelled (+)-disparlure and (-)-disparlure with *Ldis*PBPs by ^{2}H NMR spectroscopy. The results from NMR studies were correlated with the results from docking simulations of (+)-disparlure and (-)-disparlure bound to one internal site and multiple external sites of *Ldis*PBP1 and *Ldis*PBP2. These results indicated that (+)-disparlure and (-)-disparlure adopt different conformations and orientations in the binding pockets of *Ldis*PBP1 and *Ldis*PBP2.

Most of the reported work on PBPs focuses on the pheromone binding affinities of PBPs. However, the pheromone-PBP interactions require more than half an hour to establish equilibrium, whereas male moths respond to female pheromones in milliseconds. Therefore, the interactions between pheromones and olfactory components such as PBPs and pheromone receptors may not be under thermodynamic control. In this thesis, we aimed to provide a dynamic perspective of pheromone-PBP interactions and to link these to the functions of PBPs. We have studied thermodynamic (K_d) and kinetic properties (k_{on} and k_{off}) of *Ldis*PBPs-disparlure enantiomer interaction by fluorescence binding assays and kinetic experiments using fluorophore-tagged disparlure enantiomers. The result indicated that the binding preference of disparlure enantiomers to *Ldis*PBPs. Based on the kinetic data of *Ldis*PBPs with fluorophore-tagged disparlure enantiomers, we propose a kinetic model that includes a two-step binding process. Each of these two steps may contribute to a different function of the *Ldis*PBPs.

Keywords: Gypsy moth; *Ldis*PBP1 and *Ldis*PBP2; ^{2}H NMR; (+)-disparlure and (-)-disparlure probes; fluorescence-based binding assays and kinetics

Dedication

To my wonderful family with love and gratitude for all their support and encouragement

Acknowledgements

I wish to express many thanks to all individuals who offered me help and support in completing this thesis. First, I am truly grateful to Dr. Erika Plettner, my supervisor, for her guidance, encouragement, and personal and professional growth opportunities throughout my doctoral program. I sincerely appreciate her input and training that enabled me to grow assertiveness and confidence.

I am grateful for the constructive feedback and suggestions from Dr. Peter D. Wilson, Dr. Bingyun Sun, and Dr. Robert A. Britton from the supervisory committee. I thank Dr. David Vocadlo, who, amidst his busy timeline, sacrificed his time to be my internal examiner, and Dr. Jan Heinrich Bergmann for accepting to be my external examiner.

I appreciate the efforts and help from Dr. Andrew Lewis, Dr. Eric Yu, and Mr. Colin Zhang in ^{2}H and ^{17}O NMR experimental set up, and Mr. Hongwen Chen for conducting mass spectroscopy procedures, and Mr. Fred Chen for technical assistance. I would not have succeeded in achieving my study objectives without the great assistance in carrying out field trials and data analysis offered by Dr. Kirk N. Hillier from Acadia University and Dr. David R. Lance from the USDA Otis laboratory. I acknowledge the continued assistance from Ms. Nathalie Fournier, Ms. Amber Schroeder, and Ms. Jen Jackson, along with Ms. Anise Ladha, the library thesis assistant, for her primary role in formatting my thesis.

I have had a chance to work alongside many brilliant people throughout my Ph.D. program. I appreciate Dr. Mailyn Terrado for granting me the gypsy moth pheromone-binding proteins, guiding me through the stopped-flow instrument, and contributing thoughtful suggestions and comments on my write-up. I would also like to recognize my lab mate, who has been my friend, Priyadarshini Balaraman for her motivation, thoughtful comments, and suggestions. I thank Dr. Venugopal Rao Challa and his family for their friendship throughout my program.

I convey special regards and thankfulness to past and current group members of the Plettner laboratory Dr. Yang Yu, Dr. Abdul Rehman, Shaima Kammonnah, Dr. Jurgen Sanes Soniya Dawdani, Dr. Arasakumar Thangaraj, Dr. Jorge Macias, Ashna Aulakh, Nicole Gkaleni and Shubhra Srivastava for their beneficial advice and support, together

with their friendship, generosity, and patience. Finally, I acknowledge the love and encouragement from my family and friends who inspired me to be the best I can be.

Table of Contents

List of Tables

List of Figures

List of Schemes

List of Acronyms

Ac	Acetate
ACN	Acetonitrile
AMA	Aminoanthracene
ANOVA	Analysis of variance
ANS	8-Anilino-1-naphthalene sulfonate
AOX	Antennal aldehyde oxidase
Aq	Aqueous
BLAST	Basic local alignment search
Bn	Benzyl
BT	Bacillus thuringiensis
D_2	Deuterium gas
DEA	Diethylamine
DIAD	Diisopropyl azodicarboxylate
DIBAL	Diisobutylaluminium hydride
DIC	Diisopropylcarbodiimide
DIPEA	*N*,*N*-Diisopropylethylamine
DMAP	4-Dimethylaminopyridine
DMSO	Dimethyl sulfoxide
dr	Diastereomeric ratio
EAG	electroantennogram
EI	Electron ionization
EtOAc	Ethyl acetate
6-FAM	6-Carboxyfluorescein
GCMS	Gas chromatography mass spectrometry
HEK	Human embryonic kidney
HMPA	Hexamethylphosphoramide
HPLC	High-performance liquid chromatography
HRMS	High resolution mass spectrometry
Hz	Hertz
IC_{50}	Half maximal inhibitory concentration
IPA	Isopropyl alcohol
K_d	Dissociation constant

K_i	Inhibitory constant
LDA	Lithium diisopropylamide
LiCl	Lithium chloride
MMFF	Merck molecular force field
MOE	Molecular operating environment
mol	Mole(s)
MOM-Cl	Methoxymethyl chloride
mmol	Millimole(s)
NaOCl	Sodium hypochlorite
NBD	Nitrobenzoxadiazole
NBS	*N*-bromosuccinimide
NCS	*N*-chlorosuccinimide
NMR	Nuclear magnetic resonance
1-NPN	N-phenyl-1-naphtylamine
OBP	Odorant-binding protein
ODE	Odorant-degrading enzyme
OR	Odorant receptor
ORCO	Odorant receptor co-receptor
OSN	Odorant sensory neuron
PAGE	Polyacrylamide gel electrophoresis
PBP	Pheromone-binding protein
PCC	Pyridinium chlorochromate
PDB	Protein data bank
PDE	Pheromone-degrading enzyme
PLB	Propensity for ligand binding
PMA	Phosphomolybdic acid
PPTS	Pyridinium p-toluenesulfonate
PR	Pheromone receptor
PTSA	*para*-Toluenesulfonic acid
R	Substituent
rt	Room temperature
S_N2	Bimolecular nucleophilic substitution
SOMO	Singly occupied molecular orbital
T1	Spin-lattice relaxation time

T2	Spin-spin relaxation time
TBAF	Tetrabutylammonium fluoride
TBDMS	*tert*-Butyldimethylsilyl
TEA	Triethylamine
TEMPO	(2,2,6,6-Tetramethylpiperidin-1-yl)oxidanyl
THF	Tetrahydrofuran
THPTA	Tris(benzyltriazolylmethyl)amine
TLC	Thin-layer chromatography
TPP	Triphenylphosphine
Ts	Tosyl
USDA	United States Department of Agriculture
VWD	Variable wavelength detector

Chapter 1.

Introduction

1.1. Lepidopteran sex pheromone communication

Olfaction or olfactory perception is the sense of smell and it plays a very important role in insects. Insects communicate with their surroundings by sensing and releasing semiochemicals, which are volatile organic compounds that act as messengers within or between species (Bowers, 2002). In moths, two types of olfactory systems have evolved: a general odorant detection system tuned for general odorants such as food-derived and host plant odorants, and a pheromone detecting system that is highly specifically tuned for each species of insect (Renou, 2014). In 1959, the word “pheromone” was proposed by chemical ecologists Karlson and Luscher (Karlson and Lüscher, 1959) based on Greek terms pherein (to carry or transfer) and hormone (to excite or stimulate). Pheromones are a subclass of semiochemicals, which are produced and released by an organism to influence the behavior of another organism of the same species (Wyatt, 2003). This subclass can be further divided by function such as sexual pheromones, aggregation pheromones and alarm pheromones. A sex pheromone can be a single compound or a blend of chemical compounds in a specific ratio and amount, which is used to attract a conspecific male for mating. In Lepidoptera (moths and butterflies) one gender produce a sex pheromone, which they use to attract mates over long distances or to excite them sexually (Wyatt, 2003). The Lepidoptera represent the second largest group of insects, which includes approximately 180,000 described species worldwide (Powell, 2009). This order within the insects contains many rare species but also many agricultural and forest pests. The latter are often monitored or even disrupted with their sex pheromone, which is why the study of these signaling compounds is so important.

In moths, the sex pheromone, which is generally produced and released by females, acts as a chemical messenger and is highly active in attracting males of the same species. This species-specific pheromone prevents inter-specific males from mating and plays a crucial role in reproductive isolation. In 1959, German chemist Adolph Butenandt (Butenandt et al., 1959) identified the first sex pheromone, which was named bombykol after *Bombyx mori*, the silk moth. The compound ((*E*,*Z*)-10,12-hexadecadien-1-ol) (**1**)

(Figure 1.1), was isolated from pheromonal glands of 331,000 female silkworm moths, *B. mori*. Since the1950s, female moth pheromones have been isolated and identified for more than 600 species, including agricultural pests, such as rice borer *Chilo suppressalis*, citrus leaf miner *Phyllocnistis citrella* and tobacco hornworm *Manduca sexta* (Ando, 2011). Sex pheromones have traditionally been considered by researchers to be emitted by organisms of one sex, in order to attract members of the opposite sex, resulting in the localization of the emitter, and subsequently, in mating. To develop a method for integrated pest management or control, sex pheromone-baited traps and lures are widely used for monitoring and mass trapping, and sprayable formulations or high-volume release dispensers are used for mating disruption of certain species of moth in the field (Ando et al., 2004).

1.1.1. Type I pheromones

The pheromones of Lepidopteran are characterized in to four types (type 0, I, II and III), based on their chemical structures (Ando et al., 2004; Löfstedt et al., 2016). The chemical structures of some moth sex pheromones are shown in Figure 1.1. Primary alcohols, aldehydes and acetates with long chain hydrocarbons (C_{10} to C_{18}) and generally conjugated double bonds (more than two C=C double bonds) have most frequently been found in the pheromone gland extracts of female moths. These chemical compounds are classified as type I pheromones, and they are the most dominant group, which comprises around 70% of known pheromones that have been identified in a variety of species of Lepidoptera, including the wild silk moth, *Antheraea polyphemus* (Kochansky et al., 1975), the domestic silkworm moth, *B. mori* (Butenandt et al., 1959), the smaller tea tortrix, *Adoxophyes honmai* (Tamaki et al., 1971), the rice stem borer moth, *C. suppressalis* (Nesbitt et al., 1975), and the citrus leaf miner moth *P. citrella* (Mafi et al., 2005; Moreira et al., 2006) (Figure 1.1).

1.1.2. Type II pheromones

Type II pheromones comprise polyunsaturated hydrocarbons and their derivatives such as epoxides with long chains (C_{17}-C_{23}, and, unusually, C_{25} and C_{27}). Type II pheromones, lacking the functional group at the end, and have been detected in highly evolved insect groups. For example, the giant looper moth, *Ascotis selenaria* (Ando et al., 1997), the tussock moth (Okinawa and Ishigaki strains), *Orgyia postica* (Chow et al., 2001;

Wakamura et al., 2001 & 2005), and the fall webworm moth *Hyphantria cunea* (Hill et al., 1982) (Figure 1.2).

1.1.3. Type III pheromones

Apart from Type I and Type II sex pheromones, branched or straight chain ketones, secondary alcohols and esters have been identified from several Lepidoptera (Ando, et al., 2004; Löfstedt et al., 2016). In addition, some moths emit methyl branched pheromones. For example, the lichen moth, *Lyclene dharma dharma* (Yamamoto et al., 2007; Adachi et al., 2010), the peach leaf miner moth, *Lyonetia clerkella* (Sugie and Tamaki, 1984), and the gypsy moth, *Lymantria dispar* (Bierl et al., 1970) produce a branched ketone, alkene and epoxide respectively (Figure 1.3).

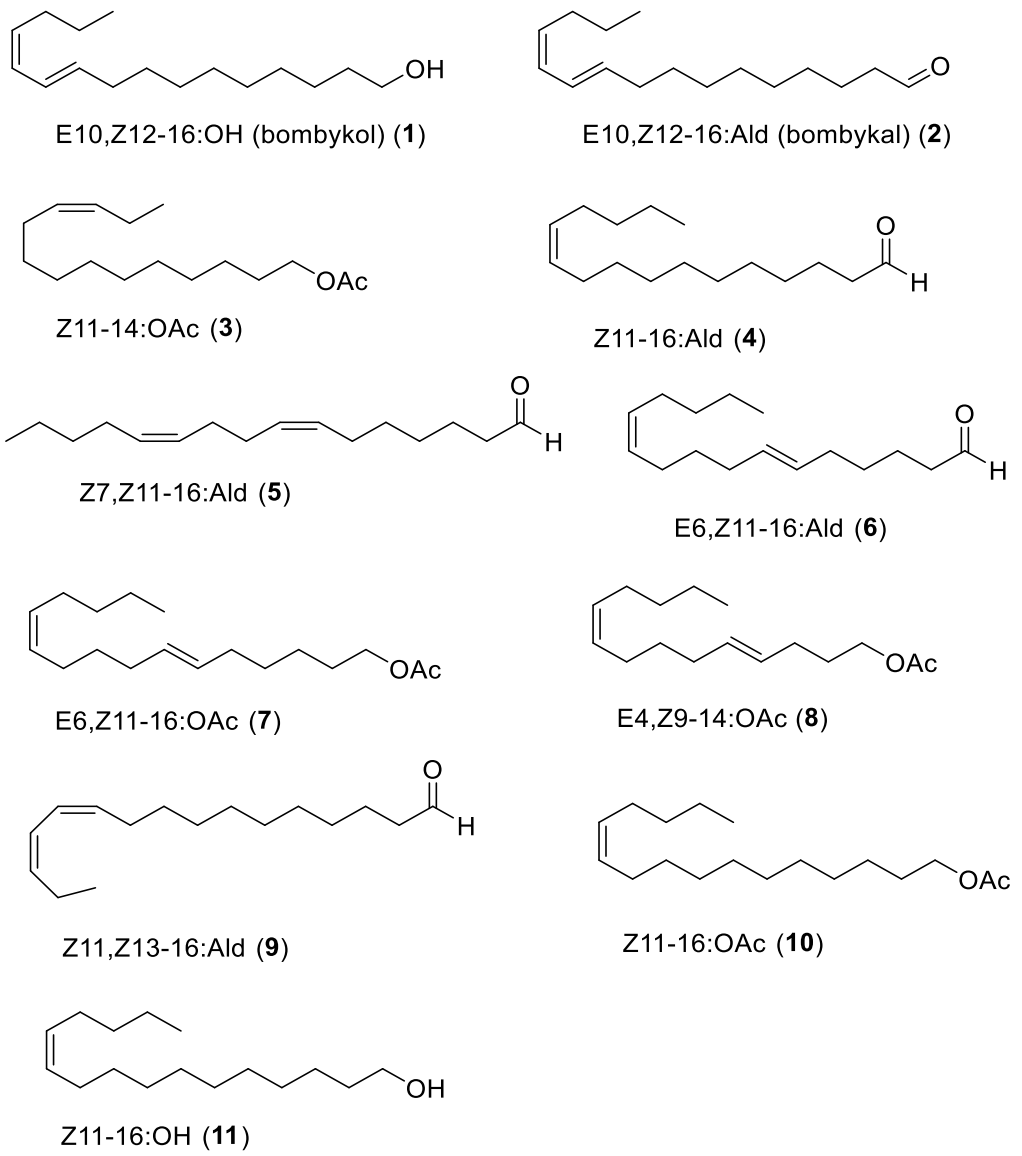

Figure 1.1 **Structures of sex pheromones from the Lepiodoptera. Shown are Type I pheromones for the silkmoth *B. mori*.(1 & 2), smaller tea tortix, *A honmal* (3), rice borer, *C. suppressalis* (4), citrus leaf miner *P. citrella* (5), giant silkmoth *A. polyphemus* (6 & 7), the Chinese tussar moth *A. pernyi* (6, 7 & 8), navel orange worm *A. transitella* (9), cabbage moth *M. brassicae* (10 & 11).**

The names of sex pheromones of Lepidoptera are abbreviated as follows: E = (*E*)-double bond, Z = (*Z*)-double bond, number after the letter Z or E = position of the double bond, number after epo = position of the epoxy ring, number after the hyphen = carbon number of the main chain, H = the hydrocarbon structure without functional groups, OH, OAc and Ald = the chemical structure with a terminal functional group (alcohol, acetate,

and aldehyde, respectively). For example, (*E*,*Z*)-10,12-hexadecadiene-1-ol and *cis*-3,4-epoxy-(6*Z*,9*Z*)-6,9-nonadecadiene are abbreviated as E10,Z12-16:OH and Z6,Z9,epo3-19:H, respectively. For the entirety of this thesis, this abbreviation system of pheromone names will be used.

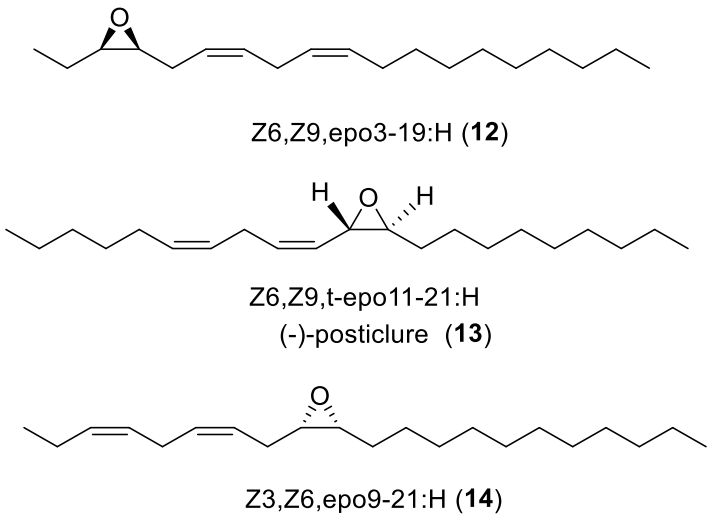

Figure 1.2 **Structures of some main components of Type II pheromones of Lepidoptera. Shown are the pheromones of the giant looper *A. selenaria* (12), the tussock moth, *O. postica* (13), and the fall webworm *H. cunea* (14).**

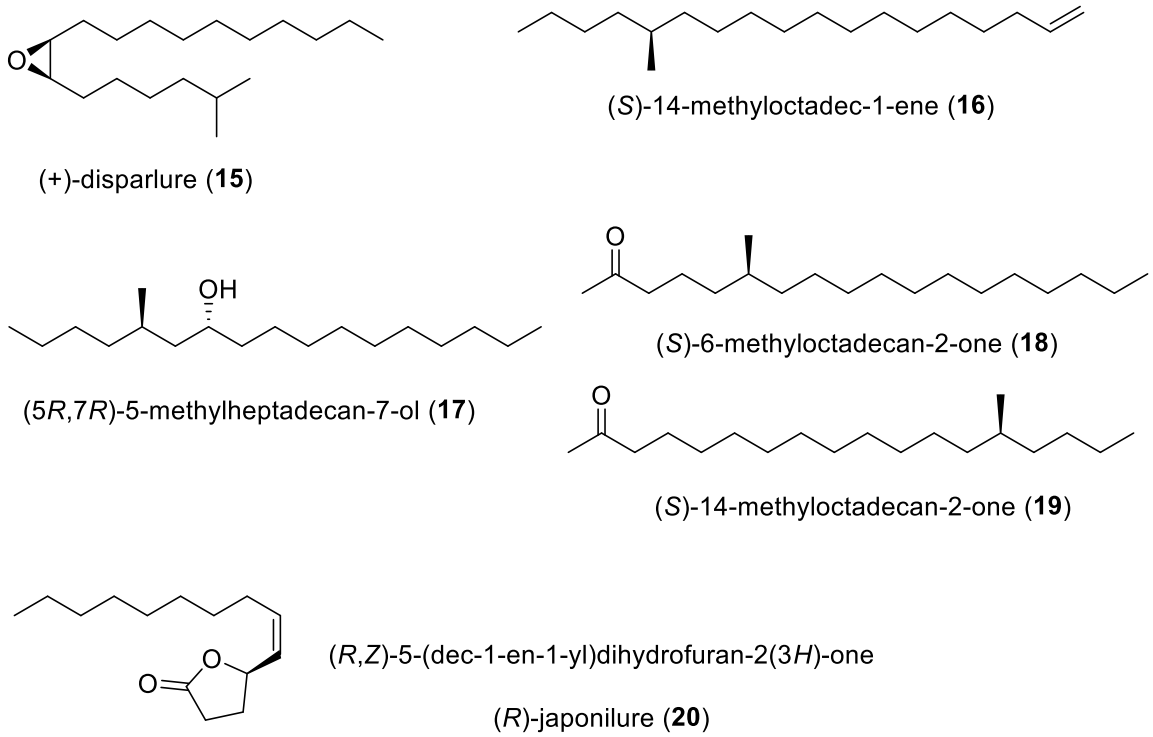

Figure 1.3 **Type III lepidopteran sex pheromones. Structures of chiral sex pheromones of the gypsymoth *L. dispar* (15), the peach leafminer moth *L. clerkella* (16), the lichen moth *M. calamina* (17), the lichen moth *L. dharma* (18 & 19), and the Japanese beetle *Popillia japonica* (20).**

1.2. Gypsy moth

The gypsy moth, *Lymantria dispar* is a harmful pest of a large variety of trees (oak, apple, maple, mountain ash, pine, and spruce), causing significant forest losses during outbreaks in Europe, Asia and North America. Since its introduction to North America (Liebhold et al.,1989), the gypsy moth has been detected in parts of the eastern Canadian provinces (Ontario, Quebec, New Brunswick, Prince Edward Island, Nova Scotia and Manitoba) and states in the northeastern U.S.A. Gypsy moth populations are established in central (Ontario and Quebec) and eastern (Nova Scotia and New Brunswick) regions of Canada. In British Colombia, a gypsy moth's egg mass was first detected on imported trees from Japan in 1911 (Lyne, 1911). Since then, the gypsy moth incursions are detected in British Colombia nearly every year, but this species has not become permanently established. The gypsy moth can have a serious economic impact mainly because of the damage it causes to trees and shrubs, and also in direct costs connected with controlling

gypsy moth populations (Tobin et al., 2004). For instance, the United States and Canada spend millions of dollars annually on controlling gypsy moths. In the United States, the gypsy moth's spread has been dramatically reduced by 50-70% since the implementation of the "slow the spread" program (Liebhold and Tobin, 2008). The main goal of this program is to slow the movement of gypsy moth populations into non-infested areas, by detecting newly infested areas using gypsy moth sex pheromone-baited traps. The newly infested areas are treated with bacterial agent *Bacillus thuringiensis* (Bt), or with a mating disruption approach that uses the racemic form of synthetic gypsy moth pheromone to confuse male moths and lower the frequency of mating.

In the late nineteenth century, with an attempt to find a method for controlling the gypsy moth, researchers of the Entomological research division of USDA (United States Department of Agriculture) at Beltsville, MD, started a study of the sex pheromones of this species. In 1960, Jacobson *et al*. isolated (Jacobson et al., 1960) one active compound from the abdominal tip extracts of 0.5 million female gypsy moths and the active compound was characterized as (*Z*)-10-acetoxy-7-hexadecen-1-ol (**21**), was named gyptol (Figure 1.4). In 1962, Jones and Jacobson synthesized the C-18 homolog of gyptol (Jacobson and Jones, 1962), (*Z*)-12-acetoxy-9-octadecen-1-ol (**22**) (gyplure). Like gyptol, this compound was found to be an extremely attractive to the males of the gypsy moth. In the following years, gyptol (**21**) and gyplure (**22**) were prepared by other researchers by different synthetic paths produced compounds that were not attractive lures to the male gypsy moths (Eiter et al., 1967). In 1970, Jacobson reinvestigated the activity of gyptol and gyplure and reported that original synthetic gyptol and gyplure were active because of the presence of an attractive substance in extremely low quantities with high biological activity (Jacobson et al., 1970). In this study, Jacobson was not able to identify the structure of the biologically attractive substance found in the synthetic gyptol and gyplure. However, he reconfirmed that the gyptol was present in the abdominal tip extracts of female gypsy moths. In the same year, Bierl *et al*. published the correct structure for the sex pheromone of the gypsy moth. They identified the sex pheromone as *cis*-7,8-epoxy-2-methyloctadecane (±)-(**15**) and named it disparlure (Bierl et al., 1970). Further studies by Iwaki *et al*. on the structure of the pheromone have shown that the compound produced by the gypsy moth is (7*R*,8*S*)-7,8-epoxy-2-mehyloctadecane or (+)-disparlure (**15**) (Iwaki et al., 1974). EAG (electroantennogram) and behavioral responses revealed that the (+)-disparlure (**15**) was attractive to male gypsy moths. The other enantiomer (-)-disparlure

(*ent*-**15**) can also be detected by male moths, but it acts as an antagonist to attractiveness of (+)-disparlure (**15**). One possible reason behind the remarkable enantioselectivity is that (-)-disparlure (*ent*-**15**) is secreted by a closely related moth species, the nun moth (*Lymantria monacha*). The nun moth is sympatric with gypsy moth in Asia and Europe where these moths are native (Miller et al., 1977).

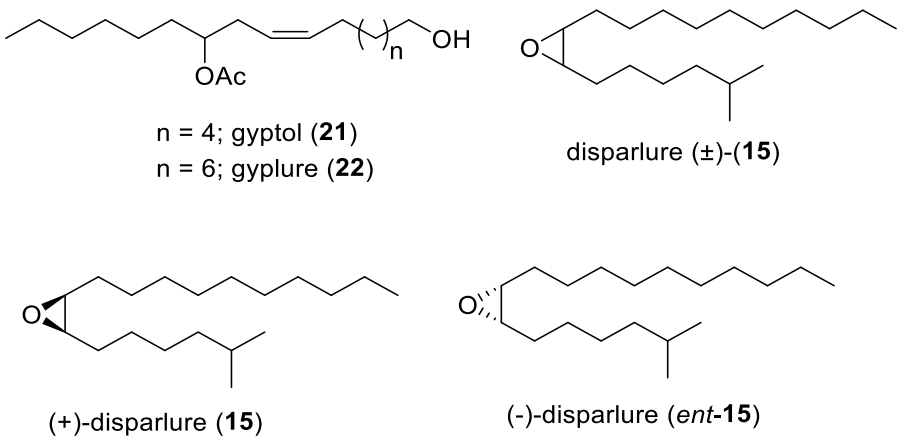

Figure 1.4 Structures of gyptol, gyplure and the disparlure enantiomers.

Controlling and monitoring gypsy moth populations has been successful mainly because of the availability of synthetic sex pheromone baited traps that are extremely effective for detecting the presence of the insect at low-density populations (Liebhold and Tobin, 2008). The unique biological activity of disparlure as sex pheromone in monitoring gypsy moth populations, as well as the insufficient quantities isolated from natural sources (each female has ~ 1 ng in the pheromone gland) have highlighted disparlure as an attractive target for several researchers over the past fifty years. In fact, since its discovery, more than fifty syntheses for enantiopure and racemic disparlure have been reported (Agustinho Fernandes et al., 2020).

Despite many reported syntheses, a short and efficient synthesis without using toxic reagents and expensive starting materials is still in demand. The building of the 2 stereocenters on the linear hydrocarbon chain of disparlure has been achieved through various synthetic strategies which include: asymmetric epoxidation (Rossiter et al., 1981; Mori and Ebata, 1981; Marczak et al., 1989; Li et al., 1997; Wang et al., 2012) and dihydroxylation (Keinan et al., 1992; Ko, 1994; Sinha-Bagchi et al., 1995), use of chiral sulfoxide auxiliaries (Satoh et al., 1989), chiral stannanes (Marshall et al., 1999), chiral

organoboranes (Hu et al., 1999), organocatalytic procedures (Chao-Xin et al., 2007; Kim, 2009; Garg et al., 2017; Klosowski and Martin, 2018), enzymatic procedures (Brevet and Mori, 1992; Fukusaki et al., 1992; Tsuboi et al., 1993; Tsuboi et al., 1997), separation of enantiomeric intermediates on microcrystalline cellulose triacetate I (MCTA-I) (Inkster et al., 2005) and usage of chiral pool starting materials (Iwaki et al., 1974; Mori et al., 1976; Paolucci et al., 1995; Koumbis and Chronopoulos, 2005; Prasad and Anbarasan, 2007; Dubey and Chattopadhyay, 2011; Bethi et al., 2014; Drop et al., 2020). The present discussion will focus on biosynthesis and some of the syntheses of disparlure that are typical of these different strategies used to prepare disparlure over the years.

1.3. Biosynthesis of (+)-disparlure

In 2003, Jurenka and co-workers (Jurenka et al., 2003) proposed a biosynthetic pathway for production of sex pheromone (+)-disparlure (**15**) in gypsy moth (Scheme 1.1). The authors demonstrate that the (+)-disparlure (**12**) was biosynthesized from the alkene precursor (*Z*)-2-methyl-7-octadecene (**28**), which was derived from valine (**23**). Thus, the biosynthetic route starts with the valine (**23**), which was first transformed into isobutyryl-CoA **24**. Then the hydrocarbon chain of isobutyryl-CoA **24** is extended to 19 carbons, followed by introduction of the *cis*-double bond with fatty acid desaturase. The resulting compound **27** is decarboxylated to the alkene, (*Z*)-2-methyl-7-octadecene (**28**). All of these steps took place in oenocyte cells that are located in the abdominal tissues, with the resulting alkene then being carried most likely by lipophorins (hemolymph proteins) to the pheromone gland (located at the tip of the abdomen) through the hemolymph. At the pheromone gland, the alkene precursor is epoxidized stereoselectively, by an unknown enzyme, before release into the air.

Jurenka and co-workers also demonstrated that it is (+)-disparlure (**15**) that is produced in the pheromone gland. They used chiral HPLC-MS (high performance liquid chromatography coupled to mass detection) technique to find out whether the female gypsy moth is producing only (+)-disparlure (**15**). Chiral resolution of disparlure that isolated from pheromone gland suggests that the predominantly (+)-disparlure (**15**) is present. Based on the electroantennogram (EAG) and behavioural assays, it has been suggested that the female gypsy moth produces only (+)-disparlure (**15**) (Hansen, 1984). Both the chiral HPLC data and behavioural data suggest that the female gypsy moth produces almost 100 % (+)-disparlure (**15**).

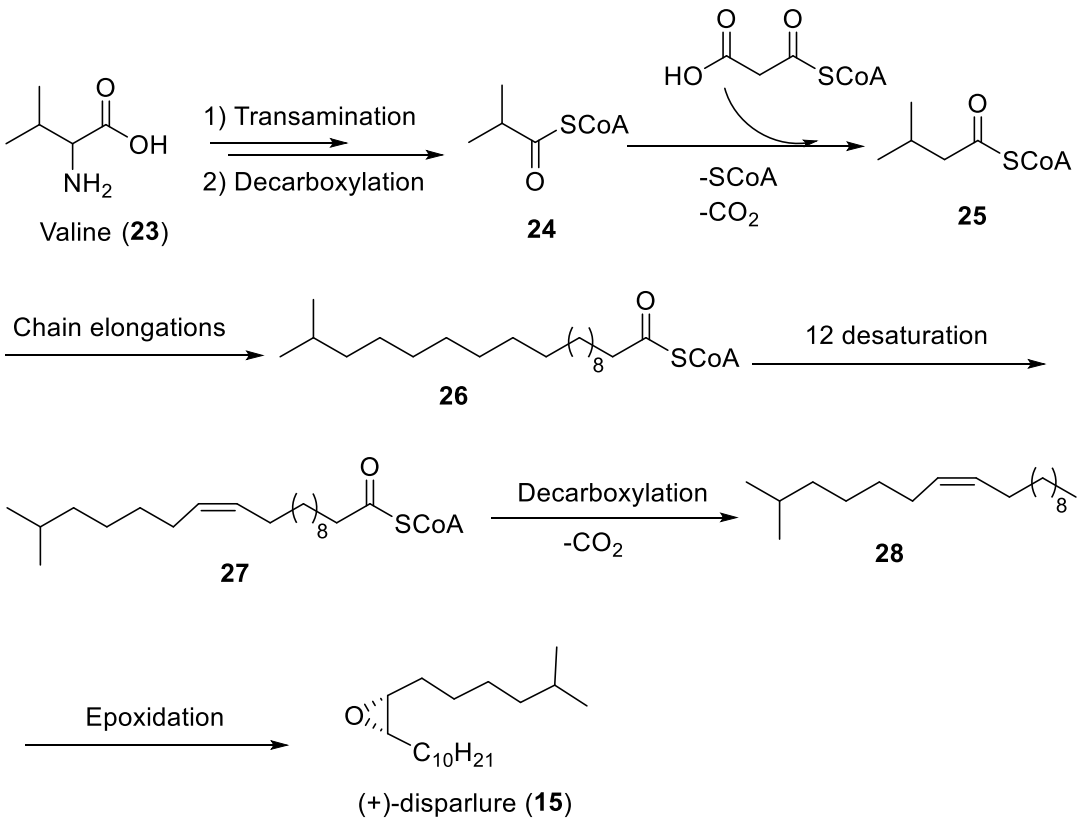

Scheme 1.1 Proposed biosynthetic route for (+)-disparlure (15) in gypsy moth

1.4. Previous syntheses of disparlure enantiomers

1.4.1. Iwaki's synthesis of (+)-disparlure (15)

In 1974, the first synthesis of the enantiomers of disparlure by Iwaki started with naturally occurring L-(+)-glutamic acid (**29**) (Iwaki et al., 1974) as shown in Scheme 1.2. That synthesis was not very stereoselective and it involved laborious separation of intermediates, diastereomeric hydroxylactones **31** & **32**. Despite the low overall yield and lengthy synthesis (12 steps & 9% overall yield), their three-step sequence (lactone reduction-Wittig olefination-hydrogenation, conversion of **34** to **37**) has been shown to be a very convenient strategy that has since been employed in many syntheses of disparlure. In addition, using a protected 1,2-diol intermediate **37** as an epoxide precursor has been demonstrated to be a common strategy in a number of asymmetric syntheses of disparlure (Kang et al., 1991; Keinan et al., 1992; Paolucci et al., 1995; Marshall et al.,1999; Koumbis and Chronopoulos, 2005; Prasad and Anbarasan, 2007; Kovalenko et al., 2009; Dubey and Chattopadhyay, 2011; Bethi et al., 2014; Drop et al., 2020).

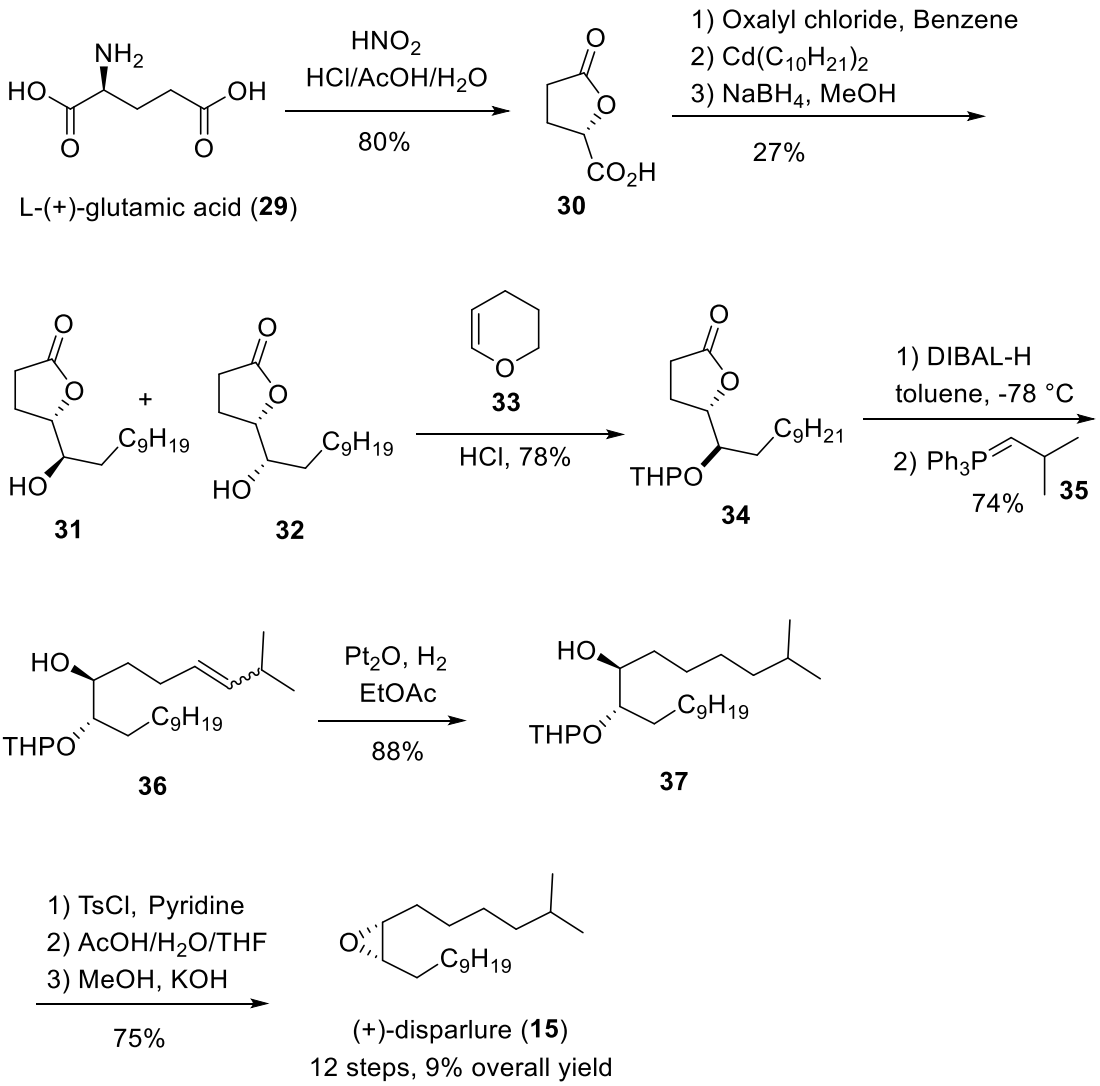

Scheme 1.2 Iwaki's synthesis of (+)-disparlure (15) from chiral pool starting material.

1.4.2. Mori's synthesis of disparlure enantiomers

In 1976, Mori described an enantioselective synthesis of disparlure enantiomers from naturally available L-(+)-tartaric acid (**38**) (Mori et al., 1976), as shown in Scheme 1.3. The elongation of the carbon chain and discrimination of the two hydroxyl groups of L-(+)-tartaric acid (**38**) were the major problems in Mori's synthesis. He converted L-(+)-tartaric acid (**38**) to the known intermediate **40** that was used in the synthesis of beetle pheromone *exo*-brevicomin. The nucleophilic substitution of tosyloxy group of intermediate **40** with an iso-pentyl group gave dimethoxy ester **41**. Demethylation of **41**

with boron trichloride followed by protection of free alcohol with THP delivered hydroxylactone **42**, which was finally converted to (+)-disparlure (**15**) via Iwaki's three step sequence (lactone reduction-Wittig olefination-hydrogenation). This synthesis involved 18 steps and produced 1.1% overall yield and it required repetitive recrystallization of hydroxylactone **42** and tosyloxy alcohol **45** to obtain optically pure (+)-disparlure (**15**). Mori also prepared (-)-disparlure (*ent*-**15**) in a similar manner by changing the order of the introduction of the alkyl groups. The tosoloxy group of intermediate **40** was substituted with an octyl group to give the compound **46** which, upon a series of transformations, gave (-)-disparlure (*ent*-**15**).

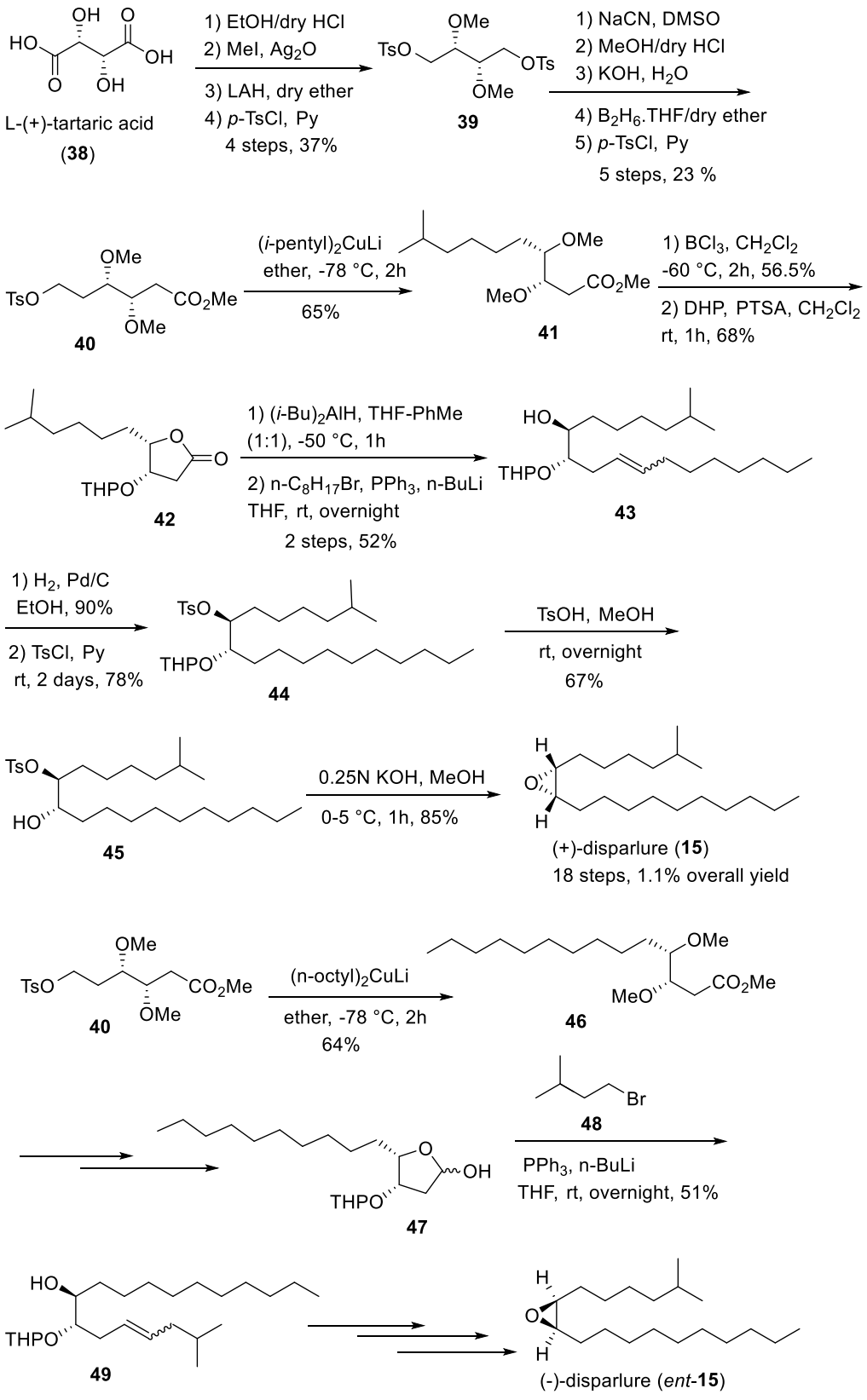

Scheme 1.3 Synthesis of disparlure enantiomers from L-(+)-tartaric acid (38).

1.4.3. Sharpless's synthesis of (+)-disparlure (15) –Asymmetric epoxidation

A few years later, Sharpless reported a successful synthesis of (+)-disparlure (**15**) by using his asymmetric epoxidation methodology (Rossiter et al., 1981) (Scheme 1.4). The alkyne anion of propargyl alcohol **50** was alkylated with decyl bromide to afford alcohol **51**, which was partially hydrogenated with Lindlar's catalyst to provide the key intermediate, *cis*-allylic alcohol **52** in 80% yield over two steps. An asymmetric epoxidation of **52** proceeded in 84% yield and produced epoxy alcohol **53** in 92% enantiomeric excess. The enantiopurity of the compound **53** was further enhanced to 95% *ee* by recrystallization. Oxidation of the enantiopure epoxy alcohol **53** by chromium trioxide led to aldehyde **54** which was converted to (+)-disparlure (**15**) through Wittig reaction with the ylide **55** followed by hydrogenation of the resulting alkene with the Wilkinson's catalyst. Thus, Sharpless synthesized (+)-disparlure (**15**) in 6 steps with 30% overall yield.

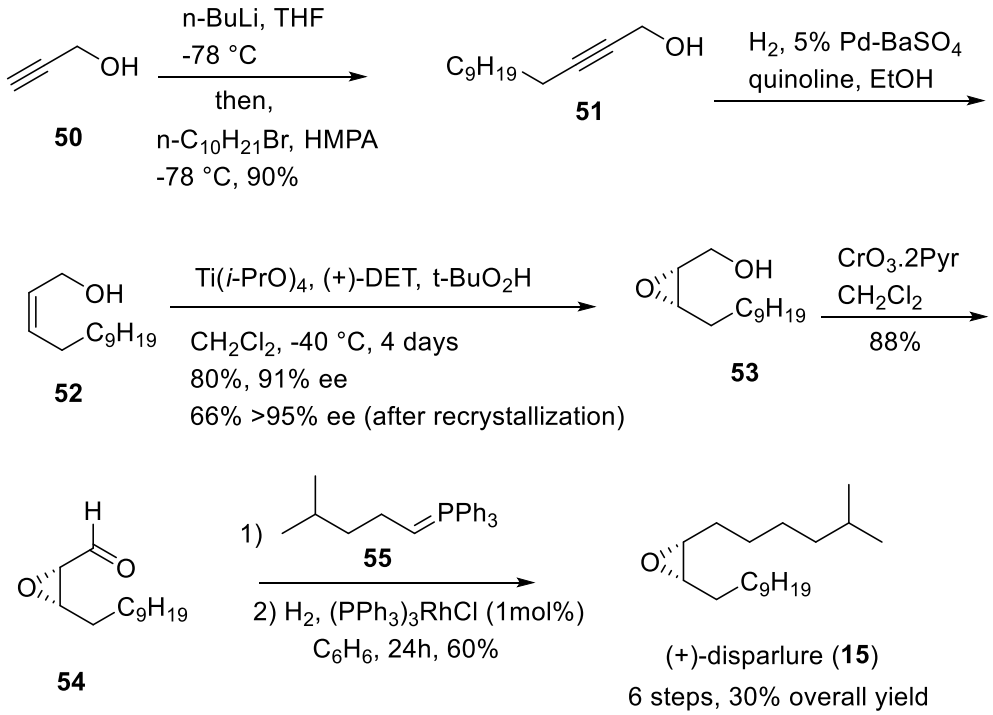

Scheme 1.4 Synthesis of optically pure disparlure (15) by Sharpless asymmetric epoxidation.

The epoxy alcohol **53** became problematic for Sharpless because it readily isomerized to a by-product ketone and it was difficult to separate from epoxy alcohol **53**.

To circumvent this problem, he treated the crude final products with the reducing agent $NaBH_4$ and separated the ketone by-product alcohol by silica column chromatography. Despite these problems, Sharpless's synthetic strategy gives an efficient route to (+)-disparlure (**15**) with high enantiopurity. In fact, this synthesis was the shortest synthetic pathway towards (+)-disparlure (**15**) to date. There have been several syntheses reported based on the Sharpless asymmetric epoxidation to obtain the required stereochemistry for (+)-disparlure but none have made significant improvements over the original synthetic route published by Sharpless (Li et al., 1997; Wang et al., 2012).

1.4.4. Sharpless synthesis of (+)-disparlure (15) – Asymmetric dihydroxylation

Later, Sharpless reported another synthesis of (+)-disparlure (**15**) that uses his asymmetric dihydroxylation (Keinan et al., 1992) as the key step to obtain the requisite stereochemistry of the (+)-disparlure (**15**). Even though this synthesis was not as short as his previous asymmetric epoxidation, its overall yield was improved. The synthesis began with undecanal (**56**) as shown in Scheme 1.5. The undecanal (**56**) was treated with Grignard reagent vinyl magnesium bromide to get allylic alcohol **57**, which was heated with triethyl orthoacetate in the presence of catalytic amount of propanoic acid to give *trans*-alkene ester **58**. Asymmetric dihydroxylation of *trans*-alkene **58** by using chiral ligand AD-mix-α furnished a hydroxyl lactone, the alcohol group of which was protected with *tert*-butyldimethylsilyl group (TBDMS) to produce **59** with 95% ee.

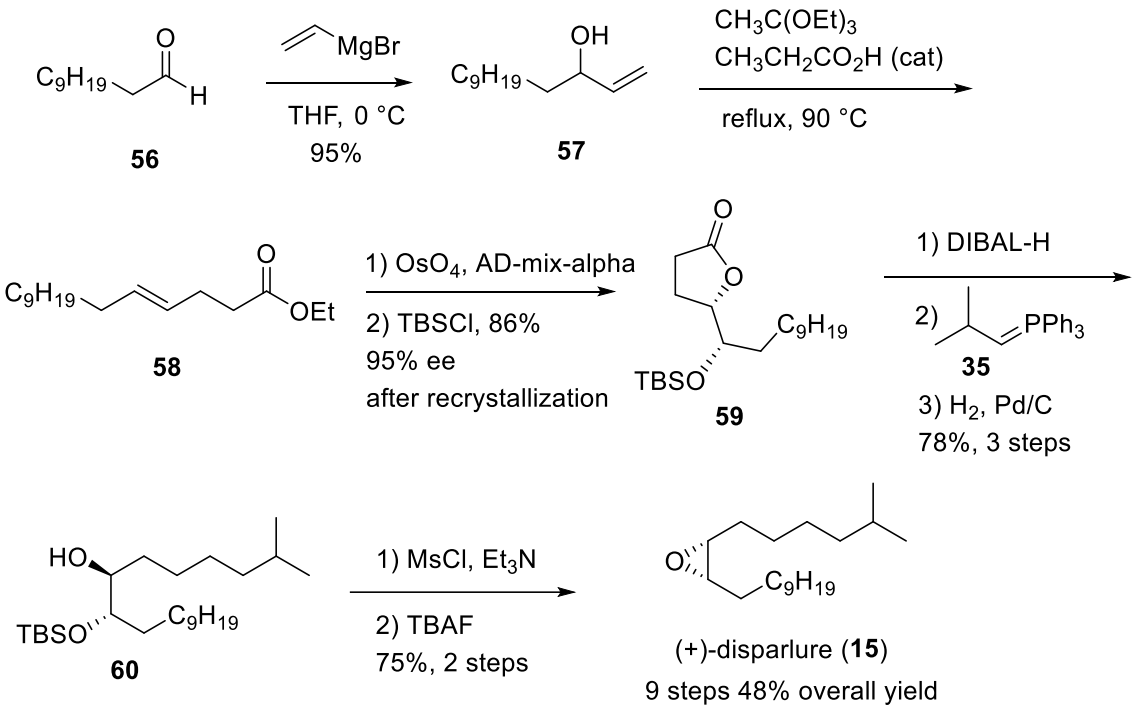

Scheme 1.5 Synthesis of optically pure disparlure (15) by Sharpless asymmetric dihydroxylation.

The enantiopurity of the lactone was further improved via recrystallization. Since Iwaki's synthesis of (+)-disparlure (**15**), a three-step sequence such as the lactone reduction-Wittig olefination-hydrogenation has become a prevalent strategy used in the synthesis of disparlure. Sharpless utilized this three-step sequence to give **60** in 78%. Finally, the synthesis was completed via mesylation of the free secondary alcohol group of **60** followed by cleavage of TBDMS protecting group with TBAF (tetrabutylammonium fluoride), which afforded enantiopure disparlure (**15**) in 9 steps with 42 % overall yield. The advent of Sharpless asymmetric dihydroxylation (AD) facilitated a number of new syntheses of disparlure enantiomers.

1.4.5. Plettner's synthesis of (+)-disparlure (15) and the analogues

In 2005, Plettner and co-workers prepared disparlure analogues **62** and **63** based on chiral separation of epoxy alcohols using microcrystalline cellulose triacetate-I (MCTA-I) column (Inkster et al., 2005) (Scheme 1.6). The allylic alcohol **52** was prepared from propargyl alcohol (**50**), which on epoxidation with meta-chloroperbenzoic acid (*m*-CPBA) gave epoxy alcohol **61**. Chiral resolution of this epoxy alcohol on MCTA-I was very poor.

Therefore, the allylic alcohol **52** was converted to allylic esters **52a-c**. These esters on epoxidation produced epoxy esters **61a-c**. Out of 3, the epoxy ester **61a** was well separated on MCTA-I to afford enantiopure epoxy esters **61a'** and *ent*-**61a'**. The epoxy ester **61a'** on basic hydrolysis produced epoxy alcohol **53**, which upon oxidation followed by Wittig reaction delivered (+)-disparlure alkene analogue **63**. The alkene **63** can be hydrogenated with Pd/C to (+)-disparlure (**15**). The epoxy alcohol **53** up on reaction with 1-bromo-3-methyl butane (**48**) produced disparlure analogue **62**.

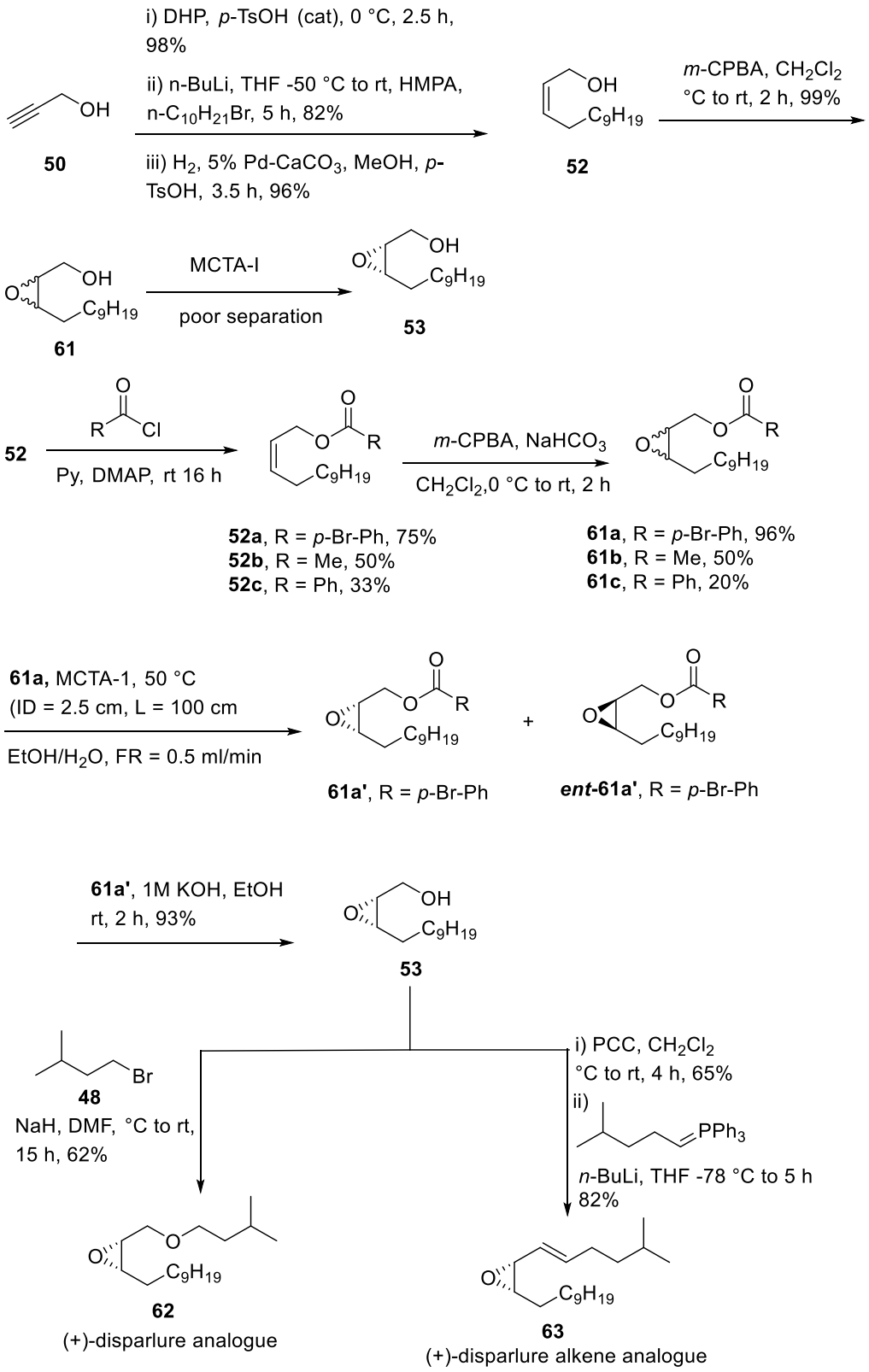

Scheme 1.6 Plettner's synthesis of oxa and alkene analogues of (+)-disparlure (15).

1.4.6. Kim's synthesis of (+)-disparlure (15)

In 2009, Kim reported a synthetic route to (+)-disparlure (**15**) based on asymmetric proline catalysis (Kim, 2009) to obtain the requisite stereochemistry of epoxide of the disparlure (Scheme 1.7). He treated the dodecanal **64** with nitrosobenzene **65** and D-proline to afford enantiopure α-aminoxylated aldehyde which on subsequent allylation with allyl bromide to give **66** as a diastereomeric mixture (4:1).

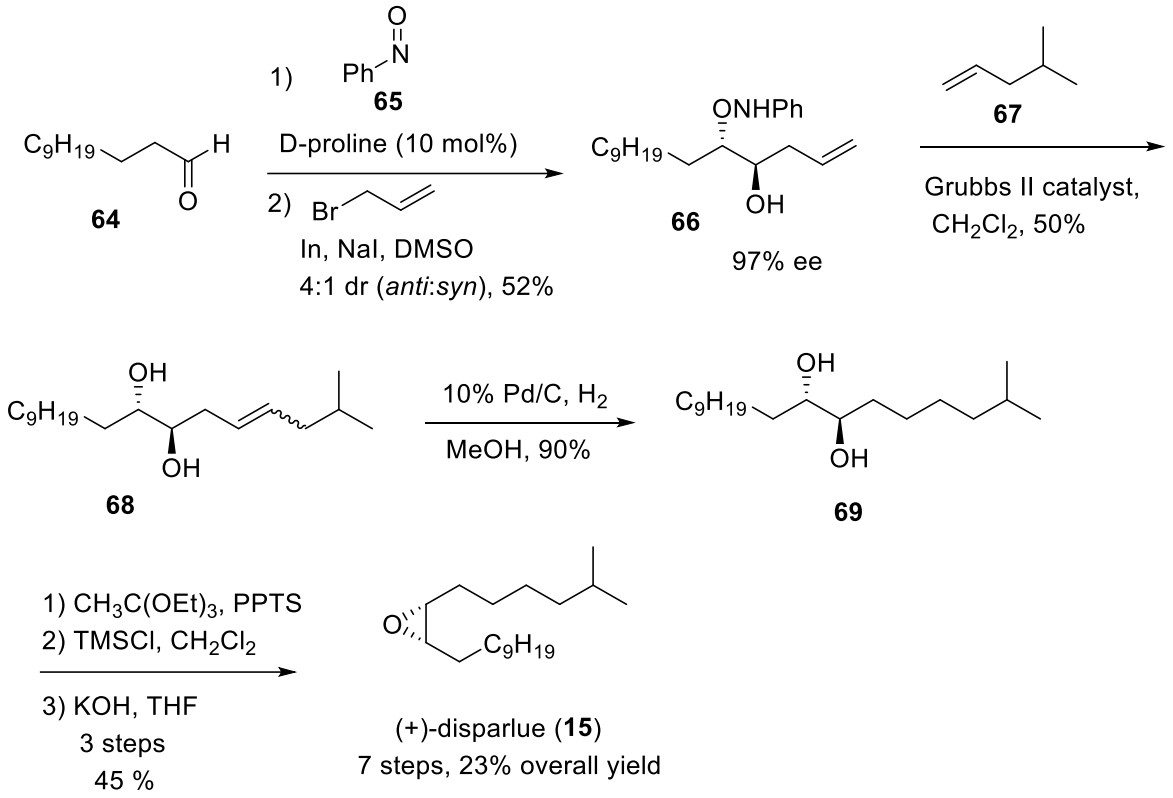

Scheme 1.7 Kim's synthesis of (+)-disparlure (15) with introduction of asymmetry through proline catalysis.

The major diastereomer (*anti*) **66** was taken forward through olefin metathesis with 4-methyl-1-pentene (**67**), which was associated with cleavage of N-O bond to afford 1,2-*anti* diol **68**. The alkene moiety of diol was then hydrogenated with Pd/C to deliver **69**, which was subjected to a three-step epoxidation sequence to produce (+)-disparlure (**15**) in 6 steps and 23% overall yield. In terms of step count, Kim's synthesis towards (+)-disparlure (**15**) was efficient. However, the key first step afforded poor diastereoselctivity and low yield.

1.4.7. Satoh's synthesis of (+)-disparlure (15)

Scheme 1.8 shows Satoh's enantioselective synthesis of (+)-disparlure (**15**) using a chiral sulfoxide auxiliary (Satoh et al., 1988) to impart asymmetry at the chiral centers. Chlorination of chiral sulfoxide **70** with NCS (*N*-chlorosuccinimide) gave chloroalkyl sulfoxide **71**. Deprotonation of **71** with base (LDA, lithium diisopropylamide) and alkylation with decyl iodide delivered **72** as a diastereomeric mixture. Next, deprotonation of **72** with LDA followed by treatment with 6-methyl-1-heptanal **73** produced **74** and **75** as a mixture of diastereomers (1:1.2), which was separated by column chromatography to deliver the desired product **75**. Then the chlorohydrin **75** was exposed to potassium *tert*-butoxide in *tert*-butanol to undergo epoxidation and afford **76**. Finally, the sulfoxide auxiliary of **76** was removed with base to deliver (+)-disparlure (**15**) in 5 steps and 11% overall yield. Satoh's use of the chiral sulfoxide auxiliary provides the shortest synthetic route to (+)-disparlure. However, the auxiliary offers poor diastereoselectivity in steps 2 and 3, and the synthesis ultimately gave low overall yield. Furthermore, the sulfoxide auxiliary detracted from the efficiency of the synthesis.

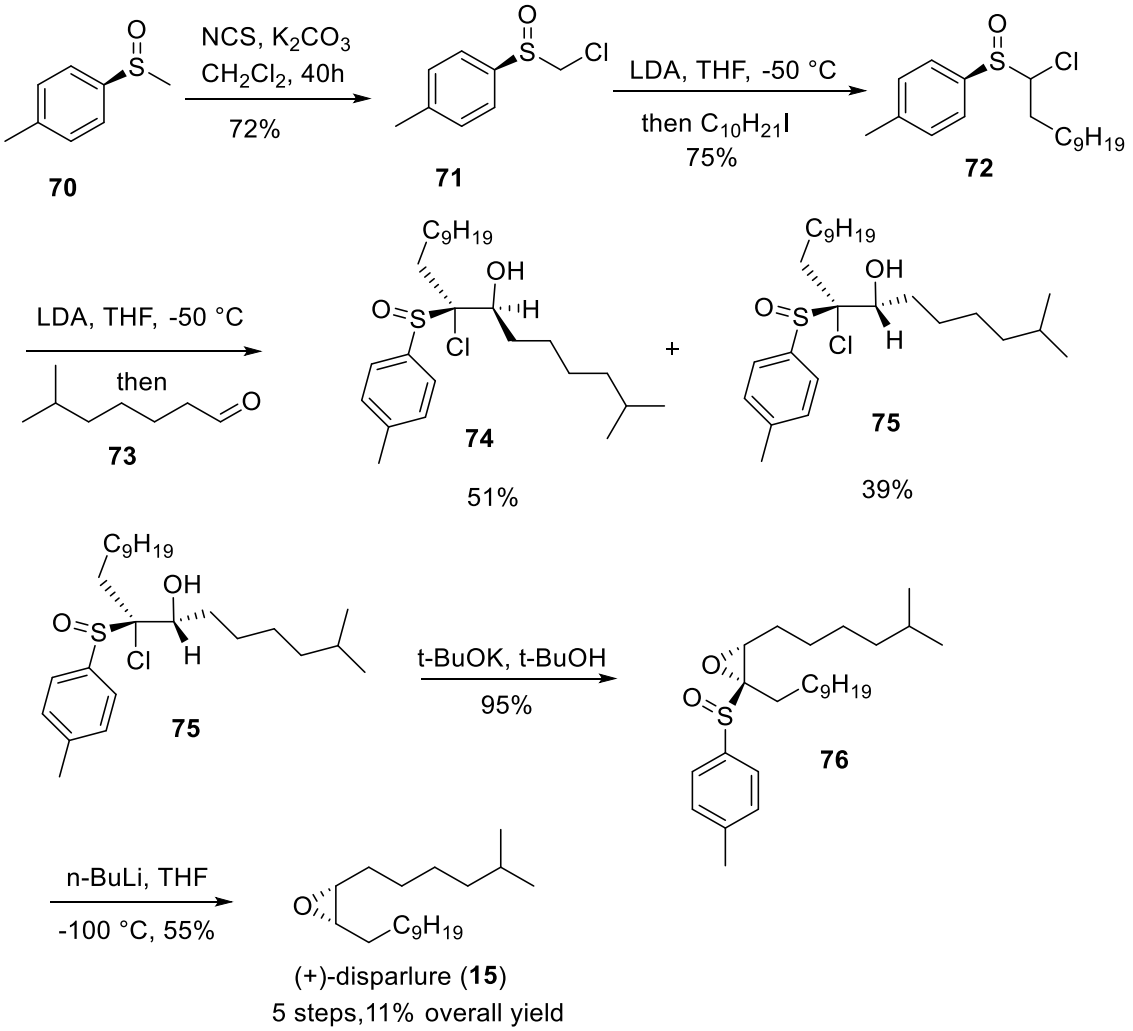

Scheme 1.8 Synthesis of (+)-disparlure (15) using chiral sulfoxide auxillary.

1.4.8. Martin's synthesis of (+)-disparlure (15)

In 2018, Martin and co-workers reported (Klosowski and Martin, 2018) an enantioselective synthetic route to (+)-disparlure (**15**) involving BINOL-amide catalysed iodolactonization as the key step (Scheme 1.9). Alkylation of alkynoic acid **77** afforded **78** which was partially hydrogenated with a Ni-catalyst to *cis*-alkene **79**. Next, enantioselective iodocyclization using BINOL-amide catalyst **80** gave **81** with high enantiomeric ratio (95: 5). Finally, compound **81** was converted to (+)-disparlure (**15**) *via* a three-step sequence including reduction of lactone with DIBAL, Wittig olefination and catalytic hydrogenation. The organocatalytic approach required 7 steps, no protecting groups involved and had 33.1 % overall yield. This is one of the most successful syntheses

that also can be easily adopted for the (-)-disparlure (*ent*-**15**) synthesis by using *ent*-**80** ligand or changing the alkyl halide in the first step.

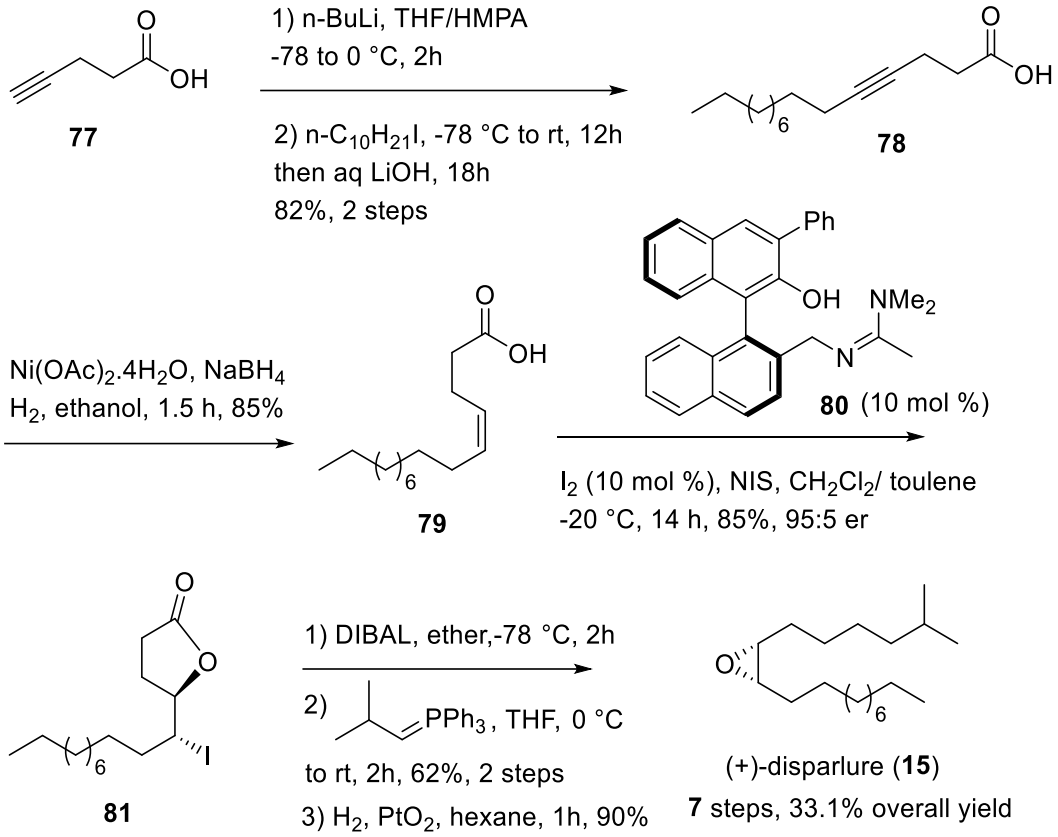

Scheme 1.9 Martin's synthesis of (+)-disparlure (15) by enenatioselective iodolactonization.

1.4.9. Summary of previous syntheses of (+)-disparlure (15)

(+)-Disparlure (**15**) has been the target of synthetic chemists for the last four decades. Despite over fifty syntheses of (+)-disparlure, there is still room for improvement because most synthetic approaches to (+)-disparlure that utilize chiral pool precursors such as L-(+)-glutamic acid, L-(+)-tartaric acid, (-)-2-deoxy-D-ribose and *S*-(-)-diethyl malate are low yielding and lengthy (see Table 1.1). Kim's synthesis of (+)-disparlure was efficient in terms of the number of steps, but his synthesis suffered from poor diastereoselectivity and low yield in the key step. Satoh's synthesis represents the shortest route to enantiopure (+)-disparlure, but his synthesis too suffers from poor diastereoselectivity in the key step and low overall yield. Sharpless' syntheses of (+)-disparlure *via* asymmetric epoxidation and dihydroxylation methods were demonstrated

to be most effective methods for building the stereocenters at epoxides. The drawbacks of previously reported approaches include the use of uncommon starting materials, low enantiomeric excess of the final (+)-disparlure, many steps and low overall yield (see Table 1.1).

Table 1.1 Summary of previous synthesis of (+)-disparlure (15) with step-count, overall yield and enantiomeric excess (*ee*)

Synthetic approach	Step-count	Overall yield (%)	[a]*ee* (%)	References
Chiral pool	12	9	88.4	Iwaki et al., 1974
	18	1.1	> 98	Mori et al., 1976
	15	20.7	> 99	(Kang et al., 1991)
	8	37.2	n.d.	Paolucci et al., 1995
	8	73	n.d.	Koumbis and Chronopoulos, 2005
	15	38.3	n.d.	Prasad and.Anbarasan, 2007
	15	3.3	~ 90	(Kovalenko, et al., 2009)
	12	11.7	n.d.	Dubey and Chattopadhyay, 2011
	8	22.6	n.d.	Bethi et al., 2014
	14	15.8	>98	Drop et al., 2020
Chiral reagents	5	11	94	Satoh et al., 1989
	9	24.4	~90	Marshall et al., 1999
	7	26.7	>99	Hu et al., 1999
Chiral separation	9	28.4	>97	Inkster et al., 2005

Metal-catalyzed (SAE[b]and SAD[c])	6	30	>95	Rossiter et al., 1981
	6	1.5	n.d.	(Odinokov et al., 1989)
	8	14.7	>95	Marczak et al., 1989
	9	28.1	>99	Guoqiang and Chunmin,1992
	12	16.5	>99	Fukusaki et al.,1992
	9	43	>99	Keinan et al., 1992
	6	26.8	> 98	(Wang et al.,2012)
Organocatalyzed	8	37.8	n.d.	Chao-Xin et al., 2007
	6	23	99	Kim, 2009
	13	18.1	n.d.	Garg et al., 2017
	7	33.1	>90	Klosowski and Martin, 2018
Enzyme-catalyzed	12	17.1	>91	Brevet et al., 1992

[a] Enantiomeric excess. [b] Sharpless asymmetric epoxidation. [c] Sharpless asymmetric hydroxylation. *n.d*. not determined

In addition to the sex pheromone-based control strategies for monitoring and controlling moth populations, a smart design of inhibitors or maskers and anti-attractants of sex pheromone perception of pest moths can disrupt the communication between moths and consequently control their population. In order to achieve this, it is essential to understand molecular mechanisms underlining the chemosensory system (olfaction and gustation) to detect either biological pheromones or their synthetic mimics.

1.5. Molecular components of pheromone reception

Moths have two important chemosensory systems, olfaction and gustation (Stocker, 1994). Pheromones might be detected by either system, but almost everything that is known about the processes behind the pheromone detection involves olfaction.

Pheromone molecules are detected by the antennae of the male moths (Kanaujia and Kaissling, 1985). On the surface of the antennae, there are thousands of olfactory sensilla divided into five structural types. The structural types are classified based on the their wall structure and morphology: chaetica, long trichodea, short trichodea, basiconica, coeloconica (Faucheux, 1985). Previous studies on moths have demonstrated that the pheromone detection is associated mainly with long sensilla trichodea (Kanaujia and Kaissling, 1985), whereas the short sensilla trichodea are involved in detection of both pheromone and other odorants (Ljungberg et al., 1993). The sensilla trichodea possess multiporous cuticular walls on their surface, having numerous tiny holes penetrating cuticle to give pheromones access the olfactory sensory neurons (OSNs) within (Boeckh et al., 1965; Schneider, 1969; Kaissling, 1971; Steinbrecht, 1997) (Figure 1.5). Generally, each sensillum is a hollow, hair-like structure, and inside the hair contains the dendrites of 2 to 4 olfactory sensory neurons bathed in the special aqueous fluid, referred to as the sensillum lymph (Chang et al., 2016). Embedded within the dendritic membrane of the OSNs are membrane proteins such as the sensory neuron membrane proteins (SNMPs), odorant receptor co-receptors (ORCO) and odorant receptors (ORs). The aqueous lymph fluid that bathes the dendritic membrane contains soluble proteins which include PBPs (pheromone-binding proteins) (Vogt and Riddiford, 1981) and PDEs (pheromone degrading enzymes) (Prestwich et al.,1989; Vogt et al., 1991). In addition to these proteins, ions such as sodium (Na^+), potassium (K^+), calcium (Ca^{2+}) and chloride (Cl^-) have also been identified in lymph (Kaissling and Thorson, 1980). Recently, endogenous fatty acids were identified and quantitated from isolated sensillar lymph droplets which contained palmitic, oleic, and stearic acids at pH 8.0-8.5 (Nardella et al., 2015). The latter result suggests that lymph contains a soap-like fatty acid emulsion (Nardella et al., 2015).

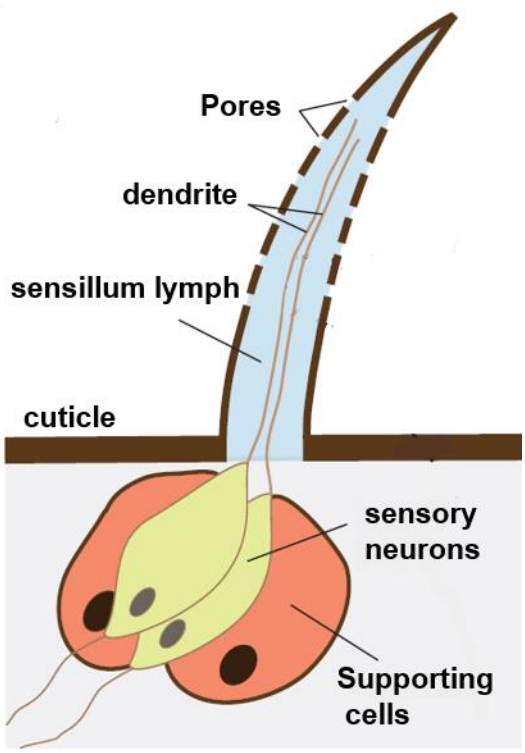

Figure 1.5 **Schematic diagram of the sensillum showing the detailed configuration of olfactory sensory neurons (OSNs) and supporting cells. Pheromne detected by pheromone receptors (PRs) expressed on the dendtric membrane of the OSNs. Adopted from the journal article (Sanchez-Gracia et al., Heredity, 2009, 103, 208-216).**

The early pheromone reception processes involve initial contact between pheromones and the molecular components of the sensilla trichodea, where the activation of signalling pathways takes place (Pelosi, 1996; Stengl et al., 1999). These processes include: 1) the adsorptive uptake of pheromone molecules from the external environment by sensilla trichodea; 2) their diffusion through the pores of the cuticle of the sensilla, towards olfactory receptor cells, 3) their interaction with various molecular components in the sensillum lymph and 4) activation of the odorant receptors (ORs) in the neuronal membrane. tetrameric proteins that form a cation channel (Butterwick et al., 2018). Activation of ORs involves specific molecular interactions within the binding site of the OR (Yuvaraj et al., 2021), which trigger the channel to open and the membrane to depolarize (Sato et al., 2008; Wicher et al., 2008). Because the direct interaction between the pheromone and OR is needed for chemoreception, the pheromone must diffuse somehow through the sensillar lymph. Considering that moth sex pheromones are very hydrophobic, as well as the presence of certain hydrolytic enzymes in the sensillum lymph, pheromones

do not diffuse easily through the hydrophilic sensillum lymph surrounding the dendritic membrane of olfactory sensory neurons. However, when the pheromones are bound to water-soluble pheromone binding proteins in the lymph, they become solubilized and most probably protected from breakdown by soluble enzymes or adsorption on cuticular surfaces. When the pheromone receptor proteins are expressed on the dendritic membrane of OSNs, and when they are activated, such that they allow influx of Ca^{+2} or Na^{+} (Sato et al., 2008; Wicher et al., 2008). This depolarizes the dendritic membrane, and this signal eventually leads to the generation of repetitive action potentials, electric signals that are transduced along the OSN's cell body and axon to the antennal lobe. After activating the pheromone receptors, the pheromone molecules are deactivated either by pheromone-degrading enzymes (PDEs) (Vogt et al.,1985) scavenging by the PBPs (Honson et al., 2003; Gong et al., 2009; 2010) or via other unknown deactivation mechanisms (Zhou, 2010; Leal, 2013; Sakurai et al., 2014).

When using olfactory proteins as molecular targets in studies aimed at the potential inhibitors of sex pheromone perception, it is important to focus on PBPs because the literature on pheromones and sensory physiology reveals that the moth PBPs are predominantly expressed in male moth antennae and are essential for pheromone detection. A better understanding of the functional role of PBPs will allow design of new insect control agents. The next sections will present details on the roles of PBPs and PDEs in pheromone perception in moths.

1.5.1. Pheromone binding proteins (PBPs)

PBPs are small (16-20 kDa), acidic, water-soluble extracellular proteins, and they are members of a unique protein super-family, the insect odorant binding proteins (OBPs). PBPs are synthesized by two olfactory auxiliary cells: tormogen and trichogen cells two types of support cells at the base of sensilla (Figure 1.5) and these cells secrete PBPs abundantly (in the range of 1-10 mM) into sensillum lymph of pheromone sensitive long sensilla trichodea (Klein, 1987; Vogt et al., 1989). In 1981, Vogt and Riddiford discovered the first PBP from antennae of the males of *A*. *polyphemus* (Vogt and Riddiford, 1981). Since 1981, a large number of PBPs have been discovered and physiologically characterized in various Lepidoptera species, including the tobacco hornworm, *M*. *sexta* (Feng and Prestwich, 1997), the European gypsy moth, *L*. *dispar dispar* (Plettner et al., 2000), the wild silk moth, *A*. *polyphemus* (Maida et al., 2003), the beet armyworm, *S*.

exigua (Xiu and Dong, 2007), the diamondback moth, *P. xyllostella* (Sun et al., 2013) and rice stem borer *C. suppressalis* (Chang et al., 2015).

1.5.2. Gypsy moth pheromone binding proteins

In 1989, Vogt *et al*. discovered two olfactory specific proteins in the gypsy moth that are exclusively associated with the male antennae (Vogt et al., 1989). These proteins are expressed in equivalent amounts in the sensilla and share 50% identity (Merritt et al., 1998). Both the proteins bound to the gypsy moth sex pheromone and shared sequence similarity with the *B. mori* PBP *Bmor*PBP. Therefore, both proteins were identified as *Ldis*PBPs and are named PBP1 and PBP2, based on their migration differences on non-denaturing-PAGE (polyacrylamide gel electrophoresis) with PBP2 being the more negatively charged of the two PBPs. PBP1 (~16 kDa) contains 143 amino acid residues whereas PBP2 (~16 kDa) contains 145 amino acid residues (Table 1.1).

Table 1.2 *Ldis*PBP1 and *Ldis*PBP2 amino acid sequence.

***Ldis*PBP1**
SKEVMKQMTINFAKPMEA**C**KQELNVPDAVMQDFFNFWKEGYQITNREAG**C**VIL**C**LAKKLELLDQDMNLH HGKAMEFAMKHGADEAMAKQLLDIKHS**C**EKVITIVADDP**C**QTMLNLAM**C**FKAEIHKLDWAPTLDVAVGEL LADT
***Ldis*PBP2**
SKDVMHQMALKFGKPIKL**C**QQELGADDSVVKEFLDFWKDGYVMKDRQTG**C**MLI**C**MAMKLELLDSAMEI HHGSTFAFAKAHGADEAMAQQIIDIVHG**C**TTTYPAAETNDP**C**QRAVNVAM**C**FKAHVHKLNWAPDVELLV ADFLAESQ

The position and disulfide connectivity of six conserved cysteine residues (or three disulfide bridges) in the primary sequence of *Ldis*PBP1 and *Ldis*PBP2 have been determined by cyanylation reactions and cyanogen bromide (CNBr) chemical cleavage, followed by mass spectrometry of the fragments (Honson and Plettner, 2006). The 6 cysteine residues are shown in bold, red type in the sequences in Table 1.1. For *Ldis*PBP1, the disulfide linkages are found between Cys19-Cys54, Cys50-Cys109 and Cys97-Cys118. As for *Ldis*PBP2, the sulfur bridges are Cys19-Cys54, Cys50-Cys110 and Cys97-Cys119.

1.5.3. Homology models of *Ldis*PBP1 and *Ldis*PBP2

To date, three dimensional structures of several insect PBPs have been elucidated by X-ray crystallography and/or NMR spectroscopy. These include PBP from *B*. *mori* *Bmor*PBP (Damberger et al., 2000; Horst et al., 2001; Lee et al., 2002), the giant silkworm moth *A*. *polyphemus* *Apol*PBP (Mohanty et al., 2004; Damberger et al., 2007), the honey bee *Apis mellifera* L. ASP1 (Birlirakis et al., 2001; Lartigue et al., 2004), the gypsy moth *L*. *dispar* *Ldis*PBP1 (Terrado et al., 2020). The structure of *Ldis*PBP2 has not yet been solved. Both *Ldis*PBP1 and *Ldis*PBP2 share sequence homology with *Apol*PBP and *Bmor*PBP (Du et al., 1994; Merritt et al., 1998). These structures reveal that insect PBPs can adopt two folded forms, known as A-form and B-form. The A-form (*e*.*g*. of *Ldis*PBP1) has 7 helices, of which 1-6 are the same as for the B-form of PBPs and the 7th is at the C-terminus (Figure 1.6A). The B-form (*e*.*g*. of *Bmor*PBP) contains 6 α-helices, and 4 of these helices connect to form a hydrophobic binding pocket (Figure 1.6C&D). In the A-form of PBPs, this pocket is partly occupied by the hydrophobic face of the 7th helix. Since insect PBPs share some sequence homology it can be believed that *Ldis*PBPs would have a similar protein structures, which both include the three conserved disulfide (-S-S-) linkages (Figure 1.6).

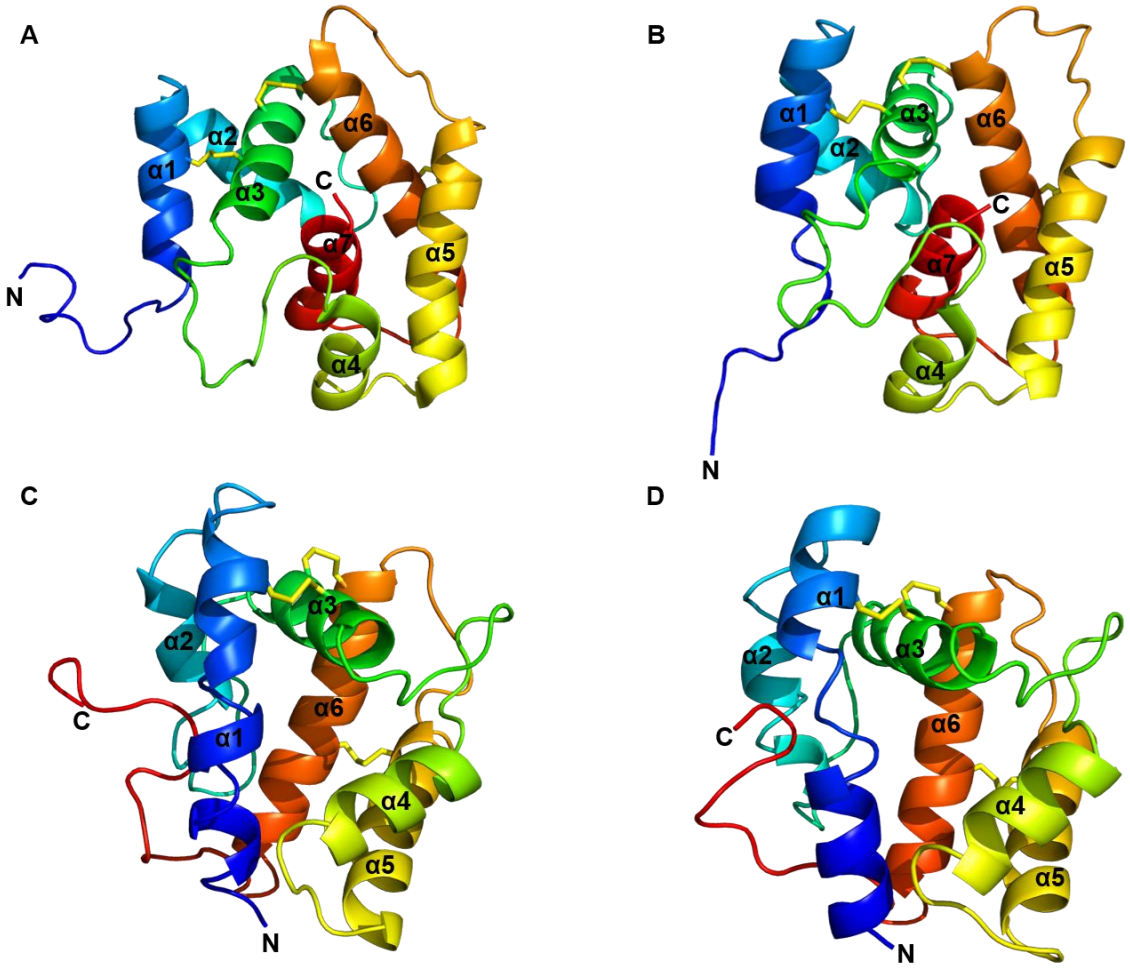

Figure 1.6 **A).The structure of *Ldis*PBP1 (A-form) (PDB ID: 6UM9) solved by NMR. B) The homology model of *Ldis*PBP2 (A-form). C) & D) The homology models of *Ldis*PBP1 and *Ldis*PBP2 (B-form), respectively.**

1.5.4. Functional role of PBPs in pheromone perception

For hydrophobic ligands such as insect sex pheromones, it has been proposed that the PBPs play a crucial role in pheromone capturing and transport to ensure that the pheromone-receptor interactions occur (Kaissling et al., 2013). However, functional studies suggest that there are 3 primary functions for PBPs, and these may play dynamic role in pheromone recognition and selectivity: 1) pheromone desorption from waxy cuticle of olfactory tubules to aqueous sensillum lymph, as suggested for gypsy moth PBPs *Ldis*PBP1 and *Ldis*PBP2 (Kowcun et al., 2001); 2) pheromone scavenging, accountable for the protection of pheromone receptors from saturation, as proposed for *Ldis*PBP2 based on a kinetic model (Gong et al., 2009); 3) pheromone recognition, as suggested for

the common fruit fly, *D*. *melanogaster* PBP (LUSH) functioning as an activator of OSNs (olfactory sensory neurons) tuned to pheromones (Laughlin et al., 2008). It is also suggested that PBPs protect pheromone molecules from deactivation or degradation by pheromone degrading enzymes during their transport, and that PBPs deliver pheromone molecules to the pheromone receptors (Kaissling, 1996 & 2001; Pophof, 2002; Leal, 2013), or form a complex with pheromones that directly activates the pheromone receptor (Pophof, 2004; Xu et al., 2005). However, it has been reported that the pheromones can activate the pheromone receptors in the absence of PBPs *in vitro* (Grosse-Wilde et al., 2006; Chang et al., 2015) and *in vivo* (Gomez-Diaz et al., 2013).

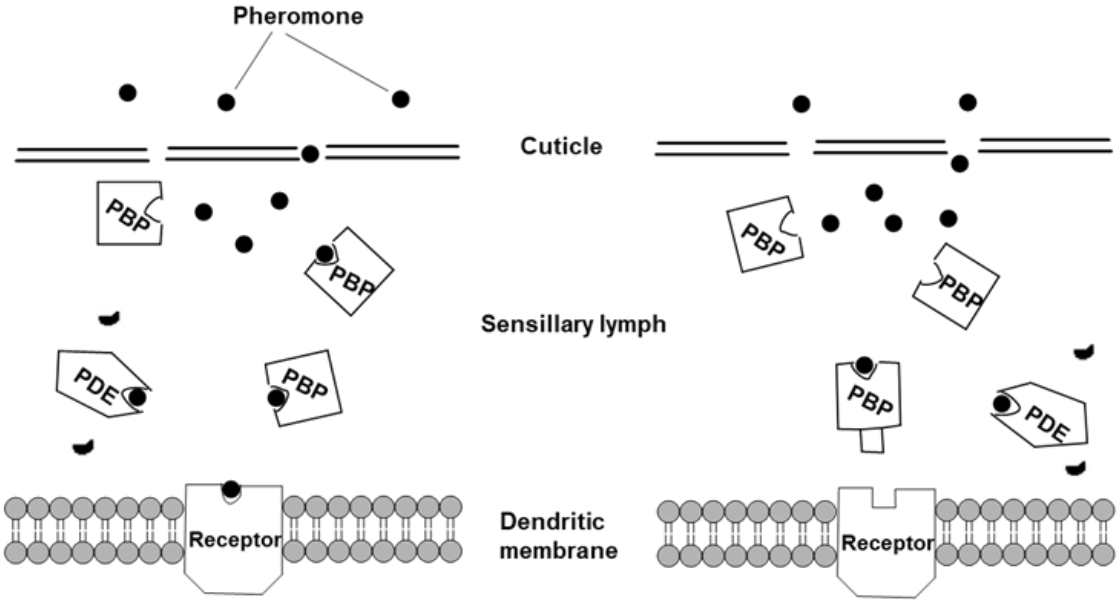

Figure 1.7 **Schematic representation of perireceptor events within the insect olfactory sensilla These events inculde interaction of pheromone molecules with PBPs which may function as carrier or/and scavengers for hydrophobic pheromones diffusing through the lymph and may even be involved in receptor activation. In some insects, pheromone degrading enzymes quickly teriminate the pheromone signal in the vicinity of pheromone receptor to allow the detection of new stimuli.**

PBP from the domestic silk moth, *B*. *mori*, *Bmor*PBP1 is an example of a PBP that is well characterized structurally and biochemically. *Bmor*PBP1 is expressed in the sensillum lymph of sensilla trichodea and selectively binds to *B*. *mori* sex pheromone bombykol (**1**) (Figure 1.1) instead of its aldehyde derivative, bombykal (**2**) (Steinbrecht et al., 1995; Laughlin et al., 2008). It binds strongly with bombykol (**1**) at physiological (pH =

7) but it shows no binding affinity when the pH changes to acidic (~4.5) (Wojtasek and Leal, 1999). It has been hypothesized that when the hydrophobic pheromone transported by PBP to the surroundings of pheromone sensory neurons where the pH is lower than in the bulk lymph, the hydrophobic pheromones will be delivered to the dendritic membrane of pheromone receptor neurons, where they can activate the pheromone receptors (Wojtasek and Leal, 1999).

Activity of pheromone receptors is detected in the absence of PBPs. For example, receptor activity studies done in frog, *Xenopus* oocyte systems (Chang et al., 2015; Zhang et al., 2014; Sun et al., 2013; Nakagawa et al., 2012; Sato et al., 2008) and HEK (human embryonic kidney) cells (Grosse-Wilde et al., 2006) expressing moth pheromone receptors reported receptor activity with addition of pheromones alone, without PBPs. It has been reported in various *in vitro* (Chang et al., 2015; Sun et al., 2013; Grosse-Wilde et al., 2007; Forstner et al., 2006) and *in vivo* (Pophof, 2002 & 2004) studies that in general, addition of PBPs enhances the sensitivity and modulates response signals of pheromone receptors. This suggests that PBPs are not merely passive pheromone carriers but play an important function in the creation of an olfaction system that is sensitive and discriminating.

However, a strong disagreement with the above studies is seen in fruit fly *Drosophila melanogaster*, with its odorant binding protein LUSH.(Xu et al., 2005). In LUSH mutants, the pheromone sensitive neurons in the mutant sensilla showed no response to the aggregation pheromone Z11-18:OAc. However, when LUSH transgene expression is rescued or recombinant LUSH protein is introduced in to the mutant sensilla, the response to aggregation pheromone is restored (Xu et al., 2005). Laughlin *et al*. demonstrated that the LUSH undergoes a pheromone specific conformational change that triggers the firing of pheromone sensitive neurons (Laughlin et al., 2008). From these studies, they concluded that the LUSH is absolutely required for detection of the aggregation pheromone Z11-18:OAc. However, Gomez-Diaz *et al*. showed that there is no conformational property of pheromone/LUSH that explains its proposed unique activated state, and a high dose of pheromone can induce neuronal activity in the absence of LUSH.(Gomez-Diaz et al., 2013).

In the past decades, PBP functional studies have also been performed in heterologous expression systems (*Xenopus oocyte* or the HEK cell system) in

combination with pheromone receptors. When pheromones are added into these systems expressing pheromone receptors either with PBPs or with bridging solvents such as DMSO (dimethyl sulfoxide), there was higher sensitivity of the pheromone receptors to pheromone in heterologous systems with PBPs than DMSO (Chang et al., 2015; Grosse-Wilde et al., 2006; Sun et al., 2013; Pophof, 2002; Forstner et al., 2009). This points towards the crucial role of PBP in dissolution of the hydrophobic pheromone in an aqueous sensillum lymph in pheromone receptor sensitivity.

Furthermore, when *B*. *mori* pheromone components bombykol (**1**) and bombykal (**2**) (oxidized form of bombykol) were delivered dissolved in dimethyl sulfoxide without *Bmor*PBPs, both pheromone components activated *Bmor*OR1 receptor expressing HEK-293 cells. However, when pheromone components were delivered dissolved with *Bmor*PBPs, without DMSO, the HEK-293 cells responded only to bombykol (**1**) (Grosse-Wilde et al., 2006). The results show that PBPs can bind, solubilize, and interact selectively with various pheromone compounds. In 2009, Forstner *et al*. also observed similar results in experiments performed on HEK-293 cells expressing *A*. *polyphemus* receptor (Forstner et al., 2009) *Apol*OR1. *A*. *polyphemus* uses a pheromone blend consisting of aldehyde E6,Z11-16:Ald (**6**) and acetate E6,Z11-16;Ac (**7**).(Figure 1.1). The authors demonstrated that *Apol*OR1 can be activated by both pheromone components **6** and **7** in solution with DMSO. Addition of *Apol*PBP1 or *Apol*PBP2 or *Apol*PBP3 with pheromone components **6** or **7** at nanomolar concentrations also elicited stronger response with *Apol*OR1. Interestingly, a selective receptor response profile was noticed at lower concentration (picomolar) of pheromone components. *Apol*PBP2 + pheromone component **6** was the only combination that elicited a response of *Apol*OR1.

In a similar experiment, utilizing *Heliothis virescens* OR13-expressing HEK cells, Grosse-Wilde *et a*l. demonstrated that the receptor responses to DMSO-solubilized major pheromone component Z11-16:Ald (**4**) (Figure 1.1) was remarkably increased by replacing DMSO with recombinant *Hvir*PBP2 (Große-Wilde et al., 2007). Interestingly, replacement of DMSO with recombinant *Hvir*PBP1 eliminated receptor responses to the major pheromone component **4**. These studies suggest a specific interplay between *Hvir*PBPs, *Hvir*OR13 and pheromone component **4**.

Another study on the interplay between PBPs and ORs from the diamondback moth *Plutella xylostella* demonstrated the effect of PBPs in receptor activation (Sun et al.,

2013). Oocyte cells expressing the odorant receptor *Pxyl*OR1 were shown to respond selectively to the major pheromone component Z11-16:Ald (**4**), the cells expressing *Pxyl*OR3 responded to the minor pheromone component. Introduction of *Pxyl*PBPs (PBP1 and PBP3) with the pheromone component **4** showed increased *Pxyl*OR4 response compared with *Pxyl*PBP3 using the same pheromone component. For *Pxyl*OR4, addition of *Pxyl*PBP2 and *Pxyl*PBP3 with minor pheromone component elicited higher responses compared with *Pxyl*PBP1.

However, Xu *et al* demonstrated that when *B*. *mori* pheromone components are placed with *Bmor*PBP1, there is no enhancement in selectivity; in contrast, both pheromone compounds were trapped by *Bmor*PBP1 leading to significantly reduced responses (Xu et al., 2012).

How the PBPs function in pheromone detection, whether the PBPs transport and deliver the pheromones to activate the pheromone sensitive neurons alone or instead as a complex is still debated. In the recent years, such functional studies have focused mainly on binding assays and PBP/OR interplay investigations have been conducted *in vitro*. In future, greater focus should be given to *in vivo* functional studies of PBPs and interactions between PBPs and ORs.

In pheromone mediated flights, moths can respond to a pheromone signal in 0.003 sec (Fadamiro et al., 1999). While flying, the moths must rest their olfactory system very quickly to detect intermittent signals encountered. For that reason, the information conveyed by pheromones require to be delivered quickly and terminated quickly. Once pheromone molecules have activated the pheromone sensitive neurons, they should be inactivated to avoid reactivation. Male antennae specific pheromone degrading enzymes (PDEs) have been considered as promising candidates to explain the rapid termination of the pheromone signal. Also, PBPs have been proposed to act as traps or scavengers for the pheromone, based on kinetic studies of ligand-PBP interactions (Gong et al., 2010).

1.5.5. Pheromone degrading enzymes

As another important component in the sensillum lymph, pheromone degrading enzymes (PDEs) have not drawn the same attention as PBPs have, since the first PDE (sensilla esterase, later renamed as *Apol*PDE) and PBP (*Aper*PBP) were co-discovered

from the wild silk moth *A*. *polyphemus* in 1981 (Vogt and Riddiford, 1981). A PDE is an enzyme, which has selectively evolved for rapid degradation of pheromone molecules and is expressed in the sensilla that detect pheromones. For example, *Apol*PDE can selectively and rapidly hydrolyze the sex pheromone component E6,Z11-16:Ac (**7**) with an estimated *in vivo* half-life rate of 15 milliseconds (Vogt and Riddiford, 1981). However, this seems contradictory to observation that the pheromone degradation on whole antennae of several moth species (*A*. *polyphemus*, *B*. *mori* and *L*. *dispar*) is very slow, with half-life rates observed in minutes (Vogt et al., 1985; Kasang, 1971; Kasang et al., 1974). One assumption for this variance in half-life rates may be attributed to the slow diffusion of the pheromone from cuticular surface into interior of the sensillum and chances that all pheromone molecules adsorbed to the antennae can reach the sensillum lymph in different times. Another possibility is that PBPs in some way participate in pheromone signal inactivation. In 1974, a model for pheromone detection in *B*. *mori* was proposed by Kaissling when the PBPs were not discovered yet. In this model, pheromone molecules were transported to the dendritic membrane via lipophilic pore tubules and involved in activation of sensory neurons and were finally inactivated through non-enzymatic processes (Kaissling, 1974) which were subsequently proposed to be assisted by PBPs (Kaissling 1986; Maida et al., 1995). All assumptions of PBP function are based on one fact: PBPs can strongly and reversibly bind pheromones.

The second characterized PDE, aldehyde oxidase (AOX), was identified in the antennae from tobacco hornworm moth *Maduca sexta*. The sex pheromone of *M*. *sexta* consists of two major components: bombykal (**2**) and (*E*,*E*,*Z*)-10,12,14-hexadecatrienal. The AOX of *Maduca sexta*, *Msex*AOX was shown to degrade the bombykal (**2**) in *in vivo*, leading to half life of 0.6 ms (Rybczynski et al., 1989).

Many moth species use a pheromone blend comprised of pheromones with diverse functional groups. Therefore, moths presumably require more than one PDE. Two similar aldehyde oxidases *Apol*AOX and *Bmor*AOX were identified in both male and female antennae of *A*. *polyphemus* and *B. mori*. Both oxidases from these species were capable of degrading aldehydes, such as the aldehyde pheromone components of those species (Rybczynski et al., 1990).

Another characterized PDE, *Pjap*PDE, is an esterase isolated from antennae of the Japanese beetle, *P. japonica. P. japonica* uses a chiral lactone (*R*,*Z*)-5-(-)-(1-decenyl)

oxacyclopentan-2-one (**20**) ((*R*)-japonilure) (Figure 1.3) as the sex pheromone.(Tumlinson et al., 1977).The other enantiomer (*S*)-japonilure acts as a behavioural antagonist to *P. japonica* but is used as a sex pheromone by closely related species Osaka beetle (Leal, 1996), *A. osakana Pjap*PDE is able to degrade the (*R*)-japonilure and other enantiomer (*S*)-japonilure with half life of ~30 and ~90 ms (Ishida and Leal, 2008). In addition to the characterized PDEs, there are other types of enzymes which specific enzymatic activities were identified in an antennal extract of several moth species. For example, the epoxide hydrolase activity has been detected in the antennal extracts of gypsy moth *Lymantria dispar*, suggesting a specialized enzyme for gypsy moth sex pheromone metabolism (Graham and Prestwich, 1992). Another, degradation of pheromonal aldehyde to acid in the tissue extracts of tobacco budworm *H. virescens* by aldehyde oxidase and dehydrogenase has been observed (Tasayco and Prestwich, 1990). Most of these enzymatic activities were seen in moths but the oxidative activity of cytochrome P450 was also identified in the antennal extracts of the scarab beetle *Phyllopertha diversa* (Wojtasek and Leal, 1999), in the mountain beetle (*Dendroctonus ponderosae*; MPB) (Chiu et al., 2019) and in the house fly *Musca domestica* (Ahmad et al., 1987) and were involved in pheromone metabolism.

These PDEs should somehow interact with PBPs in the sensillar lymph to balance pheromone degradation with the pheromone carrier and scavenging functions suggested for PBPs. However, the interaction between PDEs and PBPs is not known.

As an initial step, it was essential for my work to understand how PBPs and pheromones interact. The next section will focus on the interaction of PBPs with pheromones.

1.6. PBP-Ligand binding assays

Back in 1970s little was known about chemical structures of pheromones, let alone about their interaction with antennal components. Riddiford first used radiolabeled pheromone of the domestic silk worm *A*. *pernyi* and she successfully demonstrated its interaction with a male-specific antennal protein, later called *Aper*PBP (Riddiford, 1970). After this, numerous studies have yielded results that have been added the ligand-binding database of PBPs from various species, with either radioactive ligand techniques,

fluorescence titration assays, or gas chromatography (GC), as this has been reviewed by (Honson et al., 2005; Terrado et al., 2019).

To date, several binding assays have been reported to determine the binding of pheromones and ligands with pheromone binding proteins (PBPs). The first binding assay was reported by Vogt et al in 1989 using with radiolabeled pheromone (Vogt et al., 1989). In that assay, radiolabeled pheromone is incubated with PBP. The incubated sample is then loaded on to native polyacrylamide gel and electrophoresed. Then, the gel is either quickly stained and destained or blotted onto a membrane. The PBP band is then separated from the gel and placed in scintillation box to count radioactivity or blot is visualized by TLC (thin layer chromatography) plate scanner. This binding assay permits for only qualitative detection of pheromone binding.

In 1995, Du and Prestwich (Du and Prestwich, 1995) developed quantitative binding assay in which the radiolabeled pheromone is incubated with PBP in a plastic vial that is coated with a long-chain fatty alcohol such as 1-decanol (to prevent non-specific adsorption of pheromone to the vial surface). PBP.pheromone complexes adsorb to the surface of the plastic vial whereas the free pheromone is retained in the solution. A sample of the free pheromone is then measured for radioactivity. In subsequent assays, a filtration step utilizing size-exclusion column was introduced before counting radioactivity. In this assay, the PBP-pheromone complexes were found in the filtrate while free pheromone was retained in the column, permitting for direct estimation of bound pheromone (Plettner et al., 2000). The data from this assay give an estimate of the dissociation constant (K_d), provided the rate of dissociation of the PBP-ligand complex is much slower than the rate of separation. The disadvantage with these binding experiments was the adsorption of the hydrophobic pheromone on to the surface of plastic vial, even after coating plastic vials with 1-decanol in an effort to prevent the adsorption of the hydrophobic pheromone, Also, the synthesis of radioactive pheromones is difficult and limits the pheromone compounds tested in behavioral studies, usually the moth pheromones comprise blend of 2, 3 or even more components.

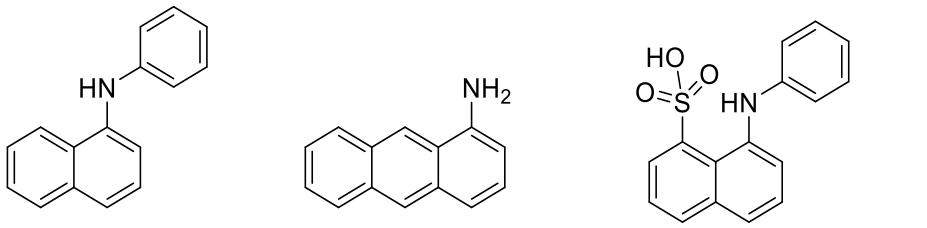

N-phenyl-1-naphthylamine (NPN) (**82**) 1-aminoanthracene (AMA) (**83**) 8-Anilino-1-naphthalene sulphonic acid (ANS) (**84**)

Figure 1.8 Structures of fluorescent probes.

Fluorescence-based binding assays between PBPs and ligands are frequently accomplished using the fluorescent probe *N*-phenylnaphthyl-1-amine (NPN) (**82**). Other, fluorescent probes sometimes used in ligand displacement assays are: 1-aminoanthracene (AMA) (**83**) and 8-anilino-1-napthalene sulphonic acid (ANS) (**84**). This assay allows determination of ligand binding affinity to PBPs at equilibrium. In fluorescence-based competitive binding experiments, the binding strength of the ligand is inferred from its ability of displacing the fluorescent probe from the PBP-ligand complex (Paolini et al., 1999; Ban et al., 2002). Generally, when the fluorescent probe binds inside the binding site of the PBP, its emission signal experiences a blue shift accompanied with an increase in fluorescence intensity. This permits easy estimation of the free and bound ligand concentrations, thus allowing the calculation of relative dissociation constant. Displacement of the fluorescent probe from the PBP binding pocket by cognate ligand causes a decrease in fluorescence intensity. This decrease is taken as measure of the binding strength of the ligand for PBP. However, the data from fluorescence-based competitive binding assay produce an approximate value of the dissociation constant (K_d) since it requires the displacement of fluorescent probe by cognate ligand is being calculated. In addition, the added pheromone can form micelles around displaced fluorescent probe, resulting in high fluorescence of the probe, and this phenomenon may give the appearance of no displacement (*i.e*. a false negative). Contrarily, if the fluorescence of the PBP-bound florescent probe is quenched by a titrated ligand, then a false positive can result. Furthermore, fluorescent reporters, such as NPN **82**, are hydrophobic molecules that can non-specifically bind to hydrophobic regions on or in the PBP structure. On the other hand, it is still possible that a cognate ligand could move into the binding pocket without displacing the fluorescent reporter. In such cases, since the

cognate ligand binding is not followed by the exit of the probe, the ligand binding affinity for the PBP could be underestimated.

There are other disadvantages with binding assays discussed above. First, since the pheromones are so hydrophobic, they stick to the plastic and glass tubes. Second (and related to the first), it is hard to estimate the bound and free pheromone concentrations because of poor solubility of pheromone in buffer. Third, it is difficult to synthesize the radiolabeled pheromone and pheromone analogues and there are increased safety, disposal and health problems associated with use of radiolabeled ligands.

The main focus of research on insect PBPs is to develop PBP-pheromone binding assays that do not involve use of radiolabeled pheromones. Although the existing fluorescent reporter displacement assay is quick and convenient to use, this assay has drawbacks that can lead to false positives and false negatives with high probability.

Fluorophore-tagged ligands are promising alternatives to radiolabeled ligands and fluorescent probes that are displaced. Assays with fluorophore-tagged ligands permit the study of protein-ligand interactions, both for thermodynamic measurements (at equilibrium) and for kinetic measurements. Additionally, the probes can be applied to insect tissues to see where they bind. Increasingly, biochemical assays using such selective fluorescent ligands have been demonstrated to be superior to radiolabeled ligand-based assays (Sridharan et al., 2014). Since most insect pheromone molecules are themselves non-fluorescent, it is necessary to change them to get the fluorescent analogues.

1.6.1. Fluorophore tagged pheromones for binding assays

Since the identification of the first insect sex pheromone, bombykol (**1**), from the silk moth *B*. *mori*, the number of characterized sex pheromones and attractants of Lepidoptera species has drastically increased. The fundamental question of pheromone-PBP and pheromone receptor interactions remain unclear. However, to develop a method which could be used to address such questions, it is extremely important to modify the natural pheromone to obtain fluorescently labelled pheromone which can retain similar binding properties to the natural pheromone. The fluorescent labelling of a pheromone

can be achieved in two ways: 1) The pheromone structure can be linked to a fluorescent moiety, or 2) the pheromone structure can be altered such that it is inherently fluorescent through a built-in chromophore. Both ways are equally feasible, but the first way has been mostly preferred because of the more predictable biological and fluorescence properties of fluorophore and the greater synthetic ease. In addition, immediate availability of diverse fluorophores and fluorescent reagents (Figure 1.9) allows the development of a series of fluorophore-tagged ligands for many potential applications, including binding assays.

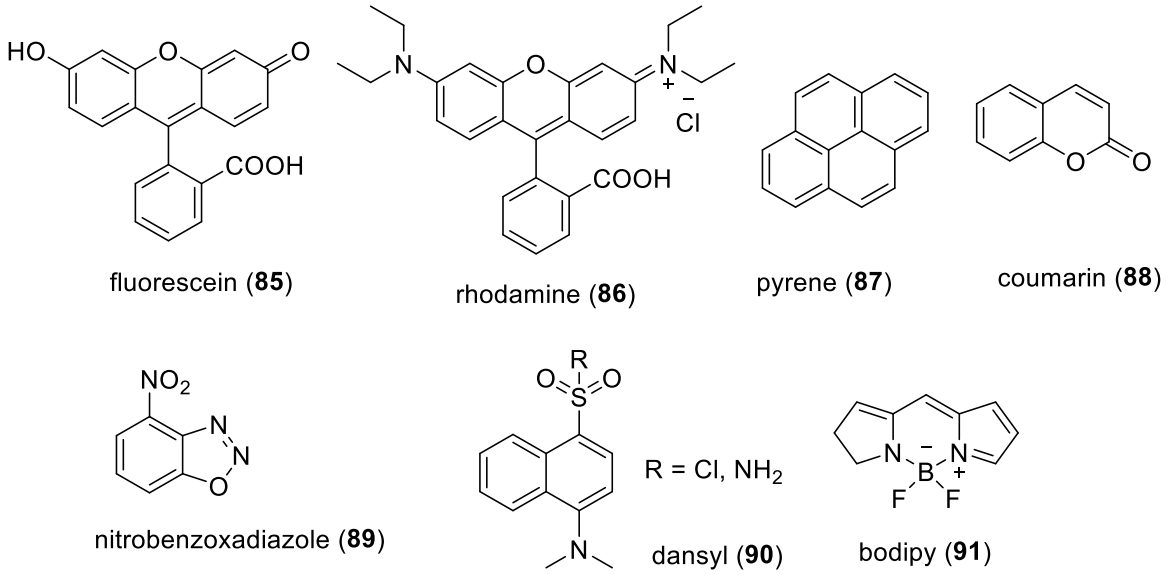

Figure 1.9 Structures of readily available fluorophores.

The main requirements in the design of the fluorescent labelled ligand include 1) retention of biological activity of the natural ligand 2) selectivity and high ligand binding affinity 3) retention of essential fluorescent properties of fluorophore for biological use including high molar absorptivity (ε), high quantum yield (ϕ), high photostability, and emission of fluorescence clearly differentiable from the target autofluorescence. These requirements can and have been achieved by linking a ligand to the bulky fluorophore with a suitable separation. The most frequently used fluorophores are: fluorescein (**85**), rhodamine (**86**), pyrene (**87**), coumarin (**88**) nitrobenzoxadiazole (NBD) (**89**), dansyl (**90**) and bodipy (**91**) (Figure 1.9).

1.6.2. Interactions of PBPs with pheromones

The binding of pheromones to pheromone binding proteins has been studied with proteins from various species of Lepidoptera (reviewed: Honson et al., 2005; Terrado et al., 2019). The calculated equilibrium dissociation constant (K_d) differ significantly. This could be due to use of different experimental methods or techniques. Most Lepidopteran PBPs bind to hydrophobic long hydrocarbon chain (C14-C16) pheromone molecules; either an unsaturated fatty alcohol like E10,Z12-16:OH (**4**) (bombykol), pheromone component of the silk moth *B. mori* (Maida et al., 1993; Leal et al., 2005); an unsaturated fatty aldehyde such as Z11-16:Ald (**3**), pheromone component of the striped rice borer *C. suppressalis* (Tatsuki et al., 1983), or an unsaturated fatty acetate such as E6,Z11-16:OAc (**7**), pheromone component of the silk moth *A. polyphemus* (Vogt and Riddiford, 1981; Maida et al., 2003). There are some changes in length of hydrophobic chain, branching chains and functional group. The properties of the pheromones that are crucial for binding to PBPs are the position and configuration of the double bonds, location of the side chains, functional groups, and chirality. Figure 1.1, 1.2 and 1.3 show examples of some major components of sex pheromones from Lepidoptera. The sex pheromone of the European gypsy moth, *L. dispar dispar* is a chiral cis epoxide, (7*R*,8*S*)-7,8-epoxy-2-methyloctadecane (**15**) (Figure 1.3).

Usually, insect sex pheromones are blends of chemical compounds that are specific to species. For instance, in the silk moth *B. mori*, the pheromone blend consists of E10,Z12-16:OH (**1**) and E10,Z12-16:Ald (**2**) (bombykal oxidized form of bombykol (**1**)) (Kaissling et al., 1978). However, only the pheromone component **1** is able to elicit mating behavior in male silk moths whereas a pheromone component **2** acts as antagonist to **1**. One crucial point, related to function of PBPs, is whether PBPs can selectively bind and discriminate between the pheromone components. There is some evidence to support the interpretation that PBPs bind these ligands selectively.

PBPs have been considered to be involved in the discrimination of pheromones based on the fact that the each moth species has more than one PBP that shows different binding strengths to different pheromone components, as has been revealed in *in vitro* binding studies utilizing several moth species (Zhang et al., 2017). For example, selective pheromone binding by PBPs has been demonstrated for PBP1, PBP2 and PBP3 of silk moth *A. polyphemus* (Maida et al., 1993; Pophof, 2002; Mohl et al., 2002; Pophof, 2004).

It was shown that PBP2 of tobacco budworm *H. virescens* selectively bound to the main component of the sex pheromone blend (Große-Wilde et al., 2007). The PBP1 and PBP2 of the Chinese oak silk moth *A. pernyi Aper*PBP1 and *Aper* PBP2 have been shown to differentially bind sex pheromone components E6,Z11-16:OAc (**7**) and E4,Z9-14:OAc (**8**) with K_d (equilibrium dissociation constant) of 0.6 and 30 mM, respectively (Du and Prestwich, 1995). K_d values in the micromolar range (μM) have been estimated with PBP1 and PBP2 of gypsy moth *L. dispar* using radio-labelled pheromone (Plettner et al., 2000). In this paper, the authors also described that both PBPs are able to discriminate between the enantiomers of pheromone. However, in most of these above binding studies, the K_d was calculated after separation of the free and bound fractions of the pheromone at equilibrium. For example, the K_d value of the PBP of the cockroach *L. maderae Lma*PBP for the pheromone component 3-hydroxy-2-butanone has been measured as 4.1 μM. It is important to note that a structurally related compound 2,3-butanediol binds to the *Lma*PBP with similar affinity, whereas, two other components of pheromone blend (senecioic acid and (*E*)-2-octenoic acid), as well as fatty acids such as lauric and palmitic acids failed to bind to *Lma*PBP (Rivière et al., 2003). This suggests that *Lma*PBP discriminates the chain lengths and functional groups.

PBPs are capable of binding several compounds with some flexibility. In a fluorescent competition-binding assay, the PBP of the tobacco hornworm *M.sexta Mbra*PBP1 binds all three pheromone components Z11-16:Ald (**4**), Z11-16:OAc (**10**), and Z11-16:OH (**11**) with K_d values between 0.18 to 0.30 μM (Campanacci et al., 2001). In the same study, the authors also show that the PBP of silk moth *A. polyphemus*, *Apol*PBP1, binds host-specific pheromone and compounds that are structurally related to the pheromone. In this case, the components of the pheromone blend E6,Z11-16:Ald (**6**), E6,Z11-16:OAc (**7**) and E4,Z9-14:OAc (**8**) show identical K_d values (0.51, 0.50 and 0.48 μM, respectively). Moreover, bombykol (**1**), the sex pheromone component of *B. mori*, and fatty acids such as palmitic acid, palmitoleic acid and oleic acid also bind strongly to *Apol*PBP1 with similar dissociation constants of 0.56 to 1.36 μM. Furthermore, the pheromone of another insect, such as (+)-disparlure (**15**) of *L. dispar* and its enantiomer (-)-disparlure (*ent*-**15**) bind to *Apol*PBP3 (Plettner et al., 2000). In this work, the authors also noticed discriminatory ability of *Apol*PBP3 towards disparlure enantiomers. The PBP1 of navel orange worm *A. transitella* can bind to host-specific pheromone Z11,Z13-16:Ald (**9**) and also to its corresponding alcohol and acetate forms (Leal et al., 2009). Similarly,

three PBPs of the diamondback moth *P. xylostella* not only bind strongly all pheromone components but also binds a series of structurally related compounds of pheromone.(Sun et al., 2013).

The results from radioligand binding assays with tritium-labelled ligand and fluorescent displacement-binding assays with fluorescent probe NPN **82** have shown that PBPs can bind strongly to several compounds that are similar to their pheromone structures. (Honson et al., 2005; Terrado et al., 2019). However, the PBPs have great selectivity towards pheromones. These binding assays demonstrated that the PBPs can discriminate compounds by variations in hydrocarbon chain lengths, functional groups and stereocenters. This suggest that PBPs act as molecular filters in the sensillum lymph. They have stronger binding affinity towards physiological ligands that elicit physiological responses. It is important to consider that the binding interaction between pheromone and PBPs is reversible process which suggests that PBP associates with and dissociates from the pheromone at different rates, that can differ by as much as 6 orders of magnitude (Gong et al., 2009).

The binding assays described above have been used for understanding various aspects of the binding interactions of PBPs with ligands. For example, the effect of salt concentrations and pH (Kowcun et al., 2001; Sanes and Plettner, 2016), as well as the effect of other lymph components such as fatty acids have been explored (Nardella et al., 2015). These equilibrium or fluorescent displacement binding assays are often coupled with molecular docking experiments. For example, docking simulations at various pH values with *Ldis*PBP1 and *Ldis*PBP2 homology models, disparlure enantiomers and their oxa and thia analogues suggest that these ligands can selectively interact with several amino acid residues in the binding pockets of the PBPs and that these interactions vary with the ligand (Sanes & Plettner, 2016). In the same study and a previous one (Y. Yu & Plettner, 2013), the authors also observed enantioselectivity of *Ldis*PBPs towards disparlure enantiomers, as well as towards enantiomers of disparlure analogs.

1.6.3. Interactions of PBPs with non-pheromonal compounds

It has been shown that PBPs are also able to bind pheromone analogues and non-pheromonal ligands besides physiological ligands. For example, PBP of *M.sexta* *Mbra*PBP1 binds to fatty acids, particularly palmitic acid with K_d value of 0.12 µM

(Campanacci et al., 2001). The odorant binding protein of the fruit fly *D. melanogaster* (OBP LUSH) binds to a library of aromatic compounds, including phthalates (Zhou et al., 2004). The PBP1 of *B.mori*, BmorPBP1 was identified to bind the sex pheromone components bombykol (**1**) and bombykal (**2**), as well as to bind strongly to the non-pheromone compound such as (10,12)-hexadeca-diyn-1-ol (Hooper et al., 2009). The gypsy moth PBPs *Ldis*PBPs showed good affinity to several ligands that are structurally related to the pheromone with enantiomer discrimination (Honson et al., 2003; Yu and Plettner, 2013; Terrado et al., 2017). The *Ldis*PBPs have also been shown to bind a series of aromatic volatiles such as di-and tri-substituted alkoxy benzenes (Paduraru et al., 2008), but these volatiles do not elicit electrophysiological responses by themselves in the moth antennae. However, they resulted in prolongation of electrophysiological responses to the sex pheromone when presented simultaneously with the sex pheromone (Plettner and Gries, 2010; Gong and Plettner, 2011). The PBP1 of *A. transitella* binds to pheromone analogue more strongly than the pheromone (Leal et al., 2009). The PBP of the *B. mori*, *Bmor*PBP binds to non-pheromone ligands such as 1-iodohexadecane (**92**), 3-isobutyl-2-methoxypyrazine (**93**) (bell pepper odorant) (Lautenschlager et al., 2007). It has been shown that PBPs are also able to bind plant volatiles. For example, the PBP of *P. xylostella*, *Pxyl*PBP1 binds to (*E*)-ß-farnesene (**94**) and benzaldehyde (**95**) (Sun et al., 2013). In the case of the pea aphid, one PBP, *Apis*PBP3 selectively binds to (*E*)-ß-farnesene (**94**) (Qiao et al., 2009). PBP1 from *M. sexta*, *A. polyphemus* and *S. exigua* binds to several fatty acids with dissociation constants (K_d) in the micromolar range (Campanacci et al., 2001; Katre et al., 2009; Liu et al., 2015).

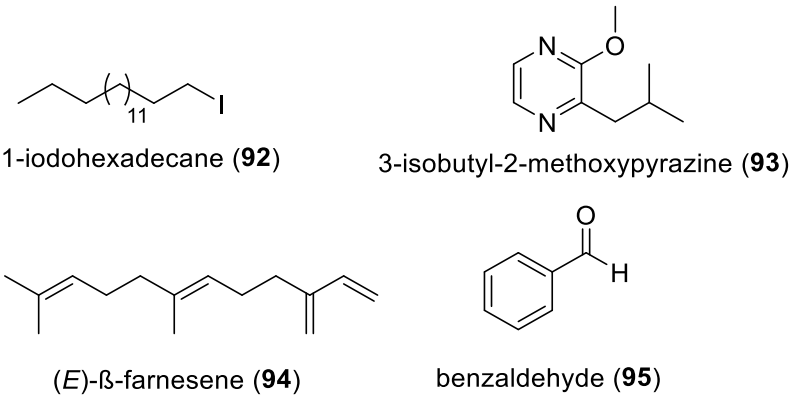

1-iodohexadecane (**92**)

3-isobutyl-2-methoxypyrazine (**93**)

(*E*)-ß-farnesene (**94**)

benzaldehyde (**95**)

Figure 1.10 Structures of non-pheromone ligands and plant volatiles.

The interactions of PBPs with ligand lead to questions on how the ligand associate with PBP and how they dissociate from the said protein. The next section will address those questions.

1.7. Pheromone association and dissociation mechanisms

Although the binding affinity (K_d) data are useful in estimating the strength of binding interaction between PBP and pheromone, the thermodynamic information is not enough to understand the time-dependency of olfaction dynamics. Therefore, it is essential to study the kinetics involved in the PBP-pheromone binding interactions, in order to link the mechanism of association and dissociation processes to what is viewed biologically.

To date, only a few studies have been reported with respect to kinetics of the PBP-pheromone interactions, namely, by estimating the association and dissociation rate constants (k_{on} and k_{off}) (Leal et al., 2005; Gong et al., 2009; Kaissling, 2009; Gong et al. 2010). For example, the k_{on}, and k_{off} values of *Apol*PBP1 with its pheromone component was estimated as 0.17 $\mu M^{-1}s^{-1}$and 0.01 s^{-1}, respectively. These k_{on} and k_{off} values were estimated, based on various electrophysiological and biochemical studies and on the hypothesis that PBP is the only carrier of pheromone in the sensillum lymph. For the interaction between the *Bmor*PBP and the pheromone component bombykol (**1**), the kinetic rate constants ($k_{on} = 6.8 \pm 1.0 \times 10^4$ $M^{-1}s^{-1}$ and $k_{off} = 0.007$ s^{-1}) have been calculated from intrinsic tryptophan quenching assay (Leal et al., 2005). In that assay, where the binding affinity of the pheromone or ligand is assumed to be able to quench the intrinsic fluorescence of the tryptophan residue within the PBP. When the pheromone or ligand interacts with the tryptophan residue, the tryptophan emission signal undergoes a blue shift associated with a decrease in fluorescence intensity. This decrease was used to measure association constant. The main issue with this assay is the relatively small change in tryptophan fluorescence, which yields large errors while measuring the binding constants.

To understand ligand association and dissociation in gypsy moth sensilla, fluorescence binding assays performed with *L. dispar* dansylated PBP2 and with disparlure enantiomers. The association and dissociation rate constants (k_{on} & k_{off}) calculated were much slower than the previous reports. The association constant (k_{on}) for

*Ldis*PBP2 for (+)-disparlure (**15**) and (-)-disparlure (*ent*-**15**) were 4.8 ± 0.4 x 10^2 M^{-1} s^{-1} and 1.6 ± 0.2 x 10^2 M^{-1} s^{-1}, respectively. The dissociation constant (k_{off}) values were 4.7 ± 0.4 x 10^{-4} s^{-1} and 5.0 ± 0.2 x 10^{-4} s^{-1}, respectively (Gong et al., 2009). In addition, the authors observed a rapid association step within first few seconds of the experiment. However, they were not able to determine the rate constant for this step due to the limitations of the technique used in that experiment. From these kinetic results, the authors proposed a two-step binding mechanism for PBP-pheromone association. In the first step, the pheromone and *Ldis*PBP quickly forms a PBP-pheromone external complex (Figure 1.11). The second step involves a slow internalization of the pheromone into the protein's binding pocket. A subsequent kinetic study with fluorescent probe such as 1-NPN **82** and *Ldis*PBPs supported the proposed first rapid association step (Gong et al., 2010). Furthermore, the authors identified a diffusion-controlled collision between the ligand and PBP prior to the ligand settling into the external binding site. In this collision step, the ligand collides with PBP resulting a PBP-ligand encounter complex (Figure 1.11).

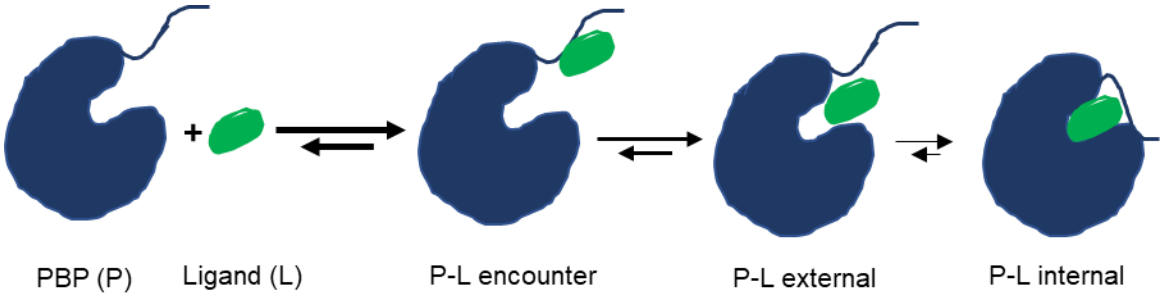

Figure 1.11 Proposed multi-step binding mechanism of ligand by *Ldis*PBPs.

The association and dissociation mechanism of PBPs is always a crucial issue. It has been proposed that, once pheromone-PBP complex reaches the vicinity of the dendritic membrane, a pH-induced conformational switch happens to release the pheromone. For instance, for the silk moth *B*. *mori*, it is proposed that the pheromone is delivered to the odorant receptors via a conformational switch of *Bmor*PBP1 by acidic pH in the vicinity of the dendritic membrane (Leal et al., 2005; Horst et al., 2001; Lautenschlager et al., 2005). It is important to note that the pH may play a role in PBP dynamics, but it cannot be the only the component that controls the association and dissociation of pheromone from PBPs. The pH of lymph from gypsy moth sensilla trichodea was measured and found to be approximately 8.5 (Nardella et al., 2015). According to another study on effect of pH and ionic strength, the high salt concentration

near the membrane, might be counteracting the effect of a slight decrease in pH (Kowcun et al., 2001). Moreover, a decrease in the pH near the dendritic membrane is estimated to be approximately 1 pH unit, and pH ~7.5 would probably not be enough to cause a conformational switch of moth PBPs from one form to an another.

Despite the number of functional and structural studies, the detailed mechanism of association and dissociation between pheromones and PBPs remains a block box. To understand pheromone binding and releasing at the high pH of lymph in gypsy moth sensilla, we have studied the kinetics of these processes using fluorescent pheromone analogs.

1.8. Thesis overview

This thesis is divided in to five chapters. Chapter 1 is an overview of the Lepidopteran sex pheromones, synthesis of gypsy moth sex pheromone (+)-disparlure and its antipode (-)-disparlure, molecular components involved in moth olfaction, and recent progress in moth PBP research.

Chapter 2 is adapted from the manuscript “Synthesis of isotopically labelled disparlure enantiomers and application to the study of enantiomer discrimination in gypsy moth pheromone binding proteins” (Pinnelli, G. R., Terrado, M., Hillier, N. K., Lance, D. R., Plettner, E. *Eur*. *J*. *Org*. *Chem*., **2019**, *40*, 6807-6821). It delineates a successfully completed synthesis of gypsy moth sex pheromone (+)-disparlure and its enantiomer, and nun moth pheromone component (+)-monachalure. This work involved the application of asymmetric SOMO catalysis to prepare the key enantiopure α-chloroaldehyde intermediate, which was rapidly converted into (+)-disparlure in excellent yield via a three step-sequence consisting of a diastereoselective nucleophilic addition, Mitsunobu reaction and hydrogenation. A critical aspect of this work involves the in-depth optimization of the diastereoselective nucleophilic addition reaction, following the groundwork in the synthesis of *trans*-epoxide containing pheromones laid out by Kang and Britton (Kang and Britton, 2007). This flexible and efficient synthetic route can be readily applied to the synthesis of isotope labelled disparlure enantiomers, and, in principle, epoxide containing insect sex pheromones.

Chapter 3 is adapted from the manuscript “Synthesis of isotopically labelled disparlure enantiomers and application to the study of enantiomer discrimination in Gypsy moth pheromone binding proteins” (Pinnelli, G. R., Terrado, M., Hillier, N. K., Lance, D. R., Plettner, E. *Eur*. *J*. *Org*. *Chem*., **2019**, *40*, 6807-6821). It describes the synthesis of the oxygen-17 or oxygen-18, and deuterium labelled disparlure enantiomers. Moreover, the binding interactions of deuterium labelled disparlure enantiomers with *Ldis*PBP1 and *Ldis*PBP2 using ^{2}H NMR spectroscopy is presented. In addition, the observed chemical shift changes of deuterated disparlure signals, from non-bound to bound, and the T1 and T2 relaxation times are correlated against the results from docking simulations of disparlure enantiomers bound to one internal site and multiple external sites of *Ldis*PBP1 and *Ldis*PBP2.

Chapter 4 delineates a successfully completed synthesis of fluorophore (6-FAM) tagged disparlure enantiomers. This chapter contains the results of fluorescence binding assay of fluorescent reporter, 6FAM tagged disparlure with *Ldis*PBP1 and *Ldis*PBP2. Moreover, the association and dissociation kinetics of 6FAM tagged disparlure enantiomers with *Ldis*PBP1 and *Ldis*PBP2 using stopped flow is presented. The structural bases of the binding interactions of between 6FAM tagged disparlure enantiomers and *Ldis*PBP1 and *Ldis*PBP2 are shown from molecular docking simulations.

The Chapter 5 focuses on the future work needed to further understand the functional role of PBPs in moth olfaction and use the pheromone probes to study the odorant receptors.

Chapter 2.

A short synthetic route to gypsy moth sex pheromone (+)-disparlure and its enantiomer (-)-disparlure, and the nun moth pheromone component (+)-monachalure

Adapted from: Pinnelli, G. R.,[1] Terrado, M.,[1] Hillier, N. K.,[2] Lance, D. R.,[3] Plettner, E.[1] (2019). European Journal of Organic Chemistry, 6807-6821.

[1] Department of Chemistry, Simon Fraser University, Burnaby, British Columbia, Canada.

[2] Department of Biology, Acadia University, 33 Westwood Ave., Wolfville, NS, B4P 2R6, Canada

[3] USDA-APHIS-PPQ CPHST Otis Laboratory, 1398 W Truck Rd, Buzzards Bay, MA 02542, USA.

GP synthesized the (+)-disparlure, (-)-disparlure and (+)-monachalure. NH and DL performed field experiments to demonstrate the attractiveness of the pheromone.

2.1. Introduction

The European gypsy moth, *Lymantria dispar dispar*, is established in several provinces of Canada (Ontario, Quebec) New Brunswick, Nova Scotia, and Prince Edward Island), and it has caused temporary outbreaks in Manitoba. It is an invasive pest of a large variety of trees and causes significant damage to Canada's forests, economy, and biodiversity. (+)-Disparlure, (7*R*,8*S*)-7,8-epoxy-2-methyloctadecane (**15**) (Figure 2.1) is the sex attractant pheromone, produced and released by female gypsy moths and detected by the male moths. Initially, disparlure was identified as *cis*-(7,8)-epoxy-2-methyloctadecane (±)-(**15**) by Bierl and coworkers (Bierl et al., 1970). Later, Iwaki *et al*. demonstrated the absolute stereochemistry of disparlure by synthesizing both enantiomers, testing them in the field, and reporting that (+)-disparlure (**15**) is more active than (-)-disparlure (*ent*-**15**) (Figure 2.1) for the attraction of the male gypsy moths (Iwaki et al., 1974). Interestingly, the synthetic version (+)-disparlure (**15**) is attractive to male moths in field studies, but naturally occurring pheromone is more attractive, suggesting that there may be a synergistic effect between (+)-disparlure (**15**) and other minor pheromone components (Gries et al., 2005; Park et al., 2019).

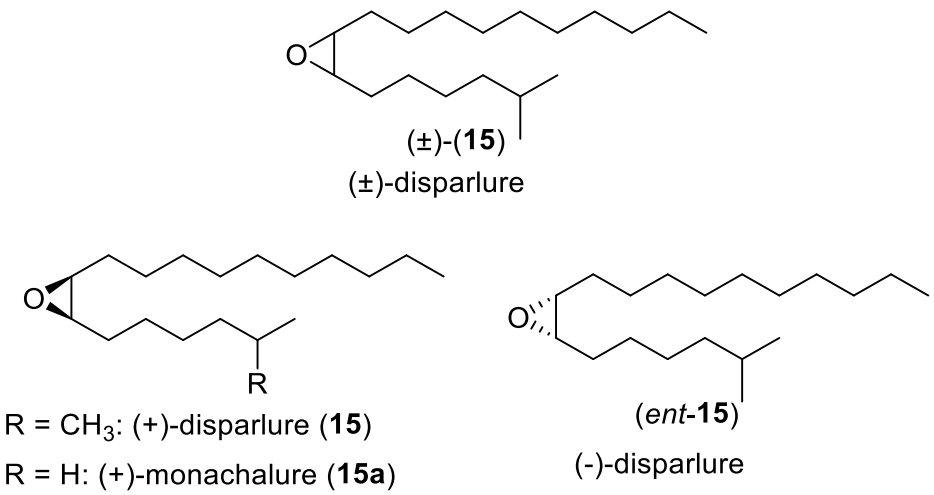

Figure 2.1 Structures of disparlure enantiomers and (+)-monachalure, prepared during optimization of disparlure synthesis.

The female gypsy moths produce and emit the sex pheromone into the wind in non-homogenous clouds, which the male moths detect with their highly sophisticated antennae to follow the pheromone and fly upwind towards its source. Because of strong

attractiveness of (+)-disparlure (**15**), it is used as a lure in traps to capture male gypsy moths. Disparlure is also used in mating disruption methods in which the chemical communication between gypsy moths is disrupted by releasing the large amounts of synthetic disparlure, and thereby preventing male moths from locating females and mating. In order to prevent gypsy moths from mating and breeding, the mating disruption technique is frequently used by saturating the area with racemic disparlure (±)-(**15**), which confuses the male moth (Leonhardt et al., 1996). Therefore, male moths cannot detect the pheromone and locate the females.

Over the past decades, significant progress has been made in the application of (+)-disparlure (**15**) in controlling and monitoring gypsy moth populations. As the commercial applications of (+)-disparlure (**15**) has expanded, its demand for larger quantities has increased, but many of the reported syntheses that use expensive and chiral pool starting material are lengthy, low yielding and of low stereochemical purity. For example, disparlure currently used for monitoring programs in the field is prepared by Sharpless epoxidation of (*Z*)-tridec-2-en-1-ol, to access the chiral epoxide ring, and Wittig olefination of the epoxy aldehyde to install the branched alkyl side chain. Typically, the overall yield of this route is 33% from non-commercially available starting material and enantiomeric excess values range from 91–95% (Rossiter et al., 1981). We have extensively investigated alternative synthetic route for the preparation of (+)-disparlure (**15**) in high yield, low step count and high stereochemical purity.

Disparlure has drawn a lot of attention from synthetic chemists due to its utility in monitoring gypsy moth populations, mating disruption treatments (Sarmiento et al., 1972) and scarcity of natural sources, leading to more than 50 synthetic routes (Introduction chapter, section 1.4). Despite these many syntheses, there is still room for improvement. We designed a synthetic route to (+)-disparlure (**15**) and (-)-disparlure (*ent*-**15**) that would have an advantage over previous syntheses in terms of enantiopurity, yield and step count. Herein we describe this five-step synthesis of (+)-disparlure (**15**), (–)-disparlure (*ent*-**15**), and (+)-monachalure (**15a**), the pheromone component of the nun moth, *Lymantria monacha*. This work has resulted in preparation of optically pure (+)-disparlure (**15**) in large quantities (>1 g). The (+)-disparlure (**15**) was tested in two infested zones, demonstrating that it is attractive towards male gypsy moths (Section 2.2.10).

2.2. Enantioselective synthesis of (+)-disparlure (15) and (-)-disparlure (*ent*-15)

2.2.1. Synthetic approach

We planned an approach where (+)-disparlure (**15**) could be synthesized from the 1,2-*syn* chlorohydrin **96**, which could be produced from the Mitsunobu inversion of the 1,2-*anti*-chlorohydrin **97** (Scheme 2.1). Our synthesis depended on the ability of a chiral imidazolidinone catalyst to promote the asymmetric α-chlorination of aldehyde **99** in highly stereoselective manner.

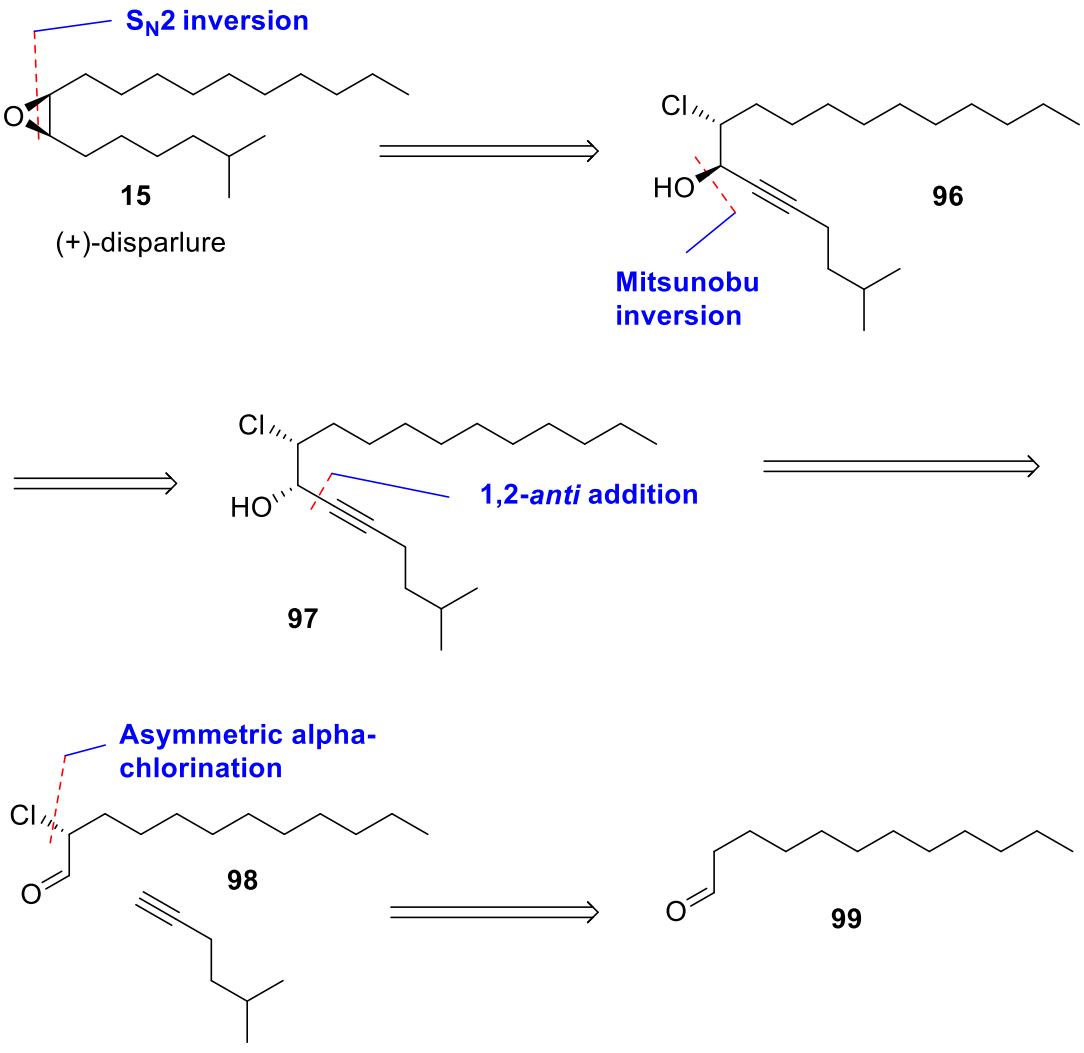

Scheme 2.1 Our retrosynthetic route to (+)-disparlure (15).

2.2.2. Asymmetric α-chlorination of aldehydes

Chiral secondary amine-catalyzed α-functionalization of aliphatic aldehydes is a versatile method for the creation of enantiomerically-enriched chiral stereogenic centers. In methods where the electrophilic chlorinating reagents such as perchlorinated quinone (**100)** *N*-chlorosuccinamide (**102**) are employed to catalyze this conversion, α-chloroaldehydes can be successfully prepared with high enantiopurity by chlorination of an enamine intermediate that the catalyst forms with the aldehyde.

In 2004, the first asymmetric α-chlorination of aliphatic aldehydes was reported by MacMillan's group (Brochu et al., 2004), almost simultaneously with Jørgensen's group (Halland et al., 2004). MacMillan and co-workers showed that the chiral imidazolidinone catalyst **101** can catalyze the asymmetric α-chlorination of aldehyde using the perchlorinated quinone (**100**) as a chlorinating agent (Scheme 2.2). In this reaction, the selection of solvent is crucial to obtain the highly enantiopure α-chlorinated product and to suppress the formation of α, α-dichlorinated product. Surveying different solvents showed that the dichlorination of the aldehyde and epimerization of the product were suppressed by acetone. Under these conditions, the chiral imidazolidinone catalyst **101** delivered the α-chlorinated aldehyde in good yield with excellent enantioselectivities (up to 95% ee).

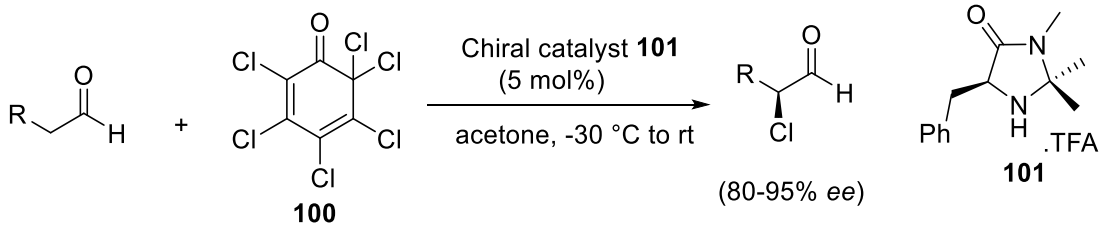

Scheme 2.2 Organocatalytic enantioselective chlorination of aldehydes by MacMillan and co-workers

Jørgensen and co-workers reported that the chiral secondary-amine catalysts such as L-proline (**103a**), 2-methyl-L-proline (**103b**), L-prolinamide (**103c**) and C_2-symmetric catalyst (2*R*,5*R*)-diphenylpyrrolidine (**104**) can catalyze the α-chlorination of aliphatic aldehydes using *N*-chlorosuccinimide (NCS) as chlorine source (Scheme 2.3). However, the enantiopurity and yield of the α-chloroaldehydes were dependent on the combination of solvent and catalyst used. Screening of the different solvents and catalysts revealed that use of catalyst **104** and 1,2-dichloroethane afforded highly enantiopure α-

chloroaldehydes (up to 97% *ee*) with good yield. Britton and co-workers also carried out the asymmetric α-chlorination of aliphatic aldehydes (Kang and Britton, 2007; Kang et al., 2009). They achieved the α-chlorination of pentanal and undecanal in 85% enantiomeric excess with a combination of organocatalyst L-prolinamide (**103c**) and *N*-chlorosuccinimide (**102**). In 2010, other organocatalyst has been reported by Zhang and co-workers for enantioselective α-chlorination of aldehydes. They identified that the pyrrolidine-thiourea **105** could easily catalyze the α-chlorination of aldehydes (Wang et al., 2010).

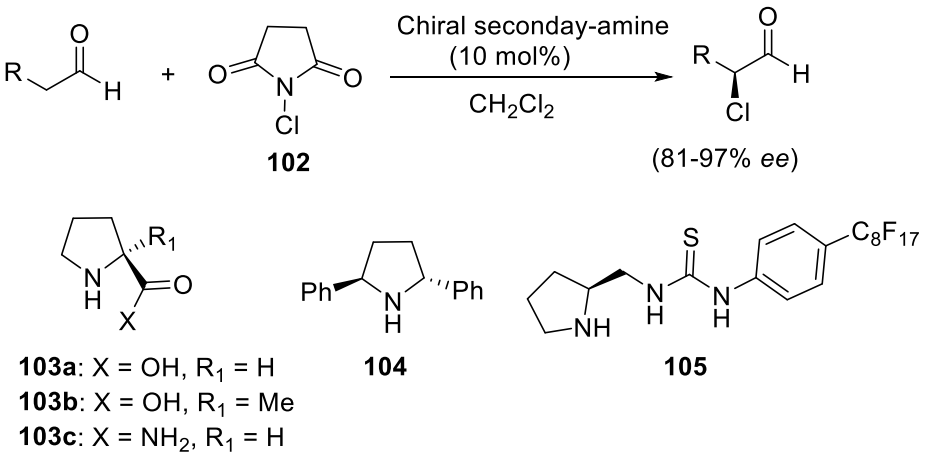

Scheme 2.3 Organocatalytic enantioselective chlorination of aldehydes by Jørgensen and co-workers

In 2009, MacMillan introduced a mode of activation in asymmetric organocatalysis named SOMO (singly occupied molecular orbital) catalysis, in which the chiral imidazolidinone catalyst (2*R*,5*S*)-2-*tert*-butyl-3,5-dimethylimidazolidin-4-one (**106**) (Scheme 2.4) reacts with substrate (aldehyde) in the presence of one electron oxidant system $Cu(TFA)_2$ and $Na_2S_2O_8$) to yield very reactive radical cationic-enamine intermediate **107** (Amatore et al., 2009). This radical cation species is more prone to subsequent radical reaction with the chlorine radical than the chloride ion (Scheme 2.4). The chlorine radical may be formed via oxidation of chloride ion with Cu^{+2} ion. Based on the DFT (density functional theory) calculations, MacMillan predicted that the chiral catalyst **106** selectively form the SOMO-activated radical cationic-enamine intermediate **107**.that projects the bond-forming site (3π-electron system) away from the *tert*-butyl group (bulky), whereas the methyl group on imidazolidinone ring shields the top *Re*-face of the π-system, leaving the bottom *Si*-face open for enantioselective chlorination to occur.

Higher levels of enantioselectivity are noticed when this reaction is attempted at lower temperatures with addition of small amount of water.

The development of SOMO catalysis has improved upon well-known enantioselective α-chlorination of aldehydes by taking advantage of cheap, low molecular weight, and environmentally friendly reagents such as lithium chloride (LiCl) and sodium chloride (NaCl) to serve as chloride sources. In general, a simple aldehyde, chiral secondary amine catalyst **106**, and an oxidant combination of copper (II) trifluoroacetate $Cu(TFA)_2$ and sodium persulfate ($Na_2S_2O_8$) yields enantiopure α-choro aldehydes in 70-90% yield and 94-97% enantiomeric excess (Scheme 2.4). In 2011, An alternative efficient organocatalytic method for asymmetric α-chlorination of aldehydes was reported by Christmann and co-workers (Winter et al., 2011). They mixed *N*-chlorosuccinimide (**102**) and MacMillan imidazolidinone catalyst **106** to achieve the efficient system. This system gave the α-chloroaldehydes with excellent enantioselectivity and yield. However, it requires high catalyst loading of up to 30% to achieve good conversion. The procedure of SOMO catalysis achieves carbon−chlorine bond formation in an efficient manner with consistently high levels of enantioinduction.

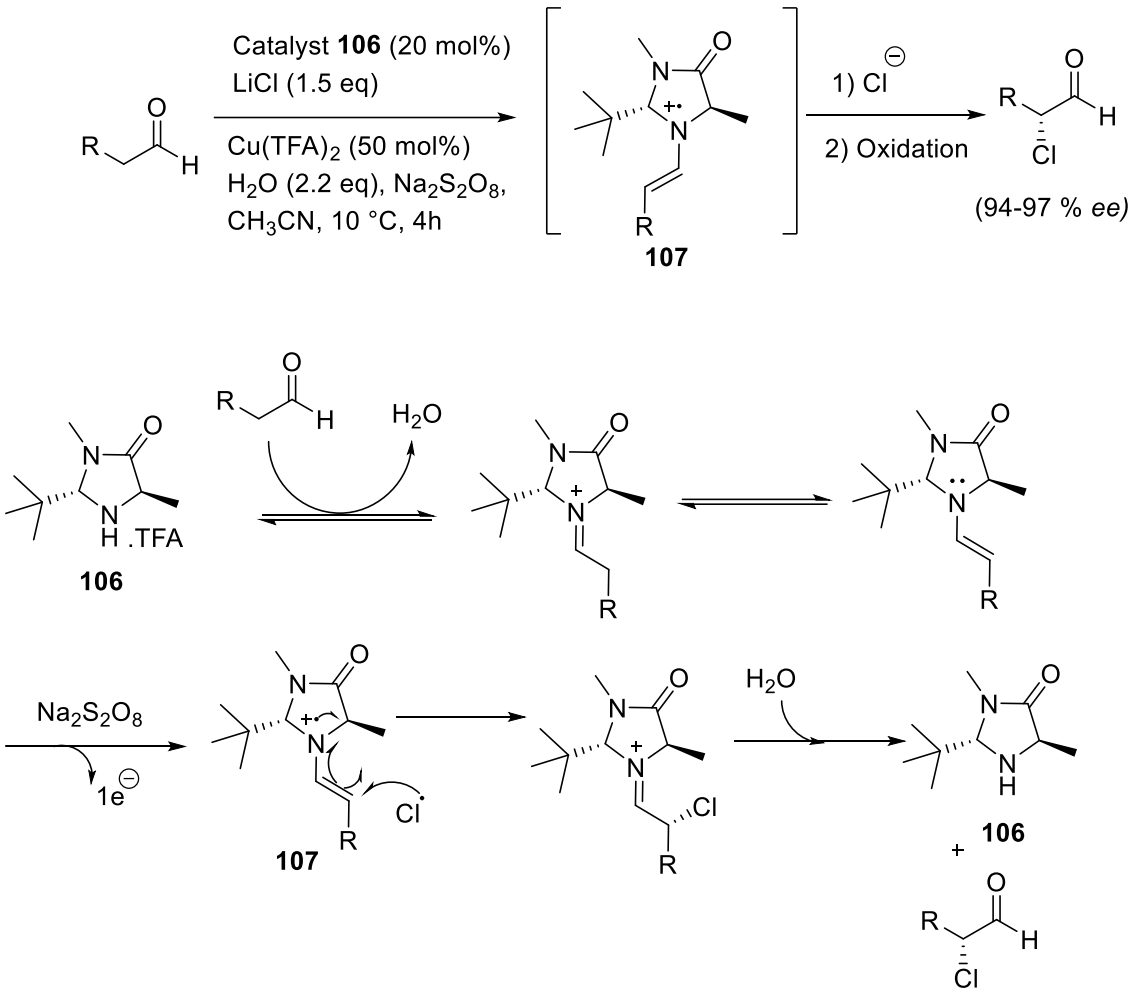

Scheme 2.4 The SOMO catalytic approach of MacMillan group for the preparation of enantiopure α-chloroaldehydes.

The enantiopure α-chloroaldehydes are very versatile and valuable synthetic intermediates, which have been used for the synthesis of number of biologically active molecules and agricultural products. .In this regard, Jørgensen and co-workers demonstrated that enantiopure α-chloroaldehydes can be efficiently converted into useful synthetic intermediates, such as enantiopure terminal epoxides, α-amino alcohols, and esters (Halland et al., 2004). Particularly, the usefulness of enantiopure α-chloroaldehydes was elegantly shown by Britton and co-workers in the total synthesis of tetrahydrofuran and pyrrolidine-containing natural products (Britton and Kang, 2013; Dhand, Chang, and Britton 2013; Dhand et al., 2013; Holmes and Britton, 2013; Chang, Hur, and Britton 2015; Holmes et al., 2015; Challa et al., 2021).

2.2.3. Synthesis of SOMO catalyst (2*R*,5*S*)-2-*tert*-butyl-3,5-dimethylimidazolidin-4-one (106)

The SOMO catalyst **106** was synthesized according to the procedure reported by MacMillan et al (Graham et al., 2011) as shown in Scheme 2.5. The synthesis consists of three sequential steps.1) an amidation of starting D-alanine methyl ester hydrochloride (**108**) with methyl amine to form amide intermediate **109**, followed by the reaction with pivaldehyde **110** to generate the imine moiety **111**, and the final cyclisation of imine **111** in the presence acetyl chloride **112** to give the SOMO catalyst **106**.

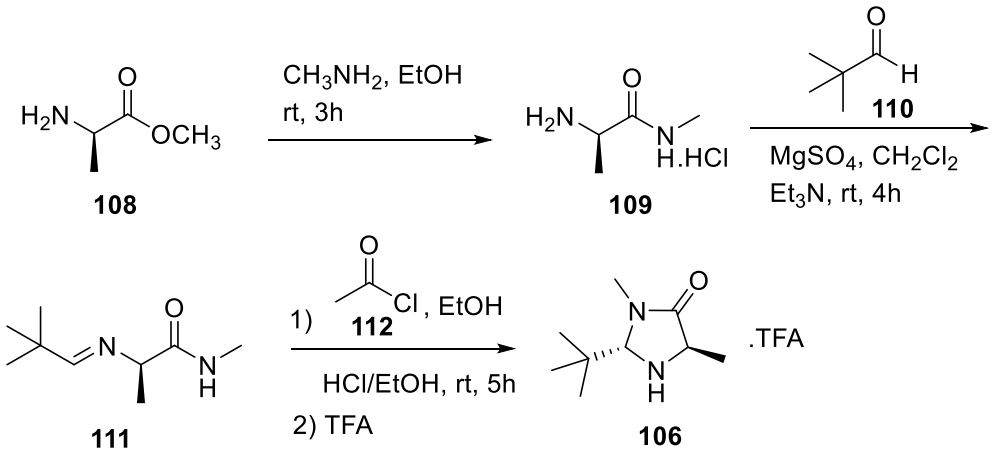

Scheme 2.5 Preparation of SOMO catalyst 106.

2.2.4. Asymmetric α-chlorination of dodecanal

Using the SOMO catalyst **106**, we explored the use of MacMillan's procedure of SOMO-activated α-chlorination of an aldehyde to prepare enantiopure α-chloroaldehyde (Amatore et al., 2009). Chlorination of dodecanal (**99**) by LiCl as the chlorine source, in the presence of SOMO catalyst **106** and an oxidant combination consisting of $Na_2S_2O_8$ and $Cu(TFA)_2$ afforded the (2*R*)-2-chlorododecanal (**113**) in 84% yield and >99% enantiomeric excess (Scheme 2.6).

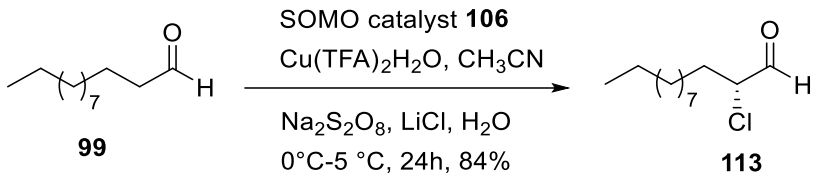

Scheme 2.6 Synthesis of enantiopure α-chlorododecanal 113.

To determine the enantiopurity of α-chlorododecanal **113**, an attempt was made for separation of scalemic α-chloroaldehyde **114** by chiral GC. The compound **114** was prepared by the reaction of dodecanol (**99**) with *N*-chlorosuccinimide (Scheme 2.7). However, the compound **114** was found to be unstable on silica and decomposed during chiral GC analysis. Then we prepared scalemic benzoate **117**, p-bromobenzoate **117a** and sulfonate **117b** from scalemic α-chloroaldehyde **114** (Scheme 2.7), and these esters are subjected to chiral HPLC. Of these three esters, benzoate **117** is well separated on chiral HPLC column (Figure 2.2).

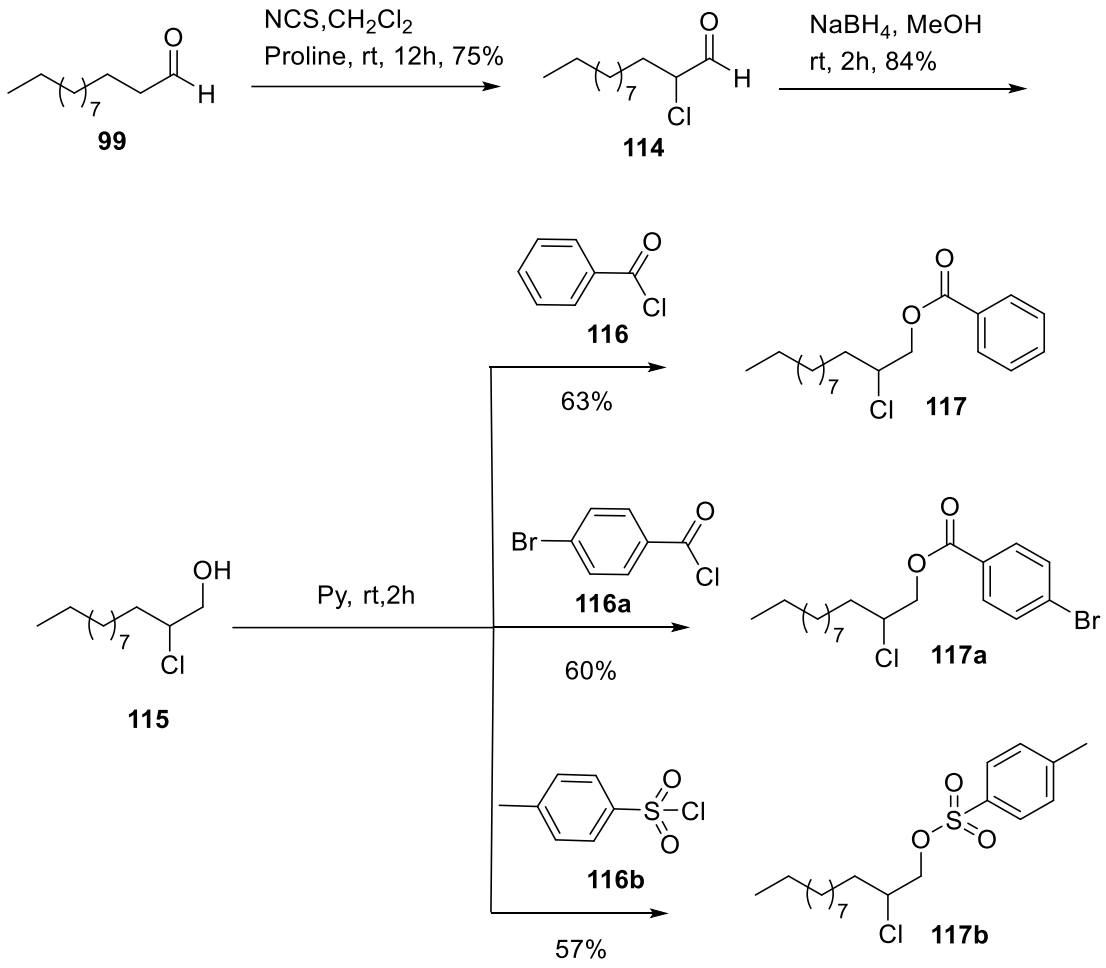

Scheme 2.7 Preparation of scalemic mixture of α-chloro benzoates (117 and 117a), and sufonate esters 117b.

The aldehyde group in scalemic α-chloroaldehyde **114** was reduced with sodium borohydride ($NaBH_4$) to give alcohol **115**. The alcohol **115** was esterified with benzoyl chloride (**116**) or 4-bromobenzoyl chloride (**116a**) or 4-methylbenzenesulfonyl chloride (**116b**) to afford the corresponding esters. Next, various solvent systems such as hexane/EtOH, hexane/ACN, hexane/IPA and hexane/IPA/TEA were evaluated for the successful separation of scalemic α-chlorobenzoates **117** and **117a** or α-chlorosulfonate **117b**. The baseline separation of scalemic α-chlorobenzoate **117** was achieved by using the solvent system containing 0.5% IPA and 99.5% hexane. The two enantiomer peaks of α-chlorobenzoate **117** eluted at 7.600 and 9.223 minutes, respectively (Figure 2.2).

As shown in Scheme 2.8, the enantiopure α-chloroaldehyde **113**, obtained via SOMO catalysis, was successfully converted into its corresponding benzoate ester **119** in

73% yield over two steps. The benzoate **119** eluted at 7.603 minutes on chiral HPLC column (Figure 2.2). The enantiomeric excess (ee) of the (2*R*)-2-chlorododecanal (**113**) was determined to be > 99% *ee*.

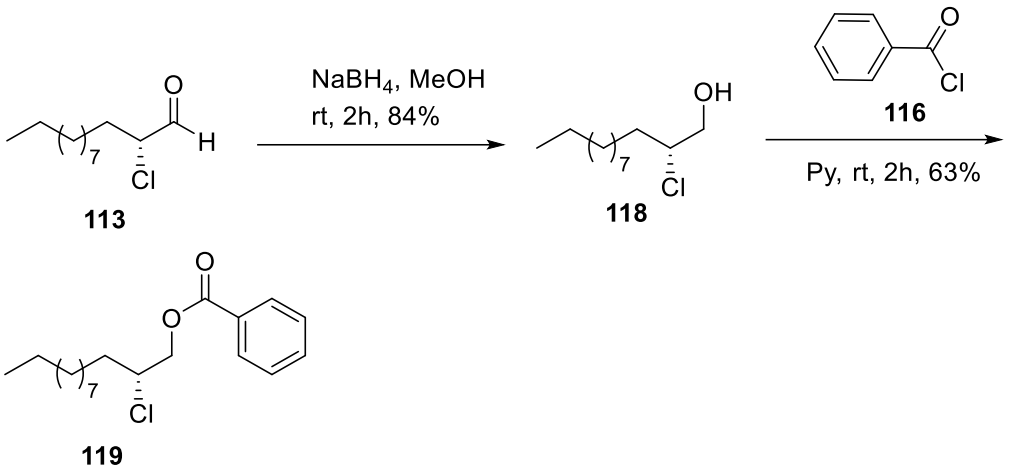

Scheme 2.8 Preparation of enantiopure α-chlorobenzoate 119.

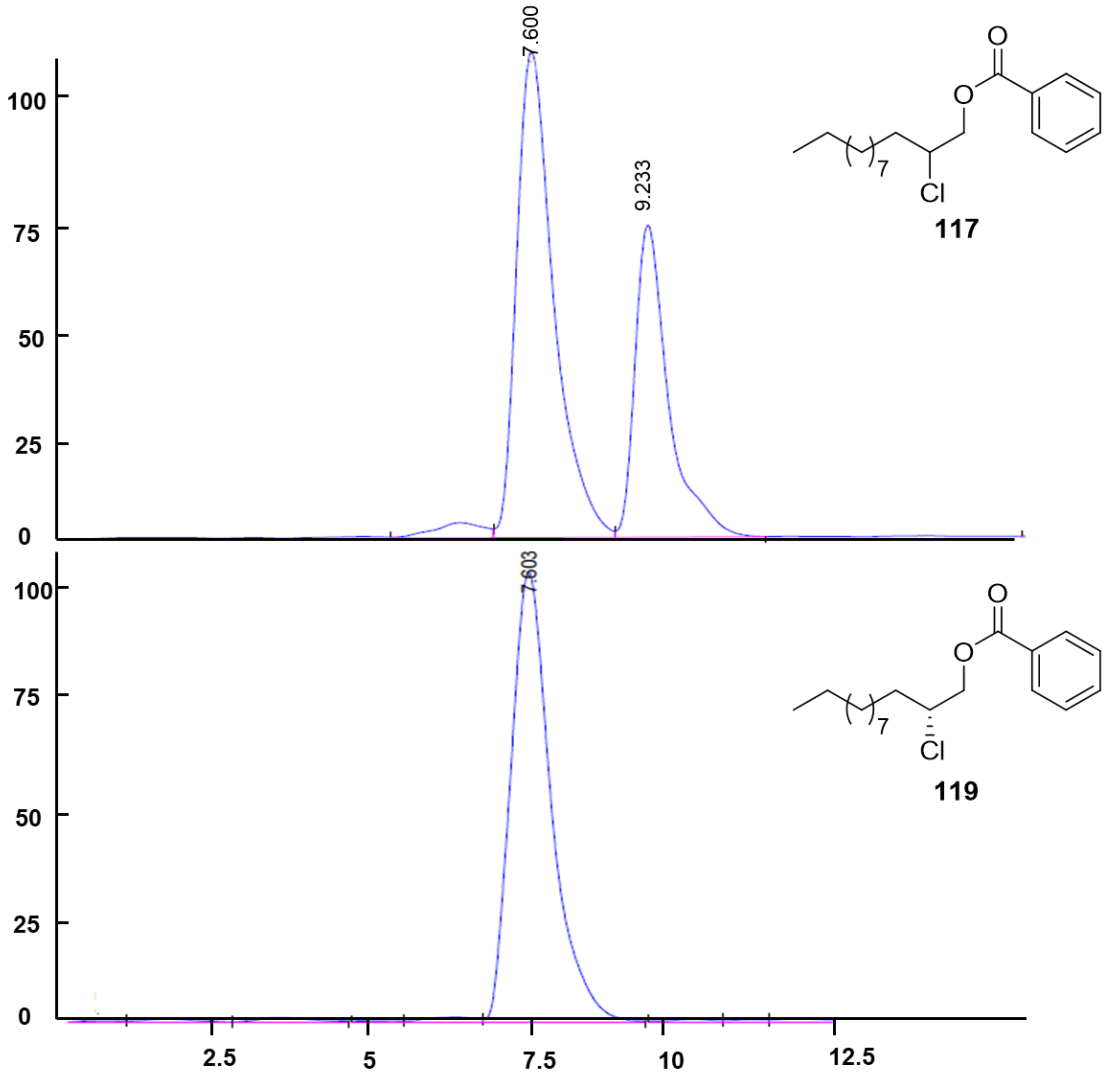

Figure 2.2 **High–performance liquid chromatographic separation of enantiomers by using Chiralcel OZ-H column a) separation of nearly racemic 2-chloro-benzoyl derivative 117 using mobile system containing 0.5% IPA in Hexane. b) Elution (2*R*)-2-chloro-benzoylderivative 119 with 0.5% IPA in Hexane.**

2.2.5. Diastereoselectivity in nucleophilic addition to α-heteroatom-substituted carbonyl compounds

This section outlines the most powerful models of 1,2-enantioinduction at carbonyl carbons, where one of the three substituents on the chiral carbon is polar (OR, NR_2 and Cl). The model utilized for predicting diastereofacial selectivity in the carbon nucleophilic additions to polar α-substituted aldehydes under non-chelating reaction conditions is the Felkin-Anh model and Cornforth-Evans model. In both models, an addition of a

nucleophile to electrophilic carbon of an aldehydes with polar α-substituent produce 1,2-*anti* isomer as the major product (Figure 2.3). These models are discussed below.

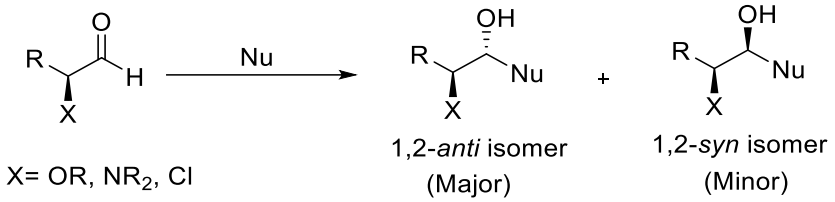

Figure 2.3 Nucleophilic addition to polar α-substituted aldehydes.

2.2.5.1. The polar Felkin-Anh (PFA) model

The polar Felkin-Anh model is the most effective model that utilized to predict the stereochemical outcome in the nucleophilic additions to aldehydes with a polar α-substituent for a long time. The first version of this model was proposed by Felkin in 1968 (Chérest et al., 1968) . Later, it was modified by Anh and Eisenstein (Anh et al., 1973; Anh and Eisenstein, 1976). In this model, both hyperconjugation interactions and torsional strain are the most important factors that stabilizes the conformation of the transition state (TS*****). The low energy orbital ($\sigma_{C\text{-}X}$*, the good vicinal acceptor orbital) of the polar α-substituent is oriented perpendicular to the plane of the carbonyl group (Figure 2.4). Anh stated that this alignment will allows maximum overlap between the π-orbital and $\sigma_{C\text{-}X}$* orbital. He also stated that delocalization of electron density by hyperconjugation between these orbitals will stabilize this conformation. In addition, the perpendicular orientation of the polar α-substituent also indicates that the orbital overlap between the $\sigma_{C\text{-}X}$* orbital and the incoming nucleophile is optimized. Then the nucleophile approaches carbonyl group along the Bürgi-Dunitz path (Burgi, Dunitz, and Shefter 1973; Burgi et al., 1974) via transition state (TS*) to minimize the steric repulsions between the nucleophile and the large substituent at α-carbon, thus yielding the 1,2-*anti* isomer (Figure 2.4).

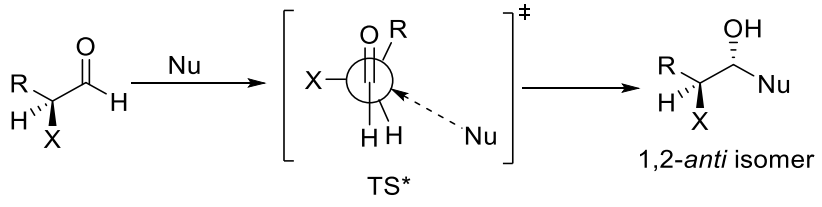

Figure 2.4 The ploar Felkin-Anh (PFA) model, X = polar substituent.

2.2.5.2. The Cornforth-Evans model

The Cornforth-Evans model was initially presented by Cornforth in 1959 (Cornforth et al., 1959), which was later revised by Evans in 2003 (Evans et al., 2003). For nucleophilic additions to polar α-substituent aldehydes and ketones, Cornforth proposed that the minimization of the dipole moment between the electronegative α-substituent and carbonyl moiety is the most important factor for predicting the stereochemical outcome of the product. However, the Cornforth model has been initially modified by introducing Bürgi-Dunitz path and altering the dihedral angle to obtain the most stable conformation (staggered) in the transition state (Paddon-Row et al., 1982) (Figure 2.5, TS*).

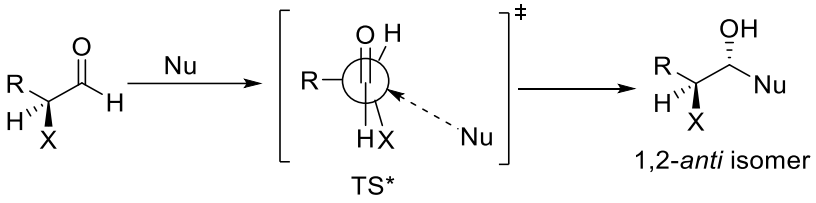

Figure 2.5 The Cornforth-Evans model, X = polar substituent.

Later, Evans and co-workers suggested a modified Cornforth model that was altered to clarify the torsional strains at the transition state by adjusting substituents at the transition state to achieve staggered conformation (Evans et al, 2003). Rather than having the polar α-substituent antiperiplanar to the approaching nucleophile to form hyperconjugative interactions as in polar Felkin-Anh model, the modified Cornforth model focuses on the dipole minimization between the carbonyl group and the polar α-substituent. Even though the polar Felkin-Anh model has been commonly used to predict the 1,2-enantioinduction of polar α-substituted aldehydes, Evans and co-workers successfully demonstrate the ability of the modified Cornforth model to predict the stereochemical outcomes of the reactions in which the nucleophile imposes a conformational restriction on the stereocenter that adjacent to the carbonyl group (Figure 2.6). This kind of restriction is wisely showed in an aldol reaction that involves the addition of *E*- and *Z*-boron enolates to the α-alkoxy aldehyde. Depending on whether the modified Cornforth or polar Felkin-Anh model was employed, the reacting polar α-substituted aldehyde with a (*E*)- or (*Z*)-enolate could be predicted to constrain destabilizing *syn*-pentane interactions between the enolate and polar α-substituent (Figure 2.6). The polar Felkin-Anh model predicts that the addition of (*E*)-enolate to the polar α-substituted

aldehyde should proceed without any destabilizing *syn*-pentane interactions to give 3,4-*anti*-product, whereas (*Z*)-enolate experiences a severe destabilizing *syn*-pentane interaction, diminishing diastereofacial selectivity. Conversely, the modified Cornforth model predicts the superior level of 3,4-*anti* selectivity from the (*Z*)-enolate because it eliminates a destabilizing *syn*-pentane interaction with the polar α-substituent at the transition state (Figure 2.6)

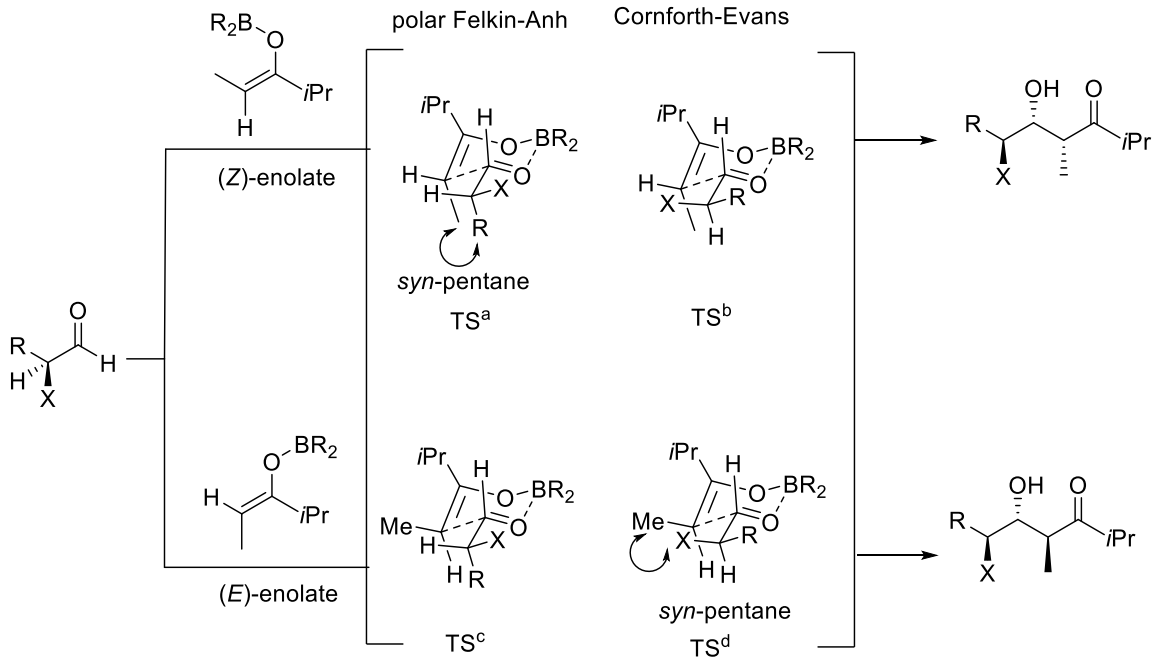

Figure 2.6 polar Felkin-Anh and modified Cornforth transition state models for the addition of (*Z*)-and (*E*)-enolates to polar α-substituted aldehydes

In a computational study, Evan and co-workers further demonstrated that the preferred model is based on the nature of the electronegative α-substituent (Cee et al., 2006). This study showed that the modified Cornforth model is valid in addition of *E*- or *Z*-boron enolates to the polar α-substituted aldehydes having more electronegative substituents (X = F, OR and Cl). On the other hand, the polar Felkin-Anh model is valid for the aldehydes with less electronegative substituents such as X = PR_2, SR and NR_2.

2.2.5.3 Aldol reactions with enantiopure α-chloroaldehydes

As discussed above, the addition of enolates to the asymmetric α-heterosubstituted aldehydes favours the *anti*-diastereomer. The Britton group has done

extensive research in relation to the aldol chemistry using enantiopure α-chloroaldehydes They noticed that the enantiopure α-chloroaldehydes reacted with lithium enolates of aliphatic and aromatic methyl ketones to afford the corresponding 1,2- *anti* β-ketochlorohydrins in high yield (63-90%) and excellent diastereoselectivity (dr >20:1, Figure 2.7) (Kang et al., 2009; Halperin et al., 2011). Snyder and co-workers successfully applied this methodology in the synthesis of cyclic bromoethers (Snyder et al., 2011).

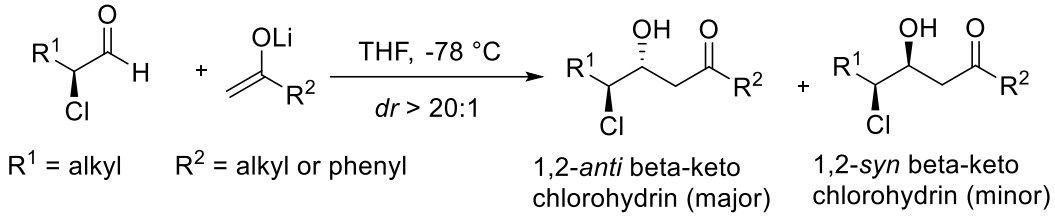

Figure 2.7 Addition of enolates to enantiopure α-chloroaldehydes

In the light of these precedents, we attempted the aldol reaction between the α-chloroaldehyde **113** with the lithium enolate of 5-methyl-2-hexanone (**120**), which furnished 1,2-*anti* β-ketochlorohydrin **121** as major product (dr = 10:1) (Scheme 2.9). The major product **121** was isolated by flash column chromatography. Our initial approach was to use a mild method for converting 1,2-*anti* β-ketochlorohydrin **121** to 1,2-*anti* chlorohydrin **123** via a two-step process involving a tosylhydrazone. First, the compound **121** is converted to the corresponding tosylhydrazone **122**, and then treatment of the tosylhydrazone **122** with the mild reducing agent sodium cyanoborohydride, under basic conditions gave compound **123** in very low yield; on the contrary, only a little yield enhancement was noticed when the reaction was heated under reflex at 100 °C (Scheme 2.9 and Table 2.1). TLC showed the full consumption of tosylhydrazone **122**, but together with the 1,2-*anti* chlorohydrin **123**, unidentified side-products were also noticed. Isolation of 1,2-*anti* chlorohydrin **123** from the complex crude reaction mixture resulted in very low yields (10-15%). Attempts to access 1,2-*anti* chlorohydrin **123** from β-keto chlorohydrin **121** under various conditions were not successful (Table 2.1). Considering very low yield we decided to not pursue this synthetic sequence any further.

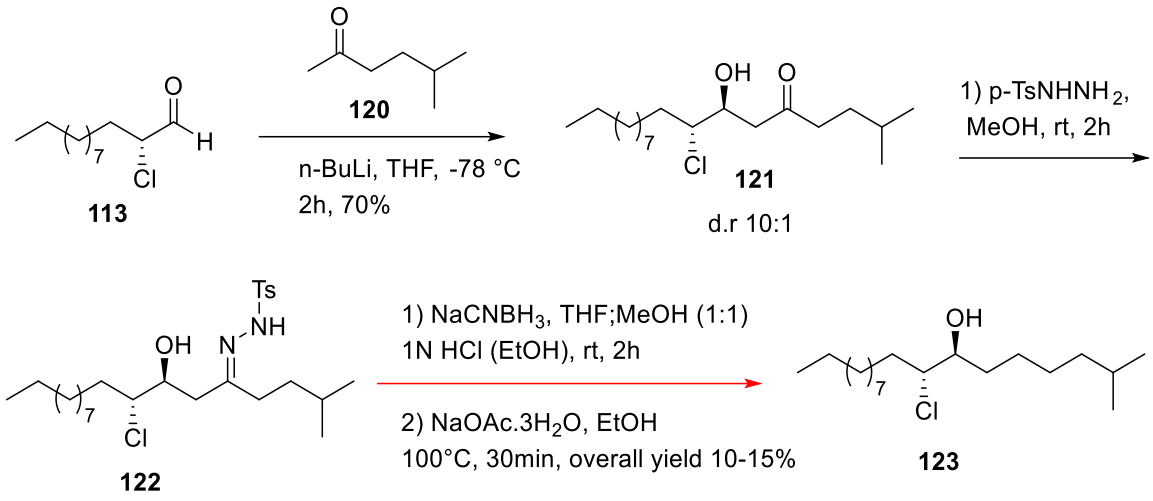

Scheme 2.9 **Preparation of *anti*-chlorohydrin 123 from β-keto *anti*chlorohydrin 121.**

Table 2.1 **Reduction of tosylhydrazone 122 to *anti*-chlorohydrin 123.**

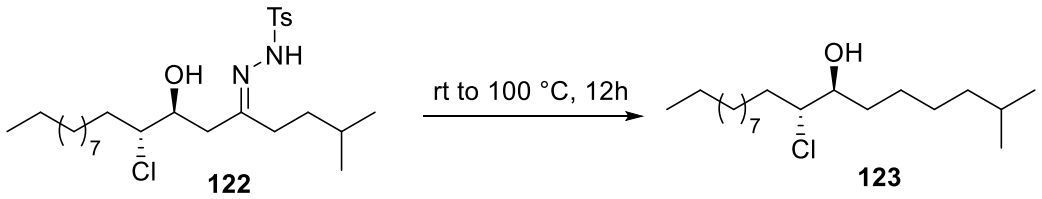

Entry	Compound	Reagent	solvent	Yield
1	**122**	$NaCNBH_3$/1N HCl, KOH	THF:MeOH (1:1), EtOH	10
2	**122**	$NaCNBH_3/ZnCl_2$	MeOH	7
3	**122**	$NaCNBH_3$/PTSA	DMF:sulfone	10
4	**122**	$NaBH_4$, KOH	ethane-1,2-diol	--
5	**122**	$NaBH(OAc)_3$, NaOAc	H_2O:EtOH (1:1)	10
6	**122**	$NaBH(OAc)_3$, $ZnCl_2$	MeOH	--

2.2.5.4 Diastereoselective addition of organometallic reagents to enantiopure α-chloroaldehydes

In 2007, Kang and Britton observed that the organolithium reagents reacted with enantiopure α-chloroaldehydes (85% *ee*) to yield the corresponding 1,2-*anti* chlorohydrin in good diastereoselectivity (dr 8:1 to 20:1). These 1,2-*anti* chlorohydrins were transformed into chiral *trans*-epoxides through base promoted S_N2 cyclization. The main objective of their work was the concise synthesis of the pine looper moth sex pheromone Z6,Z9,t-epo4-19:H (**124**) and tussock moth sex pheromone (-)-posticlure (**13**) for field trails (Figure 2.8) (Kang and Britton, 2007). Later, Vanderwal and co-workers successfully applied this procedure in the preparation of 1,2-*anti* chlorohydrin by addition of alkyne lithium to enantiopure α-chloroaldehyde (Shibuya et al., 2008)

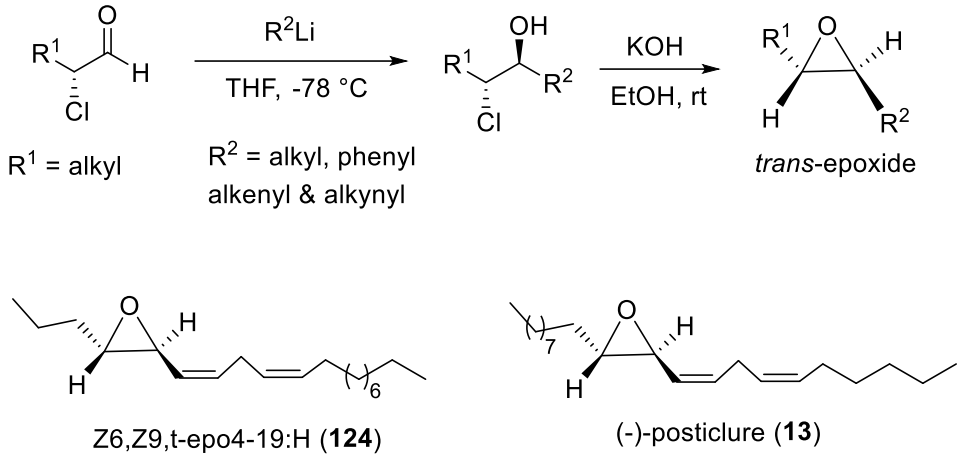

Figure 2.8 Addition of organolithium reagents to enantiopure α-chloroaldehydes. This approach was used to prepare moth sex pheromones.

With the unsuccessful attempts to access 1,2-*ant*i chlorohydrin **123**, we explored the use of Britton's procedure of an addition of Grignard and organolithium reagents to α-chloroaldehyde **113** to prepare 1,2-*anti* chlorohydrin. Treatment of enantiopure α-chloroaldehyde (>99% *ee*) **113** with either hexylmagnesium bromide or hexyllithium gave the corresponding 1,2-*anti* chlorohydrin in good yield and moderate diastereomeric excess. (Table 2.2, entries 1 & 2). We carried out this Grignard reaction in various polar aprotic solvents such as diethyl ether and 1,4-dioxane (Table 2.2, entries 3 & 4). However, changing solvent system did not improve the diastereoselectivity. In fact, the observed

diastereoselectivity of this reaction is in agreement with the previous report (Kang and Britton, 2007).

Table 2.2 Addition of organometallic reagents to enantiopure α-chloro aldehyde 113.

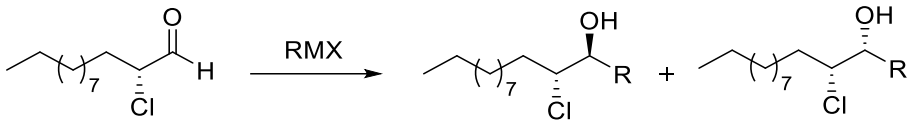

113 (1,2-*anti*) (1,2-*syn*)

Entry	RMX	Solvent	d.r. (*anti*:*syn*)[a]
1	nHexLi	THF	.10:1
2	nHexMgBr	THF	3:1
3	nHexMgBr	Ether	~3:1
4	nHexMgBr	1,4-dioxane	~3:1
3	nHexynylLi	THF	20:1
4	5-MeHexynylLi	THF	20:1

[a] Ratio of diastereomers determined by ^{1}H NMR analysis of the crude product

Then we attempted alkyne lithium anion addition to α-chloroaldehyde **113**. For the optimization of this reaction, we used the non-branched building block 1-hexyne (**125**) (Scheme 2.10, Table 2.2) that results in (+)-monachalure (**15a**), which is major pheromone component of nun moth *L. monacha.* Finally, we treated α-chloroaldehyde **113** with the alkyne lithium anion derived from 1-hexyne (**125**) or 5-methyl-1-hexyne (**126**): the reaction proceeded cleanly and the product 1,2-*anti*-chlorohydrin **127** or **128** was isolated in good yield with a 20:1 diastereoselectivity (Scheme 2.10). At this point, the diastereomers were separated by flash column chromatography.

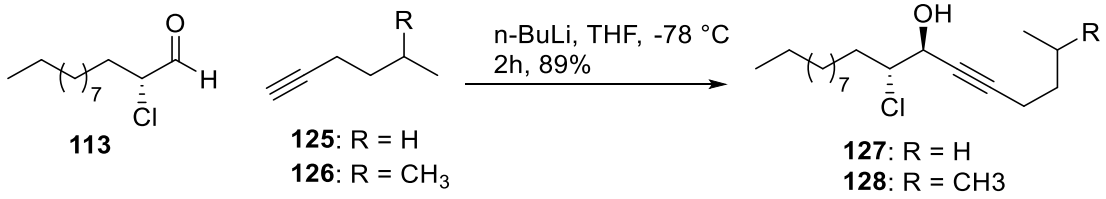

113 **125**: R = H **126**: R = CH_3 **127**: R = H **128**: R = CH3

Scheme 2.10 Synthesis of 1,2-*anti* chlorohydrin 127 or 128.

2.2.6. Mitsunobu inversion to *syn* chlorohydrins

If the 1,2-*anti* chlorohydrin **127** or **128** (Scheme 2.11) is treated with base, then a *trans* epoxide is formed. However, we require a 1,2-*syn* product to obtain the *cis* epoxide. Therefore, we need to invert the stereochemistry either at the C-7 or C-8 position of the 1,2-*anti*-chlorohydrin **127** or **128**. An attempt was made to invert the stereochemistry at the C-8 position by a Finkelstein reaction, which uses halide salt (KI or NaI) and dry acetone as nucleophile and solvent, respectively. However, the reaction was unsuccessful, and the starting material was recovered.

In order to prepare 1,2-*syn* product, the stereochemistry at the C-7 carbon of compound **127** or **128** was inverted by a Mitsunobu reaction, which is very powerful chemical tool for the inversion of stereocenters in organic synthesis. The Mitsunobu reaction of 1,2-*anti* chlorohydrin **127** or **128** with stable, cheap, and abundant nucleophile such as benzoic acid (**129**) in the presence of TPP (triphenylphosphine) DIAD (diisopropyl azadicarboxylate) produced complete inversion product **130** or **131** (Scheme 2.11), which was isolated in 80% yield.

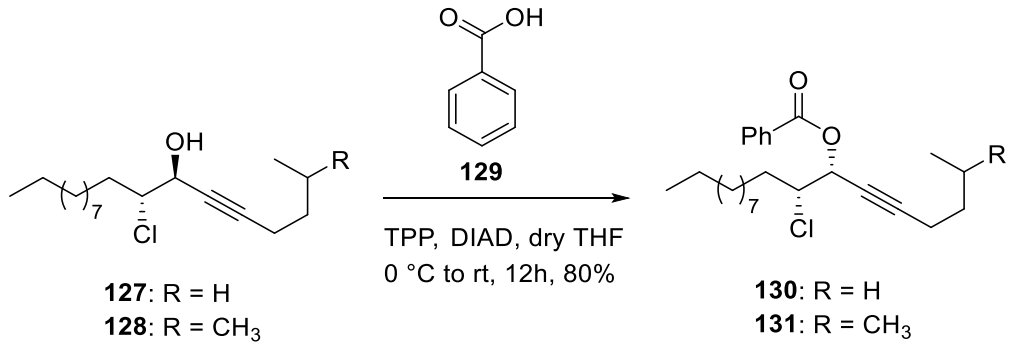

127: R = H
128: R = CH_3

130: R = H
131: R = CH_3

Scheme 2.11 Synthesis of 1,2-*syn* chloroester 130 or 131 employing benzoic acid (129) as pronucleophile.

2.2.7. Synthesis of (+)-disparlure (15) and (+)-monachalure (15a)

The resultant Mitsunobu product contained a carbon-carbon triple bond, which was subjected to hydrogenation with H_2 and catalytic Pd/C in methanol afforded reduced product **132** or **133** in 95% yield. The reduced product was treated with 4N NaOH solution in methanol to produce the final product (+)-disparlure (**15**) or (+)-monachalure (**15a**) (Scheme 2.12). On completion of the synthesis, the spectroscopic data (^{1}H NMR, ^{13}C

NMR, IR and MS) and optical rotation of the final products were compared to those reported in the literature.

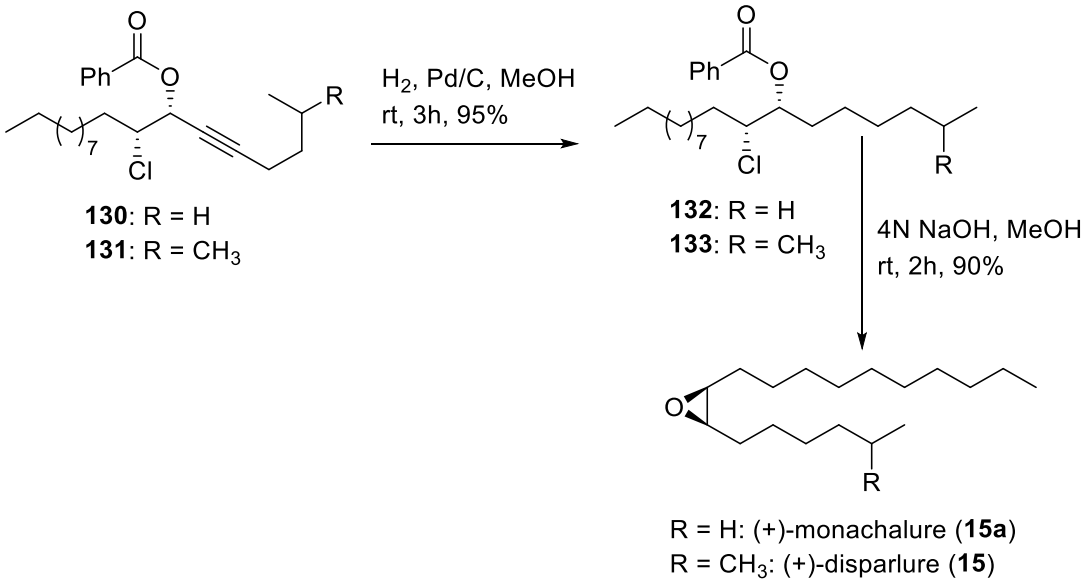

Scheme 2.12 synthesis of (+)-monachalure (15a) and (+)-disparlure (15).

2.2.8. Synthesis of (-)-disparlure (*ent*-15)

After successful synthesis and characterization of (+)-disparlure (**15**), we prepared (-)-disparlure (*ent*-**15**), which was obtained 40-45% overall yield. For the synthesis of *ent*-**15** (Scheme 2.13), SOMO catalyst (2*R*,5*S*)-2-(*tert*-butyl)-3,5-dimethylimidazolidin-4-one (*ent*-**106**) was used to prepare enantiopure α-chlorododecanal *ent*-**113**. Diastereoselective addition of lithium alkyne anion to the compound *ent*-**113** resulted in *ent*-**128** in 85% yield. Reaction of *ent*-**128** with benzoic acid (**129**) and DIAD produced the ester *ent*-**131**, which was hydrogenated with H_2 and Pd/C, then treated with NaOH to close the epoxide and furnish (–)-disparlure (*ent*-**15**) in 90% yield.

The synthesis of (+)-disparlure (**15**) and (-)-disparlure (*ent*-**15**) was achieved using commercially available dodecanal (**99**) as the starting material. This synthetic route may also be applied for the preparation of other disubstituted *cis*-epoxides. Apart from that, this route provides easy access to isotope (^{17}O, ^{18}O and ^{2}H) labelled disparlure enantiomers for studies with pheromone binding proteins (PBPs) that are present in the male gypsy moth antennae (Chapter 3).

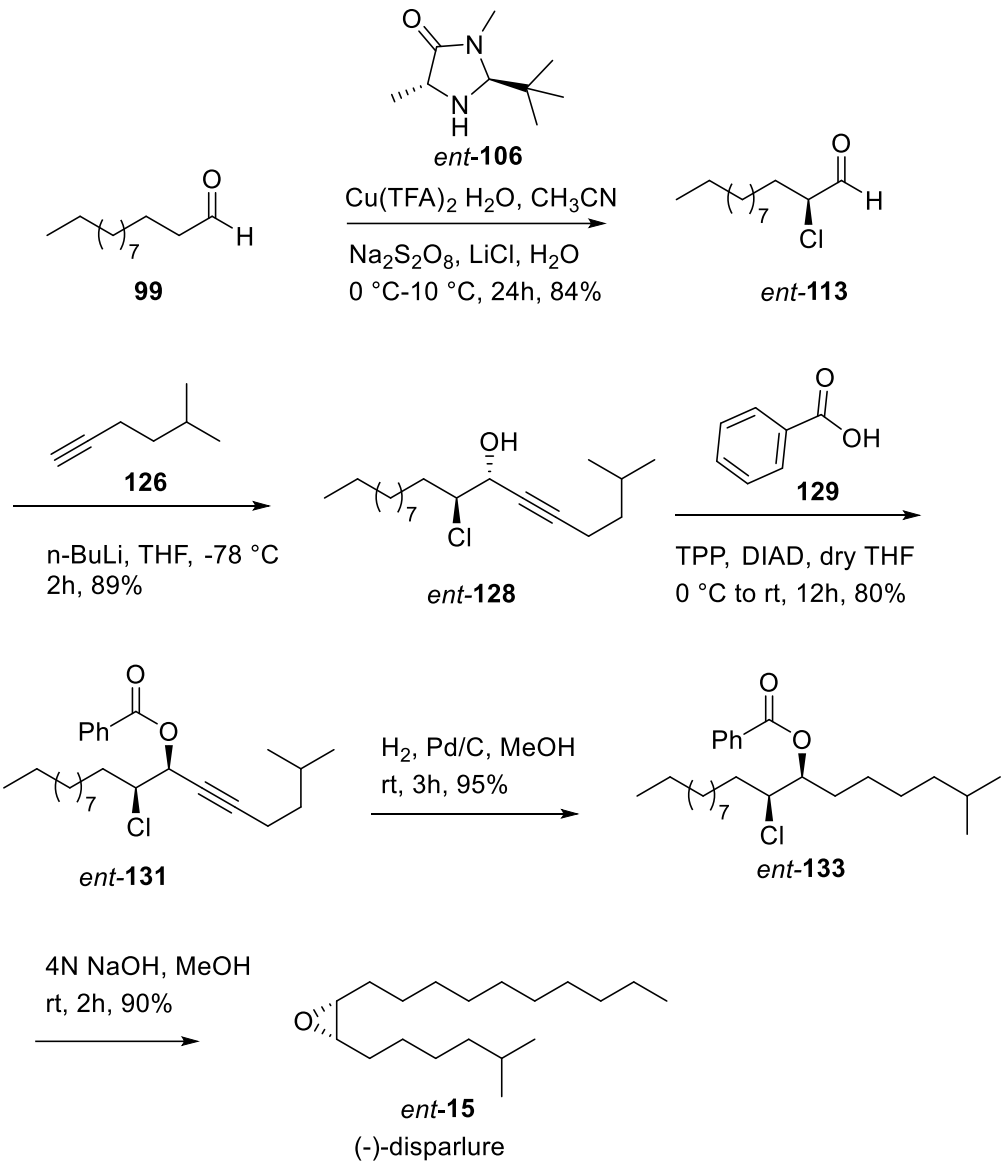

Scheme 2.13 Synthesis of (-)-disparlure (*ent*-15).

2.2.9. Determination of enantiomeric excess of (+)-disparlure (15)

To determine the enantiopurity of (+)-disparlure (**15**), An attempt was made for separation of scalemic mixture of disparlure by chiral gas chromatography. However, this was not successful. The common method for finding enantiopurity of chiral organic molecules is the transformation of enantiomers to diastereomers by establishing a second defined chiral center (Skidmore, 1993). To optimize the method used to determine enantiomeric excess of (+)-disparlure (**15**), we converted a scalemic sample of disparlure to the corresponding *cis*-N-(α-methylbenzyl)aziridines **139** and **140** with inversion of

configuration at both, the C-7 and C-8 positions (Oliver and Waters, 1995) (Scheme 2.14). The *cis* epoxide of scalemic disparlure was opened with *R*-(+)-α-methylbenzylamine **134** in the presence of trimethylaluminium, which produced a mixture of amino alcohols **135**, **136**, **137** and **138**. This mixture was treated with methanesulfonyl chloride and triethylamine, to afford a diastereomeric mixture of *cis*-N-(α-methylbenzyl) aziridines **139** and **140**.

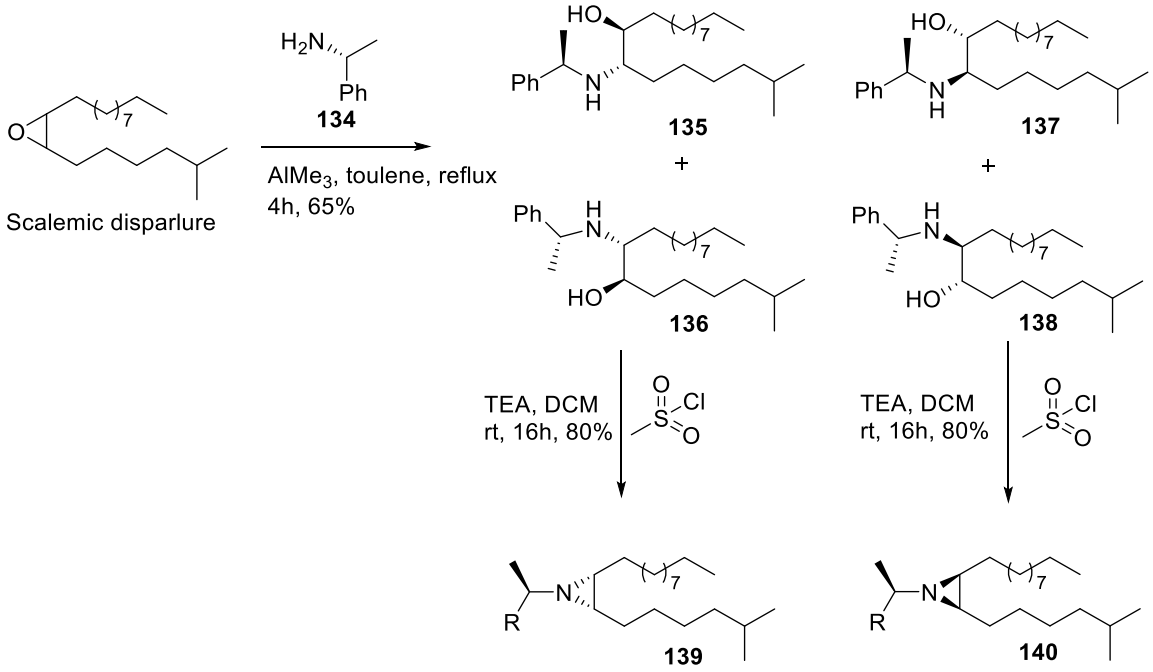

Scheme 2.14 Conversion of enantiomers to diastereomers by opening of epoxide with (+)-(*R*)-1-phenyl aminoethane (134). The diastereomeric aziridines 139 and 140 separate by gas chromatography.

Next, the addition of chiral amine **134** to (+)-disparlure (**15**) gave the amino alcohols **135** and **136** (Scheme 2.15). Treatment of the amino alcohols **135** and **136** with methane sulfonyl chloride and TEA gave *cis*-N-(α-methylbenzyl)aziridine **139**. In a similar way, (-)-disparlure (*ent*-**15**) was converted to corresponding *cis*-N-(α-methylbenzyl)aziridine **140** with inversion of configuration at both stereocenters (Scheme 2.16).

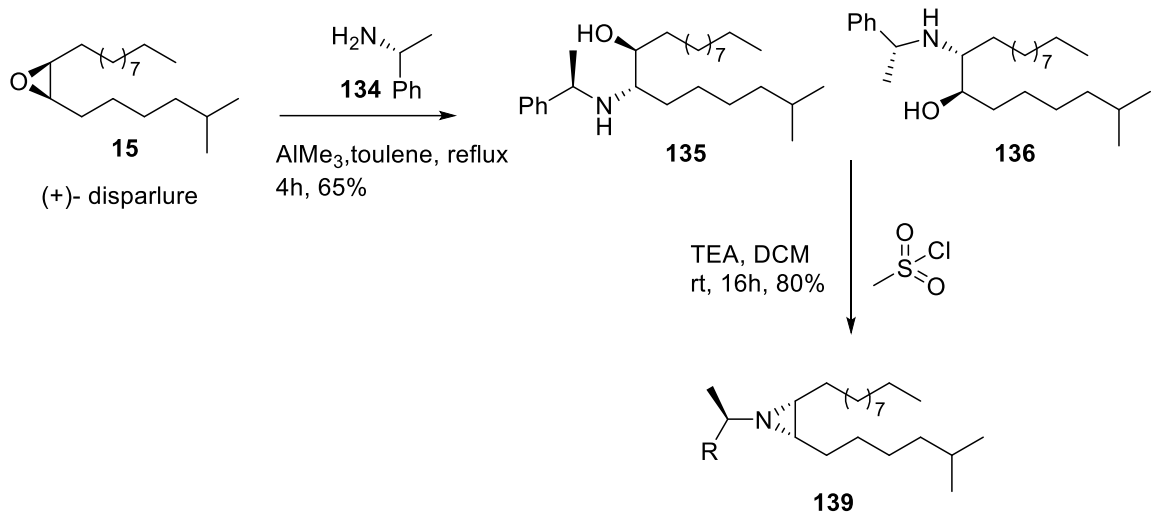

Scheme 2.15 Coversion of (+)-disparlure to *cis*-N-(α-methylbenzyl)aziridine 139.

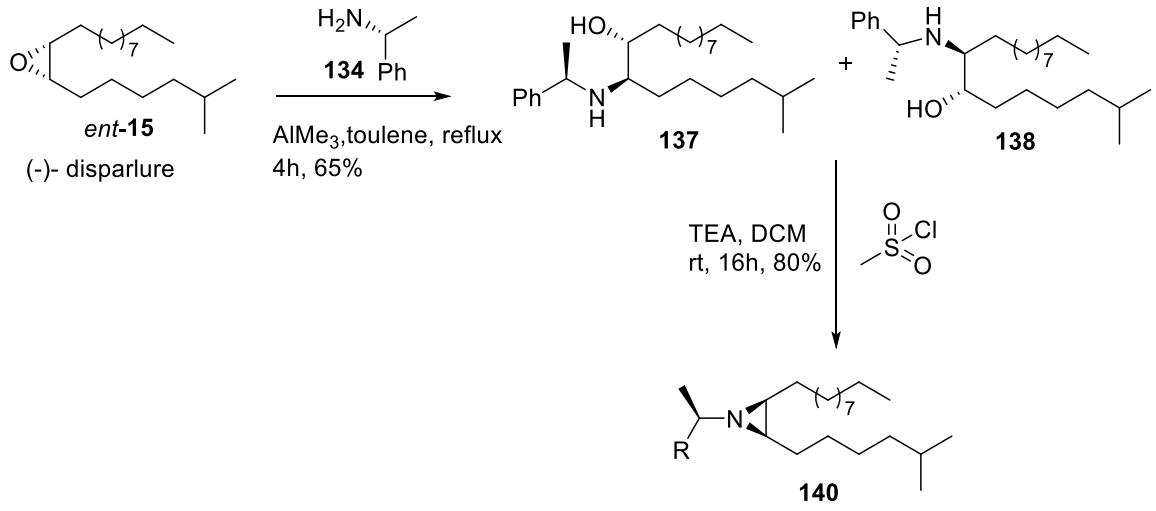

Scheme 2.16 Coversion of (-)-disparlure to *cis*-N-(α-methylbenzyl)aziridine 140.

The mixture of aziridines **139** and **140** this prepared was examined on several GC columns. Varying degrees of resolution were noticed, and it was found that a SPB-5 fused-silica capillary column (30 m × 0.25 mm i.d., film thickness 0.25 μm) achieved nearly baseline separation in over 50 min. Figure 2.9a showed nearly baseline separation of aziridine peaks, permitting us to determine the enantiomeric excess (*ee*) of the (+)-disparlure (>99% *ee*) and (-)-disparlure (~99% *ee*). Trapping of male gypsy moths with traps baited with (+)-disparlure (**15**) has been used for number of years for monitoring

gypsy moth populations. It has been reported that the presence of (-)-disparlure (*ent*- **15**), even in small amounts, (<1%), can lower the trap catch significantly (Carde et al., 1977; Miller and Roelofs, 1978). The best enantiomer discrimination is offered by the male moths themselves when pheromone is offered at high doses (>500 µg/trap).

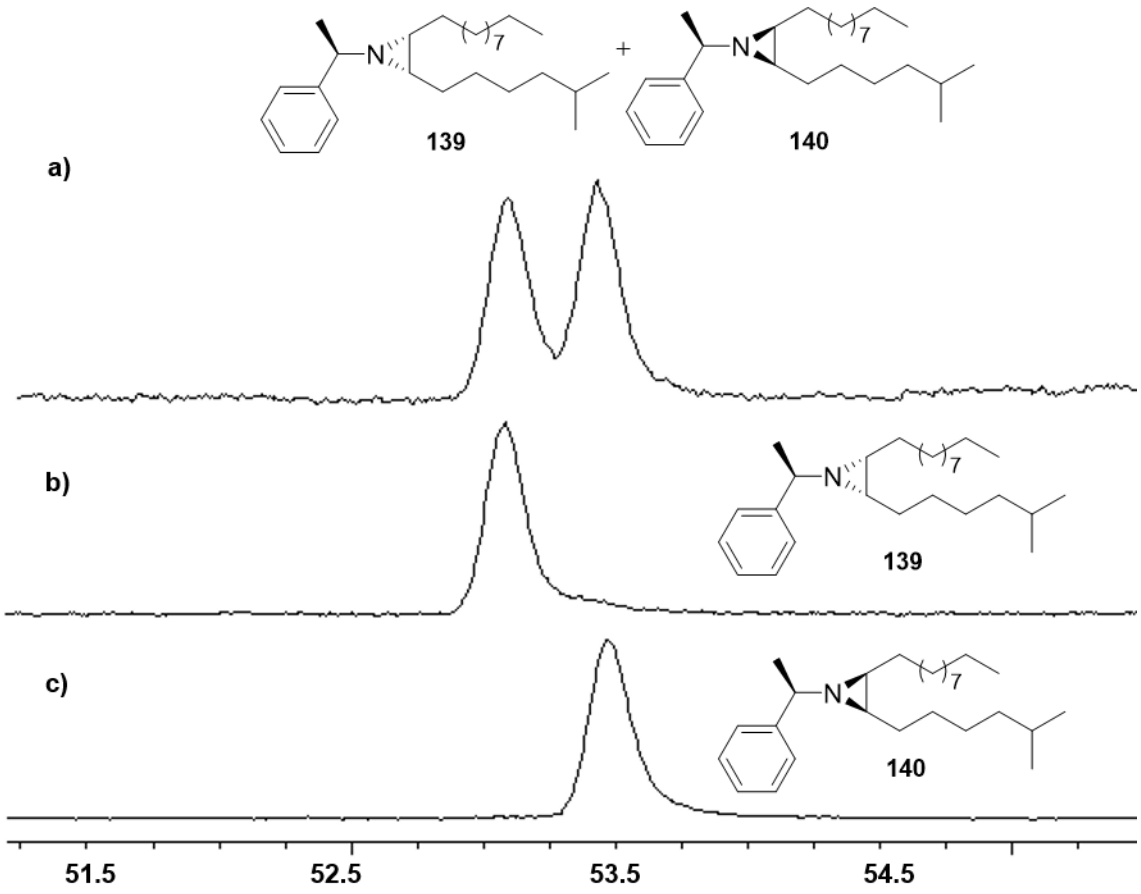

Figure 2.9 **Determination of enantiomeric excess of synthesized (+)-disparlure (15). Resolution of diastereomers of *cis*-N-(α-methylbenzyl)aziridine on GC column (SPB-5 fused capillary silica column), prepared from a) Racemic disparlure (±)-15 b) (-)-disparlure (*ent*-15) c) (+)-disparlure (15).**

2.2.10. Field trials

(+)-Disparlure (**15**) prepared herein was tested in two infested zones, located in Massachusetts (USA) and Nova Scotia (Canada), to demonstrate activity against male gypsy moths. We used delta sticky traps baited with either white rubber septa (Nova Scotia) or milk carton traps baited with impregnated dental cotton (Massachusetts), in both cases dosed with 500 µg of (+)-disparlure (**15**) or 500 µg of paraffin oil in hexanes as a

control. In Massachusetts, milk carton traps with cotton wick dispensers were used and left for 4 days. Three different doses (100, 500 and 1000 µg) were tested against a control with mineral oil. The 100 and 1000 µg treatments were from a commercial standard, and the 500 µg dose was from this study. The control did not catch any moths, and the pheromone-baited traps caught the same number of moths within limits of error (F = 2.27; *d.f.* = 2, 8; P = 0.17) (Table 2.3). Significant contamination with (–)-disparlure (due to insufficiently high *ee*) on a 500 µg wick would normally suppress trap catch to levels significantly below those obtained with highly pure (+)-disparlure at either 100 µg or 1000 µg loadings. In Nova Scotia, red delta traps with rubber septum dispensers were used and left for 10 days. Three of the treatment traps were lost due to predation. Nonetheless, the treatment traps caught significantly more moths than the control (Table 2.3). Observation on the first day suggested that traps saturated with moths within a matter of hours. The traps attracted moths within minutes of being deployed. Traps in the two locations caught different total numbers of moths due to two factors: 1) different infestation levels and 2) different dispensers and traps.

Table 2.3 Summary of field trials.

Location	Trap type	Dispenser	Treatment	Dose (µg)	Moths caught (mean ± SEM, n=10)
Massachusetts	Milk carton	Cotton wick	Control (mineral)	500	0 ± 0
			(+)-disparlure (commercial standard)	100	52 ± 15
			(+)-disparlure (this study)	500	70 ± 8
			(+)-disparlure (commercial standard)	1000	82 ± 17
Nova Scotia	Delta	Rubber septum	Control (mineral)	500	0.9 ± 0.4
			(+)-disparlure (this study)	500	22 ± 2

2.3. Conclusion

In conclusion, concise and efficient synthetic route to bioactive (+)-disparlure (**15**), (-)-disparlure (*ent*-**15**) and (+)-monachalure (**15a**) were completed in high overall yields from commercially available dodecanal. Key steps in the synthesis involved MacMillan's

SOMO-activated α-chlorination of the aldehyde, which was shown to be a highly effective means for preparing enantiopure α-chloroaldehyde (>99% ee), and Mitsunobu inversion. This synthetic route provides convenient platform to isotopically (^{17}O, ^{18}O and ^{2}H) labelled derivatives of disparlure enantiomers for studies with pheromone binding proteins (PBPs) that are present in the male gypsy moth antennae (see Chapter 3). The results from both infested zones showed that the (+)-disparlure (**15**) synthesized here significantly attracted male gypsy moths, consistent with the *ee* of the final product of >99%.

2.4. General experimental methods

All reactions were carried out in the presence of a nitrogen atmosphere and at room temperature (22 °C) unless the reactions were performed in aqueous media or unless otherwise specified. Reactions carried out at -78 °C used a bath of dry ice in acetone. Reactions undertaken at 0 °C utilized a bath of water and ice. Hexanes and ethyl acetate were distilled prior to use. THF was distilled over sodium benzophenone. Chemicals and Reagents were used without further purification and were purchased from Sigma-Aldrich. Syringes and cannulas were used to transfer reagents. Reactions were monitored by thin layer chromatography (TLC) on aluminum baked silica plates (Merck Silica Gel 60 F254) and products were visualized under UV (λ = 254 nm) or stained with phosphomolybdic acid (PMA), anisaldehyde or potassium permanganate, followed by exposure of the stained plates to heat. Silica flash chromatography (Fisher Silica Gel 60 40-63 μm) was undertaken to purify crude reaction mixtures using hexanes/ethyl acetate mixture. The enantiomeric excess (ee) was analyzed on an Agilent 1100 HPLC equipped with a chiral column (Phenomenex Lux 5μm Cellulose-2) and variable wavelength detector (VWD). The HPLC chromatograph was programmed isocratically with hexanes/isopropanol (99:1). Optical rotations were recorded on a Perkin-Elmer Polarimeter 340 thermostatted to 20 ºC, using the sodium D line.

The ^{1}H NMR spectra were obtained on Bruker DRX 400 and 500 MHz spectrometers in $CDCl_3$. Chemical shifts are reported in parts per million (ppm) relative to the reference TMS (Trimethylsilane). The coupling constants are reported in hertz (Hz). ^{1}H NMR data was reported as follows: chemical shift values (ppm), multiplicity (s = singlet, d = doublet, t = triplet, q = quartet, m = multiplet). ^{13}C NMR spectra were recorded in $CDCl_3$ or CD_3OD by using a Bruker DRX 400 MHz or DRX 500 MHz.^{13}C NMR data was reported as chemical shift values (ppm). IR spectra were obtained with a Perkin-Elmer Spectrum

One FT-IR spectrometer and samples were directly placed on the KBr plates. High-resolution mass spectra (HRMS) were obtained by using positive electrospray ionization and by TOF method (Bruker Impact QTOF). The GC-MS analysis was performed on GC-MS (Varian CP-3800 GC, interfaced with a Varian Saturn 2000 MS) using a SPB-5 fused silica capillary column (30 m × 0.25 mm i.d., film thickness 0.25 µm, Supelco, Bellefonte, PA, USA) with positive electron ionization (EI). The GC-MS analysis was performed on GC-MS (Varian CP-3800) using a SPB-5 fused silica capillary column (30 m × 0.25 mm i.d., film thickness 0.25 µm, Supelco, Bellefonte. PA, USA) with positive electron ionization (EI). Samples were diluted in n-hexanes and injected with a 1:10 split ratio. The injector temperature was programmed to 250 °C. The oven temperature was held at 80 °C for 50 sec and raised to 200 °C at 14 °C/min which was held for 15 min. Then finally 2 °C/ min to 260 °C which was held for 5 min. The MS conditions were: Solvent - delay time 6 min and scanned mass range (m/z) 50-500.

2.5. Experimental procedures

2.5.1. Preparation of (*S*,*E*)-2-((2,2-dimethylpropylidene)amino)-N-methylpropanamide (111)

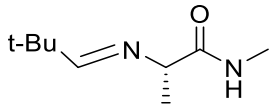

A 100 mL round bottom flask equipped with stir bar was charged with a 33 wt% solution of methylamine in ethanol (14 mL, 10.63 g, 0.107 mol) and placed in an ice-cold water bath. L-alanine methyl ester hydrochloride (**108**) (5 g, 0.036 mol) was added to the cold, stirred solution. The reaction mixture was brought to room temperature and stirred for 5 h. Afterward, the reaction mixture was concentrated under reduced pressure to give a wet solid (8.1 g). Toluene (20 mL) was added to the mixture, which was then concentrated *in vacuo*.to provide a wet solid (8.1 g). The toluene (20 mL) flush was repeated, and the mixture was concentrated to 6.0 g of solids, which were dried in high vacuum for 5 h to produce the crude (*S*)-2-amino-N-methylpropanamide (**109**) as a pasty solid (5.6 g).

To a stirred solution of (*S*)-2-amino-N-methylpropanamide (**109**) (5.6 g, 0.040 mol) in dichloromethane (25 mL) was added anhydrous magnesium sulfate (4 g) The reaction mixture was treated sequentially with pivaldehyde (**110**) (4.25 mL, 3.4 g, 0.04 mol) and

triethylamine (8.3 mL, 6.0 g, 0.06 mol) and stirred at room temperature for 4 h. The reaction mixture was then filtered through a Büchner funnel to remove the magnesium sulfate and triethylamine hydrochloride salt. The filter cake was washed with toluene (40 mL). The combined filtrate was dried over $MgSO_4$ and concentrated under reduced pressure to provide (*S*,*E*)-2-(2,2-dimethylpropylidene)amino)-N-methylpropanamide (**111**) as a yellow oil (5.2 g, 85%).

^{1}H NMR (500 MHz, CD_3OD) δ 7.54 (s, 1H), 7.0 (bs, 1H), 3.70 (q, *J* = 7.1 Hz, 1H), 2.86 (d, *J* = 4.9 Hz, 3H), 1.33 (d, *J* = 7.0 Hz, 3H), 1.09 (s, 9H).

^{13}C NMR (125 MHz, CD_3OD) δ 174.9, 173.4, 67.9, 36.7, 27.1, 26.0, 21.8.

2.5.2. Preparation of (2*R*,5*S*)-2-tert-butyl-3,5-dimethylimidazolidin-4-one (106)

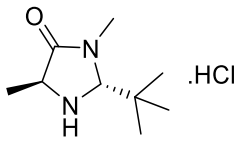

To a cold (0 °C) stirred suspension of (*S*,*E*)-2-(2,2-dimethylpropylidene)amino)-N-methylpropanamide (**111**) in ethanol (5 g, 0.029 mol), acetyl chloride (2.3 mL, 2.54 g, 0.032 mol) was added dropwise over 30 min. The reaction temperature rose to 30 °C during the addition of acetyl chloride. The reaction mixture was heated to 75 °C for 1 h. After this time, the reaction mixture was allowed to cool to room temperature and stirring was continued for 4 h. The resulting white crystals were filtered using a Büchner funnel. The filter cake was washed with ethanol (3 × 10 mL), and vacuum dried to afford (2*R*,5*S*)-2-*tert*-butyl-3,5-dimethylimidazolidin-4-one (**106**) (5.7 g, 90%) as white crystalline material. The spectroscopic data of the obtained compound **3** agree with the literature data (Graham, Horning, and MacMillan 2011).

^{1}H NMR (500 MHz, CD_3OD) δ 4.81 (s, 1H), 4.29 (q, *J* = 7.0 Hz, 1H), 3.10 (s, 3H), 1.60 (d, *J* = 7.0 Hz, 3H), 1.20 (s, 9H).

^{13}C NMR (125 MHz, CD_3OD) δ 171.5, 82.1, 55.0, 37.9, 32.7, 25.5, 15.1.

IR (neat): 2879, 2645, 2520, 1720, 1586 cm^{-1}.

HRMS (ESI) *m/z* calculated for $C_9H_{19}N_2O$ [M+H]: 171.1492, found 171.1491.

$[\alpha]_D^{20}$: -44.1 (*c* 1.0, CH_3OH).

2.5.3. General procedure for preparation of (2*R*)-2-chlorododecanal (113) and (2*S*)-2-chlorododecanal (*ent*-113)

To a cold (0 °C), stirred suspension of lithium chloride (0.016 mol) in acetonitrile (50 mL), was added copper (II) trifluoroacetate hydrate (0.004 mol) and sodium persulfate (0.004 mol) followed by H_2O (0.017 mol). The reaction mixture was stirred for 5 min and then the SOMO catalyst (2*S*,5*R*)-2-(*tert*-butyl)-3,5-dimethylimidazolidin-4-one (**106**) or (2*R*,5*S*)-2-(*tert*-butyl)-3,5-dimethylimidazolidin-4-one (*ent*-**106**) (0.0016 mol) was added. After stirring for 5 min at 0 °C, dodecanal (**99**) (0.008 mmol) was added. The reaction mixture was stirred for 1 h and then allowed to slowly warm to 5 °C over the course of 24 h. The mixture was stirred at 5 °C until dodecanal had been completely consumed (as determined by ^1H NMR spectroscopy). After this time, the reaction mixture was treated with water (20 mL) and diluted with ethyl acetate (50 mL), and the phases were separated. The aqueous phase was extracted with ethyl acetate (3 × 50 mL) and the combined organic phases were washed with brine (20 mL), dried over $MgSO_4$, and concentrated to give the crude chloroaldehyde. Purification of the crude product by flash chromatography afforded the desired products.

(2*R*)-2-chlorododecanal (113)

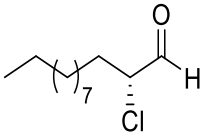

(Eluent: 1% EA/hexane), 1.03 g, 87%, pale yellow oil: ^1H NMR (500 MHz, $CDCl_3$) δ: 9.48 (d, 1H, *J* = 2.5 Hz), 4.15 (ddd, 1H, *J* = 8.5 Hz, 5.5 Hz, 3 Hz), 1.99-1.92 (dddd, 1H, *J* = 16 Hz, 11.5 Hz, 10.5 Hz, 6Hz), 1.84-1.78 (dddd, 1H, *J* = 18.5 Hz, 14 Hz, 8.5 Hz, 5 Hz), 1.54-1.48 (m, 1H), 1.44-1.37 (m, 1H), 1.25 (m, 14H), 0.88 (t, 3H, *J* = 7 Hz).

^{13}C NMR (125 MHz, $CDCl_3$) δ 194.7, 63.4, 31.4, 31.3, 28.9, 28.8, 28.7 (2C), 28.3, 24.9, 22.0, 13.5.

IR (neat): 2955, 2925, 2855, 2718, 1736, 1466, 759 cm^{-1}.

HRMS (ESI) m/z calculated for $C_{12}H_{23}ClO$ [M-H] 217.1359; found: 217.1362.

$[\alpha]_D^{20}$: +10 (c 0.5, $CHCl_3$).

(2*S*)-2-chlorododecanal (*ent*-113)

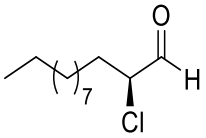

(Eluent: 1% EA/hexane), 1.0 g, 84%, pale yellow oil: ^{1}H NMR (500 MHz, $CDCl_3$) δ 9.48 (d, 1H, *J* = 2.5 Hz), 4.17-4.14 (ddd, 1H, *J* = 8.5 Hz, 5.5 Hz, 3 Hz), 2.02-1.93 (dddd, 1H, *J* = 16 Hz, 11.5 Hz, 10.5 Hz, 6Hz), 1.86-1.77 (dddd, 1H, *J* = 18.5 Hz, 14 Hz, 8.5 Hz, 5 Hz), 1.68-1.57 (m, 1H), 1.53-1.39 (m, 1H), 1.26 (m, 14H), 0.87 (t, 3H, *J* = 7 Hz).

^{13}C NMR (125 MHz, $CDCl_3$) δ: 195.3, 63.8, 31.9, 31.7, 29.4, 29.3, 29.2 (2C), 28.8, 25.4, 22.6, 14.0.

IR (neat): 2957, 2928, 2855, 2718, 1738, 1466, 759 cm^{-1}.

HRMS (ESI) m/z calculated for $C_{12}H_{23}ClO$ [M-H] 217.1359; found: 217.1362.

$[\alpha]_D^{20}$: -9.9 (c 0.5, $CHCl_3$).

2.5.4. Preparation of 2-chlorododecanal (114)

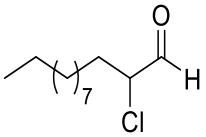

To a cold (0 ^{o}C), stirred solution of dodecanal (**99**) (150 mg, 0.8152 mmol) in dichloromethane (10 mL) *N*-chlorosuccinimide (130 mg, 0.9782 mmol) and proline (47 mg, 0.4076 mmol) were added. After stirring for 5 min at 0 ^{o}C, the reaction mixture was allowed to slowly warm to room temperature. Then the mixture was stirred at room temperature until dodecanal had been completely consumed (as determined by ^{1}H NMR spectroscopy). After this time, the reaction mixture was treated with water (20 mL) and diluted with ethyl acetate (50 mL), and the phases were separated. The aqueous phase

was extracted with ethyl acetate (3 × 50 mL) and the combined organic phases were washed with brine (20 mL), dried over $MgSO_4$, and concentrated to give the crude chloroaldehyde. Purification of the crude product by flash chromatography (silica gel, 99:1 hexane: ethyl acetate) afforded 2-chlorododecanal (**114**) as a colourless oil (143 mg, 81%).

^{1}H NMR (500 MHz, $CDCl_3$) δ: 9.48 (d, 1H, *J* = 2.5 Hz), 4.15 (ddd, 1H, *J* = 8.5 Hz, 5.5 Hz, 3Hz), 1.99-1.92 (dddd, 1H, *J* = 16Hz, 11.5 Hz, 10.5Hz, 6Hz), 1.84-1.78 (dddd, 1H, *J* = 18.5Hz, 14Hz, 8.5Hz, 5Hz), 1.54-1.48 (m, 1H), 1.44-1.37 (m, 1H), 1.25 (m, 14H), 0.88 (t, 3H, *J* = 7 Hz).

^{13}C NMR (125 MHz, $CDCl_3$) δ 194.7, 63.4, 31.4, 31.3, 28.9, 28.8, 28.7 (2C), 28.3, 24.9, 22.0, 13.5.

IR (neat): 2955, 2925, 2855, 2718, 1736, 1466, 759 cm^{-1}.

HRMS (ESI) m/z calculated for $C_{12}H_{23}ClO$ [M-H] 217.1359; found: 217.1362.

2.5.5. General procedure for preparation of 2-chlorododecanol (115) and (2*R*)-2-chlorododecanol (118)

To a cold (0 ^{o}C) stirred solution of chloroaldehyde **113** or **114** (100 mg, 0.458 mmol) in MeOH (2 mL), sodium borohydride (34 mg, 0.916 mmol) was added. After stirring for 5 min at 0 ^{o}C the resulting reaction mixture was allowed to stir at room temperature for 2h. Then the reaction mixture was quenched with ice cold water (5 mL) and diluted with ethyl acetate (10 mL). The aqueous layer was removed and extracted with ethyl acetate (2 × 5 mL) and the combined organic layers were dried over $MgSO_4$, concentrated under reduced pressure afforded crude product. Purification of the crude product by flash chromatography (silica gel, 95:5 hexanes: ethyl acetate) yielded 2-chlorododecanol (**115**) or (2*R*)-2-chlorododecanol (**118**) as a colourless oil.

2-chlorododecanol (115)

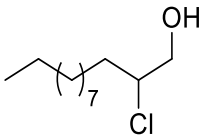

(Eluent: 5% EA/hexane), 82 mg, 81%, colorless oil. ^{1}H NMR (500 MHz, $CDCl_3$) δ: 4.04 (m, 1H), 3.80 (dd, 1H, *J* = 12Hz, 3.5 Hz), 3.68 (dd, 1H, *J* = 12Hz, 7 Hz), 1.81-1.74 (m, 2H), 1.59-1.50 (m, 1H), 1.41-1.37 (m, 1H), 1.28 (m, 15H), 0.90 (t, 3H, *J* = 7 Hz).

^{13}C NMR (125 MHz, $CDCl_3$) δ 67.2, 65.6, 34.3, 31.9, 29.6 (2C), 29.4, 29.3, 29.1, 26.4, 22.7, 14.2. IR (neat): 3369, 2954, 2924, 2854, 1465, 721 cm^{-1}.

HRMS (ESI) m/z calculated for $C_{12}H_{25}ClONH_3$ [M+NH_3]: 237.1594; found: 237.1205.

(2*R*)-2-chlorododecanol (118)

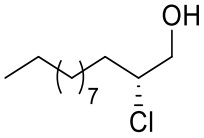

(Eluent: 5% EA/hexane), 85 mg, 84%, colorless oil.^{1}H NMR (500 MHz, $CDCl_3$) δ: 4.04 (m, 1H), 3.80 (dd, 2H, *J* = 12Hz, 3.5 Hz), 3.68 (dd, 2H, *J* = 12Hz, 7 Hz), 1.81-1.74 (m, 2H), 1.59-1.50 (m, 1H), 1.41-1.37 (m, 1H), 1.28 (m, 15H), 0.90 (t, 3H, *J* = Hz).

^{13}C NMR (125 MHz, $CDCl_3$) δ: 67.0, 65.3, 34.2, 31.8, 29.5 (2C), 29.4, 29.2, 29.0, 26.3, 22.6, 14.0.

IR (neat): 3369, 2954, 2924, 2854, 1465, 721 cm^{-1}.

HRMS (ESI) m/z calculated for $C_{12}H_{25}ClONH_3$ [M+NH_3]: 237.1594; found: 237.1205.

$[\alpha]_D^{20}$: +10 (c 0.5, $CHCl_3$).

2.5.6. General procedure for the preparation of 2-chlorododecyl benzoate (117), 2-chlorododecyl-4-bromobenzoate (117a), 2-chlorododecyl-4-methylbenzenesulfonate (117b) and (2*R*)-2-chlorododecylbenzoate (119)

To a cold (0 ^{o}C) stirred solution of chlorododecanol **115** or **118** (85 mg, 0.386 mmol) in pyridine (2 mL), benzoyl chloride (**116**) (81 mg, 0.579 mmol) or 4-bromobenzenesulfonyl chloride (**116a**) (137 mg, 0.579 mmol) or 4-methylbenzenesulfonyl chloride (**116b**) (103 mg, 0.579 mmol) was added. The reaction mixture was stirred for 5 min at 0 ^{o}C and then at room temperature for 2h. Then the reaction mixture was quenched with saturated sodium bicarbonate ($NaHCO_3$) solution and diluted with ethyl acetate (10 mL). The aqueous layer was removed and extracted with ethyl acetate (2 × 5 mL) and the combined organic layers were washed with 1N HCl (5 mL) and brine solution (5 mL), dried over $MgSO_4$, concentrated under reduced pressure afforded crude product. Purification of the crude product by flash chromatography yielded 2-chlorododecyl benzoate (**117**), or 2-chlorododecyl-4-bromobenzenesulfonate (**117a**) or 2-chlorododecyl-4-methylbenzenesulfonate (**117b**) or (2*R*)-2-chlorododecylbenzoate (**119**).

2-chlorododecyl benzoate (117)

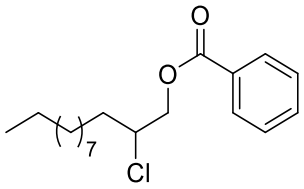

Chlorododecanol **115** (85 mg, 0.386 mmol), benzoyl chloride (81 mg, 0.579 mmol), Pyridine (2 mL). (Eluent: 1% EA/hexane), 82 mg, 65.4%, colorless oil. ^{1}H NMR (500 MHz, $CDCl_3$) δ: 8.08 (d, 2H, = 8Hz), 7.58 (t, 2H, *J* = 7.5 Hz), 7.46 (t, 2H, *J* = 7.5 Hz), 4.51-4.47 (dd, 1H, *J* = 11.5 Hz, 5.5 Hz), 4.46-4.42 (dd, 1H, *J* = 11.5 Hz, 6.5 Hz), 4.23-4.16 (m, 1H), 1.91-1.85 (m, 1H), 1.81-1.74 (m, 1H), 1.65-1.55 (m, 1H), 1.50-1.41 (m, 1H), 1.25 (m, 14 H), 0.87 (t, 3H, *J* = 7Hz).

^{13}C NMR (125 MHz, $CDCl_3$) δ: 166.7, 133.0, 129.7 (3C), 128.4 (2C), 67.9, 59.2, 34.7, 31.8, 29.5, 29.4, 29.3, 29.2, 29.0, 26.0, 22.6, 14.0.

IR (neat): 2994, 2953, 2926, 2855, 1727, 1465, 1452, 1271, 1113, 710 cm^{-1}.

HRMS (ESI) m/z calculated for $C_{19}H_{29}ClO_2Na$ [M+Na] 347.1754; found: 347.1741.

2-chlorododecyl-4-bromobenzoate (117a)

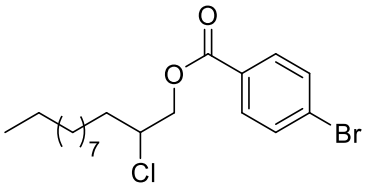

(85 mg, 0.386 mmol), 4-bromobenzoyl chloride (137 mg, 0.579 mmol), Pyridine (2 mL). (Eluent: 1% EA/hexane), 87 mg, 56.1%, colorless oil. ^{1}H NMR (500 MHz, $CDCl_3$) δ: 7.92 (d, *J* = 8.6 Hz, 2H), 7.60 (d, *J* = 8.6 Hz, 2H), 4.52-4.41 (m, 2H), 4.21-4.16 (m, 1H), 1.91-1.73 (m, 3H), 1.45 (qt, *J* = 10.1, 4.3 Hz, 1H), 1.28 (d, *J* = 18.6 Hz, 19H), 0.88 (t, *J* = 6.9 Hz, 4H).

^{13}C NMR (125 MHz, $CDCl_3$) δ: 165.42, 131.83 (2C), 131.24 (2C), 128.62, 128.42, 68.25, 59.26, 34.74, 31.90, 29.57, 29.52, 29.41, 29.31, 29.05, 26.08, 22.68, 14.12.

IR (neat): 2995, 2954, 2927, 2854, 1730, 1464, 1451, 1270, 1113, 711 cm^{-1}.

HRMS (ESI) m/z calculated for $C_{19}H_{29}ClO_2Na$ [M+Na] 403.7850; found: 403.7855.

2-chlorododecyl-4-methylbenzenesulfonate (117b)

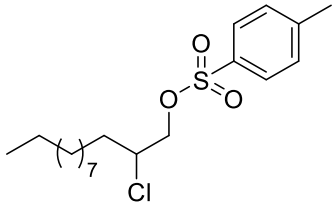

(85 mg, 0.386 mmol), 4-methylbenzeneshulfonyl chloride (103 mg, 0.579 mmol), Pyridine (2 mL). (Eluent: 1% EA/hexane), 94 mg, 65.2%, colorless oil. ^{1}H NMR (500 MHz, $CDCl_3$) δ: 7.81 (d, *J* = 8.3 Hz, 2H), 7.36 (d, *J* = 8.0 Hz, 2H), 4.11 (tt, *J* = 10.4, 5.2 Hz, 2H), 4.01-3.96 (m, 1H), 2.46 (s, 4H), 1.80 (qd, *J* = 10.0, 5.6 Hz, 1H), 1.65-1.43 (m, 2H), 1.25 (s, 13H), 0.88 (t, *J* = 7.0 Hz, 3H).

^{13}C NMR (125 MHz, $CDCl_3$) δ: 145.14, 132.64, 129.94 (2C), 128.01 (2C), 72.11, 58.05, 34.14, 31.90, 29.56, 29.51, 29.37, 29.31, 28.94, 25.72, 22.68, 21.69, 14.12.

IR (neat): 2992, 2953, 2926, 2855, 1727, 1465, 1452, 1365, 1177, 1271, 1113, 912, 710 cm^{-1}.

HRMS (ESI) m/z calculated for $C_{19}H_{29}ClO_2Na$ [M+Na] 374.9640; found: 374.9647.

(2*R*)-2-chlorododecylbenzoate (119)

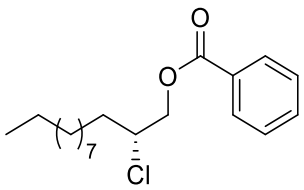

(Eluent: 1% EA/hexane), 79 mg, 63%, colorless oil. ^{1}H NMR (500 MHz, $CDCl_3$) δ: 8.08 (d, 2H, *J* = 8Hz), 7.58 (t, 2H, *J* = 7.5 Hz), 7.46 (t, 2H, *J* = 7.5 Hz), 4.51-4.47 (dd, 1H, *J* = 11.5 Hz, 5.5 Hz), 4.46-4.42 (dd, 1H, *J* = 11.5 Hz, 6.5 Hz), 4.23-4.16 (m, 1H), 1.91-1.85 (m, 1H), 1.81-1.74 (m, 1H), 1.65-1.55 (m, 1H), 1.50-1.41 (m, 1H), 1.25 (m, 14H), 0.87 (t, 3H, *J* = 7Hz).

^{13}C NMR (125 MHz, $CDCl_3$) δ: 166.1, 133.2, 129.7 (3C), 128.4 (2C), 68.0, 59.4, 34.8, 31.9, 29.6, 29.5, 29.4, 29.3, 29.0, 26.1, 22.7, 14.1.

IR (neat): 3064, 2953, 2926, 2855, 1727, 1465, 1452, 1271, 1113, 710 cm^{-1}.

HRMS (ESI) m/z calculated for $C_{19}H_{29}ClO_2Na$ [M+Na] 347.1754; found: 347.1741.

$[\alpha]_D^{20}$: +10 (c 0.5, $CHCl_3$).

2.5.7. Preparation of (7*S*,8*R*)-8-chloro-7-hydroxy-2-methyloctadecan-5-one (121)

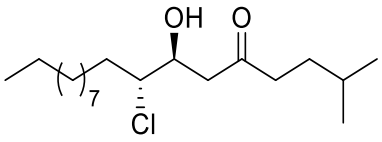

To a cold (-78 °C), stirred solution of 5-methyl-2-hexanone (**120**) (495 mg, 4.335 mmol) in dry THF (10 mL) was added lithium diisopropylamide (1.66 mL, 4.335 mmol, 2.5 M in hexanes). After 45 minutes of stirring at -78 °C, a solution of the chlorododecanol **113** (950

mg, 4.335 mmol) in dry THF (5 mL) was slowly added dropwise to the reaction mixture. After a further 45 minutes stirring at the same temperature, the reaction mixture was quenched with a saturated aqueous solution of NH_4Cl (15 mL), diluted with ethyl acetate (50 mL) and water (20 mL). The phases were separated, and the aqueous phase was extracted with ethyl acetate (3 × 50 mL). The combined organic layers were washed with brine (30 mL), dried over $MgSO_4$, and concentrated under reduced pressure, which afforded crude product (d.r. 10:1 determined by ^{1}H NMR analysis of the crude reaction mixture). Purification of the crude product by flash chromatography afforded (silica gel, 90:10 hexanes: ethyl acetate) yielded **121** (1.01 g, 70%) as a colourless oil.

^{1}H NMR (500 MHz, $CDCl_3$)δ: 4.10 (dddd, *J* = 8.3, 6.1, 5.0, 3.3 Hz, 1H), 3.91 (ddd, *J* = 9.5, 6.1, 3.3 Hz, 1H), 3.30 (d, *J* = 5.0 Hz, 1H), 2.82 (dd, *J* = 17.6, 3.3 Hz, 1H), 2.75 (dd, *J* = 17.6, 8.1 Hz, 1H), 2.47 (t, *J* = 7.5 Hz, 2H), 1.95-1.81 (m, 1H), 1.71-1.51 (m, 1H), 1.55 (m, 2H), 1.25 (m, 17H), 0.90 (d, 6H, *J* = 6.6 Hz), 0.89 (t, 3H, *J* = 7 Hz).

2.5.8. Preparation of N'-((7*S*,8*R*,*E*)-8-chloro-7-hydroxy-2-methyloctadecan-5-ylidene)-4-methylbenzenesulfonohydrazide (122)

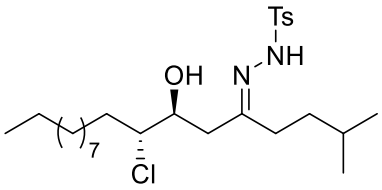

To a stirred solution of β-keto-chlorohydrin **121** (100 mg, 0.3003 mmol) in MeOH (5 mL) was added *p*-toluenesulfonyl hydrazide (56 mg, 0.3003.) and the resulting reaction mixture was stirred at room temperature for 2 h. The reaction mixture was diluted with dichloromethane (20 mL) and white precipitate was filtered off. The filtrate was dried over Na_2SO_4 and the concentrated under reduced pressure to afford the crude product. The crude was carried to next step.

2.5.9. General procedure for preparation of 127, 128 and *ent*-128

To a cold (-78 ^{o}C), stirred solution of 1-hexyne (**125**) or 5-methyl-1-hexyne (**126**) (0.015 mol) in THF (20 mL), a solution of *n*-butyllithium (2.5 M in hexanes, 0.014 mmol) was added dropwise. The resulting mixture was stirred at -78 ^{o}C for 1h. After this time, a

solution of **113** or *ent*-**113** (0.008 mol) in THF (10 mL) was added dropwise and the reaction mixture was stirred for an additional 1h. Then the reaction mixture was quenched with a saturated aqueous solution of NH_4Cl (10 mL), diluted with ethyl acetate (50 mL) and water (20 mL). The phases were separated, and the aqueous phase was extracted with ethyl acetate (3 × 50 mL). The combined organic layers were washed with brine (30 mL), dried over $MgSO_4$, and concentrated under reduced pressure, which afforded crude product The ^1H NMR analysis of the crude product showed a diastereomeric ratio (*d*.*r*) approximately 20:1 (*anti*:*syn*). The diastereomeric ratio of 1,2-*anti* and 1,2-*syn* isomers was determined based on the proton signals from CH group (CH-OH or CH-Cl). Purification of the crude product by flash chromatography afforded (silica gel, 95:5 hexanes: ethyl acetate) yielded **127** or **128** or ***ent*-128**.

(7*S*,8*R*)-8-chloro-octadec-5-yn-7-ol (127)

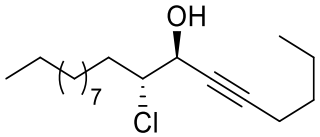

(Eluent: 5% EA/hexane), 1.94 g, 89%, pale yellow oil: ^1H NMR (500 MHz, $CDCl_3$) δ: 4.50 (dt, 1H, *J* = 3.6, 1.9 Hz), 4.0 (ddd, 1H, *J* = 9.3, 4.4, 3.5 Hz), 2.24 (td, 2H, *J* = 7.4 Hz, 2.0 Hz),1.82 (m, 2H),1.70 (m, 1H),1.56 (m, 2H),1.27 (m, 17H), 0.90 (t, 3H, *J* = 7 Hz), 0.89 (t, 3H, *J* = 7 Hz).

^{13}C NMR (125 MHz, $CDCl_3$) δ: 87.9, 76.8, 67.6, 66.4, 37.5, 33.7, 32.0, 29.7, 29.7, 29.5, 29.4, 29.2, 27.3, 26.6, 22.8, 22.2, 14.2, 13.2.

IR (neat): 3416, 2956, 2926, 2855, 2237, 1466, 1042, 759 cm^{-1}.

HRMS (ESI) m/z calculated for $C_{18}H_{33}ClONa$ [M+Na]: 323.9008; found: 323.9015.

(7*S*,8*R*)-8-chloro-2-methyloctadec-5-yn-7-ol (128)

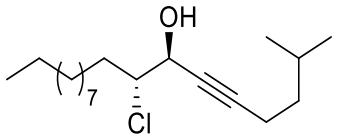

(Eluent: 5% EA/hexane), 1.94 g, 89%, pale yellow oil: ^{1}H NMR (500 MHz, $CDCl_3$) δ: 4.50 (dt, 1H, *J* = 3.6, 1.9 Hz), 4.0 (ddd, 1H, *J* = 9.3, 4.4, 3.5 Hz), 2.24 (td, 2H, *J* = 7.4 Hz, 2.0 Hz),1.82 (m, 2H),1.70 (m, 1H),1.56 (m, 2H),1.27 (m, 17H), 0.90 (d, 6H, *J* = 6.6 Hz), 0.89 (t, 3H, *J* = 7 Hz).

^{13}C NMR (125 MHz, $CDCl_3$) δ: 87.9, 76.8, 67.6, 66.4, 37.5, 33.7, 32.0, 29.7, 29.7, 29.5, 29.4, 29.2, 27.3, 26.6, 22.8, 22.2, 16.8, 14.2.

IR (neat): 3416, 2956, 2926, 2855, 2237, 1466, 1042, 759 cm^{-1}.

HRMS (ESI) m/z calculated for $C_{19}H_{35}ClONa$ [M+Na]: 337.2274; found: 337.1042.

(7*R*,8*S*)-8-chloro-2-methyloctadec-5-yn-7-ol (*ent*-128)

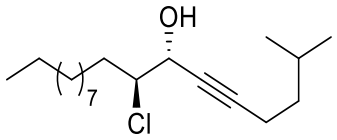

(Eluent: 5% EA/hexane), 1.88 g, 86%, pale yellow oil: ^{1}H NMR (500 MHz, $CDCl_3$) δ: 4.50 (dt, 1H, *J* = 3.6, 1.9 Hz), 4.03-3.99 (ddd, 1H, *J* = 9.3, 4.4, 3.5 Hz), 2.26-2.22 (td, 2H, *J* = 7.4 Hz, 2.0 Hz),1.88-1.75 (m, 2H),1.72-1.66 (m, 1H),1.63-1.52 (m, 2H),1.26 (m, 17H), 0.90 (d, 6H, *J* = 6.6 Hz), 0.86 (t, 3H, *J* = 7 Hz).

^{13}C NMR (125 MHz, $CDCl_3$) δ: 87.7, 76.8, 67.4, 66.2, 37.5.6, 33.5, 31.8, 30.4, 29.5, 29.4, 29.3, 29.2, 29.0, 26.3, 22.6, 21.8, 18.2, 14.0, 13.4.

IR (neat): 3417, 2957, 2926, 2855, 2237, 1466, 1042, 759 cm^{-1}.

HRMS (ESI) m/z calculated for $C_{19}H_{35}ClONa$ [M+Na]: 337.2274; found: 337.1042.

2.5.10. General procedure for preparation of 130, 131 and *ent*-131

To an ice cold, stirred solution of triphenylphosphine (0.0082 mol) in dry THF (20 mL), benzoic acid (**129**) (0.0082 mol) and the solution of **127** or **128** or *ent*-**128** (0.0041 mol) in

dry THF (10 mL) were added slowly to the reaction flask under an inert N_2 atmosphere. The resulting mixture was stirred at 0 ^oC for 5 minutes. After this time, a solution of diisopropyl azodicarboxylate (0.0082 mol) in dry THF (5 mL) was added dropwise and the reaction mixture was stirred at room temperature for 12 h. The reaction solvent was removed by evaporation under reduced pressure and diluted with ethyl acetate (50 mL) and water (20 mL). The phases were separated, and the aqueous phase was extracted with ethyl acetate (3 × 50 mL). The combined organic layers were washed with brine (20 mL), dried over $MgSO_4$, and concentrated under reduced pressure, which afforded crude product. Purification of the crude product by flash chromatography (silica gel, 99:1 hexane: ethyl acetate) afforded the desired target compounds.

(7*R*,8*R*)-8-chloro-octadec-5-yn-7-yl benzoate (130)

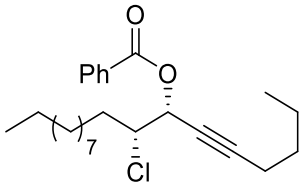

(Eluent: 1% EA/hexane), 1.25 g, 73%, pale yellow oil: ^1H NMR (500 MHz, $CDCl_3$) δ: 8.09 (d, 2H, *J* = 7.2 Hz), 7.58 (t, 1H, *J* = 7.4 Hz), 7.46 (t, 2H, *J* = 7.7 Hz), 5.74 (dt, 1H, *J* = 6.1 Hz, 1.9 Hz), 4.09 (ddd, 1H, *J* = 9.6 Hz, 6.2 Hz, 3.4 Hz), 2.24 (td, 2H, *J* = 7.4 Hz, 1.9 Hz), 2.02 (m, 1H), 1.84 (m, 1H), 1.66 (m, 2H), 1.43 (dd, 2H, *J* = 14.5 Hz, 7.3 Hz), 1.26 (m, 14H), 1.16 (m, 2H), 0.89 (t, 3H, *J* = 6.3 Hz), 0.87 (t, 3H, *J* = 5.9 Hz).

^{13}C NMR (125 MHz, $CDCl_3$) δ: 165.1, 133.3, 130.0, 128.5, 88.7, 77.1, 74.4, 67.8, 62.5, 37.2, 33.8, 32.0, 29.7, 29.6, 29.6, 29.5 29.4, 29.1, 27.3, 26.1 22.7, 22.2, 16.8, 14.2.

IR (neat): 2941, 2879, 2238, 1727, 1261, 1103, 1093, 956, 708 cm^{-1}.

$[\alpha]_D^{20}$: + 5.7 (c 0.8, CCl_4).

(7*R*,8*R*)-8-chloro-2-methyloctadec-5-yn-7-yl benzoate (131)

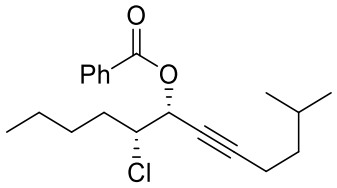

(Eluent: 1% EA/hexane), 1.37 g, 80%, pale yellow oil: ^{1}H NMR (500 MHz, $CDCl_3$) δ: 8.09 (d, 2H, *J* = 7.2 Hz), 7.58 (t, 1H, *J* = 7.4 Hz), 7.46 (t, 2H, *J* = 7.7 Hz), 5.74 (dt, 1H, *J* = 6.1 Hz, 1.9 Hz), 4.09 (ddd, 1H, *J* = 9.6 Hz, 6.2 Hz, 3.4 Hz), 2.24 (td, 2H, *J* = 7.4 Hz, 1.9 Hz), 2.02 (m, 1H), 1.84 (m, 1H), 1.66 (m, 2H), 1.43 (dd, 2H, *J* = 14.5 Hz, 7.3 Hz), 1.26 (m, 14H), 1.16 (m, 2H), 0.89 (t, 3H, *J* = 6.3 Hz), 0.88 (d, 6H, *J* = 6.6 Hz).

^{13}C NMR (125 MHz, $CDCl_3$) δ: 165.1, 133.3, 130.0, 129.5, 128.5, 88.7, 77.1, 74.4, 67.8, 62.5, 37.2, 33.8, 32.0, 29.7, 29.6, 29.6, 29.5, 29.4, 29.1, 27.3, 26.1 22.7, 22.2, 16.8, 14.2.

IR (neat): 2941, 2879, 2238, 1727, 1261, 1103, 1093, 956, 708 cm^{-1}.

HRMS (ESI) m/z calculated for $C_{26}H_{39}ClO_2$ [M+H]: 419.2701; found: 419.2696.

$[\alpha]_D^{20}$: + 5.7 (c 0.8, CCl_4).

(7*S*,8*S*)-8-chloro-octadec-5-yn-7-yl benzoate (*ent*-131)

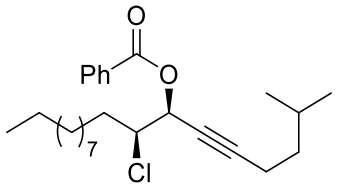

(Eluent: 1% EA/hexane), 1.30 g, 76%, pale yellow oil: ^{1}H NMR (500 MHz, $CDCl_3$) δ: 8.09-8.07 (d, 2H, *J* = 7.2 Hz), 7.60-7.56 (t, 1H, *J* = 7.4 Hz), 7.46-7.44 (t, 2H, *J* = 7.7 Hz), 5.75-5.74 (dt, 1H, *J* = 6.1 Hz, 1.9 Hz), 4.12-4.07 (ddd, 1H, *J* = 9.6 Hz, 6.2 Hz, 3.4 Hz), 2.26-2.22 (td, 2H, *J* = 7.4 Hz, 1.9 Hz), 2.07-1.99 (m, 1H), 1.89-1.79 (m, 1H), 1.66 (m, 2H), 1.43 (dd, 2H, *J* = 14.5 Hz, 7.3 Hz), 1.26 (m, 14H), 0.89 (t, 3H, *J* = 6.3 Hz), 0.88 (d, 6H, *J* = 6.6 Hz).

^{13}C NMR (125 MHz, $CDCl_3$) δ: 165.1, 133.2, 130.0, 129.5, 128.3, 88.4, 77.1, 74.2, 67.7, 62.4, 37.1, 33.7, 32.0, 29.5, 29.4, 29.3, 29.2, 29.0, 27.1, 26.0 22.6, 22.0, 16.7, 14.0.

IR (neat): 2941, 2879, 2238, 1727, 1261, 1103, 1093, 956, 708 cm^{-1}.

HRMS (ESI) m/z calculated for $C_{26}H_{39}ClO_2$ [M+H]: 419.2701; found: 419.2696.

$[\alpha]_D^{20}$: - 5.67 (c 0.8, CCl_4).

2.5.11. General procedure for preparations of 132, 133 and *ent*-133

A 100 mL round bottom flask was charged with methanol or benzene. The flask was evacuated and back filled with nitrogen gas. After two vacuum/ nitrogen cycles to replace air with nitrogen inside the reaction flask, the compound **130** or **131** or ***ent*-131** (0.0028 mol), 20% Pd/C (240 mg, 20 wt % of compound) were added. The reaction mixture was vigorously stirred at room temperature under atmospheric hydrogen for 3 h. After that the reaction mixture was filtered through a celite pad, and the filtrate was concentrated on a rotary evaporator to afford crude product. The crude product was carried to the next step without further purification.

(7*R*,8*R*)-8-chloro-octadecan-7-yl benzoate (132)

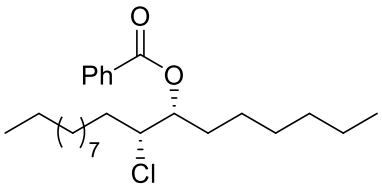

Yield 1.03 g, 86%, colorless oil: ^{1}H NMR (500 MHz, $CDCl_3$) δ: 8.09 (d, 2H, *J* = 7.2 Hz), 7.58 (t, 1H, *J* = 7.4 Hz), 7.45 (t, 2H, *J* = 7.7 Hz), 5.28 (dt, 1H, *J* = 7.2 Hz, 3.2 Hz), 4.06 (dt, 1H, *J* = 9.1 Hz, 4.0 Hz), 1.82 (m, 4H), 1.50 (m, 1H), 1.41 (m, 1H), 1.34 (m, 4H), 1.23 (m, 15H), 1.16 (m, 2H), 0.89 (t, 3H, *J* = 6.3 Hz), 0.87 (t, 3H, *J* = 5.9 Hz).

^{13}C NMR (125 MHz, $CDCl_3$) δ: 166.0, 133.1, 130.0, 128.5, 75.7, 63.9, 38.7, 34.6, 32.0, 31.4, 29.6, 29.5, 29.5, 29.4, 29.3, 29.0, 27.9, 27.2, 26.7, 25.7, 22.7, 22.6, 22.5, 14.1.

IR (neat): 2945, 2880, 1721, 1266, 1108, 1069, 709 cm^{-1}.

$[\alpha]_D^{20}$: +6.4 (c 0.68, CCl_4).

(7*R*,8*R*)-8-chloro-2-methyloctadecan-7-yl benzoate (133)

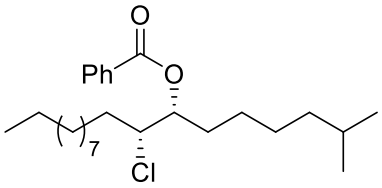

Yield 1.14 g, 95%, colorless oil: ^{1}H NMR (500 MHz, $CDCl_3$) δ: 8.09 (d, 2H, *J* = 7.2 Hz), 7.58 (t, 1H, *J* = 7.4 Hz), 7.45 (t, 2H, *J* = 7.7 Hz), 5.28 (dt, 1H, *J* = 7.2 Hz, 3.2 Hz), 4.06 (dt, 1H, *J* = 9.1 Hz, 4.0 Hz), 1.82 (m, 4H), 1.50 (m, 1H), 1.41 (m, 1H), 1.34 (m, 4H), 1.23 (m, 15H), 1.16 (m, 2H),0.87 (t, 3H, *J* = 6.3 Hz), 0.84 (d, 6H, *J* = 6.6 Hz).

^{13}C NMR (125 MHz, $CDCl_3$) δ: 166.0, 133.1, 130.0, 128.5, 75.7, 63.9, 38.7, 34.6, 32.0, 31.4, 29.6, 29.5, 29.5, 29.4, 29.3, 29.0, 27.9, 27.2, 26.7, 25.7, 22.7, 22.6, 22.5, 14.1.

IR (neat): 2945, 2880, 1721, 1266, 1108, 1069, 709 cm^{-1}.

HRMS (ESI) m/z calculated for $C_{26}H_{43}ClO_2$ [M+H]: 424.0792.; found: 424.2289.

$[\alpha]_D^{20}$: +6.4 (c 0.68, CCl_4).

(7*S*,8*S*)-8-chloro-2-methyloctadecan-7-yl benzoate (*ent*-133)

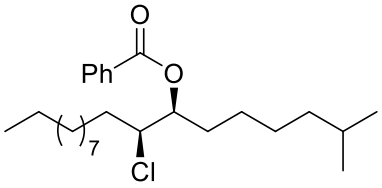

Yield 1.10 g, 90%, colorless oil: ^{1}H NMR (500 MHz, $CDCl_3$) δ: 8.09-8.08 (d, 2H, *J* = 7.2 Hz), 7.57 (t, 1H, *J* = 7.4 Hz), 7.48-7.45 (t, 2H, *J* = 7.7 Hz), 5.31-5.28 (dt, 1H, *J* = 7.2 Hz, 3.2 Hz), 4.08-4.04 (dt, 1H, *J* = 9.1 Hz, 4.0 Hz), 1.88-1.80 (m, 4H), 1.69-1.53 (m, 1H), 1.41 (m, 1H), 1.34 (m, 4H), 1.24 (m, 15H), 0.89 (t, 3H, *J* = 6.3 Hz), 0.85 (d, 6H, *J* = 6.6 Hz).

^{13}C NMR (125 MHz, $CDCl_3$) δ: 165.9, 133.0, 130.0, 129.7, 128.3, 75.6, 63.7, 38.7, 34.4, 31.8, 31.3, 29.6, 29.5, 29.4, 29.4, 29.3, 29.2, 29.0, 27.8, 27.1, 26.5, 25.5, 22.6, 22.5, 22.4, 14.0.

IR (neat): 2945, 2880, 1721, 1266, 1108, 1069, 709 cm^{-1}.

HRMS (ESI) m/z calculated for $C_{26}H_{43}ClO_2$ [M+H]: 424.0792.; found: 424.2289.

$[\alpha]_D^{20}$: -6.35 (c 0.68, CCl_4).

2.5.12. General procedure for preparation of (15a), (15), and (*ent*-15)

To an ice cold, stirred solution of **132** or **133** or *ent*-**133** (0.9456 mmol) in methanol (6 mL), 4N NaOH in methanol (4 mL) was added slowly to the reaction flask. The resulting mixture was stirred at room temperature for 2 h. The reaction solvent was removed by evaporation under reduced pressure and diluted with ethyl acetate (20 mL) and water (10 mL). The phases were separated, and the aqueous phase was extracted with ethyl acetate (3 × 20 mL). The combined organic layers were washed with brine (10 mL), dried over $MgSO_4$, and concentrated under reduced pressure. Purification of the crude product by flash chromatography (silica gel, 100% hexanes) afforded (+)-monachalure (**15a**) or (+)-disparlure (**15**).and (-)-disparlure (*ent*-**15**).

(7*R*,8*S*)-7,8-epoxy-2-octadecane (15a)

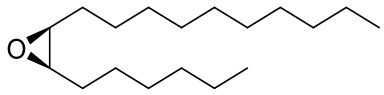

(Eluent: 100% hexane), 0.242 g, 91%, clear oil: ^{1}H NMR (500 MHz, $CDCl_3$) δ: 2.92-2.88 (m, 2H), 1.56-1.18 (m, 27H), 0.90-0.85 (m, 6H).

^{13}C NMR (125 MHz, $CDCl_3$) δ: 57.4, 39.0, 32.0, 29.7, 29.7, 28.0, 27.9, 27.0, 26.7, 22.8, 22.7, 22.7, and 14.2.

IR (neat): 2954, 2923, 2854, 1466, 1082, 1029, 721 cm^{-1}.

$[\alpha]_D^{20}$: +0.55 (c 0.56, CCl_4).

(7*R*,8*S*)-7,8-epoxy-2-methyloctadecane (15)

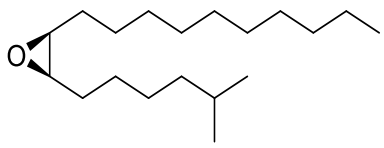

(Eluent: 100% hexane), 0.240 g, 90%, clear oil: ^{1}H NMR (500 MHz, $CDCl_3$) δ: 2.92-2.88 (m, 2H), 1.56-1.18 (m, 27H), 0.90-0.85 (m, 9H).

^{13}C NMR (125 MHz, $CDCl_3$) δ: 57.4, 39.0, 32.0, 29.7, 29.7, 28.0, 27.9, 27.0, 26.7, 22.8, 22.7, 22.7, and 14.2.

IR (neat): 2954, 2923, 2854, 1466, 1082, 1029, 721 cm^{-1}.

HRMS (ESI) m/z calculated for $C_{19}H_{38}O$ [M+H]: 283.3001; found: 283.2985.

$[\alpha]_D^{20}$: +0.54 (c 0.56, CCl_4).

(7*S*,8*R*)-7,8-epoxy-2-methyloctadecane (*ent*-15)

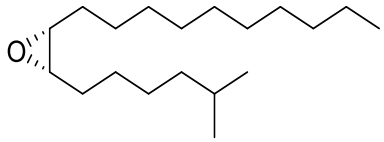

(Eluent: 100% hexane), 0.240 g, 90%, clear oil: ^1H NMR (500 MHz, $CDCl_3$) δ: 2.91-2.87 (m, 2H), 1.53-1.19 (m, 27H), 0.89-0.86 (m, 9H).

^{13}C NMR (125 MHz, $CDCl_3$) δ: 57.2, 57.0, 38.8, 31.8, 29.7, 29.1, 27.9, 27.8, 27.7, 27.6, 27.2, 26.7, 26.4, 22.6, 22.5, 22.5, 22.4, 14.2, 14.01.

IR (neat): 2954, 2923, 2854, 1466, 1082, 1029, 721 cm^{-1}.

HRMS (ESI) m/z calculated for $C_{19}H_{38}O$ [M+H]: 283.3001; found: 283.2985.

$[\alpha]_D^{20}$: -0.537 (c 0.56, CCl_4).

2.5.13. General procedure for preparation of *cis*-N-(α-methylbenzyl)aziridine 139 and 140

To a stirred solution of (+)-(*R*)-α-methylbenzylamine (**134**) (0.0883 mmol) in toluene (0.5 ml), trimethylaluminum in hexane (0.1060 mmol) was added dropwise at 0 °C under nitrogen atmosphere. After, a solution of racemic disparlure ((±)-**15**) or (+)-disparlure (**15**) or (-)-disparlure (*ent*-**15**) in toluene (0.0883 mmol) was added and the reaction mixture was heated at reflux for 4 h. After cooling, the reaction mixture was diluted with water and extracted with three portions of hexanes, and the combined extracts were rinsed well with water, dried, concentrated, and flash chromatographed (silica gel, 80:20 hexanes: ethyl acetate) to give N-substituted 1,2-amino alcohols.

A solution of N-substituted 1,2-amino alcohols (22 mg) in dichloromethane (0.5 ml), trimethylamine (25 µl) and methanesulfonyl chloride (5 µl) were added. After stirring 16 h, the reaction mixture was diluted with saturated aqueous sodium carbonate solution (1 mL) and extracted with three portions of pentanes (3 × 2 mL), and the combined extracts were rinsed with water, dried, concentrated and purified by flash column chromatography technique (silica gel, 95:5 hexanes: ethyl acetate) afforded cis-N-(α-methylbenzyl)aziridine **139** or **140**.

(2*R*,3*S*)-1-((*R*)-1-phenylethyl)-2-decyl-3-(5-methylhexyl)aziridine (139)

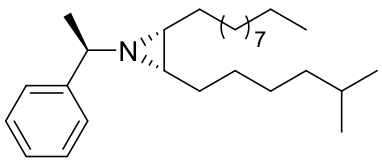

^{1}H NMR (500 MHz, $CDCl_3$) δ: 7.34-7.25 (m, 5H), 2.45 (q, 1H, *J* = 6.6 Hz), 1.55 (m, 2H), 1.43 (m, 6H), 1.37 (m, 4H), 1.27 (m, 14H), 1.06 (m, 6H), 0.89 (m, 6H), 0.80 (d, 3H, *J* = 6.6 Hz).

IR (neat): 2954, 2923, 2854, 1466, 1385, 1029, 721 cm^{-1}.

HRMS (ESI) m/z calculated for $C_{27}H_{47}N$ [M+H]: 386.3742; found: 386.3788.

(2*S*,3*R*)-1-((*R*)-1-phenylethyl)-2-decyl-3-(5-methylhexyl)aziridine (140)

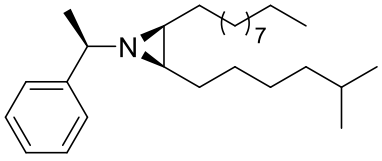

^{1}H NMR (500 MHz, $CDCl_3$) δ: 7.34-7.25 (m, 5H), 2.45 (q, 1H, *J* = 6.6 Hz), 1.55 (m, 2H), 1.43 (m, 6H), 1.37 (m, 4H), 1.27 (m, 14H), 1.06 (m, 6H), 0.89 (m, 6H), 0.80 (d, 3H, *J* = 6.6 Hz).

IR (neat): 2954, 2923, 2854, 1466, 1385, 1029, 721 cm^{-1}.

HRMS (ESI) m/z calculated for $C_{27}H_{47}N$ [M+H]: 386.3742; found: 386.3788.

2.5.14. GC-MS Method for separating diastereomers of *cis*-N-(α-methylbenzyl)aziridine 139 and 140

The GC-MS analysis was performed on GC-MS (Varian CP-3800) using a SPB-5 fused silica capillary column (30 m × 0.25 mm i.d., film thickness 0.25 µm, Supelco, Bellefonte. PA, USA) with positive electron ionization (EI). Samples were diluted in n-hexanes and injected with a 1:10 split ratio. The injector temperature was programmed to 250 °C. The oven temperature was held at 80 °C for 50 sec and raised to 200 °C at 14 °C/min which was held for 35 min. Then finally 2 °C/ min to 260 °C which was held for 10 min. The total programming time was 84.07 min. The MS conditions were: Solvent - delay time 6 min and scanned mass range (m/z) 50-500.

2.5.15. Lure efficacy in trapping

In Massachusetts, cotton dental wicks (1 cm diameter x 2.5 cm) were dosed with 100, 500, or 1000 µg of disparlure, or 500 µg mineral oil, in hexane. The 100 and 1000 µg loadings were from available (+)-disparlure standards (Sigma-Aldrich), and material for the 500 µg disparlure loading was synthesized as described here. The wicks were suspended at the height of the entry ports within USDA milk carton traps, 20 of which were hung at 40-m intervals along unpaved roads in a wooded section of the Massachusetts National Cemetery, Bourne, MA (41°40′21″N 70°35′11″W). A 2.5- x 10-cm plastic strip impregnated with 10% DDVP (Vaportape II, Hercon Environmental, Emigsville, PA) killed moths that entered the trap. A complete randomized block design was used (n = 5), where each block contained one trap for each of the four lure treatments. Traps were deployed from July 30 to August 3, 2015. Moths in traps were counted after 1 and 4 days. At the day 1 check, traps were emptied, wicks replaced, and positions of traps within lines were re-randomized. Data for each trap were pooled across checks, converted to ln(n+1), and analyzed by ANOVA (General Linear Model routine in SYSTAT 13 [Systat Software, San Jose, CA]). Differences between treatment means were not significant ($F = 2.27$; d.f. = 2, 8; $P = 0.17$; the control caught no moths and was excluded from the analysis).

Nova Scotia. Efficacy of synthesized (+)-disparlure (**15**) was evaluated using rubber septa loaded with 500 µg (+)-disparlure in 100 µL of HPLC grade hexane. Treatment lures were deployed individually in Delta wing traps (Great Lakes IPM, Vestaburg, MI). In addition, control lures treated with 500 µg paraffin oil in hexane as

solvent control were also deployed in a similar manner. Ten sites were selected within a 10 km radius of Wolfville, Nova Scotia (45.0833° N, 64.3667° W), which have maintained historical infestations of *L*. *dispar*. At each site, two prospective host trees of the same species were selected (either maple (3 site), oak (3 sites), poplar (3 sites) or ash (1 site), with diameter a breast height between 20-60 cm). One control and one treatment trap were deployed on individual trees, by attaching the trap to the trunk of the tree at 1.5 m above the ground. Control and treatment trees at each site were separated by a minimum of 40 m. All traps were deployed from August 17-26, 2016. Traps were observed at the end of the first day and counted on the last day when traps were retrieved.

Chapter 3.

Application of isotope labelled disparlure enantiomers to study enantiomer discrimination in the gypsy moth PBPs

Adapted from: Pinnelli, G. R.,[1] Terrado, M.,[1] Hillier, N. K.,[2] Lance, D. R.,[3] Plettner, E.[1] (2019). European Journal of Organic Chemistry, 6807-6821.

[1] Department of Chemistry, Simon Fraser University, Burnaby, British Columbia, Canada.

[2] Department of Biology, Acadia University, 33 Westwood Ave., Wolfville, NS, B4P 2R6, Canada.

[3] USDA-APHIS-PPQ CPHST Otis Laboratory, 1398 W Truck Rd, Buzzards Bay, MA 02542, USA.

GP synthesized the isotope labelled disparlure enantiomers and performed NMR binding experiments. MT prepared the *Ldis*PBP1 and *Ldis*PBP2, performed stopped-flow kinetic experiment and prepared Figure 3.9. EP performed molecular docking experiments and prepared Table 3.5, Figures 3.10, 3.11 and 3.12.

3.1. Introduction

Pheromones are detected by moths using a very organized system (Krieger and Breer, 1999). They are chemical signals that are transformed into electrical signals by pheromone sensory neurons found specifically in the antennae of male moths. Male moths have a pair of antennae, surrounded by a cuticle and covered in sensilla, which allow the diffusion of pheromones through the cuticular pores leading to the pheromone receptors (PRs). The latter sit on the dendritic end of pheromone sensory neurons and are bathed in aqueous sensillum lymph where they become activated upon landing of the pheromone. There are 3 important proteins that involve in the detection of the pheromone signal and the initiation of electrical response by the pheromone sensory neurons: pheromone

binding proteins (PBPs), pheromone receptors (PRs) and pheromone degrading enzymes (PDEs).

The first insect olfactory binding protein to be discovered was the pheromone-binding protein (PBP) of the giant silk moth *Antheraea polyphemus* (Vogt and Riddiford, 1981). This small (16-kDa) protein was identified uniquely in the extracellular fluid of sensilla trichodea of male moths. Since then, PBPs have been discovered in several moths; they are expressed during adult development, just before pupation (Vogt et al., 1989). An immunological assay gave confirmation that the PBPs are prepared by the tormogen and trichogen supporting cells of the sensilla trichodea (Steinbrecht et al., 1995).

The PBPs are believed to solubilize the hydrophobic pheromones in the sensillum lymph of sensilla trichodea by making PBP-pheromone complexes. These complexes may travel across the sensillum lymph to vicinity of pheromone receptors. Electrophysiological recording of individual olfactory hairs that are filled with pheromone, displayed significant increase in the physiological response when PBP is added (van den Berg and Ziegelberger, 1991). However, it is unclear whether the increased physiological response noticed is based exclusively on increased solubility of the pheromone during its journey through the lymph to the dendrite or on a more specific detection by a pheromone receptor. Moreover, when pheromones are introduced in heterologous systems (*Xenopus* oocyte and HEK-293 cells) expressing pheromone receptors without PBPs, there was less pheromone sensitivity observed than in systems that contained PBPs (Pophof, 2002; Grosse-Wilde et al., 2006; Grosse-Wilde et al., 2007; Chang et al., 2015) .This suggest that PBPs are not only passive carriers for hydrophobic pheromone molecules, but rather discriminative for certain ligands, thus acting as a filter, which binds, and therefore transport, selectively physiologically relevant ligands.

It is not clear whether the PBPs play a role in translocating pheromones from the sensillar cuticle to receptor sites on the dendrite or whether PBPs act as scavengers, protecting the sensory neuron from saturating at high pheromone doses or removing the pheromone from receptor sites, in conjunction with pheromone degrading enzymes. In principle, PBPs could also contribute to both, transport and scavenging functions simultaneously, as they are known to bind pheromones at external sites and in one internal site (Gong et al., 2009; 2010). Despite the significant body of work on insect PBPs, their function is still debated.

3.2. Interaction of gypsy moth pheromone binding proteins with disparlure enantiomers

In the gypsy moth, *Lymantria dispar*, two PBPs have been discovered, *Ldis*PBP1 and *Ldis*PBP2 (Vogt et al., 1989). Both proteins share 50% identity and belong to the insect odorant-binding proteins (OBP) family with a long C-terminus. The *Ldis*PBP1 and *Ldis*PBP2 contain 143 and 145 amino acid residues, respectively. Homology models of *Ldis*PBPs (created from Bombyx mori PBP template (PDB: 1LS.1.A)) show a highly helical structure, stabilized by 3 disulfide bridges (Chapter 1, Figure 1.6) (Honson and Plettner, 2006). Structural analysis of *Ldis*PBP revealed the presence of conserved phenylalanine amino acid residues that are highly conserved among Lepidoptera PBPs: Phe12, Phe36, Phe76, Phe119 for PBP1 and Phe120 for PBP2 (Figure 3.1). These residues interact with the hydrophobic region (hydrocarbon chains) of the ligands (Sandler et al., 2000; Honson et al., 2003; Sanes and Plettner, 2016). Furthermore, the binding site residues that vary between *Ldis*PBPs were found to be: Asn35, Ala73, Leu91, and Ala135 in *Ldis*PBP1 whereas in *Ldis*PBP2 these residues were substituted with Asp35, Thr73, Ile91 and Leu136 (Sanes and Plettner, 2016). Previously, our group have shown that (+)-disparlure (**15**), the gypsy moth sex pheromone, and its enantiomer (-)-disparlure (*ent*-**15**) (Figure 3.2) bind strongly to *Ldis*PBP1 and *Ldis*PBP2, with opposite enantioselectivity. *Ldis*PBP1 has higher affinity for (-)-disparlure (*ent*-**15**), whereas *Ldis*PBP2 has higher affinity for (+)-disparlure (**15**) (Plettner et al., 2000; Yu and Plettner, 2013). The remarkable enantiomer discrimination between (+)-disparlure (**15**) and (–)-disparlure (*ent*-**15**) is governed by the selectivity and sensitivity of neurons of the olfactory receptors. In addition, the two proteins differ in their ligand binding association and dissociation kinetics: PBP2 binds ligands at its internal binding site very slowly, whereas PBP1 has much faster association and dissociation kinetics (Gong et al., 2009; 2010). The interaction and discrimination of these two PBPs towards disparlure enantiomers are not completely understood due to lack of crystal or NMR-based structures.

```
LdisPBP1    SKEVMKQMTINFAKPMEACKQELNVPDAVMQDFFNFWKEGYQITNREAGC  50
LdisPBP2    SKDVMHQMALKFGKPIKLCQQELGADDSVVKEFLDFWKDGYVMKDRQTGC  50
BmorPBP     SQEVMKNLSLNFGKALDECKKEMTLTDAINEDFYNFWKEGYEIKNRETGC  50
ApolPBP1    SPEIMKNLSNNFGKAMDQCKDELSLPDSVVADLYNFWKDDYVMTDRLAGC  50
AtraPBP1    SPEIMKDLSINFGKALDTCKKELDLPDSINEDFYKFWKEDYEITNRLTGC  50

LdisPBP1    VILCLAKKLELLDQDMNLHHGKAMEFAMKHGADEAMAKQLLDIKHSCEKV 100
LdisPBP2    MLICMAMKLELLDSAMEIHHGSTFAFAKAHGADEAMAQQIIDIVHGCTTT 100
BmorPBP     AIMCLSTKLNMLDPEGNLHHGNAMEFAKKHGADETMAQQLIDIVHGCEKS 100
ApolPBP1    AINCLATKLDVVDPDGNLHHGNAKDFAMKHGADETMAQQLVDIIHGCEKS 100
AtraPBP1    AIKCLSEKLEMVDADGKLHHGNAREFAMKHGADDAMAKQLVDLIHGCEKS 100

LdisPBP1    ITIV-ADDPCQTMLNLAMCFKAEIHKLDWAPTLDVAVGELLADT- 143
LdisPBP2    YPAAETNDPCQRAVNVAMCFKAHVHKLNWAPDVELLVADFLAESQ 145
BmorPBP     TP-A-NDDKCIWTLGVATCFKAEIHKLNWAPSMDVAVGEILAEV- 142
ApolPBP1    AP-P-NDDKCMKTIDVAMCFKKEIHKLNWVPNMDLVIGEVLAEV- 142
AtraPBP1    IP-P-NDDRCMEVLSIAMCFKKEIHNLKWAPNMEVVVGEVLAEV- 142
```

Figure 3.1 **Sequence alignment of lepidopteran PBPs. *Ldis*PBP, *L. dispar*; *Bmor*PBP, *B. mori*; *Apol*PBP, *A. polyphemus*; *Atra*PBP, *A. transitella*. Fully conserved cysteine residues are highlighted in yellow. Fully conserved residues of phenylalanine are highlighted in bright green. Histidine (69, 70, 80 and 95), glycine (71), alanine (141) are in bold letters.**

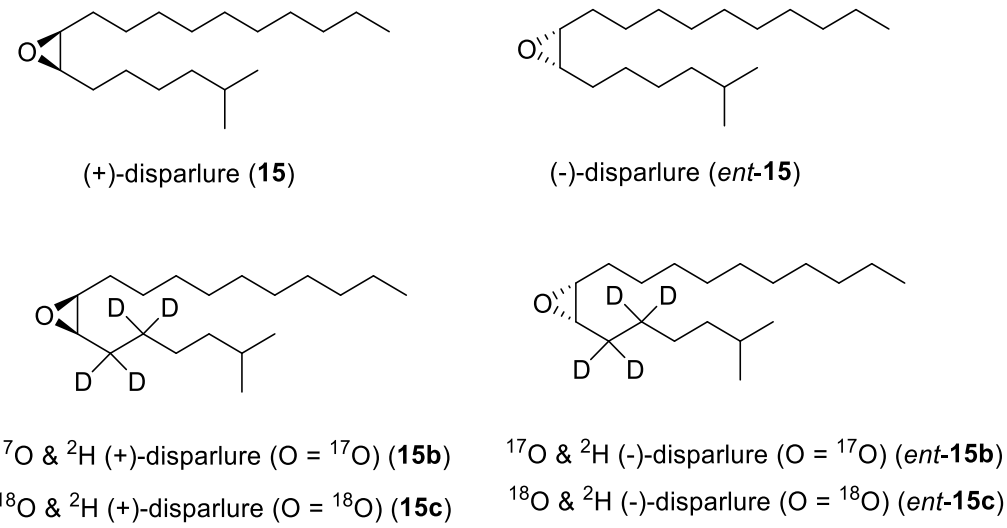

Figure 3.2 **Structures of (+)-disparlure (15), (-)-disparlure (*ent*-15) and isotope labelled disparlure enantiomers.**

Our group proposed previously a two-step association mechanism, based on kinetic studies with ligand and PBPs. The kinetic data suggested that a ligand will interact with the protein on an external site before entering the internal binding pocket (Gong et al., 2009). Once the ligand reaches the internal pocket we know that the two gypsy moth PBPs differ in their affinity for the disparlure enantiomers, but we only have *in-silico* docking models of the PBP-bound pheromones (Yu and Plettner, 2013; Sanes and Plettner, 2016). The challenge of binding studies of PBP-ligand interactions using already known assays is to probe the equilibrating PBP-ligand mixture without excessively disturbing it and to detect the bound ligand.

Several synthetic epoxides that are structurally relevant to disparlure showed that a few essential features of the disparlure molecule are critical for biological activity. For example, two hydrocarbon chains (long and short) of the pheromone and position of methyl substituent, as well as *cis*- configuration of the epoxide are the key features. Moreover, number of studies have demonstrated the importance of epoxy group since its relocation results in significant loss of biological activity. Therefore, we aimed to label the disparlure with specific focus on the incorporation of ^{17}O or ^{18}O oxygen isotopes into the epoxy ring, as well as deuterium at C-5 and C-6 positions. The ^{17}O or ^{18}O & ^{2}H labelled disparlure permits the study of binding orientations with *Ldis*PBP1 and *Ldis*PBP2 by ^{17}O or ^{2}H NMR (Nuclear Magnetic Resonance) spectroscopy. Both isotopes, with quadrupolar nucleus, are suitable for NMR studies, particularly as oxygen-17 shows a wide chemical shift range (~ 2000 ppm). The oxygen-18 isotope is not directly detectable by NMR but does induce isotopic shifts in carbon-13 NMR spectra that can be used analytically (Risley and Van Etten, 1989). The oxygen-18 and hydrogen-2 isotopes can be used as isotopic markers for mass spectroscopic studies (Ye et al., 2009). A convenient synthetic route to oxygen-17 or 18 and hydrogen-2 labelled disparlure has been discussed in this chapter, involving Mitsunobu inversion of secondary alcohol group of chlorohydrin with oxygen-17 or 18 benzoic acid and hydrogenation of alkyne with D_2

We performed experiments in which we studied the binding of ^{17}O & ^{2}H (+)-disparlure (**15b**) to PBP1 and of ^{18}O & ^{2}H labelled disparlure enantiomers (**15c** and *ent*-**15c**) (Figure 3.2) to both *Ldis*PBPs. With the latter, two types of analysis were done on the data: 1) chemical shift changes between disparlure in buffer *vs*. bound to *Ldis*PBP were correlated with the location of the deuterium labels in PBP-ligand structures obtained through docking simulations, and 2) the measurement of longitudinal relaxation (T_1) and

transverse relaxation (T_2) times. Docking simulations of both enantiomers were done with homology models of *Ldis*PBP1 and PBP2, at one internal and two external binding sites. These were used to interpret the position of disparlure ligands relative to aromatic residues in the protein and the level of mobility of the labeled positions of disparlure under various conditions (in organic solvent, in buffer and bound to the PBPs). We then correlated the simulations with the observed NMR parameters. We detected differences between the enantiomers of disparlure interacting with the two proteins. This is discussed in the context of differences detected in other assays.

3.3. Results and discussion

3.3.1. Synthesis and characterization of isotope (^{17}O or ^{18}O &^{2}H) labelled (+)-disparlure (15b or 15c).

Our aim was to prepare isotopically labeled derivatives of disparlure with specific focus on the incorporation of oxygen-17 or 18 into the epoxy ring, as well as hydrogen-2 at C-5 and C-6 positions. The synthetic routes for the convenient synthesis of these isotopically labelled disparlure were presented, applying Mitsunobu reaction with ^{17}O or ^{18}O labelled benzoic acid for the installment of the ^{17}O or ^{18}O- label and Wilkinson's catalyst ($RhCl(PPh_3)_3$-chlorotris(triphenylphosphine)rhodium(I)) catalyzed deuteration of alkyne for the introduction of ^{2}H-label.

Synthesis of ^{17}O or ^{18}O enriched compounds usually involves water, carbon monoxide and [$^{17/18}O$] enriched starting materials, which are expensive. The most convenient precursor to prepare $^{17/18}O$ enriched compounds is labelled water, which is commercially available with various enrichment levels starting from 10 to 97%. For efficient incorporation of ^{18}O or ^{17}O into benzoic acid, the reaction between benzoyl chloride (**141**) and ^{17}O or ^{18}O water appeared the most promising method. Accordingly, benzoyl chloride (**141**) was converted into ^{17}O or ^{18}O labelled benzoic acid by action of $H_2{}^{17}O$ (20 atom-% ^{17}O) or H_2O^{18} (97 atom-% ^{18}O) (Scheme 3.1). Although gas chromatography (GC) would not resolve the oxygen-16 and oxygen-17 or oxygen-18 containing benzoic acid the mass spectra showed that the ^{17}O and ^{18}O benzoic acid consisted of about 20% $^{17}O_2$ and 97% of $^{18}O_2$ label, respectively (Scheme 3.1).

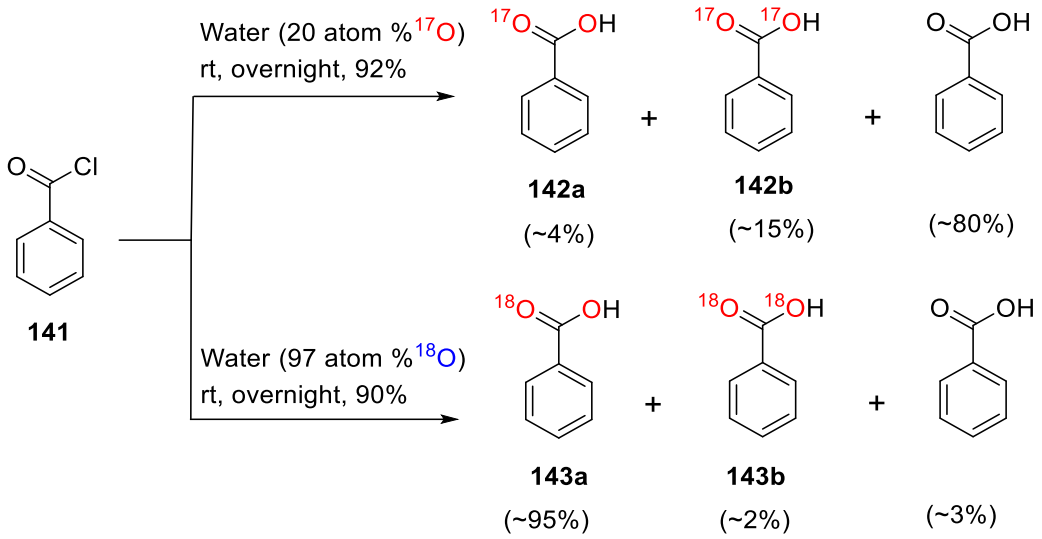

Scheme 3.1 Synthesis of ^{17}O and ^{18}O labelled benzoic acid.

The infra-red (IR) spectra of the ^{17}O and ^{18}O enriched and normal benzoic acid (obtained from the reaction between benzoyl chloride and tap water) are compared (Figure 3.3) as solutions in chloroform. The Figure 3.3 shows that the IR spectra of oxygen enriched, and the normal benzoic acids are not identical. There are minor differences in the frequencies of carbonyl (C=O) and C-O bands. The carbonyl stretching mode at 1680 cm^{-1} was shifted downwards by almost 19 cm^{-1} for ^{18}O labelled benzoic acid and 7cm^{-1} for ^{17}O labelled benzoic acid. The C-O stretching frequency at 1288 cm^{-1} was shifted to 1273 cm^{-1} for ^{18}O benzoic acid whereas the smallest frequency shift 1 cm^{-1} observed for ^{17}O benzoic acid (Figure 3.3).

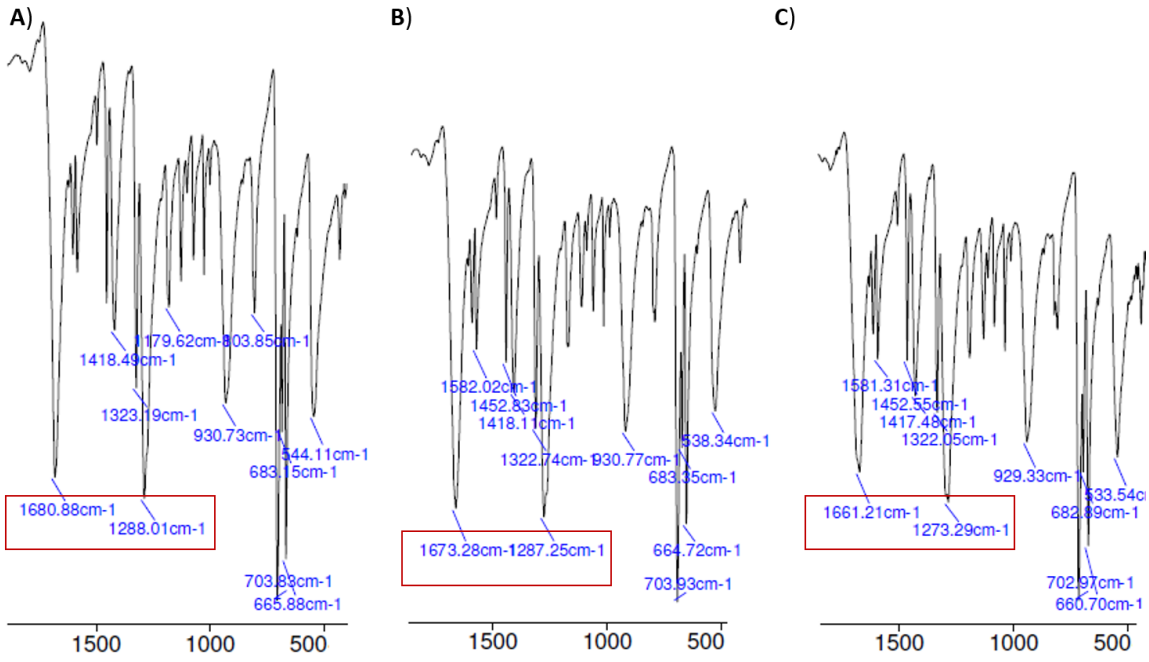

Figure 3.3 **The infra-red spectrum in solution of A) normal benzoic acid B)^{17}O enriched benzoic acid C) ^{18}O benzoic acid.**

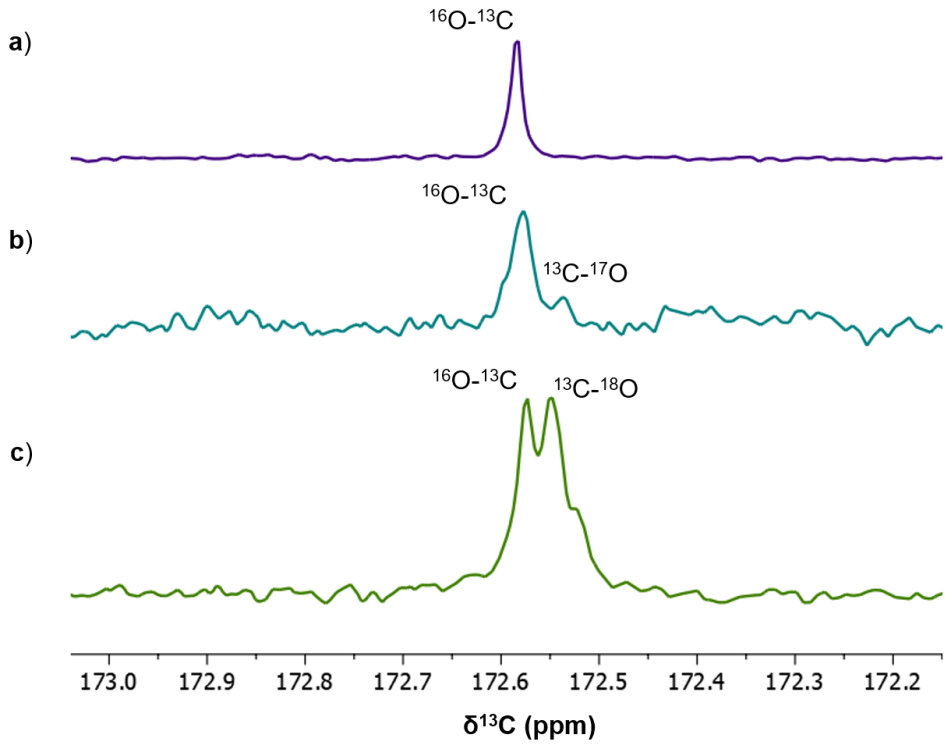

Figure 3.4 **The region of ^{13}C NMR spectra (125 MHz, $CDCl_3$) corresponding to the carboxy carbon of a) natural benzoic acid b) ^{17}O labelled benzoic acid c) ^{18}O labelled benzoic acid. The ^{13}C NMR signals of the carboxy carbon are shifted upfield by ~ 0.030 ppm upon ^{17}O or ^{18}O substitution.**

Comparison of ^{13}C NMR spectra of oxygen isotope ($^{17}O_2$ & $^{18}O_2$) enriched and natural benzoic acid showed that the oxygen isotope induced chemical shift of the carboxyl carbon in benzoic acid (Figure 3.4). The magnitude of oxygen-isotope induced shift agrees with the isotope shifts reported previously for carboxylic acids (Risley and Van Etten, 1980; 1981). In case of carboxylate ion, the carboxyl carbon signal of $^{18}O_2$ enriched sodium formate was moved upfield 0.025ppm. ^{13}C NMR signal of benzoic acid was shifted upfield a significant great amount, 0.031ppm. The upfield shift showed by the ^{17}O benzoic acid is ~ 0.031ppm relative to the resonance position of the unlabeled benzoic acid. These valves are same within experimental error. This upfield shift allowed us to determine oxygen isotopic enrichment in benzoic acid. On the NMR time scale, the 2 oxygen atoms of the benzoic acid are equivalent. Therefore, substitution by two equivalent isotopic oxygen atoms result in a shift of the carboxyl carbon ^{13}C NMR signal upfield by identical amounts upon each isotopic substitution.

The synthetic method used for the incorporation of ^{17}O or ^{18}O isotopes into disparlure was dictated by the availability of $^{17}O_2$ or $^{18}O_2$ labelled benzoic acid. The method finally adopted was based on that described in the Chapter 2 (Schemes 2.10 & 2.11) for the preparation of 1,2-*syn* chloroester. The outline of this method is as follows: enantiopure α-chloroaldehyde **113** was converted to 1,2-*anti* chlorohydrin **128**, which was treated with ^{17}O labelled benzoic acid or ^{18}O labelled benzoic acid in the presence of TPP (triphenyl phosphine) and DIAD (diisopropyl azodicarboxylate).to form $^{17}O_2$ or $^{18}O_2$ labelled 1,2-*anti* chloroester **144** or **145** (Scheme 3.2).

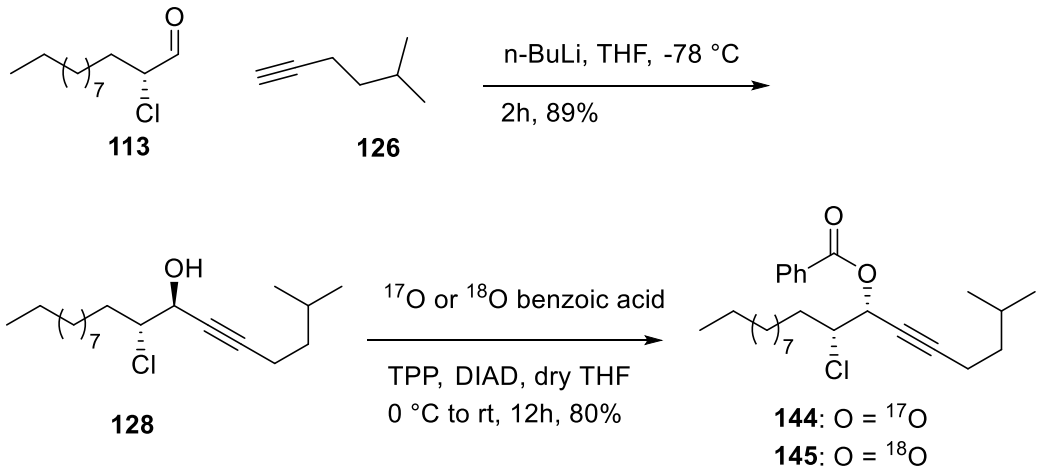

Scheme 3.2 Insertion of ^{17}O or ^{18}O isotope via Mitsunobu inversion.

The oxygen isotope labelled intermediates **144** and **145** were obtained as liquids. This reaction gave isolated yield of 80%. Following column purification, the isotopic enrichment of the intermediates **144** and **145** was determined by ^{13}C NMR spectroscopy. The incorporation of ^{17}O or ^{18}O caused a readily detectable isotopic shift of the carbon-7 (C-O) and carboxy carbon (-C=O) ^{13}C resonance (Figure 3.5). ^{17}O and ^{18}O enrichment was calculated by the relative peak areas for the ^{13}C-signal of the ^{16}O- and ^{17}O- or ^{18}O-isotopomers. The ^{17}O and ^{18}O enriched intermediates **144** and **145** contained approximately 50% ^{18}O and 8-10% ^{17}O at either one of the benzoate oxygens (Figure 3.5).

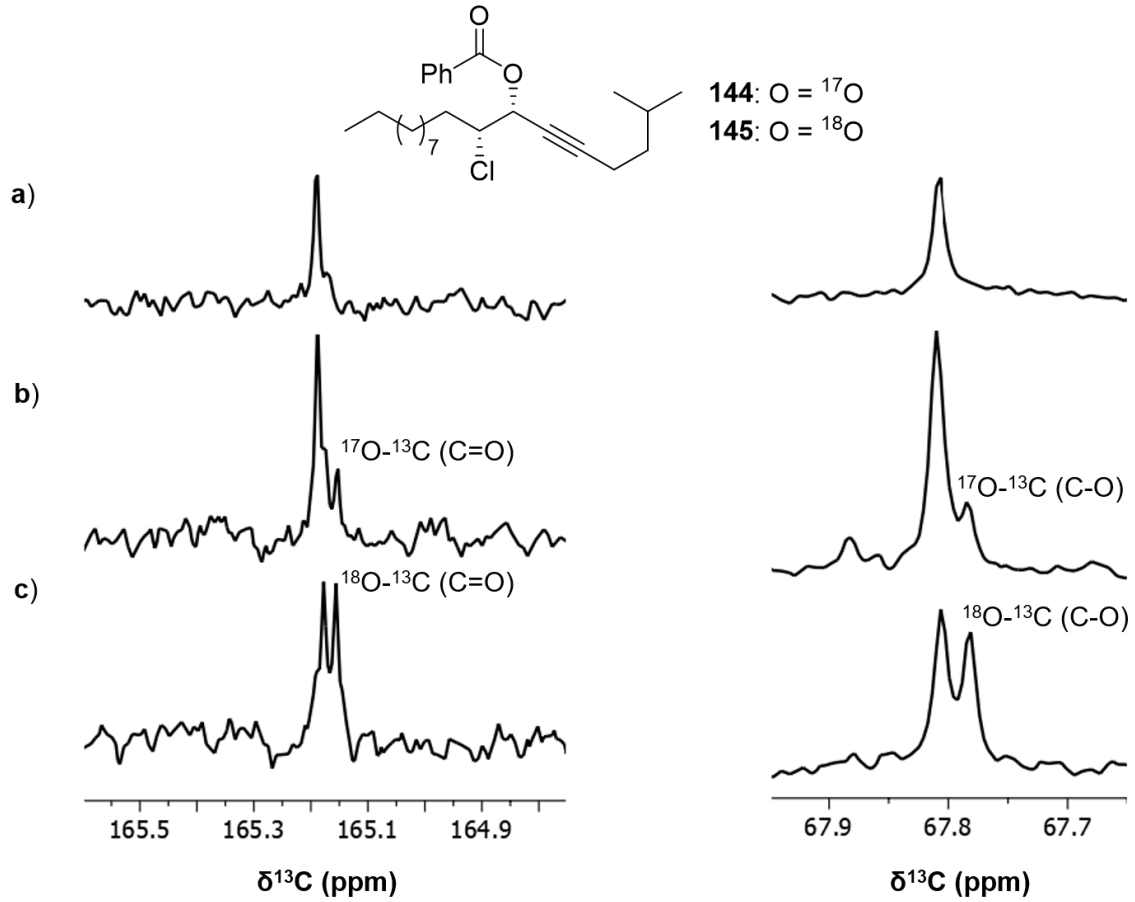

Figure 3.5 **^{13}C NMR signal of the carboxyl carbon (-C=O) and C-O carbon of the ^{17}O or ^{18}O labelled syn chloroesters 144 or 145 was shifted upfield 0.030 ppm with respect to the unlabelled (^{16}O) compound. a) unlabelled b) ^{17}O labelled and c) ^{18}O labelled compounds.**

The synthesis of ^{17}O or ^{18}O and ^{2}H labelled (+)-disparlure **15b** or **15c** was carried out as shown in Scheme 3.3. Deuteration of oxygen isotope labelled 1,2-*anti* chloroesters **144** or **145** with deuterium gas (D_2) in the presence of Wilkinson's catalyst ($RhCl(PPh_3)_3$) afforded isotope labelled compounds **146** or **147**. Use of the Wilkinson's catalyst avoided the occurrence of deuterium scrambling (Figure 3.6). Once the alkyne functionality was deuterated, basic hydrolysis of the ester group of compounds **146** or **147** with 4N NaOH using methanol as solvent afforded ^{17}O & ^{2}H (+)-disparlure **15b** or ^{18}O & ^{2}H (+)-disparlure **15c** (Scheme 3.3).

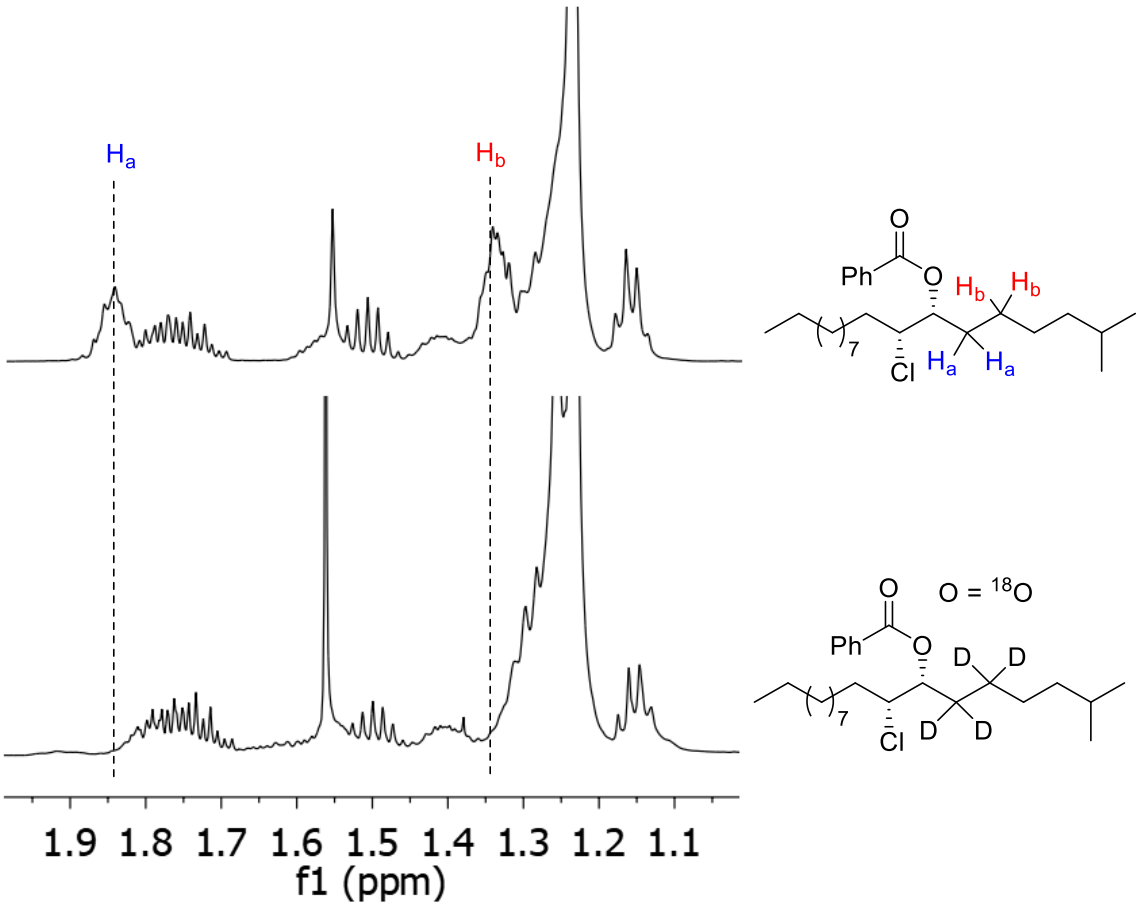

Figure 3.6 **^{1}H NMR spectra of non-labelled compound 131 (top) and deuterated compound 147 (bottom) with H_a and H_b signal assignement.**

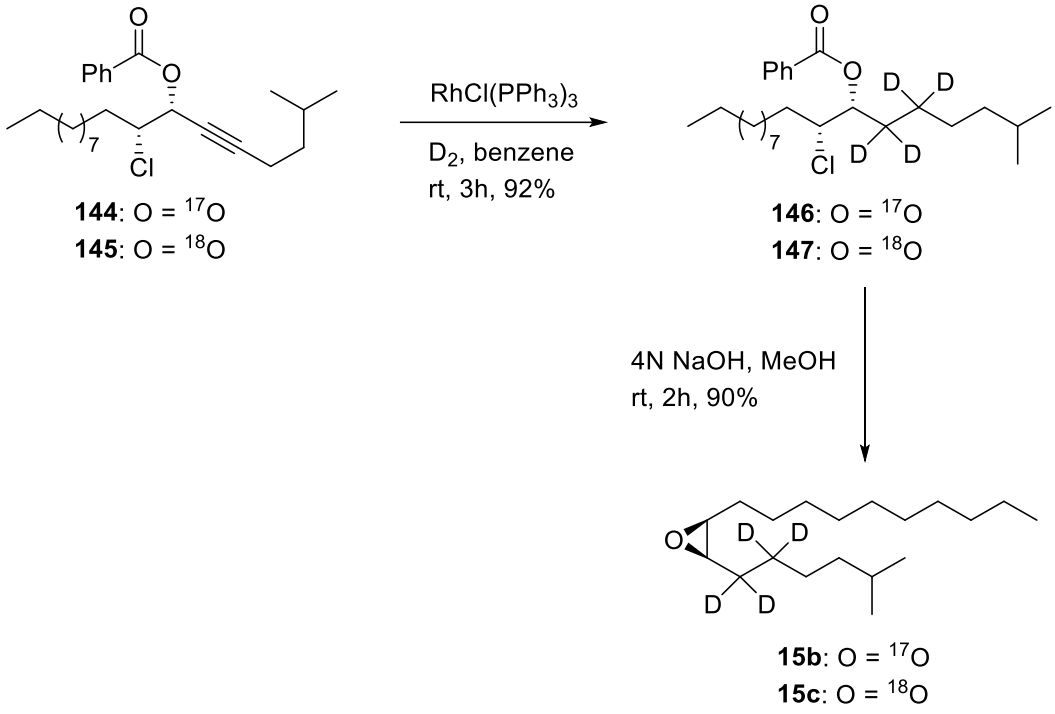

Scheme 3.3 Synthesis of isotope (^{17}O or ^{18}O & ^{2}H) labelled (+)-disparlure.

3.3.2. Synthesis of isotope labelled (^{17}O or ^{18}O & ^{2}H) (-)-disparlure (*ent*-15b or *ent*-15c)

For the synthesis of ^{17}O or ^{18}O deuterated (-)-disparlure *ent*-**15b** or *ent*-**15c** (Figure 3.2), the Mitsunobu reaction between 1,2-*anti*-chlorohydrin *ent*-**128** (Scheme 3.4) and ^{17}O or ^{18}O labelled benzoic acid followed by reduction of triple bond with D_2 were performed first giving the ^{17}O or ^{18}O and deuterium labelled intermediates *ent*-**146** or *ent*-**147**. The isotope labelled (-)-disparlure *ent*-**15b** or *ent*-**15c** were obtained after basic hydrolysis of the ester group in intermediates *ent*-**146** or *ent*-**147**.

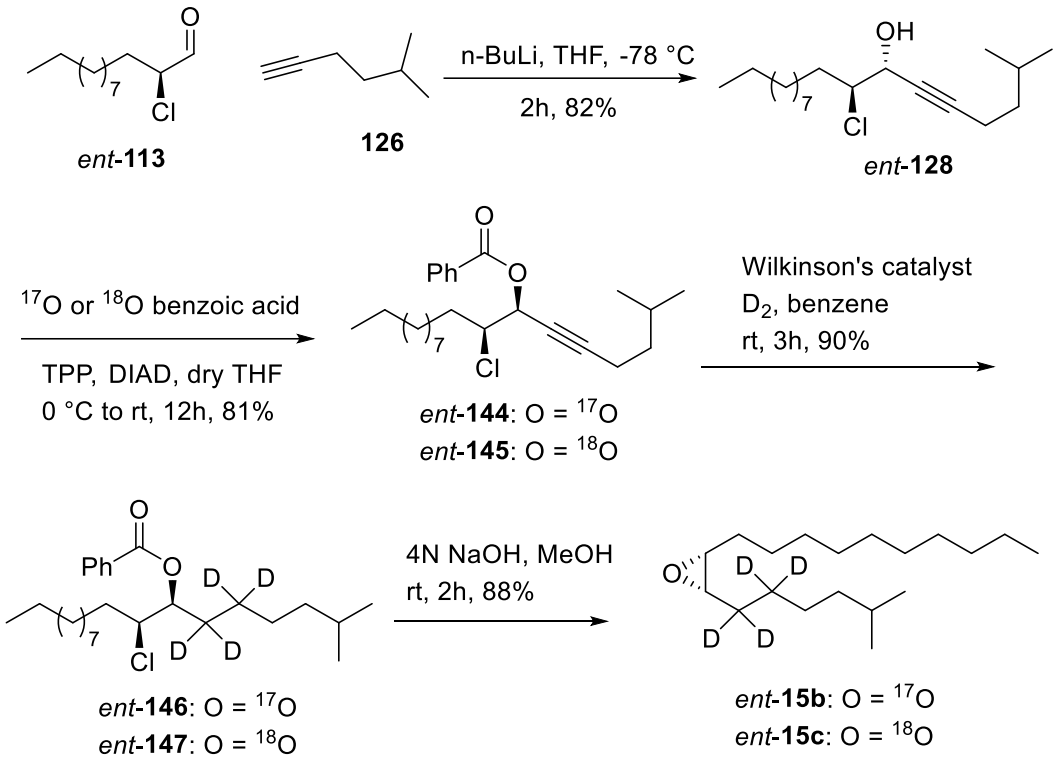

Scheme 3.4 Synthetic route to ^{17}O or ^{18}O & ^{2}H labelled (-)-disparlure.

The percentages of ^{17}O or ^{18}O at the epoxide oxygen of the **15b**, **15c**, *ent*-**15b** and *ent*-**15c** were calculated from the area of the shifted carbon signal in their ^{13}C NMR spectra and from HR-MS (Figure 3.7, Table 3.1). The ^{17}O NMR spectrum was obtained for the ^{17}O labelled (+)-disparlure. In ^{18}O labelled (+)-disparlure, the signals for the oxirane ring carbon atoms were seen upfield from those of the non-labelled variant due to the isotope effect on the chemical shift.

Table 3.1 Oxygen and hydrogen isotope enrichment of (+)-and (-)-disparlure (15 and *ent*-15)

		Isotope enrichment (%)		
Entry	**Compound**	**^{17}O**	**^{18}O**	**^{2}H (C-5 & C-6)**
1	(+)-disparlure (**15**)	8-10		>99
2	(+)-disparlure (**15**)		~50	>99
3	(-)-disparlure (*ent*-**15**)	8-10		>99
4	(-)-disparlure (*ent*-**15**)		~50	>99

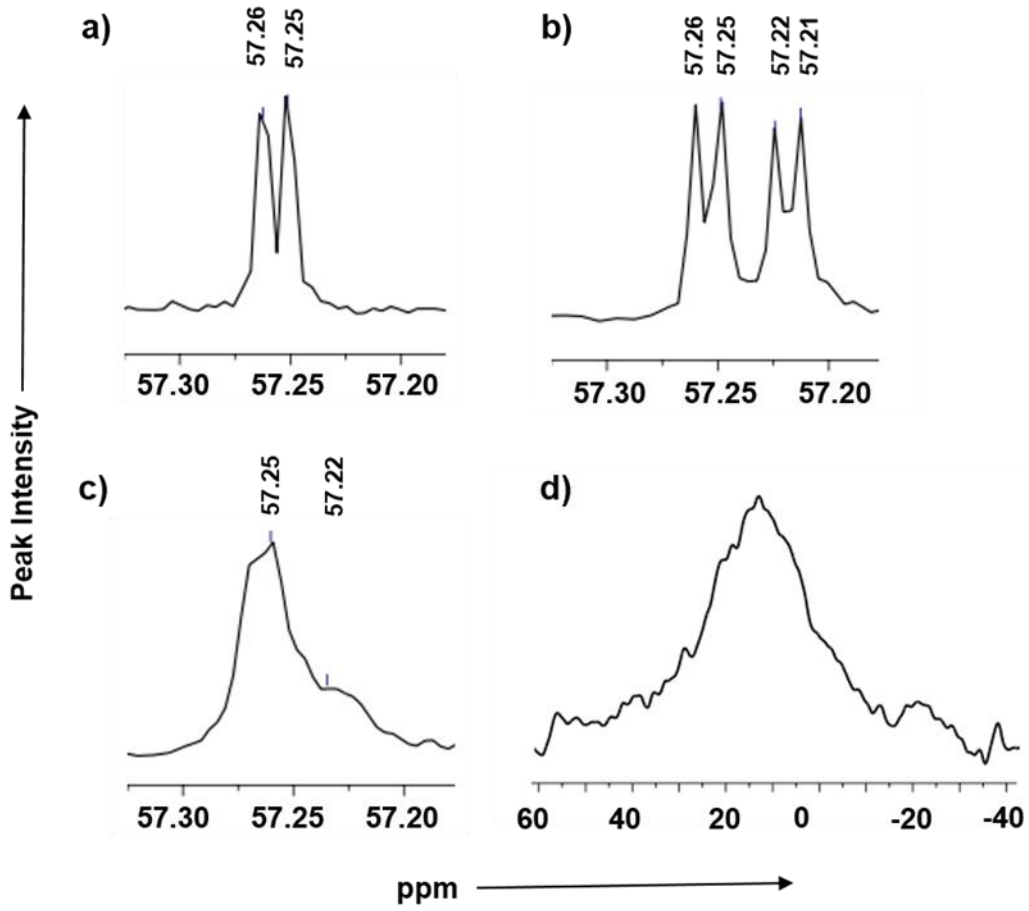

Figure 3.7 **^{13}C NMR signals of epoxy carbons of a) (+)-disparlure, b) ^{18}O (+)-disparlure c) ^{17}O (+)-disparlure, and d) ^{17}O NMRspectrum of ^{17}O (+)-disparlure in $CDCl_3$**

3.3.3. Heteronuclear NMR studies of disparlure binding to *Ldis*PBPs

The binding of disparlure enantiomers to pheromone binding proteins of male gypsy moth was studied by NMR spectroscopy. First, we studied binding of ^{17}O (+)-disparlure **15b** to *Ldis*PBP1, as well as ^{17}O (+)-disparlure **15b** by itself in $CDCl_3$ (Figure 3.7) and in buffer. The ^{17}O signal was broad, as expected, in $CDCl_3$, but completely disappeared when disparlure was placed in buffer with fatty acid salts as emulsifier and a

bridging solvent (acetonitrile). We chose to use fatty acid micelles to disperse disparlure in the aqueous buffer, because previous studies from our laboratory have shown that gypsy moth sensilla contain high quantities of fatty acids in the lymph (Nardella et al., 2015). The result suggests that disparlure mobility would have decreased significantly in the fatty acid micelles and, therefore, the ^{17}O signal is so broad that it cannot be detected.

Because ^{17}O was difficult to detect, we decided to use ^{2}H labelled disparlure enantiomers **15c** and *ent*-**15c** (Scheme 3.3 and 3.4) in our binding studies. We used 92 MHz deuterium NMR to observe binding-induced chemical shift change of the deuterium signals of the deuterated disparlure enantiomers. The ^{2}H chemical shift of the deuterium labelled disparlure enantiomers **15c** or *ent*-**15c** resonance in the presence and absence of *Ldis*PBPs was monitored. It was possible to distinguish the more shielded 5-D signals from the 6-D signals (Figure 3.8). We have named these signals 5-D_a, 5-D_b, 6-D_a and 6-D_b. In a solvent ($CDCl_3$, toluene or phosphate buffer) the majority of disparlure molecules will adopt a conformation around the epoxide at or near the global energy minimum.(Yu and Plettner, 2013). In that conformation, **15c** has the 5-*pro*-R H atom in the shielding zone above the epoxide ring and the 5-*pro*-S H atom in the deshielding zone at the edge of the epoxide ring, along the C-O bond (Tori et al., 1966). In our data, 5-D_a is more shielded than 5-D_b (Table 3.2), so 5-D_a must correspond to the *pro*-R D atom and 5-D_b must be the *pro*-S. For *ent*-**15c**, the 5-*pro*-S H atom is in the epoxide shielding zone (above the oxirane ring) and the 5-*pro*-R H is in the deshielding zone at the global minimum (Yu and Plettner, 2013). Therefore, for this compound, 5-D_a must correspond to the *pro*-S D, whereas 5-D_b must correspond to the *pro*-R D. Using the same approach, we assign the deuterium atoms at the 6 position as 6-D_a = 6-D_S and 6-D_b = 6-D_R for **15c**, and 6-D_a = 6-D_R and 6-D_b = 6-D_S *ent*-**15c**. In the chiral protein binding pockets this assignment can change, because there are numerous anisotropic effects (from aromatic side chains and carbonyl groups), apart from the anisotropic effect of the oxirane ring (see below).

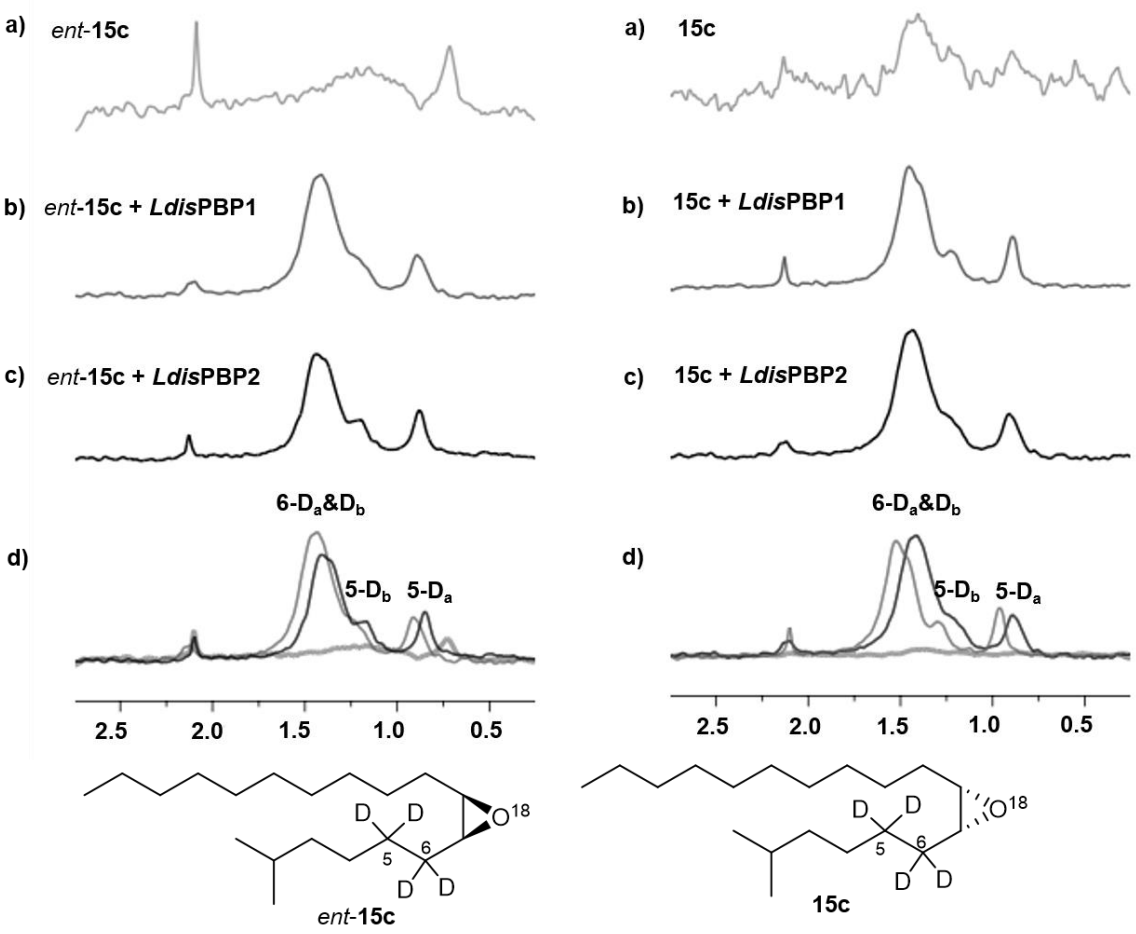

Figure 3.8 **The 92 MHz ^{2}H NMR spectra recorded for deuterium labelled disparlure enantiomers with and without *Ldis*PBPs in phosphate buffer at pH 8. The chemical shift scales of the above spectra are aligned on the basis of the deuterium resonance (2.10 ppm) of internal standard CH_3CN. a) The region of the ^{2}H NMR spectra of deuterium labelled disparlure enantiomers and acetonitrile resonances are shown in the absence of *Ldis*PBPs, b) & c) downfield shifting of the deuterium signals of the disparlure enantiomers by *Ldis*PBP1 and *Ldis*PBP2, respectively. d) superimposed spectra of a), b) and c). The same buffer (50 mM sodium phosphate pH 8.0) was used for all these spectra.**

The ^{2}H NMR spectrum of the compounds **15c** and *ent*-**15c** in buffer, in the absence of *Ldis*PBPs showed two peaks, but these were not well resolved due to poor solubility of the compounds in the phosphate buffer solution (Figure 3.8). The most shielded 5-D signal was sharper than the 6-D and the second 5-D signals. One explanation is that disparlure forms micelles in the aqueous environment and the mobility of the 6-position is more restricted than that of the 5-position. Furthermore, the hydrophobic disparlure molecule

adsorbs on glass surfaces (Nardella et al., 2015), and the adsorbed molecules will have very restricted mobility and, therefore, broad signals. Addition of *Ldis*PBPs causes an increase in solubility of the **15c** and *ent*-**15c** in the phosphate buffer solution (Plettner et al., 2000; Nardella et al., 2015) and deuterium resonances to shift downfield (Figure 3.8, Table 3.2, 3.3 and 3.4). The ^{2}H chemical shift changes of the bound **15c** and *ent*-**15c** noticed were typically of the order of 0.07 to 0.29 ppm (Table 3.4). The deuterium signals of **15c** were more deshielded than signals of *ent*-**15c** by *Ldis*PBP1 and *Ldis*PBP2. The apparent bound chemical shift difference of the compounds **15c** and *ent*-**15c** deuterium signals shows that the binding (and therefore local variations in the magnetic field) of disparlure enantiomers to *Ldis*PBP1 is different from binding to *Ldis*PBP2.

Table 3.2 The ^{2}H chemical shifts of 5,6-D_4 15c and *ent*-15c in the presence and absence of *Ldis*PBPs

Compound	Position signal & assignment [a]	δ $CDCl_3$	δ Toluene	δ Phosphate buffer (pH 8)	δ Phosphate buffer (pH 8) + *Ldis*PBP1 [b]	δ Phosphate buffer (pH 8) + *Ldis*PBP2 [b]
15c	5-D_a (*pro*-R)	0.8	0.94	0.73	0.96 (*pro*-R)	0.89 (*pro*-S)
	5-D_b (*pro*-S)	1.07	1.26	0.98	1.3 (*pro*-S)	1.17 (*pro*-R)
	6-D_a (*pro*-S)	1.25	1.46	1.16	1.45 (*pro*-S)	1.41 (*pro*-S)
	6-D_b (*pro*-R)	1.34	1.56	1.38	1.52 (*pro*-R)	1.45 (*pro*-R)
ent-**15c**	5-D_a (*pro*-S)	0.8	0.94	0.73	0.91 (*pro*-R)	0.85 (*pro*-R)
	5-D_b (*pro*-R)	1.07	1.26	0.98	1.21 (*pro*-S)	1.17 (*pro*-S)
	6-D_a (*pro*-R)	1.25	1.46	1.16	1.43 (*pro*-R)	1.37 (*pro*-S)
	6-D_b (*pro*-S)	1.34	1.56	1.38	1.49 (*pro*-S)	1.41 (*pro*-R)

[a] Assignments of the 5 and 6 deuterium atom signals for disparlure in solvent, based on the global energy minimum around the epoxide found in ab initio calculations in (Yu and Plettner, 2013)and the anisotropic effect of the oxirane ring (Tori et al., 1966). [b] Chemical shifts and assignment, based on averaged protein-bound conformations of the disparlure enantiomers, chemical shift differences between protein-bound and solvent (Table 3.3) and anisotropic effects of the oxirane and the proteins (see Figure 3.8).

Table 3.3 Chemical shift differences, relative to the CD_3CN signal, used as an internal standard and net shifts of 15c and *ent*-15c in buffer and PBP-bound

Condition	δ δ (CD_3CN-5-D_a) ppm	δ δ (CD_3CN-5-D_b) ppm	δ δ (CD_3CN-6-D_a) ppm	δ δ (CD_3CN-6-D_b) ppm
$CDCl_3$	1.3	1.03	0.85	0.76
Toluene	1.16	0.84	0.64	0.54
Phosphate buffer	1.37	1.12	0.94	0.72
***Ldis*PBP1 + 15c**	1.14	0.85	0.65	0.58
***Ldis*PBP2 +-15c**	1.21	0.93	0.69	0.65
***Ldis*PBP1 + *ent*-15c**	1.19	0.89	0.67	0.61
***Ldis*PBP2 + *ent*-15c**	1.25	0.93	0.73	0.69

Table 3.4 Net shifts of 15c and *ent*-15c in buffer and PBP bound

Condition	δ δ (*Ldis*PBP1-buffer), ppm				δ δ (*Ldis*PBP2-buffer), ppm			
	5-D_a	5-D_b	6-D_a	6-D_b	5-D_a	5-D_b	6-D_a	6-D_b
***Ldis*PBP + Buffer + 15c**	0.23	0.32	0.29	0.14	0.16	0.19	0.25	0.10
***Ldis*PBP + Buffer + *ent*-15c**	0.18	0.20	0.27	0.11	0.12	0.19	0.21	0.07

Both *Ldis*PBPs have one internal binding site and multiple external binding sites (Yu and Plettner, 2013) which interact with a ligand in a stepwise manner, fast external binding, followed by slow internalization (Gong et al., 2009). The apparent equilibrium constant for the external sites, K_d', is the ratio of the dissociation and association rate constants, k_{off}/k_{on}, for the first external binding step (Figure 3.9). From (Gong et al., 2009) we had data for PBP2, but for PBP1 we lacked data because this protein interacts with ligands much faster than PBP2 (Gong et al., 2010) Therefore, we used stopped-flow experiments to obtain k_{off} and k_{on} for PBP1 and the disparlure enantiomers from competitive kinetics between a fluorescent reporter ligand (1-phenylnaphthylamine, NPN) and **15** or *ent*-**15**. This information was required to process the *in silico* ligand docking data (see Section 3.4). For the measurement of association, NPN bound to PBP is displaced with disparlure (which causes NPN fluorescence to decrease). For measurement of disparlure dissociation, disparlure bound to PBP is displaced with NPN (which causes NPN fluorescence to increase. Both measurements can be done simultaneously in

experiments wherein NPN and disparlure compete for the binding sites on the protein (Figure 3.9).

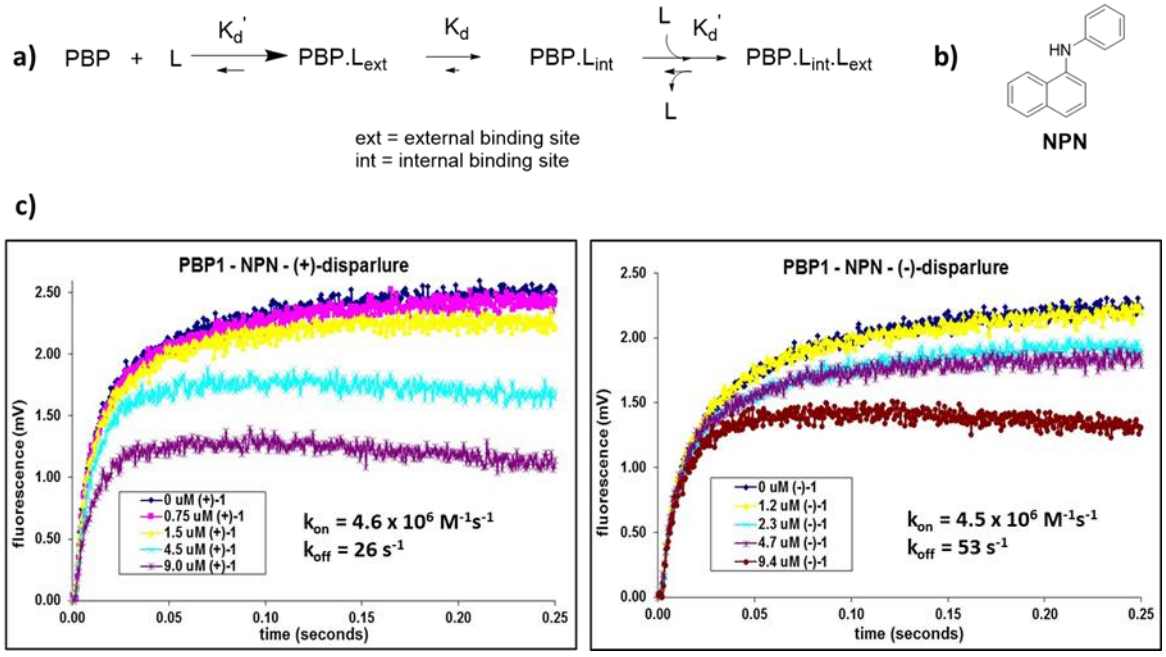

Figure 3.9 **Association and dissociation kinetics of PBPs and cognate ligands. a) Kinetic scheme for ligand-PBP interaction. The ligand first binds externally in a rapid, reversible manner, and then slowly diffuses into the internal binding site of the PBP. b) Structure of NPN, the competitive fluorescent reporter ligand used in PBP1-ligand association kinetics experiments in a stopped-flow apparatus. c) Stopped-flow kinetics with fluorescence reporting of PBP1 with either 15 or *ent*-15 and NPN. Both association (k_{on}) and dissociation (k_{off}) rate constants can be obtained from non-linear fitting of the traces at different concentrations of ligand and constant concentration of NPN reporter.**

3.4. *In-silico* docking simulations of disparlure into homology models of LdisPBPs

To understand the chemical shift changes observed, we performed *in-silico* docking simulations of **15** and *ent*-**15** into homology models of PBP1 and PBP2. We docked both ligands into the internal binding site (site 1) and the two largest external sites (sites 2 and 3). The two external sites were assumed to contribute randomly (*i.e*. equally). Structures that were calculated to be populated > 5% were examined with regard to the interactions of the focal hydrogen atoms, at the 5 and 6 positions of disparlure, with the

protein. Anisotropic effects from aromatic side chains and carbonyl groups within a range of 4.5 Å around the focal H atoms were scored (Experimental section 3.7.6), along with the anisotropic effect from the oxirane ring. Scores were weighted according to their proportion at the docking site, and internal vs. external sites were weighted according to their proportion (Table 3.5). The patterns obtained for the *pro*-R and *pro*-S hydrogen atoms at each position allowed us to assign signals in the PBP-ligand treatments.

Table 3.5 Dissociation constants used in the calculation of ligand distribution between internally, externally bound and free states. Distributions between states obtained for each PBP with both disparlure enantiomers.

Protein	Ligand	K_d [µM][a]	K_d' [µM][b]	Ref K_d	% bound Internal[c]	% bound External[d]	% free
PBP1	15	6.8	56.5	This work	48.9	43.8	7.3
	ent-15	6.0	11.8	This work	49.0	49.1	1.9
PBP2	15	2.2	..1.1	(Gong et al., 2009)	49.6	50.2	0.2
	ent-15	4.7	..1.6	(Gong et al., 2009)	49.2	50.5	0.3

[a] From Terrado et al (2017). [b] Calculated as k_{off}/k_{on}, the ratio of association and dissociation rate constants. [c] $[PBP]_{total}$ = 300 µm; $[L]_{total}$ = 600 µm. [d] Since there are two external binding sites, their combined concentration is 600 µm.

As shown in Figure 3.10, the assignments for D_a and D_b were reversed in some cases of PBP-bound disparlure enantiomers, relative to those at the global minima. Specifically, for (-)-disparlure (*ent*-**15**) bound to PBP1, 5-D_a is *pro*-R and 5-D_b is *pro*-S. For (+)-disparlure (**15)** bound to PBP2, 5D_a is *pro*-S and 5-D_b is *pro*-R. Finally, for *ent*-**15** bound to PBP2, 5-D_a = *pro*-R, 5-D_b = *pro*-S, 6-D_a = *pro*-S and 6-D_b = *pro*-R. There are two factors which influence the chemical shifts of the 5 and 6 protons of disparlure when bound to the PBPs: 1) the conformation of the pheromone and 2) the shielding and deshielding effects of nearby groups on the protein, particularly carbonyl or phenyl groups. For example, Figure 3.11 shows the most populated pose at the internal binding site for the four cases studied here. The disparlure enantiomers are clearly not bound at a minimum conformation calculated in (Yu and Plettner, 2013). For the PBP1 and *ent*-**15** case, one can see that 5-H_R is in the weak shielding zone near the oxirane, and 5-H_S is in the deshielding zone around the oxirane C-O bond, the reverse of the arrangement in the global minimum. Also, 5-H_S is in the deshielding zones of Phe 119 and Trp 37, which reinforce the oxirane deshielding effect.

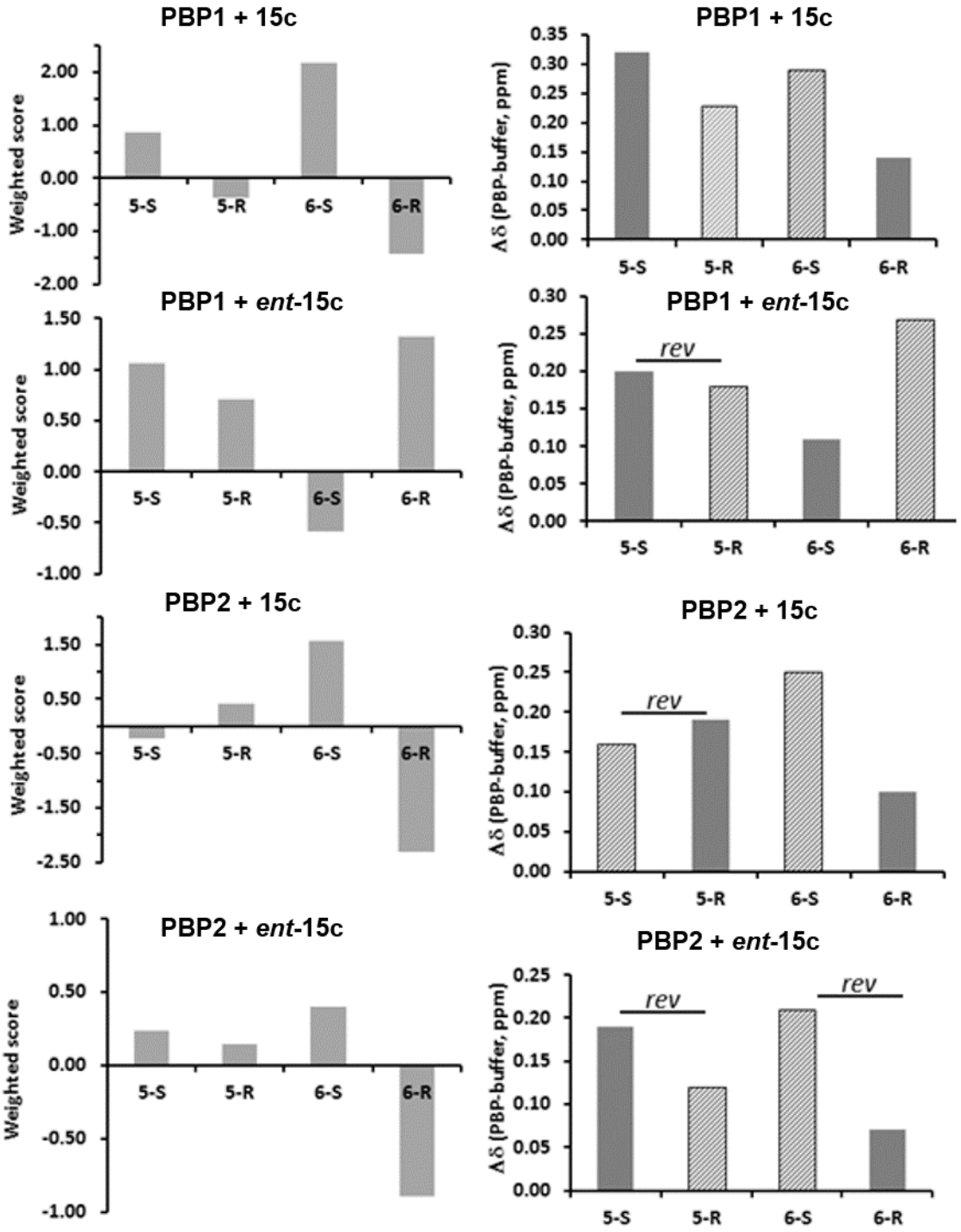
PBP1 + 15c
Weighted score
2.00
1.00
0.00
-1.00
-2.00
5-S
5-R
6-S
6-R
PBP1 + 15c
Δδ (PBP-buffer, ppm)
0.35
0.30
0.25
0.20
0.15
0.10
0.05
0.00
5-S
5-R
6-S
6-R
PBP1 + ent-15c
Weighted score
1.50
1.00
0.50
0.00
-0.50
-1.00
5-S
5-R
6-S
6-R
PBP1 + ent-15c
Δδ (PBP-buffer, ppm)
0.30
0.25
0.20
0.15
0.10
0.05
0.00
rev
5-S
5-R
6-S
6-R
PBP2 + 15c
Weighted score
1.50
0.50
-0.50
-1.50
-2.50
5-S
5-R
6-S
6-R
PBP2 + 15c
Δδ (PBP-buffer, ppm)
0.30
0.25
0.20
0.15
0.10
0.05
0.00
rev
5-S
5-R
6-S
6-R
PBP2 + ent-15c
Weighted score
1.00
0.50
0.00
-0.50
-1.00
5-S
5-R
6-S
6-R
PBP2 + ent-15c
Δδ (PBP-buffer, ppm)
0.25
0.20
0.15
0.10
0.05
0.00
rev
rev
5-S
5-R
6-S
6-R

Figure 3.10 **Left: weighted scores for shielding (< 0) or deshielding (> 0) effects, from docking simulations, weighted for distribution of poses at the internal and the two external sites and weighted for the distribution of the ligand between external and internal sites as shown in Table 3.5. Right: chemical shift differences (∆δ) between disparlure bound to PBP and disparlure in buffer. The hatched bars correspond to the signal labelled D_a and the dark gray bars correspond to the signal labelled D_b. Bars labelled "rev" exhibited a reversed assignment of prochirality for the D_a and D_b signals, relative to the assignment in an isotropic medium (Table 3.2).**

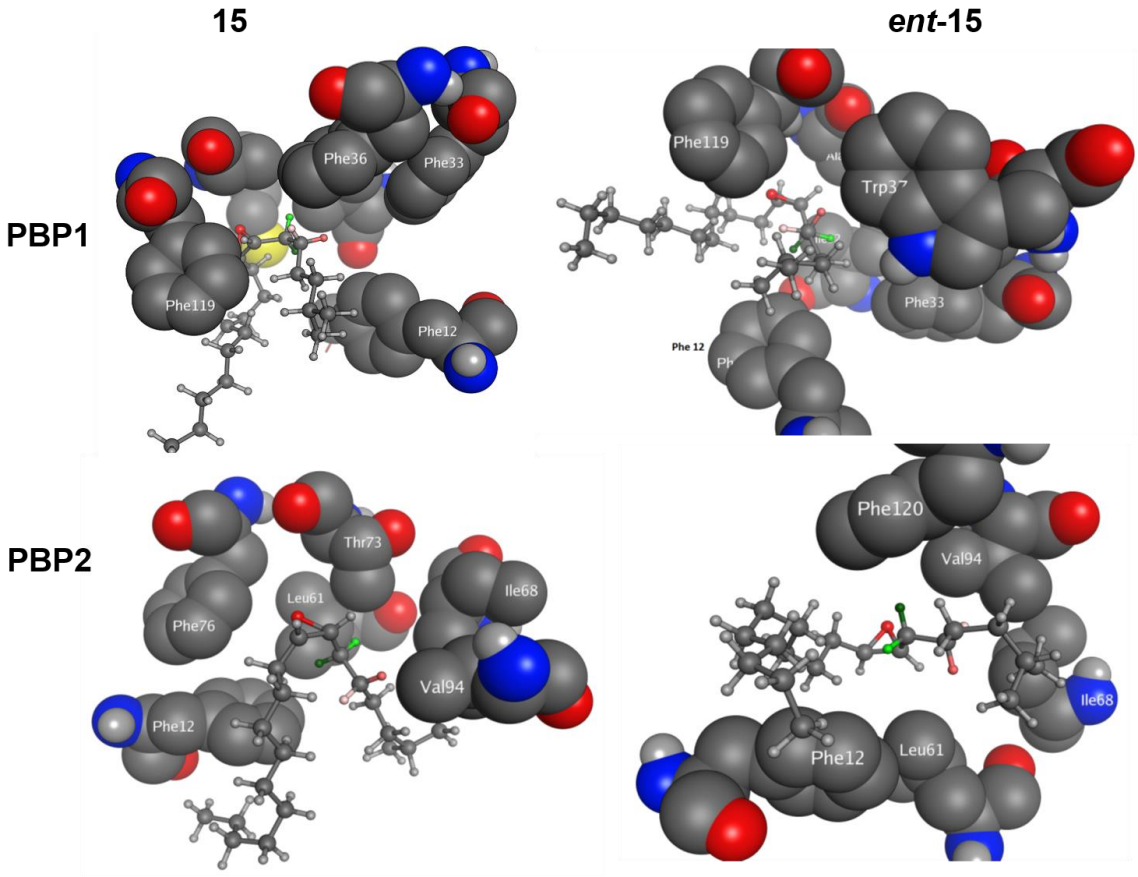

Figure 3.11 **Interactions at the internal binding site of the most populated pose for each combination of protein and ligand. Top row: PBP1, bottom row: PBP2. The disparlure chain is shown in ball-and-stick format, with the epoxide colored red, 6-H_S = light green, 6-H_R = dark green, 5-H_S light pink, 5-H_R = dark pink. Residues that have a part interacting with any of the focal hydrogen atoms within a 4.5 Å radius are shown in space-filling format, without their hydrogen atoms.**

We also determined the spin-lattice relaxation time, T_1, and the transverse relaxation time T_2 for the two 5-D signals and the combined 6-D signals (Figure 3.12), to better understand how the hydrogen atoms at the 5 and 6 positions of the disparlure enantiomers interact locally with the two binding proteins. T_1 reflects the longitudinal relaxation of the magnetic field in the z direction to its equilibrium value. This process is influenced by the local fluctuations in the magnetic field around the nucleus being observed. The frequencies of these fluctuations depend on the local density of the medium around the nucleus: the greater the density and viscosity (i.e. the lower the mobility), the larger T_1 (Cantor et al., 1980). The transverse relaxation process reflects the decay of the phasing of nuclei in the xy plane. It depends on the fluctuations in the local magnetic field and on spin exchange between neighboring nuclei of opposite spin. In the gas phase, the local fluctuations average and $2T_1 \cong T_2$. At increasing viscosity in a condensed phase, the local magnetic fluctuations do not average, spin exchange occurs and T_2 decreases (Cantor et al., 1980). Thus, the two relaxation times give insight into the mobility around the focal nucleus. In our molecular models, we checked the number of interactions between the focal hydrogen atoms and groups either on the protein or the twisted chain of disparlure. All interactions within a 4 Å radius were counted, and an estimate of the local mobility was obtained as the inverse of that number of interactions. This was done for each retained pose at each of the three sites, and mobility was averaged for each site and across sites, as described in the experimental. The inverse of the averaged mobility is a measure of the local viscosity: the more interactions, the lower the mobility and the higher the local viscosity.

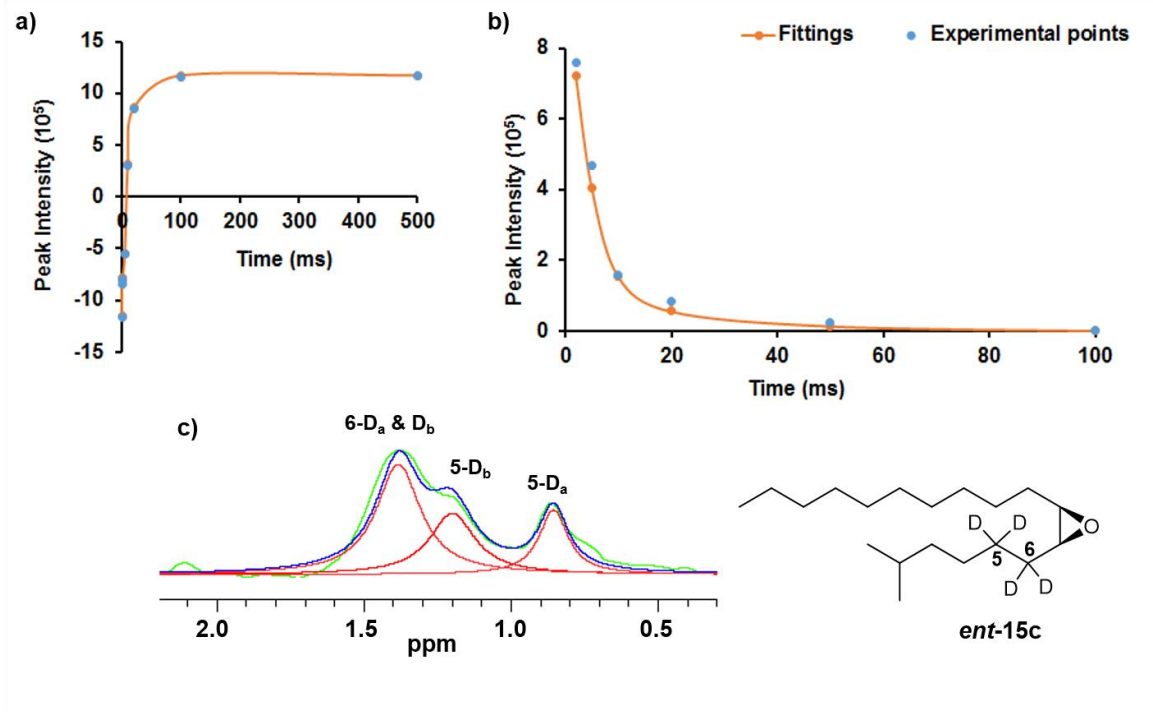

Figure 3.12 **Determination of relaxation times T_1 and T_2. a) Example of a T_1 determination for 5-D_a of *ent*-15c with *Ldis* PBP1 (phosphate buffer, pH 8) by following the re-establishment of the magnetization after a 90° pulse (see Appendix B7 for traces) b) Example of a T_2 determination for 5D_a of *ent*-15c with *Ldis* PBP1 (phosphate buffer, pH 8) by following the decay of the signal intensity after a 180° pulse. c) Example of signal deconvolution for 5-D_a, 5-D_b and 6-$D_{a/b}$.**

3.5. Determination of relaxation times (T_1 & T_2) for deuterium atoms of bound disparlure

Figure 3.12 shows an example of T_1 and T_2 determination for 5-D_a of (-)-disparlure *ent*-**15c** in the presence of *Ldis*PBP1 (phosphate buffer, pH 8). The T_1 values for the four combinations of PBP and disparlure enantiomers are shown in Figure 3.13 and Table 3.6. Because $CDCl_3$ and buffer are non-chiral, isotropic media, we only performed the measurements with one of the two enantiomers, *ent*-**15c**. It is interesting to note that both solvent systems gave the same T_1 values within limits of error. In buffer, the signals were much weaker than in $CDCl_3$ or in the protein-bound cases (Figure 3.8), because in buffer disparlure has a strong tendency to adsorb on the walls of the vial. Signal from adsorbed disparlure is not detectable, since its mobility is completely restricted and T_1 is very long, T_2 is very short, both outside of the range of this experiment. Thus, in buffer, we detected only the disparlure that was dissolved in the aqueous phase.

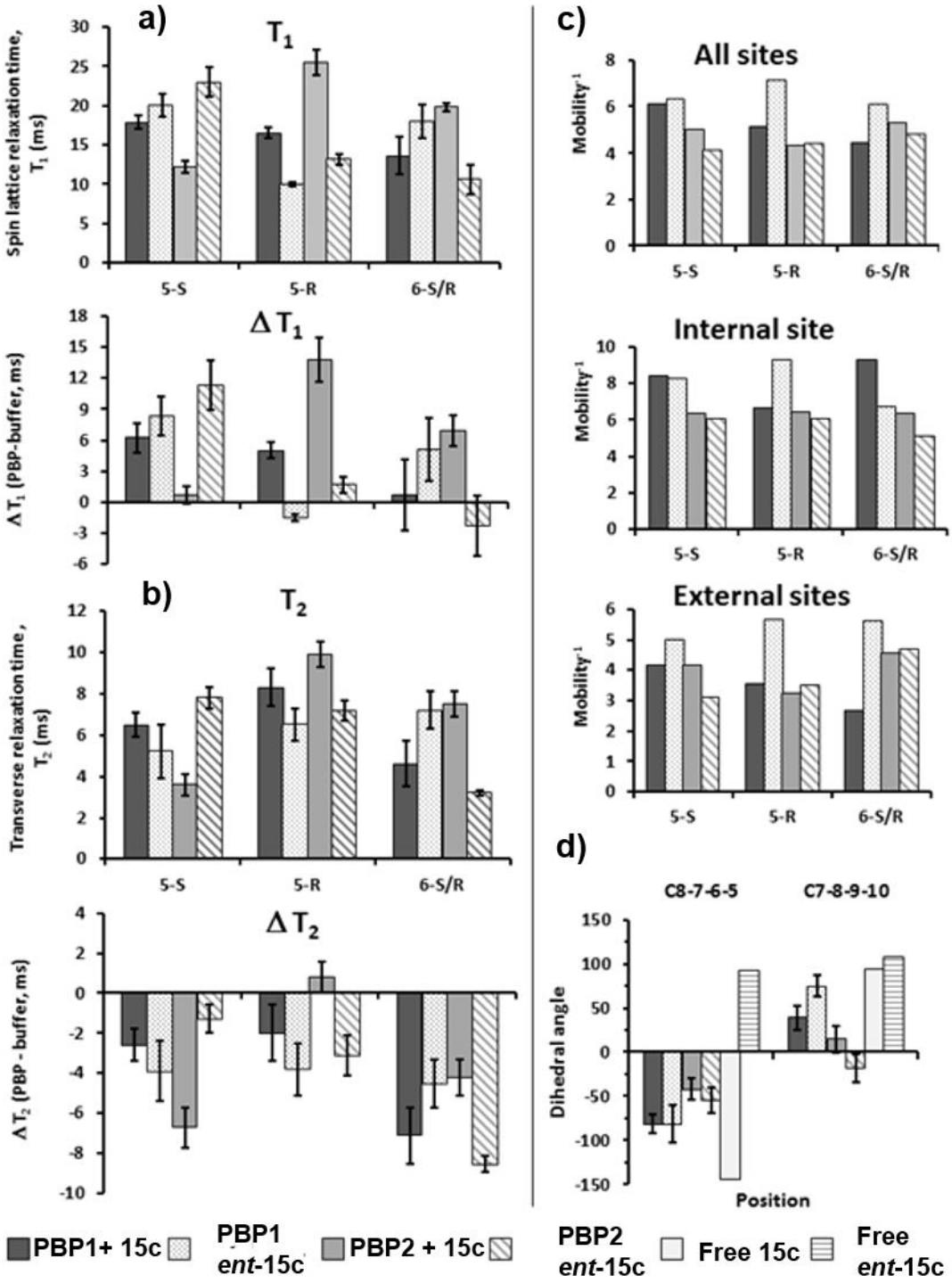
a)
T_1
Spin lattice relaxation time, T_1 (ms)
5-S
5-R
6-S/R
ΔT_1
ΔT_1 (PBP-buffer, ms)
b)
T_2
Transverse relaxation time, T_2 (ms)
ΔT_2
ΔT_2 (PBP - buffer, ms)
c)
All sites
Internal site
External sites
Mobility^{-1}
d)
C8-7-6-5
C7-8-9-10
Dihedral angle
Position
PBP1+ 15c
PBP1 *ent*-15c
PBP2 + 15c
PBP2 *ent*-15c
Free 15c
Free *ent*-15c

Figure 3.13 **Left: spin relaxation data from ^{2}H NMR experiments with PBP1 and PBP2 with 15c or *ent*-15c bound. Right: measurements obtained from docking simulations of the ligands into one internal and two external sites on PBP1 and PBP2. Dark gray = PBP1 and 15c, stippled = PBP1 and *ent*-15c, medium gray = PBP2 and 15c, hatched = PBP2 and *ent*-15c. a) Top: Spin lattice relaxation time,T_1, in ms. Bars represent the average value from fitting of decay data, and the error bars denote the fitting error. Bottom: difference in T_1 between PBP-bound ligand and the ligand in buffer. Error bars are the sum of both errors. b) Top: transverse relaxation time,T_2, in ms. Bars represent the average value from fitting of decay data, and the error bars denote the fitting error. Bottom: difference in T_2 between PBP-bound ligand and the ligand in buffer. Error bars are the sum of both errors. c) Inverse mobility (which is approximately the average number of interactions and is proportional to the local viscosity) detected at all three sites (weighted for population of the sites – see text), at the internal site and at the two external sites (average of both sites). d) Average dihedral angles around C8–7–6–5 and C7–8–9–10, i.e. around the epoxide moiety. For the PBP-bound disparlure enantiomers the color scheme is the same as for the other graphs. Bars represent the weighted averages of all dihedral angles of retained poses, weighted by pose at each site and by site distribution (see text). Error bars represent the S. D. The light gray bars represent the dihedral angles at the global minimum for 15c and the horizontally striped bars represent the dihedral angles at the global minimum for *ent*-15c as calculated in (Y. Yu & Plettner, 2013).**

Table 3.6 **Spin-lattice relaxation (T_1) of 5,6-D_4 15c and *ent*-15c in $CDCl_3$, buffer and PBP-bound**

Condition	5-D_a		5-D_b		6-D_a & 6-D_b	
	15c	*ent*-15c	15c	*ent*-15c	15c	*ent*-15c
$CDCl_3$		13.6 ± 2.6		12.7± 0.7		11.6 ± 1.5
Phosphate buffer		11.5 ± 0.1		11.7 ± 0.5		12.9 ± 1.0
Buffer+ *Ldis*PBP1	16.5 ± 0.7	10.0 ± 0.2	17.9 ± 0.9	20.05 ± 1.42	13.6 ± 2.4	18.0 ± 2.1
Buffer+ *Ldis*PBP2	12.2 ± 0.7	13.2 ± 0.7	25.5 ± 1.6	23.0 ± 1.9	19.8 ± 0.5	10.6 ± 1.9

Comparing T_1 values obtained for PBP-bound disparlure enantiomers, and the value obtained for the free disparlure in solvent (Figure 3.13a) we see that, in general, there was an increase in T_1 upon binding of disparlure to the PBPs. This suggests that, generally, the mobility of the focal hydrogen atoms decreased upon binding to the protein. However, the signal intensity increased relative to buffer (Figure 3.8), and this is because

PBPs help to desorb pheromones from solid surfaces, thus brining the hydrophobic pheromone into solution (Plettner et al., 2000; Nardella et al., 2015). Exceptions to the general increase in T_1 upon protein binding were: 5-H_S in PBP2 with **15c**, 6-$H_{S/R}$ in PBP1 with **15c** and 6-$H_{S/R}$ in PBP2 with *ent*-**15c**, all of which did not differ from the T_1 value seen in buffer. Thus, for these exceptional cases the local viscosity around the focal hydrogen atom in the protein-bound ligand was the same as that of free ligand.

The site-averaged inverted mobility patterns obtained from modelling (Figure 3.13c) parallel the patterns seen for T_1 with the exception of 5-H_S in PBP2 with *ent*-**15c**, 5-H_R in both PBP1 with *ent*-**15c** and PBP2 with **15c**. For 5-H_S in PBP2 with *ent*-**15c** the inverted mobility (local viscosity) was lower than reflected in the T_1. Interaction at the internal binding site between 5-H_S and the two methyl groups of the side chain of Val 94 (both within van der Waals radius) contributes to restriction in the mobility of 5-H_S much more than is estimated by simple counting of interactions. Similarly, for 5-H_R in PBP2 with **15c**, the methyl groups of Val 94 or of Leu 52 clamp around that hydrogen atom in the three most populated poses at the internal binding site.

Additionally, methyl groups or Ile 68 and Thr 73 also surround that hydrogen atom in those internal poses. Conversely, 5-H_R of PBP1 with *ent*-**15c** only has weak interactions with Phe 36 and Phe 119 on the protein and intramolecular interactions with 7-H, 3-H_S and 2-H. Counting these interactions overestimates their contribution to the relative local viscosity.

Comparing T_2 values obtained for PBP-bound disparlure enantiomers, and the value obtained for the free disparlure in solvent (Figure 3.13b, Table 3.7) we see that, in general, there was a decrease in T_2 upon binding of disparlure to the PBPs. This suggests that, generally, the mobility of the focal hydrogen atoms decreased upon binding to the protein, consistent with the conclusion from T_1 data. The only case in which T_2 in the protein-bound disparlure and the solvent did not differ was 5-H_R in PBP2 with **15c**. This is interesting, because we know from T_1 and the modelling that 5-H_R in this case is very strongly restricted in its mobility at the internal binding site, so T_2 should be short and not detected. From kinetic data we know that, for PBP2, once disparlure is bound internally it dissociates only very slowly (with a rate constant of $4.7 \pm 0.4 \times 10^{-4}$ s^{-1}) (Gong et al., 2009), too slow for T_2 to be detectable in the current experiment. At the external sites in this case, interactions with 5-H_R in PBP2 with **15c** are weak, and anisotropic effects cancel

each other, so fluctuations in the magnetic field would be averaged as they would in a solvent.

Table 3.7 Spin-Spin (transverse) relaxation (T_2) of 5,6-D_4 15c and *ent*-15c in the presence and absence of *Ldis*PBPs

Condition	5-D_a		5-D_b		6-D_a & 6-D_b	
	15c	*ent*-**15c**	**15c**	*ent*-**15c**	**15c**	*ent*-**15c**
$CDCl_3$		12.0 ± 0.1		11.4 ± 0.6		10.2 ± 0.1
Phosphate buffer		10.3 ± 0.5		9.1 ± 0.2		11.7 ± 0.3
Buffer+ *Ldis*PBP1	8.3 ± 0.9	6.5 ± 0.8	6.5 ± 0.6	5.2 ± 1.3	4.6 ± 1.1	7.2 ± 0.9
Buffer+ *Ldis*PBP2	3.6 ± 0.5	7.2 ± 0.5	9.9 ± 0.6	7.8 ± 0.5	7.5 ± 0.6	3.2 ± 0.1

Another interesting case is 6-$H_{S/R}$ in PBP1 with **15c**, in which T_2 decreased significantly relative to solvent but T_1 was no different than in solvent. This pattern can be explained by a high number of interactions with 6-$H_{S/R}$ at the internal binding site. PBP1 associates with and dissociates from ligand much faster than PBP2, so that internal binding contributions would be detectable in the pattern of T_2. PBP1 binds **15c** more weakly than *ent*-**15c**, at internal (Plettner et al., 2000; Terrado et al., 2017) and external (this study) binding sites. Thus, for PBP1 and the two enantiomers, the T_2 pattern is likely dominated by contributions from internal binding, and the inverted mobility pattern (or local viscosity) (Figure 3.13c) perfectly explains the T_2 pattern: more viscosity (lower T_2) for **15c** and lower local viscosity (higher T_2) for *ent*-**15c**.

Finally, the case of 6-$H_{S/R}$ in PBP2 with *ent*-**15c** is also interesting. The T_1 for this case did not change significantly from solvent (Figure 3.13a), but T_2 significantly decreased upon protein binding (Figure 3.13b). In external site 2 of PBP2, the Lys 2 ε-NH_3^+ is H-bonded to the epoxide of *ent*-**15c** and the δ-CH_2 of Lys 2 packs near 6-H_S in the model. Both 6-H_S and 6-H_R pack with the β-CH_2 of Asp 132. These interactions could restrict mobility of the 6-$H_{S/R}$ of *ent*-**15c**, such that the T_2 value detected is shorter than the one detected with **15c**, which does not interact in that way with site 2 of PBP2.

PBP1 only had a significant difference in T_1 between bound enantiomers of disparlure at 5-H_R, whereas PBP2 showed enantiomer differences at 5-H_S, 5-H_R and 6-$H_{S/R}$ (Figure 3.13a). For T_2, PBP1 showed significant differences between enantiomers for

5-H_R and 6-$H_{S/R}$, and PBP2 again showed significant differences between enantiomers for all three signals (Figure 3.13b). This is consistent with the body of previous studies on PBP1 and PBP2 interactions with the enantiomers of disparlure. PBP1 interacts more weakly overall but with greater differences in equilibrium dissociation constants than PBP2 (Plettner et al., 2000; Yu and Plettner, 2013; Sanes and Plettner, 2016; Terrado et al., 2017) and PBP1 associates with and dissociates from disparlure enantiomers faster and more selectively than PBP2 (Gong et al., 2009; 2010). The slower kinetic regime followed by PBP2 is consistent with the greater number of significant differences between enantiomers in T_1 and T_2 detected here. PBP1 binds (-)-disparlure (*ent*-**15**) more strongly at equilibrium than (+)-disparlure (**15**), and PBP2 is the opposite (Plettner et al., 2000; Yu and Plettner, 2013; Terrado et al., 2017).

3.6. Conclusion

The binding interactions between *Ldis*PBP1 and *Ldis*PBP2 and disparlure enantiomers were studied by ^{2}H NMR using deuterated disparlure enantiomers. Changes in chemical shifts in free vs. bound disparlure, spin-lattice relaxation (T_1) and spin-spin relaxation (T_2) times of deuterium atoms of deuterated (+)-disparlure or (-)-disparlure showed that the binding of (+)-disparlure and (-)-disparlure to *Ldis*PBP1 differs from binding to *Ldis*PBP2. Furthermore, the results from NMR studies were correlated with the results from docking simulations of (+)-disparlure (**15**) and (-)-disparlure (*ent*-**15**) bound to one internal site and multiple external sites of *Ldis*PBP1 and *Ldis*PBP2. We showed that (+)-disparlure (**15**) and (-)-disparlure (*ent*-**15**) adopt different conformations and orientations in the binding pockets of *Ldis*PBP1 and *Ldis*PBP2. The chemical shift, T_1 and T_2 data, along with the models, demonstrate that the PBPs discriminate the disparlure enantiomers not only by binding differently to the epoxide moiety, but also by interacting with subtle differences at positions 5 and 6, which were identified in 1977 as important general odotopes of disparlure in an electrophysiology structure-activity study with racemic disparlure analogs (Schneider et al., 1977).

This is the first report on a study of interactions between isotope labelled disparlure enantiomers and *Ldis*PBPs of gypsy moth by using ^{2}H NMR spectroscopy. The present study confirms that the 5 and 6 positions on the hydrophobic short side chain of the disparlure enantiomers play an important role in recognition of the disparlure enantiomers in the binding site of the *Ldis*PBPs.

3.7. Experimental section

3.7.1. General

Chemicals and reagents were obtained from Sigma-Aldrich (St. Louis, MO, USA) and used without further purification. Isotopically enriched water was sourced from ICON stable isotopes (Old Kings Highway, Mt. Marion, NY, USA). Isotopic enrichments were 20 atom % for $H_2{}^{17}O$ and 99% for $H_2{}^{18}O$. Deuterium gas (99 atom %) was purchased from Sigma-Aldrich (St. Louis, MO, USA). All preparations with isotopically labelled compounds were first carried out with non-labelled compounds and products were confirmed by spectroscopy. The NMR (^1H, ^2H, ^{13}C and ^{17}O) spectra were obtained on Bruker DRX 400 and 500 MHz spectrometers in $CDCl_3$. Chemical shifts and coupling constants are reported in parts per million (ppm) and hertz (Hz) respectively. ^1H NMR data was reported as follows: chemical shift values (ppm), multiplicity (s = singlet, d = doublet, t = triplet, q = quartet, m = multiplet). Isotopically labelled products were characterized by ^{13}C NMR using a Bruker DRX 500 spectrometer at 125 MHz in order to confirm the isotopic enrichment. IR spectra were obtained with a Perkin-Elmer Spectrum One FT-IR spectrometer and samples were directly placed on the KBr plates. High-resolution mass spectra (HRMS) were obtained by using positive electrospray ionization and by TOF method. The GC-MS analysis was performed on GC-MS (Varian CP-3800 GC, interfaced with a Varian Saturn 2000 MS) using a SPB-5 fused silica capillary column (30 m × 0.25 mm i.d., film thickness 0.25 µm, Supelco, Bellefonte, PA, USA) with positive electron ionization (EI). The GC-MS analysis was performed on GC-MS (Varian CP-3800) using a SPB-5 fused silica capillary column (30 m × 0.25 mm i.d., film thickness 0.25 µm, Supelco, Bellefonte. PA, USA) with positive electron ionization (EI). Samples were diluted in n-hexanes and injected with a 1:10 split ratio. The injector temperature was programmed to 250 °C. The oven temperature was held at 80 °C for 50 sec and raised to 200 °C at 14 °C/min which was held for 15 min. Then finally 2 °C/ min to 260 °C which was held for 5 min. The MS conditions were: Solvent - delay time 6 min and scanned mass range (m/z) 50-500.

3.7.2. Sample preparation for ^2H NMR studies

The stock solutions of poorly water soluble deuterated disparlure enantiomers were prepared by dissolving the pheromone in acetonitrile. Phosphate buffer (50 mM) of pH 8 was prepared by using mono and dibasic sodium phosphate. The protein (*Ldis*PBPs)

solutions (0.3 mM) were incubated with deuterium labelled disparlure enantiomers (0.6 mM) in ice cold water for 3 h. The *Ldis*PBPs (*Ldis*PBP1 and *Ldis*PBP2) were expressed and purified according to the protocol described by Plettner *et al* (Plettner et al., 2000). The protein-ligand interaction process was monitored through acquisition of ^{2}H NMR spectra. The ^{2}H NMR relaxation spectra of the deuterated disparlure enantiomers/*Ldis*PBPs system were obtained using a Bruker-600 NMR spectrometer equipped with QCI probe. The T_1 (relaxation) times were measured by using with the standard inversion-recovery pulse sequence (180°- τ - 90°) (Vold et al., 1968) The T_2 (transverse relaxation) times were measured using with Carr-Purcell-Meiboom-Gill pulse sequence (90° (τ-180°-τ) n) (Meiboom and Gill, 1958). The delay times in between 180°C were used as 0.42ms. T_1 and T_2 relaxation curves were fitted to the equation 1 and 2 respectively.

$$M_z(t) = M_z(0)\ (1\text{-}\exp\ (-t/T_1) \qquad \text{(Eq.1)}$$

$$M_{xy}(t) = M_{xy}(0)\ (\exp\ (-t/T_2) \qquad \text{(Eq.2)}$$

3.7.3. Stopped flow kinetics

Kinetics experiments were performed in a Chirascan stopped-flow instrument (Applied Photophysics Ltd, UK). For the competition kinetics, N-phenyl-1-naphthylamine (1-NPN) was used as the fluorescent reporter. First, the association and dissociation rate constants of 1-NPN were determined by association and the values were used as constraints for calculating the k_{on} and k_{off} of the ligands. In the competitive assay, one reservoir was filled with the PBP1 solution (0.50 µM PBP1 in 20 mM Tris/HCl buffer pH 8.0 with 180 mM KCl, 25 mM NaCl, and 0.1% ethanol) while the second reservoir contained the solution of NPN (0.50 µM) mixed with various concentrations of **15** or *ent*-**15** in the same buffer. The NPN was added from a 0.50 mM NPN in methanol stock. Six microliters of **15** or *ent*-**15** was added from stock solutions in ethanol (0.20 mM to 1.6 mM). The stopped-flow instrument mixed the solutions in 1:1 volume ratio from the two reservoirs. The final concentrations of the participating components were the following: (1) PBP1 0.25 µM, (2) NPN 0.25 µM, and (3) **15** or *ent*-**15** 0 to 9.4 µM. NPN fluorescence was observed using 337 nm excitation and the emission detected using long pass filter disc with 395 nm cut-off. The experiment was performed at constant temperature, 22 °C. The

fluorescent traces were fitted using kinetics of competitive binding model in GraphPad Prism 5 (GraphPad Software Inc., California).

3.7.4. Homology models of *Ldis*PBP1 and *Ldis*PBP2

The gypsy moth PBP1 and PBP2 share 61.7 % and 48.9 % similarity with Bombyx mori PBPs respectively (Figure 3.1). The homology models of *Ldis*PBP1 and *Ldis*PBP2 were created based on the crystal structures of Bombyx mori PBP (PDB ID: 1LS8.1. A) by using SWISS MODEL (expasy.org) (Merritt et al., 1998; Biasini et al., 2014). The models were corrected for lacking hydrogen atoms, using the “Protonate 3D” function at pH 8 and with 0.10 M salt concentration. Using the MMFF94X force field, protonate 3D function assigns the location of hydrogen atoms and ionization states in the protein structure. After protonation, energy minimization was applied to the protein structures.

3.7.5. Molecular docking simulations

The homology models were docked with disparlure enantiomers by using an induced fit protocol. Docking stimulations were performed with the MMFF94X force field of Molecular Operating Environment (MOE) using default parameters (Refinement: Force field, Placement: Triangle Matcher). Two scoring functions (Rescoring 1: London dG and Rescoring 2: GBVI/WSA dG) were used for this docking protocol. The ligand binding sites of protein were detected in MOE by using geometric algorithm based on Edelsbrunner’s Alpha Shapes called Site Finder in MOE.

3.7.6. Evaluation of molecular docking simulation data

The simulations were programmed such that the fit of the ligand into the binding site was induced and up to 30 poses of the ligand were retained. We obtained between 18 and 30 poses, which were evaluated for the total potential energy. Using the assumption that all the poses can equilibrate with the pose of lowest energy, a distribution of poses was calculated for each case.

Next, all poses that were found to be populated above 5% were examined with regard to molecular interactions with the epoxide and the 5_S, 5_R, 6_S and 6_R hydrogen atoms. To perform this inspection, binding pocket residues and functional groups within a

4.5 Å of the focal atoms were selected. Distances of nearby hydrogen atoms to the 5 and 6 H atoms were measured, both on the protein and on disparlure itself. We also checked whether the focal hydrogen atoms are within the shielding or deshielding zones of nearby phenyl or indole systems of phenylalanine or tryptophan residues or of carbonyl groups (in the backbone or aspartate, glutamate, asparagine, or glutamine side chains). We also assessed every focal hydrogen atom with regard to its position relative to the oxirane ring's shielding and deshielding zones (Kleinpeter et al., 2015) The interactions found were tabulated and scored according to the following scale: 0 = neither shielding nor deshielding; -1 = weak shielding; 1 = weak deshielding; -2 moderate shielding; 2 = moderate deshielding; -3 = strong shielding; 3 = strong deshielding. This assessment was performed for each enantiomer in each relevant retained pose (populated > 5%). Weighted averages were calculated for each enantiomer at each site.

Finally, a global weighting was done for internal and external sites, taking into consideration that the ligand can partition between external sites and the internal one, according to previous kinetic binding experiments (Gong et al., 2009), and overall equilibrium binding constants determined recently at pH 8.0 (Terrado et al., 2017) The overall binding constants determined at equilibrium were taken to reflect the affinity of the proteins for internally bound ligands. Affinity of the external sites for the ligands was determined here for PBP1, using a fluorescent displacement assay in a stopped-flow apparatus and from our previous study (Gong et al., 2009) for PBP2. Dissociation constants for external binding were estimated as k_{off}/k_{on}, the ratio of the dissociation and association rate constants. Shielding and deshielding contributions from the three sites were weighted according to the percentages shown in Table 3.5.

3.7.7. General procedure for preparation of ^{17}O labelled benzoic acid and ^{18}O labelled benzoic acid

Benzoyl chloride (**141**) (0.41 mL, 0.5 g, 3.557 mmol) was suspended in ^{17}O water (20 atom % ^{17}O) (67.65 µl, 3.557 mmol) or ^{18}O water (98 atom % ^{18}O) (71.2 µl, 3.557 mmol) in 10 mL round bottom flask, and the reaction mixture was stirred for 12 h at room temperature. After stirring, the resulting colourless needles were filtered off and dried *in vacuo* to afford ^{17}O labelled benzoic acids **142a** and **142b** or ^{18}O labelled benzoic acids **143a** and **143b**.

^{17}O labelled benzoic acids (142a&b)

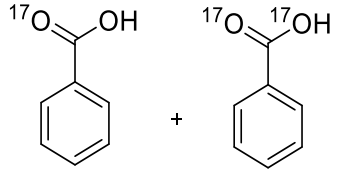

142a **142b**

0.4 g, 91%, colorless solid: ^{1}H NMR (500 MHz, $CDCl_3$) δ 12.21 (bs, 1H), 8.15 (d, *J* = 7.9 Hz, 2H), 7.63 (t, *J* = 7.4 Hz, 1H), 7.49 (t, *J* = 7.7 Hz, 2H).

^{13}C NMR (125 MHz, $CDCl_3$) δ 172.58, 172.55 ($^{13}C_{carboxy\ carbon}$-^{17}O) 134.66, 131.09, 130.14, 129.37.

IR (neat): 2544, 1673, 1417, 1287, 930, 704, 683, 664 cm^{-1}. HRMS (ESI) m/z calculated for $C_7H_7{}^{17}O$ [M-H]: 122.0410; found: 122.0328 and $C_7H_7{}^{17}O_2$ [M-H]: 123.0452; found: 123.0331.

^{18}O labelled benzoic acids (143a&b)

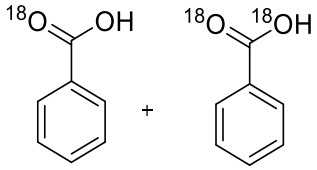

143a **143b**

0.41g, 93%, colourless solid: ^{1}H NMR (500 MHz, $CDCl_3$) δ 8.13 (d, *J* = 7.0 Hz, 1H), 7.62 (t, *J* = 7.4 Hz, 1H), 7.49 (t, *J* = 7.8 Hz, 1H).

^{13}C NMR (125 MHz, $CDCl_3$) δ 172.57, 172.55 ($^{13}C_{carboxy\ carbon}$-^{18}O), 133.87, 130.26, 129.37, 128.53.

IR (neat): 2535, 1660, 1416 1273, 929, 703, 682, 664 cm^{-1}. HRMS (ESI) m/z calculated for $C_7H_7{}^{18}O$ [M-H]: 123.0410; found: 123.0329 and $C_7H_7{}^{18}O_2$ [M-H]: 125.0453; found: 125.0368.

3.7.8. General procedure for preparation of 144, *ent*-144, 145 and *ent*-145

To an ice cold, stirred solution of triphenylphosphine (0.0082 mol) in dry THF (20 mL), benzoic acid or $^{17}O_2$ or $^{18}O_2$ benzoic acid (0.0082 mol) and the solution of **128** or *ent*-**128** (0.0041 mol) in dry THF (10 mL) were added slowly to the reaction flask under an inert N_2 atmosphere. The resulting mixture was stirred at 0 ^oC for 5 minutes. After this time, a solution of diisopropyl azodicarboxylate (0.0082 mol) in dry THF (5 mL) was added dropwise and the reaction mixture was stirred at room temperature for 12 h. The reaction solvent was removed by evaporation under reduced pressure and diluted with ethyl acetate (50 mL) and water (20 mL). The phases were separated, and the aqueous phase was extracted with ethyl acetate (3 × 50 mL). The combined organic layers were washed with brine (20 mL), dried over $MgSO_4$, and concentrated under reduced pressure, which afforded crude product. Purification of the crude product by flash chromatography (silica gel, 99:1 hexane: ethyl acetate) afforded the desired target compounds.

(7*R*,8*R*)-8-chloro-2-methyloctadec-5-yn-7-yl benzoate-$^{17}O_2$ (144)

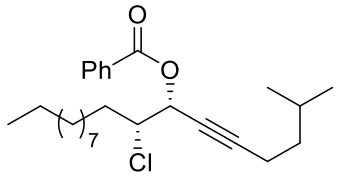

144: O = ^{17}O

Triphenylphosphine (0.00127 mol), $^{17}O_2$ benzoic acid (0.00127 mol) and **128** (0.000636 mol). (Eluent: 1% EA/hexane), 0.208 g, 78%, pale yellow oil: ^1H NMR (500 MHz, $CDCl_3$) δ: 8.09-8.08 (d, 2H, *J* = 7.2 Hz), 7.60-7.57 (t, 1H, *J* = 7.4 Hz), 7.47-7.44 (t, 2H, *J* = 7.7 Hz), 5.75-5.74 (dt, 1H, *J* = 6.1 Hz, 1.9 Hz), 4.12-4.08 (ddd, 1H, *J* = 9.6 Hz, 6.2 Hz, 3.4 Hz), 2.26-2.23 (td, 2H, *J* = 7.4 Hz, 1.9 Hz), 2.07-2.00 (m, 1H), 1.88-1.80 (m, 1H), 1.70-1.65 (m, 1H), 1.26 (m, 18H), 0.89 (t, 3H, *J* = 6.3 Hz), 0.87 (d, 6H, *J* = 6.6 Hz).

^{13}C NMR (125 MHz, $CDCl_3$) δ: 165.05, 165.02 ($^{13}C_{benzoate}$-^{17}O), 133.2, 129.8, 129.5, 128.3, 88.4, 77.1, 74.2, 67.7, 67.6 ($^{13}C_{benzoate}$-^{17}O), 62.4, 37.1, 33.6, 31.8, 29.5, 29.4, 29.3 29.2, 28.9, 27.1, 25.9 22.6, 22.0, 16.7, 14.0.

IR (neat): 2947, 2882, 2238, 1721, 1260, 1103, 1093, 956, 708 cm^{-1}.

$[\alpha]_D^{20}$: + 5.7 (c 0.8, CCl_4).

(7*R*,8*R*)-8-chloro-2-methyloctadec-5-yn-7-yl benzoate-$^{18}O_2$ (145)

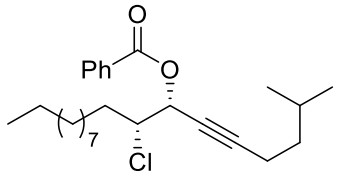

145: O = ^{18}O

Triphenylphosphine (0.00127 mol), $^{18}O_2$ benzoic acid (0.00127 mol) and **128** (0.000636 mol). (Eluent: 1% EA/hexane), 0.213 g, 80%, pale yellow oil: ^1H NMR (500 MHz, $CDCl_3$) δ: 8.09-8.08 (d, 2H, *J* = 7.2 Hz), 7.60-7.57 (t, 1H, *J* = 7.4 Hz), 7.47-7.44 (t, 2H, *J* = 7.7 Hz), 5.75-5.73 (dt, 1H, *J* = 6.1 Hz, 1.9 Hz), 4.12-4.08 (ddd, 1H, *J* = 9.6 Hz, 6.2 Hz, 3.4 Hz), 2.25-2.22 (td, 2H, *J* = 7.4 Hz, 1.9 Hz), 2.06-2.02 (m, 1H), 1.88-1.80 (m, 1H), 1.70-1.65 (m, 1H), 1.30-1.26 (m, 18H), 0.89 (t, 3H, *J* = 6.3 Hz), 0.87 (d, 6H, *J* = 6.6 Hz).

^{13}C NMR (125 MHz, $CDCl_3$) δ: 165.05, 165.03 ($^{13}C_{benzoate}$-^{18}O), 133.2, 129.8, 128.3, 88.4, 77.1, 74.2, 67.7, 67.6 ($^{13}C_{benzoate}$-^{18}O), 62.4, 37.1, 33.6, 31.8, 29.5, 29.4, 29.3 29.2, 28.9, 27.1, 26.0 22.6, 22.0, 16.7, 14.0.

IR (neat): 2945, 2879, 2238, 1712, 1243, 1103, 1093, 956, 708 cm^{-1}.

HRMS (ESI) m/z calculated for $C_{26}H_{39}ClNa^{18}O_2$ [M+Na]: 443.2573; found: 443.2574.

$[\alpha]_D^{20}$: + 5.7 (c 0.8, CCl_4).

(7*S*,8*S*)-8-chloro-octadec-5-yn-7-yl benzoate-$^{17}O_2$ (*ent*-144)

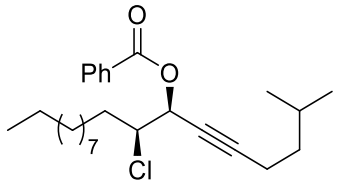

ent-**144**: O = ^{17}O

Triphenylphosphine (0.00127 mol), $^{17}O_2$ benzoic acid (0.00127 mol) and *ent*-**128** (0.000636 mol). (Eluent: 1% EA/hexane), 0.208 g, 78%, pale yellow oil. ^1H NMR (500

MHz, $CDCl_3$) δ: 8.09-8.08 (d, 2H, *J* = 7.2 Hz), 7.60-7.56 (t, 1H, *J* = 7.4 Hz), 7.46-7.44 (t, 2H, *J* = 7.7 Hz), 5.76-5.73 (dt, 1H, *J* = 6.1 Hz, 1.9 Hz), 4.12-4.07 (ddd, 1H, *J* = 9.6 Hz, 6.2 Hz, 3.4 Hz), 2.26-2.23 (td, 2H, *J* = 7.4 Hz, 1.9 Hz), 2.07-1.99 (m, 1H), 1.89-1.79 (m, 1H), 1.71-1.63 (m, 1H), 1.26 (m, 18H), 0.89 (t, 3H, *J* = 6.3 Hz), 0.87 (d, 6H, *J* = 6.6 Hz).

^{13}C NMR (125 MHz, $CDCl_3$) δ: 165.0, 164.9 ($^{13}C_{benzoate}$-^{17}O), 133.1, 129.7, 129.5, 128.2, 88.3, 77.1, 74.2, 67.7, 67.6 ($^{13}C_{benzoate}$-^{17}O), 62.4, 37.0, 33.6, 31.8, 29.5, 29.4, 29.3 29.2, 28.9, 27.1, 25.9 22.6, 22.0, 16.7, 13.9.

IR (neat): 2947, 2882, 2238, 1721, 1260, 1103, 1093, 956, 708 cm^{-1}.

$[\alpha]_D^{20}$: - 5.67 (c 0.8, CCl_4).

(7*S*,8*S*)-8-chloro-octadec-5-yn-7-yl benzoate-$^{18}O_2$ (*ent*-145)

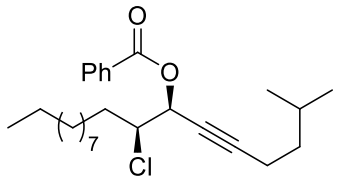

ent-**145**: O = ^{18}O

Triphenylphosphine (0.00127 mol), $^{18}O_2$ benzoic acid (0.00127 mol) and *ent*-**128** (0.000636 mol). (Eluent: 1% EA/hexane), 0.213 g, 80%, pale yellow oil. ^1H NMR (500 MHz, $CDCl_3$) δ: 8.10-8.07 (d, 2H, *J* = 7.2 Hz), 7.60-7.56 (t, 1H, *J* = 7.4 Hz), 7.48-7.44 (t, 2H, *J* = 7.7 Hz), 5.75-5.74 (dt, 1H, *J* = 6.1 Hz, 1.9 Hz), 4.12-4.07 (ddd, 1H, *J* = 9.6 Hz, 6.2 Hz, 3.4 Hz), 2.26-2.22 (td, 2H, *J* = 7.4 Hz, 1.9 Hz), 2.07-1.99 (m, 1H), 1.89-1.79 (m, 1H), 1.71-1.64 (m, 1H), 1.30-1.26 (m, 18H), 0.89 (t, 3H, *J* = 6.3 Hz), 0.87 (d, 6H, *J* = 6.6 Hz).

^{13}C NMR (125 MHz, $CDCl_3$) δ: 165.05, 165.03 ($^{13}C_{benzoate}$-^{18}O), 133.2, 129.8, 128.3, 88.4, 77.1, 74.2, 67.7, 67.6 ($^{13}C_{benzoate}$-^{18}O), 62.4, 37.1, 33.6, 31.8, 29.5, 29.4, 29.3 29.2, 28.9, 27.1, 26.0 22.6, 22.0, 16.7, 14.0.

IR (neat): 2945, 2879, 2238, 1712, 1243, 1103, 1093, 956, 708 cm^{-1}.

HRMS (ESI) m/z calculated for $C_{26}H_{39}ClNa^{18}O_2$ [M+Na]: 443.2573; found: 443.2574.

$[\alpha]_D^{20}$: - 5.67 (c 0.8, CCl_4).

3.7.9. General procedure for preparation of 146, *ent*-146, 147 and *ent*-147

A 100 mL round bottom flask was charged with benzene. The flask was evacuated and back filled with nitrogen gas. After two vacuum/nitrogen cycles to replace air with nitrogen inside the reaction flask, the compound **144,** *ent*-**144, 145** and *ent*-**145** (0.0028 mol), $RhCl(PPh_3)_3$ (10 mol%) were added. The reaction mixture was vigorously stirred at room temperature under atmospheric deuterium pressure (balloon) for 3 h. After that the reaction mixture was filtered through a celite pad, and the filtrate was concentrated on a rotary evaporator to afford crude product. The crude product was carried to the next step without further purification.

(7*R*,8*R*)-8-chloro-2-methyloctadecan-7-yl benzoate-d_4, $^{17}O_2$ (146)

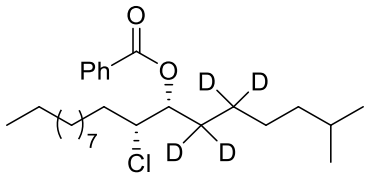

146: O = ^{17}O

The compound **144** (0.00024 mol) and $RhCl(PPh_3)_3$ (10 mol%). 0.093 g, 92%, colorless oil: ^1H NMR (500 MHz, $CDCl_3$) δ: 8.10-8.08 (d, 2H, *J* = 7.2 Hz), 7.59-7.56 (t, 1H, *J* = 7.4 Hz), 7.48-7.45 (t, 2H, *J* = 7.7 Hz), 5.30-5.28 (m, 1H), 4.08-4.05 (dt, 1H, *J* = 9.1 Hz, 4.0 Hz), 1.83-1.69 (m, 3H), 1.53-148 (m, 1H), 1.33-1.24 (m, 19H), 0.87 (t, 3H, *J* = 6.3 Hz), 0.84 (d, 6H, *J* = 6.6 Hz).

^{13}C NMR (125 MHz, $CDCl_3$) δ: 165.9, 165.8 ($^{13}C_{benzoate}$-^{17}O), 133.0, 129.9, 129.7, 129.6, 128.3, 75.5, 75.4 ($^{13}C_{benzoate}$-^{17}O), 63.7, 38.6, 34.4, 31.8, 29.5, 29.4, 29.3, 29.2 28.9, 27.7, 26.5, 22.6, 22.5, 22.4, 14.0.

IR (neat): 2945, 2880, 1720, 1260, 1108, 1069, 709 cm^{-1}.

$[\alpha]_D^{20}$: +6.4 (c 0.68, CCl_4).

(7*R*,8*R*)-8-chloro-2-methyloctadecan-7-yl benzoate-d_4, $^{18}O_2$ (147)

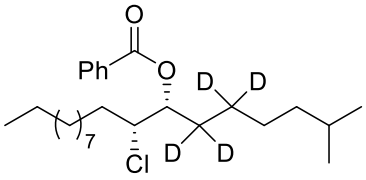

147: O = ^{18}O

The compound **145** (0.00024 mol) and $RhCl(PPh_3)_3$ (10 mol%) 0.093g, 92%, colorless oil: ^1H NMR (500 MHz, $CDCl_3$) δ: 8.09-8.08 (d, 2H, *J* = 7.2 Hz), 7.59-7.56 (t, 1H, *J* = 7.4 Hz), 7.48-7.45 (t, 2H, *J* = 7.7 Hz), 5.29-5.27 (m, 1H), 4.07-4.04 (dt, 1H, *J* = 9.1 Hz, 4.0 Hz), 1.81-1.69 (m, 2H), 1.53-1.47 (m, 1H), 1.30-1.23 (m, 20H), 0.87 (t, 3H, *J* = 6.3 Hz), 0.85 (d, 6H, *J* = 6.6 Hz).

^{13}C NMR (125 MHz, $CDCl_3$) δ: 165.9, 165.8 ($^{13}C_{benzoate}$-^{18}O), 133.0, 129.9, 129.7, 128.3, 75.5, 75.4 ($^{13}C_{benzoate}$-^{18}O), 63.7, 38.6, 34.4, 31.8, 29.5, 29.4, 29.3 29.2, 28.9, 27.8, 26.5, 22.6, 22.5, 22.4, 14.0.

IR (neat): 2955, 2888, 1711, 1242, 1110, 1080, 709 cm^{-1}.

HRMS (ESI) m/z calculated for $C_{26}H_{39}ClKD_4{}^{18}O_2$ [M+K]: 467.2888.; found: 467.2876.

$[\alpha]_D{}^{20}$: +6.4 (c 0.68, CCl_4).

(7*S*,8*S*)-8-chloro-2-methyloctadecan-7-yl benzoate-d_4, $^{17}O_2$ (*ent*-146)

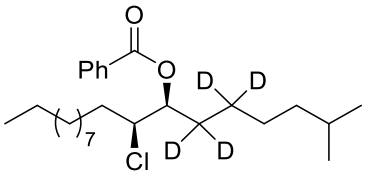

ent-**146**: O = ^{17}O

The compound *ent*-**144** (0.00024 mol) and $RhCl(PPh_3)_3$ (10 mol%). 0.093 g, 92%, colorless oil: ^1H NMR (500 MHz, $CDCl_3$) δ: 8.09-8.08 (d, 2H, *J* = 7.2 Hz), 7.60-7.56(t, 1H, *J* = 7.4 Hz), 7.48-7.44 (t, 2H, *J* = 7.7 Hz), 5.31-5.27 (m, 1H), 4.08-4.04 (dt, 1H, *J* = 9.1 Hz, 4.0 Hz), 1.87-1.71 (m, 3H), 1.54-147 (m, 1H), 1.34-1.23 (m, 19H), 0.87 (t, 3H, *J* = 6.3 Hz), 0.84 (d, 6H, *J* = 6.6 Hz).

^{13}C NMR (125 MHz, $CDCl_3$) δ: 165.9, 165.8 ($^{13}C_{benzoate}$-^{17}O), 133.0, 129.9, 129.7, 129.6, 128.3, 75.5, 75.4 ($^{13}C_{benzoate}$-^{17}O), 63.7, 38.6, 34.4, 31.8, 29.5, 29.4, 29.3, 29.2 28.9, 27.7, 26.5, 22.6, 22.5, 22.4, 14.0.

IR (neat): 2945, 2880, 1721, 1260, 1108, 1069, 709 cm^{-1}.

$[\alpha]_D^{20}$: -6.37 (c 0.68, CCl_4).

(7*S*,8*S*)-8-chloro-2-methyloctadecan-7-yl benzoate-d$_4$, $^{18}O_2$ (*ent*-147)

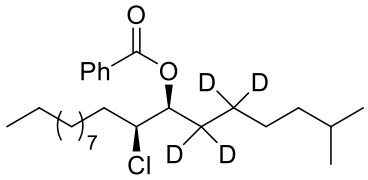

ent-**147**: O = ^{18}O

The compound *ent*-**145** (0.00024 mol) and $RhCl(PPh_3)_3$ (10 mol%). 0.093 g, 92%, colorless oil: ^{1}H NMR (500 MHz, $CDCl_3$) δ: 8.10-8.08 (d, 2H, *J* = 7.2 Hz), 7.60-7.56 (t, 1H, *J* = 7.4 Hz), 7.48-7.45 (t, 2H, *J* = 7.7 Hz), 5.31-5.28 (m, 1H), 4.08-4.04 (dt, 1H, *J* = 9.1 Hz, 4.0 Hz), 1.83-1.71 (m, 2H), 1.53-1.47 (m, 1H), 1.30-1.23 (m, 20H), 0.87 (t, 3H, *J* = 6.3 Hz), 0.85 (d, 6H, *J* = 6.6 Hz).

^{13}C NMR (125 MHz, $CDCl_3$) δ: 165.9, 165.8 ($^{13}C_{benzoate}$-^{18}O), 133.0, 129.9, 129.7, 128.3, 75.5, 75.4 ($^{13}C_{benzoate}$-^{18}O), 63.7, 38.6, 34.4, 31.8, 29.5, 29.4, 29.3 29.2, 28.9, 27.8, 26.5, 22.6, 22.5, 22.4, 14.0.

IR (neat): 2955, 2888, 1711, 1242, 1110, 1080, 709 cm^{-1}.

HRMS (ESI) m/z calculated for $C_{26}H_{39}ClKD_4{}^{18}O_2$ [M+K]: 467.2888.; found: 467.2876.

$[\alpha]_D^{20}$: -6.4 (c 0.68, CCl_4).

3.7.10. General procedure for preparation of 15b, *ent*-15b, 15c and *ent*-15c

To an ice cold, stirred solution of **146,** *ent*-**146, 147** and *ent*-**147** (0.9456 mmol) in methanol (6 mL), 4N NaOH in methanol (4 mL) was added slowly to the reaction flask. The resulting mixture was stirred at room temperature for 2 h. The reaction solvent was

removed by evaporation under reduced pressure and diluted with ethyl acetate (20 mL) and water (10 mL). The phases were separated, and the aqueous phase was extracted with ethyl acetate (3 × 20 mL). The combined organic layers were washed with brine (10 mL), dried over $MgSO_4$, and concentrated under reduced pressure. Purification of the crude product by flash chromatography (silica gel, 100% hexanes) afforded the desired targets.

(7*R*,8*S*)-7,8-epoxy-2-methyloctadecane-d_4,^{17}O (15b)

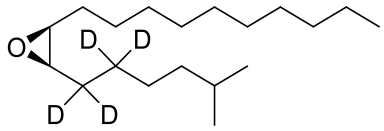

15b: O = ^{17}O

The compound **146** (0.000163 mol) and 4N NaOH. (Eluent: 100% hexane), 0.042 g, 90%, clear oil: ^{1}H NMR (500 MHz, $CDCl_3$) δ: 2.92-2.88 (m, 2H), 1.56-1.16 (m, 23H), 0.89-0.86 (m, 9H).

^{13}C NMR (125 MHz, $CDCl_3$) δ: 57.2-57.0 ($^{13}C_{epo}$-^{2}H & $^{13}C_{epo}$-^{17}O), 38.8, 31.8, 29.5, 29.4, 29.2, 27.8, 27.7, 26.5, 22.6, 22.6, 22.5, and 14.0.

IR (neat): 2954, 2923, 2854, 1466, 1080, 1029, 721 cm^{-1}.

HRMS (ESI) m/z calculated for $C_{19}H_{35}D_4{}^{17}O$ [M+H]: 288.3281; found: 288.3288.

$[\alpha]_D^{20}$: +0.54 (c 0.56, CCl_4).

(7*R*,8*S*)-7, 8-epoxy-2-methyloctadecane-d_4,^{18}O (15c)

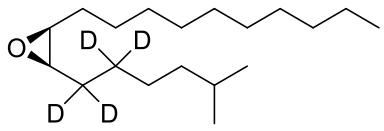

15c: O = ^{18}O

The compound **147** (0.000163 mol) and 4N NaOH. (Eluent: 100% hexane), 0.042 g, 89.5%, clear oil: ^{1}H NMR (500 MHz, $CDCl_3$) δ: 2.92-2.89 (m, 2H), 1.56-1.18 (m, 23H), 0.90-0.85 (m, 9H).

^{13}C NMR (125 MHz, $CDCl_3$) δ: 57.2-57.0 ($^{13}C_{epo}$-^{2}H & $^{13}C_{epo}$-^{18}O), 39.0, 32.0, 29.7, 29.5, 29.4, 29.2, 27.8, 27.7, 26.5, 22.6, 22.5, 22.4, and 14.0. IR (neat): 2954, 2923, 2854, 1466, 1385, 1029, 721 cm^{-1}.

HRMS (ESI) m/z calculated for $C_{19}H_{34}D_4Na^{18}O$ [M+Na]: 311.3120; found: 311.3108.

IR (neat): 2954, 2923, 2854, 1466, 1066, 1029, 721 cm^{-1}.

$[\alpha]_D^{20}$: +0.54 (c 0.56, CCl_4).

(7*S*,8*R*)-7, 8-epoxy-2-methyloctadecane- d_4,^{17}O (*ent*-15b)

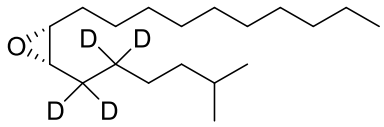

***ent*-15b**: O = ^{17}O

The compound *ent*-**146** (0.000163 mol) and 4N NaOH. (Eluent: 100% hexane), 0.039 mg, 83%, clear oil: ^{1}H NMR (500 MHz, $CDCl_3$) δ: 2.92-2.89 (m, 2H), 1.56-1.16 (m, 23H), 0.89-0.86 (m, 9H).

^{13}C NMR (125 MHz, $CDCl_3$) δ: 57.2-57.0 ($^{13}C_{epo}$-^{2}H & $^{13}C_{epo}$-^{17}O), 38.8, 31.8, 29.5, 29.4, 29.2, 27.8, 27.7, 26.5, 22.6, 22.6, 22.5, and 14.0.

IR (neat): 2954, 2923, 2854, 1466, 1080, 1029, 721 cm^{-1}.

HRMS (ESI) m/z calculated for $C_{19}H_{35}D_4{}^{17}O$ [M+H]: 287.5365; found: 287.5368.

$[\alpha]_D^{20}$: -0.535 (c 0.56, CCl_4).

(7*S*,8*R*)-7, 8-epoxy-2-methyloctadecane d_4,^{18}O (*ent*-15c)

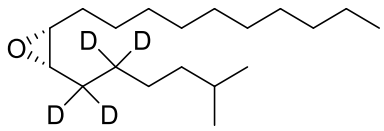

***ent*-15c**: O = ^{18}O

The compound *ent*-**147** (0.000163 mol) and 4N NaOH. (Eluent: 100% hexane), 0.041g, 87%, clear oil: ^{1}H NMR (500 MHz, $CDCl_3$) δ: 2.92-2.89 (m, 2H), 1.56-1.18 (m, 23H), 0.90-0.85 (m, 9H).

^{13}C NMR (125 MHz, $CDCl_3$) δ: 57.2-57.0 ($^{13}C_{epo}$-^{2}H & $^{13}C_{epo}$-^{18}O), 39.0, 32.0, 29.7, 29.5, 29.4, 29.2, 27.8, 27.7, 26.5, 22.6, 22.5, 22.4, and 14.0.

IR (neat): 2954, 2923, 2854, 1466, 1066, 1029, 721 cm^{-1}.

HRMS (ESI) m/z calculated for $C_{19}H_{34}D_4Na^{18}O$ [M+Na]: 288.5366; found: 288.5367. $[\alpha]_D^{20}$: -0.535 (c 0.56, CCl_4).

Chapter 4.

Design, synthesis and use of fluorescently tagged disparlure enantiomers to study pheromone interaction kinetics of pheromone binding proteins from the gypsy moth.

4.1. Introduction

Ligand-binding experiments between pheromone binding proteins (PBPs) and hydrophobic ligands (*e.g*. pheromones) can be performed in two general ways: 1) the ligand and protein are equilibrated in buffer, and protein-bound ligand is then separated from the free ligand using filteration (Plettner et al., 2000) or 2) the protein is titrated with a fluorescent reporter such as NPN (N-phenyl-1-napthylamine), and the NPN is then displaced by titration of the PBP-NPN complex with the ligand of interest (Ban et al., 2002; Gong et al., 2010; Gong and Plettner, 2011). Disadvantages of equilibrium binding assays are the adsorption of hydrophobic ligands to the vial surfaces and the potential loss of bound ligand during the filtration step, which leads to underestimates of binding affinity. Determination of binding constants of PBP-ligand complex in the second type of experiment depends on displacement of the fluorescent reporter by a competing ligand with a concomitant decrease in NPN fluorescence. This type of binding experiment does not require any physical separation of bound ligand from unbound ligand (Ban et al., 2002). However, this approach needs the availability of a fluorescent reporter equipped with good binding strength for the PBP under study, whose fluorescence emission spectrum is significantly changed when the reporter binds inside the binding pocket of PBP.

The disadvantage of the use of fluorescent reporters in ligand-binding assays is that various compounds differ in their ability to displace the reporter (due to kinetic factors and incomplete equilibrium between aliquot additions during these experiments), rather than reporting the binding strength of the ligand of interest to the PBP. Another disadvantage is the strong fluorescent emission of the reporter in the presence of ligands or pheromone compounds that are capable of forming micelles (*e.g*. fatty acids or amphiphilic pheromones). In this case, the reporter can occupy the hydrophobic core of

the micelle, producing a strong fluorescent peak, similar to that emitted in the binding pocket of the PBP. An example of this problem can be seen in the study by McAfee et.al.(McAfee et al., 2018) when they titrated OBPs 16 and 18 from the honey bee (*Apis mellifera* L.) with the oleic acid. Given these drawbacks, it would be necessary to conduct binding assays between pheromone and PBPs with different fluorescent reporters linked to the ligand of interest.

The utility of fluorophore-tagged ligands for studying receptor-ligand interactions has been acknowledged for several decades (Melamed, Lahav, and Atlas 1976; Atlas and Levitzki, 1977; Daly and McGrath, 2003; Middleton and Kellam, 2005; Soave et al. 2020). The most frequently used fluorophores are: fluorescein (**85**), rhodamine (**86**), pyrene (**87**), coumarin (**88**) nitrobenzoxadiazole (NBD) (**89**), dansyl (**90**) and bodipy (**91**) (Chapter 1, Figure 1.9). The main feature of these fluorophores is their ease of availability with the required photophysical and chemical properties and the small size. The feasibility of utilizing a particular fluorophore relies on the chemical properties and photophysical properties such as excitation maximum wavelength (λ_{ex}), emission maximum wavelength (λ_{em}), molar absorptivity (ε) and quantum efficiency (ϕ). The value of quantum efficiency multiplied by molar absorptivity ($\phi \times \varepsilon$) is generally used to estimate the sensitivity of the fluorophore. The photophysical properties of the most commonly used fluorophores are shown in Table 4.1.

Table 4.1 Photophysical properties of variuos fluorophores

Fluorophore	**λ_{ex} (nm)**	**λ_{em} (nm)**	**(φ)**	**ε [M^{-1} cm^{-1}]**
Pyranine (8-hydroxy-1,3,6-pyrenetrisulfonate	340	376	0.75	2.5×10^4
7-hydroxy-4-methylcoumarin	360	450	0.63	1.7×10^3
NBD chloride	465	535	0.30	2.2×10^4
Dansyl chloride	336	520	0.27	6.1×10^3
6-Carboxyfluorescein (6-FAM)	494	520	0.93	9.3×10^4
6-Carboxy-X-rhodamine (6-ROX)	570	591	0.88	7.6×10^4
BODIPY FL	505	511	0.94	9.1×10^4

λ_{ex}, excitation maximum; λ_{em}, emission maximum; ε, molar absorptivity; Φ, quantum efficiency

We have covalently linked 6-carboxyfluorescein (6-FAM) to the gypsy moth sex pheromone (+)-disparlure (**15**) and to its enantiomer (-)-disparlure (*ent*-**15**) (Figure 4.1) by adding a linker with a terminal alkyne moiety to disparlure and performing a click reaction of the alkyne and 6-carboxyfluorescein azide (6-FAM azide). We choose 6-Carboxyfluorescein (6-FAM) as a fluorescent reporter because of its high fluorescence quantum yield (0.93) (Table 4.1), good water solubility and its derivatives, such as 6-FAM azide, are commercially available. In addition to the high quantum yield, it has excellent absorption and emission properties (Sjöback et al., 1995; Zhang et al., 2014).

This is the first report describing the synthesis of a fluorophore-tagged insect pheromone. We expect that these fluorophore-tagged pheromones will provide researchers with a viable alternative to the radiolabeled pheromones and fluorescent probes such as 1-NPN that are used in PBP-pheromone binding assays. To date, the use of fluorophore tagged pheromones as a fluorescent reporter in the study of pheromone binding protein kinetics has not been reported.

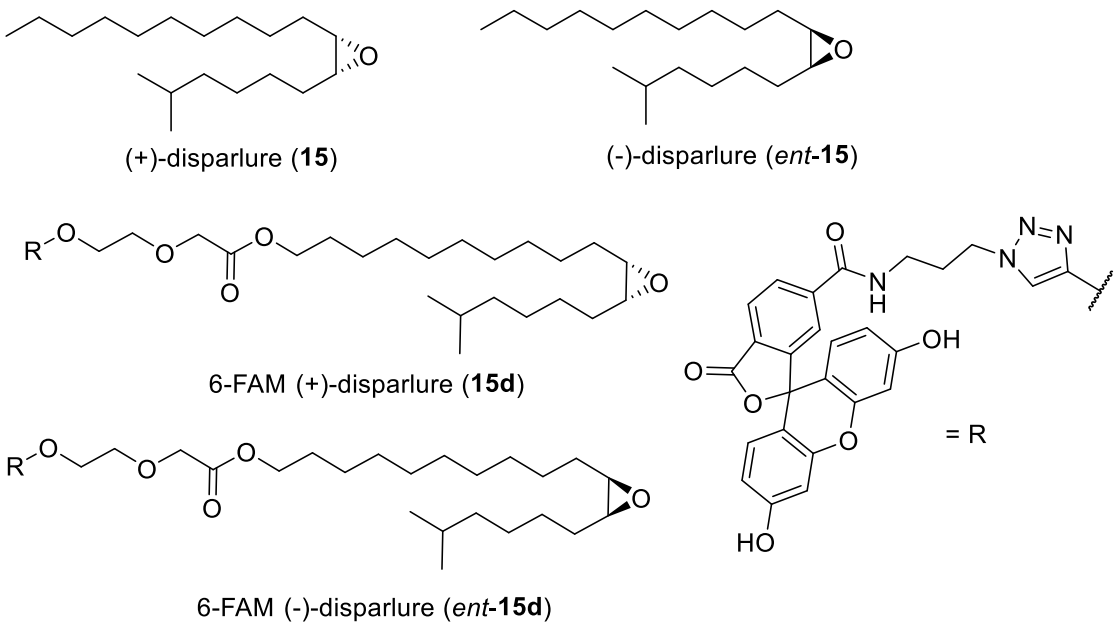

Figure 4.1 Structures of disparlure enantiomers and their fluorescent analogues.

In this Chapter, I report the design, synthesis and spectroscopic characterization of fluorophore-tagged disparlure enantiomers 6FAM (+)-disparlure (**15d**) and 6FAM (-)-disparlure (*ent*-**15d**) (Figure 4.1), and their binding affinities to two pheromone binding

proteins *Ldis*PBP1 and *Ldis*PBP2 of gypsy moth, *Lymantria dispar*. Furthermore, the kinetic rate constants k_{on} and k_{off} were obtained for *Ldis*PBPs with 6-FAM disparlure enantiomers listed in Figure 4.1. The fluorescence-based binding assays and kinetic experiments were monitored in a fluorescence spectrometer and stopped-flow instrument, respectively. The disparlure binding to *Ldis*PBPs was determined by changes in fluorescence emission intensity of the solution containing *Ldis*PBPs and 6-FAM disparlure. The relative changes in fluorescence intensity reflecting binding to *Ldis*PBP1 or *Ldis*PBP2 are quantitated as a function of increasing 6FAM (+)-disparlure (**15d**) or 6-FAM (-)-disparlure (*ent*-**15d**) concentration. I have presented a two-step mechanism for the disparlure binding to *Ldis*PBP1 and *Ldis*PBP2 based on the kinetic studies with 6-FAM disparlure enantiomers and *Ldis*PBPs. In this mechanism, the disparlure ligands interact with the *Ldis*PBP on an external site before moving into the *Ldis*PBP internal binding site. This two-step binding mechanism is consistent with previous kinetic studies, obtained using different techniques, indicating that the ligand binding at the *Ldis*PBP internal site is multi-step mechanism that proceeds through an external binding site (see Section 4.2.10) (Gong et al., 2009, 2010).

4.2. Results and discussion

4.2.1. Design of 6-FAM tagged disparlure enantiomers

Herein, I describe the design and convergent synthesis of 6-carboxyfluorescein (6-FAM)-tagged (+)-disparlure analogue **15d** taking advantage of the copper (I)-catalyzed Huisgen 1,3-dipolar cycloaddition (also known as click reaction). The target molecule has been divided in to three parts: (+)-disparlure (**15**) (pheromone, recognition part) for the selective binding towards its pheromone binding protein, 6-FAM moiety for the fluorescence detection, and finally between two parts, a diethylene glycol linker to increase the hydrophilicity of the final target molecule and provide some separation between the recognition part and the fluorophore (Figure and Scheme 4.1).

The design for 6-FAM (+)-disparlure (**15d**) is outlined in Scheme 4.1. We believed that the target molecule **15d** could be prepared by the click reaction between the 6-carboxyfluorescein azide (6-FAM azide) **148** and epoxy alkyne intermediate **149** which could be assembled by esterification of epoxy alcohol **150** and the alkyne acid **151**. On

the other hand, propargylation reaction between ethylene glycol and propargyl bromide followed by oxidation would furnish the alkyne acid **151**.

The retrosynthetic analysis of epoxy alcohol fragment **150** reveals that this could be synthesized from1,2-*syn* chlorohydrin **152** which could be obtained by Mitsunobu inversion of 1,2-*anti* chlorohydrin **153**. We envisioned that the stereocenter at carbon-8 of 1,2-*anti* chlorohydrin **153** could be introduced by utilizing a diastereoselective nucleophilic addition reaction between enantiopure α-chloroaldehyde **154** and acetylide anion. The enantiopure α-chloroaldehyde **154** could be prepared from aldehyde intermediate **155** via asymmetric α-chlorination. We used the same approach to prepare (+)-and (-)-disparlure enantiomers (Pinnelli et al., 2019). The asymmetric α-chlorination of an aldehyde was also used previously in the synthesis of the posticlure enantiomers, which have a *trans* epoxide moiety (Kang and Britton, 2007). To obtain the *cis* epoxide of disparlure we had to invert the configuration of the intermediate *anti* chlorohydrin (Pinnelli et al., 2019).

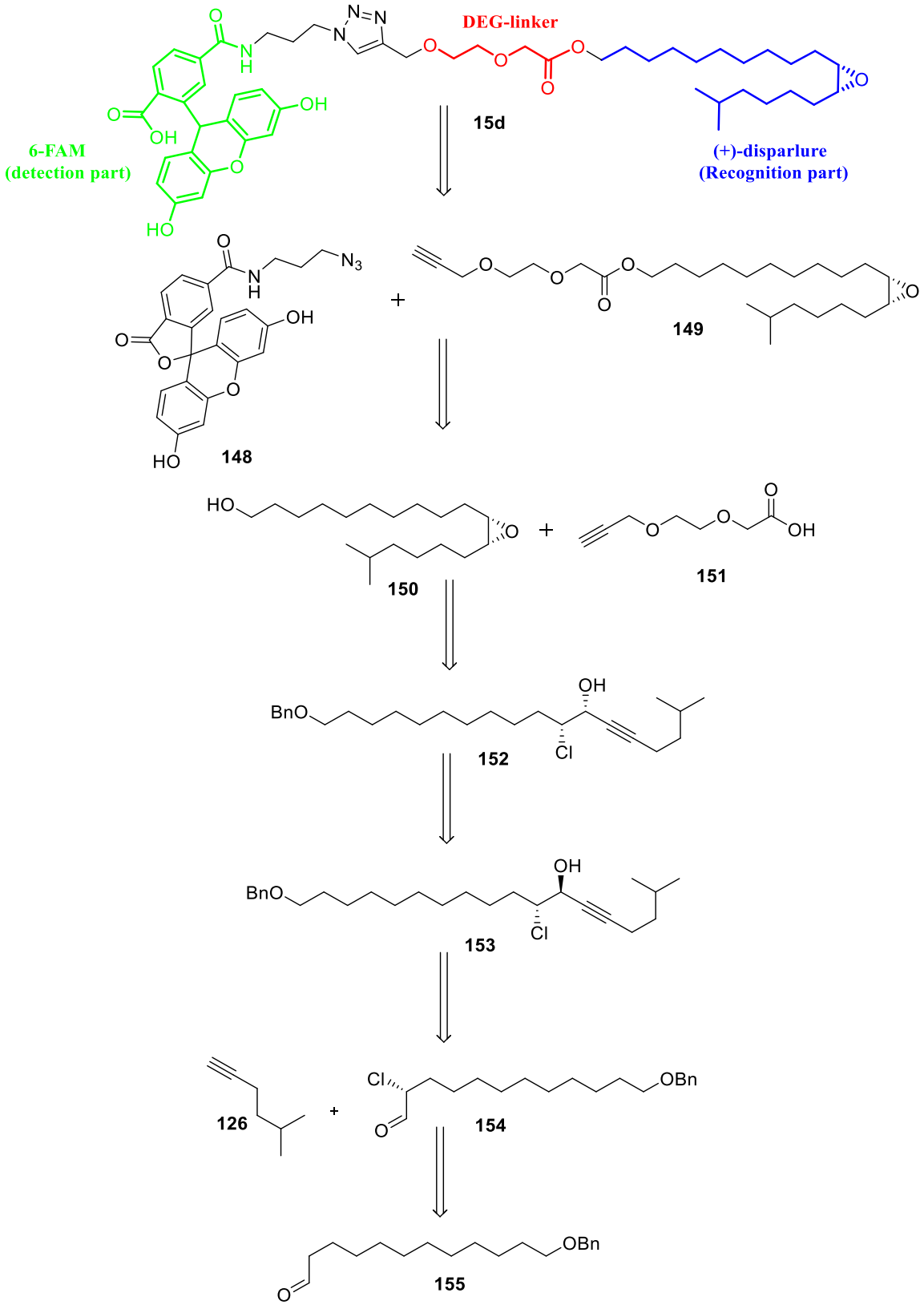

Scheme 4.1 Retereosynthetic design for 6FAM tagged (+)-disparlure (15d).

4.2.2. Synthesis of key fragment, enantiopure *cis*-epoxy alcohol 150

To accomplish the synthesis of the 6-FAM (+)-disparlure (**15d**), two key fragments (*i.e.*, enantiopure *cis*-epoxy alcohol **150** and ethylene glycol linker **151**) have been prepared and their synthetic routes are discussed below. The first task of the synthesis was the preparation of enantiopure epoxy alcohol fragment **150**, which began from commercially available 1,12-dodecanediol (**156**) (Scheme 4.2). The diol **156** was treated with chloromethyl methyl ether (MOM-Cl) or tert-Butyldimethylchlorosilane (TBDMS-Cl) to afford the mono MOM or TBDMS protected alcohol **157** or **158**. Subsequent oxidation of compound **157** or **158** with pyridinium chlorochromate (PCC) furnished the aldehyde **159** or **160**. We attempted to asymmetrically chlorinate aldehydes **159** or **160**, using previously reported asymmetric chlorination reaction (Amatore et al., 2009; Pinnelli et al., 2019). In this reaction chiral amine (2*R*, 5*S*)-2-*tert*-butyl-3,5-dimethylimidazolidin-4-one (**106**) and LiCl are used as catalyst and chlorinating agent, respectively. However, this reaction gave a mixture of decomposition products and failed to provide the desired product **161** or **162** (Scheme 4.2). The ^{1}H NMR analysis of the crude product showed deprotection of the MOM or TBDMS group, which lead to the formation of decomposition products.

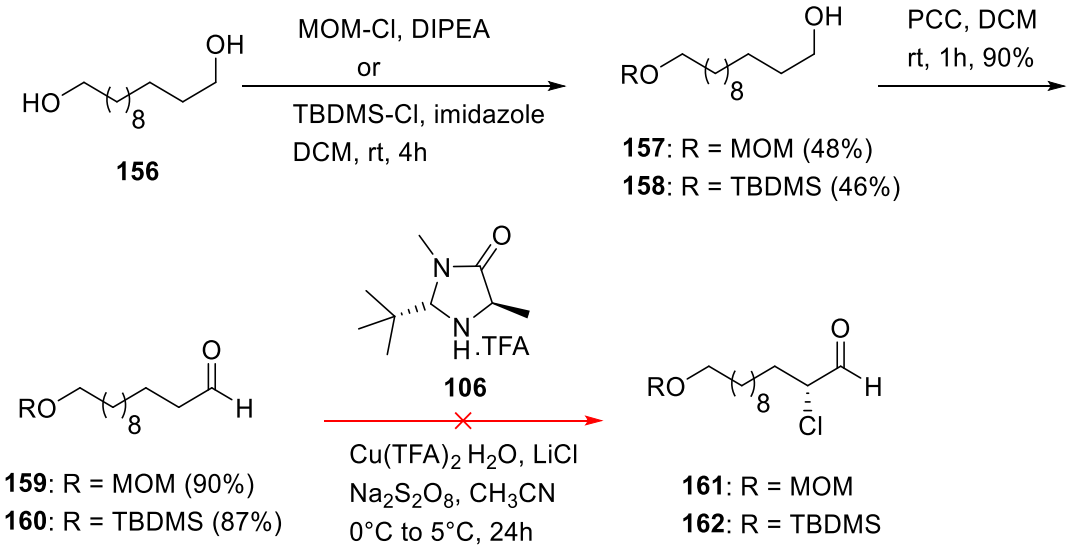

Scheme 4.2 Attempted asymmetric α-chlorination of MOM or TBDMS protected aldehyde with SOMO catalyst.

To overcome this problem, an alternative approach was employed in which benzyl protecting group was utilized during protection of the diol **156**. The monobenzylated alcohol **164** is prepared by benzylation of diol **156** with benzylbromide **163** in the presence of NaH/THF at 70°C (Scheme 4.3). ^{1}H NMR analysis of the crude reaction mixture indicated approximately 1:1 ratio of mono and dibenzylated products. Upon purification by flash column chromatography, 44% yield of the monobenzylated alcohol **164** was isolated. The resulting monobenzylated alcohol **164** was oxidized with PCC under standard conditions to its corresponding aldehyde **165**, followed by asymmetric α-chlorination with SOMO catalyst **106** to afford enantiopure α-chloroaldehyde **166** in 85% yield and >98% ee (see Appendix C2).

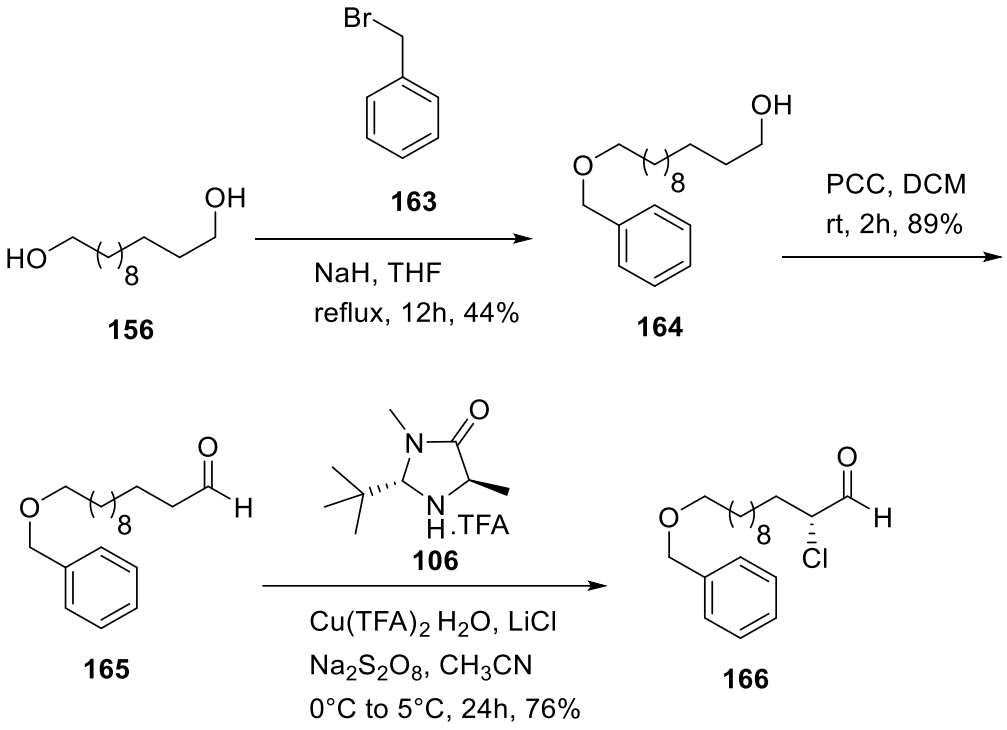

Scheme 4.3 Synthesis of enantiopure α-chloroaldehyde 166.

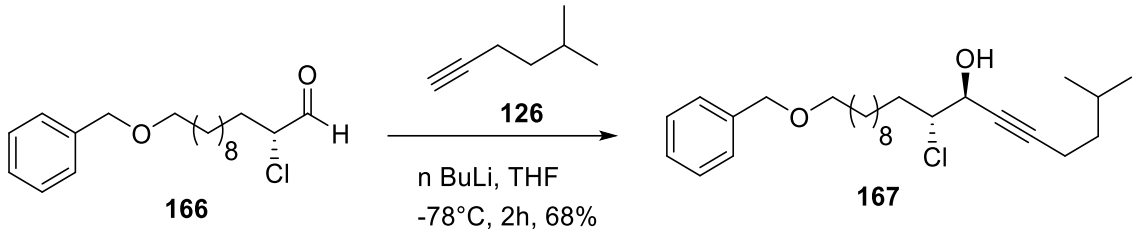

Scheme 4.4 Preparation of 1,2-*anti* chlorohydrin 167 from enantiopure α-chloroaldehyde 166.

With the required enantiopure α-chloroaldehyde **166**, we proceeded to prepare the 1,2-*anti* chlorohydrin **167** as shown in Scheme 4.4. Previous literature shows that addition of nucleophile to enantiopure α-chloroaldehyde delivers predominantly 1,2-*anti*-chlorohydrin (Kang and Britton, 2007; Shibuya, Kanady, and Vanderwal 2008; Pinnelli et al., 2019) . Therefore, the 5-methyl-1-hexyne **126** was treated with *n*-butyllithium followed by slow addition of enantiopure α-chloroaldehyde **166** to afford 1,2-*anti* chlorohydrin **167**. ^{1}H NMR data of the crude reaction mixture revealed a diastereomeric ratio (d.r) of ~ 20:1 (*anti*:*syn*). The crude reaction mixture was subjected to column chromatography yielding the 1,2-*anti* chlorohydrin **167** as pale-yellow oil in 68% yield.

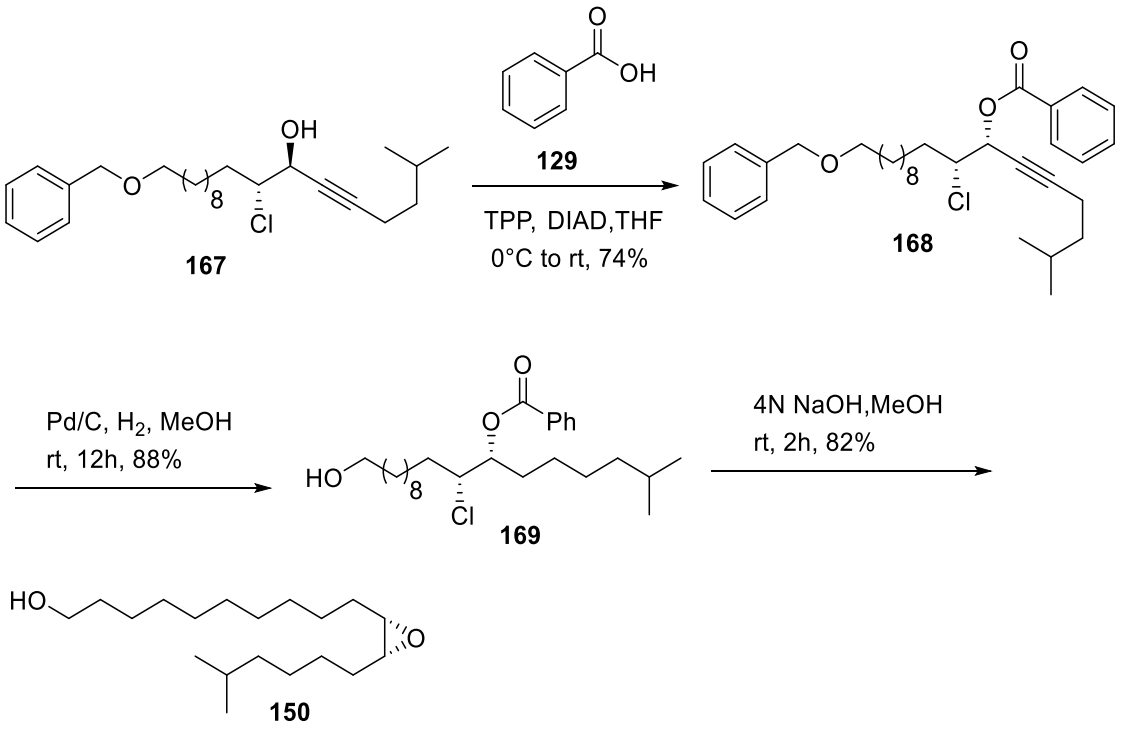

Scheme 4.5 Synthesis of key fragment epoxy alcohol 150.

It has been reported that the 1,2-*anti* chlorohydrins produce *trans* epoxides when treated with base (e.g., Kang and Britton 2007). However, we require a 1,2-*syn* chlorohydrin to obtain the key intermediate epoxy alcohol **150**. To prepare the 1, 2-*syn* chlorohydrin, the stereochemistry at the C-8 carbon of 1,2-*anti* chlorohydrin **167** was inverted under Mitsunobu conditions (Scheme 4.5). Therefore, compound **167** was treated with benzoic acid (**129**), tri-phenylphosphine (TPP) and diisopropyl azadicarboxylate (DIAD) in dry THF under an inert atmosphere. This resulted in the completely inverted product **168**, which was obtained in 80% yield. Then, a one-pot deprotection of the benzyl group and alkyne reduction of the 1,2-*syn* chloroester **168** was carried out, using 10% Pd/C in MeOH in the presence of hydrogen (1 atm, balloon). Thus, formation of the compound **169**, using Pd/C and followed by basic hydrolysis of benzoate of 1,2-*syn* chloroester **169**, led to the key fragment, enantiopure *cis*-epoxy alcohol **150** in good yield.

4.2.3. Synthesis of ethylene glycol linker 151

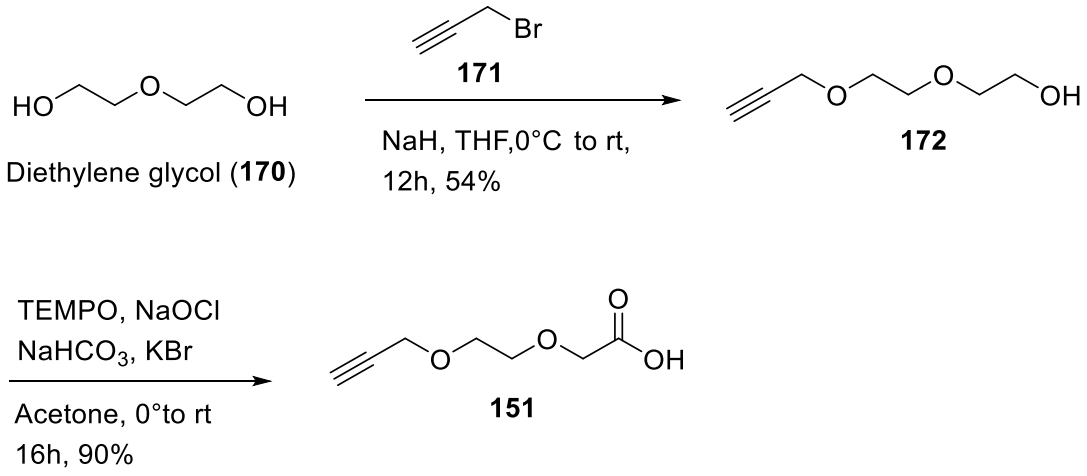

Scheme 4.6 Synthetic route to ethylene glycol linker 151.

The required ethylene glycol linker for esterification of enantiopure epoxy alcohol **150** was prepared by the synthetic pathway shown above (Scheme 4.6). The monopropargylation of diethylene glycol (**170**) was achieved using equimolar amounts of propargyl bromide **171** and NaH, which led to the propargyl ether precursor **172** with 54 % yield. The alcohol **172** was efficiently converted to the corresponding acid **151** by treating it with oxidizing agent NaOCl (sodium hypochlorite) and TEMPO (2,2,6,6-Tetramethylpiperidin-1-yl) oxidanyl) as a catalyst.

4.2.4. Synthesis of 6FAM-tagged (+)-disparlure (15d)

Finally, the key fragments **150** and **151** were coupled under Steglich conditions, which involve DIC (*N*,*N*′-diisopropylcarbodiimide) as coupling reagent and DMAP (*N*,*N*′-dimethylaminopyridine as a catalyst, leading to the required alkyne ester **149** with good yield, thus building the appropriate alkyne partner for the copper-catalyzed Huisgen 1,3-dipolar cycloaddition (click reaction) employing 6-FAM azide **173** as the coupling partner (Scheme 4.8).

The 1,3-dipolar cycloaddition (also known as Huisgen's cycloaddition) between the alkyne and azide to deliver 1,4- or 1,5-disubstituted triazoles, was developed predominantly by Rolf Huisgen (Scheme 4.7a) (Huisgen, 1963). The major disadvantages of this reaction are the lack of regioselectivity, elevated temperatures and long reaction times. In 2002, Sharpless's and Meldal's groups (Rostovtsev et al., 2002; Tornøe et al., 2002) separately reported the identification of copper (I) catalysis in Huisgen's 1,3-diploar cycloaddition reaction between alkyne and azide. This copper (I) catalysis not only improved the regioselectivity to exclusively yield 1,4-disubstituted triazole (Scheme 4.7b), but also increased the reaction rate by a factor of almost 10^7 compared to Huisgen's 1,3-dipolar cycloaddition.

a) Huisgen's 1,3-dipolar cycloaddition reaction

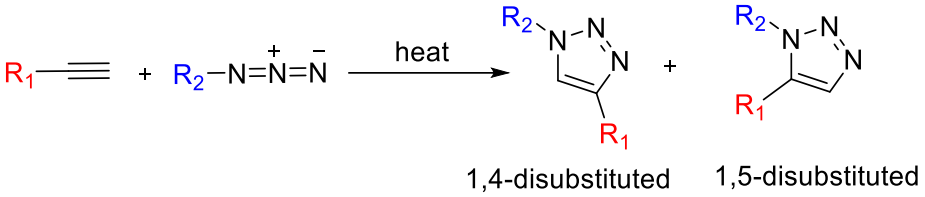

b) Copper-catalysed alkyne-azide cycloaddition (CuAAC) reaction

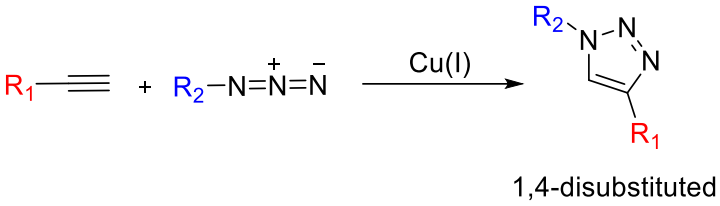

Scheme 4.7 a) & b) Huisgen's 1,3-dipolar cycloaddition and CuAAC reaction, respectively.

From the alkyne **149**, the (+)-disparlure-based fluorescent probe **15d** was synthesized (Scheme 4.8). The alkyne **149** and 6-FAM azide **173** were subjected to the copper-catalyzed alkyne-azide cycloaddition using THPTA (tris(benzyltriazolylmethyl)amine), sodium ascorbate and copper (II) sulphate in an equimolar mixture of water and tert-butanol, at room temperature. This reaction led to the 1,4-disubstitued triazole **15d** with 57% yield.

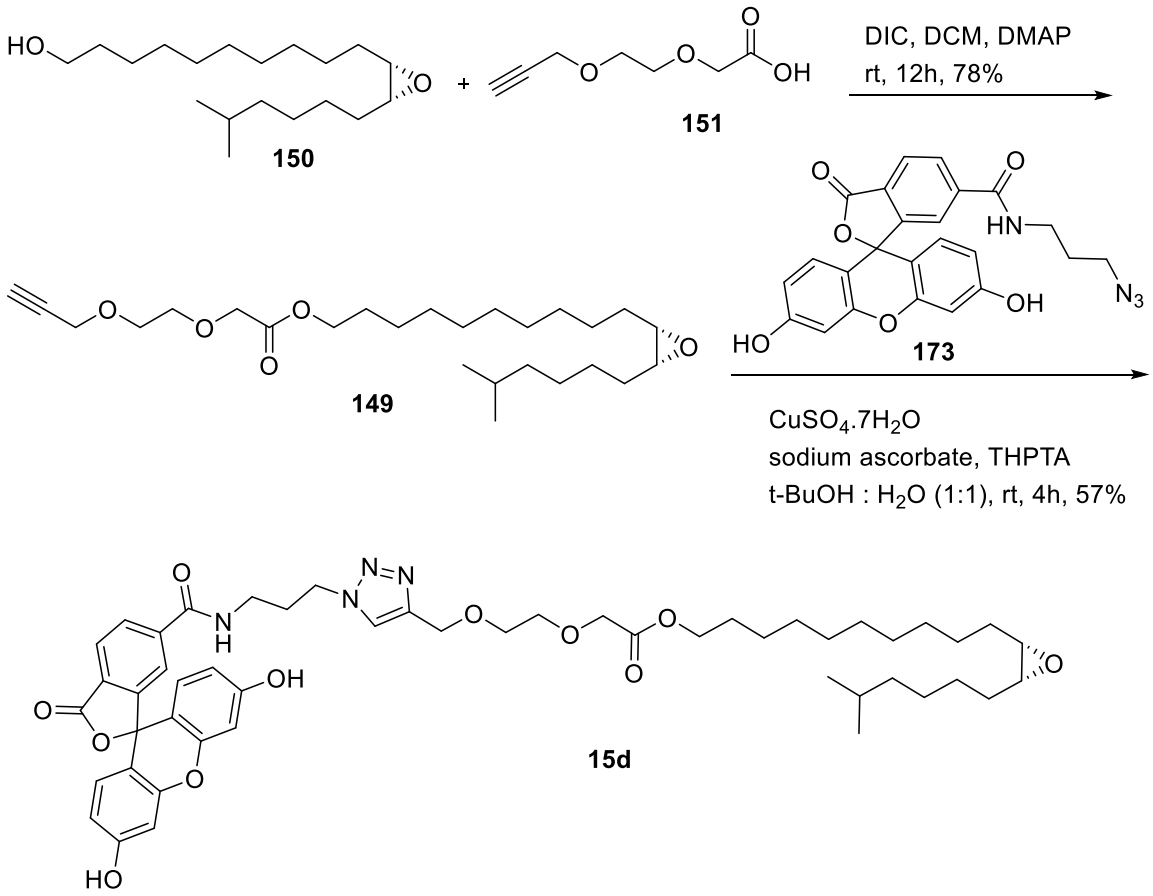

Scheme 4.8 Synthesis of 6FAM-tagged (+)-disparlure (15d).

4.2.5. Synthesis of 6FAM-tagged (-)-disparlure (*ent*-15d)

After the successful synthesis of (+)-disparlure fluorescent probe **15d**, we proceeded to synthesize the (-)-disparlure fluorescent probe *ent*-**15d** as shown in Scheme 4.10. The aldehyde **165** was treated with SOMO catalyst *ent*-**106** under asymmetric α-chlorination conditions to afford enantiopure α-chloroaldehyde *ent*-**166** (Scheme 4.9) (for enantiomeric excess, see Appendix C2). Then, α-chloroaldehyde *ent*-**106** was treated with acetylide anion which is generated from reaction between 5-methyl-1-hexyne **126**, to afford 1,2-*anti* chlorohydrin *ent*-**167**. Next, Mitsunobu inversion of the1,2-*anti* chlorohydrin *ent*-**167** with benzoic acid **129** afforded the desired 1,2-*syn* chloroester *ent*-**168** in 70% yield.

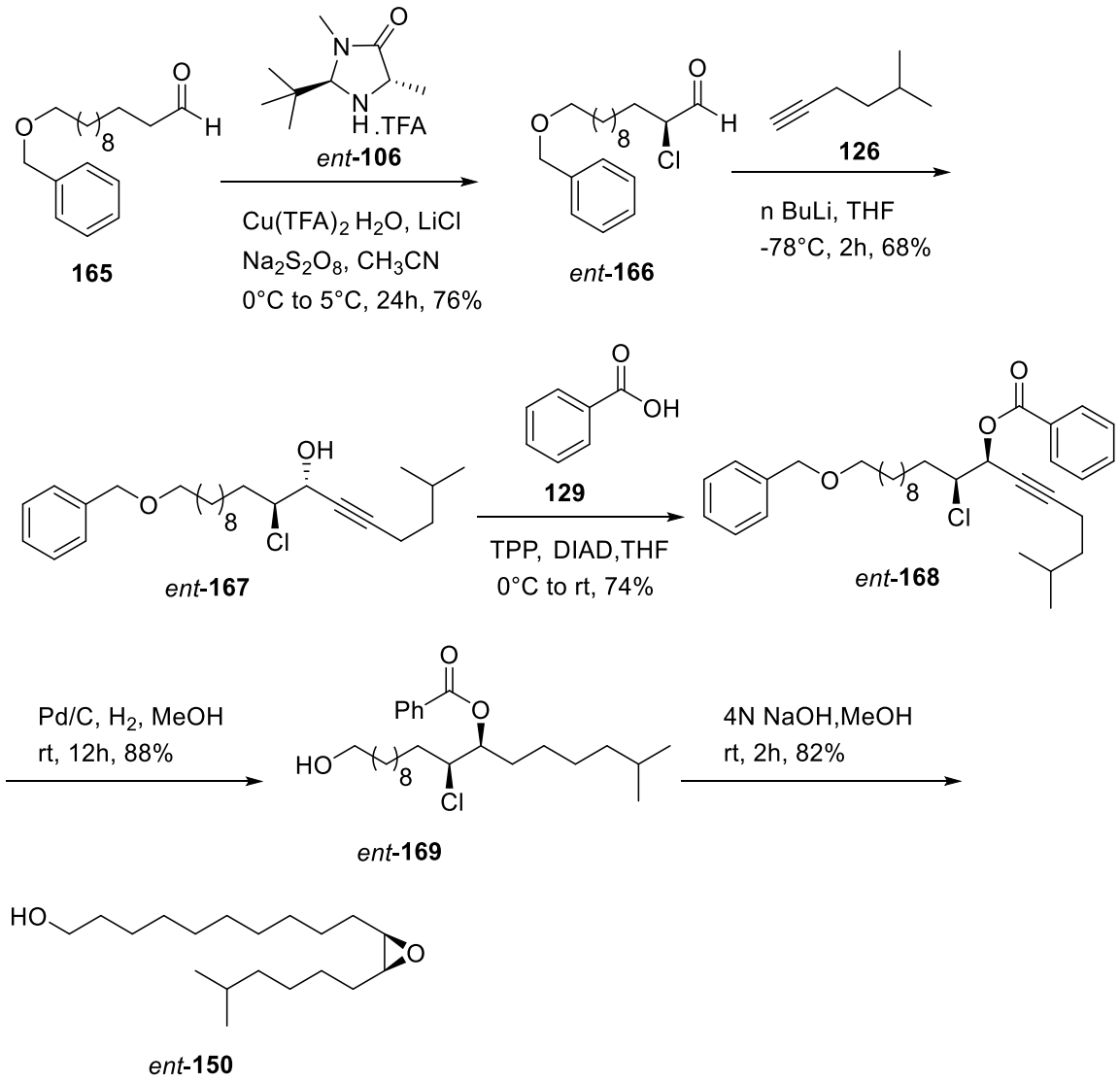

Scheme 4.9 Synthesis of key intermediate *cis*-epoxy alcohol *ent*-150.

Subsequently, 1,2-*syn* chloroester *ent*-**168** was subjected to the hydrogenation with Pd/C, followed by basic hydrolysis with 4N NaOH to afford epoxy alcohol *ent*-**150** in 82% yield (Scheme 4.9).

Next, Steglich esterification between the resulting epoxy alcohol *ent*-**150** and acid **151** in the presence of DIC and catalytic amount of DMAP yielded the required alkyne intermediate *ent*-**149**, a key precursor for the click reaction. Finally, the alkyne partner *ent*-**149** was coupled with 6-FAM azide **173** under click reaction conditions to deliver 6-FAM tagged (-)-disparlure *ent*-**15d** (Scheme 4.10).

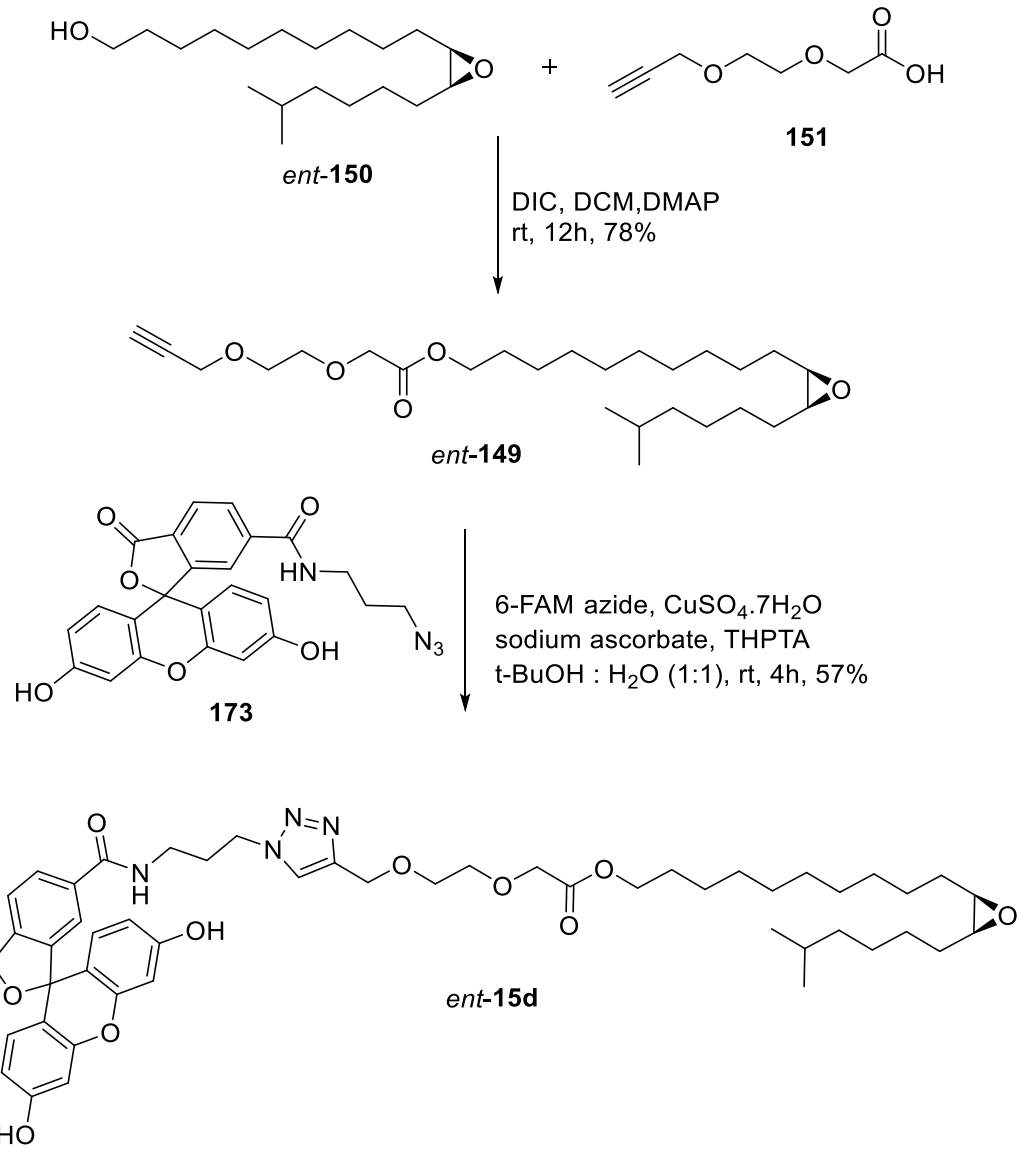

Scheme 4.10 Synthesis of 6FAM linked (-)-disparlure *ent*-15d.

4.2.6. Determination of enantiomeric excess of epoxy alkynes 149 and *ent*-149

In order to determine the enantiomeric excess for the target molecules 6-FAM (+)-disparlure (**15d**) and 6-FAM (-)-disparlure (*ent*-**15d**), the scalemic sample of epoxy alkyne **174** (Scheme 4.11) was prepared by mixing nearly equal amounts of enantiopure epoxy alkynes **149** and *ent*-**149** (Scheme 4.8 and 4.10). This scalemic epoxy alkyne **174** was later subjected to the click reaction using 4-bromophenylazide **175** as coupling partner to give corresponding scalemic triazole **176**. On the other hand, the enantiopure epoxy

alkynes **149** and *ent*-**149** were transformed to their corresponding triazoles **177** and *ent*-**177** using the same click reaction conditions as shown in Scheme 4.12.

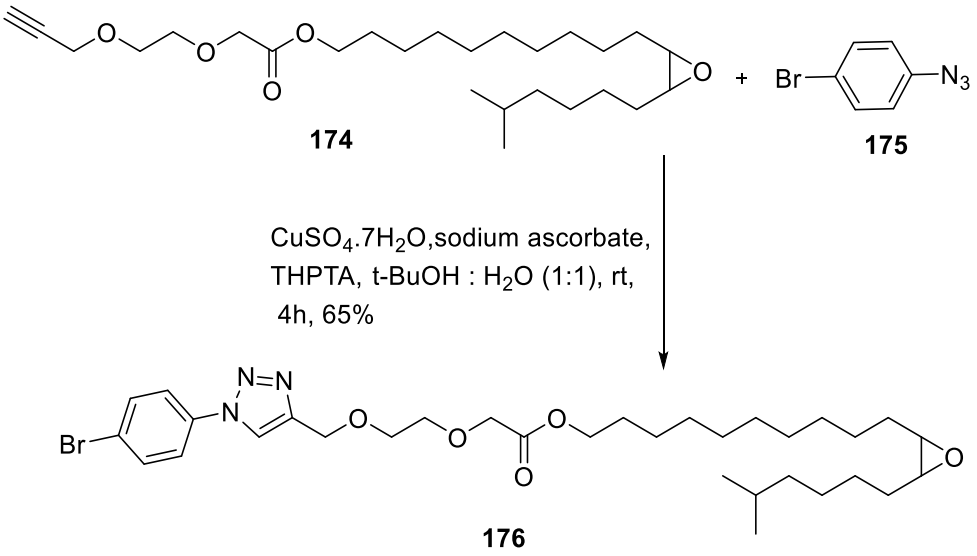

Scheme 4.11 Determination of enantiomeric excess by forming of phenyl triazole.

The resulting triazoles **176**, **177** and *ent*-**177** are UV absorbing compounds, which are amenable to separation by HPLC and detection by variable wavelength detector (VWD). The scalemic triazole **176** was separated on a chiral HPLC column (Phenomenex Lux 5µm Cellulose-2). The enantiopure triazoles **177** and *ent*-**177** were eluted at 5.55 min and 6.56 min, respectively (see Appendix C1). The enantiomeric excess of epoxy alkyne **149** and *ent*-**149** was determined to be greater than 98%.

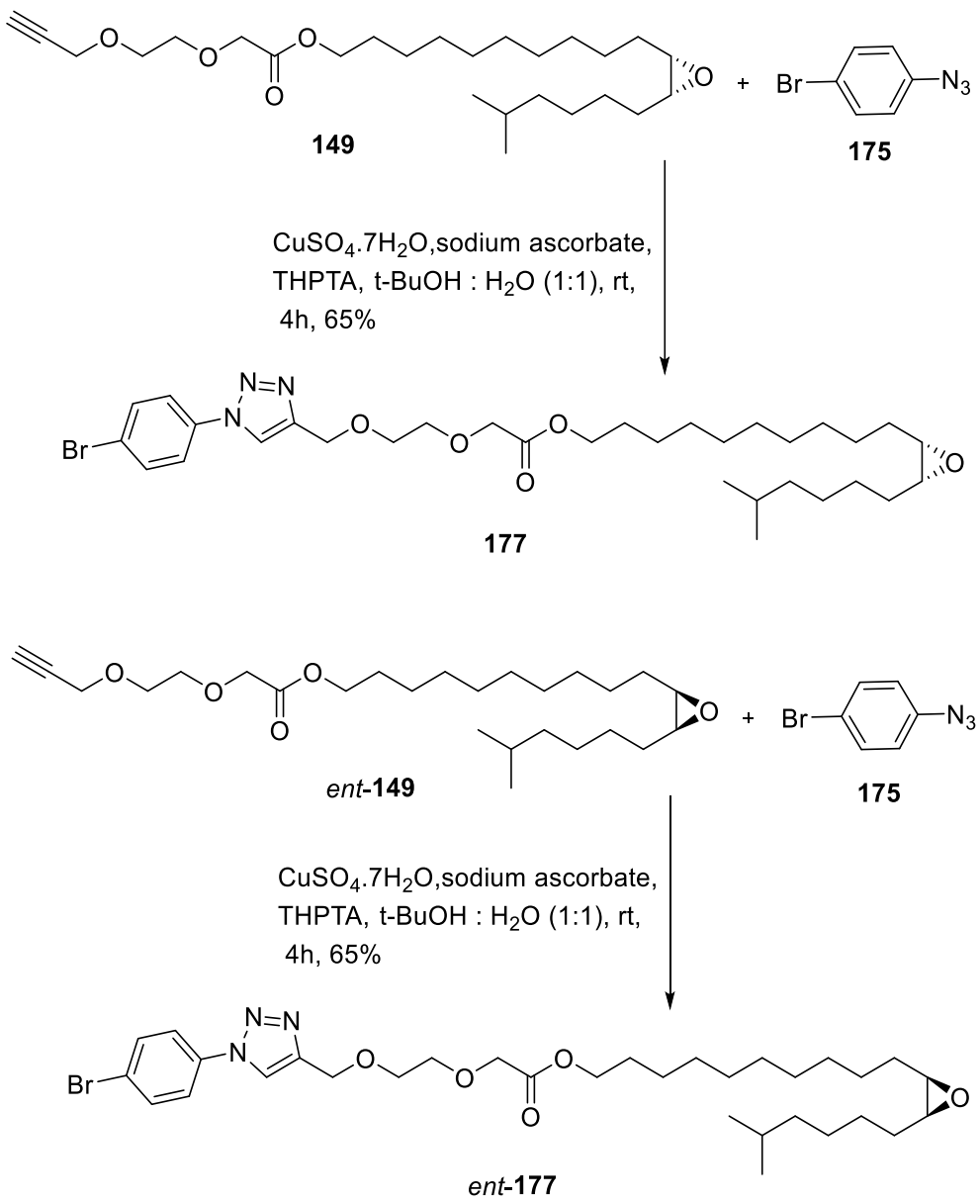

Scheme 4.12 Determination of enantiomeric excess of epoxy alkynes 149 and *ent*-149 by forming of phenyl triazoles.

4.2.7. Characterization of 6-FAM (+)-disparlure (15d)

The absorbance and emission spectra of 6-FAM (+)-disparlure **15d** were recorded in phosphate buffer (pH 8) and in 1-heptanol. A shift of 9 nm was noticed when comparing the excitation maximum of **15d** in 1-heptanol (λ_{max} 485) with that in phosphate buffer (λ_{max} 494). The molar absorptivity (ε) of **15d** was determined in 1-heptanol ($\varepsilon_{485\ nm}$ = 3021 M^{-1} cm^{-1}) and in phosphate buffer ($\varepsilon_{497\ nm}$ = (1.7 ± 0.03) × 10^4 M^{-1} cm^{-1}) from absorption spectra

recorded at different concentrations of **15d**. Compound **15d** shows maximum emission at 515 nm with a 30 nm Stokes shift and quantum efficiency of (Φ) 0.62 in 1-heptanol, whereas it exhibits maximum emission at 520 nm with a Stokes shift of 26 nm and quantum efficiency of (Φ) 0.86 in phosphate buffer (Table 4.2).

Table 4.2 Absorption and fluorescence properties of 6-FAM (+)-disparlure 15d in phosphate buffer (pH 8) and in 1-heptanol.

	λ_{ex} [nm]	λ_{em} [nm]	SS [nm]	$\varepsilon_{497\ nm}$ [M^{-1} cm^{-1}][b]	Φ[b]
Phosphate buffer (pH 8)	494	520	26	$(1.7 \pm 0.03) \times 10^4$	0.86 ± 0.02
1-heptanol	485	519	34	$(3.0 \pm 0.06) \times 10^3$	0.62 ± 0.08

SS, Stokes shift; ε, molar absorptivity; Φ, quantum yield. [b] Values are reported ± standard error (SE) of 3 replicates

4.2.8. Fluorescence emission of 6-FAM tagged disparlure enantiomers upon binding to *Ldis*PBPs

We have examined the binding affinity of 6-FAM tagged disparlure enantiomers **15d** and *ent*-**15d** to *Ldis*PBP1 and *Ldis*PBP2 in a binding assay, in which the change in fluorescence as the ligand binds to the protein is followed. When excited at 494 nm, fluorescent probes 6-FAM (+)-disparlure **15d** and 6-FAM (+)-disparlure *ent*-**15d** in phosphate buffer (pH 8) show a fluorescence emission with maximum at 520 nm. For example, Figure 4.3A shows the emission spectra of fluorescent probe **15d** in phosphate buffer and in presence of *Ldis*PBP1. We can observe an increase in fluorescence emission intensity as fluorescent probe **15d** concentration increases (Figure 4.3B).

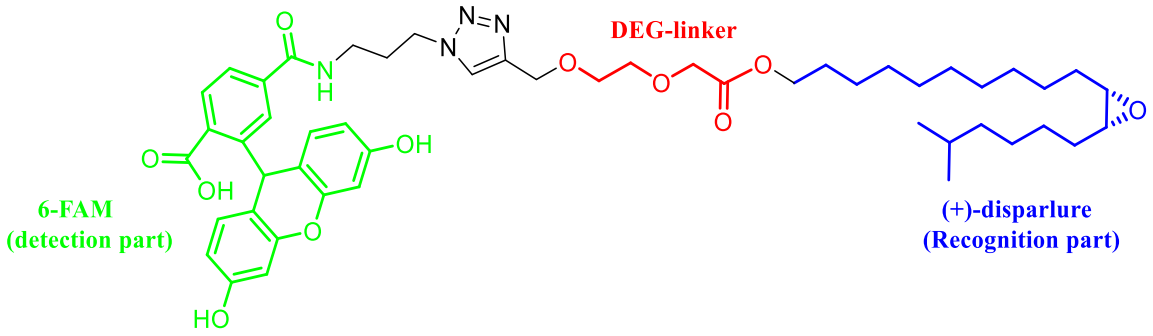

Figure 4.2 Structure of 6-FAM tagged (+)-disparlure 15d

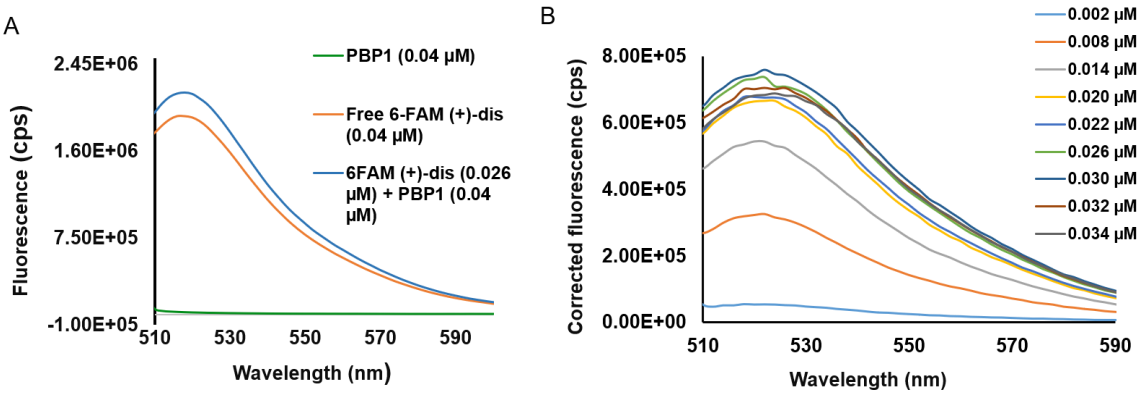

Figure 4.3 **A) 6-FAM (+)-disparlure 15d emission spectra. 1a bound to *Ldis*PBP1 was excited at 494 nm and its emission spectrum (blue trace) was recorded. The red trace shows the emission spectrum of 15d in buffer and the green trace shows the emission background obtained with only PBP in buffer. B) Fluorescence emission spectra were recorded with increasing doses of 6-FAM (+)-disparlure 15d, titrated into *Ldis*PBP1. The fluorescence emission from 6-FAM (+)-disparlure 15d / *Ldis*PBP1 complex determined by substracting the bottom trace (red) from the upper trace (blue) in part A.**

The increase in fluorescence intensity is a probable consequence of restricted rotation of the fluorophore upon binding to PBP. It has been reported that the fluorescent probes show weak fluorescence in buffer due to fast vibrational relaxation of singlet excited state through internal bond rotations (Haidekker and Theodorakis, 2007; Yu et al. 2015). When the fluorescent probe binds to the protein, a large fluorescence increase can be noticed due to restricted bond rotation of the fluorophore.

The increase in fluorescence intensity allows measurements of interaction between the probes and the proteins. Therefore, I titrated the *Ldis*PBP1 and *Ldis*PBP2 with 6-FAM (+)-disparlure **15d** and 6-FAM (-)-disparlure *ent*-**15d** to determine the dissociation constants (K_d) as a measure of the strength of binding. The smaller the K_d, the stronger the interaction. Figure 4.4 shows the isotherms for *Ldis*PBP/fluorescent disparlure enantiomer pair, for both of which we could detect significant binding affinities. The concentration dependence of fluorescent disparlure enantiomers binding to *Ldis*PBP can be described by a hyperbolic curve, as expected for one-site binding model (Figure 4.4). Based on those titration data, dissociation constants (K_d) were calculated. The novel fluorescent disparlure compounds appeared to be much stronger ligands for the *Ldis*PBP1 and *Ldis*PBP2, with dissociation constants in the nanomolar range (Figure 4.4, Table 4.3),

compared to the fluorescent probe NPN (which had K_d values 1.3 ± 0.3 µM for *Ldis*PBP1 and 8.6 ± 0.6 µM for *Ldis*PBP2 (Gong et al., 2010)).

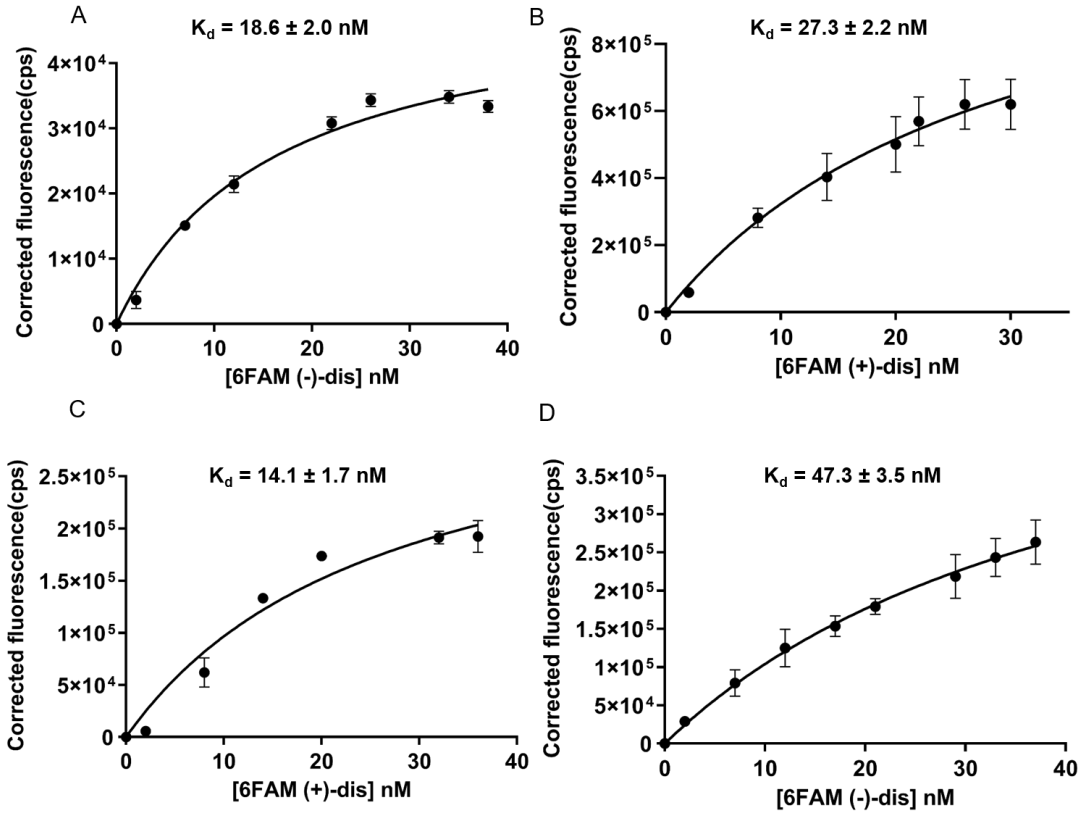

Figure 4.4 **Binding curves for 6-FAM tagged disparlure enantiomers binding with purified gypsy moth pheromone binding proteins (*Ldis*PBPs) at pH 8. A) & B) Titration of *Ldis*PBP1 with 6FAM (-)-disparlure *ent*-15d and (+)-disparlure 15d, respectively. B) & C) Titration of *Ldis*PBP2 with 6FAM (+)-disparlure 15d and (-)-disparlure *ent*-15d, respectively. Data represent the mean of three independent measurements. Standard errors are indicated by error bars.**

Table 4.3 Binding of 6-FAM disparlure enantiomers 15d and *ent*-15d to gypsy moth pheromone binding proteins *Ldis*PBP1 and *Ldis*PBP2.

Protein	Ligand	K_d (nM)[a]	Enantiomeric excess of the 15d and *ent*-15d[b]
*Ldis*PBP1	6-FAM (+)-disparlure **15d**	27.3 ± 2.2	98.4%
	6-FAM (-)-disparlure *ent*-**15d**	18.6 ± 2.0	98.8%
*Ldis*PBP2	6-FAM (+)-disparlure **15d**	14.1 ± 1.7	98.4%
	6-FAM (-)-disparlure *ent*-**15d**	47.3 ± 3.5	98.8%

[a] Values represent the mean ±S.E of 3 replicates. [b] For enantiomeric excess, see Section 4.2.6 and Appendix C1.

The results show that the 6-FAM tagged disparlure enantiomers **15d** and *ent*-**15d** bound to both *Ldis*PBP1 and *Ldis*PBP2 with nanomolar dissociation constants. When binding affinities of the *Ldis*PBPs for the 6-FAM tagged disparlure enantiomers were compared, *Ldis*PBP1 had significantly higher affinity towards 6-FAM (-)-disparlure whereas *Ldis*PBP2 bound the 6-FAM (+)-disparlure more strongly (Table 4.3). This is consistent with the body of previous equilibrium dissociation studies on *Ldis*PBP1 and *Ldis*PBP2 with (+)-disparlure (**15**) and (-)-disparlure (*ent*-**15**). *Ldis*PBP1 binds preferentially to (-)-disparlure (*ent*-**15**) whereas *Ldis*PBP2 prefers (+)-disparlure (**15**) (Plettner et al., 2000; Yu and Plettner, 2013). Furthermore, the remarkable selectivity of PBPs towards pheromones has been observed in systems from other moths, e.g. PBP2 and PBP3 from Chinese silk oak moth, *Antheraea pernyi* and the giant silk moth, *Antheraea polyphemus*. The PBP2 form these species preferentially binds to the aldehyde pheromone component, whereas PBP3 preferres the acetate pheromone component (Maida, et al., 2003). A difference in pheromone binding affinity has been observed for PBP3 from *Ostrinia furnacalis* which binds strongly to sex pheromone components E12-14:OAc and Z11-14:OAc, but PBP4 and PBP5 binds selectively to E12-14:OAc and Z11-14:OAc, respectively (Zhang et al., 2017). Similarly, selective sex pheromone binding by PBPs has been observed for PBP1 and PBP2 of the tea geometrid moth *Ectropis obliqua* (Sun et al., 2019; Yan et al., 2020) and PBP2 of the tobacco budworm *H. virescens* (Große-Wilde et al., 2007). This indicates that members from the gene family of insect odorant-binding proteins (OBPs), of which PBPs are a subset, can selectively bind different ligands. Our results of fluorescence binding assay suggest that *Ldis*PBPs selectively bind to disparlure enantiomers, which would be useful if they function as molecular filters in the process of pheromone perception.

4.2.9. Displacement of 6-FAM tagged disparlure by disparlure

The fluorescence of bound fluorescent probes 6-FAM (+)-disparlure **15d** and 6-FAM (-)-disparlure *ent*-**15d** were displaced by titration of non-labelled disparlure enantiomers (same enantiomer as the probe), to measure the binding affinities of disparlure enantiomers to *Ldis*PBP1 and *Ldis*PBP2.

In order to check whether fluorescent probes **15d** and *ent*-**15d** bind within the binding pocket of *Ldis*PBPs, we titrated the equimolar mixture of *Ldis*PBPs and fluorescent probes with disparlure and monitored fluorescence emission spectra at 520 nm. The fluorescence emission spectra of the mixture decreased in intensity upon addition of disparlure (Figure 4.5A). The decrease in fluorescence emission intensity suggests that the disparlure was displacing the fluorescent disparlure from the binding pocket of *Ldis*PBPs as it was titrated into the mixture. This decrease can be taken as a measure binding affinity of disparlure for *Ldis*PBPs.

The displacement constant (K_i) values determined for the disparlure enantiomers in competition with fluorescent probes **15d** and *ent*-**15d** binding to *Ldis*PBPs in a range between 132 and 211 nM. For *Ldis*PBP1, the (+)-disparlure and (-)-disparlure exhibit different fluorescent probe displacement properties with K_i values of 165 and 132 nM, respectively. In the case of *Ldis*PBP2, the best fluorescent probe competitor was found to be (+)-disparlure (K_i = 144 nM) (Figure 4.5 and Table 4.4). These K_i data show that the disparlure enantiomers can effectively displace the corresponding enantiomer of the fluorescent probe from the binding pocket. This assumption is further supported by molecular docking simulations (see below), which show that disparlure and the disparlure portion of 6-FAM disparlure are competing for the same binding site and closely interacting with the same residues (see Section 4.2.11). Furthermore, an estimate of the K_d values for the free disparlure enantiomers from the displacement data (see derivation below) gave K_d values (Table 4.4) within the range observed previously by other methods (*e*.*g*. Plettner et al., 2000). The enantiomer selectivity is also consistent with previous studies.

$$K_d \text{ (disparlure)} = K_i \times K_d \text{ (6-FAM-disparlure)}$$

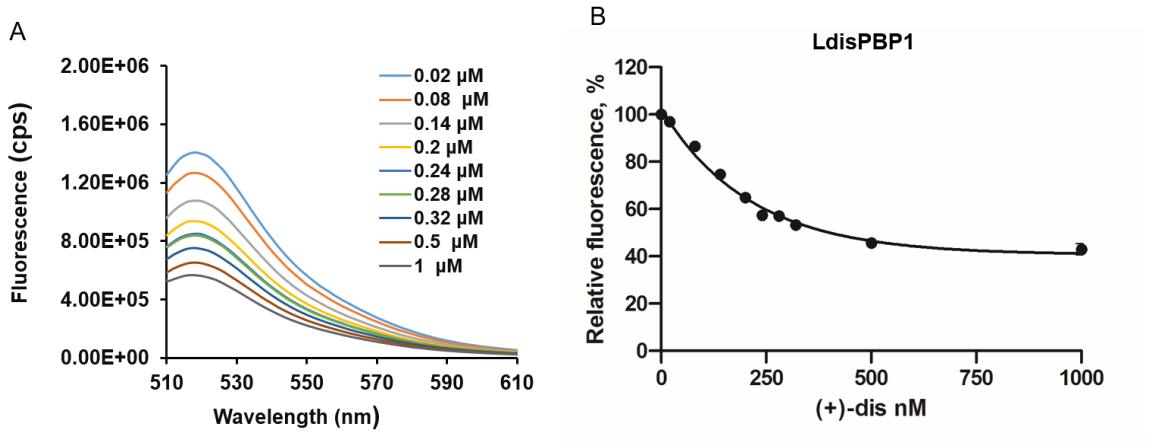

Figure 4.5 **A) Example of the decrease of 6-FAM (+)-disparlure/*Ldis*PBP1 florescence emission intensity at maximum (520 nm) at increasing concentrations of competitor (+)-disparlure (15). B) Competition of 6-FAM (+)-disparlure 15d binding to *Ldis*PBP1 (see Appendix C6 for competition binding curves of 6-FAM (-)-disparlure *ent*-15d with *Ldis*PBP1 and 6-FAM disparlure enantiomers with *Ldis*PBP2) Data shown are the mean of 3 independent measurements. Points represent means ± S. E of 3 replicates.**

Table 4.4 **Inhibition of 6-FAM disparlure binding to *Ldis*PBPs by disparlure enantiomers. Competitor concentrations causing a decay of fluorescence emission to half maximal intensity were determined as IC_{50} values from curves resulting from competition binding assays as shown in Figure 4.5.**

Protein	Competitor	IC_{50} (nM) [a]	K_i (nM) [b]	K_d (µM) [c]
*Ldis*PBP1	(+)-disparlure **15**	410 ± 4.6	165 ± 1.9	4.5 ± 0.4
	(-)-disparlure *ent*-**15**	414 ± 9.8	132 ± 2.3	2.5 ± 0.3
*Ldis*PBP2	(+)-disparlure **15**	556 ± 10	144 ± 2.6	2.0 ± 0.3
	(-)-disparlure *ent*-**15**	210 ± 4.8	211 ± 4.9	10.0 ± 6.4

[a] Values are the ± S. E of 3 replicates. [b] Calculated from the IC_{50} and dissociation constants of the ligand (see experimental section 4.4.21). [c] Calculated from the $K_i \times K_d$ (6-FAM-dis) = K_d (disparlure).

4.2.10. Rate constants of 6-FAM disparlure enantiomers with *Ldis*PBP1 and *Ldis*PBP2

To study the rates of association of the two *L. dispar* PBPs and the two enantiomeric fluorescent probes, stopped flow-kinetic fluorescence traces were obtained

by mixing *Ldis*PBP1 or *Ldis*PBP2 and 6-FAM (+)-disparlure **15d** or 6-FAM (-)-disparlure *ent*-**15d** at pH 8. Figure 4.6A shows the the kinetic fluorescence traces of fluorescent probe **15d** in phosphate buffer (pH 8) and in the presence of protein (*Ldis*PBP1). The fluorescence signal intensity of probe **15d** significantly increased in the presence of *Ldis*PBP1 compared to free ligand. We observed that this increase in fluorescence intensity was directly proportional to the ligand concentration (Figure 4.6B). To understand the order in protein and ligand of the association process, two series of stopped-flow experiments were done: 1) maintenance of constant concentration of the PBP and variation of the probe's concentration and 2) maintenance of constant concentration of the probe and variation of the protein's concentration. In all cases, the initial velocity of ligand binding to the protein, V_0, was determined from the best linear fit of the linear portion of the progress curves. An example of progress curves from an experiment with *Ldis*PBP1 (constant) and 6-FAM (+)-disparlure (variable) is shown in Fig. 4.6.

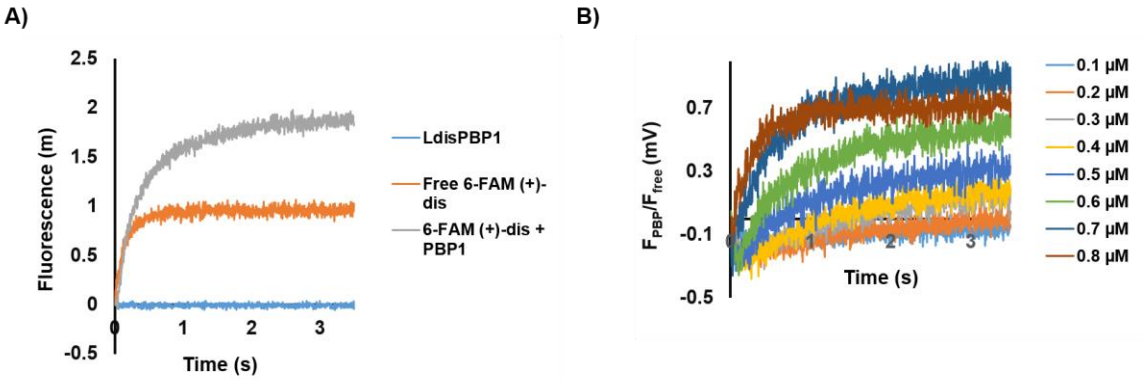

Figure 4.6 **A) Fluoresence traces of 6-FAM (+)-disparlure 15d with phosphate buffer and *Ldis*PBP1 B) Fluorescence traces of 15d association kinetics with *Ldis*PBP1. Varied concentrations of 15d was used to generate traces for protein shown in the plot. The final *Ldis*PBP1 concentartion per trace was 0.6 µM. The net fluorescence intensity increased as 15d concentration increased.**

The data of initial velocity and substrate concentration thus obtained were analyzed in two ways: 1) From experiments of type 1 (constant PBP, variable probe) plots of V_0 *vs*. ligand concentration (which were sigmoidal – see below) and double logarithm plots of the data from both types of experiments (to obtain the order in the probe and the protein, respectively). The second type of analysis is based on the expression of the rate of association shown in Equation 4.1.

$V_0 = k_{on} [P]_0^m [L]_0^n$…………………………………………….. (4.1)

Where V_0 = Initial velocity
k_{on} = association rate constant
P_0 = initial protein concentration, m = order of the protein
L_0 = initial ligand concentration, n = order of the ligand

Taking the logarithm, we get:

$\log V_0 = \log k_{on} + m\log[P]_0 + n\log[L]_0$…………………………..(4.2)

For the type 1 experiment (constant P and variable L), the slope of the line is n, the order in ligand, and the intercept is: $\log k_{on} + m\log[P]_0$. For the type 2 experiment (constant L and variable P), the slope of the line is m, the order in protein, and the intercept is: $\log k_{on} + n\log[L]_0$.

In the first analysis, initial association rates plotted versus the concentration of fluorescent probe and the association binding fit a sigmoidal curve. In all the cases, we observed a saturable curve, in which the rate of binding (as detected through an increase in fluorescence) was clearly dependent on the concentration of fluorescent probe at lower probe concentrations and independent of the probe’s concentration at higher concentrations (Figure 4.7).

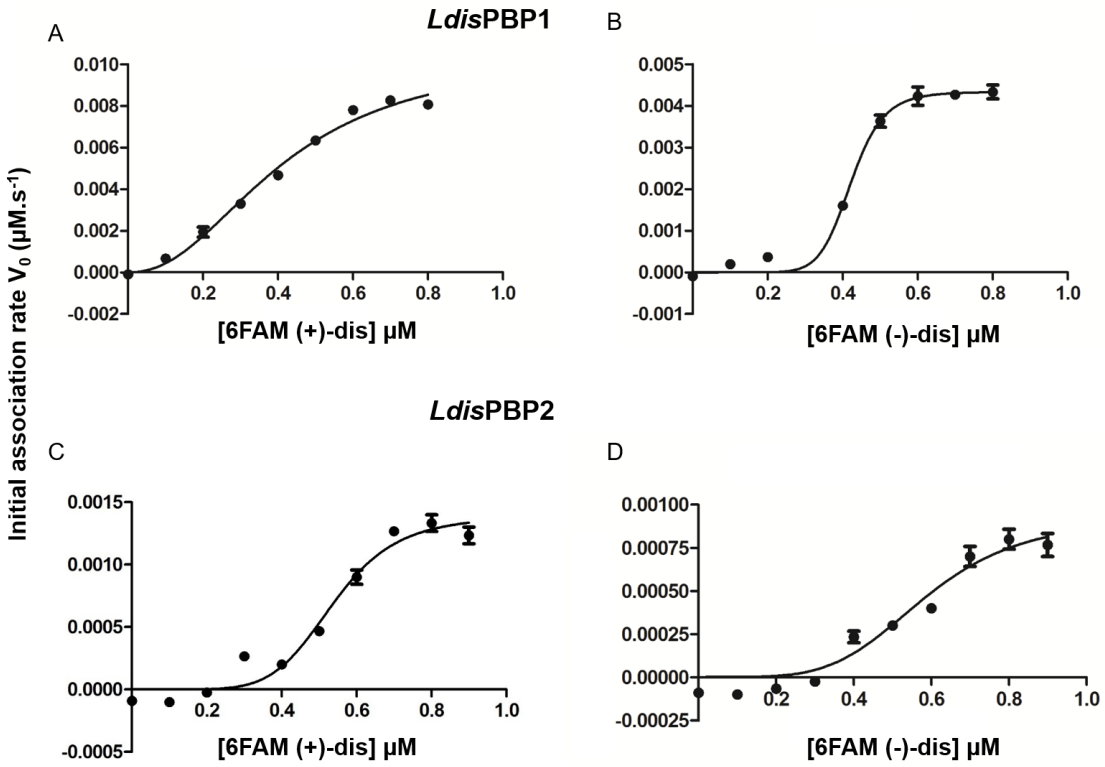

Figure 4.7 **Binding association rates of *Ldis*PBPs with 6-FAM disparlure enantiomers. The plot of initial velocity V_0 versus L_0 when the protein concentration was 0.6 μM and the fluorescent ligand concentration was varied between 0 and 0.8 μM. V_{max} is the maximum rate of flurescent ligand binding at ligand saturation. Curves are fitted to the sigmoidal equation (4.3) (A, *Ldis*PBP1 and 6-FAM (+)-disparlure; B, *Ldis*PBP1 and 6-FAM (-)-disparlure; C, *Ldis*PBP2 and 6-FAM (+)-disparlure; D, *Ldis*PBP2 and 6-FAM (-)-disparlure).Data represents the mean of at least three independent experiments, each performed in triplicate.**

With increasing the 6-FAM disparlure concentration (0.1-0.8 μM, 0.6 μM *Ldis*PBPs), the initial rates of the binding reaction increased. We observed a sigmoidal relationship between the initial rate and ligand concentration (Figure 4.7). The initial rates, V_0, were fit into a nonlinear allosteric kinetic model. Fitting of these initial rates allowed calculation of V_{max} and K':

$$V_0 = V_{max}[L]^h/(K' + [L]^h) \quad \text{.....(4.3)}$$

Where V_0 is the initial velocity obtained from the family of progress curves from the type 1 experiment (constant P and variable L), h is the Hill coefficient, a measure of the steepness of the curve. When h = 1, the equation is the same as the Michaelis-Menten

formula for enzyme kinetics without allostery. K' is the concentration of L at which half-maximal velocity is reached (*i.e*. the K_m) raised to the power of h, $K' = K_m^h$. The maximal velocity, V_{max} is the rate constant of the rate-limiting step, k_{on}, multiplied by the concentration of protein, $V_{max} = k_{on}[P]$. The saturability of V_0 in all four cases (Figure 4.7) indicates that the protein and ligand association process observed in the experiment must have two steps: a rapid, reversible first step and a rate-limiting second step, as shown below:

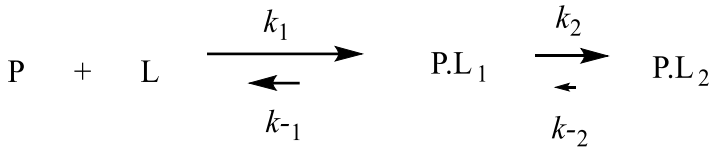

In this model, the protein and ligand associate to form a first complex, $P.L_1$ *e.g.* with the ligand bound at an external binding site that is more accessible than the internal one, and decay to a second complex, $P.L_2$, *e.g.* with the ligand bound internally. The formation of $P.L_1$ is rapid and reversible, whereas the formation of $P.L_2$ is slower and much less reversible. The net formation of $P.L_2$ at saturation is the constant for this rate-limiting step (k_{rla}) x the concentration of $P.L_1$, which equals the rate of formation of $P.L_2$ from $P.L_1$ minus its rate of backreaction to $P.L_1$ (Equation 4.4):

$$V_{max} = k_{rla} \times [P.L_1] = k_2[P.L_1] - k_{-2}[P.L_2] \quad \text{.....(4.4)}$$

Because we are measuring initial rates, one can assume that the amount of $P.L_2$ that can react back to $P.L_1$ is negligible, so equation 2 is simplified to $V_{max} \approx k_2[P.L_1]$. The rate constant k_{on} is the overall rate constant at saturation, from P to $P.L_2$, and this should be dominated by the rate-limiting constant, k_2.

From the V_{max}, we obtained the association rate constant for the rate-limiting association step k_{on} for the fluorescent probes **15d** and *ent*-**15d**. From the slope of plots (Figure 4.8), the association order for the fluorescent probe and protein was obtained. The order in both protein and ligand was found to be 1 within limits of error for *Ldis*PBP1 (Table 4.5). This result can be interpreted as there being one protein molecule and one ligand molecule interacting at the rate-limiting step. This, in turn, means that the positive cooperativity in the rate of association (Fig. 4.8) does not come from multiple protein molecules interacting and affecting the rate of association. One possibility is that the protein needs to change

conformation after the initial binding step, to allow the hydrophobic pheromone chain to diffuse into the internal binding site. This is consistent with the previous kinetic studies, suggesting that pheromone binding at the PBP internal site is multi-step process that proceeds via an external site (Gong et al., 2009; 2010).

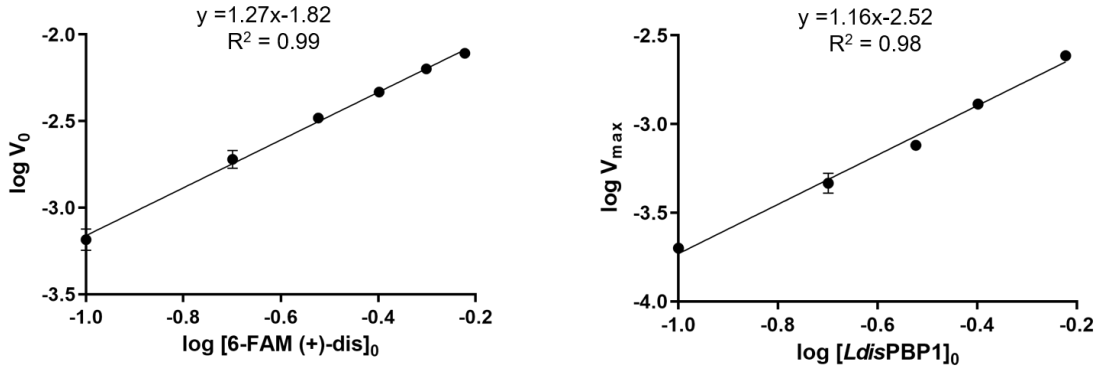

Figure 4.8 The association orders for 6-FAM (+)-disparlure 15d and *Ldis*PBP1. A) the plot of $logV_0$ verses $log[L]_0$ when the protein concentration was kept constant at 0.6 µM and the ligand concentration was varied (0.1-0.8 µM). B) the plot of log V_{max} against log P_0 when the ligand concentration was held constant 0.6 µM and the protein concentration was varied (0.1-0.8 µM). The slopes of plot A and B give the association order in 6-FAM (+)-disparlure 15d and *Ldis*PBP1, respectively.

Using fluorophore tagged disparlure enantiomers 6-FAM (+)-disparlure **15d** and 6-FAM (-)-disparlure *ent*-**15d** as fluorescent probes, the association and dissociation rate constants between disparlure enantiomers and *Ldis*PBPs were determined. Figure 4.6B and Appendix C13 and C14 show the association fluorescence traces of 6-FAM (+)-disparlure **15d** and 6-FAM (-)-disparlure *ent*-**15d** with *Ldis*PBP1, respectively. The association fluorescence traces of *Ldis*PBP2 with 6-FAM disparlure enantiomers are shown in Appendix C15 and C16. The fluorescence signals increased proportionally as 6-FAM disparlure concentration increases. Global fitting of these fluorescence traces permitted estimation of rate constant for the rapid first step.

Although dissociation rate constant (k_{off}) values can be obtained from association fitting, a separate kinetic experiment was carried out to determine the dissociation rate constant between fluorescent probe and *Ldis*PBPs. In this experiment, the fluorescent probe-*Ldis*PBP complex was allowed to form by incubating fluorescent probe **15d** or *ent*-**15d** with *Ldis*PBP1 or *Ldis*PBP2 for 45 minutes followed by dilution to promote fluorescent

probe dissociation and monitoring a decrease in the fluorescence of the probe with time. Global fitting of the fluorescence traces to a first-order exponential decay allowed calculation of dissociation rate constants, which are shown in the table 4.5. Our association and dissociation rate constants for fluorescent probe binding and release give dissociation constants ($K_d = k_{off}/k_{on}$, Table 4.5) that are ~10-15 times higher than the values derived from saturation binding assay. However, the selectivity between these fluorescent probes was preserved. That is, *Ldis*PBP1 prefers 6-FAM (-)-disparlure *ent*-**15d** and *Ldis*PBP2 binds selectively to 6-FAM (+)-disparlure **15d**, either from saturation binding assay or as shown from the derived association and dissociation rate constants.

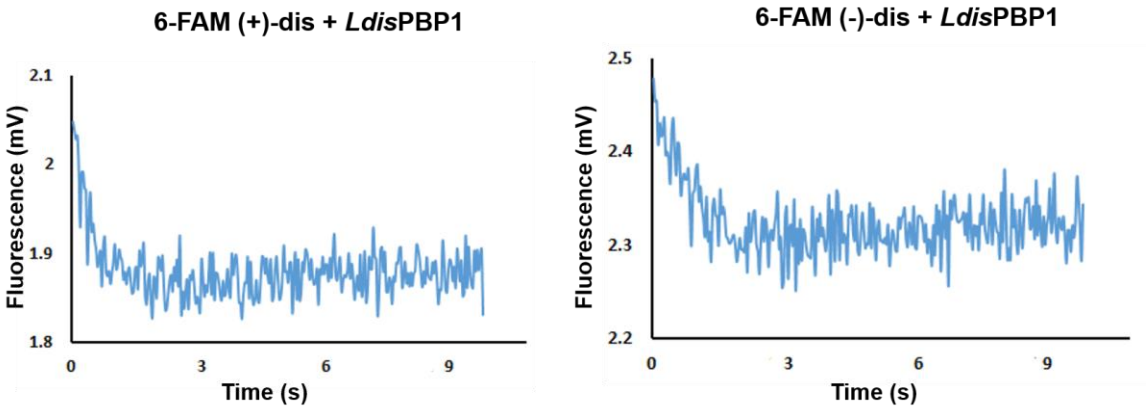

Figure 4.9 Fluorescence traces of 6-FAM disparlure enantiomers dissociation kinetics with *Ldis*PBP1. Concentrations of 6-FAM disparlure and *Ldis*PBP1 were 250 nM, respectively.

The association rate constant for rate-limiting step k_2 for fluorescent probes **15d** and *ent*-**15d** ranged from 1.6×10^{-3}-8.8×10^{-3} s^{-1} (Table 4.5). The small rate constant value was from 6-FAM (+)-disparlure **15d** and *Ldis*PBP1 whereas the large k_{on} value was calculated for *Ldis*PBP1 and 6-FAM (-)-disparlure *ent*-**15d**. Interestingly, significant differences in association rate values were noticed between 6-FAM disparlure enantiomers with *Ldis*PBPs. For *Ldis*PBP1, 6-FAM (-)-disparlure *ent*-**15d** has significantly greater rate constant compared to 6-FAM (+)-disparlure **15d**. For *Ldis*PBP2, 6-FAM (+)-disparlure **15d** has larger k_{on} compared to its enantiomer **15d**. These k_{on} values indicate that *Ldis*PBP1 binds faster to (-)-disparlure, whereas *Ldis*PBP2 binds faster to (+)-disparlure.

Table 4.5 Summary of 6-FAM disparlure-binding kinetics and thermodynamics for *Ldis*PBP1 and *Ldis*PBP2.

Measurement		Ligand	
		6-FAM (+)-disparlure 15d	**6-FAM (-)-disparlure *ent*-15d**
K_d (nM)	*Ldis*PBP1	27.3 ± 2.2	18.6 ± 2.0
	*Ldis*PBP2	14.1 ± 1.7	47.3 ± 3.5
V_{max} (μM/s)	*Ldis*PBP1	$(1.0 \pm 0.24) \times 10^{-3}$	$(5.3 \pm 0.44) \times 10^{-3}$
	*Ldis*PBP2	$(1.6 \pm 0.12) \times 10^{-3}$	$(0.9 \pm 0.10) \times 10^{-3}$
k_1($M^{-1}s^{-1}$)[a]	*Ldis*PBP1	$(1.4 \pm 0.10) \times 10^{6}$	$(3.0 \pm 0.09) \times 10^{6}$
	*Ldis*PBP2	$(2.9 \pm 0.14) \times 10^{6}$	$(1.6 \pm 0.07) \times 10^{6}$
k_2 (s^{-1})	*Ldis*PBP1	$(2.6 \pm 0.40) \times 10^{-3}$	$(8.8 \pm 0.74) \times 10^{-3}$
	*Ldis*PBP2	$(2.7 \pm 0.20) \times 10^{-3}$	$(1.6 \pm 0.10) \times 10^{-3}$
k_{off} (s^{-1})	*Ldis*PBP1	$(5.3 \pm 0.29) \times 10^{-1}$	$(4.8 \pm 0.1) \times 10^{-1}$
	*Ldis*PBP2	$(7.0 \pm 0.66) \times 10^{-1}$	$(8.2 \pm 1.2) \times 10^{-1}$
K_d (nM)[a]	*Ldis*PBP1	379 ± 10	155 ± 7.0
	*Ldis*PBP2	236 ± 8.0	338 ± 13
n[b]	*Ldis*PBP1	1.23 ± 0.21	1.07 ± 0.08
m[c]		1.17 ± 0.08	1.30 ± 0.05
n[b]	*Ldis*PBP2	N.D.	N.D.
m[c]		N.D.	N.D.

[a] $K_d = k_{off}/k_{on}$ [b] n = order of ligand, [c] m = order of protein. N.D. = not determined (due to machine non-availability)

The k_{off} values ranged from 4.8×10^{-1}-8.2×10^{-1} s^{-1}. A significantly large k_{off} value was obtained for 6-FAM (-)-disparlure **15d** with *Ldis*PBP2. Interestingly, a small k_{off} value was observed for 6-FAM (-)-disparlure **15d** with *Ldis*PBP1. A significant difference in the k_{off} was observed between 6-FAM (+)-disparlure **15d** and 6-FAM (-)-disparlure *ent*-**15d** with *Ldis*PBP1 and *Ldis*PBP2. 6-FAM (+)-disparlure **15d** has greater k_{off} compared to 6-FAM (-)-disparlure *ent*-**15d** with *Ldis*PBP1, whereas 6-FAM (-)-disparlure *ent*-**15d** has higher k_{off} value compared to 6-FAM (+)-disparlure **15d** with *Ldis*PBP2. These k_{off} values suggest that the dissociation rate of 6-FAM (+)-disparlure **15d** with *Ldis*PBP1 and 6-FAM

(-)-disparlure *ent*-**15d** with *Ldis*PBP2 are faster than their respective enantiomer. These kinetic rate constants (k_{on} & k_{off}) and equilibrium binding constants (K_d) suggest that *Ldis*PBP1 interacts with disparlure enantiomers differently from *Ldis*PBP2. *Ldis*PBP1 preferentially binds to the (-)-disparlure (*ent*-**15**), whereas *Ldis*PBP2 prefers the (+)-disparlure. This is consistent with previous kinetic and equilibrium binding studies (see below).

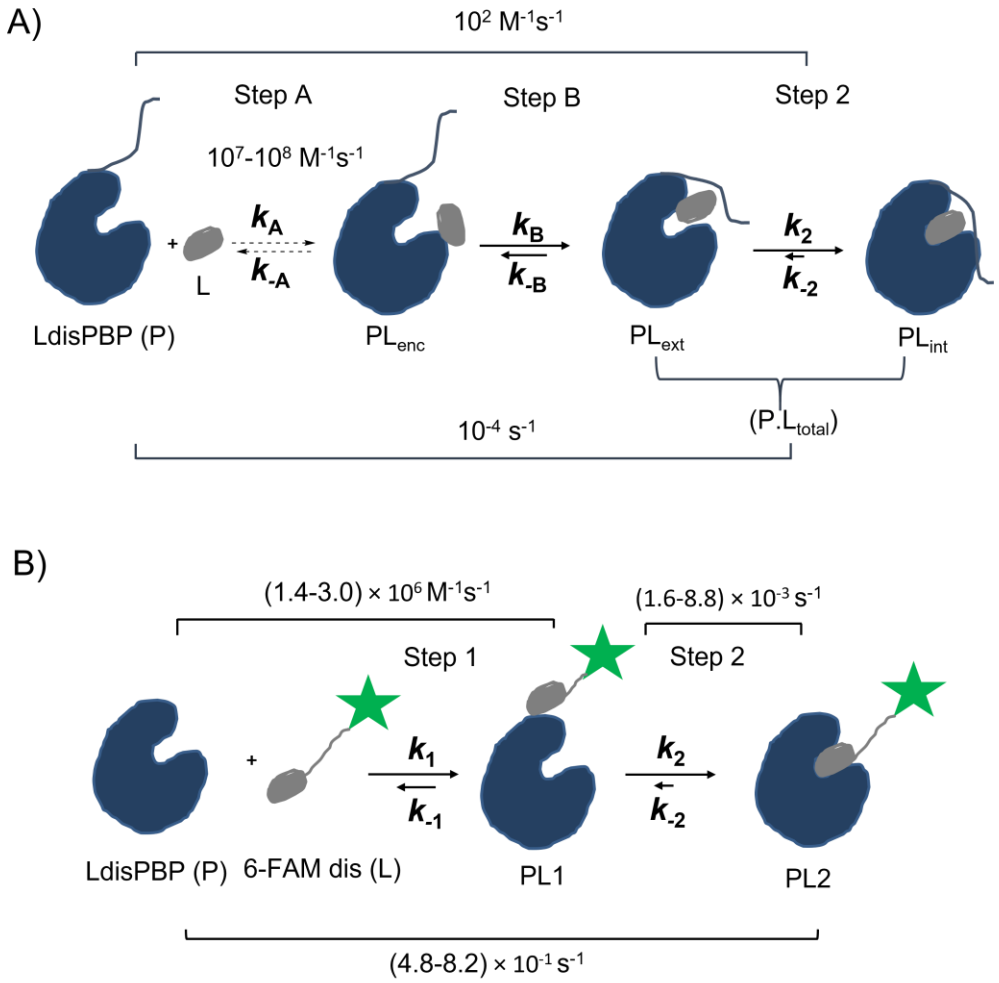

Figure 4.10 **A multi-step mechanism of ligand binding to *Ldis*PBPs (*Ldis*PBP1 and *Ldis*PBP2) proposed by Plettner and co-workers ((Gong et al., 2009, 2010). A two-step kinetic model proposed based on assocation and dissociation kinetics of *Ldis*PBPs with 6-FAM disparlure enantiomers.**

Previous studies on the kinetics of association of disparlure enantiomers (**15** and *ent*-**15**) with dansylated *Ldis*PBP2 revealed saturable binding kinetics, which led the

authors to infer that a multi-step interaction process for ligand association, with a fast initial step, followed by a slow rate-determining step, was taking place (Figure 4.10A) (Gong et al. 2009). A very rapid association step was also observed, within the first few seconds of the progress curves. However, the kinetic constant for this step could not be determined with the method used in that study. The results show that *Ldis*PBP2 binds (+)-disparlure (**15**) and (-)-disparlure (*ent*-**15**) in a fast step, followed by a slow step to the final form detected in the experiment. The rate-determining step (slow step) was the one identified to be consistent with selectivity of *Ldis*PBP2 for (+)-disparlure (**15**) over (-)-disparlure (*ent*-**15**) (Gong et al., 2009).

In the second kinetic experiment with *Ldis*PBP1 or *Ldis*PBP2 and the fluorescent reporter 1-NPN, the initial association step was divided into two sub-steps: a diffusion-controlled step that involves ligand colliding with *Ldis*PBP, and which results in an encounter complex ($P.L_{enc}$) (Figure 4.10A). A slower decay of the encounter complex leads to a new protein-ligand complex, interpreted to be the externally bound ligand complex ($P.L_{ext}$) (Gong et al.,2010). In the kinetic study, it was extremely difficult to observe internalization of the fluorescent reporter (1-NPN **82**) because of the way in which 1-NPN reports on binding. When 1-NPN shifts from a polar environment (aqueous) to non-polar environment such as the surface of a PBP or its binding pocket, its fluorescence increases significantly. In the kinetic study, the authors observed an increase in fluorescence of 1-NPN upon formation of the $P.L_{enc}/P.L_{ext}$ complex. However, they did not observe a change in 1-NPN fluorescence upon internalization, so they could not monitor the slow binding step seen in the earlier study.

From these kinetic studies, The authors observed a slow association of *Ldis*PBP2 to disparlure enantiomers. They frequently noticed a non-zero physical quantity which suggested some rapid kinetic behaviour of *Ldis*PBP2. However, they were unable to resolve this kinetic behaviour with the experimental time scale (≤5s). Because of the limitations in this experiment and faster kinetic behaviour of *Ldis*PBP1, they studied a fast association of *Ldis*PBP2 to ligand as well as association kinetics of *Ldis*PBP1 using the fluorescent probe 1-NPN **82**. In this kinetic experiment, the authors observed a fast association of ligand to the *Ldis*PBPs. However, they did not observe a slow association step (rate determining step). From these two kinetic studies, the authors proposed a multi-step binding model for *Ldis*PBP-pheromone association (Figure 4.10A). The major drawback of using 1-NPN **82** to probe the PBP-ligand association and dissociation

processes is that 1-NPN is non-natural ligand. Therefore, I have studied the association and dissociation kinetics between *Ldis*PBP1 and *Ldis*PBP2 and disparlure enantiomers using fluorophore-tagged disparlure enantiomers 6-FAM (+)-disparlure **15d** and 6-FAM (-)-disparlure *ent*-**15d** as fluorescent reporters. In this study, I have observed a fast association of 6-FAM disparlure to *Ldis*PBPs is then followed by a slow association (Figure 4.10B). Both *Ldis*PBP1 and *Ldis*PBP2 showed different association modes at the initial encounter step as well as at the slow step (rate-determining step). The fast process observed for the *Ldis*PBP1 with 6-FAM (-)-disparlure *ent*-**15d** and *Ldis*PBP2 with 6-FAM (+)-disparlure **15d**. This observation is consistent with the slow step (Figure 4.10B). The overall association process is consistent with the disparlure binding preferences for *Ldis*PBPs, as described in section 4.2.8. The present kinetic study with fluorescent disparlure enantiomers is consistent with the *Ldis*PBP2 having slower overall association than *Ldis*PBP1 (Gong et al., 2009; 2010).

Previous dissociation kinetic studies between *Ldis*PBP2 and disparlure enantiomers suggested that the disparlure enantiomers dissociate from *Ldis*PBP2 with extremely slow and similar kinetics (for (+)-disparlure (**15**) and (-)-disparlure (*ent*-**15**) were 4.7×10^{-4} s^{-1} and 5.0×10^{-4} s^{-1}, respectively) (Gong et al., 2009). However, the slight discrimination between (+)-and (-)-disparlure was preserved. In that study, the authors could not measure the association/dissociation rate constants for *Ldis*PBP1 with disparlure enantiomers, because the *Ldis*PBP1 interacts with the ligands faster than *Ldis*PBP2. Using the 6-FAM-tagged disparlure enantiomers as fluorescent robes, I have measured the dissociation rate constant (k_{off}) between *Ldis*PBPs (*Ldis*PBP1 and *Ldis*PBP2) and disparlure enantiomers (Table 4.5). I have observed the difference in dissociation rates between *Ldis*PBPs and 6-FAM disparlure enantiomers. The slower off-rates were noticed for 6-FAM (-)-disparlure *ent*-**15d** and 6-FAM (+)-disparlure **15d** with *Ldis*PBP1 and *Ldis*PBP2, respectively. These slower off-rates suggest that the *Ldis*PBP1 binds 6-FAM (-)-disparlure *ent*-**15d** more strongly at equilibrium than 6-FAM (+)-disparlure **15d**, and *Ldis*PBP2 is the opposite. This is consistent with the previous equilibrium studies (Gong et al., 2009; Plettner et al., 2000).

Rapid pheromone detection and inactivation is required for the orientation of moth flights towards the pheromone source (Leal, 2004). It has been proposed that the hydrophobic pheromone requires transport by the PBP through the aqueous lymph and release of the pheromone at the dendritic membrane, which was thought to be induced by

pH-dependent, rapid conformational change (Wojtasek and Leal, 1999; Damberger et al., 2000; Horst et al., 2001; Lee et al., 2002; Damberger et al., 2007; Xu et al., 2011; Luccio et al., 2013). These authors suggested that the C-terminal region of PBP forms an α-helix at low pH, which occupies the binding pocket. Therefore, the formed α-helix is proposed to be responsible for the release of the pheromone near the dendritic membrane in on the side of the sensillum lymph, where the pH is assumed to be lower than in the bulk sensillum lymph. However, the pH of sensillum lymph from gypsy moth sensilla has been tested and found to be approximately 8.5, as discussed in the introduction chapter (Nardella et al., 2015). In addition, the change in pH near dendritic membrane has been estimated to be very small (~ 0.5-1 pH unit, Kowcun et al., 2001), and this small pH change is not sufficient to cause conversion of a moth PBP from one form to an another. An alternative picture of pheromone transport and release emerges from kinetic studies, such as the ones described here. The rapid association of pheromone and PBP at an external site on the protein could serve a transport function, whereas dissociation would serve the release function. Pheromone molecules could bounce between PBP, fatty acid micelles and aqueous medium in a random walk as they diffuse through the lymph to the receptors. It has been demonstrated that lymph is a complex emulsion with high levels of fatty acid salts at pH 8 or higher (Nardella et al., 2015). The fatty acid salts can act like soap and help to emulsify hydrophobic odorants. Thus, solubilization and transport of odorants is not the only role of OBPs in olfactory sensilla. Furthermore, the OBP-ligand complex diffuses much more slowly than an odorant by itself, due to the much larger molecular mass of the complex. Thus, OBPs should also have functions other than odorant transport through aqueous compartments.

Because most pheromones are hydrophobic, they do not easily cross the hydrophilic sensillum lymph and reach the pheromone receptors on the dendritic membrane of pheromone sensory neurons. It has been believed that PBPs solubilize the hydrophobic pheromones and transport them across the hydrophilic lymph to pheromone receptors on the dendritic membrane of pheromone sensory neurons (K. Kaissling, 1986; K.-E. Kaissling, 2013; Vogt & Riddiford, 1981). It has also been suggested that the PBPs participate in scavenging of excess pheromone molecules near the dendritic membrane to prevent the pheromone sensory neurons from saturating (N. Honson et al., 2003). However, It has also been proposed that the sensillum lymph fluid contains large amounts of fatty acids and these can increase the diffusion of hydrophobic pheromones in to

aqueous lymph (Nardella et al., 2015). The authors demonstrated that these fatty acids promote the pheromone interactions with the PBP. The transporter and scavenger functions of PBPs were studied by Terrado et al. using the disparlure and their oxa and thia analogues (Terrado et al., 2017). The authors measured the equilibrium dissociation constant (K_d) for the disparlure and their analogues with *Ldis*PBPs and EAG (electroantennogram) responses of male gypsy moth antennae to these compounds. They observed a negative correlation between K_d values and EAG response lag times, which suggested both transporting and scavenging functions of PBPs. In addition, the positive correlation between K_d values and depolarization rates and the negative correlation between K_d values and repolarization rates suggest the transporting and scavenging functions of PBPs, respectively.

In this kinetic study, the first step appears to be connected to the pheromone binding at an external site of *Ldis*PBP, through a rapid interaction between pheromone and *Ldis*PBP. From the above kinetic model (Figure 4.10), the slow step appears to be crucial for accommodating the cognate ligand within the internal binding site of the PBP. Internal binding produces a kinetically stable-pheromone-PBP complex. We studied the binding interactions between *Ldis*PBPs and disparlure enantiomers by ^{2}H NMR using deuterium labelled disparlure enantiomers (see Chapter 3). In this study, the chemical shift changes (free vs bound disparlure), spin-lattice relaxation (T_1) and spin-spin relaxation (T_2) times of deuterium atoms of disparlure enantiomers showed that the binding of disparlure enantiomers to *Ldis*PBP1 differs from binding to *Ldis*PBP2. The results from NMR studies are correlated with the results from docking simulations (docking models of disparlure bound to one internal site and multiple external sites of *Ldis*PBP1 and *Ldis*PBP2 were constructed). The pattern in spin-lattice relaxation times (T_1) for the deuterium atoms at carbon-6 in the disparlure enantiomers demonstrates the external binding interactions with *Ldis*PBP2, whereas the pattern in transverse relaxation times (T_2) for these deuterium atoms at C-6 shows the internal binding interactions with *Ldis*PBP1. The difference in the kinetic constants (k_{on} and k_{off}) and T_1 and T_2 relaxations times supports the multi-step binding mechanism for *Ldis*PBP1 and *Ldis*PBP2. These different binding and association steps could serve different function: the rapid, easily reversible step on the exterior of the protein could serve transport functions, whereas slow internalization step could serve ligand-selective scavenging function.

4.2.11. *In-silico* docking simulations of 6-FAM tagged disparlure enantiomers to homology models of *Ldis*PBP1 and *Ldis*PBP2

To understand the structural basis of *Ldis*PBPs (*Ldis*PBP1 and *Ldis*PBP2) and ligand interactions, binding of natural ligands ((+)-disparlure **15** and (-)-disparlure *ent*-**15**) and fluorescent probes (**15d** and *ent*-**15d**) was explored using molecular docking simulations with homology models. The homology models for both *Ldis*PBP1 and *Ldis*PBP2 were generated, based on template from silkmoth, *Bombyx mori* PBP *Bmor*PBP (PDB ID: 1LS8.1.A).

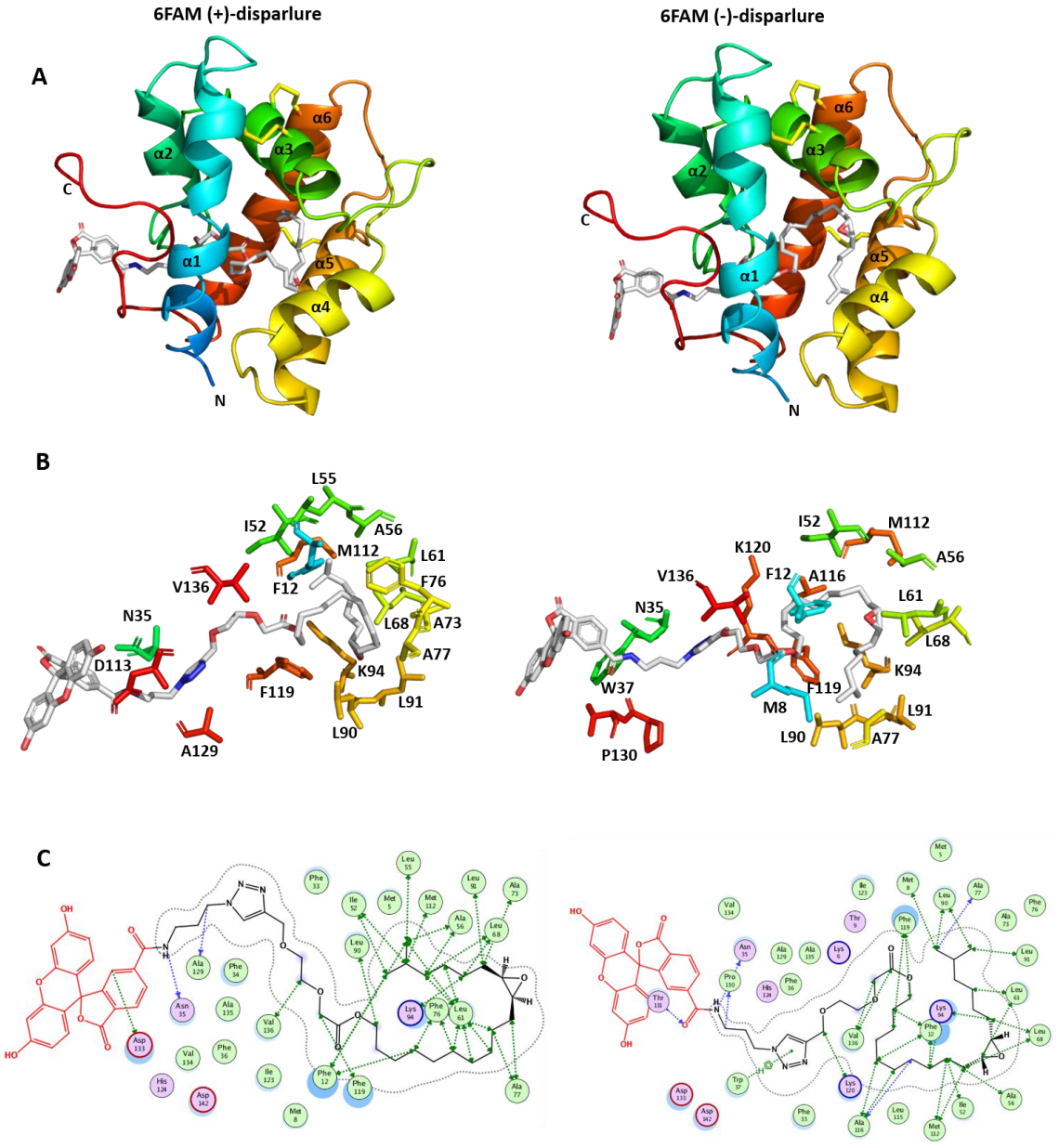

Figure 4.11 **Docking of 6-FAM tagged disparlure enentiomers on to *Ldis*PBP1 homology model using MOE. A.** Left side: 6-FAM (+)-disparlure; right side: 6-FAM (-)-disparlure. Ligands are shown as grey sticks model inside the binding site. The homology model of *Ldis*PBP1 contains 6 helices labelled as α1-α6. The disorderd C-terminus (red, labelled as C) which located outside the binding site. N-terminus (labelled as N) is strctured helix (blue). **B.** Binding site residues in contact with 6-FAM (+)-disparlure or 6-FAM (-)-disparlure are all hydrophobic except the Lys 94. **C.** Protein-ligand interactions map of binding site residues in contact with 6-FAM (+)-disparlure or 6-FAM (-)-disparlure. Residues in green background are nonpolar whereas residues in purple are polar. The ligand atoms in red background and residues with blue clouds are exposed to the solvent.

Results of 6-FAM disparlure enantiomers docking with *Ldis*PBPs homology models are shown in Figure 4.11 and 4.12. In both figures, A) show bound 6-FAM disparlure and *Ldis*PBP complex B) represent the residues of binding site involved in 6-FAM disparlure interactions (within 4.5 Å) C) show the *Ldis*PBP-6-FAM disparlure interaction maps which were exported from MOE (molecular operating environment) program.

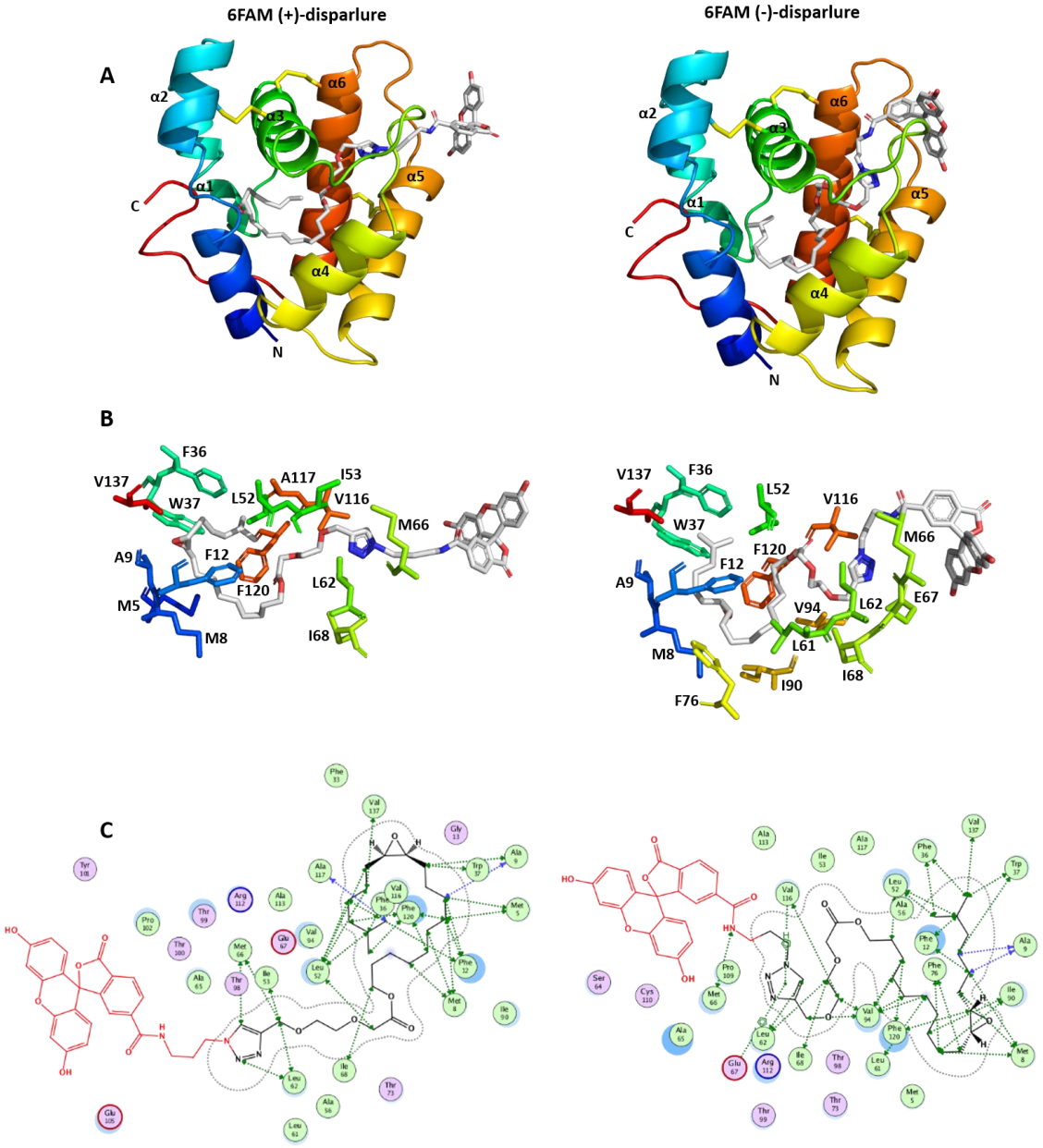

Figure 4.12 Docking of 6FAM disparlure enantiomers onto *Ldis*PBP2 homology model using MOE.

4.2.12. Disparlure and 6-FAM disparlure interactions with *Ldis*PBP1

Molecular docking of disparlure or 6FAM disparlure enantiomers showed different conformations of ligand inside the binding site of *Ldis*PBP1. The orientations were never the same for each of enantiomer of disparlure or 6-FAM disparlure and these enantiomers were in completely opposite orientations. For the 6-FAM (+)-disparlure **15d**, shorter carbon chain (C1-C6) (Table 4.6) interacted with nonpolar regions of the amino acid residues Met 112, Leu 91, Lys 94, Ala 73, Leu 68, Leu 61, Ala 56, Leu 55, Leu 52, Ile 53 and Phe 12. For 6-FAM (-)-disparlure *ent*-**15d**, the residues Lys 94, Leu 91, Leu 90, Leu 68, Leu 61, Ala 77 and Met 8 were involved (Figure 4.13, Table 4.6). The longer hydrocarbon chain (C9-C18) of **15d** interacted with hydrophobic parts of residues Leu 90, Phe 76, Ala 77, Leu 61 and Phe 12 whereas *ent*-**15d** showed interaction with Phe 119, Leu 68, Ala 116, Met 112, Leu 68, Ile 52 and Phe 12 (Figure 4.13, Table 4.7). Interestingly, for bound conformations of **15d** and *ent*-**15d**, the residues involved in interactions with the shorter hydrocarbon chain of one enantiomer were those that interacted with the longer hydrocarbon chain of the other enantiomer. Therefore, the ligand bound confirmation of **15d** was inverted in comparison with *en*t-**15d**. Most of the residues interacted differently with **15d** and *ent*-**15d**. For example, Phe 12, and Lys 94 have different interactions with two enantiomers. With **15d**, Phe 12 had an interaction with carbon 1 and carbon 15 whereas with *ent*-**15d**, it showed interaction with carbons 11, 14 and 18. In both enantiomers, Lys 94 had a different interaction with the ligand, at carbon 5 with **15d** and at carbon 6 with *ent*-**15d**. This is consistent with docking studies on *Ldis*PBP1 with (+)-disparlure (Figure 4.13 & Table 4.6). From the molecular docking studies with the disparlure enantiomers binding at internal binding pocket of *Ldis*PBP2 (Chapter 3), Val 94 or Leu 52 had a different interaction at carbon-5 with disparlure enantiomers (Pinnelli et al. 2019).

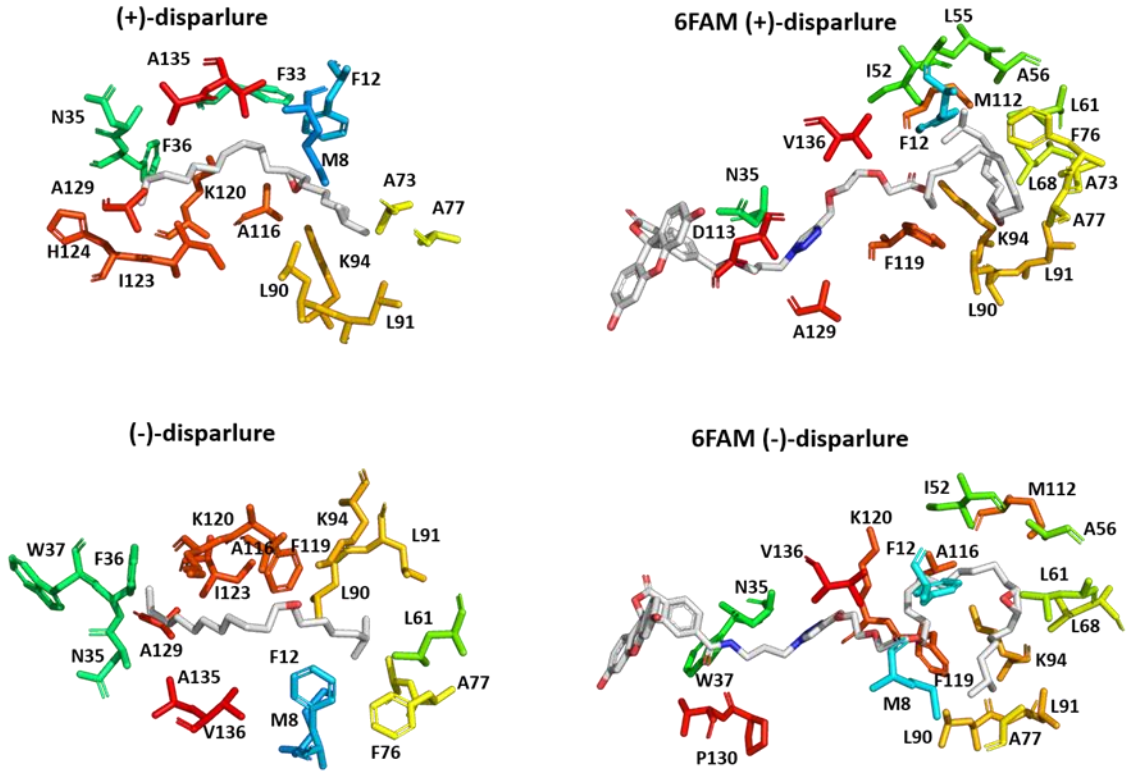

Figure 4.13 **Comparision of *Ldis*PBP1 binding pocket residues in contact with natural ligands and 6-FAM disparlure enantiomers.**

Table 4.6 ***Ldis*PBP1 docking. Binding pocket residues involved in interactions with short chain of ligand.**

	C1	C2	C2'	C3	C4	C5	C6	C7	O
15	Met 8 Leu 90	Leu 90	Ala 73 Ala 77 Leu 91		Lys 94	Phe 12 Lys 94	Lys 94		Lys 94
***ent*-15**	Met 8 Phe 76 Ala 77	Phe 76	Leu 90 Leu 91	Leu 61		Lys 94	Phe 119		
15d	Ile 53 Phe 12	Leu 52 Met 112	Leu 55 Leu 61 Ala 56	Ala 56 Leu 61 Lue 68	Leu 61	Lys 94 Leu 68	Ala 73 Leu 91		
***ent*-15d**	Met 8 Ala 77 Leu 90		Leu 90 Leu 91		Leu 61		Leu 68 Lys 94		

When comparing bound conformations of natural ligand (+)-disparlure **15** and 6-FAM tagged (+)-disparlure **15d**, Phe 12, Ala 73, Ala 77, Leu 90, Leu 91 and Lys 94 involved in interactions with both **15** and **15d** (Table 4.6 and 4.7). Both ligands were oriented in the same direction. Interestingly, hydrogen bonding was noticed between Lys 94 and oxygen of the epoxide for **15**. This interaction was absent for **15d**. When comparing *ent*-**15** and *ent*-**15d**, the common residues that interacted with both ligands were: Met 8, Phe12, Leu 61, Ala 77, Leu 90, Leu 91, Lys 94, Ala 116 and Phe 119. For both *ent*-**15** and *ent*-**15d**, the hydrogen bonding was not observed with Lys 94. These binding interactions are consistent with findings from previous molecular docking studies with (+)-disparlure **15** and (-)-disparlure *ent*-**15** (Chapter 3). The docking results indicated that both disparlure and disparlure portion of 6-FAM tagged disparlure are consistent in orientation and overlapped in the same tunnel of the binding pocket.

Table 4.7 *Ldis*PBP1 docking. Binding pocket residues involved in interactions with long chain of ligand.

	C9	C10	C11	C13	C14	C15	C16	C17	C18
15	Ala 116	Phe 12	Phe 33 Val 136	Lys 120		Ile 123	Asn 35 Ile 123 Ala 129 Ala 135	Phe 36	His 124
***ent*-15**	Phe 12	Ala 116	Lys 120		Ala 135	Asn 35 Phe 36	Ile 123 Ala 129 Ala 135	Phe 36 Ala 129	Phe 36 Trp 37 Ile 123
15d	Ala 77	Leu 61 Ala 77	Leu 61	Leu 61 Phe 76		Phe 12 Phe 76			Leu 90
***ent*-15d**	Leu 68 Met 112	Ile 52 Met 112	Phe 12	Ala 116	Ala 116 Phe 12		Phe 119	Phe 12	Phe 119

4.2.13. Disparlure and 6-FAM disparlure interactions with *Ldis*PBP2

For *Ldis*PBP2 binding with disparlure and 6-FAM disparlure, two different conformations were observed (Figure 4.14). (+)-disparlure **15** and 6-FAM (+)-disparlure **15d** followed one conformation whereas (-)-disprlure *ent*-**15** and 6FAM (-)-disparlure *ent*-**15d** followed the inverted form of the other conformation. For **15d**, the amino acid residues Phe12, Phe36, Leu 52, Ala 56, Ala 117, Phe 120 and Val 137 interacted with shorter hydrocarbon chain. The longer hydrocarbon chain interacted with Met 5, Met 8, Ala 9, Phe 12, Trp 37, Ile 68 and Phe 120. Participation of these amino acid residues with respective hydrocarbon chains was inverted for *ent*-**15d**. For **15** and *ent*-**15**, the residues involved in

interactions with short and long hydrocarbon chains were presented on Table 4.8 and 4.9. No Lys94 interaction was noticed for epoxide oxygen atom across all four ligands. Furthermore, the chiral carbons at C-7 and C-8 were stabilized by residues Leu 52 and Phe112 for **15**, Met 8 for *ent*-**15**, Phe 120 for *ent*-**15d** but no interactions were noticed for **15d**.

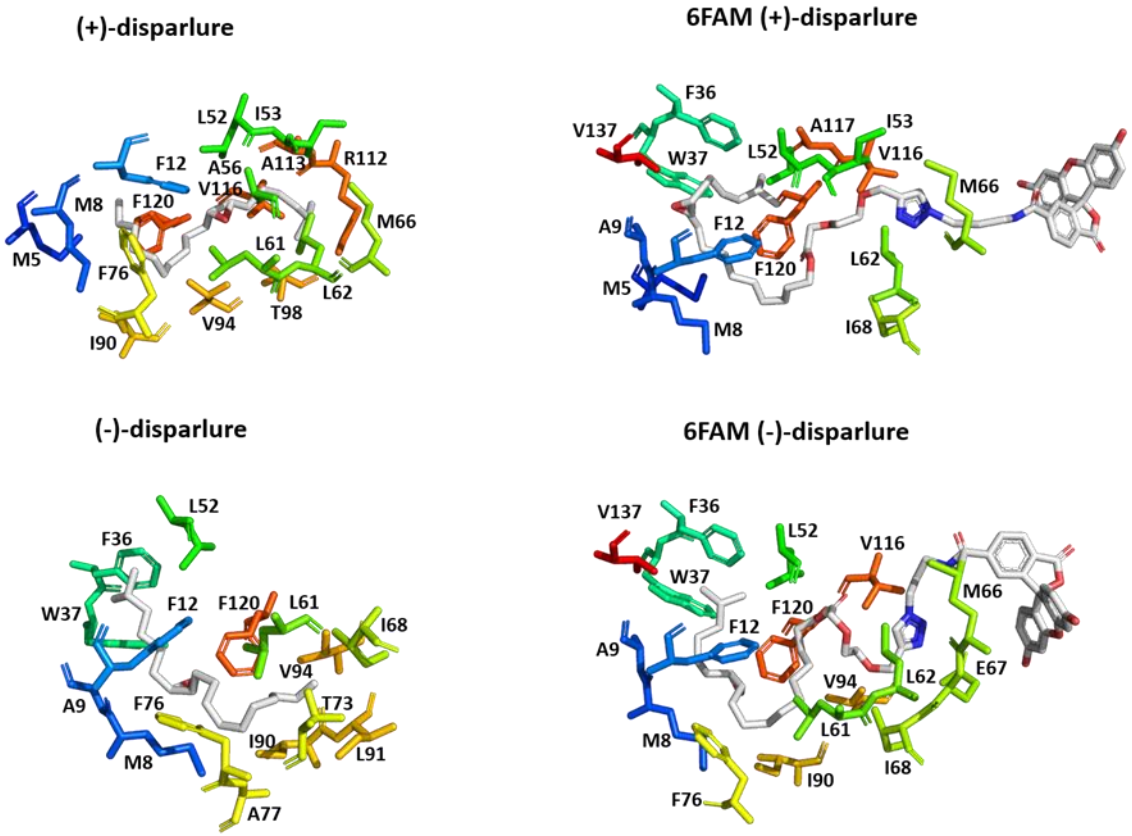

Figure 4.14 Comparision of *Ldis*PBP2 binding pocket residues in contact with natural ligands and 6-FAM disparlure enantiomers.

Table 4.8 *Ldis*PBP2 docking interactions with short chain of the ligand.

	C1	C2	C2'	C3	C4	C5	C6	C7	C8
15	Lue 62 Thr 98 Val 116	Arg 112	Met 66 Ala 113 Val 116	Leu 52 Ile 53 Met 66	Ile 53 Ala113	Leu 52 Ile 53 Ala 56	Val 116	Leu 52	Phe 112
***ent*-15**	Phe 36		Phe 36 Trp 37	Phe 12 Leu 52	Trp 37		Met 8 Ala 9 Phe 12		Met 8
15d	Phe12 0	Phe 36 Leu 52	Phe 12 Ala 117 Ala 56	Phe 120	Phe 12 Leu 52	Leu 52 Val 137	Leu 52		
***ent*-15d**	Phe 36 Leu 52	Phe 12 Leu 52	Phe 36 Trp 37 Val 137		Ala 9 Trp 37	Met 8 Ala 9 Phe 12	Met 8	Phe 120	

Table 4.9 *Ldis*PBP2 docking. Interactions with long chain of the ligand.

	C9	C10	C11	C12	C13	C14	C16	C17	C18
15		Val 94	Leu 61		Ile 90	Leu 61 Phe 76	Phe 12	Met 5 Met 8	Met 5 Phe 12 Phe 120
***ent*-15**			Phe 76 Ile 90		Ala 77	Leu 61 Thr 73 Phe 76	Val 94 Phe 120	Val 94 Ile 90 Ile 91	Ile 68 Ile 91 Val 94
15d	Ala 9 Trp 37		Met 5 Ala 9 Phe 12	Met 5 Met 8 Phe 120	Met 8	Phe 120			Ile 68
***ent*-15d**	Phe 76	Met 8 Phe 76 Ile 90	Ile 90	Ala 116	Leu 61 Val 94	Val 94	Val 94 Phe 120	Leu 52	

Molecular docking studies of fluorescent probes 6FAM (+)-disparlure **15d** and 6-FAM (-)-disparlure *ent*-**15d** to homology models of *Ldis*PBP1 and *Ldis*PBP2 revealed that the disparlure enantiomers adopt different conformations in the binding pocket, resulting in enantiomer discrimination of *Ldis*PBPs towards disparlure.

4.2.14. Conclusion

The two gypsy moth pheromone binding proteins *Ldis*PBP1 and *Ldis*PBP2 have different binding affinities with fluorescent probes 6-FAM (+)-disparlure and 6-FAM (-)-disparlure. *Ldis*PBP1 has stronger affinity for 6-FAM (-)-disparlure, whereas *Ldis*PBP2 has stronger affinity for 6-FAM (+)-disparlure, consistent with the findings from previous study with disparlure enantiomers. The Molecular docking results showed that *Ldis*PBP1

and *Ldis*PBP2 have different recognition mechanism for 6-FAM disparlure enantiomers. The association rate constant (k_{on}) values indicates that 6-FAM (+)-disparlure binds faster to *Ldis*PBP1 and *Ldis*PBP2 compared to 6-FAM (-)-disparlure. The dissociation rate constant (k_{off}) values suggest that the dissociation rate of 6-FAM (+)-disparlure with *Ldis*PBP1 and 6-FAM (-)-disparlure with *Ldis*PBP2 are faster than their respective enantiomer. These binding affinities and kinetic constants confirm that *Ldis*PBP1 and *Ldis*PBP2 differ in their preferences for (+)-disparlure and (-)-disparlure.

4.3. General experimental

All reactions were carried out in the presence of a nitrogen atmosphere and at room temperature unless the reactions were performed in aqueous media or unless otherwise specified. Reactions carried out at -78 °C used a bath of dry ice in acetone. Reactions undertaken at 0 °C utilized a bath of water and ice. Hexanes and ethyl acetate were distilled prior to use. Chemicals and Reagents were used without further purification and were purchased from Sigma-Aldrich (Oakville, ON, Canada). Syringes and cannulas were used to transfer reagents. Reactions were monitored by thin layer chromatography (TLC) on aluminum baked silica plates (Merck Silica Gel 60 F254) and products were visualized under UV or stained with phosphomolybdic acid (PMA), anisaldehyde and potassium permanganate followed by exposure of the stained plates to heat. Silica flash chromatography (Fisher Silica Gel 60 40-63 μm) was undertaken to purify crude reaction mixtures using hexanes/ethyl acetate mixture. The enantiomeric excess (*ee*) was analyzed on an Agilent 1260 HPLC equipped with a chiral column (Phenomenex, Lux 5u cellulose-2, 250×4.60 mm) and variable wavelength detector (VWD). The HPLC chromatograph was programmed with hexanes/isopropanol/DEA (90:10:0.1). Optical rotations were recorded on a Perkin-Elmer Polarimeter 340 thermostatted to 20 ºC, using the sodium D line.

The ^{1}H NMR spectra were obtained on Bruker DRX 400 and 500 MHz spectrometers in $CDCl_3$. Chemical shifts are reported in parts per million (ppm) relative to the reference TMS (Trimethylsilane). The coupling constants are reported in hertz (Hz). ^{1}H NMR data was reported as follows: chemical shift values (ppm), multiplicity (s = singlet, d = doublet, t = triplet, q = quartet, m = multiplet). ^{13}C NMR spectra were recorded in $CDCl_3$ by using a Bruker DRX 400 MHz or DRX 500 MHz.^{13}C NMR data was reported as chemical shift values (ppm). IR spectra were obtained with a Perkin-Elmer Spectrum One

FT-IR spectrometer and samples were directly placed on the KBr plates. High-resolution mass spectra (HRMS) were obtained by using positive electrospray ionization (EI) and by the time of flight (TOF) method (Brucker impact QTOF). The GC-MS analysis was performed using Clarus 690-GC and Clarus SQ8T-MS systems (Perkin Elmer, MA, USA). GC-MS equipped with a SPB-5 fused silica capillary column (SPB-5, 30 m × 0.25 mm i.d., film thickness 0.25 μm, Supelco, Bellefonte. PA, USA) with positive electron ionization (EI). Samples were diluted in dichloromethane and injected with a 1:10 split ratio. The injector temperature was programmed to 250 °C. The oven temperature was held at 80 °C for 50 sec and raised to 200 °C at 14 °C/min which was held for 15 min. Then finally 2 °C/ min to 260 °C which was held for 5 min. The MS conditions were: Solvent - delay time 6 min and scanned mass range (m/z) 50-500.

4.4. Experimental procedures

4.4.1. General synthetic procedure for preparation of protected alcohols 157, 158 or 164

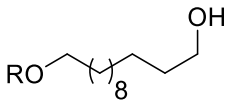

157: R = MOM
158: R = TBDMS
164: R = Bn

Three protection groups were tried for the single protection of 1,12-dodecanediol: methoxymethyl (MOM), t-butyldimethylsilyl (TBDMS) or benzyl (Bn) (Scheme 4.3). To a nitrogen flushed 50 mL flask was added 1, 12-dodecanediol (**156**) (200 mg, 0.990 mmol) *N*,*N*'-Diisopropylethylamine (DIPEA, 130 mg, 0.990 mmol) or imidazole (67.4 mg, 0.990 mmol), and dichloromethane (2 mL). Next, either methoxymethyl chloride (MOM-Cl, 80 mg, 0.990 mmol) or t-butyldimethylsilyl chloride (TBDMS-Cl, 150 mg, 0.990 mmol) was added, and the reaction mixture was allowed to stir at room temperature for 4h. The resulting reaction mixture was diluted with dichloromethane (20 mL) and washed with water (10 mL), and saturated NaCl solution (10 mL). The organic phase was dried over Na2SO4, filtered and concentrated in vacuo. The resulting crude product was purified by silica flash column chromatography (15% EtOAc/hexane) to yield the product **157** (116 mg, 48%) or **158** (145 mg, 46%).

Compound 157: ^{1}H NMR (400 MHz, $CDCl_3$) δ: 4.60 (s, 2H), 3.61 (t, *J* = 6.6 Hz, 2H), 3.50 (t, *J* = 6.7 Hz, 2H), 3.34 (s, 3H), 1.57 (m, 4H), 1.28 (m 14H). ^{13}C NMR (125 MHz, $CDCl_3$) δ 96.49, 68.01, 63.13, 55.19, 32.92, 29.86, 29.70, 29.69, 29.68, 29.67, 29.55, 26.32, 25.87.

Compound 158:^{1}H NMR (400 MHz, $CDCl_3$) δ: 3.66-3.62 (t, *J* = 6.6 Hz, 2H), 3.61-3.57 (t, *J* = 6.6 Hz, 2H), 1.60-1.48 (m, 4H), 1.31-1.25 (m, 14H), 0.89 (s, 9H), 0.05 (s, 6H).

Compound 164: To a cold (0 °C) stirred suspension of NaH (0.534 g, 24.75 mmol) in anhydrous THF (100 mL), 1, 12-dodecanediol (**156**) (5 g, 24.75 mmol) was added. After 30 mins stirring at rt, the benzyl bromide (**163**) (4.24 g, 24.75 mmol) was added dropwise, and the reaction mixture was refluxed at 70 °C for 12 h. Then the reaction was quenched with ice-cold water and diluted with EtOAc (100 mL). The aqueous layer was separated and extracted with ethyl acetate (2×50 mL). The organic layers were pooled, washed with brine solution (50 mL), dried over Na_2SO_4, and concentrated under reduced pressure to afford crude product. Purification of the crude product by flash chromatography (silica gel, 80: 20 hexanes: ethyl acetate) yielded 12-(benzyloxy) dodecan-1-ol (**164**) as a colourless solid (3.2 g, 44%).

^{1}H NMR (500 MHz, $CDCl_3$) δ 7.37-7.32 (d, *J* = 4.4 Hz, 4H), 7.30-7.26 (m, 1H), 4.52-4.49 (s, 2H), 3.66-3.61 (t, *J* = 6.7 Hz, 2H), 3.48-3.44 (t, *J* = 6.7 Hz, 2H), 1.64-1.54 (m, 4H), 1.50- 1.40 (s, 1H), 1.38-1.26 (m, 16H). ^{13}C NMR (125 MHz, $CDCl_3$) δ 138.64, 128.25, 127.53, 127.37, 72.77, 70.46, 62.99, 32.74, 29.70, 29.52, 29.50, 29.49, 29.48, 29.40, 29.35, 26.12, 25.67. IR (neat): 3360, 2922, 2849, 2794, 1116, 1058, 956, 735 cm^{-1}. GCMS (EI) m/z calculated for $C_{19}H_{32}O_2$ $[M]^{+\cdot}$: 292.24; found: 292.30.

4.4.2. General procedure for synthesis of MOM or TBDMS protected aldehyde 159, 160 or 165

Compounds **159**, **160** or **165** were prepared by oxidation of the alcohol group of compounds **157**, **158** or **164** with pyridinium chlorochromate (Scheme 4.3).

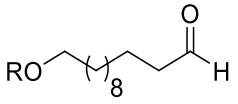

159: R = MOM
160: R = TBDMS
165: R = Bn

The procedure was the same for all three compounds; the one for **164** is given in detail. To a stirred solution of 12-(benzyloxy) dodecan-1-ol (**164**) (2.2 g, 7.48 mmol) in dichloromethane (50 mL), pyridinium chlorochromate (1.93 g, 8.97 mmol) was added portion wise at room temperature. After that, the reaction mixture was stirred at rt for 2h. The resulting gummy black residue was diluted with dichloromethane (50 mL) and the supernatant liquid decanted from the gummy black residue. The black residue was washed with dichloromethane (2×50 mL). The combined dichloromethane solution was filtered through the pad of alumina, dried over Na_2SO_4, and concentrated in vacuo to yield crude product. Purification of the crude product by flash chromatography (silica gel, 90:10 hexanes: ethyl acetate) yielded 12-(benzyloxy) dodecanal (**165**) as a colourless semi solid (1.94 g, 89%).

^{1}H NMR (500 MHz, $CDCl_3$) δ: 9.76 (s, 1H), 7.35-7.27 (m, 5H), 4.50 (s, 2H), 3.46 (s, 2H), 2.41 (s, 2H), 1.61 (t, *J* = 13.4 Hz, 5H), 1.28 (d, *J* = 13.6 Hz, 18H). ^{13}C NMR (125 MHz, $CDCl_3$) δ: 202.82, 138.63, 128.23, 127.51, 127.35, 72.76, 70.43, 43.83, 29.46, 29.41, 29.37, 29.31, 29.25, 29.07, 27.28, 26.10, 22.00. IR (neat): 2925, 2853, 1725, 1101, 735 cm^{-1}. GCMS (EI) m/z calculated for $C_{19}H_{30}O_2$ $[M]^{+\cdot}$: 290.22; found: 290.10.

Compound 159: The compound **157** (100 mg, 0.406 mmol), Pyridinium chlorochromate (PCC) (87 mg, 0.406 mmol), DCM (2 mL). (Eluent: 7% EA/hexane), 80 mg, 81%. ^{1}H NMR (400 MHz, $CDCl_3$) δ: 9.75 (t, *J* = 1.9 Hz, 1H), 4.61 (s, 2H), 3.50 (t, *J* = 6.6 Hz, 2H), 3.35 (s, 3H), 2.40 (td, *J* = 7.4, 1.9 Hz, 2H), 1.59-1.54 (m, 4H), 1.36-1.26 (m, 14H). ^{13}C NMR (125 MHz, $CDCl_3$) δ 203.05, 96.51, 77.36, 68.00, 55.20, 44.04, 29.87, 29.68, 29.63, 29.55, 29.52, 29.47, 29.29, 26.34, 22.21.

Compound 160: The compound **158** (100 mg, 0.316 mmol), Pyridinium chlorochromate (PCC) (68 mg, 0.406 mmol), DCM (2 mL). (Eluent: 5% EA/hexane), 80 mg, 92%. ^{1}H NMR (500 MHz, $CDCl_3$) δ: 9.75 (s, 1H), 3.60-3.56 (t, *J* = 6.7 Hz, 2H), 2.43-2.39 (t, *J* = 8.2 Hz, 2H), 1.64-1.58 (p, *J* = 7.3 Hz, 2H), 1.52-1.46 (p, *J* = 6.6 Hz, 2H), 1.30-1.23 (m, 14H), 0.88 (s, 9H), 0.03 (s, 6H). ^{13}C NMR (125 MHz, $CDCl_3$) δ 203.23, 63.46, 44.06, 32.99, 29.72, 29.64, 29.55, 29.54, 29.49, 29.28, 26.11, 25.90, 22.18, -5.12.

4.4.3. Preparation of (*R*)-12-(benzyloxy)-2-chlorododecanal (166)

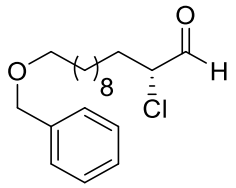

166

The three aldehydes **159**, **160** and **165** were subjected to α-chlorination. The procedure for conversion of **165** to **166** is given. Aldehydes 159 and 160 did not react (Scheme 4.2). The D-SOMO catalyst **106** (1.10 g, 3.81 mmol) was added to a stirred ice cooled solution of the 12-(benzyloxy) dodecanal (**165**) (2.2 g, 7.65 mmol) in acetonitrile (50 mL) and water (0.3 mL) followed by the addition of $Cu(TFA)_2.H_2O$ (0.430 g, 1.517 mmol), LiCl (0.640 g, 1.517 mmol) and $Na_2S_2O_8$ (2.16 g, 9.103 mmol). The reaction mixture was stirred at 5 ^oC until dodecanal had been completely consumed (as determined by ^1H NMR spectroscopy). After this time, the reaction mixture was treated with water (20 mL) and diluted with ethyl acetate (50 mL), and the phases were separated. The aqueous phase was extracted with ethyl acetate (3×50 mL). The combined organic phases were washed with brine (100 mL), dried over Na_2SO_4, and concentrated in vacuo to produce the crude chloroaldehyde. Purification of the crude product by flash chromatography afforded the (*R*)-12-(benzyloxy)-2-chlorododecanal (**166**) as a pale yellow liquid (1.45g, 53.1%).

^1H NMR (500 MHz, $CDCl_3$) δ: 9.49 (s, 1H), 7.34 (d, *J* = 4.4 Hz, 5H), 4.51 (s, 3H), 4.19-4.12 (m, 1H), 3.47 (t, *J* = 6.6 Hz, 3H), 1.94 (s, 1H), 1.82 (d, *J* = 37.7 Hz, 1H), 1.62 (d, *J* = 28.2 Hz, 3H), 1.28 (s, 22H). ^{13}C NMR (125 MHz, $CDCl_3$) δ: 195.28, 138.63, 128.24, 127.52, 127.37, 72.77, 70.42, 63.92, 31.98, 29.69, 29.41, 29.35, 29.31, 29.18, 28.84, 26.10, 25.45.

IR (neat): 2926, 2854, 1725, 1102, 735, 698 cm^{-1}. GCMS (EI) m/z calculated for $C_{19}H_{29}ClO_2$ [M+1]: 325.19; found: 325.30. $[\alpha]^{25}{}_D$: + 13.4 (c 0.8, $CHCl_3$).

4.4.4. Preparation of (7*S*, 8*R*)-18-(benzyloxy)-8-chloro-2-methyloctadec-5-yn-7-ol (167)

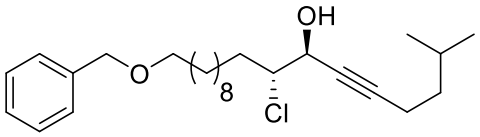

167

To a cold (-78 °C), stirred solution of 5-methyl-1-hexyne (**126**) (1 g, 10.4 mmol) in dry THF (35 mL), a solution of *n*-butyllithium (2.5 M in hexanes, 3.75 mL, 9.37 mmol) was added dropwise. The resulting mixture was stirred at -78 °C for 45 minutes. After this time, a solution of (*R*)-12-(benzyloxy)-2-chlorododecanal (**166**) (1.71 g, 5.208 mmol) in THF (5 mL) was added dropwise and the reaction mixture was stirred for an additional 45 minutes. Then the reaction mixture was quenched with a saturated aqueous solution of NH_4Cl (20 mL), diluted with ethyl acetate (50 mL) and water (20 mL). The phases were separated, and the aqueous phase was extracted with ethyl acetate (3×50 mL). The combined organic layers were washed with brine (100 mL), dried over Na_2SO_4, and concentrated under reduced pressure, which afforded crude product (d.r. 20:1 determined by ^1H NMR analysis of the crude reaction mixture). Purification of the crude product by flash chromatography afforded (silica gel, 95:10 hexanes: ethyl acetate) (7*S*, 8*R*)-18-(benzyloxy)-8-chloro-2-methyloctadec-5-yn-7-ol (**167**) (1.64 g, 68.3%).

^1H NMR (500 MHz, $CDCl_3$) δ: 7.36-7.32 (m, 5H), 4.53-4.49 (s, 3H), 4.04-3.97 (ddd, *J* = 9.4, 4.5, 3.5 Hz, 1H), 3.48-3.45 (d, *J* = 6.6 Hz, 2H), 2.29-2.19 (td, *J* = 7.4, 2.0 Hz, 2H), 1.89-1.75 (m, 2H), 1.72-1.56 (m, 6H), 1.36-1.24 (m, 17H), 0.9-0.88 (d, *J* = 6.7 Hz, 6H). ^{13}C NMR (125 MHz, $CDCl_3$) δ 138.59, 128.24, 127.53, 127.37, 87.74, 76.60, 72.76, 70.41, 67.52, 66.20, 37.26, 33.49, 29.67, 29.46, 29.38, 29.29, 27.17, 27.00, 26.39, 26.10, 22.07, 22.01, 16.65, 16.60.

IR (neat): 3461, 2927, 2855, 2223, 1275, 713, 649 cm^{-1}. GCMS (EI) m/z calculated for $C_{26}H_{41}ClO_2$ $[M]^{+\cdot}$: 420.28; found: 421.20. $[\alpha]^{25}{}_D$: + 9.8 (c 1.54, $CHCl_3$).

4.4.5. Preparation of (7*R*, 8*R*)-18-(benzyloxy)-8-chloro-2-methyloctadec-5-yn-7-yl benzoate (168)

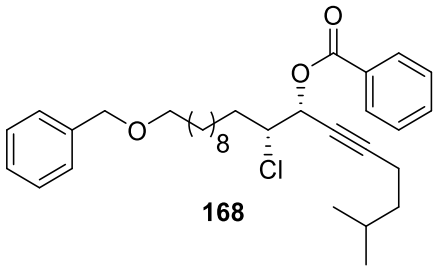

168

To a cold (0°C), stirred solution of (7*S*,8*R*)-18-(benzyloxy)-8-chloro-2-methyloctadec-5-yn-7-ol (**167**) (1.64 g, 3.88 mmol) and triphenylphosphine (2.03 g, 7.763 mmol) in dry THF (30 mL) under N_2 atmosphere, benzoic acid (**129**) was added (0.947 g, 7.763 mmol). The mixture was stirred 10 min. at same temperature and then DIAD (Diisopropyl azodicarboxylate) (1.35 g, 7.763 mmol) was added dropwise. After, the reaction mixture was stirred for 16h at room temperature. Then the solvent (THF) was removed by rotovap and the crude was purified by flash column chromatography (silica gel, 95:5 hexanes: ethyl acetate) to afford (7*R*, 8*R*)-18-(benzyloxy)-8-chloro-2-methyloctadec-5-yn-7-yl benzoate (**168**) (1.52 g, 74%).

^{1}H NMR (500 MHz, $CDCl_3$) δ: 8.14-8.09 (m, 2H), 7.52-7.45 (m, 3H), 7.37-7.32 (m, 5H), 4.51-4.50 (s, 3H), 4.04-3.99 (m, 1H), 3.48-3.45 (t, *J* = 6.7 Hz, 2H), 2.27-2.21 (td, *J* = 7.4, 2.0 Hz, 3H), 1.89-1.74 (m, 3H), 1.71-1.55 (m, 5H), 1.35-1.25 (s, 16H), 0.91-0.89 (d, *J* = 6.6 Hz, 6H). ^{13}C NMR (125 MHz, $CDCl_3$) δ: 171.85, 138.57, 133.76, 133.64, 130.20, 130.05, 129.23, 128.45, 128.36, 128.26, 127.56, 127.40, 87.81, 76.57, 72.76, 70.42, 67.52, 67.26, 66.23, 37.27, 33.51, 29.67, 28.98, 27.18, 27.02, 22.08, 22.03, 16.62.

IR (neat): 2926, 2854, 2249, 1729, 1263, 1103, 734, 710 cm^{-1}. GCMS (EI) m/z calculated for $C_{33}H_{45}ClO_3$ $[M]^{+\cdot}$: 524.31; found: 524.20. $[\alpha]^{25}{}_D$: + 11.3 (c 1.38, $CHCl_3$).

4.4.6. Preparation of (7*R*, 8*R*)-8-chloro-18-hydroxy-2-methyloctadecan-7-yl benzoate (169)

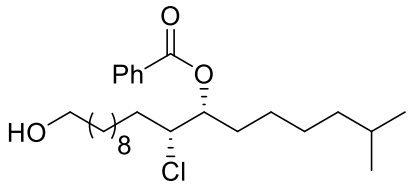

169

To a stirred solution of (7*R*,8*R*)-18-(benzyloxy)-8-chloro-2-methyloctadec-5-yn-7-yl benzoate (**168**) (0.8 g, 1.526 mmol) in methanol (20 mL) at room temperature, 10% Pd/C (80 mg) was added. The reaction mixture was hydrogenated under balloon pressure for 12h. After, Pd/C was removed by filteration and rinsing with 10% MeOH/ DCM (3×20 mL). Then the pooled filtrate was evaporated under reduced pressure to afford the crude product. The crude was purified by flash column chromatography (silica gel, 95:5 hexanes: ethyl acetate) to yield (7*R*, 8*R*)-8-chloro-18-hydroxy-2-methyloctadecan-7-yl benzoate (**169**) (0.591 g, 88%).

^{1}H NMR (500 MHz, $CDCl_3$) δ: 8.10-8.07 (d, *J* = 7.4 Hz, 2H), 7.60-7.55 (d, *J* = 7.4 Hz, 1H), 7.47-7.44 (m, 2H), 5.33-5.26 (dt, *J* = 7.4, 3.1 Hz, 1H), 4.09-4.02 (dt, *J* = 7.2, 3.2 Hz, 1H), 3.72-3.59 (s, 2H), 1.88-1.81 (s, 2H), 1.79-1.71 (d, *J* = 38.7 Hz, 2H), 1.62-1.54 (s, 3H), 1.52-1.47 (s, 1H), 1.37-1.24 (m, 19H), 0.86-0.83 (d, *J* = 6.6 Hz, 6H). ^{13}C NMR (125 MHz, $CDCl_3$) δ: 165.91, 130.07, 129.87, 129.77, 129.61, 128.36, 128.30, 75.63, 63.87, 62.90, 38.63, 34.45, 32.59, 31.32, 29.39, 29.26, 28.89, 27.84, 27.68, 27.08, 26.53, 25.70, 25.60, 25.55, 22.51, 22.48.

IR (neat): 3446, 2926, 2855, 1721, 1268, 1109, 1069, 1026, 711 cm^{-1}. GCMS (EI) m/z calculated for $C_{26}H_{43}ClO_3$ $[M]^{+\cdot}$: 438.29; found: 438.20. $[\alpha]^{25}{}_{D}$: + 10.9 (c 1.52, $CHCl_3$).

4.4.7. Preparation of (11*S*, 12*R*)-11,12-epoxy-17-methyl-octadecan-1-ol (150)

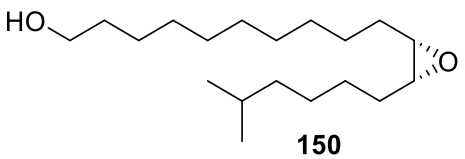

150

To a stirred solution of (7*R*,8*R*)-8-chloro-18-hydroxy-2-methyloctadecan-7-yl benzoate (**169**) (0.55 g, 1.254 mmol) in methanol (4 mL) at room temperature, 4N NaOH (4 mL) was added. This reaction mixture was stirred for 2h. After this time, the solvent was removed by roto evaporation. The resulting residue was diluted with ethyl acetate (50 mL) and water (15 mL). The phases were separated, and the aqueous phase was extracted with ethyl acetate (3×20 mL). The combined organic layers were washed with brine (50 mL), dried over Na_2SO_4, and concentrated under reduced pressure, which afforded crude product. The crude was purified by flash column chromatography (silica gel, 95:5 hexanes: ethyl acetate) to yield (11*S*, 12*R*)-11,12-epoxy-17-methyl-octadecan-1-ol (**150**) (0.308 g, 82%).

^{1}H NMR (500 MHz, $CDCl_3$) δ: 3.67-3.61 (t, *J* = 6.6 Hz, 2H), 2.95-2.86 (m, 2H), 1.63-1.46 (m, 10H), 1.40-1.26 (m, 17H), 0.89-0.85 (d, *J* = 6.6 Hz, 7H). ^{13}C NMR (125 MHz, $CDCl_3$) δ: 62.98, 57.16, 38.80, 32.70, 29.45, 29.43, 29.36, 29.30, 27.80, 27.76, 27.72, 27.22, 26.76, 26.50, 25.62, 22.52, 22.51.

IR (neat): 3404, 2924, 2854, 1366, 1267, 1095, 1058 cm^{-1}. GCMS (EI) m/z calculated for $C_{19}H_{38}O_2$ $[M]^{+\cdot}$: 298.29; found: 298.30. $[\alpha]^{25}{}_{D}$: + 5.7 (c 1.5, $CHCl_3$).

4.4.8. Preparation of 2-(2-(prop-2-yn-1-yloxy)ethoxy)acetic acid (172)

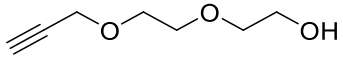

172

Diethylene glycol (**170**) (1.5 g, 14.15 mmol) was dissolved in anhydrous THF (50 mL) in a round bottom flask. To this homogeneous solution, NaH was added (0.34 g, 1415 mmol) at 0°C under inert atmosphere. After half an hour of stirring, the propargyl bromide (**171**) (1.18 g, 14.15 mmol) was added dropwise to the flask and the mixture was stirred

at room temperature for 16h. Then the reaction was poured into the ice-cold water and diluted with EtOAc (50 mL). The aqueous layer was separated and extracted with ethyl acetate (2×50 mL). The combined organic layers were washed with brine solution (50 mL), dried over Na_2SO_4, and concentrated under reduced pressure, which afforded crude product. The crude product was purified through flash column chromatography (silica gel, 80: 20 hexanes: ethyl acetate) to yield 2-(2-(prop-2-yn-1-yloxy) ethoxy) ethan-1-ol (**172**) (1.1 g, 54%).

^{1}H NMR (500 MHz, $CDCl_3$) δ: 4.08-4.04 (d, *J* = 2.4 Hz, 2H), 3.59-3.51 (m, 6H), 3.46-3.43 (m, 2H), 3.27-3.20 (s, 1H), 2.41-2.36 (t, *J* = 2.4 Hz, 1H). ^{13}C NMR (125 MHz, $CDCl_3$) δ: 79.06, 74.39, 72.13, 69.61, 68.58, 61.00, 57.84.

IR (neat): 3288, 2924, 2857, 2117, 1066, 1045cm^{-1}. GCMS (EI) m/z calculated for $C_7H_{12}O_3$ [M-C_3H_4]: 104.06; found: 104.10.

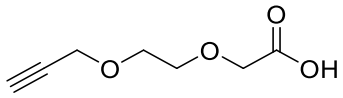

151

To a stirred solution of 2-(2-(prop-2-yn-1-yloxy) ethoxy) ethan-1-o l (**172**) (0.3 g, 2.083 mmol) in acetone (10 mL) at 0° C 10 % $NaHCO_3$ solution was added. The reagent 2, 2, 6, 6-Tetramethylpiperidin-1-yl (TEMPO, 0.358 g, 2.283 mmol) was added to the heterogeneous reaction mixture followed by KBr (0.0024 g, 0.283 mmol). After that, sodium hypochlorite (NaOCl, 10% solution, 1.95 mL, and 2.625mmol) was added dropwise at 0° C, and the reaction mixture was stirred at room temperature for 16h. The reaction mixture was diluted with H_2O (10 mL) and EtOAc (50 mL). The organic and aqueous layers were separated, and the aqueous layer was extracted with ethyl acetate (2×10 mL). All the organic layers were combined, washed with saturated NaCl solution, dried over Na_2SO_4 and concentrated in *vacuo*. After, the residue was purified by flash chromatography (silica gel, 80: 20 hexanes: ethyl acetate) it yielded 2-(2-(prop-2-yn-1-yloxy)ethoxy)acetic acid (**151**) (0.298 g, 90%).

^{1}H NMR (500 MHz, $CDCl_3$) δ: 7.92 (s, 2H), 4.21-4.15 (m, 4H), 3.78-3.70 (m, 4H), 2.45 (t, *J* = 2.3 Hz, 1H). ^{13}C NMR (125 MHz, $CDCl_3$) δ: 174.26, 79.02, 75.01, 74.80, 70.69, 68.77, 68.17, 58.29.

IR (neat): 2989, 2925, 2857, 2117, 1729, 1249, 1094 cm^{-1}.GCMS (EI) m/z calculated for $C_7H_{10}O_4$ [M-C_3H_4]: 118.03; found: 118.10.

4.4.9. Preparation of 10-((2*S*,3*R*)-3-(5-methylhexyl)oxiran-2-yl)decyl 2-(2-(prop-2-yn-1-yloxy)ethoxy)acetate (149)

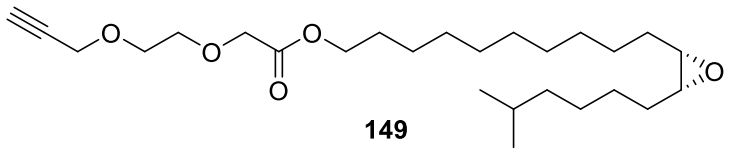

149

To a stirred solution (11*S*, 12*R*)-11,12-epoxy-17-methyl-octadecan-1-ol (**150**) (0.1 g, 0.3355 mmol) in dichloromethane (5 mL), 2-(2-(prop-2-yn-1-yloxy) ethoxy) acetic acid (**151**) (0.107 g, 0.6711 mmol) was added at room temperature. Then *N*,*N*'-diisopropylcarbodiimide (DIC, 0.845 g, 0.6711 mmol) and *N*,*N*'-dimethyl-4-aminopyridine (DMAP, 8.2 mg, 0.0671 mmol) were added and the resulting homogeneous reaction mixture was stirred at room temperature for overnight. The dichloromethane solvent that was removed under reduced pressure afforded oily residue, which after column purification by flash chromatography (silica gel, 95:5 hexanes: ethyl acetate) yielded 10-((2*S*, 3*R*)-3-(5-methylhexyl) oxiran-2-yl) decyl 2-(2-(prop-2-yn-1-yloxy) ethoxy) acetate (**149**) (0.114 g, 78%).

^{1}H NMR (500 MHz, $CDCl_3$) δ: 4.24-4.19 (d, *J* = 2.4 Hz, 2H), 4.17-4.12 (m, 4H), 3.79-3.71 (m, 4H), 2.94-2.86 (m, 2H), 2.45-2.41 (t, *J* = 2.4 Hz, 1H), 1.67-1.61 (m, 2H), 1.55-1.45 (m, 7H), 1.40-1.24 (m, 18H), 0.89-0.86 (d, *J* = 6.6 Hz, 6H).^{13}C NMR (125 MHz, $CDCl_3$) δ: 170.35, 79.37, 74.50, 70.56, 68.99, 68.54, 64.87, 58.27, 57.11, 38.78, 29.41, 29.33, 29.08, 28.45, 27.77, 27.74, 27.70, 27.20, 26.74, 26.50, 25.71, 22.50, 22.49.

IR (neat): 2925, 2855, 2115, 1752, 1203, 1146, 1103 1032 cm^{-1}. GCMS (EI) m/z calculated for $C_{26}H_{46}O_5$ [M+1]: 438.33; found: 439.30. [α]$^{25}{}_D$: + 3.7 (c 0.5, $CHCl_3$).

4.4.10. Preparation of fluorescently tagged (+)-disparlure (15d)

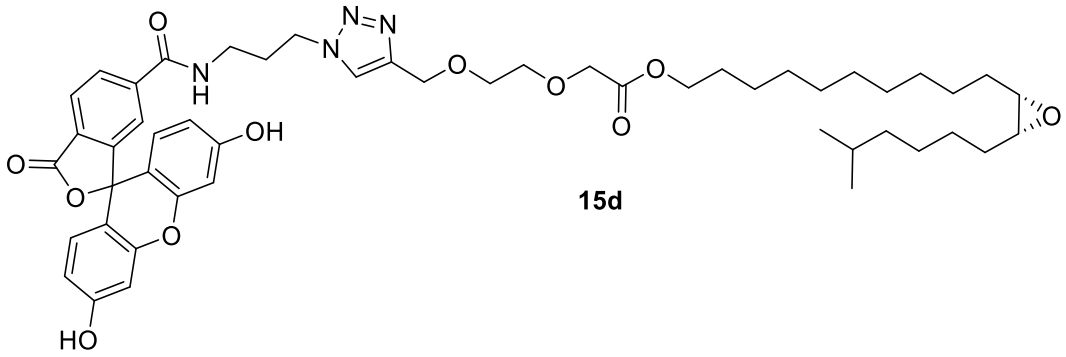

15d

In a 2 mL reaction vial, 6-FAM azide **173** (1 mg, 0.0022 mmol) and 10-((2*S*,3*R*)-3-(5-methylhexyl)oxiran-2-yl)decyl 2-(2-(prop-2-yn-1-yloxy)ethoxy)acetate (**149**) (5 mg, 0.0114 mmol) were added to the mixture of tris(3-hydroxypropyltriazolylmethyl)amine (THPTA, 1 mg, 0.0023 mmol) sodium ascorbate (28 mg, 0.01144 mmol), and copper (II) sulfate heptahydrate (1.1 mg, 0.0057 mmol) dissolved in ratio of 1:1 volume of t-BuOH and water (1 mL) at room temperature. The reaction mixture was stirred at room temperature for 1h. After this time, the t-BuOH was removed and the resulting residue was diluted with water and dichloromethane. The aqueous layer was extracted with 10% MeOH/DCM (4×10 mL). The pooled organic layers were washed with saturated sodium chloride solution, dried over Na_2SO_4 and concentrated in *vacuo*. The crude residue was purified by column chromatography on neutral alumina (10% MeOH/DCM) yielded 6-FAM tagged (+)-disparlure **15d** (1.12 mg, 57.4%).

^{1}H NMR (600 MHz, $CDCl_3$) δ: 8.17-8.07 (m, 4H), 8.07 (s, 1H), 7.63 (s, 2H), 6.73-6.53 (m, 6H), 4.79 (s, 2H), 4.18-4.08 (m, 4H), 3.78 (td, *J* = 5.4, 3.5 Hz, 4H), 3.41 (t, *J* = 6.9 Hz, 2H), 3.36 (t, *J* = 6.7 Hz, 2H), 2.90 (t, *J* = 3.9 Hz, 2H), 1.82 (p, *J* = 6.8 Hz, 2H), 1.63 (dt, *J* = 13.7, 6.7 Hz, 4H), 1.54-1.45 (m, 7H), 1.38-1.22 (m, 17H), 0.87 (d, *J* = 6.6 Hz, 6H).

IR (neat): 3570-3245 (O-H & N-H str), 2924-2856 (C-H str), 1771, 1749, 1690, 1625, 1591, 1524, 1456, 1439, 1250, 1213, 1148, 1104 1029 cm^{-1}. HRMS (ESI) m/z calculated for $C_{50}H_{65}N_4O_{11}$ [M+H]: 897.4650; found: 897.4662.

4.4.11. Preparation of (*S*)-12-(benzyloxy)-2-chlorododecanal (*ent*-166)

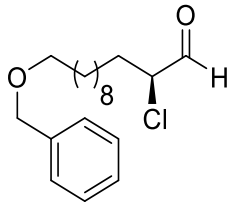

ent-**166**

The compound *ent*-**166** was prepared according to the procedure described in the experimental section **4**.**4**.**3**. 12-(benzyloxy) dodecanal (**165**) (7.241 mmol), L-SOMO *ent*-**106** (1.448 mmol), $Cu(TFA)_2.H_2O$ (3.62 mmol), LiCl (14.48 mmol) and $Na_2S_2O_8$ (8.68 mmol). (Eluent: 20% EA/hexane), 1.35 g, 57%, pale yellow oil.

^{1}H NMR (500 MHz, $CDCl_3$) δ: 9.50-9.47 (d, *J* = 2.5 Hz, 1H), 7.36-7.32 (m, 5H), 4.51-4.50 (s, 2H), 4.17-4.13 (ddd, *J* = 8.1, 5.4, 2.4 Hz, 1H), 3.49-3.45 (t, *J* = 6.6 Hz, 3H), 2.01-1.94 (m, 1H), 1.87-1.79 (m, 1H), 1.64-1.60 (m, 2H), 1.31-1.26 (m, 12H).^{13}C NMR (125 MHz, $CDCl_3$) δ: 195.28, 138.63, 128.24, 127.52, 127.37, 77.20, 77.15, 76.95, 76.69, 72.77, 70.42, 63.92, 31.98, 29.69, 29.41, 29.35, 29.31, 29.18, 28.84, 26.10, 25.45.

IR (neat): 2925, 2854, 1725, 1102, 1028, 735, 697 cm^{-1}.GCMS (EI) m/z calculated for $C_{19}H_{29}ClO_2$ [M+1]: 325.19; found: 325.30. $[\alpha]^{25}{}_D$: - 13.28 (c 0.8, $CHCl_3$).

4.4.12. Preparation of (7*R*, 8*S*)-18-(benzyloxy)-8-chloro-2-methyloctadec-5-yn-7-ol (*ent*-167)

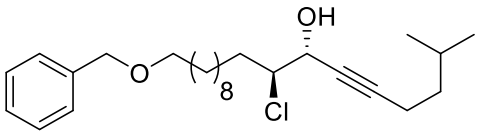

ent-**167**

The compound *ent*-**167** was prepared according to the procedure described in the experimental section **4**.**4**.**4**. 5-methyl-1-hexyne (**126**) (4.147 mmol), *n*-butyllithium (3.732 mmol), (*S*)-12-(benzyloxy)-2-chlorododecanal (*ent*-**166**) (4.147 mmol). (Eluent: 10% EA/hexane), 1.30 g, 75%, colorless oil.

^{1}H NMR (500 MHz, $CDCl_3$) δ: 7.36-7.34 (d, *J* = 4.4 Hz, 4H), 7.31-7.27 (dt, *J* = 8.8, 4.3 Hz, 1H), 4.53-4.50 (s, 2H), 4.53- 4.49 (dt, *J* = 9.5, 4.1 Hz, 1H), 4.04-3.98 (dt, *J* = 9.5, 4.1 Hz, 1H), 3.49-3.46 (t, *J* = 6.7 Hz, 2H), 2.52-2.36 (s, 1H), 2.27-2.21 (m, 2H), 1.91-1.74 (m, 2H), 1.74-1.65 (m, 1H), 1.67-1.58 (m, 4H), 1.34-1.24 (s, 16H), 0.91-0.89 (d, *J* = 6.6 Hz, 6H).^{13}C NMR (125 MHz, $CDCl_3$) δ: 138.59, 128.24, 127.53, 127.37, 87.74, 77.20, 76.95, 76.69, 76.60, 72.76, 70.41, 67.52, 66.20, 37.26, 33.49, 29.67, 29.46, 29.38, 29.29, 27.17, 27.00, 26.39, 26.10, 22.07, 22.01, 16.65, 16.60.

IR (neat): 3404, 2926, 2854, 2238, 1275, 1100, 735, 697 cm^{-1}. GCMS (EI) m/z calculated for $C_{26}H_{41}ClO_2$ $[M]^{+\cdot}$: 420.28; found: 421.20. $[\alpha]^{25}{}_{D}$: - 9.6 (c 1.54, $CHCl_3$).

4.4.13. Preparation of (7S, 8S)-18-(benzyloxy)-8-chloro-2-methyloctadec-5-yn-7-yl benzoate (*ent*-168)

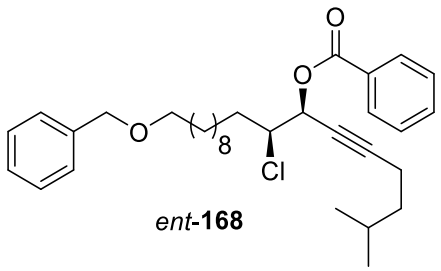

ent-**168**

The compound *ent*-**168** was prepared according to the procedure described in the experimental section **4.4.5**. (7*R*,8*S*)-18-(benzyloxy)-8-chloro-2-methyloctadec-5-yn-7-ol (*ent*-**167**) (3.095 mmol), triphenylphosphine (6.190 mmol), benzoic acid **129** (6.190 mmol) and DIAD (6.190 mmol). (Eluent: 10% EA/hexane), 1.12 g, 69%, colorless oil.

^{1}H NMR (500 MHz, $CDCl_3$) δ: 8.11-8.08 (d, *J* = 7.1 Hz, 2H), 7.60-7.57 (t, *J* = 7.4 Hz, 1H), 7.49-7.44 (t, *J* = 7.8 Hz, 2H), 7.36-7.34 (d, *J* = 4.4 Hz, 4H), 7.31-7.27 (m, 1H), 5.78-5.74 (dt, *J* = 6.1, 2.0 Hz, 1H), 4.52-4.51 (s, 2H), 4.14-4.08 (ddd, *J* = 9.6, 6.2, 3.4 Hz, 1H), 3.49-3.46 (t, *J* = 6.6 Hz, 2H), 2.28-2.23 (td, *J* = 7.4, 2.0 Hz, 2H), 2.08-2.01 (m, 1H), 1.89-1.81 (m, 1H), 1.72-1.59 (m, 4H), 1.40-1.24 (m, 15H), 0.91-0.88 (d, *J* = 6.6 Hz, 6H). ^{13}C NMR (125 MHz, $CDCl_3$) δ: 165.06, 138.64, 133.20, 129.82, 129.55, 128.33, 128.24, 127.51, 127.36, 88.46, 77.20, 77.15, 76.95, 76.69, 74.27, 72.77, 70.42, 67.70, 62.45, 37.09, 33.65, 29.69, 29.47, 29.40, 29.39, 29.31, 28.94, 27.16, 26.11, 25.97, 22.04, 16.69.

IR (neat): 2926, 2854, 2245, 1727, 1263, 1095, 1068, 734, 710, 697 cm^{-1}.GCMS (EI) m/z calculated for $C_{33}H_{45}ClO_3$ $[M]^{+\cdot}$: 524.31; found: 524.20. $[\alpha]^{25}{}_{D}$: - 11.06 (c 1.38, $CHCl_3$).

4.4.14. Preparation of (7*S*, 8*S*)-8-chloro-18-hydroxy-2-methyloctadecan-7-yl benzoate (*ent*-169).

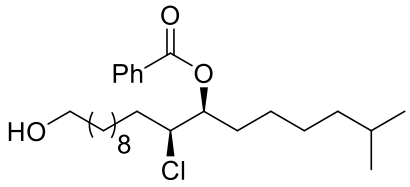

ent-**169**

The compound *ent*-**169** was prepared according to the procedure described in the experimental section **4.4.6**. (7*S*,8*S*)-18-(benzyloxy)-8-chloro-2-methyloctadec-5-yn-7-yl benzoate (*ent*-**168**) (0.9532 mmol) and 10% Pd/C (10 mol %). (Eluent: 20% EA/hexane), 0.350 g, 84%, colorless oil.

^{1}H NMR (500 MHz, $CDCl_3$) δ: 8.14-8.06 (d, *J* = 8.9 Hz, 2H), 7.61-7.55 (t, *J* = 7.3 Hz, 1H), 7.49-7.43 (t, *J* = 7.7 Hz, 2H), 5.33-5.27 (m, 1H), 4.09-4.03 (m, 1H), 3.68-3.61 (t, *J* = 6.6 Hz, 2H), 1.88-1.81 (m, 2H), 1.81-1.68 (m, 2H), 1.60-1.45 (m, 4H), 1.37-1.23 (m, 19H), 0.87-0.81 (d, *J* = 6.6 Hz, 6H). ^{13}C NMR (125 MHz, $CDCl_3$) δ: 165.91, 130.07, 129.87, 129.77, 129.61, 128.36, 128.30, 75.63, 63.87, 62.90, 38.63, 34.45, 32.59, 31.32, 29.39, 29.26, 28.89, 27.84, 27.68, 27.08, 26.53, 25.70, 25.60, 25.55, 22.51, 22.48.

IR (neat): 3449, 2926, 2854, 1723, 1268, 1110, 1071, 1026, 711 cm^{-1}.GCMS (EI) m/z calculated for $C_{26}H_{43}ClO_3$ $[M]^{+\cdot}$: 438.29; found: 438.20. $[\alpha]^{25}{}_{D:}$ + 10.78 (c 1.52, $CHCl_3$).

4.4.15. Preparation of (11*R*, 12*S*)-11,12-epoxy-17-methyl-octadecan-1-ol (*ent*-150)

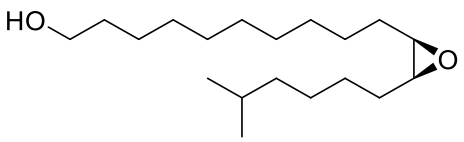

ent-**150**

The compound **37** was prepared according to the procedure described in the experimental section **4**.**4**.**7**. (7*S*, 8*S*)-8-chloro-18-hydroxy-2-methyloctadecan-7-yl benzoate (*ent*-**169**) (0.798 mmol) and 4N NaOH (4 mL). (Eluent: 25% EA/hexane), 0.187 g, 79%, colorless oil.

^{1}H NMR (500 MHz, $CDCl_3$) δ: 3.64-3.58 (t, *J* = 6.7 Hz, 2H), 2.92-2.85 (p, *J* = 4.1 Hz, 2H), 1.60-1.42 (m, 11H), 1.36-1.30 (m, 7H), 1.29-1.25 (m, 8H), 1.22-1.13 (m, 3H), 0.87-0.84 (d, *J* = 6.6 Hz, 6H). ^{13}C NMR (125 MHz, $CDCl_3$) δ: 77.20, 76.95, 76.69, 62.89, 57.07, 38.91, 38.80, 38.74, 32.83, 32.70, 32.54, 29.44, 29.37, 29.32, 27.87, 27.72, 27.22, 26.76, 26.50, 25.79, 22.53, 22.50.

IR (neat): 3410, 2925, 2855, 1367, 1267, 1095, 1058 cm^{-1}.GCMS (EI) m/z calculated for $C_{19}H_{38}O_2$ $[M]^{+\cdot}$: 298.29; found: 298.30. $[\alpha]^{25}{}_{D}$: - 5.64 (c 1.5, $CHCl_3$).

4.4.16. Preparation of 10-((2*R*,3*S*)-3-(5-methylhexyl)oxiran-2-yl)decyl 2-(2-(prop-2-yn-1-yloxy)ethoxy)acetate (*ent*-149)

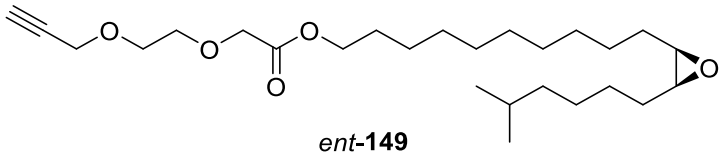

ent-**149**

The compound *ent*-**149** was prepared according to the procedure described in the experimental section **4**.**4**.**9**. 10-((2*R*, 3*S*)-3-(5-methylhexyl) oxiran-2-yl) decan-1-ol (*ent*-**150**) (0.251 mmol), 2-(2-(prop-2-yn-1-yloxy) ethoxy) acetic acid (**151**) (0.276 mmol), DIC (0.502 mmol) and DMAP (0.0502 mmol). (Eluent: 30% EA/hexane), 0.089 g, 81%, colorless oil.

^{1}H NMR (500 MHz, $CDCl_3$) δ: 4.21-4.19 (s, 2H), 4.15-4.13 (t, *J* = 3.2 Hz, 4H), 3.75-3.73 (m, 4H), 2.90-2.87 (m, 2H), 2.43-2.41 (t, *J* = 2.4 Hz, 1H), 1.66-1.59 (m, 3H), 1.51-1.46 (m, 6H), 1.36-1.27 (m, 16H), 1.20-1.13 (m, 3H), 0.87-0.85 (d, *J* = 6.6 Hz, 6H). ^{13}C NMR (125 MHz, $CDCl_3$) δ: 170.38, 79.39, 77.20, 77.15, 76.95, 76.69, 74.54, 70.59, 69.01, 68.56, 64.90, 58.30, 57.14, 38.81, 29.43, 29.36, 29.11, 28.48, 27.80, 27.77, 27.73, 27.22, 26.76, 26.52, 25.74, 22.53, 22.52.

IR (neat): 2925, 2855, 2115, 1753, 1202, 1147, 1104 1029 cm^{-1}.GCMS (EI) m/z calculated for $C_{26}H_{46}O_5$ [M+1]: 438.33; found: 439.30. [α]$^{25}{}_{D}$: + 3.66 (c 0.5, $CHCl_3$).

4.4.17. Preparation of fluorescently tagged (-)-disparlure (*ent*-15d)

The compound *ent*-**15d** was prepared according to the procedure described in the experimental section **4**.**4**.**12**.

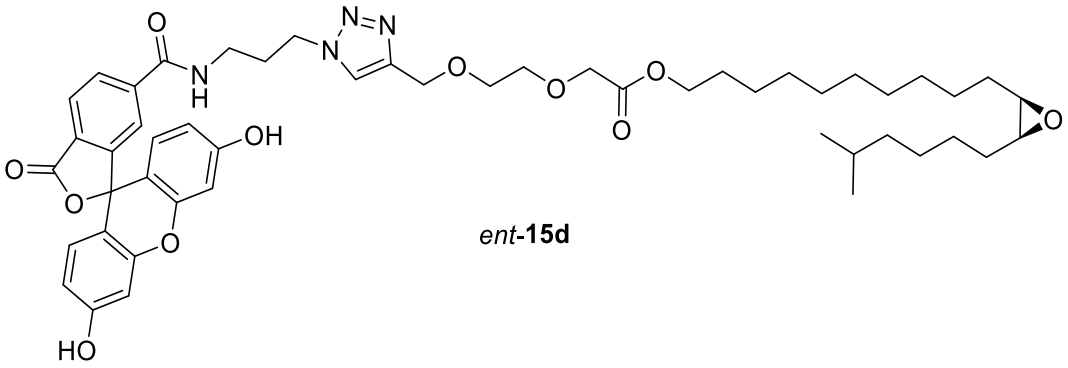

ent-**15d**

The compound *ent*-**15d** was prepared according to the procedure described in the experimental section **4**.**4**.**10**. 6-FAM azide **173** (1 mg, 0.0022 mmol), 10-((2*R*,3*S*)-3-(5-methylhexyl)oxiran-2-yl)decyl 2-(2-(prop-2-yn-1-yloxy)ethoxy)acetate (*ent*-**149**) (5 mg, 0.0114 mmol), tris(3-hydroxypropyltriazolylmethyl)amine (THPTA, 1 mg, 0.0023 mmol), sodium ascorbate (28 mg, 0.01144 mmol), and copper (II) sulfate heptahydrate (1.1 mg, 0.0057 mmol). (Eluent: 10% MeOH/DCM), 1.12 mg, 57.4%.

^{1}H NMR (600 MHz, $CDCl_3$) δ: 8.17-8.06 (m, 4H), 8.06 (s, 1H), 7.63 (s, 2H), 6.72-6.52 (m, 4H), 4.79 (s, 2H), 4.14 (d, *J* = 6.3 Hz, 4H), 3.80-3.76 (m, 4H), 3.40 (t, *J* = 6.8 Hz, 2H), 3.36 (t, *J* = 6.6 Hz, 2H), 2.91-2.88 (m, 2H), 1.82 (p, *J* = 6.7 Hz, 2H), 1.63 (dt, *J* = 14.3, 6.7 Hz, 4H), 1.55-1.46 (m, 7H), 1.36-1.27 (m, 17H), 0.87 (d, *J* = 6.6 Hz, 6H).

IR (neat): 3572-3244 (O-H & N-H str), 2925-2855 (C-H str), 1771, 1750, 1691, 1625, 1590, 1524, 1456, 1439, 1250, 1213, 1148, 1104 1029 cm^{-1}. HRMS (ESI) m/z calculated for $C_{50}H_{65}N_4O_{11}$ [M+H]: 897.4650; found: 897.4662.

4.4.18. General procedure for the synthesis of the compounds 176, 177 and *ent*-177

In a 2 mL reaction vial, 4-bromophenyl azide (**175**) (1 mg, 0.0022 mmol) and 10-((2*S*,3*R*)-3-(5-methylhexyl)oxiran-2-yl)decyl2-(2-(prop-2-yn-1-yloxy)ethoxy)acetate (**174**) or 10-((2*R*,3*S*)-3-(5-methylhexyl)oxiran-2-yl)decyl 2-(2-(prop-2-yn-1-yloxy)ethoxy)acetate (**149**) or 10-(3-(5-methylhexyl)oxiran-2-yl)decyl 2-(2-(prop-2-yn-1-yloxy)ethoxy)acetate (*ent*-**149**) (5 mg, 0.0114 mmol) were added to the mixture of tris(3-hydroxypropyltriazolylmethyl)amine (THPTA, 1 mg, 0.0023 mmol) sodium ascorbate (28 mg, 0.01144 mmol), and copper (II) sulfate heptahydrate (1.1 mg, 0.0057 mmol) dissolved in ratio of 1:1 volume of t-BuOH and water (1 mL) at room temperature. The reaction mixture was stirred at room temperature for 1h. After this time, the t-BuOH was removed, and the resulting residue was diluted with water and dichloromethane. The aqueous layer was extracted with 10% MeOH/DCM (4×10 mL). The pooled organic layers were washed with saturated sodium chloride solution, dried over Na_2SO_4 and concentrated in *vacuo*. The crude residue was purified by column chromatography on neutral alumina (70% EtoAc/hexane) yielded **176**, or **177** or *ent*-**177**.

10-(3-(5-methylhexyl)oxiran-2-yl)decyl 2-(2-((1-(4-bromophenyl)-1H-1,2,3-triazol-4-yl)methoxy)ethoxy)acetate (176)

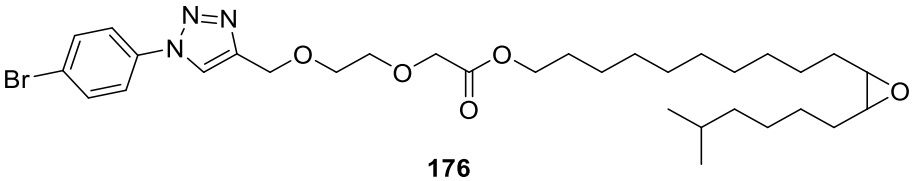

176

The compound **174** (4.2 mg, 58.3%): ^{1}H NMR (500 MHz, $CDCl_3$) δ: 8.08-8.05 (s, 1H), 7.66-7.65 (s, 4H), 4.80-4.78 (s, 2H), 4.15 (s, 2H), 4.15-4.12 (t, *J* = 5.7 Hz, 2H), 3.80-3.76 (td, *J* = 5.4, 3.5 Hz, 4H), 2.92-2.87 (m, 2H), 1.66-1.59 (m, 4H), 1.56-1.46 (m, 7H), 1.38-1.26 (m, 16H), 0.88-0.85 (d, *J* = 6.6 Hz, 6H). ^{13}C NMR (150 MHz, $CDCl_3$) δ: 170.40, 136.04, 132.86, 122.32, 121.88, 120.69, 70.86, 69.87, 68.65, 65.00, 64.67, 57.21, 38.88,

29.51, 29.43, 29.18, 28.56, 27.87, 27.85, 27.81, 27.30, 26.84, 26.60, 25.81, 22.60, 22.59. IR (neat): 2924, 2856, 1753, 1635, 1590, 1456, 1439, 1200, 1148, 1104 1029 cm^{-1}.

10-((2*S*,3*R*)-3-(5-methylhexyl)oxiran-2-yl)decyl 2-(2-((1-(4-bromophenyl)-1H-1,2,3-triazol-4-yl)methoxy)ethoxy)acetate (177)

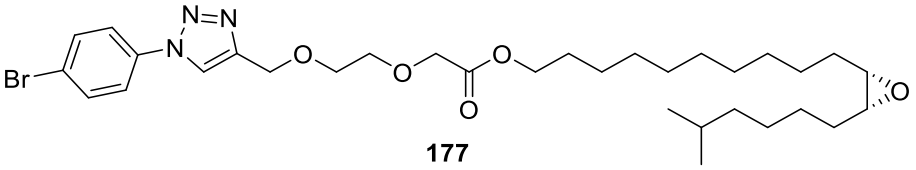

177

The compound **149** (3.9 mg, 54.1%): ^{1}H NMR (500 MHz, $CDCl_3$) δ: 8.08-8.05 (s, 1H), 7.66-7.65 (s, 4H), 4.80-4.78 (s, 2H), 4.15 (s, 2H), 4.15-4.12 (t, *J* = 5.7 Hz, 2H), 3.80-3.76 (td, *J* = 5.4, 3.5 Hz, 4H), 2.92-2.87 (m, 2H), 1.66-1.59 (m, 4H), 1.56-1.46 (m, 7H), 1.38-1.26 (m, 16H), 0.88-0.85 (d, *J* = 6.6 Hz, 6H). ^{13}C NMR (150 MHz, $CDCl_3$) δ: 170.40, 136.04, 132.86, 122.32, 121.88, 120.69, 70.86, 69.87, 68.65, 65.00, 64.67, 57.21, 38.88, 29.51, 29.43, 29.18, 28.56, 27.87, 27.85, 27.81, 27.30, 26.84, 26.60, 25.81, 22.60, 22.59. IR (neat): 2924, 2856, 1753, 1635, 1590, 1456, 1439, 1200, 1148, 1104 1029 cm^{-1}.

10-((2*R*,3*S*)-3-(5-methylhexyl)oxiran-2-yl)decyl 2-(2-((1-(4-bromophenyl)-1H-1,2,3-triazol-4-yl)methoxy)ethoxy)acetate (*ent*-177)

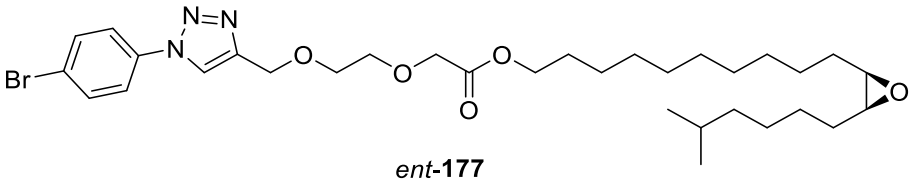

ent-**177**

The compound *ent*-**149** (4.0 mg, 55.5%): ^{1}H NMR (500 MHz, $CDCl_3$) δ: 8.08-8.06 (s, 1H), 7.66-7.65 (s, 4H), 4.80-4.78 (s, 2H), 4.15 (s, 2H), 4.15-4.12 (t, *J* = 5.7 Hz, 2H), 3.80-3.76 (m, 4H), 2.92-2.87 (m, 2H), 1.65-1.59 (m, 4H), 1.55-1.46 (m, 7H), 1.38-1.26 (m, 16H), 0.88-0.85 (d, *J* = 6.6 Hz, 6H). ^{13}C NMR (150 MHz, $CDCl_3$) δ: 170.40, 136.04, 132.86, 122.32, 121.88, 120.69, 70.86, 69.87, 68.65, 65.00, 64.67, 57.21, 38.88, 29.51, 29.43, 29.18, 28.56, 27.87, 27.85, 27.81, 27.30, 26.84, 26.60, 25.81, 22.60, 22.59. IR (neat): 2924, 2856, 1753, 1635, 1590, 1456, 1439, 1200, 1148, 1104 1029 cm^{-1}.

4.4.19. HPLC method for separating enantiomers of epoxy phenyltriazoles 176, 177 and *ent*-177

The resulting triazoles **176**, **177** and *ent*-**177** are UV absorbing compounds, which are amenable to separation by HPLC and detection by variable wavelength detector (VWD). The scalemic triazole **176** was separated by chiral HPLC using a chiral column (Phenomenex Lux 5µm Cellulose-2). The flow rate was set to be 0.2 mL/min. The solvent system IPA/hexane/DEA used as eluent. The enantiopure triazoles **177** and *ent*-**177** were eluted at 5.55 min and 6.56 min, respectively (Appendix C1). The enantiomeric excess of epoxy alkyne **149** and *ent*-**149** was determined to be greater than 98%.

4.4.20. Determination of Quantum Yield (Φ) and Molar Extinction Coefficient (ε) for 6-FAM (+)-disparlure (15d)

In order to determine the quantum yield (Φ) for the 6-FAM (+)-disparlure (**15d**), the 6-FAM azide was used as reference fluorophore as it has the same excitation and emission wavelengths as the 6-FAM (+)-disparlure. The quantum yield of 6-FAM azide is 0.90 at the excitation wavelength of 494 nm. In this experiment, the solutions of the reference and the sample (6-FAM (+)-disparlure) with the absorbance values from 0.01 to 0.04 were considered to minimize the fluorescence inner-filter effect (IFE). A series of four standard solutions in phosphate buffer or 1-heptanol were prepared each for 6-FAM (+)-disparlure and 6-FAM azide, with the absorbance values between 0.01 to 0.04. The absorption spectra of these solutions were recorded on VWR UV-6300PC double beam spectrophotometer (VWR, PA, USA) at excitation wavelength of 494 nm (Appendix C7). The fluorescence emission spectra of both reference and samples solutions were recorded on fluorescent spectrophotometer (PTI-QunataMaster) over the wavelength range 450 to 600 nm at excitation wavelength 494 nm (Appendix C8). The plots of integrated fluorescence intensity of the emission spectra against the absorbance of the both 6-FAM azide and 6-FAM (+)-disparlure showed a linear relationship (Appendix C9). The slope of the liner fit for the 6-FAMazide and 6-FAM (+)-disparlure is used to calculate the quantum yield (Φ) of 6-FAM (+)-disparlure according to the equation below.

$$\Phi FD = \Phi FA\ (mFD/mFA)\ (\eta 2FD/\eta 2FA) \quad \ldots\ldots\ldots\ldots\ldots\ldots\ldots\ldots (4.5)$$

Where ΦFD is the quantum yield of 6-FAM (+)-disparlure, ΦFA is the quantum yield of the 6-FAM azide (standard), mFD and mFA are the slope of the linear fit for the 6-

FAM (+)-disparlure and 6-FAM azide, respectively, and η2FD and η2FA are the refractive indices of the 6-FAM (+)-disparlure and 6-FAM azide solutions, respectively. Since the same buffer was used for both fluorophores, the term η2FD/η2FA = 1 and we get:

ΦFD = ΦFA (mFD/mFA)…….. (4.6)

To determine the molar extinction coefficient (ε) for 6-FAM (+)-disparlure 1a, a series of four sample solutions was prepared by diluting the 6-FAM (+)-disparlure in phosphate buffer (pH 8) or 1-heptanol. The absorption spectra for these solutions were recorded on UV/vis spectrophotometer at excitation wavelength of 494 nm. The plot of concentration of 6-FAM (+)-disparlure against the absorbance showed a linear relationship (Appendix C10). According to the Beer-Lambert law (A = εbc), where b is the path length of the cuvette which is equal to 1 in most instances. Therefore, the slope of absorbance (A) vs concentration plot is equal to the molar extinction coefficient.

4.4.21. Fluorescence binding assay

To determine the binding affinity of disparlure enantiomers to pheromone binding proteins (*Ldis* PBP1 and *Ldis* PBP2), fluorescence binding assays was conducted on a fluorescent spectrophotometer (PTI-QuantaMaster) using 6-FAM tagged disparlure enantiomers **15d** and *ent*-**15d** as fluorescent probes. The fluorescence spectra were recorded at room temperature with a silica quartz cuvette (light path = 1 cm). The protein (0.04 μm), *Ldis*PBP1 or *Ldis*PBP2 in 50 mM phosphate buffer (pH 8.0) was titrated with fluorescent probes **15d** or *ent*-**15d** to final concentrations 2-60nM. The fluorescent probes/*Ldis*PBPs complex was excited at 494 nm and the fluorescence emission spectra were monitored between 450 to 600 nm.

To measure the dissociation constant (K_d) of the complex, the values of florescent intensity of fluorescent probes at the emission maximum (after buffer and protein background correction) were plotted against total fluorescent probe concentrations and the data were fitted into nonlinear regression model (curve fit) using GraphPad Prism 5 (GraphPad Software LLC). To determine the K_d for the competitor ligands, (+)-disparlure (**15**) and (-)-disparlure (*ent*-**15**) the competitive binding assay was performed. Aliquots of the competitor ligand aliquots in ethanol were added to the solution containing 0.04 μM protein and fixed concentration of fluorescent probe (60 nM). A decrease in the relative

fluorescence intensity suggested that the competitor removed the fluorescent probe from the binding site of the protein. The inhibitory constant (K_i), which is dissociation constant (K_d) of the competitor, was calculated based on the competitor IC_{50} value using the following equation. $K_i = [IC_{50}]/(1+[6\text{-FAM dis}]/(K_{6\text{-FAM dis}})$. [6-FAM dis] = free 6-FAM dis concentration; $K_{6\text{-FAM}}$ dis = dissociation constant (K_d) for *Ldis*PBP/6-FAM dis (see below).

$$K_i = [IC_{50}]/1 + [F]/K_{dF}, \quad (4.7)$$

where [F] is the total fluorescent probe concentration and K_{dF} is the binding constant of the fluorescent probe to the *Ldis*PBPs. The dissociation constant of the ligand (K_{dL}, see Eq. 4.8 below) can then be obtained as follows. The equilibrium between P.F (the protein – fluorescent probe complex), L (the ligand of interest) and F (the fluorescent reporter) is:

$$P.F + L \leftrightarrow P.L + F$$

$$K_i = [P.F][L]/[P.L][F] \quad (4.8)$$

The equilibria between the probe and the protein, as well as the ligand and the protein are:

$$F + P \leftrightarrow P.F \quad K_{dF} = [P][F]/[P.F] \quad (4.9)$$

$$L + P \leftrightarrow P.L \quad K_{dL} = [P][L]/[P.L] \quad (4.10)$$

Substituting Eq. 4.9 and 4.10 into Eq. 4.8, we get:

$$K_i \times K_{dF} = K_{dL} \quad (4.11)$$

4.4.22. Stopped flow kinetics of *Ldis*PBPs and 6-FAM disparlure

The fluorescent traces of 6-FAM disparlure association and dissociation with *Ldis*PBPs were collected using stopped flow apparatus (Chirascan CS/SF, Applied Photophysics Ltd., United Kingdom). The kinetic experiments were performed at room temperature with the following parameters: excitation 494 nm, external trigger, data collection until 3.2 second with 1000 data points and 8 repeats. The 8 repeats/run were averaged to give the mean average fluorescent trace. This average fluorescent trace was considered as single

result. For the association kinetics, three trials were performed, respectively. For the association kinetics, *Ldis*PBP1 or *Ldis*PBP2 (1.2 µM) solution was prepared using 50 mM phosphate buffer (pH 8). This solution was loaded to one of the two reservoirs of the instrument while the second reservoir contained the solutions of various concentrations (0 to 1.6 µM) of 6-FAM (+)-disparlure **15d** or 6FAM (-)-disparlure *ent*-**15d** in the same buffer. The stopped-flow apparatus mixes the solutions in an equal volume ratio (1:1) from the two reservoirs. The final concentrations of protein and ligand were the following: (1) *Ldis*PBP1 or *Ldis*PBP2 0.6 µM, (2) 6FAM (+)-disparlure **15d** or 6FAM (-)-disparlure *ent*-**15d** 0 to 0.8 µM. After each run, the system was washed with water and buffer.

The initial velocity (V_0) of 6-FAM disparlure binding to *Ldis*PBP was determined from the best linear fit of the linear portion of the progress curves. The progress curves were obtained by plotting the (F_A/F_c) vs time.

Where $F_A = F_{obs}/F_{blank} = F_{6\text{-FAM dis}/Ldis\text{PBP}}/F_{6\text{-FAM dis}}$ and F_c = fluorescence constant, which is the slope of the linear portion of the saturation binding curve of 6-FAM dis and *Ldis*PBP.

The initial velocities of 6-FAM dis binding to *Ldis*PBP were fit into non-linear allosteric sigmoidal model. Fitting of these rates allowed calculation of V_{max}. The association rate constant (k_2) is calculated from the equation 4.4 (see Section 4.2.10).

For dissociation kinetic experiment, an equimolar solution of *Ldis*PBP1 or *Ldis*PBP2 (250 nM) and 6FAM (+)-disparlure **15d** or 6FAM (-)-disparlure *ent*-**15d** (250 nM) was prepared and equilibrated for 60 minutes at rt. In this experiment, the phosphate buffer solution was loaded in reservoir 1 and the equilibrated solution of *Ldis*PBP1 or *Ldis*PBP2 and 6FAM (+)-disparlure **15d** or 6FAM (-)-disparlure *ent*-**15d** placed in reservoir 2. After each run, the system was washed with water and buffer. The processed dissociation fluorescent traces were fitted in GraphPad Prism 9 (GraphPad Software, San Diego, California) kinetics binding dissociation one phase exponential decay to calculate k_{off} Value.

4.4.23. In Silico docking simulations of disparlre and 6FAM disparlure enantiomers

Disparlure and 6FAM disparlure docking experiments were simulated onto one of the two conformation (B-form) of *Ldis*PBPs. The homology models of *Ldis*PBP1and *Ldis*PBP2 were created by the SWISS-MODEL (expasy.org) using the *Bmor*PBP (*Bombyx*

mori) as a template (PDB ID: 1LS8.1.A). *Bmor*PBP was identified the closet sequence similarity for *Ldis*PBP1 and *Ldis*PBP2.by BLAST (basic local alignment search tool) protocol. The molecular docking experiments were performed in Molecular Operating Environment (MOE) using disparlure and 6FAM disparlure enantiomers as ligands. Before docking, the homology models of *Ldis*PBP1 and *Ldis*PBP2 were subjected to protonation using protonate 3D. The protonate 3D method predicts the hydrogen coordinates and ionization states to the protein structure using the molecular force field (MMFF94). The assignment of hydrogen coordinates includes determination of rotamers of –CH3, -NH3, -OH and –SH functional groups, ionization states of acids (Arg, Asp, Glu, and Lys) and base (His), and the tautomers of carboxylic acids (Asp) and imidazoles (His). Following protonation, protein models and ligands were energy minimized. The ligand binding sites were detected by application of MOE Site Finder and the results were ranked according to the PLB (Propensity for Ligand Binding) score. Ligands placement in the active site were performed using the Triangle Matcher method and ranked with London dG scoring function. The ligand possess were then ranked according to the calculated S score. The top pose (according to the S scoring function energies) was selected for protein-ligand interaction analysis.

The interactions of natural ligands and 6-FAM disparlure enantiomers with amino acid residues of *Ldis*PBPs were observed in MOE through the ligand interaction options. The interactions of side chain donors and acceptors, and of backbone donors and acceptors can be seen in Figures 4.11, 4.12, 4.13 and 4.14. The binding pocket residues of *Ldis*PBP1 and *Ldis*PBP2 shown to interact with respective atoms of natural ligands and 6-FAM disparlure enantiomers are summarized in Figure 4.13, Table 4.6 and 4.7 for *Ldis*PBP1 and Figure 4.14, Table 4.8 and 4.9 for *Ldis*PBP2.

Chapter 5.

Future work

In this thesis work, we have shown a concise total synthesis of gypsy moth sex pheromone (+)-disparlure, and its enantiomer (-)-disparlure. Apart from that, our synthetic route gave easy access not only to disparlure enantiomers but also to isotope labelled disparlure enantiomers and fluorescent probes which mimic (+)-disparlure and (-)-disparlure. Our flexible synthetic strategy would now allow us to investigate the synthesis of pheromone components of several bark beetle and moth species. For example, synthesis of bark beetle pheromones such as (+)-*exo*-brevicomin (**178**), (-)-*exo*-brevicomin (*ent*-**178**), (+)-*endo*-brevicomin (**179**) and (-)-*endo*-brevicomin (*ent*-**179**) (Figure 5.1).

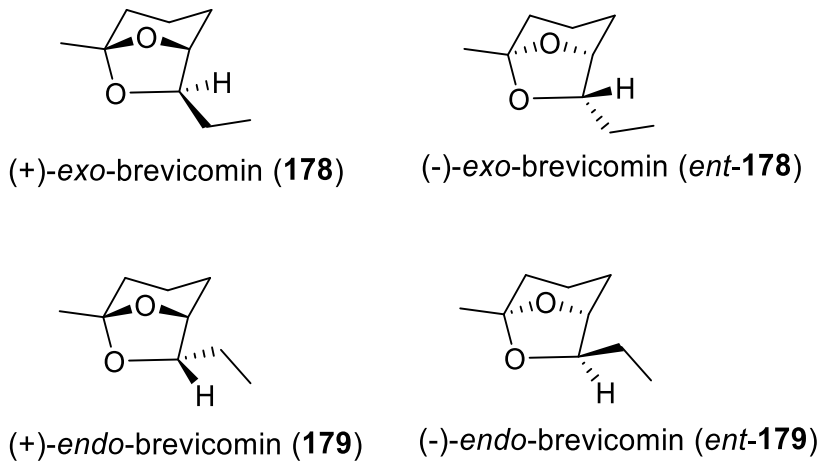

Figure 5.1 Structures of bark beetle pheromone components.

The enantiopure *exo*-and *endo*-isomers of brevicomins are the pheromone components of several species of pine and bark beetles and these brevicomins have been shown to be very important for their communication. For instance, the (+)-*exo*-brevicomin (**178**) is a major sex attractant of the western pine beetle, *Dendroctonus brevicomis,* which attacks the pine trees (Silverstein et al., 1968; Wood et al. 1976). The (-)-*exo*-brevicomin (*ent*-**178**) has been reported to be an aggregation pheromone for southern pine beetle *Dendroctonus frontalis* (Dickens and Payne, 1977). The (+)-*endo*-brevicomin (**3**) was identified to be a minor pheromone component in the natural pheromone blend produced

by the western pine beetle *D*. *brevicomics* (Silverstein et al., 1968; Bellas, Brownlee and Silverstein, 1969). The (+)-*endo*-brevicomin (**179**) enhances the response of pine beetle, *D*. *frontalis,* to their sex pheromone component frontaline, which is the isomer of brevicomin, whereas (-)-*endo*-brevicomin (*ent*-**179**) significantly inhibits this response (Vité et al., 1985).

These brevicomins have the bicyclic skeleton and all these have been target of several synthetic and entomological studies because of their utility in control of several bark beetle species. We propose the synthesis of enantiopure *exo*-and *endo*-isomers of brevicomin starting from *n*-butanal (**180**). Our synthetic strategy is shown in Scheme 5.1.

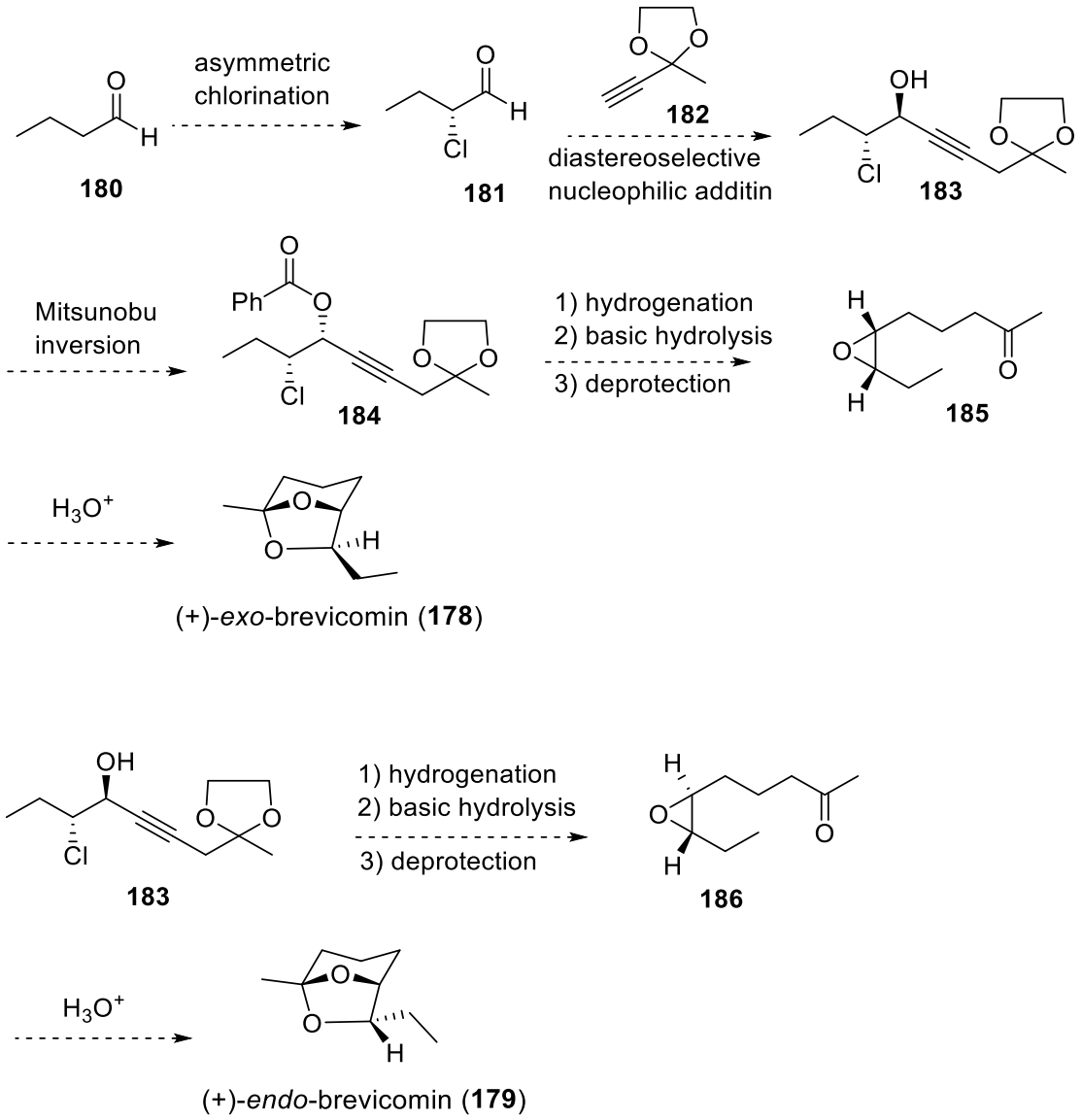

Scheme 5.1 Proposed synthesis of (+)-*exo*-brevicomin (178) and (+)-*endo*-brevicomin (179).

Our approach will begin with asymmetric α-chlorination of n-butanal (**180**) to afford the enantiopure α-chloroaldehyde **181**. Next, we will use diastereoselective addition to add the alkyne **182** to α-chloroaldehyde **181** and anticipate that this stereoselectivity of this reaction should favour the production of desired 1,2-*anti* chlorohydrin **183**. Subsequently, Mitsunobu inversion of the compound **183** would yield the 1,2-*syn* chloroester **184**. The hydrogenation of the alkyne moiety of the ester **184**, followed by basic hydrolysis to afford the *cis*-epoxide **185**. The acid-catalysed ring opening of epoxide with water should then yield (+)-*exo*-brevicomin (**178**). On other hand, the 1,2-*anti*

chlorohydrin **183** can be converted to *trans*-epoxide **186** and subsequent epoxide opening with water should then afford the (+)-*endo*-brevicomin (**179**). This synthetic approach can be easily adopted for the (-)-*exo*- and (-)-*endo* brevicomin (*ent*-**178** & **179**, respectively) synthesis by preparing the *ent*-**181** in the first step.

It has been demonstrated that insect olfactory neurons have specific types of olfactory receptor cells for each component of their pheromone and related compounds, such as isomers. The gypsy moth, *Lymantria dispar*, has a chiral epoxide, (+)-disparlure as sex attractant pheromone, produced and released by females and attractive to the males. Each enantiomer of disparlure delivers specific information to the insects, for example, attraction of males by (+)-disparlure, aggregation inhibition of females by (+)-disparlure and disruption of attraction by (-)-disparlure. Pheromones are detected by specific receptor cells expressed in the male gypsy moth antennae. We hypothesize that the two enantiomers of disparlure are perceived by separate receptors. The results from Chapter **3** and **4** demonstrated that the two pheromone binding proteins of gypsy moth (*Ldis*PBP1 and *Ldis*PBP2) selectively bind and interact with disparlure enantiomers. The LdisPBP1 binds selectively to (-)-disparlure, while LdisPBP2 prefers the sex pheromone (+)-disparlure. The existence of two PBPs on the antennae of *L*. *dispar* and selective binding interactions of these PBPs with disparlure enantiomers supports the hypothesis that the two enantiomers of disparlure are perceived by separate receptor neurons.

Future work should, therefore, attempts to identify the disparlure receptors on the antennae of *L*. *dispar*, in order to evaluate their functional properties with disparlure enantiomers and their possible interplay with *Ldis*PBP1 and *Ldis*PBP2. The receptors of disparlure enantiomers can be identified through chemical proteomics approach, which involves two steps: 1) biotinylated probe design and synthesis and 2) target fishing and identification. In chemical proteomics approach, designing and preparing the biotinylated probe is the first and crucial step for target identification. A biotinylated probe often consists of 3 parts: 1) a reactive head part, which is the structure of parent molecule and ensures that it keeps its ability to bind target proteins 2) an affinity tag such as biotin, for purification of target proteins with streptavidin beads 3) a spacer, to link the reactive head part and biotin, and this spacer should be long enough to avoid steric hindrance between reactive part and biotin (Sieber and Cravatt, 2006; Yang and Liu, 2015). I have designed and synthesized biotinylated disparlure probes **187** and **188** based on the synthetic schemes discussed in Chapter 4.

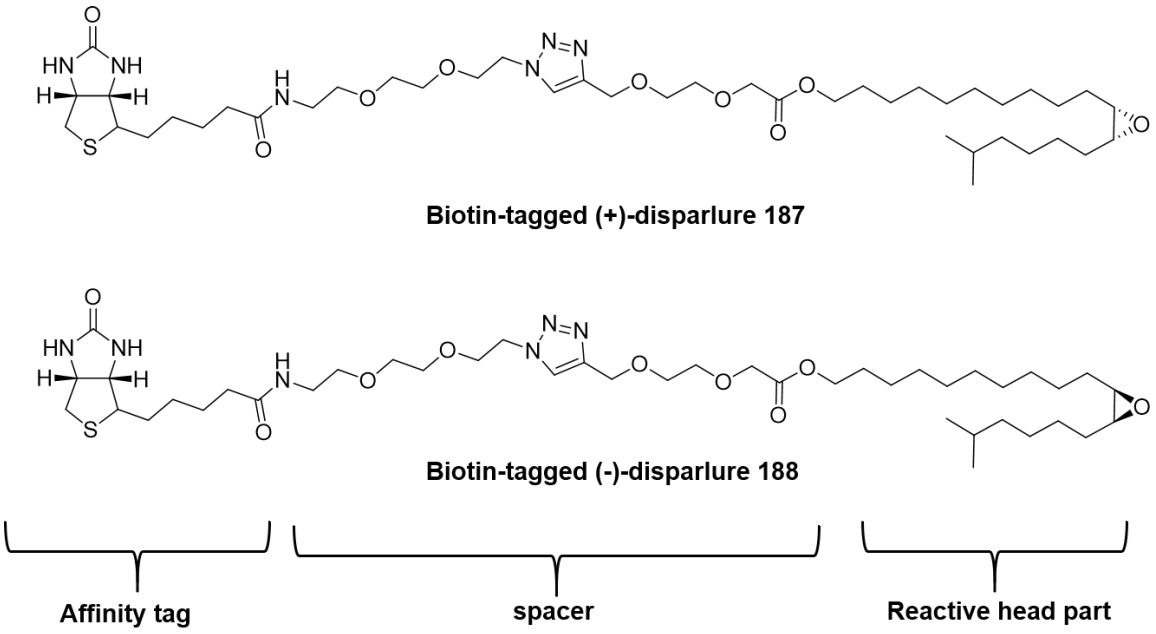

Figure 5.2 Structures of biotinylated disparlure probes.

A typical target fishing and identification procedure involves several steps as shown in Scheme 5.2. In this procedure, the reporter tag such as biotin acts as an affinity tag which can permits isolation of biotinylated probe-bound proteins with streptavidin beads. Washing of streptavidin beads can remove non-specific binding. The biotinylated probe-bound proteins could then be eluted from the beads and separated through SDS-PAGE or two-dimensional electrophoresis. Silver staining or Coomassie brilliant blue staining procedures can be used to detect the probe-bound proteins. The unique protein bands can be digested with trypsin. Finally, the digested peptide fragments can be identified with mass spectrometry and verified through protein bank for identity.

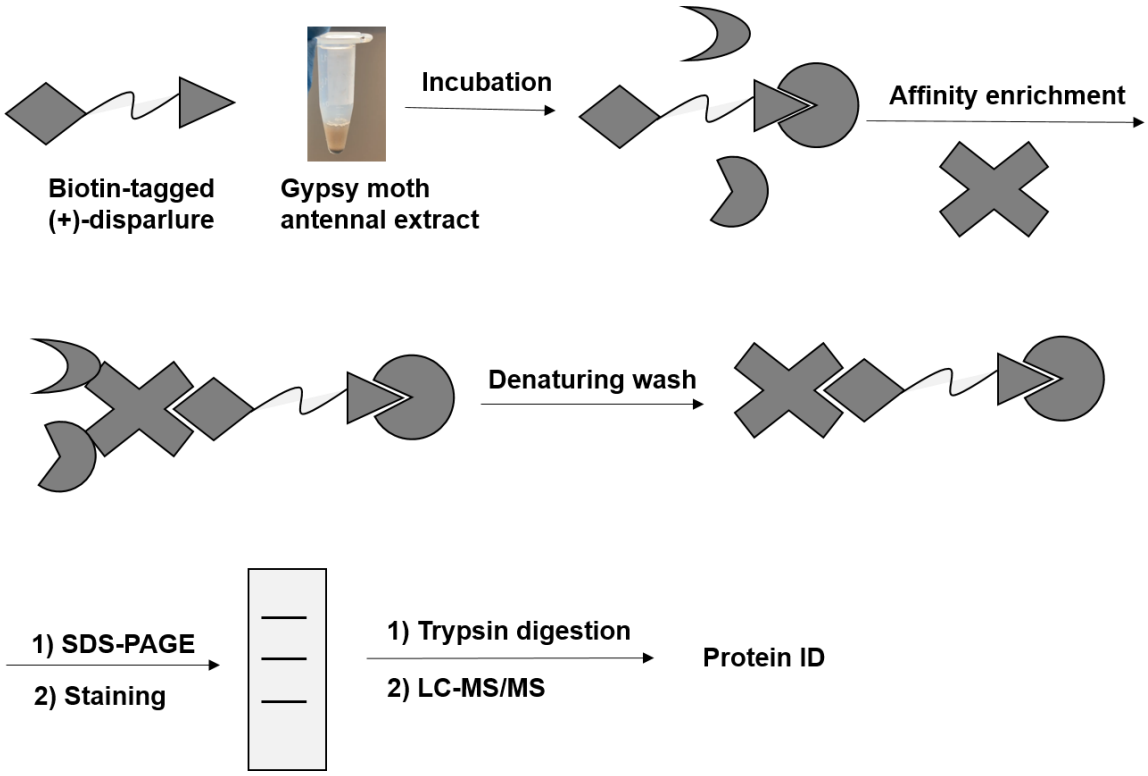

Scheme 5.2 Schematic of target identification with biotinylated probe.

References

Adachi, Y., Do, N. D., Kinjo, M., Makisako, S., Yamakawa, R., Mori, K., & Ando, T. (2010). Positions and stereochemistry of methyl branches in the novel sex pheromone components produced by a lichen moth, lyclene dharma dharma. *Journal of Chemical Ecology*. https://doi.org/10.1007/s10886-010-9813-3

Ahmad, S., Kirkland, K. E., & Blomquist, G. J. (1987). Evidence for a sex pheromone metabolizing cytochrome P-450 mono-oxygenase in the housefly. *Archives of Insect Biochemistry and Physiology*, *6*(2), 121–140. https://doi.org/10.1002/arch.940060206

Amatore, M., Beeson, T. D., Brown, S. P., & MacMillan, D. W. C. (2009). Enantioselective Linchpin Catalysis by SOMO Catalysis: An Approach to the Asymmetric α-Chlorination of Aldehydes and Terminal Epoxide Formation. *Angewandte Chemie International Edition*, *48*(28), 5121–5124. https://doi.org/10.1002/anie.200901855

Ando, T. (2011). *Internet database, 2011*. (http://www.tuat.ac.jp/~antetsu/Lists.htm)

Ando, T., Inomata, S.-I., & Yamamoto, M. (2004). *Lepidopteran Sex Pheromones*. https://doi.org/10.1007/b95449

Ando, T., Ohtani, K., Yamamoto, M., Miyamoto, T., Qin, X.-R., & Witjaksono. (1997). Sex Pheromone of Japanese Giant Looper, Ascotis selenaria cretacea: Identification and Field Tests. *Journal of Chemical Ecology*, *23*(10), 2413–2423. https://doi.org/10.1023/B:JOEC.0000006683.58028.1e

Anh, N. T., & Eisenstein, O. (1976). Induction asymetrique 1–2: Comparaison ab initio des modeles de cram, de cornforth, de karabatsos et de felkin. *Tetrahedron Letters*, *17*(3), 155–158. https://doi.org/10.1016/0040-4039(76)80002-0

Atlas, D., & Levitzki, A. (1977). Probing of β-adrenergic receptors by novel fluorescent β-adrenergic blockers. *Proceedings of the National Academy of Sciences*, *74*(12), 5290–5294.

Ban, L., Zhang, L., Yan, Y., & Pelosi, P. (2002). Binding properties of a locust's chemosensory protein. *Biochemical and Biophysical Research Communications*, *293*(1), 50–54. https://doi.org/10.1016/S0006-291X(02)00185-7

Bellas, T. E., Brownlee, R. G., & Silverstein, R. M. (1969). Synthesis of brevicomin, principal sex attractant in the frass of the female western pine beetle. *Tetrahedron*, *25*(21), 5149–5153. https://doi.org/10.1016/0040-4020(69)80035-9

Bethi, V., Kattanguru, P., & Fernandes, R. A. (2014). Domino Recombinant γ-Isomerization and Reverse Wacker Oxidation of γ-Vinyl-γ-butyrolactone: Synthesis of (+)- *trans*- , (-)- and (+)-Disparlures: Synthesis of Disparlures. *European Journal of Organic Chemistry*, *2014*(15), 3249–3255. https://doi.org/10.1002/ejoc.201400021

Biasini, M., Bienert, S., Waterhouse, A., Arnold, K., Studer, G., Schmidt, T., Kiefer, F., Gallo Cassarino, T., Bertoni, M., Bordoli, L., & Schwede, T. (2014). SWISS-MODEL: Modelling protein tertiary and quaternary structure using evolutionary information. *Nucleic Acids Research*, *42*(Web Server issue), W252-258. https://doi.org/10.1093/nar/gku340

Bierl, B. A., Beroza, M., & Collier, C. W. (1970). Potent Sex Attractant of the Gypsy Moth: Its Isolation, Identification, and Synthesis. *Science*, *170*(3953), 87–89. https://doi.org/10.1126/science.170.3953.87

Birlirakis, N., Briand, L., Pernollet, J.-C., & Guittet, E. (2001). Letter to the Editor: 1H, 13C and 15N chemical shift assignment of the honeybee pheromone carrier protein ASP1. *Journal of Biomolecular NMR*, *20*(2), 183–184. https://doi.org/10.1023/A:1011243815544

Boeckh, J., Kaissling, K. E., & Schneider, D. (1965). *Insect olfactory receptors*.

Bowers, W. S. (2002). Insect Physiology and Biochemistry. *Journal of Chemical Ecology*, *28*(12), 2633–2635. https://doi.org/10.1023/A:1021485306837

Brevet, J.-L., & Mori, K. (1992). Pheromone Synthesis; CXXXIX. Enzymatic Preparation of (2S,3R)-4-Acetoxy-2,3-epoxybutan-1-ol and Its Conversion to the Epoxy Pheromones of the Gypsy Moth and the Ruby Tiger Moth. *Synthesis*, *1992*(10), 1007–1012. https://doi.org/10.1055/s-1992-26290

Britton, R., & Kang, B. (2013). α-Haloaldehydes: Versatile building blocks for natural product synthesis. *Natural Product Reports*, *30*(2), 227–236. https://doi.org/10.1039/C2NP20108A

Brochu, M. P., Brown, S. P., & MacMillan, D. W. C. (2004). Direct and Enantioselective Organocatalytic α-Chlorination of Aldehydes. *Journal of the American Chemical Society*, *126*(13), 4108–4109. https://doi.org/10.1021/ja049562z

B:urgi, H. B., Dunitz, J. D., Lehn, J. M., & Wipff, G. (1974). Stereochemistry of reaction paths at carbonyl centres. *Tetrahedron*, *30*(12), 1563–1572. https://doi.org/10.1016/S0040-4020(01)90678-7

Burgi, H. B., Dunitz, J. D., & Shefter, Eli. (1973). Geometrical reaction coordinates. II. Nucleophilic addition to a carbonyl group. *Journal of the American Chemical Society*, *95*(15), 5065–5067. https://doi.org/10.1021/ja00796a058

Butenandt et al., V. A. (1959). Uber den sexsual-lockstoff des seidenspinners Bombyx mori. *Reindarstellung Und Konstitution. Z. Naturforschg, b*, *14*, 283.

Campanacci, V., Krieger, J., Bette, S., Sturgis, J. N., Lartigue, A., Cambillau, C., Breer, H., & Tegoni, M. (2001). Revisiting the Specificity of Mamestra brassicaeand Antheraea polyphemus Pheromone-binding Proteins with a Fluorescence Binding Assay. *Journal of Biological Chemistry*, *276*(23), 20078–20084. https://doi.org/10.1074/jbc.M100713200

Cantor, C. R., Cantor, R. C., & Schimmel, P. R. (1980). *Biophysical Chemistry: Part I: The Conformation of Biological Macromolecules*. W. H. Freeman.

CardÉ, R. T., Doane, C. C., Baker, T. C., Iwaki, S., & Marumo, S. (1977). Attractancy of Optically Active Pheromone for Male Gypsy Moths12. *Environmental Entomology*, *6*(6), 768–772. https://doi.org/10.1093/ee/6.6.768

Cee, V. J., Cramer, C. J., & Evans, D. A. (2006). Theoretical Investigation of Enolborane Addition to α-Heteroatom-Substituted Aldehydes. Relevance of the Cornforth and Polar Felkin−Anh Models for Asymmetric Induction. *Journal of the American Chemical Society*, *128*(9), 2920–2930. https://doi.org/10.1021/ja0555670

Challa, V. R., Kwon, D., Taron, M., Fan, H., Kang, B., Wilson, D., Haeckl, F. P. J., Keerthisinghe, S., Linington, R. G., & Britton, R. (2021). Total synthesis of biselide A. *Chemical Science*, *12*(15), 5534–5543. https://doi.org/10.1039/D0SC06223E

Chang, H., Guo, M., Wang, B., Liu, Y., Dong, S., & Wang, G. (2016). Sensillar expression and responses of olfactory receptors reveal different peripheral coding in two Helicoverpa species using the same pheromone components. *Scientific Reports*, *6*(1), 18742. https://doi.org/10.1038/srep18742

Chang, H., Liu, Y., Yang, T., Pelosi, P., Dong, S., & Wang, G. (2015). Pheromone binding proteins enhance the sensitivity of olfactory receptors to sex pheromones in Chilo suppressalis. *Scientific Reports*, *5*(1), 13093. https://doi.org/10.1038/srep13093

Chang, S., Hur, S., & Britton, R. (2015). Total Synthesis and Configurational Assignment of Ascospiroketal A. *Chemistry – A European Journal*, *21*(46), 16646–16653. https://doi.org/10.1002/chem.201502754

Chao-Xin, Z., Shi-Jun, D. A., Hua-Bing, Z., Bin, S. U. N., & Ying, L. I. (2007). Asymmetric Total Synthesis of (＋)-Disparlure: (＋)-(7R,8S)-cis-7,8- ep-oxy-2-methyloctadecane. *Acta Chimica Sinica*, *65*(21), 2433.

Chérest, M., Felkin, H., & Prudent, N. (1968). Torsional strain involving partial bonds. The stereochemistry of the lithium aluminium hydride reduction of some simple open-chain ketones. *Tetrahedron Letters*, *9*(18), 2199–2204. https://doi.org/10.1016/S0040-4039(00)89719-1

Chiu, C. C., Keeling, C. I., & Bohlmann, J. (2019). The cytochrome P450 CYP6DE1 catalyzes the conversion of α-pinene into the mountain pine beetle aggregation pheromone trans -verbenol. *Scientific Reports*, *9*(1), 1–10. https://doi.org/10.1038/s41598-018-38047-8

Chow, Y. S. (2001). Preliminary identification of the sex pheromone of Orgyia postica (Walker) (Lepidoptera: Lymantriidae). *Entomol. Sin.*, *8*(Suppl.), 13–20.

Cornforth, J. W., Cornforth, R. H., & Mathew, K. K. (1959). 24. A General Stereoselective Synthesis of olefins. *J. Chem. Soc.,* 112–127.

Daly, C. J., & McGrath, J. C. (2003). Fluorescent ligands, antibodies, and proteins for the study of receptors. *Pharmacology & Therapeutics*, *100*(2), 101–118. https://doi.org/10.1016/j.pharmthera.2003.08.001

Damberger, F. F., Ishida, Y., Leal, W. S., & Wüthrich, K. (2007). Structural Basis of Ligand Binding and Release in Insect Pheromone-binding Proteins: NMR Structure of Antheraea polyphemus PBP1 at pH 4.5. *Journal of Molecular Biology*, *373*(4), 811–819. https://doi.org/10.1016/j.jmb.2007.07.078

Damberger, F., Nikonova, L., Horst, R., Peng, G., Leal, W. S., & Wüthrich, K. (2000). NMR characterization of a pH-dependent equilibrium between two folded solution conformations of the pheromone-binding protein from Bombyx mori. *Protein Science: A Publication of the Protein Society*, *9*(5), 1038–1041. https://doi.org/10.1110/ps.9.5.1038

Dhand, V., Chang, S., & Britton, R. (2013). Total Synthesis of the Cytotoxic Anhydrophytosphingosine Pachastrissamine (Jaspine B). *The Journal of Organic Chemistry*, *78*(16), 8208–8213. https://doi.org/10.1021/jo4013223

Dhand, V., Draper, J. A., Moore, J., & Britton, R. (2013). A Short, Organocatalytic Formal Synthesis of (−)-Swainsonine and Related Alkaloids. *Organic Letters*, *15*(8), 1914–1917. https://doi.org/10.1021/ol400566j

Dickens, J. C., & Payne, T. L. (1977). Bark beetle olfaction: Pheromone receptor system in Dendroctonus frontalis. *Journal of Insect Physiology*, *23*(4), 481–489. https://doi.org/10.1016/0022-1910(77)90258-X

Drop, A., Wojtasek, H., & Frąckowiak-Wojtasek, B. (2020). Synthesis of disparlure and monachalure enantiomers from 2,3-butanediacetals. *Beilstein Journal of Organic Chemistry*, *16*(1), 616–620. https://doi.org/10.3762/bjoc.16.57

Du, G., Ng, C.-S., & Prestwich, G. D. (1994). Odorant Binding by a Pheromone Binding Protein: Active Site Mapping by Photoaffinity Labeling. *Biochemistry*, *33*(16), 4812–4819. https://doi.org/10.1021/bi00182a009

Du, G., & Prestwich, G. D. (1995). Protein structure encodes the ligand binding specificity in pheromone binding proteins. *Biochemistry*, *34*(27), 8726–8732. https://doi.org/10.1021/bi00027a023

Dubey, A. K., & Chattopadhyay, A. (2011). An enantiodivergent synthesis of both (+)- and (−)-disparlure from (R)-2,3-cyclohexylideneglyceraldehyde. *Tetrahedron: Asymmetry*, *22*(14), 1516–1521. https://doi.org/10.1016/j.tetasy.2011.08.013

Eiter, K., Truscheit, E., & Boneβ, M. (1967). Neuere Ergebnisse der Chemie von Insektensexuallockstoffen. Synthesen von D,L-10-Acetoxy-hexadecen-(7-cis)-ol-(1), 12-Acetoxy-octadecen-(9-cis)-ol-(1) („Gyplure") und 1-Acetoxy-10-propyl-tridecadien-(5-trans. 9)—Eiter—1967—Justus Liebigs Annalen der Chemie—Wiley Online Library. https://onlinelibrary.wiley.com/doi/10.1002/jlac.19677090104

Evans, D. A., Siska, S. J., & Cee, V. J. (2003). Resurrecting the Cornforth Model for Carbonyl Addition: Studies on the Origin of 1,2-Asymmetric Induction in Enolate Additions to Heteroatom-Substituted Aldehydes. *Angewandte Chemie International Edition*, *42*(15), 1761–1765. https://doi.org/10.1002/anie.200350979

Fadamiro, H. Y., Cossé, A. A., & Baker, T. C. (1999). Fine-scale resolution of closely spaced pheromone and antagonist filaments by flying male Helicoverpa zea. *Journal of Comparative Physiology A*, *185*(2), 131–141. https://doi.org/10.1007/s003590050372

Faucheux, M. J. (1985). Morphology and distribution of antennal sensilla in the female and male clothes moth, Tineola bisselliella Humm. (Lepidoptera: Tineidae). *Canadian Journal of Zoology*, *63*(2), 355–362. https://doi.org/10.1139/z85-054

Feng, L., & Prestwich, G. D. (1997). Expression and characterization of a lepidopteran general odorant binding protein. *Insect Biochemistry and Molecular Biology*, *27*(5), 405–412. https://doi.org/10.1016/S0965-1748(97)00012-X.

Forstner, M., Breer, H., & Krieger, J. (2009). A receptor and binding protein interplay in the detection of a distinct pheromone component in the silkmoth Antheraea polyphemus. *International Journal of Biological Sciences*, *5*(7), 745–757.

Fernandes, R.A., Chandra, N., & Gangani, J.A. (2020). Three Decades of Disparlure and Analogue Synthesis. *New Journal of Chemistry*. https://doi.org/10.1039/D0NJ03582C

Forstner, M., Gohl, T., Breer, H., & Krieger, J. (2006). Candidate pheromone binding proteins of the silkmoth Bombyx mori. *Invertebrate Neuroscience*, *6*(4), 177–187. https://doi.org/10.1007/s10158-006-0032-0

Fukusaki, E., Senda, S., Nakazono, Y., Yuasa, H., & Omata, T. (1992). Large-scale preparation of (+)-disparlure, the gypsy moth pheromone, by a practical chemico-enzymatic procedure. *Journal of Fermentation and Bioengineering*, *73*(4), 284–286. https://doi.org/10.1016/0922-338X(92)90184-V

Garg, Y., Kumar Tiwari, A., & Kumar Pandey, S. (2017). Enantioselective total synthesis of cis -(+)- and trans -(+)-disparlure. *Tetrahedron Letters*, *58*(34), 3344–3346. https://doi.org/10.1016/j.tetlet.2017.07.024

Gomez-Diaz, C., Reina, J. H., Cambillau, C., & Benton, R. (2013). Ligands for Pheromone-Sensing Neurons Are Not Conformationally Activated Odorant Binding Proteins. *PLOS Biology*, *11*(4), e1001546. https://doi.org/10.1371/journal.pbio.1001546

Gong, Y., Pace, T. C. S., Castillo, C., Bohne, C., O'Neill, M. A., & Plettner, E. (2009). Ligand-Interaction Kinetics of the Pheromone- Binding Protein from the Gypsy Moth, L. dispar: Insights into the Mechanism of Binding and Release. *Chemistry & Biology*, *16*(2), 162–172. https://doi.org/10.1016/j.chembiol.2009.01.005

Gong, Y., & Plettner, E. (2011). Effects of aromatic compounds on antennal responses and on the pheromone-binding proteins of the gypsy moth (Lymantria dispar). *Chemical Senses*, *36*(3), 291–300. https://doi.org/10.1093/chemse/bjq130

Gong, Y., Tang, H., Bohne, C., & Plettner, E. (2010). Binding Conformation and Kinetics of Two Pheromone-Binding Proteins from the Gypsy Moth Lymantria dispar with Biological and Nonbiological Ligands. *Biochemistry*, *49*(4), 793–801. https://doi.org/10.1021/bi901145a

Graham, S. M., & Prestwich, G. D. (1992). Tissue distribution and substrate specificity of an epoxide hydrase in the gypsy moth,Lymantria dispar. *Experientia*, *48*(1), 19–21. https://doi.org/10.1007/BF01923597

Graham, T. H., Horning, B. D., & MacMillan, D. W. C. (2011). The preparation of (2R,5S)-2-t-butyl-3,5-dimethylimidazolidin-4-one. *Organic Syntheses*, *88*, 42. https://doi.org/10.15227/orgsyn.088.0042

Gries, R., Khaskin, G., Schaefer, P. W., Hahn, R., Gotoh, T., & Gries, G. (2005). (7*R*,8*S*)-cis-7,8-epoxy-2-methyloctadec-17-ene: A novel trace component from the sex pheromone gland of gypsy moth, Lymantria dispar. *Journal of Chemical Ecology*, *31*(1), 49–62. https://doi.org/10.1007/s10886-005-0973-5

Große-Wilde, E., Gohl, T., Bouché, E., Breer, H., & Krieger, J. (2007). Candidate pheromone receptors provide the basis for the response of distinct antennal neurons to pheromonal compounds. *European Journal of Neuroscience*, *25*(8), 2364–2373. https://doi.org/10.1111/j.1460-9568.2007.05512.x

Grosse-Wilde, E., Svatos, A., & Krieger, J. (2006). A pheromone-binding protein mediates the bombykol-induced activation of a pheromone receptor in vitro. *Chemical Senses*, *31*(6), 547–555. https://doi.org/10.1093/chemse/bjj059

Haidekker, M. A., & Theodorakis, E. A. (2007). Molecular rotors—Fluorescent biosensors for viscosity and flow. *Organic & Biomolecular Chemistry*, *5*(11), 1669–1678. https://doi.org/10.1039/B618415D

Halland, N., Braunton, A., Bachmann, S., Marigo, M., & Jørgensen, K. A. (2004). Direct Organocatalytic Asymmetric α-Chlorination of Aldehydes. *Journal of the American Chemical Society*, *126*(15), 4790–4791. https://doi.org/10.1021/ja049231m

Halperin, S. D., Kang, B., & Britton, R. (2011). Lithium Aldol Reactions of α-Chloroaldehydes Provide Versatile Building Blocks for Natural Product Synthesis. *Synthesis*, *2011*(12), 1946–1953. https://doi.org/10.1055/s-0030-1260032

Hansen, K. (1984). Discrimination and production of disparlure enantiomers by the gypsy moth and the nun moth. *Physiological Entomology*, *9*(1), 9–18. https://doi.org/10.1111/j.1365-3032.1984.tb00676.x

Hill, A. S., Kovalev, B. G., Nikolaeva, L. N., & Roelofs, W. L. (1982). Sex pheromone of the fall webworm moth,Hyphantria cunea. *Journal of Chemical Ecology*, *8*(2), 383–396. https://doi.org/10.1007/BF00987787

Holmes, M., Kwon, D., Taron, M., & Britton, R. (2015). Total Synthesis of Amphirionin-4. *Organic Letters*, *17*(15), 3868–3871. https://doi.org/10.1021/acs.orglett.5b01844

Holmes, M. T., & Britton, R. (2013). Total Synthesis and Structural Revision of Laurefurenynes A and B. *Chemistry – A European Journal*, *19*(38), 12649–12652. https://doi.org/10.1002/chem.201302352

Honson, N., Johnson, M. A., Oliver, J. E., Prestwich, G. D., & Plettner, E. (2003). Structure–Activity Studies with Pheromone-binding Proteins of the Gypsy Moth, Lymantria dispar. *Chemical Senses*, *28*(6), 479–489. https://doi.org/10.1093/chemse/28.6.479

Honson, N. S., Gong, Y., & Plettner, E. (2005). Structure and Function of Insect Odorant and Pheromone-Binding Proteins (OBPs and PBPs) and Chemosensory-Specific Proteins (CSPs). In *Recent Advances in Phytochemistry* (Vol. 39, pp. 227–268). Elsevier. https://doi.org/10.1016/S0079-9920(05)80010-3

Honson, N. S., & Plettner, E. (2006). Disulfide connectivity and reduction in pheromone-binding proteins of the gypsy moth, Lymantria dispar. *Naturwissenschaften*, *93*(6), 267–277. https://doi.org/10.1007/s00114-006-0096-z

Hooper, A. M., Dufour, S., He, X., Muck, A., Zhou, J.-J., Almeida, R., Field, L. M., Svatos, A., & Pickett, J. A. (2009). High-throughput ESI-MS analysis of binding between the Bombyx mori pheromone-binding protein BmorPBP1, its pheromone components and some analogues. *Chemical Communications (Cambridge, England)*, *38*, 5725–5727. https://doi.org/10.1039/b914294k

Horst, R., Damberger, F., Luginbühl, P., Güntert, P., Peng, G., Nikonova, L., Leal, W. S., & Wüthrich, K. (2001). NMR structure reveals intramolecular regulation mechanism for pheromone binding and release. *Proceedings of the National Academy of Sciences*, *98*(25), 14374–14379. https://doi.org/10.1073/pnas.251532998

Hu, S., Jayaraman, S., & Oehlschlager, A. C. (1999). An Efficient Enantioselective Synthesis of (+)-Disparlure. *The Journal of Organic Chemistry*, *64*(10), 3719–3721. https://doi.org/10.1021/jo9820871

Huisgen, R. (1963). 1,3-Dipolar Cycloadditions. Past and Future. *Angewandte Chemie International Edition in English*, *2*(10), 565–598. https://doi.org/10.1002/anie.196305651

Inkster, J. A. H., Ling, I., Honson, N. S., Jacquet, L., Gries, R., & Plettner, E. (2005). Synthesis of disparlure analogues, using resolution on microcrystalline cellulose triacetate-I. *Tetrahedron: Asymmetry*, *16*(23), 3773–3784. https://doi.org/10.1016/j.tetasy.2005.10.031

Ishida, Y., & Leal, W. S. (2008). Chiral discrimination of the Japanese beetle sex pheromone and a behavioral antagonist by a pheromone-degrading enzyme. *Proceedings of the National Academy of Sciences of the United States of America*, *105*(26), 9076–9080. https://doi.org/10.1073/pnas.0802610105

Iwaki, S., Marumo, S., Saito, T., Yamada, M., & Katagiri, K. (1974). Synthesis and activity of optically active disparlure. *Journal of the American Chemical Society*, *96*(25), 7842–7844. https://doi.org/10.1021/ja00832a055

Jacobson, M., Beroza, M., & Jones, W. A. (1960). Isolation, Identification, and Synthesis of the Sex Attractant of Gypsy Moth. *Science*, *132*(3433), 1011–1012. https://doi.org/10.1126/science.132.3433.1011

Jacobson, M., & Jones, W. A. (1962). Insect Sex Attractants. II. The Synthesis of a Highly Potent Gypsy Moth Sex Attractant and Some Related Compounds1. *The Journal of Organic Chemistry*, *27*(7), 2523–2524. https://doi.org/10.1021/jo01054a052

Jacobson, M., Schwarz, M., & Waters, R. M. (1970). Gypsy Moth Sex Attractants: A Reinvestigation. *Journal of Economic Entomology*, *63*(3), 943–945. https://doi.org/10.1093/jee/63.3.943

Jurenka, R. A., Subchev, M., Abad, J.-L., Choi, M.-Y., & Fabrias, G. (2003). Sex pheromone biosynthetic pathway for disparlure in the gypsy moth, Lymantria dispar. *Proceedings of the National Academy of Sciences*, *100*(3), 809–814. https://doi.org/10.1073/pnas.0236060100

Kaissling, K. (1986). Chemo-Electrical Transduction in Insect Olfactory Receptors. *Annual Review of Neuroscience*, *9*(1), 121–145. https://doi.org/10.1146/annurev.ne.09.030186.001005

Kaissling, K. E. (1996). Peripheral mechanisms of pheromone reception in moths. *Chemical Senses*, *21*(2), 257–268. https://doi.org/10.1093/chemse/21.2.257

Kaissling, K. E., Kasang, G., Bestmann, H. J., Stransky, W., & Vostrowsky, O. (1978). A new pheromone of the silkworm moth Bombyx mori. *Naturwissenschaften*, *65*, 382–384. https://doi.org/10.1007/BF00439702

Kaissling, K.-E. (1971). Insect Olfaction. In J. E. Amoore, M. G. J. Beets, J. T. Davies, T. Engen, J. Garcia, R. C. Gesteland, P. P. C. Graziadei, K.-E. Kaissling, R. A. Koelling, J. LeMagnen, P. MacLeod, D. G. Moulton, M. M. Mozell, D. Ottoson, T. S. Parsons, S. F. Takagi, D. Tucker, B. M. Wenzel, & L. M. Beidler (Eds.), *Olfaction* (pp. 351–431). Springer. https://doi.org/10.1007/978-3-642-65126-7_14

Kaissling, K.-E. (2001). Olfactory Perireceptor and Receptor Events in Moths: A Kinetic Model. *Chemical Senses*, *26*(2), 125–150. https://doi.org/10.1093/chemse/26.2.125

Kaissling, K.-E. (2009). Olfactory perireceptor and receptor events in moths: A kinetic model revised. *Journal of Comparative Physiology A*, *195*(10), 895–922. https://doi.org/10.1007/s00359-009-0461-4

Kaissling, K.-E. (2013). Kinetics of olfactory responses might largely depend on the odorant–receptor interaction and the odorant deactivation postulated for flux detectors. *Journal of Comparative Physiology A*, *199*(11), 879–896. https://doi.org/10.1007/s00359-013-0812-z

Kaissling, K.-E. (1974). Sensory Transduction in Insect Olfactory Receptors. In L. Jaenicke (Ed.), *Biochemistry of Sensory Functions* (pp. 243–273). Springer. https://doi.org/10.1007/978-3-642-66012-2_15

Kaissling, K.-E., & Thorson, J. (1980). Insect Olfactory Sensilla: Structural, Chemical and Electrical Aspects of the Functional Organisation. *Receptors for Neurotransmitters, Hormones and Pheromones in Insects*, 261–282.

Kanaujia, S., & Kaissling, K. E. (1985). Interactions of pheromone with moth antennae: Adsorption, desorption and transport. *Journal of Insect Physiology*, *31*(1), 71–81. https://doi.org/10.1016/0022-1910(85)90044-7

Kang, B., & Britton, R. (2007). A General Method for the Synthesis of Nonracemic trans-Epoxides: Concise Syntheses of trans-Epoxide-Containing Insect Sex Pheromones. *Organic Letters*, *9*(24), 5083–5086. https://doi.org/10.1021/ol702273n

Kang, B., Mowat, J., Pinter, T., & Britton, R. (2009). Development of a Concise and General Enantioselective Approach to 2,5-Disubstituted-3-hydroxytetrahydrofurans. *Organic Letters*, *11*(8), 1717–1720. https://doi.org/10.1021/ol802711s

Kang, S.-K., Kim, Y.-S., Lim, J.-S., Kim, K.-S., & Kim, S.-G. (1991). Synthesis of chiral epoxy alcohols: Synthesis of (+)-disparlure. *Tetrahedron Letters*, *32*(3), 363–366. https://doi.org/10.1016/S0040-4039(00)92629-7

Karlson, P., & Lüscher, M. (1959). 'Pheromones': A New Term for a Class of Biologically Active Substances. *Nature*, *183*(4653), 55–56. https://doi.org/10.1038/183055a0

Kasang, G. (1971). Bombykol reception and metabolism on the antennae of the silkmoth Bombys mori. In *In Gustation and Olfaction* (pp. 245–250). Academic Press, London/New York, 1971.

Kasang, G., Knauer, B., & Beroza, M. (1974). Uptake of the sex attractant3H-disparlure by male gypsy moth antennae(Lymantria dispar) [=Porthetria dispar-]. *Experientia*, *30*(2), 147–148. https://doi.org/10.1007/BF01927698

Katre, U. V., Mazumder, S., Prusti, R. K., & Mohanty, S. (2009). Ligand Binding Turns Moth Pheromone-binding Protein into a pH Sensor. *The Journal of Biological Chemistry*, *284*(46), 32167–32177. https://doi.org/10.1074/jbc.M109.013383

Keinan, E., Sinha, S. C., Sinha-Bagchi, A., Zhi-Min, W., Xiu-Lian, Z., & Sharpless, K. B. (1992). Synthesis of all four isomers of disparlure using osmium-catalyzed asymmetric dihydroxylation. *Tetrahedron Letters*, *33*(43), 6411–6414. https://doi.org/10.1016/S0040-4039(00)79002-2

Kim, S.-G. (2009). Concise Total Synthesis of (+)-Disparlure and its trans-Isomer Using Asymmetric Organocatalysis. *Synthesis*, *2009*(14), 2418–2422. https://doi.org/10.1055/s-0029-1216855

Klein, U. (1987). Sensillum-lymph proteins from antennal olfactory hairs of the moth Antheraea polyphemus (Saturniidae). *Insect Biochemistry*, *17*(8), 1193–1204. https://doi.org/10.1016/0020-1790(87)90093-X

Kleinpeter, E., Krüger, S., & Koch, A. (2015). Anisotropy Effect of Three-Membered Rings in 1H NMR Spectra: Quantification by TSNMRS and Assignment of the Stereochemistry. *The Journal of Physical Chemistry A*, *119*(18), 4268–4276. https://doi.org/10.1021/acs.jpca.5b03078

Klosowski, D. W., & Martin, S. F. (2018). Synthesis of (+)-Disparlure via Enantioselective Iodolactonization. *Organic Letters*, *20*(5), 1269–1271. https://doi.org/10.1021/acs.orglett.7b03911

Ko, S. Y. (1994). Cis-epoxides via sharpless' asymmetric dihydroxylation reaction: Synthesis of (+)-disparlure. *Tetrahedron Letters*, *35*(21), 3601–3604. https://doi.org/10.1016/S0040-4039(00)73251-5

Kochansky, J., Tette, J., Taschenberg, E. F., Cardé, R. T., Kaissling, K.-E., & Roelofs, W. L. (1975). Sex pheromone of the moth, Antheraea polyphemus. *Journal of Insect Physiology*, *21*(12), 1977–1983. https://doi.org/10.1016/0022-1910(75)90230-9

Koumbis, A. E., & Chronopoulos, D. D. (2005a). A short and efficient synthesis of (+)-disparlure and its enantiomer. *Tetrahedron Letters*, *46*(25), 4353–4355. https://doi.org/10.1016/j.tetlet.2005.04.081

Koumbis, A. E., & Chronopoulos, D. D. (2005b). A short and efficient synthesis of (+)-disparlure and its enantiomer. *Tetrahedron Letters*, *46*(25), 4353–4355. https://doi.org/10.1016/j.tetlet.2005.04.081

Kovalenko, V. N., Masalov, N. V., & Kulinkovich, O. G. (2009). Synthesis of (+)-disparlure from diethyl (−)-malate via opening and fragmentation of the three-membered ring in tertiary cyclopropanols. *Russian Journal of Organic Chemistry*, *45*(9), 1318. https://doi.org/10.1134/S1070428009090036

Kowcun, A., Honson, N., & Plettner, E. (2001). Olfaction in the Gypsy Moth, *Lymantria dispar*: Effect of pH, ionic strength, and reductants on pheromone transport by pheromone-binding proteins. *Journal of Biological Chemistry*, *276*(48), 44770–44776. https://doi.org/10.1074/jbc.M104688200

Krieger, J., & Breer, H. (1999). Olfactory reception in invertebrates. *Science (New York, N.Y.)*, *286*(5440), 720–723. https://doi.org/10.1126/science.286.5440.720

Lartigue, A., Gruez, A., Briand, L., Blon, F., Bézirard, V., Walsh, M., Pernollet, J.-C., Tegoni, M., & Cambillau, C. (2004). Sulfur Single-wavelength Anomalous Diffraction Crystal Structure of a Pheromone-Binding Protein from the Honeybee Apis mellifera L. *Journal of Biological Chemistry*, *279*(6), 4459–4464. https://doi.org/10.1074/jbc.M311212200

Laughlin, J. D., Ha, T. S., Jones, D. N. M., & Smith, D. P. (2008). Activation of Pheromone-Sensitive Neurons Is Mediated by Conformational Activation of Pheromone-Binding Protein. *Cell*, *133*(7), 1255–1265. https://doi.org/10.1016/j.cell.2008.04.046

Lautenschlager, C., Leal, W. S., & Clardy, J. (2005). Coil-to-helix transition and ligand release of Bombyx mori pheromone-binding protein. *Biochemical and Biophysical Research Communications*, *335*(4), 1044–1050. https://doi.org/10.1016/j.bbrc.2005.07.176

Lautenschlager, C., Leal, W. S., & Clardy, J. (2007). Bombyx mori pheromone-binding protein binding nonpheromone ligands: Implications for pheromone recognition. *Structure (London, England: 1993)*, *15*(9), 1148–1154. https://doi.org/10.1016/j.str.2007.07.013

Leal, W. S. (1996). Chemical communication in scarab beetles: Reciprocal behavioral agonist-antagonist activities of chiral pheromones. *Proceedings of the National Academy of Sciences of the United States of America*, *93*(22), 12112–12115. https://doi.org/10.1073/pnas.93.22.12112

Leal, W. S. (2004). Pheromone Reception. In S. Schulz (Ed.), *The Chemistry of Pheromones and Other Semiochemicals II* (Vol. 240, pp. 1–36). Springer Berlin Heidelberg. https://doi.org/10.1007/b98314

Leal, W. S. (2013). Odorant Reception in Insects: Roles of Receptors, Binding Proteins, and Degrading Enzymes. *Annual Review of Entomology*, *58*(1), 373–391. https://doi.org/10.1146/annurev-ento-120811-153635

Leal, W. S., Chen, A. M., Ishida, Y., Chiang, V. P., Erickson, M. L., Morgan, T. I., & Tsuruda, J. M. (2005). Kinetics and molecular properties of pheromone binding and release. *Proceedings of the National Academy of Sciences*, *102*(15), 5386–5391. https://doi.org/10.1073/pnas.0501447102

Leal, W. S., Ishida, Y., Pelletier, J., Xu, W., Rayo, J., Xu, X., & Ames, J. B. (2009). Olfactory Proteins Mediating Chemical Communication in the Navel Orangeworm Moth, Amyelois transitella. *PLOS ONE*, *4*(9), e7235. https://doi.org/10.1371/journal.pone.0007235

Lee, D., Damberger, F. F., Peng, G., Horst, R., Güntert, P., Nikonova, L., Leal, W. S., & Wüthrich, K. (2002). NMR structure of the unliganded Bombyx mori pheromone-binding protein at physiological pH. *FEBS Letters*, *531*(2), 314–318. https://doi.org/10.1016/S0014-5793(02)03548-2

Leonhardt, B. A., Mastro, V. C., Leonard, D. S., McLane, W., Reardon, R. C., & Thorpe, K. W. (1996). Control of low-density gypsy moth (Lepidoptera: Lymantriidae) populations by mating disruption with pheromone. *Journal of Chemical Ecology*, *22*(7), 1255–1272. https://doi.org/10.1007/BF02266964

Li, L. H., Wang, D., & Chan, T. H. (1997). Asymmetric epoxidation of nearly symmetrical cis-alkenes. Sharpless epoxidation of (1,2-dialkyl)vinylsilanols. *Tetrahedron Letters*, *38*(1), 101–104. https://doi.org/10.1016/S0040-4039(96)02226-5

Liebhold, A. M., & Tobin, P. C. (2008). Population Ecology of Insect Invasions and Their Management. *Annual Review of Entomology*, *53*(1), 387–408. https://doi.org/10.1146/annurev.ento.52.110405.091401

Liebhold, A., Mastro, V., & Schaefer, P. w. (1989). Learning from the Legacy of Léopold Trouvelot. *Bulletin of the Entomological Society of America*, *35*(2), 20–22. https://doi.org/10.1093/besa/35.2.20

Liu, N.-Y., Yang, F., Yang, K., He, P., Niu, X.-H., Xu, W., Anderson, A., & Dong, S.-L. (2015). Two subclasses of odorant-binding proteins in Spodoptera exigua display structural conservation and functional divergence. *Insect Molecular Biology*, *24*(2), 167–182. https://doi.org/10.1111/imb.12143

Ljungberg, H., Anderson, P., & Hansson, B. S. (1993). Physiology and morphology of pheromone-specific sensilla on the antennae of male and female Spodoptera littoralis (Lepidoptera: Noctuidae). *Journal of Insect Physiology*, *39*(3), 253–260. https://doi.org/10.1016/0022-1910(93)90096-A

Löfstedt, C., Wahlberg, N., & Millar, J. G. (2016). Evolutionary Patterns of Pheromone Diversity in Lepidoptera. *In Pheromone Communication in Moths : Evolution, Behavior and Application*, 43–78.

Luccio, E. di, Ishida, Y., Leal, W. S., & Wilson, D. K. (2013). Crystallographic Observation of pH-Induced Conformational Changes in the Amyelois transitella Pheromone-Binding Protein AtraPBP1. *PLOS ONE*, *8*(2), e53840. https://doi.org/10.1371/journal.pone.0053840

Lyne, W. H. (1911). Insects Infecting Imported Nursery Stock, Fruit, and Grain, Received at the Provincial Fumigation and Inspection Station, Vancouver, B.C. *Journal of the Entomological Society of British Columbia*, *1*(0), 26–30.

Mafi, S. A., Vang, L. V., Nakata, Y., Ohbayashi, N., Yamamoto, M., & Ando, T. (2005). Identification of the Sex Pheromone of the Citrus Leafminer (*Phyllocnistis citrella* Stainton, Lepidoptera: Gracillariidae) with a Trial of Control by the Communication Disruption Method. *Journal of Pesticide Science*, *30*(4), 361–367. https://doi.org/10.1584/jpestics.30.361

Maida, R., Steinbrecht, A., Ziegelberger, G., & Pelosi, P. (1993). The pheromone binding protein of Bombyx mori: Purification, characterization and immunocytochemical localization. *Insect Biochemistry and Molecular Biology*, *23*(2), 243–253. https://doi.org/10.1016/0965-1748(93)90005-D

Maida, R., Ziegelberger, G., & Kaissling, K. E. (1995). Esterase activity in the olfactory sensilla of the silkmoth Antheraea polyphemus. *Neuroreport*, *6*(5), 822–824. https://doi.org/10.1097/00001756-199503270-00029

Maida, R., Ziegelberger, G., & Kaissling, K.-E. (2003). Ligand binding to six recombinant pheromone-binding proteins of Antheraea polyphemus and Antheraea pernyi. *Journal of Comparative Physiology B*, *173*(7), 565–573. https://doi.org/10.1007/s00360-003-0366-4

Marczak, S., Masnyk, M., & Wicha, J. (1989). Synthesis of (+)-disparlure using the reaction of 6-methylheptyl phenyl sulphone with trimethylsilyl ethylene oxide and asymmetric epoxidation. *Tetrahedron Letters*, *30*(21), 2845–2846. https://doi.org/10.1016/S0040-4039(00)99140-8

Marshall, J. A., Jablonowski, J. A., & Jiang, H. (1999a). Total Synthesis of the Gypsy Moth Pheromones (+)- and (−)-Disparlure from a Single Nonracemic α-Silyloxy Allylic Stannane. *The Journal of Organic Chemistry*, *64*(6), 2152–2154. https://doi.org/10.1021/jo982353a

Marshall, J. A., Jablonowski, J. A., & Jiang, H. (1999b). Total Synthesis of the Gypsy Moth Pheromones (+)- and (−)-Disparlure from a Single Nonracemic α-Silyloxy Allylic Stannane. *The Journal of Organic Chemistry*, *64*(6), 2152–2154. https://doi.org/10.1021/jo982353a

McAfee, A., Chapman, A., Iovinella, I., Gallagher-Kurtzke, Y., Collins, T. F., Higo, H., Madilao, L. L., Pelosi, P., & Foster, L. J. (2018). A death pheromone, oleic acid, triggers hygienic behavior in honey bees (Apis mellifera L.). *Scientific Reports*, *8*(1), 5719. https://doi.org/10.1038/s41598-018-24054-2

Meiboom, S., & Gill, D. (1958). Modified Spin-Echo Method for Measuring Nuclear Relaxation Times. *Review of Scientific Instruments*, *29*(8), 688–691. https://doi.org/10.1063/1.1716296

Melamed, E., Lahav, M., & Atlas, D. (1976). Direct localisation of β-adrenoceptor sites in rat cerebellum by a new fluorescent analogue of propranolol. *Nature*, *261*(5559), 420–422. https://doi.org/10.1038/261420a0

Merritt, T. J., LaForest, S., Prestwich, G. D., Quattro, J. M., & Vogt, R. G. (1998). Patterns of gene duplication in lepidopteran pheromone binding proteins. *Journal of Molecular Evolution*, *46*(3), 272–276. https://doi.org/10.1007/pl00006303

Merritt, T. J. S., LaForest, S., Prestwich, G. D., Quattro, J. M., & Vogt, R. G. (1998). Patterns of Gene Duplication in Lepidopteran Pheromone Binding Proteins. *Journal of Molecular Evolution*, *46*(3), 272–276. https://doi.org/10.1007/PL00006303

Middleton, R. J., & Kellam, B. (2005). Fluorophore-tagged GPCR ligands. *Current Opinion in Chemical Biology*, *9*(5), 517–525. https://doi.org/10.1016/j.cbpa.2005.08.016

Miller, J. R., Mori, K., & Roelofs, W. L. (1977). Gypsy moth field trapping and electroantennogram studies with pheromone enantiomers. *Journal of Insect Physiology*, *23*(11), 1447–1453. https://doi.org/10.1016/0022-1910(77)90171-8

Miller, J. R., & Roelofs, W. L. (1978). Gypsy Moth 1 Responses to Pheromone Enantiomers as Evaluated in a Sustained-Flight Tunnel. *Environmental Entomology*, *7*(1), 42–44. https://doi.org/10.1093/ee/7.1.42

Mohanty, S., Zubkov, S., & Campos-Olivas, R. (2003). Letter to the Editor: 1H, 13C and 15N backbone assignments of the pheromone binding protein from the silk moth Antheraea polyphemus (ApolPBP). *Journal of Biomolecular NMR*, *27*(4), 393–394. https://doi.org/10.1023/A:1025880932197

Mohanty, S., Zubkov, S., & Gronenborn, A. M. (2004). The Solution NMR Structure of Antheraea polyphemus PBP Provides New Insight into Pheromone Recognition by Pheromone-binding Proteins. *Journal of Molecular Biology*, *337*(2), 443–451. https://doi.org/10.1016/j.jmb.2004.01.009

Mohl, C., Breer, H., & Krieger, J. (2002). Species-specific pheromonal compounds induce distinct conformational changes of pheromone binding protein subtypes from Antheraea polyphemus. *Invertebrate Neuroscience*, *4*(4), 165–174. https://doi.org/10.1007/s10158-002-0018-5

Moreira, J. A., McElfresh, J. S., & Millar, J. G. (2006). Identification, Synthesis, and Field Testing of the Sex Pheromone of the Citrus Leafminer, Phyllocnistis citrella. *Journal of Chemical Ecology*, *32*(1), 169–194. https://doi.org/10.1007/s10886-006-9359-6

Mori, K., & Ebata, T. (1981). Synthesis of optically active pheromones with an epoxy ring, (+)-disparlure and the saltmarsh caterpillar moth pheromone [(Z,Z)-3,6-cis-1-9,10-epoxyheneicosadiene]. *Tetrahedron Letters*, *22*(43), 4281–4282. https://doi.org/10.1016/S0040-4039(01)82934-8

Mori, K., Takigawa, T., & Matsui, M. (1976). Stereoselective synthesis of optically active disparlure, the pheromone of the gypsy moth (Porthetria dispar L.). *Tetrahedron Letters*, *17*(44), 3953–3956. https://doi.org/10.1016/S0040-4039(00)92545-0

Nakagawa, T., Pellegrino, M., Sato, K., Vosshall, L. B., & Touhara, K. (2012). Amino Acid Residues Contributing to Function of the Heteromeric Insect Olfactory Receptor Complex. *PLOS ONE*, *7*(3), e32372. https://doi.org/10.1371/journal.pone.0032372

Nardella, J., Terrado, M., Honson, N. S., & Plettner, E. (2015). Endogenous fatty acids in olfactory hairs influence pheromone binding protein structure and function in Lymantria dispar. *Archives of Biochemistry and Biophysics*, *579*, 73–84. https://doi.org/10.1016/j.abb.2015.05.007

Nesbitt, B. F., Beevor, P. S., Hall, D. R., Lester, R., & Dyck, V. A. (1975). Identification of the female sex pheromones of the moth, Chilo suppressalis. *Journal of Insect Physiology*, *21*(12), 1883–1886. https://doi.org/10.1016/0022-1910(75)90218-8

Nguyen Trong Anh, ., Eisenstein, O., Lefour, J. M., & Tran Huu Dau, M. E. (1973). Orbital factors and asymmetric induction. *Journal of the American Chemical Society*, *95*(18), 6146–6147. https://doi.org/10.1021/ja00799a068

Odinokov, V. N., Akhmetova, V. R., Khasanov, Kh. D., Abduvakhabov, A. A., Kuchin, A. V., Andreeva, N. I., & Tolstikov, G. A. (1989). Insect pheromones and their analogs. *Chemistry of Natural Compounds*, *25*(5), 610–613. https://doi.org/10.1007/BF00598087

Oliver, J. E., & Waters, R. M. (1995). Determining enantiomeric composition of disparlure. *Journal of Chemical Ecology*, *21*(2), 199–211. https://doi.org/10.1007/BF02036651

Paddon-Row, M. N., Rondan, N. G., & Houk, K. N. (1982). Staggered models for asymmetric induction: Attack trajectories and conformations of allylic bonds from ab initio transition structures of addition reactions. *Journal of the American Chemical Society*, *104*(25), 7162–7166. https://doi.org/10.1021/ja00389a045

Paduraru, P. M., Popoff, R. T. W., Nair, R., Gries, R., Gries, G., & Plettner, E. (2008). Synthesis of Substituted Alkoxy Benzene Minilibraries, for the Discovery of New Insect Olfaction or Gustation Inhibitors. *Journal of Combinatorial Chemistry*, *10*(1), 123–134. https://doi.org/10.1021/cc700139y

Paolucci, C., Mazzini, C., & Fava, A. (1995). Dihydro- and Tetrahydrofuran Building Blocks from 1,4:3,6-Dianhydrohexitols. 2. Synthesis of Acetal, Alcohol, Diol, Epoxide, Hydrocarbon, and Lactone Pheromones. *The Journal of Organic Chemistry*, *60*(1), 169–175. https://doi.org/10.1021/jo00106a030

Park, I.-K., Lee, H.-R., Jung, C.-S., & Koh, S.-H. (2019). Synergic effect of sex pheromone (7R,8S)-cis-7,8-epoxy-2-methyloctadec-17-ene on (+)-disparlure of the Asian gypsy moth, Lymantria dispar, in Korea. *Journal of Forestry Research*, *30*(3), 1119–1122. https://doi.org/10.1007/s11676-018-0668-8

Pelosi, P. (1996). Perireceptor events in olfaction. *Journal of Neurobiology*, *30*(1), 3–19. https://doi.org/10.1002/(SICI)1097-4695(199605)30:1<3::AID-NEU2>3.0.CO;2-A

Pinnelli, G. R., Terrado, M., Hillier, N. K., Lance, D. R., & Plettner, E. (2019). Synthesis of Isotopically Labelled Disparlure Enantiomers and Application to the Study of Enantiomer Discrimination in Gypsy Moth Pheromone-Binding Proteins. *European Journal of Organic Chemistry*, *2019*(40), 6807–6821. https://doi.org/10.1002/ejoc.201901164

Plettner, E., & Gries, R. (2010). Agonists and antagonists of antennal responses of gypsy moth (Lymantria dispar) to the pheromone (+)-disparlure and other odorants. *Journal of Agricultural and Food Chemistry*, *58*(6), 3708–3719. https://doi.org/10.1021/jf904139e

Plettner, E., Lazar, J., Prestwich, E. G., & Prestwich, G. D. (2000). Discrimination of Pheromone Enantiomers by Two Pheromone Binding Proteins from the Gypsy Moth Lymantria dispar. *Biochemistry*, *39*(30), 8953–8962. https://doi.org/10.1021/bi000461x

Pophof, B. (2002). Moth pheromone binding proteins contribute to the excitation of olfactory receptor cells. *Naturwissenschaften*, *89*(11), 515–518. https://doi.org/10.1007/s00114-002-0364-5

Pophof, B. (2004). Pheromone-binding proteins contribute to the activation of olfactory receptor neurons in the silkmoths antheraea polyphemus and Bombyx mori. *Chemical Senses*, *29*(2), 117–125. https://doi.org/10.1093/chemse/bjh012

Powell, J. A. (2009). Chapter 151 - Lepidoptera: Moths, Butterflies. In V. H. Resh & R. T. Cardé (Eds.), *Encyclopedia of Insects (Second Edition)* (pp. 559–587). Academic Press. https://doi.org/10.1016/B978-0-12-374144-8.00160-0

Prasad, K. R., & Anbarasan, P. (2007). Enantiodivergent Synthesis of Both Enantiomers of Gypsy Moth Pheromone Disparlure. *The Journal of Organic Chemistry*, *72*(8), 3155–3157. https://doi.org/10.1021/jo070060o

Prestwich, G. D., Graham, S. M., & König, W. A. (1989). Enantioselective opening of (+)- and (–)- disparlure by epoxide hydrase in gypsy moth antennae. *Journal of the Chemical Society, Chemical Communications*, *9*, 575–577. https://doi.org/10.1039/C39890000575

Qiao, H., Tuccori, E., He, X., Gazzano, A., Field, L., Zhou, J.-J., & Pelosi, P. (2009). Discrimination of alarm pheromone (E)-β-farnesene by aphid odorant-binding proteins. *Insect Biochemistry and Molecular Biology*, *39*(5), 414–419. https://doi.org/10.1016/j.ibmb.2009.03.004

Renou, M. (2014). Pheromones and General Odor Perception in Insects. In C. Mucignat-Caretta (Ed.), *Neurobiology of Chemical Communication*. CRC Press/Taylor & Francis. http://www.ncbi.nlm.nih.gov/books/NBK200986/

Riddiford, L. M. (1970). Antennal proteins of saturniid moths—Their possible rôle in olfaction. *Journal of Insect Physiology*, *16*(4), 653–660. https://doi.org/10.1016/0022-1910(70)90098-3

Risley, J. M., & Van Etten, R. L. (1980). Oxygen-18 isotope effect in carbon-13 nuclear magnetic resonance spectroscopy. 2. The effect of structure. *Journal of the American Chemical Society*, *102*(14), 4609–4614. https://doi.org/10.1021/ja00534a007

Risley, J. M., & Van Etten, R. L. (1981). Oxygen-18 isotope effect in carbon-13 nuclear magnetic resonance spectroscopy. 4. Oxygen exchange of [1-13C,18O2]acetic acid in dilute acid. *Journal of the American Chemical Society*, *103*(15), 4389–4392. https://doi.org/10.1021/ja00405a017

Risley, J. M., & Van Etten, R. L. (1989). [19] Mechanistic studies utilizing oxygen-18 analyzed by carbon-13 and nitrogen-15 nuclear magnetic resonance spectroscopy. In *Methods in Enzymology* (Vol. 177, pp. 376–389). Academic Press. https://doi.org/10.1016/0076-6879(89)77021-X

Rivière, S., Lartigue, A., Quennedey, B., Campanacci, V., Farine, J.-P., Tegoni, M., Cambillau, C., & Brossut, R. (2003). A pheromone-binding protein from the cockroach Leucophaea maderae: Cloning, expression and pheromone binding. *Biochemical Journal*, *371*(Pt 2), 573–579. https://doi.org/10.1042/BJ20021877

Rossiter, B. E., Katsuki, T., & Sharpless, K. B. (1981). Asymmetric epoxidation provides shortest routes to four chiral epoxy alcohols which are key intermediates in syntheses of methymycin, erythromycin, leukotriene C-1, and disparlure. *Journal of the American Chemical Society*, *103*(2), 464–465. https://doi.org/10.1021/ja00392a038

Rostovtsev, V. V., Green, L. G., Fokin, V. V., & Sharpless, K. B. (2002). A Stepwise Huisgen Cycloaddition Process: Copper(I)-Catalyzed Regioselective “Ligation” of Azides and Terminal Alkynes. *Angewandte Chemie International Edition*, *41*(14), 2596–2599. https://doi.org/10.1002/1521-3773(20020715)41:14<2596::AID-ANIE2596>3.0.CO;2-4

Rybczynski, R., Reagan, J. A., & Lerner, M. R. (1989). A pheromone-degrading aldehyde oxidase in the antennae of the moth Manduca sexta. *The Journal of Neuroscience : The Official Journal of the Society for Neuroscience*. https://doi.org/10.1523/JNEUROSCI.09-04-01341.1989

Rybczynski, R., Vogt, R. G., & LernerS, M. R. (1990). *Antennal-specific Pheromone-degrading Aldehyde Oxidases from the Moths Antheraea polyphemus and Bombyx mori*. *265*(32), 19712–19717.

Sakurai, T., Namiki, S., & Kanzaki, R. (2014). Molecular and neural mechanisms of sex pheromone reception and processing in the silkmoth Bombyx mori. *Frontiers in Physiology*, *5*. https://doi.org/10.3389/fphys.2014.00125

Sandler, B. H., Nikonova, L., Leal, W. S., & Clardy, J. (2000). Sexual attraction in the silkworm moth: Structure of the pheromone-binding-protein–bombykol complex. *Chemistry & Biology*, *7*(2), 143–151. https://doi.org/10.1016/S1074-5521(00)00078-8

Sanes, J. T., & Plettner, E. (2016). Gypsy moth pheromone-binding protein-ligand interactions: PH profiles and simulations as tools for detecting polar interactions. *Archives of Biochemistry and Biophysics*, *606*, 53–63. https://doi.org/10.1016/j.abb.2016.07.008

Sarmiento, R., Beroza, M., Bierl, B. A., & Tardif, J. G. R. (1972). Activity of Compounds Related to Disparlure, the Sex Attractant of the Gypsy Moth. *Journal of Economic Entomology*, *65*(3), 665–667. https://doi.org/10.1093/jee/65.3.665

Sato, K., Pellegrino, M., Nakagawa, T., Nakagawa, T., Vosshall, L. B., & Touhara, K. (2008). Insect olfactory receptors are heteromeric ligand-gated ion channels. *Nature*, *452*(7190), 1002–1006. https://doi.org/10.1038/nature06850

Satoh, T., Oohara, T., Ueda, Y., & Yamakawa, K. (1988). The practical procedure for a preparation of 1-chloroalkyl p-tolyl sulfoxides in high optically active form: A very short synthesis of optically active disparlure. *Tetrahedron Letters*, *29*(3), 313–316. https://doi.org/10.1016/S0040-4039(00)80083-0

Satoh, T., Oohara, T., Ueda, Y., & Yamakawa, K. (1989). .Alpha.,.beta.-Epoxy sulfoxides as useful intermediates in organic synthesis. 21. A novel approach to the asymmetric synthesis of epoxides, allylic alcohols, .alpha.-amino ketones, and .alpha.-amino aldehydes from carbonyl compounds through .alpha.,.beta.-epoxy sulfoxides using the optically active p-tolylsulfinyl group to induce chirality. *The Journal of Organic Chemistry*, *54*(13), 3130–3136. https://doi.org/10.1021/jo00274a032

Schneider, D. (1969). Insect Olfaction: Deciphering System for Chemical Messages. *Science*, *163*(3871), 1031–1037. https://doi.org/10.1126/science.163.3871.1031

Schneider, D., Kafka, W. A., Beroza, M., & Bierl, B. A. (1977). Odor receptor responses of male gypsy and nun moths (Lepidoptera, Lymantriidae) to disparlure and its analogues. *Journal of Comparative Physiology*, *113*(1), 1–15. https://doi.org/10.1007/BF00610450

Shibuya, G. M., Kanady, J. S., & Vanderwal, C. D. (2008). Stereoselective Dichlorination of Allylic Alcohol Derivatives to Access Key Stereochemical Arrays of the Chlorosulfolipids. *Journal of the American Chemical Society*, *130*(37), 12514–12518. https://doi.org/10.1021/ja804167v

Sieber, S. A., & Cravatt, B. F. (2006). Analytical platforms for activity-based protein profiling – exploiting the versatility of chemistry for functional proteomics. *Chemical Communications*, *22*, 2311–2319. https://doi.org/10.1039/B600653C

Silverstein, R. M., Brownlee, R. G., Bellas, T. E., Wood, D. L., & Browne, L. E. (1968). Brevicomin: Principal Sex Attractant in the Frass of the Female Western Pine Beetle. *Science*, *159*(3817), 889–891. https://doi.org/10.1126/science.159.3817.889

Sinha-Bagchi, A., Sinha, S. C., & Keinan, E. (1995). A practical approach to enantiomerically pure cis-epoxides. Synthesis of (+)-disparlure. *Tetrahedron: Asymmetry*, *6*(12), 2889–2892. https://doi.org/10.1016/0957-4166(95)00405-X

Sjöback, R., Nygren, J., & Kubista, M. (1995). Absorption and fluorescence properties of fluorescein. *Spectrochimica Acta Part A: Molecular and Biomolecular Spectroscopy*, *51*(6), L7–L21. https://doi.org/10.1016/0584-8539(95)01421-P

Skidmore, M. W. (1993). *Derivatives for chromatographic resolution of optically active compounds. Balu. K and Halket. J. M. (eds.). Handbbok of Derivatives for Chromatography, 2nd ed. John Wiley & Sons, New York.* Wiley.Com. https://www.wiley.com/en-us/Handbook+of+Derivatives+for+Chromatography%2C+2nd+Edition-p-9780471926993

Snyder, S. A., Treitler, D. S., Brucks, A. P., & Sattler, W. (2011). A General Strategy for the Stereocontrolled Preparation of Diverse 8- and 9-Membered *Laurencia* -Type Bromoethers. *Journal of the American Chemical Society*, *133*(40), 15898–15901. https://doi.org/10.1021/ja2069449

Soave, M., Briddon, S. J., Hill, S. J., & Stoddart, L. A. (2020). Fluorescent ligands: Bringing light to emerging GPCR paradigms. *British Journal of Pharmacology*, *177*(5), 978–991. https://doi.org/10.1111/bph.14953

Sridharan, R., Zuber, J., Connelly, S. M., Mathew, E., & Dumont, M. E. (2014). Fluorescent Approaches for Understanding Interactions of Ligands with G Protein Coupled Receptors. *Biochimica et Biophysica Acta*, *1838*(1 0 0), 15–33. https://doi.org/10.1016/j.bbamem.2013.09.005

Steinbrecht, R. A. (1997). Pore structures in insect olfactory sensilla: A review of data and concepts. *International Journal of Insect Morphology and Embryology*, *26*(3), 229–245. https://doi.org/10.1016/S0020-7322(97)00024-X

Steinbrecht, R. A., Laue, M., & Ziegelberger, G. (1995). Immunolocalization of pheromone-binding protein and general odorant-binding protein in olfactory sensilla of the silk moths Antheraea and Bombyx. *Cell and Tissue Research*, *282*(2), 203–217. https://doi.org/10.1007/BF00319112

Stengl, M., Ziegelberger, G., Boekhoff, I., & Krieger, J. (1999). Perireceptor Events and Transduction Mechanisms in Insect Olfaction. In B. S. Hansson (Ed.), *Insect Olfaction* (pp. 49–66). Springer. https://doi.org/10.1007/978-3-662-07911-9_3

Stocker, R. F. (1994). The organization of the chemosensory system in Drosophila melanogaster: A rewiew. *Cell and Tissue Research*, *275*(1), 3–26. https://doi.org/10.1007/BF00305372

Sugie, H., & Tamaki, Y. (National I. of A.-E. S. (1984). Sex pheromone of the peach leafminer moth, Lyonetia clerkella Linne: Isolation and identification. *Applied Entomology and Zoology (Japan)*. http://agris.fao.org/agris-search/search.do?recordID=JP8602330

Sun, L., Wang, Q., Zhang, Y., Tu, X., Yan, Y., Wang, Q., Dong, K., Zhang, Y., & Xiao, Q. (2019). The sensilla trichodea-biased EoblPBP1 binds sex pheromones and green leaf volatiles in Ectropis obliqua Prout, a geometrid moth pest that uses Type-II sex pheromones. *Journal of Insect Physiology*, *116*, 17–24. https://doi.org/10.1016/j.jinsphys.2019.04.005

Sun, M., Liu, Y., Walker, W. B., Liu, C., Lin, K., Gu, S., Zhang, Y., Zhou, J., & Wang, G. (2013). Identification and Characterization of Pheromone Receptors and Interplay between Receptors and Pheromone Binding Proteins in the Diamondback Moth, Plutella xyllostella. *PLOS ONE*, *8*(4), e62098. https://doi.org/10.1371/journal.pone.0062098

Sun, M., Liu, Y., & Wang, G. (2013). Expression patterns and binding properties of three pheromone binding proteins in the diamondback moth, Plutella xyllotella. *Journal of Insect Physiology*, *59*(1), 46–55. https://doi.org/10.1016/j.jinsphys.2012.10.020

Tamaki, Y., Noguchi, H., Yushima, T., & Hirano, C. (1971). Two Sex Pheromones of the Smaller Tea Tortrix: Isolation, Identification, and Synthesis. *Applied Entomology and Zoology*, *6*(3), 139–141. https://doi.org/10.1303/aez.6.139

Tasayco, M. L., & Prestwich, G. D. (1990). Aldehyde-oxidizing enzymes in an adult moth: In vitro study of aldehyde metabolism in Heliothis virescens. *Archives of Biochemistry and Biophysics*, *278*(2), 444–451. https://doi.org/10.1016/0003-9861(90)90283-5

Tatsuki, S., Kurihara, M., Usui, K., Ohguchi, Y., Uchiumi, K., Arai, K., Yabuki, S., & Tanaka, F. (1983). Sex Pheromone of the Rice Stem Borer, Chilo suppressalis (WALKER) (Lepidoptera: Pyralidae) : the Third Component, Z-9-Hexadecenal. *Applied Entomology and Zoology*, *18*(3), 443–446. https://doi.org/10.1303/aez.18.443

Terrado, M., Okon, M., McIntosh, L. P., & Plettner, E. (2020). Ligand- and pH-Induced Structural Transition of Gypsy Moth Lymantria dispar Pheromone-Binding Protein 1 (LdisPBP1). *Biochemistry*, *59*(37), 3411–3426. https://doi.org/10.1021/acs.biochem.0c00592

Terrado, M., Pinnelli, G. R., Sanes, J., & Plettner, E. (2019). Binding Interactions, Structure-Activity Relationships and Blend Effects in Pheromone and Host Olfactory Detection of Herbivorous Lepidoptera. In J.-F. Picimbon (Ed.), *Olfactory Concepts of Insect Control—Alternative to insecticides: Volume 2* (pp. 265–310). Springer International Publishing. https://doi.org/10.1007/978-3-030-05165-5_11

Terrado, M., Yu, Y., & Plettner, E. (2017). Correlation of pheromone-binding protein–ligand equilibrium dissociation constants with electroantennogram response patterns. *Canadian Journal of Chemistry*. https://doi.org/10.1139/cjc-2017-0339

Tobin, P. C., Sharov, A. A., Liebhold, A. A., Leonard, D. S., Roberts, A. E., & Learn, M. R. (2004). Management of the Gypsy Moth through a Decision Algorithm under the STS Project. *American Entomologist*, *50*(4), 200–209. https://doi.org/10.1093/ae/50.4.200

Tori, K., Aono, K., Kitahonoki, K., Muneyuki, R., Takano, Y., Tanida, H., & Tsuji, T. (1966). NMR studies of bridged ring systems. X. Long-range anisotropic shielding effects of an epoxide and an aziridine ring. *Tetrahedron Letters*, *7*(25), 2921–2926. https://doi.org/10.1016/S0040-4039(01)99888-0

Tornøe, C. W., Christensen, C., & Meldal, M. (2002). Peptidotriazoles on Solid Phase: [1,2,3]-Triazoles by Regiospecific Copper(I)-Catalyzed 1,3-Dipolar Cycloadditions of Terminal Alkynes to Azides. *The Journal of Organic Chemistry*, *67*(9), 3057–3064. https://doi.org/10.1021/jo011148j

Tsuboi, S., Furutani, H., Ansari, M. H., Sakai, T., Utaka, M., & Takeda, A. (1993). Highly enantioselective reduction of 3-chloro-2-oxoalkanoates with fermenting bakers' yeast. A new synthesis of optically active 3-chloro-2-hydroxyalkanoates and glycidic esters. *The Journal of Organic Chemistry*, *58*(2), 486–492. https://doi.org/10.1021/jo00054a036

Tsuboi, S., Yamafuji, N., & Utaka, M. (1997). Lipase-catalyzed kinetic resolution of 3-chloro-2-hydroxyalkanoates. Its application for the synthesis of (−)-disparlure. *Tetrahedron: Asymmetry*, *8*(3), 375–379. https://doi.org/10.1016/S0957-4166(96)00529-0

Tumlinson, J. H., Klein, M. G., Doolittle, R. E., Ladd, T. L., & Proveaux, A. T. (1977). Identification of the Female Japanese Beetle Sex Pheromone: Inhibition of Male Response by an Enantiomer. *Science*, *197*(4305), 789–792. https://doi.org/10.1126/science.197.4305.789

van den Berg, M. J., & Ziegelberger, G. (1991). On the function of the pheromone binding protein in the olfactory hairs of Antheraea polyphemus. *Journal of Insect Physiology*, *37*(1), 79–85. https://doi.org/10.1016/0022-1910(91)90022-R

Vité, J. P., Billings, R. F., Ware, C. W., & Mori, K. (1985). Southern pine beetle: Enhancement or inhibition of aggregation response mediated by enantiomers of endo-brevicomin. *Naturwissenschaften*, *72*(2), 99–100. https://doi.org/10.1007/BF00508146

Vité, J. P., Billings, R., Ware, C., & Mori, K. (2004). Southern pine beetle: Enhancement or inhibition of aggregation response mediated by enantiomers of endo-brevicomin. *Naturwissenschaften*. https://doi.org/10.1007/BF00508146

Vogt, R. G., Kohne, A. C., Dubnau, J. T., & Prestwich, G. D. (1989). Expression of pheromone binding proteins during antennal development in the gypsy moth Lymantria dispar. *Journal of Neuroscience*, *9*(9), 3332–3346. https://doi.org/10.1523/JNEUROSCI.09-09-03332.1989

Vogt, R. G., & Riddiford, L. M. (1981). Pheromone binding and inactivation by moth antennae. *Nature*, *293*(5828), 161–163. https://doi.org/10.1038/293161a0

Vogt, R. G., Riddiford, L. M., & Prestwich, G. D. (1985). Kinetic properties of a sex pheromone-degrading enzyme: The sensillar esterase of Antheraea polyphemus. *Proceedings of the National Academy of Sciences*, *82*(24), 8827–8831. https://doi.org/10.1073/pnas.82.24.8827

Vogt, R. G., Rybczynski, R., & Lerner, M. R. (1991). Molecular cloning and sequencing of general odorant-binding proteins GOBP1 and GOBP2 from the tobacco hawk moth Manduca sexta: Comparisons with other insect OBPs and their signal peptides. *Journal of Neuroscience*, *11*(10), 2972–2984. https://doi.org/10.1523/JNEUROSCI.11-10-02972.1991

Vold, R. L., Waugh, J. S., Klein, M. P., & Phelps, D. E. (1968). Measurement of Spin Relaxation in Complex Systems. *The Journal of Chemical Physics*, *48*(8), 3831–3832. https://doi.org/10.1063/1.1669699

Wakamura, S., Arakaki, N., Yamamoto, M., Hiradate, S., Yasui, H., Kinjo, K., Yasuda, T., Yamazawa, H., & Ando, T. (2005). Sex Pheromone and Related Compounds in the Ishigaki and Okinawa Strains of the Tussock Moth Orgyia postica (Walker) (Lepidoptera: Lymantriidae). *Bioscience, Biotechnology, and Biochemistry*, *69*(5), 957–965. https://doi.org/10.1271/bbb.69.957

Wakamura, S., Arakaki, N., Yamamoto, M., Hiradate, S., Yasui, H., Yasuda, T., & Ando, T. (2001). Posticlure: A novel trans-epoxide as a sex pheromone component of the tussock moth, Orgyia postica (Walker). *Tetrahedron Letters*, *42*(4), 687–689. https://doi.org/10.1016/S0040-4039(00)02038-4

Wang, L., Cai, C., Curran, D. P., & Zhang, W. (2010). Enantioselective α-Chlorination of Aldehydes with Recyclable Fluorous (S)-Pyrrolidine-Thiourea Bifunctional Organocatalyst. *Synlett*, *2010*(3), 433–436. https://doi.org/10.1055/s-0029-1219198

Wang, Z., Zheng, J., & Huang, P. (2012). Asymmetric Synthesis of Both Enantiomers of Disparlure. *Chinese Journal of Chemistry*, *30*(1), 23–28. https://doi.org/10.1002/cjoc.201100482

Wicher, D., Schäfer, R., Bauernfeind, R., Stensmyr, M. C., Heller, R., Heinemann, S. H., & Hansson, B. S. (2008). Drosophila odorant receptors are both ligand-gated and cyclic-nucleotide-activated cation channels. *Nature*, *452*(7190), 1007–1011. https://doi.org/10.1038/nature06861

Winter, P., Swatschek, J., Willot, M., Radtke, L., Olbrisch, T., Schäfer, A., & Christmann, M. (2011). Transforming terpene-derived aldehydes into 1,2-epoxides via asymmetric α-chlorination: Subsequent epoxide opening with carbon nucleophiles. *Chemical Communications*, *47*(44), 12200–12202. https://doi.org/10.1039/C1CC15173H

Wojtasek, H., & Leal, W. S. (1999a). Degradation of an alkaloid pheromone from the pale-brown chafer, Phyllopertha diversa (Coleoptera: Scarabaeidae), by an insect olfactory cytochrome P450. *FEBS Letters*, *458*(3), 333–336. https://doi.org/10.1016/S0014-5793(99)01178-3

Wojtasek, H., & Leal, W. S. (1999b). Conformational change in the pheromone-binding protein from Bombyx mori induced by pH and by interaction with membranes. *The Journal of Biological Chemistry*, *274*(43), 30950–30956. https://doi.org/10.1074/jbc.274.43.30950

Wood, D. L., Browne, L. E., Ewing, B., Lindahl, K., Bedard, W. D., Tilden, P. E., Mori, K., Pitman, G. B., & Hughes, P. R. (1976). Western pine beetle: Specificity among enantiomers of male and female components of an attractant pheromone. *Science*, *192*(4242), 896–898. https://doi.org/10.1126/science.1273574

Wyatt, T. D. (2003). *Pheromones and Animal Behaviour: Communication by Smell and Taste*. Cambridge University Press. https://doi.org/10.1017/CBO9780511615061

Xiu, W.-M., & Dong, S.-L. (2007). Molecular Characterization of Two Pheromone Binding Proteins and Quantitative Analysis of their Expression in the Beet Armyworm, Spodoptera exigua Hübner. *Journal of Chemical Ecology*, *33*(5), 947–961. https://doi.org/10.1007/s10886-007-9277-2

Xu, P., Atkinson, R., Jones, D. N. M., & Smith, D. P. (2005). Drosophila OBP LUSH Is Required for Activity of Pheromone-Sensitive Neurons. *Neuron*, *45*(2), 193–200. https://doi.org/10.1016/j.neuron.2004.12.031

Xu, P., Hooper, A. M., Pickett, J. A., & Leal, W. S. (2012). Specificity Determinants of the Silkworm Moth Sex Pheromone. *PLOS ONE*, *7*(9), e44190. https://doi.org/10.1371/journal.pone.0044190

Xu, W., Xu, X., Leal, W. S., & Ames, J. B. (2011). Extrusion of the C-terminal Helix in Navel Orangeworm Moth Pheromone-Binding Protein (AtraPBP1) Controls Pheromone Binding. *Biochemical and Biophysical Research Communications*, *404*(1), 335–338. https://doi.org/10.1016/j.bbrc.2010.11.119

Yamamoto, M., Kamata, T., Do, N. D., Adachi, Y., Kinjo, M., & Ando, T. (2007). A Novel Lepidopteran Sex Pheromone Produced by Females of a Lithosiinae Species, Lyclene dharma dharma, in the Family of Arctiidae. *Bioscience, Biotechnology, and Biochemistry*, *71*(11), 2860–2863. https://doi.org/10.1271/bbb.70551

Yan, Y., Zhang, Y., Tu, X., Wang, Q., Li, Y., Li, H., Wang, Q., Zhang, Y., & Sun, L. (2020). Functional characterization of a binding protein for Type-II sex pheromones in the tea geometrid moth Ectropis obliqua Prout. *Pesticide Biochemistry and Physiology*, *165*, 104542. https://doi.org/10.1016/j.pestbp.2020.02.008

Yang, P., & Liu, K. (2015). Activity-Based Protein Profiling: Recent Advances in Probe Development and Applications. *ChemBioChem*, *16*(5), 712–724. https://doi.org/10.1002/cbic.201402582

Ye, X., Luke, B., Andresson, T., & Blonder, J. (2009). 18O Stable Isotope Labeling in MS-based Proteomics. *Briefings in Functional Genomics and Proteomics*, *8*(2), 136–144. https://doi.org/10.1093/bfgp/eln055

Yu, W.-T., Wu, T.-W., Huang, C.-L., Chen, I.-C., & Tan, K.-T. (2015). Protein sensing in living cells by molecular rotor-based fluorescence-switchable chemical probes. *Chemical Science*, *7*(1), 301–307. https://doi.org/10.1039/C5SC02808F

Yu, Y., & Plettner, E. (2013). Enantiomer and conformer recognition of (+) and (-)-disparlure and their analogs by the pheromone binding proteins of the gypsy moth, Lymantria dispar. *Bioorganic and Medicinal Chemistry*. https://doi.org/10.1016/j.bmc.2013.01.043

Zhang, T., Sun, Y., Wanner, K. W., Coates, B. S., He, K., & Wang, Z. (2017). Binding affinity of five PBPs to Ostrinia sex pheromones. *BMC Molecular Biology*, *18*. https://doi.org/10.1186/s12867-017-0079-y

Zhang, X.-F., Zhang, J., & Liu, L. (2014). Fluorescence Properties of Twenty Fluorescein Derivatives: Lifetime, Quantum Yield, Absorption and Emission Spectra. *Journal of Fluorescence*, *24*(3), 819–826. https://doi.org/10.1007/s10895-014-1356-5

Zhang, Y.-N., Zhang, J., Yan, S.-W., Chang, H.-T., Liu, Y., Wang, G.-R., & Dong, S.-L. (2014). Functional characterization of sex pheromone receptors in the purple stem borer, Sesamia inferens (Walker). *Insect Molecular Biology*, *23*(5), 611–620. https://doi.org/10.1111/imb.12109

Zhou, J.-J. (2010). Odorant-Binding Proteins in Insects. In *Vitamins & Hormones* (Vol. 83, pp. 241–272). Elsevier. https://doi.org/10.1016/S0083-6729(10)83010-9

Zhou, J.-J., Zhang, G.-A., Huang, W., Birkett, M. A., Field, L. M., Pickett, J. A., & Pelosi, P. (2004). Revisiting the odorant-binding protein LUSH of Drosophila melanogaster: Evidence for odour recognition and discrimination. *FEBS Letters*, *558*(1–3), 23–26. https://doi.org/10.1016/S0014-5793(03)01521-7

APPENDIX A. Chapter 2 supporting information

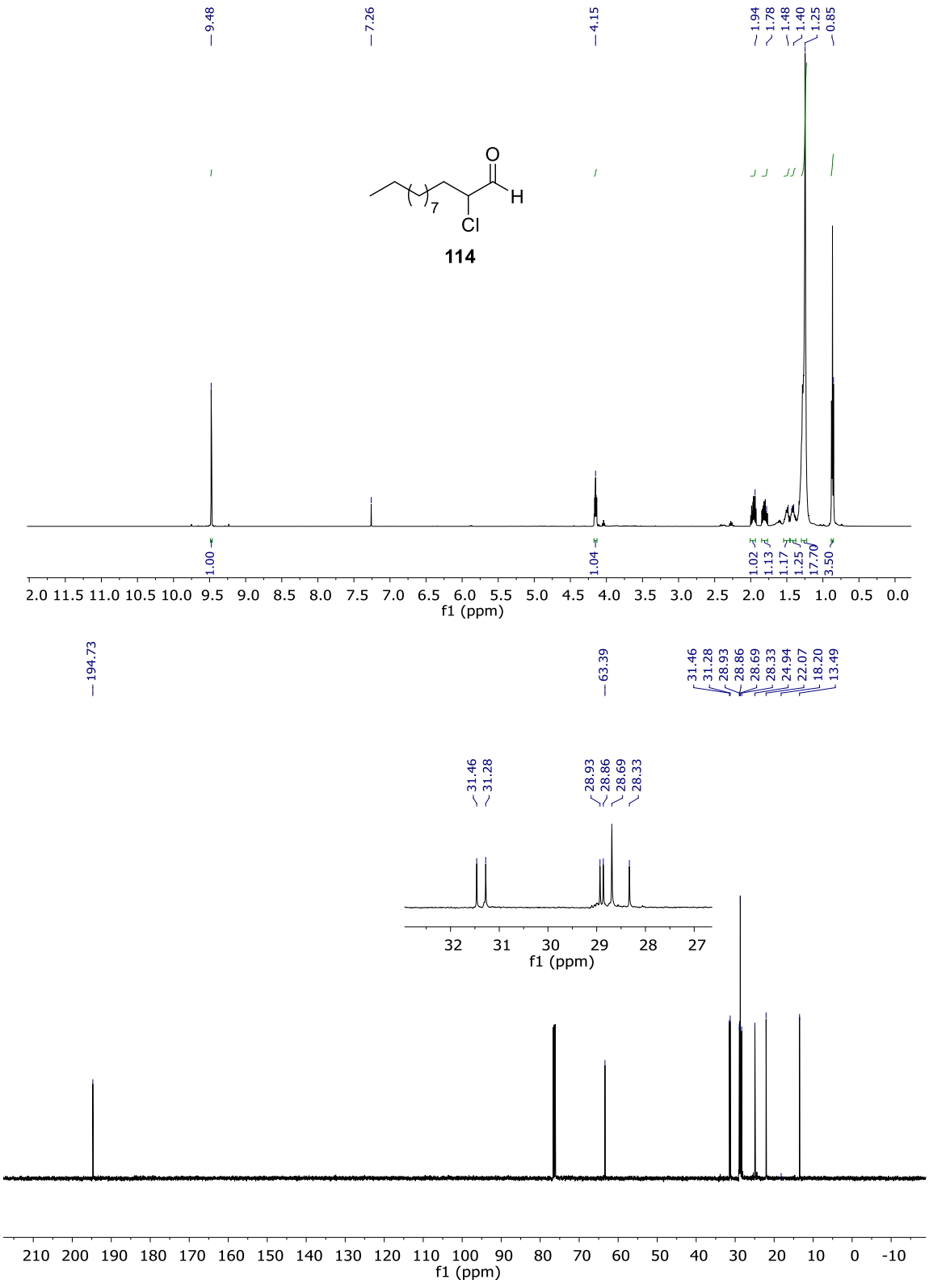

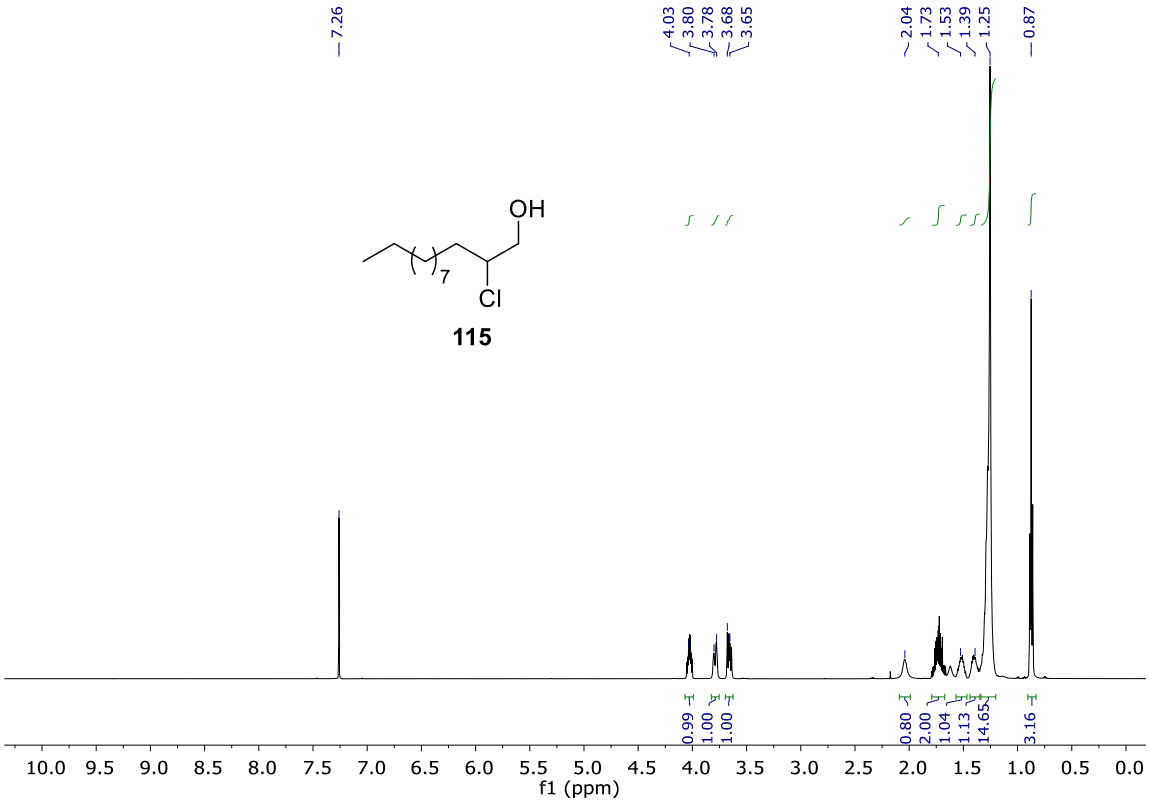
7.26
4.03
3.80
3.78
3.68
3.65
2.04
1.73
1.53
1.39
1.25
0.87
OH
Cl
7
115
0.99
1.00
1.00
0.80
2.00
1.04
1.13
14.65
3.16
f1 (ppm)

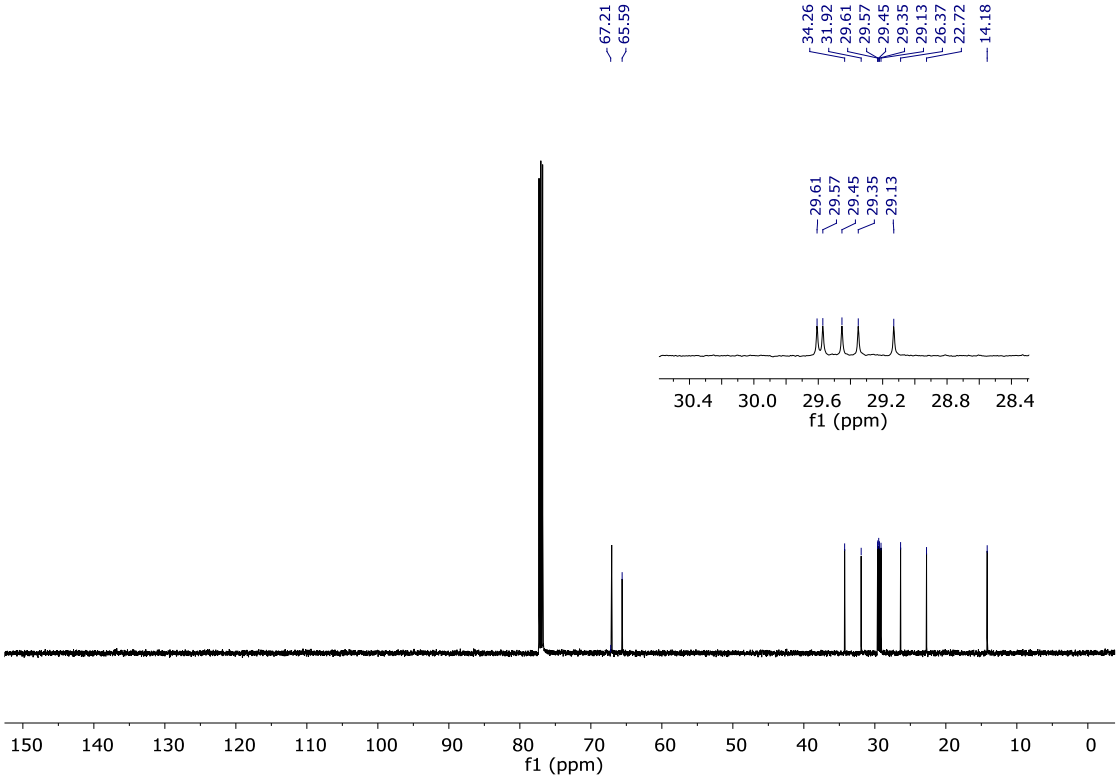
67.21
65.59
34.26
31.92
29.61
29.57
29.45
29.35
29.13
26.37
22.72
14.18
29.61
29.57
29.45
29.35
29.13
f1 (ppm)
f1 (ppm)

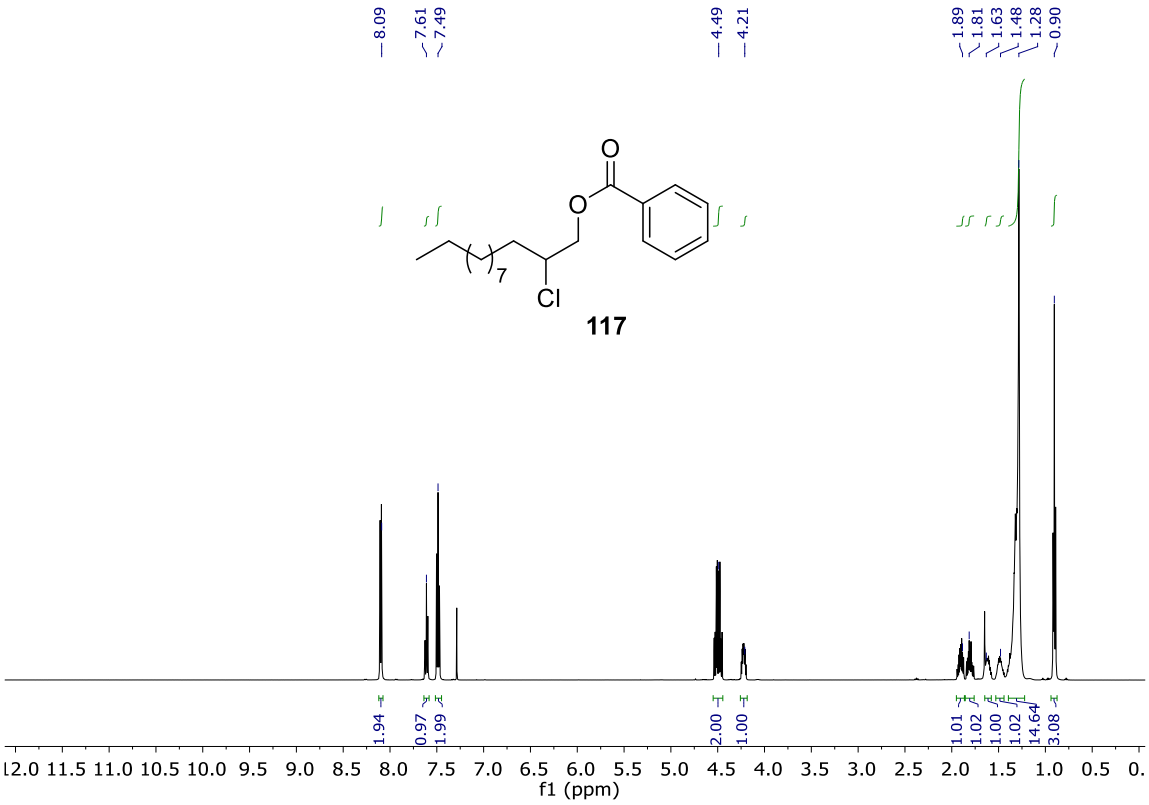
8.09
7.61
7.49
4.49
4.21
1.89
1.81
1.63
1.48
1.28
0.90
O
O
7
Cl
117
1.94
0.97
1.99
2.00
1.00
1.01
1.02
1.00
1.02
14.64
3.08
f1 (ppm)

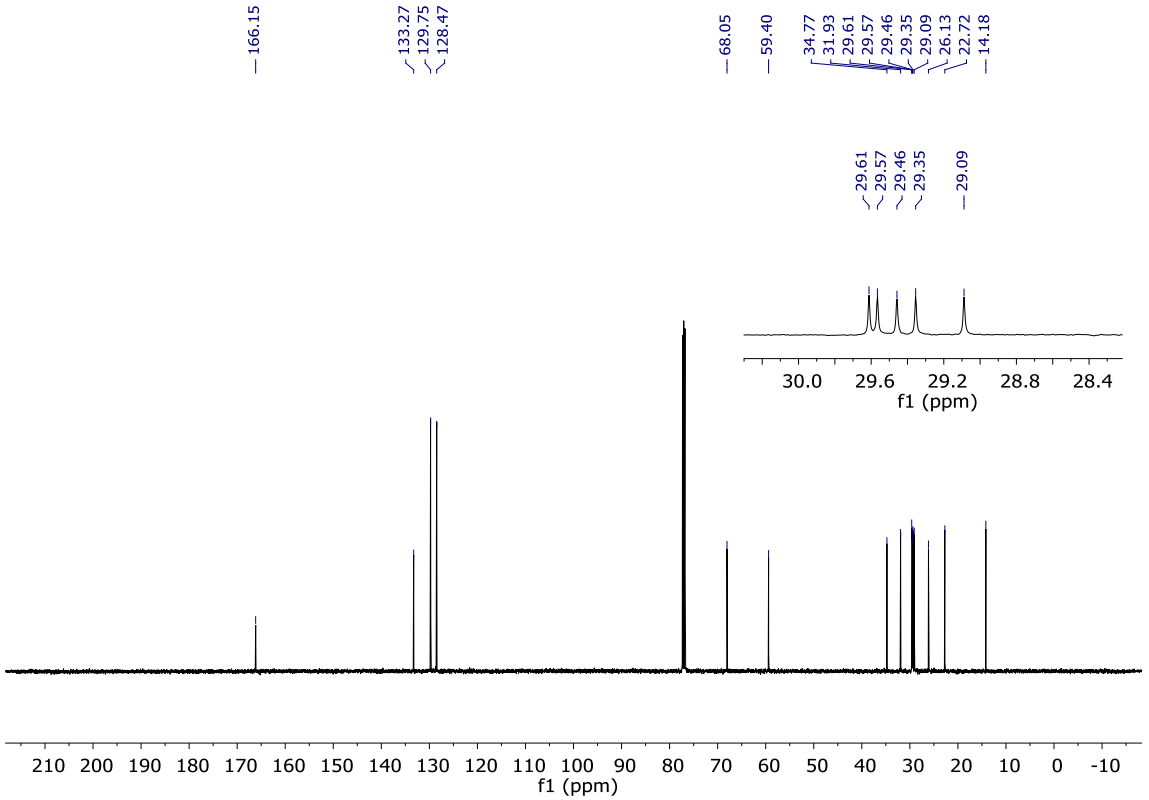
166.15
133.27
129.75
128.47
68.05
59.40
34.77
31.93
29.61
29.57
29.46
29.35
29.09
26.13
22.72
14.18
29.61
29.57
29.46
29.35
29.09
30.0
29.6
29.2
28.8
28.4
f1 (ppm)
f1 (ppm)

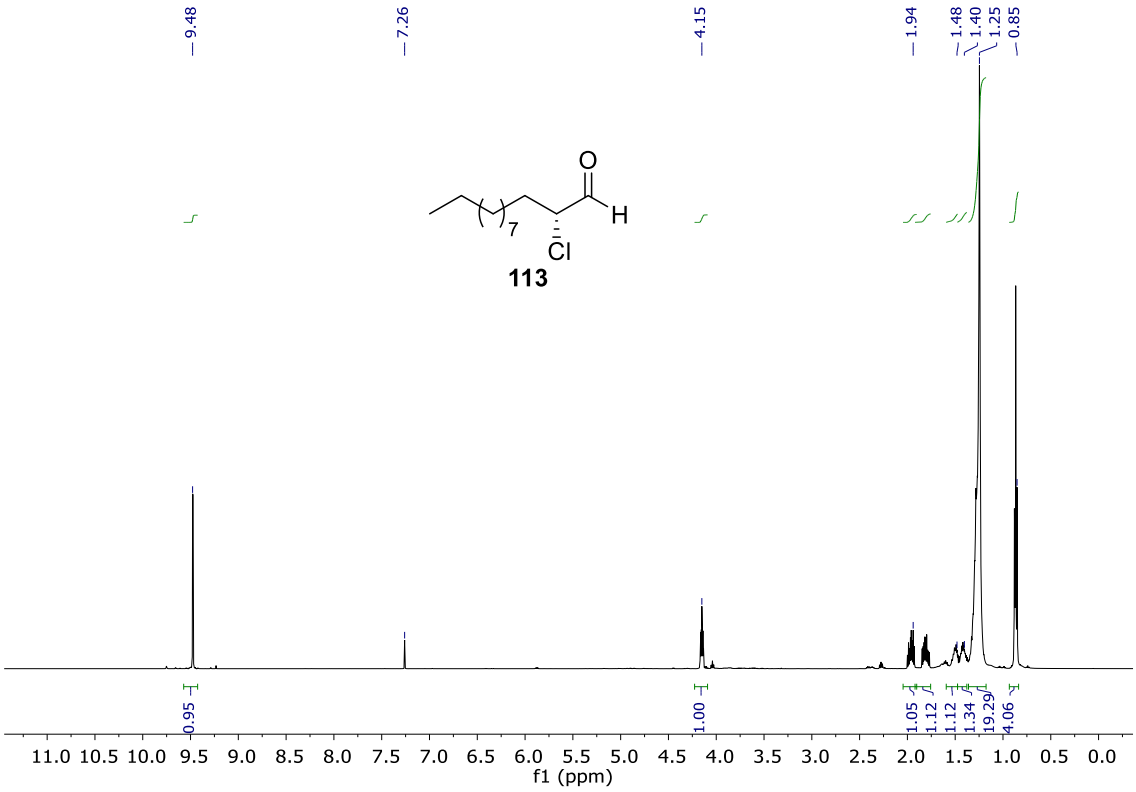
9.48
7.26
4.15
1.94
1.48
1.40
1.25
0.85
O
H
7
Cl
113
0.95
1.00
1.05
1.12
1.12
1.34
19.29
4.06
11.0 10.5 10.0 9.5 9.0 8.5 8.0 7.5 7.0 6.5 6.0 5.5 5.0 4.5 4.0 3.5 3.0 2.5 2.0 1.5 1.0 0.5 0.0
f1 (ppm)

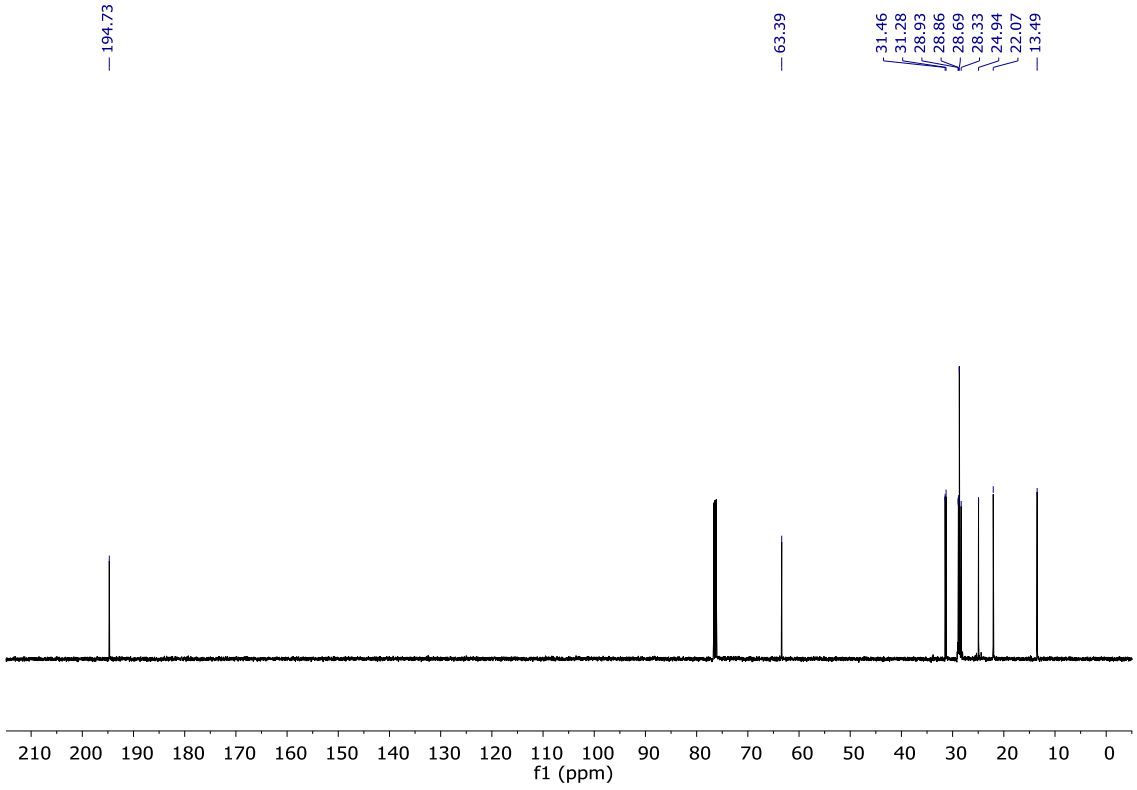
194.73
63.39
31.46
31.28
28.93
28.86
28.69
28.33
24.94
22.07
13.49
210 200 190 180 170 160 150 140 130 120 110 100 90 80 70 60 50 40 30 20 10 0
f1 (ppm)

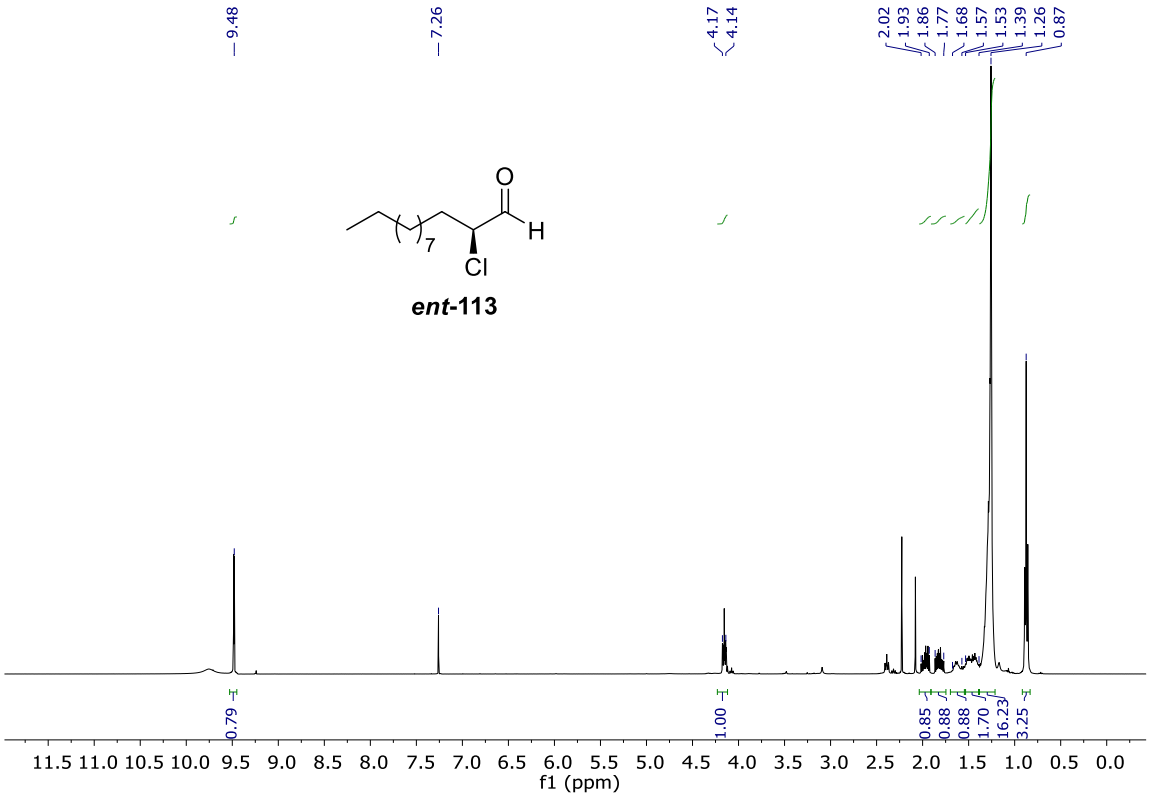
9.48
7.26
4.17
4.14
2.02
1.93
1.86
1.77
1.68
1.57
1.53
1.39
1.26
0.87
O
H
Cl
7
0.79
1.00
0.85
0.88
0.88
1.70
16.23
3.25
11.5 11.0 10.5 10.0 9.5 9.0 8.5 8.0 7.5 7.0 6.5 6.0 5.5 5.0 4.5 4.0 3.5 3.0 2.5 2.0 1.5 1.0 0.5 0.0
f1 (ppm)

***ent*-113**

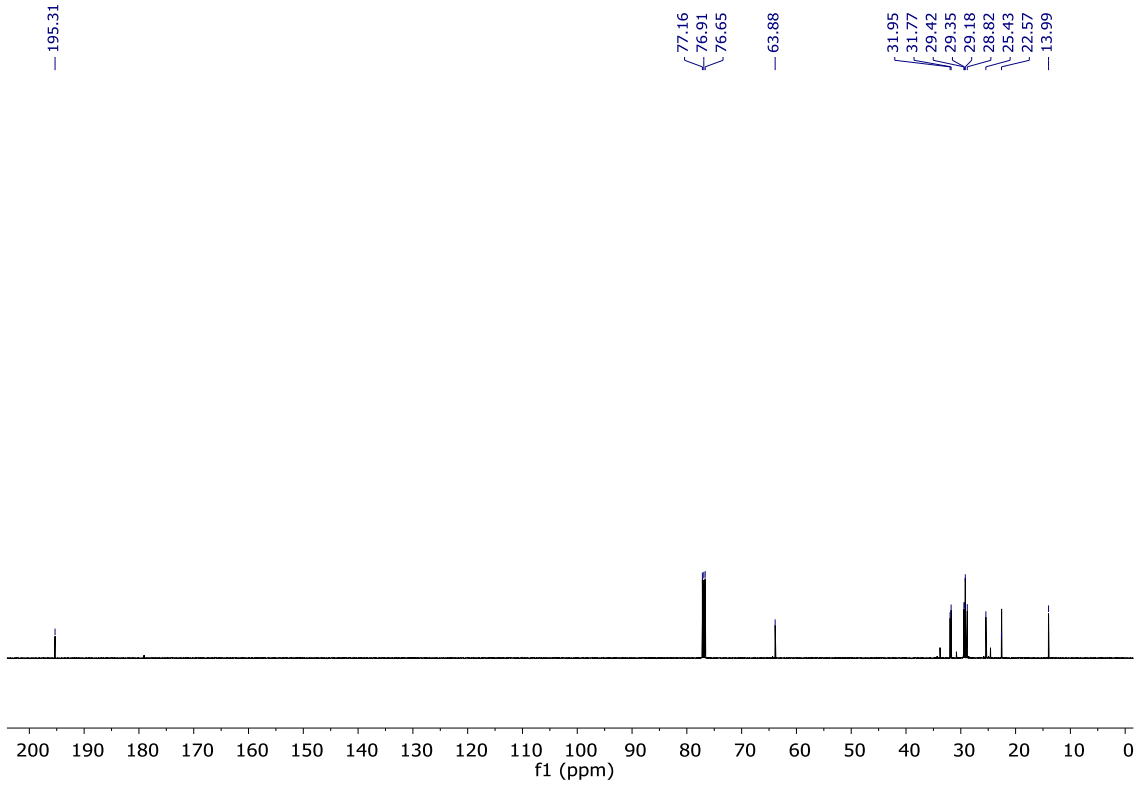
195.31
77.16
76.91
76.65
63.88
31.95
31.77
29.42
29.35
29.18
28.82
25.43
22.57
13.99
200 190 180 170 160 150 140 130 120 110 100 90 80 70 60 50 40 30 20 10 0
f1 (ppm)

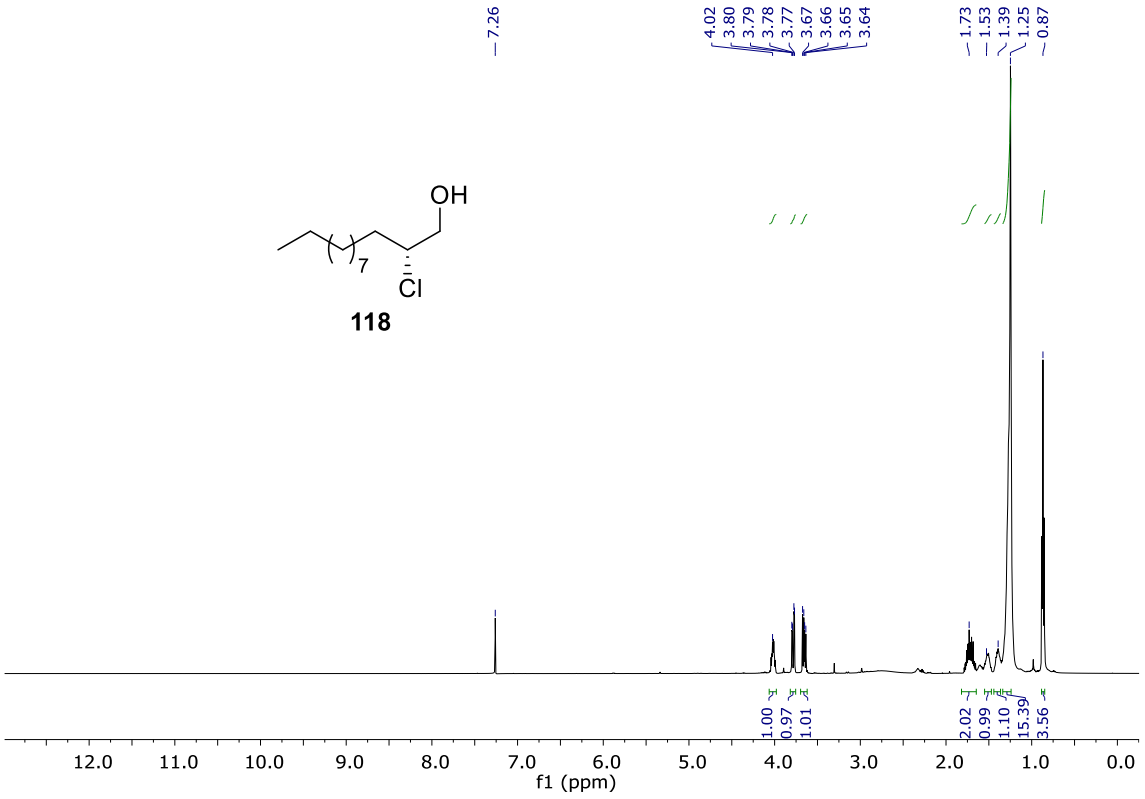
7.26
4.02
3.80
3.79
3.78
3.77
3.67
3.66
3.65
3.64
1.73
1.53
1.39
1.25
0.87
OH
7
Cl
1.00
0.97
1.01
2.02
0.99
1.10
15.39
3.56
12.0
11.0
10.0
9.0
8.0
7.0
6.0
5.0
4.0
3.0
2.0
1.0
0.0
f1 (ppm)

118

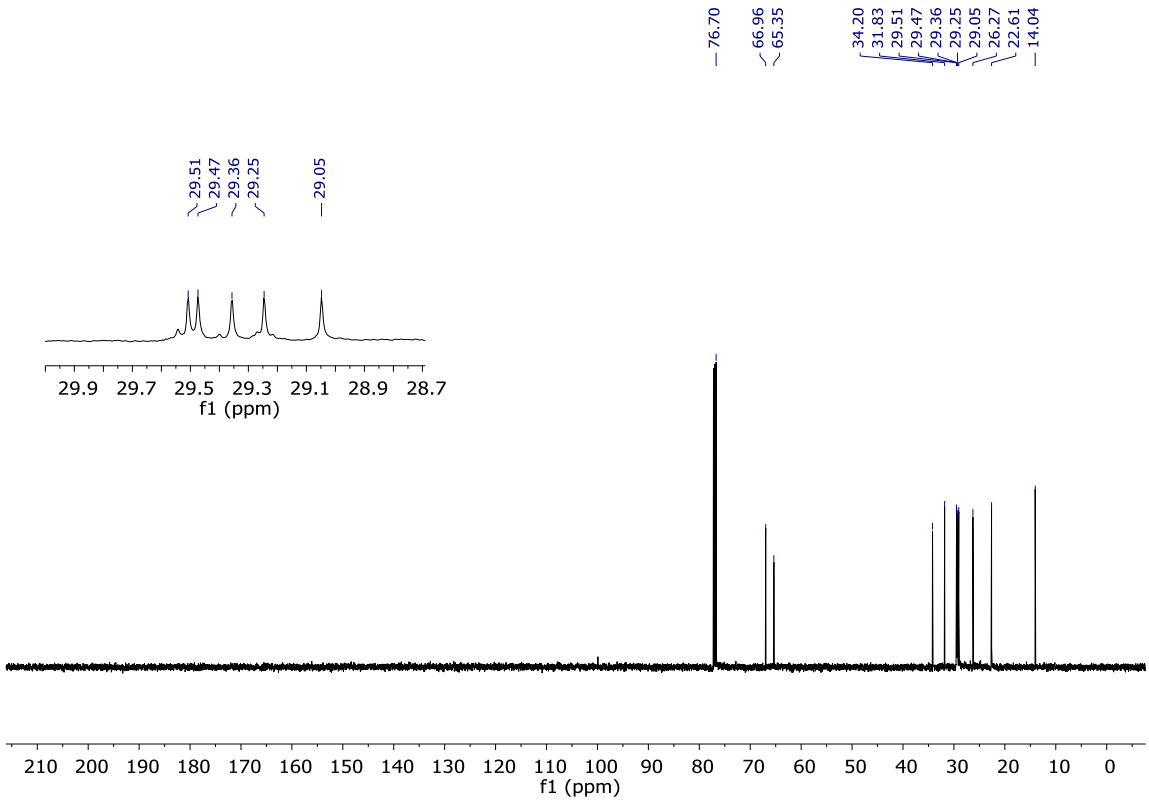
76.70
66.96
65.35
34.20
31.83
29.51
29.47
29.36
29.25
29.05
26.27
22.61
14.04
29.51
29.47
29.36
29.25
29.05
29.9
29.7
29.5
29.3
29.1
28.9
28.7
f1 (ppm)
210
200
190
180
170
160
150
140
130
120
110
100
90
80
70
60
50
40
30
20
10
0
f1 (ppm)

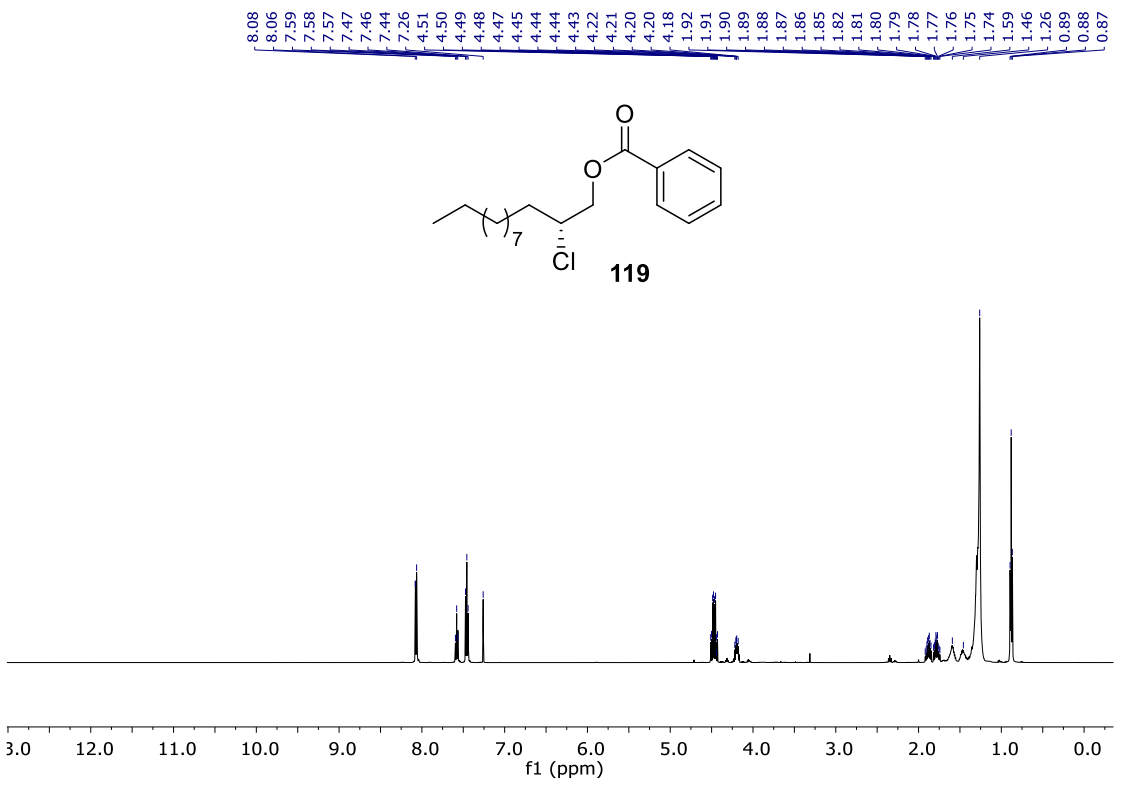
8.08
8.06
7.59
7.58
7.57
7.47
7.46
7.44
7.26
4.51
4.50
4.49
4.48
4.47
4.45
4.44
4.44
4.43
4.22
4.21
4.20
4.20
4.18
1.92
1.91
1.90
1.89
1.88
1.87
1.86
1.85
1.82
1.81
1.80
1.79
1.78
1.77
1.76
1.75
1.74
1.59
1.46
1.26
0.89
0.88
0.87
O
O
7
Cl
119
3.0
12.0
11.0
10.0
9.0
8.0
7.0
6.0
5.0
4.0
3.0
2.0
1.0
0.0
f1 (ppm)

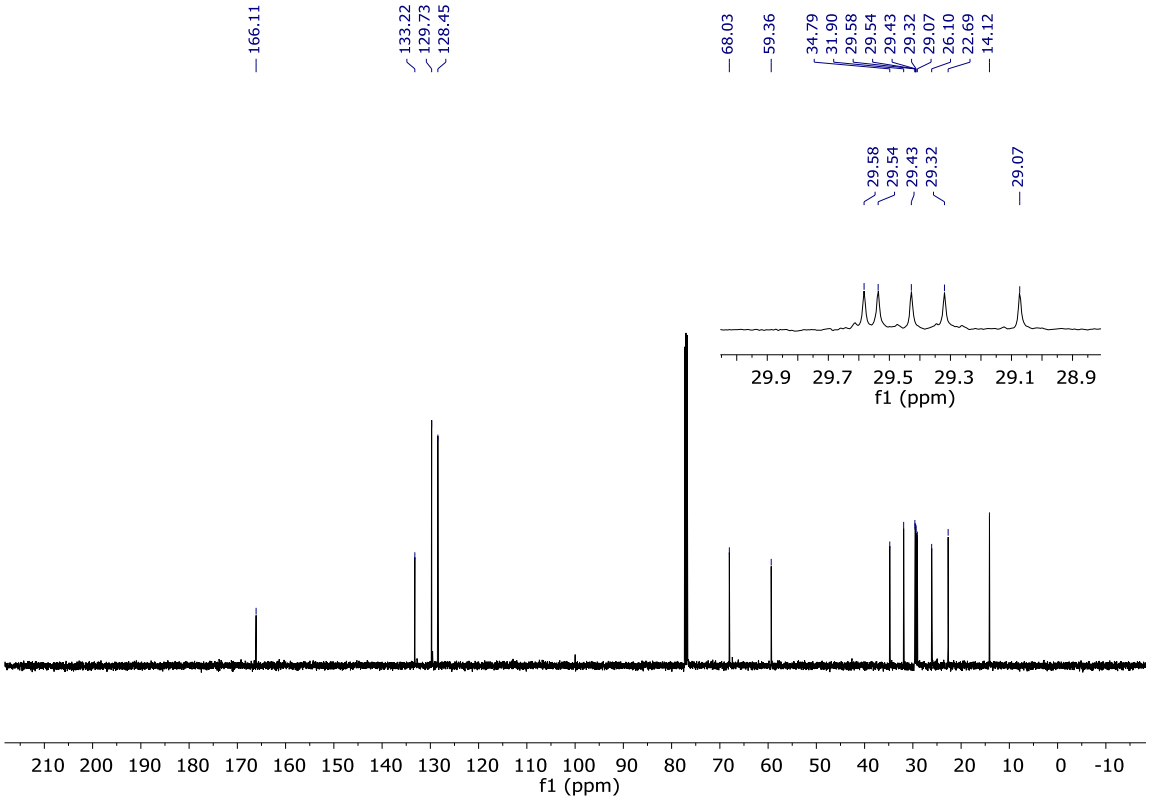
166.11
133.22
129.73
128.45
68.03
59.36
34.79
31.90
29.58
29.54
29.43
29.32
29.07
26.10
22.69
14.12
29.58
29.54
29.43
29.32
29.07
29.9
29.7
29.5
29.3
29.1
28.9
f1 (ppm)
210
200
190
180
170
160
150
140
130
120
110
100
90
80
70
60
50
40
30
20
10
0
-10
f1 (ppm)

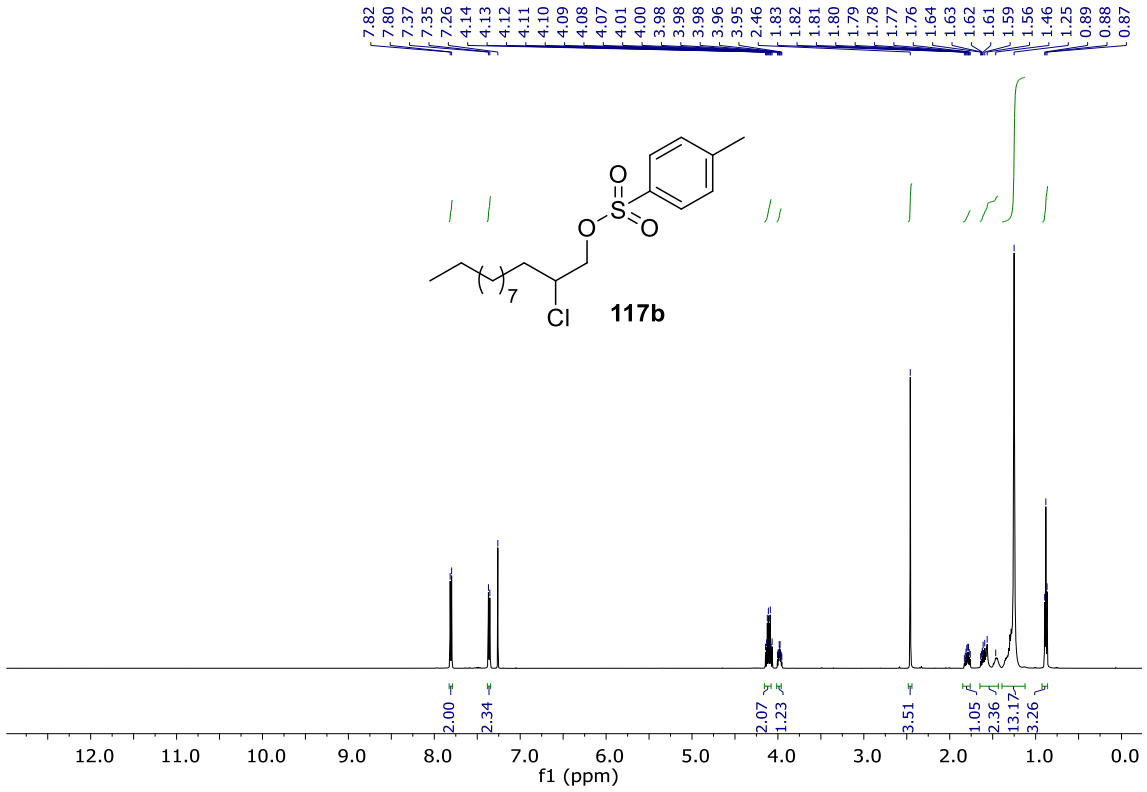
7.82
7.80
7.37
7.35
7.26
4.14
4.13
4.12
4.11
4.10
4.09
4.08
4.07
4.01
4.00
3.98
3.98
3.98
3.96
3.95
2.46
1.83
1.82
1.81
1.80
1.79
1.78
1.77
1.76
1.64
1.63
1.62
1.61
1.59
1.56
1.46
1.25
0.89
0.88
0.87
O
S
O
O
7
Cl
117b
2.00
2.34
2.07
1.23
3.51
1.05
2.36
13.17
3.26
12.0
11.0
10.0
9.0
8.0
7.0
6.0
5.0
4.0
3.0
2.0
1.0
0.0
f1 (ppm)

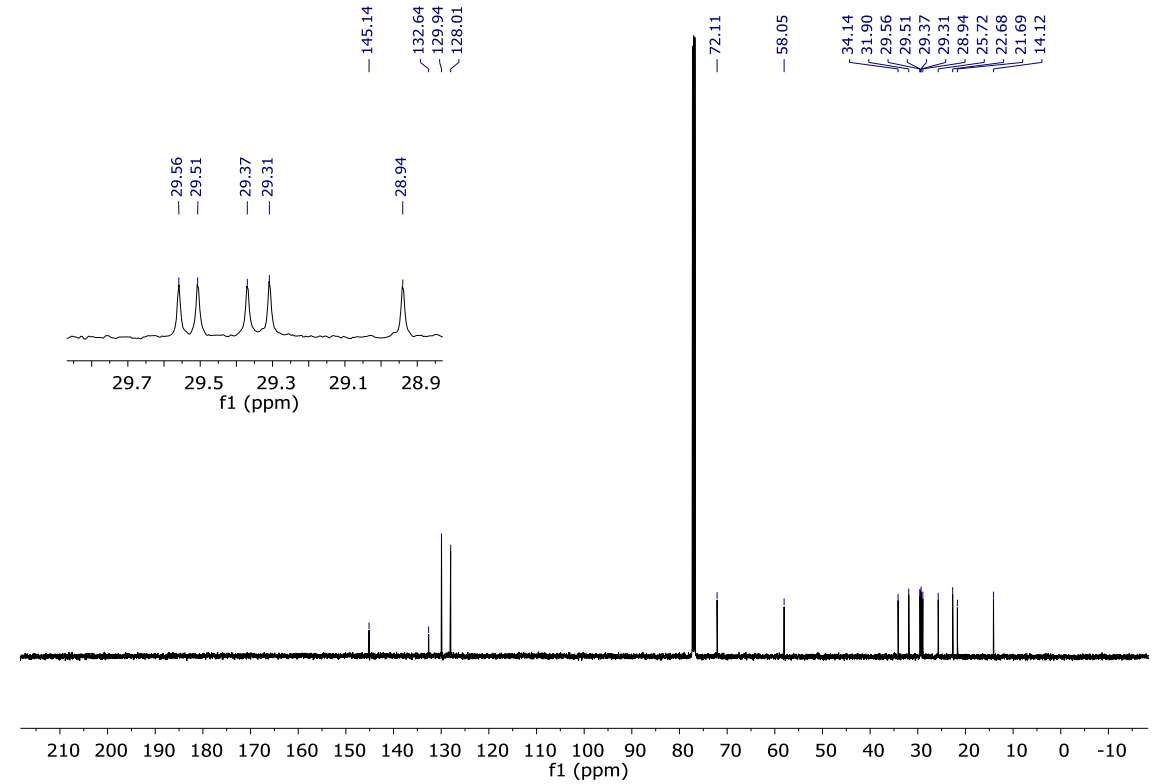
145.14
132.64
129.94
128.01
72.11
58.05
34.14
31.90
29.56
29.51
29.37
29.31
28.94
25.72
22.68
21.69
14.12
29.56
29.51
29.37
29.31
28.94
29.7
29.5
29.3
29.1
28.9
f1 (ppm)
210
200
190
180
170
160
150
140
130
120
110
100
90
80
70
60
50
40
30
20
10
0
-10
f1 (ppm)

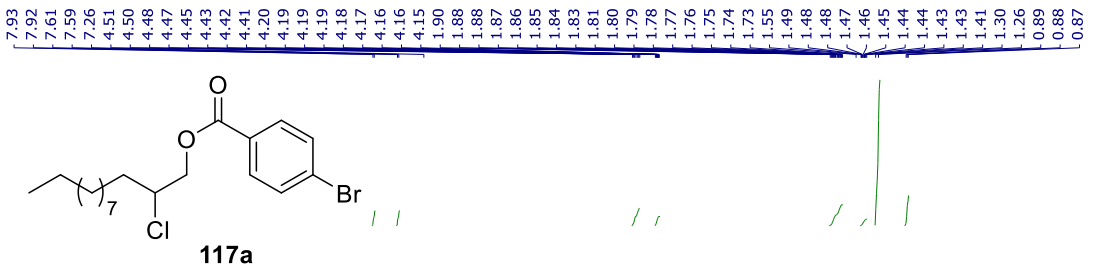
7.93 7.92 7.61 7.59 7.26 4.51 4.50 4.48 4.47 4.45 4.43 4.42 4.41 4.20 4.19 4.19 4.19 4.18 4.17 4.16 4.16 4.15 1.90 1.88 1.88 1.87 1.86 1.85 1.84 1.83 1.81 1.80 1.79 1.78 1.77 1.76 1.75 1.74 1.73 1.55 1.49 1.48 1.48 1.47 1.46 1.45 1.44 1.44 1.43 1.43 1.41 1.30 1.26 0.89 0.88 0.87
O
O
Br
7
Cl

117a

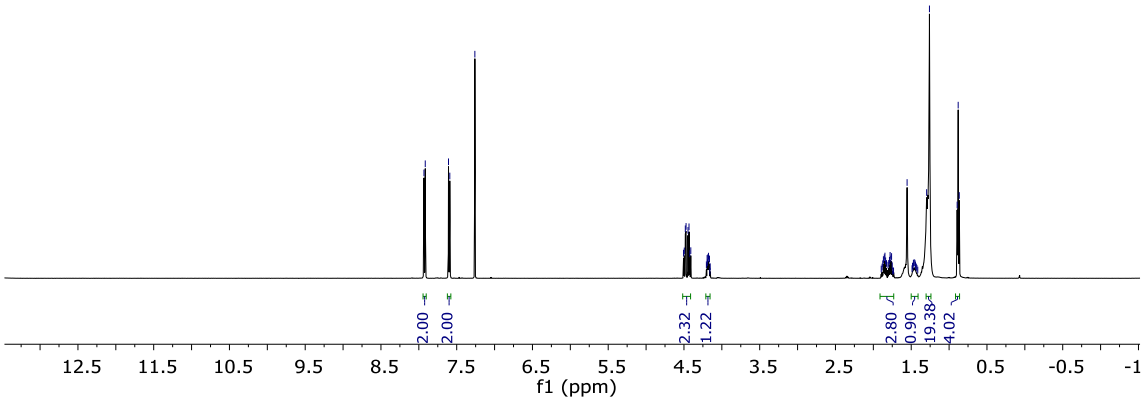
2.00
2.00
2.32
1.22
2.80
0.90
19.38
4.02
12.5 11.5 10.5 9.5 8.5 7.5 6.5 5.5 4.5 3.5 2.5 1.5 0.5 -0.5 -1
f1 (ppm)

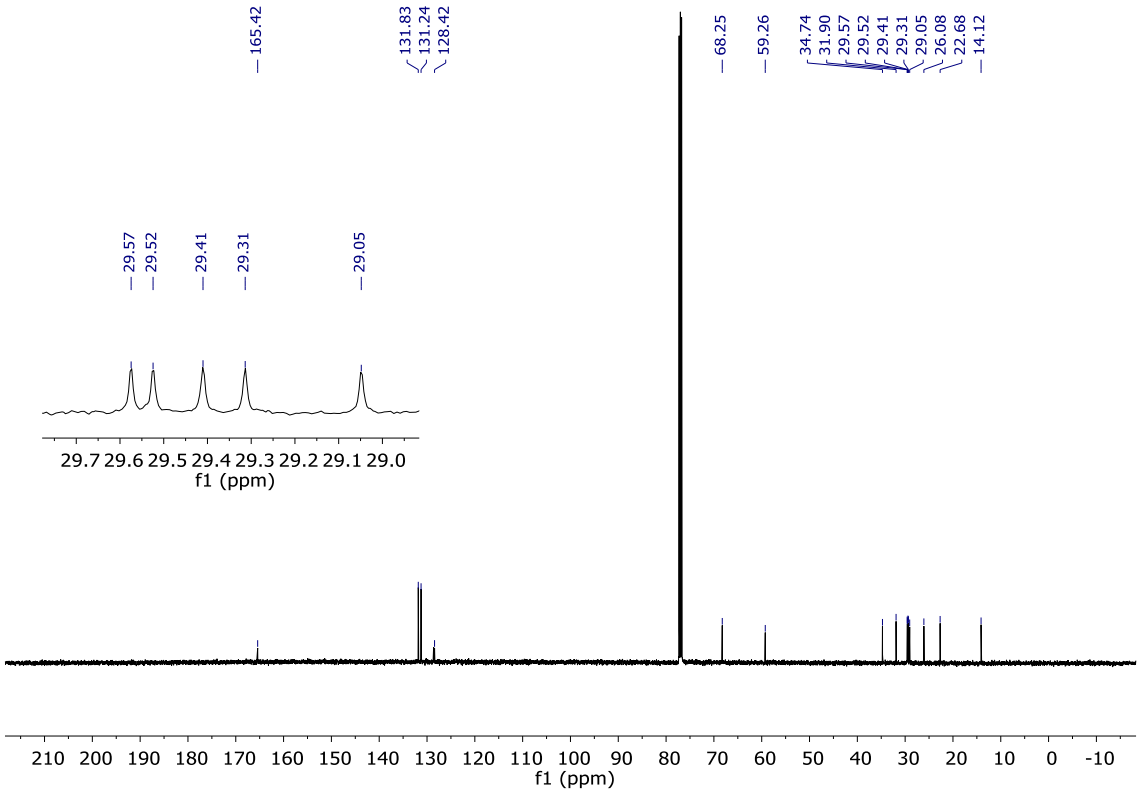
165.42
131.83
131.24
128.42
68.25
59.26
34.74
31.90
29.57
29.52
29.41
29.31
29.05
26.08
22.68
14.12
29.57
29.52
29.41
29.31
29.05
29.7 29.6 29.5 29.4 29.3 29.2 29.1 29.0
f1 (ppm)
210 200 190 180 170 160 150 140 130 120 110 100 90 80 70 60 50 40 30 20 10 0 -10
f1 (ppm)

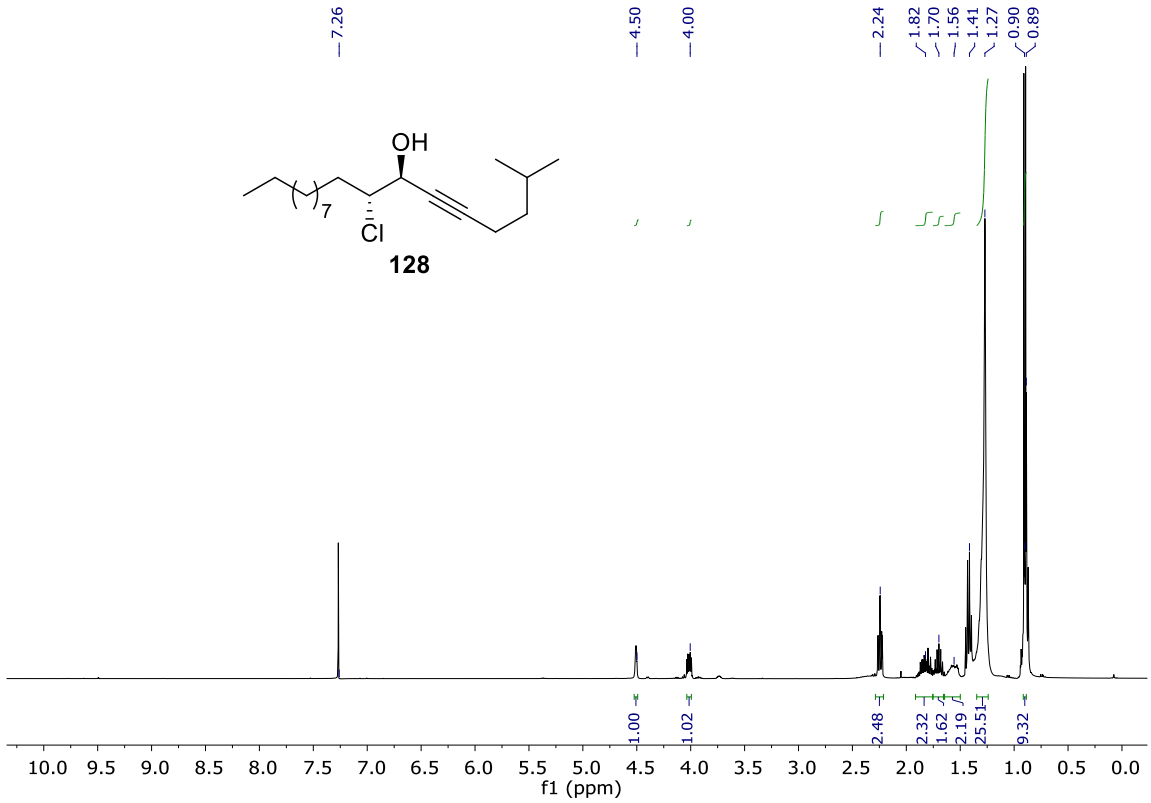
7.26
4.50
4.00
2.24
1.82
1.70
1.56
1.41
1.27
0.90
0.89
OH
Cl
7
128
1.00
1.02
2.48
2.32
1.62
2.19
25.51
9.32
f1 (ppm)

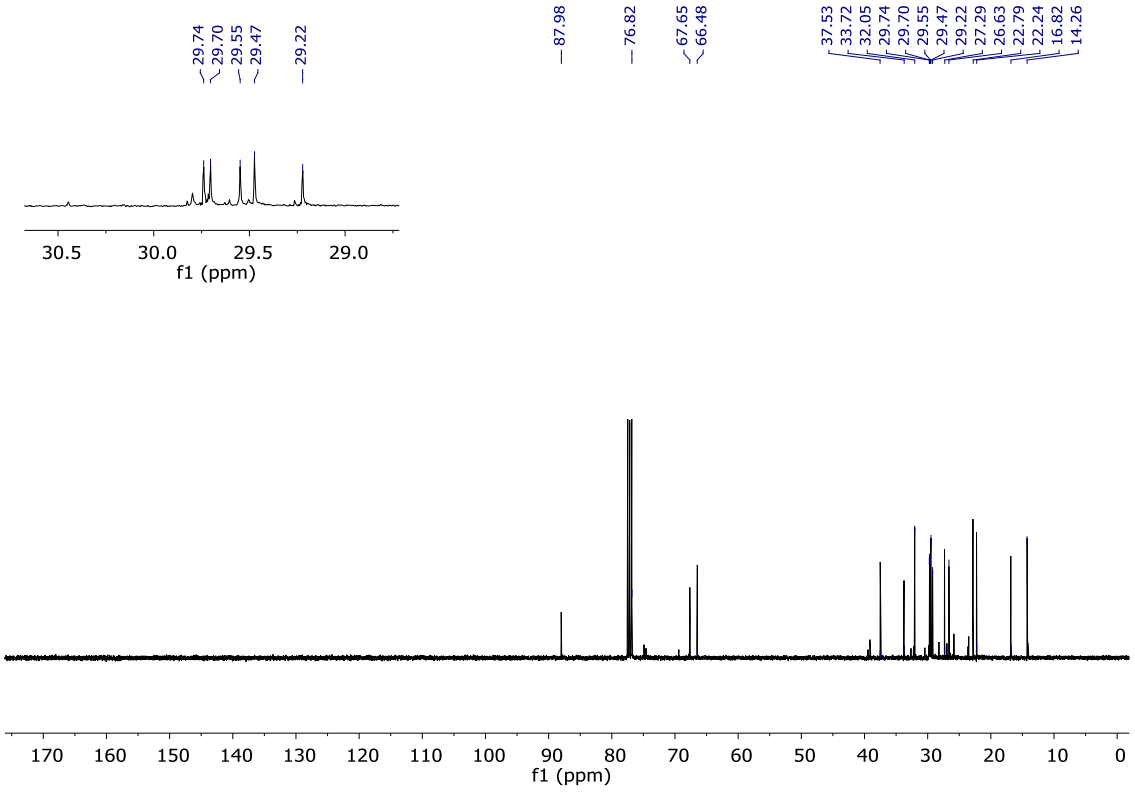
29.74
29.70
29.55
29.47
29.22
87.98
76.82
67.65
66.48
37.53
33.72
32.05
29.74
29.70
29.55
29.47
29.22
27.29
26.63
22.79
22.24
16.82
14.26
f1 (ppm)
f1 (ppm)

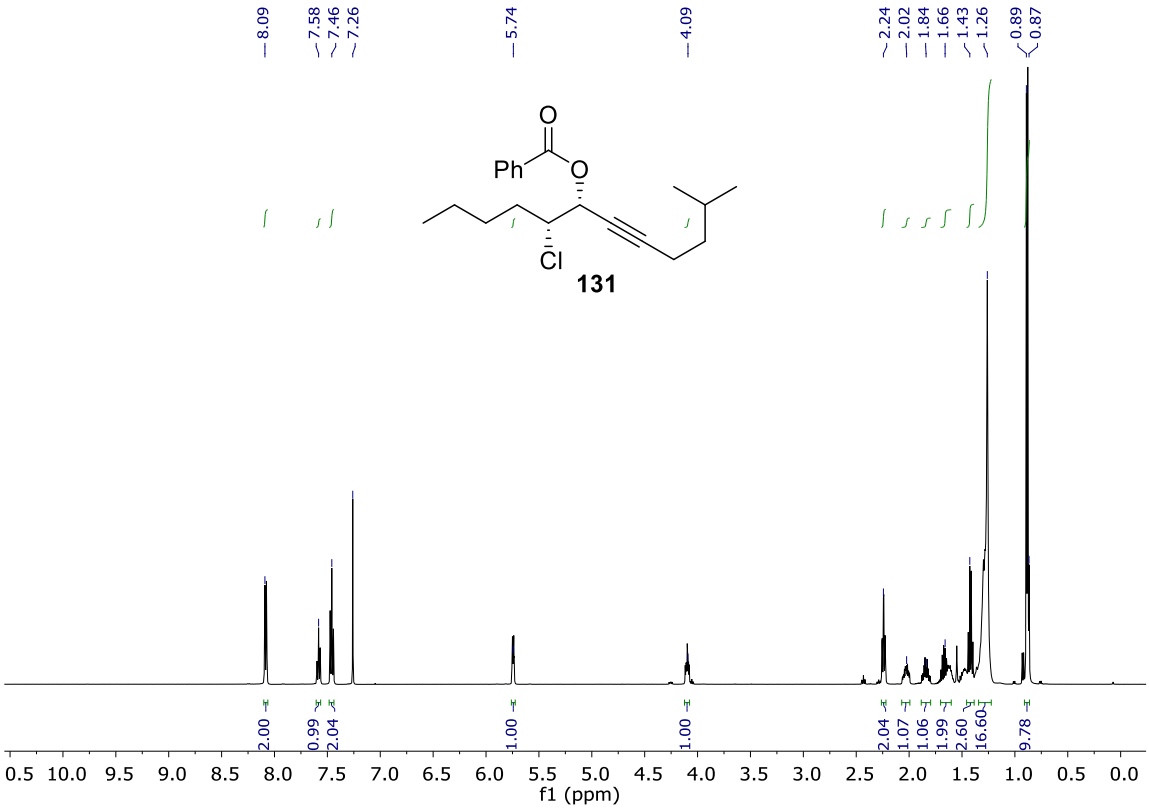
8.09
7.58
7.46
7.26
5.74
4.09
2.24
2.02
1.84
1.66
1.43
1.26
0.89
0.87
O
Ph
O
Cl
131
2.00
0.99
2.04
1.00
1.00
2.04
1.07
1.06
1.99
2.60
16.60
9.78
0.5 10.0 9.5 9.0 8.5 8.0 7.5 7.0 6.5 6.0 5.5 5.0 4.5 4.0 3.5 3.0 2.5 2.0 1.5 1.0 0.5 0.0
f1 (ppm)

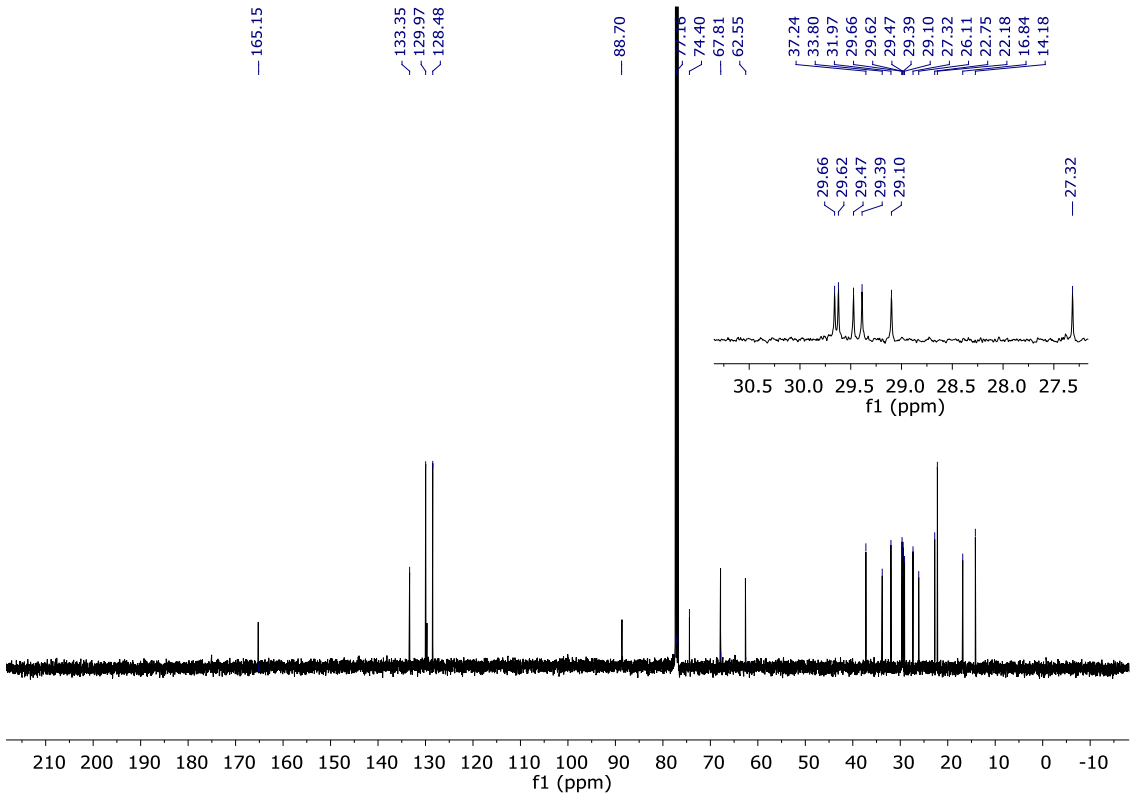
165.15
133.35
129.97
128.48
88.70
77.16
74.40
67.81
62.55
37.24
33.80
31.97
29.66
29.62
29.47
29.39
29.10
27.32
26.11
22.75
22.18
16.84
14.18
29.66
29.62
29.47
29.39
29.10
27.32
30.5 30.0 29.5 29.0 28.5 28.0 27.5
f1 (ppm)
210 200 190 180 170 160 150 140 130 120 110 100 90 80 70 60 50 40 30 20 10 0 -10
f1 (ppm)

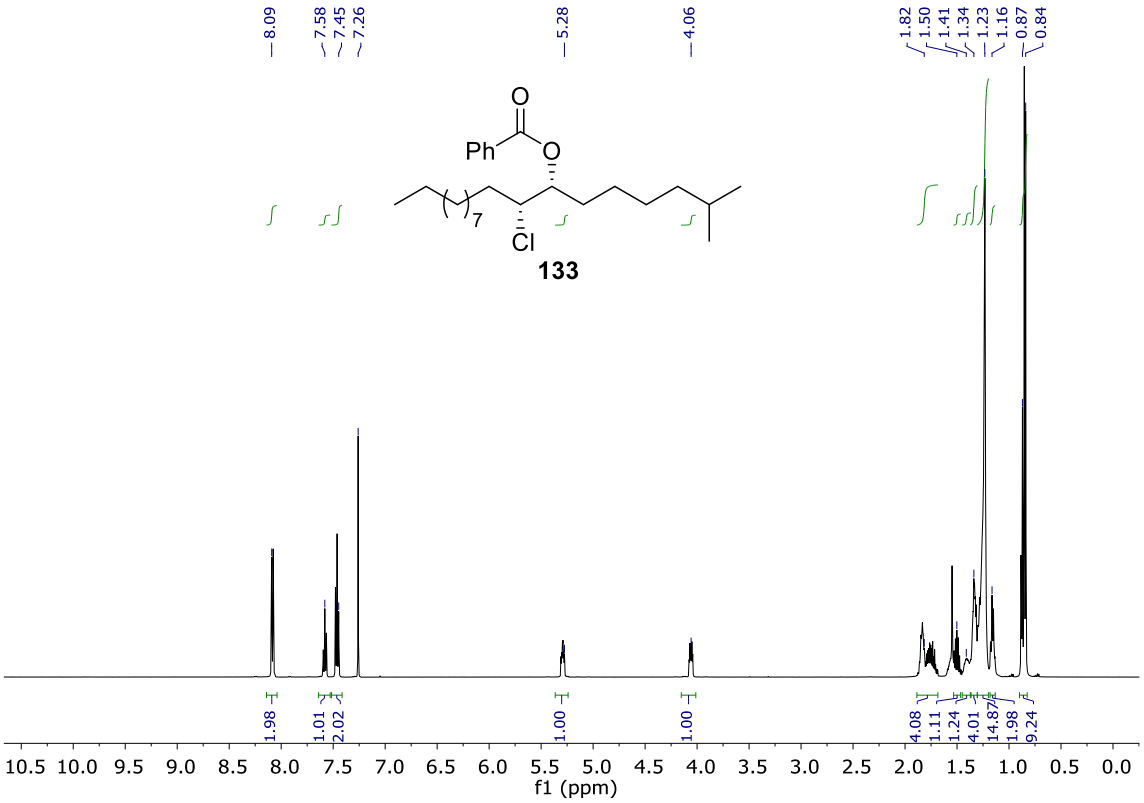
8.09
7.58
7.45
7.26
5.28
4.06
1.82
1.50
1.41
1.34
1.23
1.16
0.87
0.84
O
Ph
O
7
Cl
133
1.98
1.01
2.02
1.00
1.00
4.08
1.11
1.24
4.01
14.87
1.98
9.24
10.5 10.0 9.5 9.0 8.5 8.0 7.5 7.0 6.5 6.0 5.5 5.0 4.5 4.0 3.5 3.0 2.5 2.0 1.5 1.0 0.5 0.0
f1 (ppm)

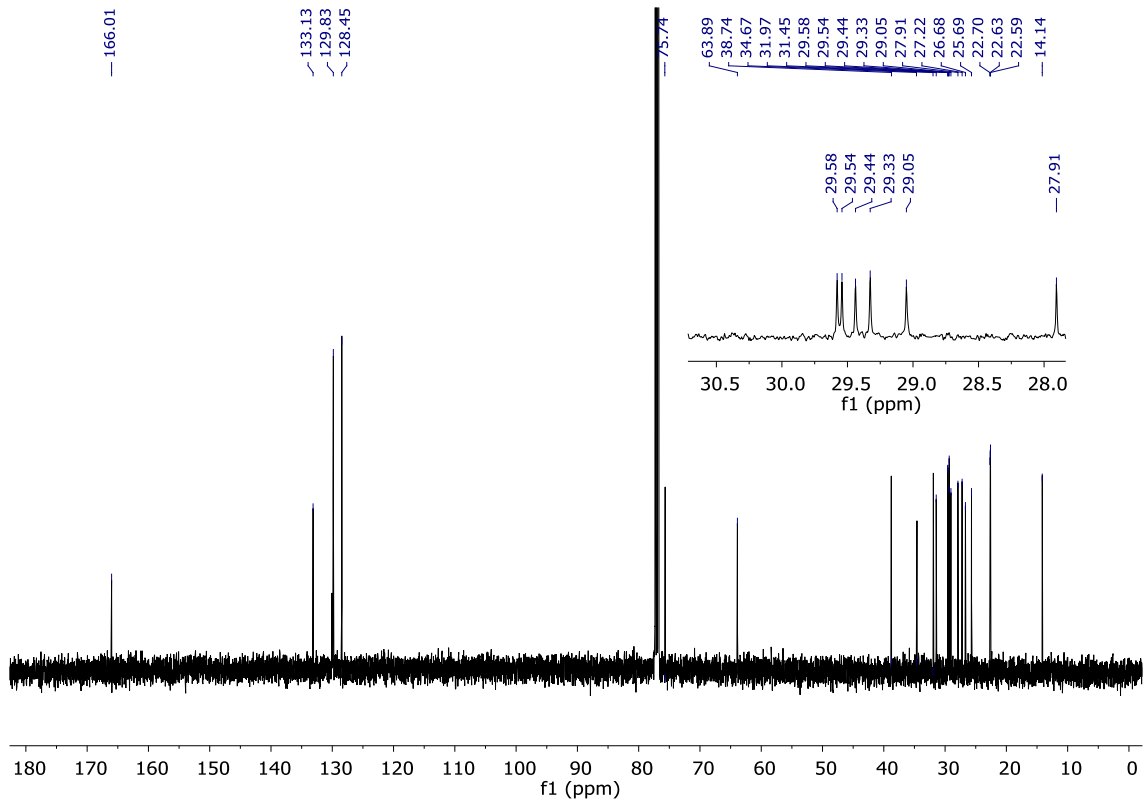
166.01
133.13
129.83
128.45
75.74
63.89
38.74
34.67
31.97
31.45
29.58
29.54
29.44
29.33
29.05
27.91
27.22
26.68
25.69
22.70
22.63
22.59
14.14
29.58
29.54
29.44
29.33
29.05
27.91
30.5 30.0 29.5 29.0 28.5 28.0
f1 (ppm)
180 170 160 150 140 130 120 110 100 90 80 70 60 50 40 30 20 10 0
f1 (ppm)

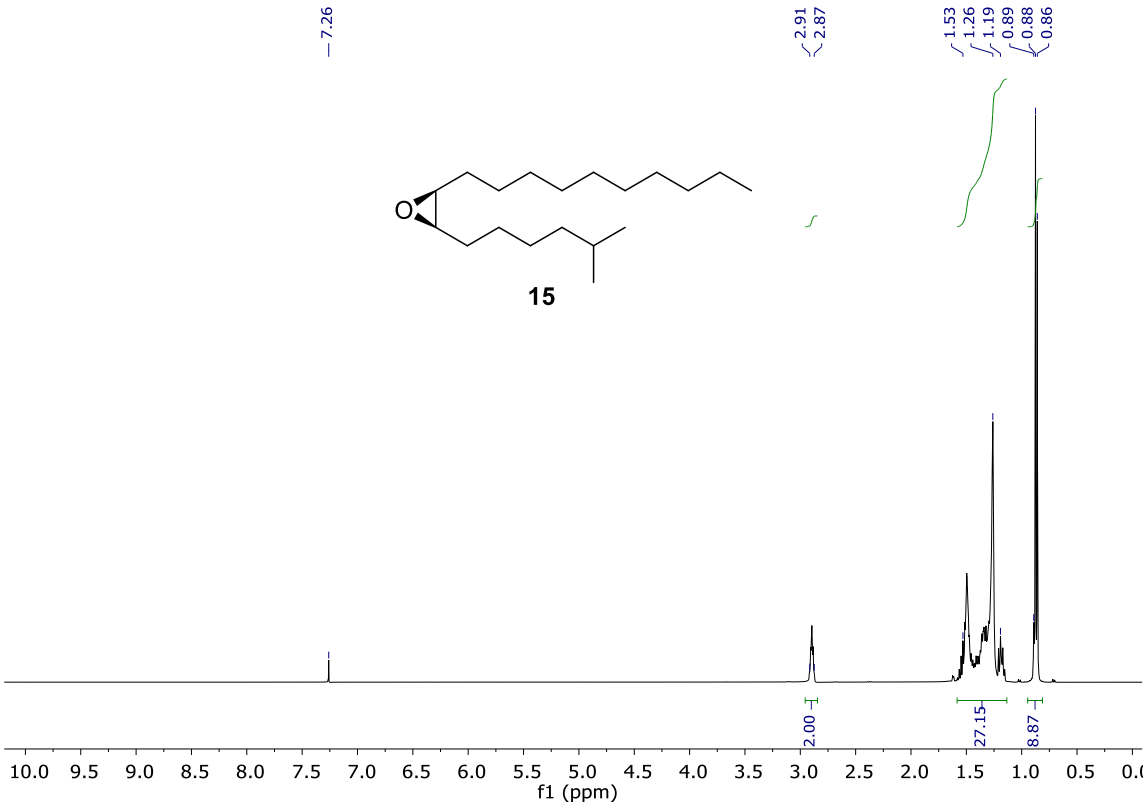
7.26
2.91
2.87
1.53
1.26
1.19
0.89
0.88
0.86
15
2.00
27.15
8.87
f1 (ppm)

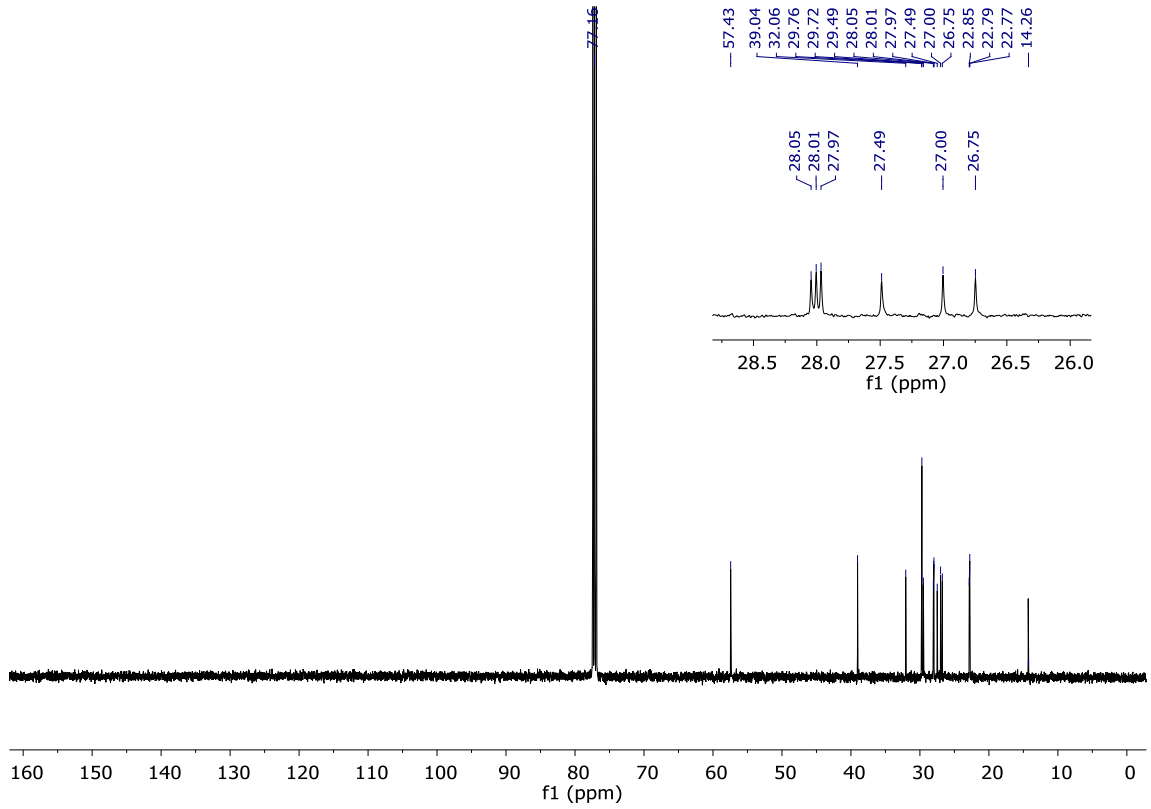
77.16
57.43
39.04
32.06
29.76
29.72
29.49
28.05
28.01
27.97
27.49
27.00
26.75
22.85
22.79
22.77
14.26
f1 (ppm)

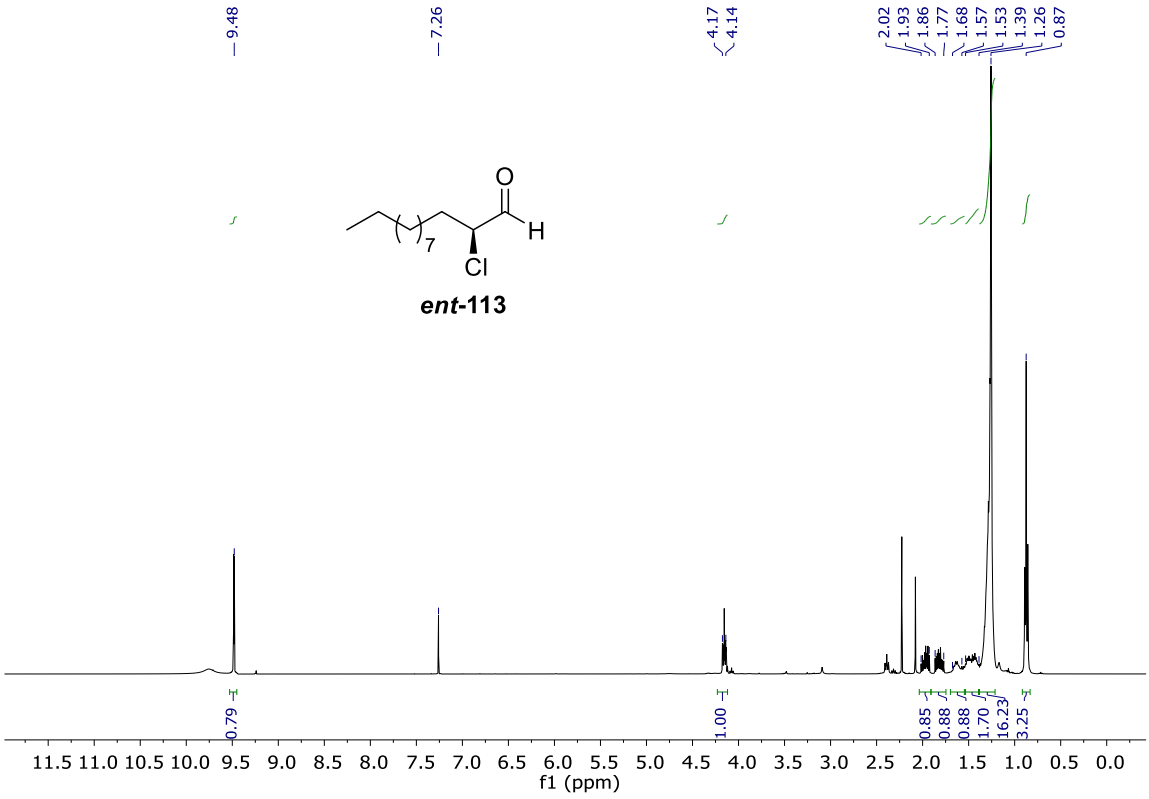
9.48
7.26
4.17
4.14
2.02
1.93
1.86
1.77
1.68
1.57
1.53
1.39
1.26
0.87
O
H
Cl
7
0.79
1.00
0.85
0.88
0.88
1.70
16.23
3.25
11.5 11.0 10.5 10.0 9.5 9.0 8.5 8.0 7.5 7.0 6.5 6.0 5.5 5.0 4.5 4.0 3.5 3.0 2.5 2.0 1.5 1.0 0.5 0.0
f1 (ppm)

***ent*-113**

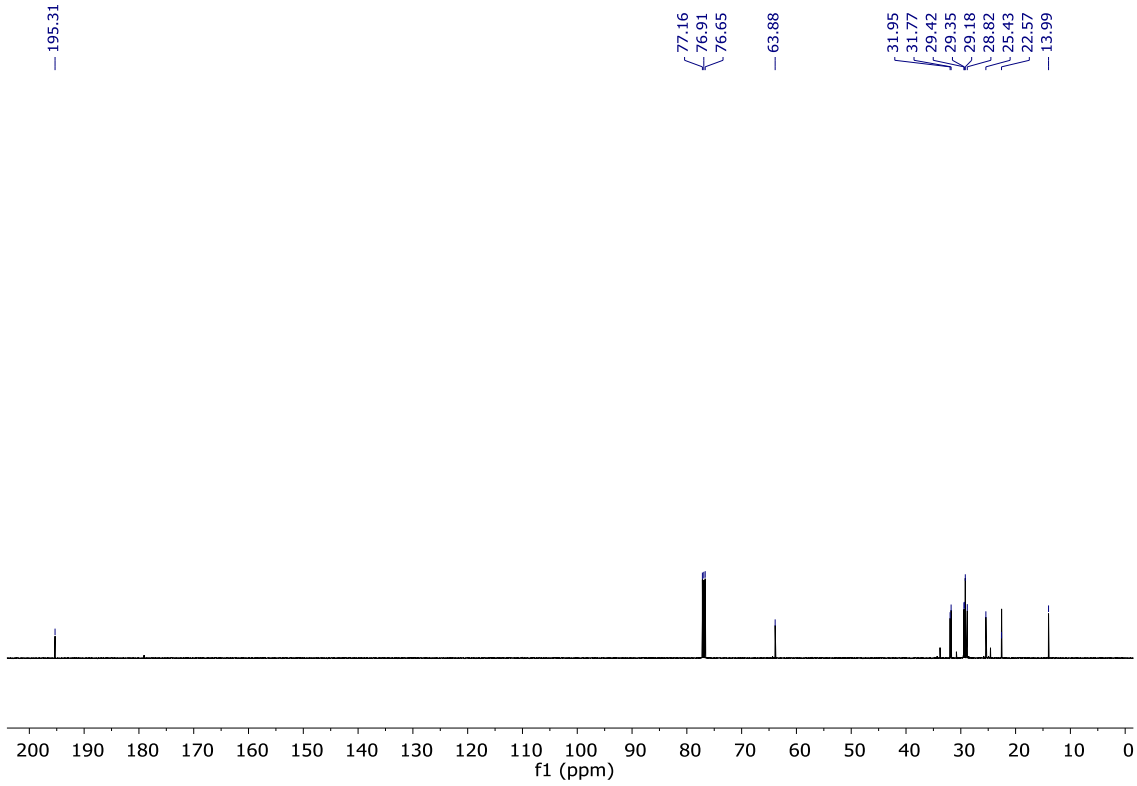
195.31
77.16
76.91
76.65
63.88
31.95
31.77
29.42
29.35
29.18
28.82
25.43
22.57
13.99
200 190 180 170 160 150 140 130 120 110 100 90 80 70 60 50 40 30 20 10 0
f1 (ppm)

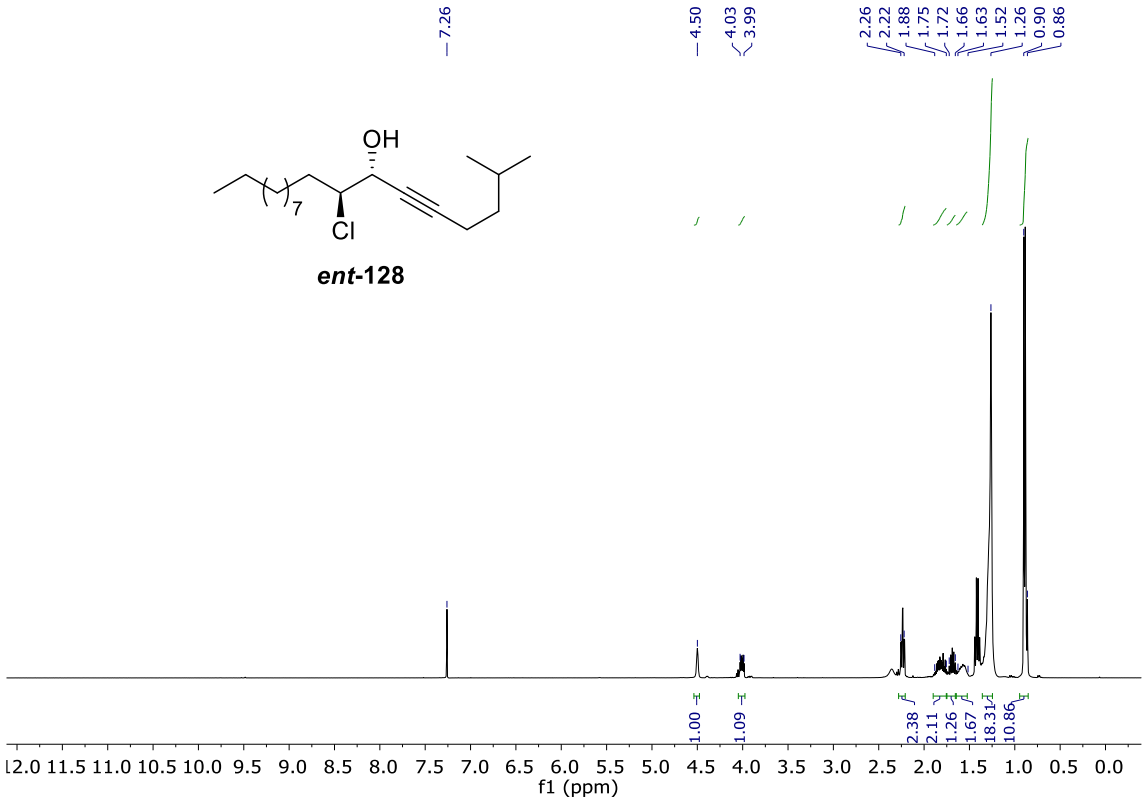
7.26
4.50
4.03
3.99
2.26
2.22
1.88
1.75
1.72
1.66
1.63
1.52
1.26
0.90
0.86
OH
Cl
7
1.00
1.09
2.38
2.11
1.26
1.67
18.31
10.86
f1 (ppm)

***ent*-128**

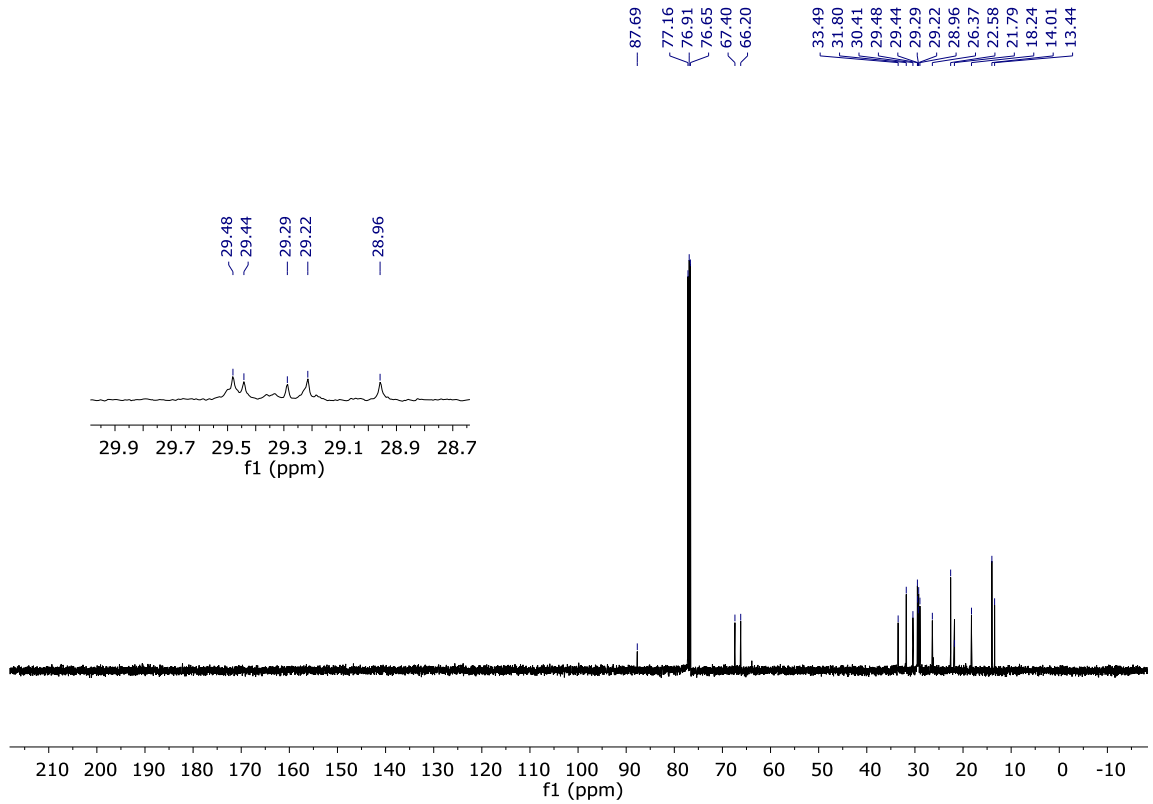
87.69
77.16
76.91
76.65
67.40
66.20
33.49
31.80
30.41
29.48
29.44
29.29
29.22
28.96
26.37
22.58
21.79
18.24
14.01
13.44
29.48
29.44
29.29
29.22
28.96
f1 (ppm)

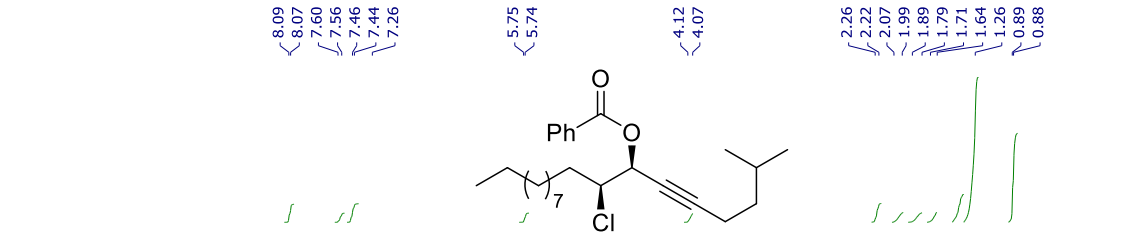
8.09
8.07
7.60
7.56
7.46
7.44
7.26
5.75
5.74
4.12
4.07
2.26
2.22
2.07
1.99
1.89
1.79
1.71
1.64
1.26
0.89
0.88
O
Ph
O
7
Cl

***ent*-131**

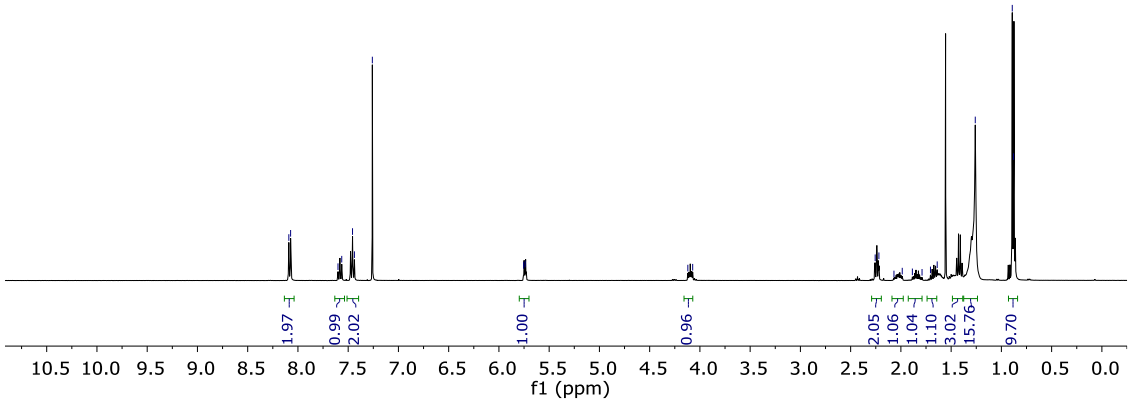
1.97
0.99
2.02
1.00
0.96
2.05
1.06
1.04
1.10
3.02
15.76
9.70
10.5 10.0 9.5 9.0 8.5 8.0 7.5 7.0 6.5 6.0 5.5 5.0 4.5 4.0 3.5 3.0 2.5 2.0 1.5 1.0 0.5 0.0
f1 (ppm)

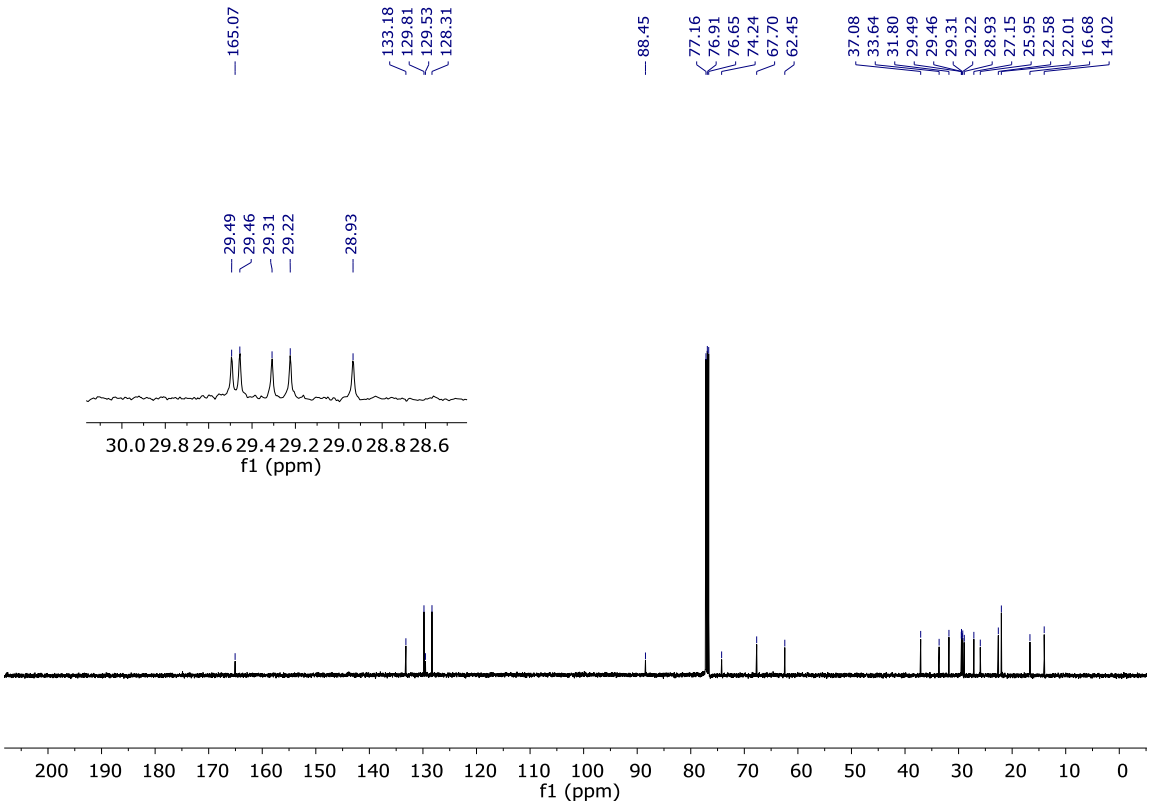
165.07
133.18
129.81
129.53
128.31
88.45
77.16
76.91
76.65
74.24
67.70
62.45
37.08
33.64
31.80
29.49
29.46
29.31
29.22
28.93
27.15
25.95
22.58
22.01
16.68
14.02
29.49
29.46
29.31
29.22
28.93
30.0 29.8 29.6 29.4 29.2 29.0 28.8 28.6
f1 (ppm)
200 190 180 170 160 150 140 130 120 110 100 90 80 70 60 50 40 30 20 10 0
f1 (ppm)

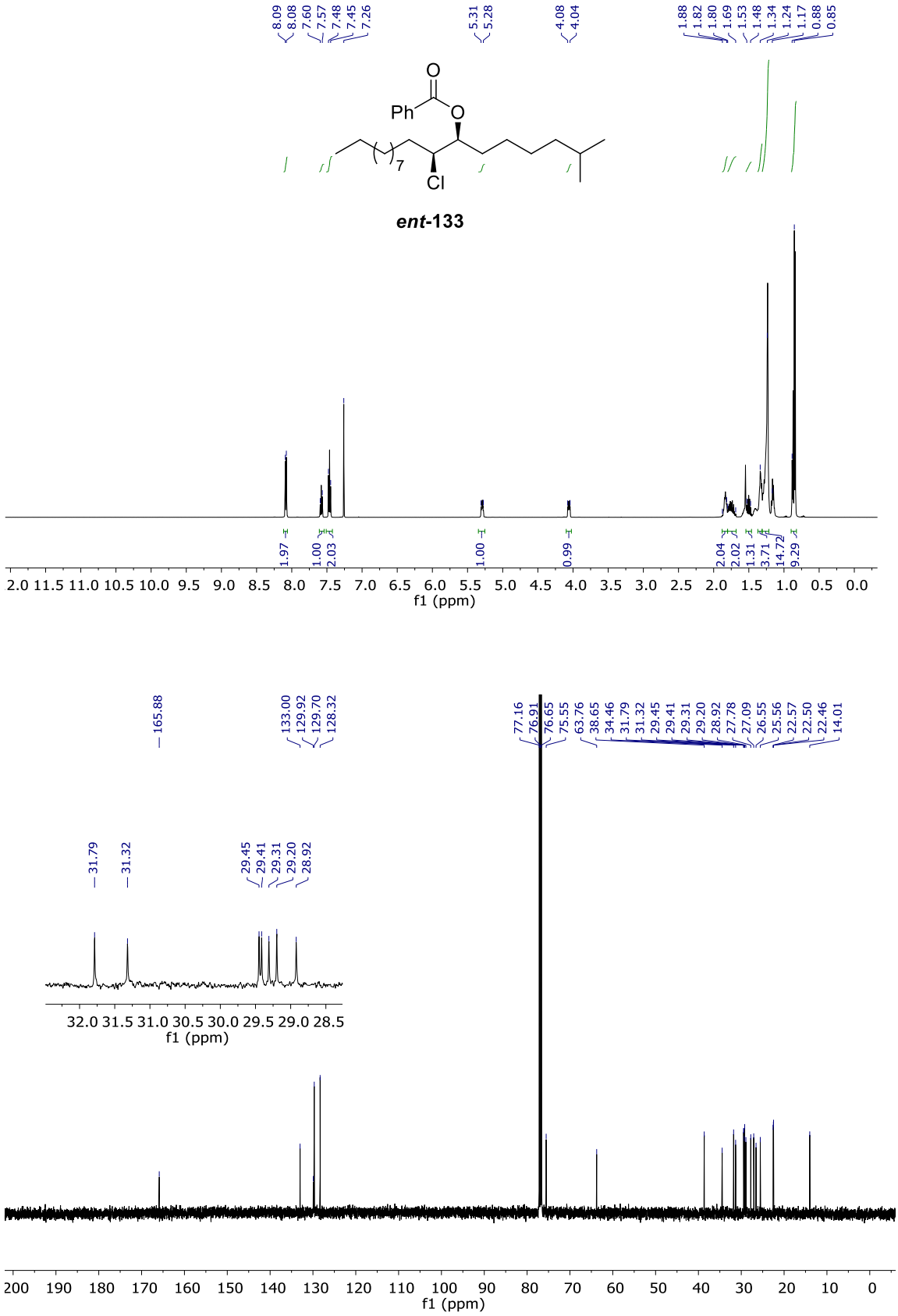
8.09
8.08
7.60
7.57
7.48
7.45
7.26
5.31
5.28
4.08
4.04
1.88
1.82
1.80
1.69
1.53
1.48
1.34
1.24
1.17
0.88
0.85
O
Ph
O
7
Cl
1.97
1.00
2.03
1.00
0.99
2.04
2.02
1.31
3.71
14.72
9.29
2.0 11.5 11.0 10.5 10.0 9.5 9.0 8.5 8.0 7.5 7.0 6.5 6.0 5.5 5.0 4.5 4.0 3.5 3.0 2.5 2.0 1.5 1.0 0.5 0.0
f1 (ppm)
165.88
133.00
129.92
129.70
128.32
77.16
76.91
76.65
75.55
63.76
38.65
34.46
31.79
31.32
29.45
29.41
29.31
29.20
28.92
27.78
27.09
26.55
25.56
22.57
22.50
22.46
14.01
31.79
31.32
29.45
29.41
29.31
29.20
28.92
32.0 31.5 31.0 30.5 30.0 29.5 29.0 28.5
f1 (ppm)
200 190 180 170 160 150 140 130 120 110 100 90 80 70 60 50 40 30 20 10 0
f1 (ppm)

***ent*-133**

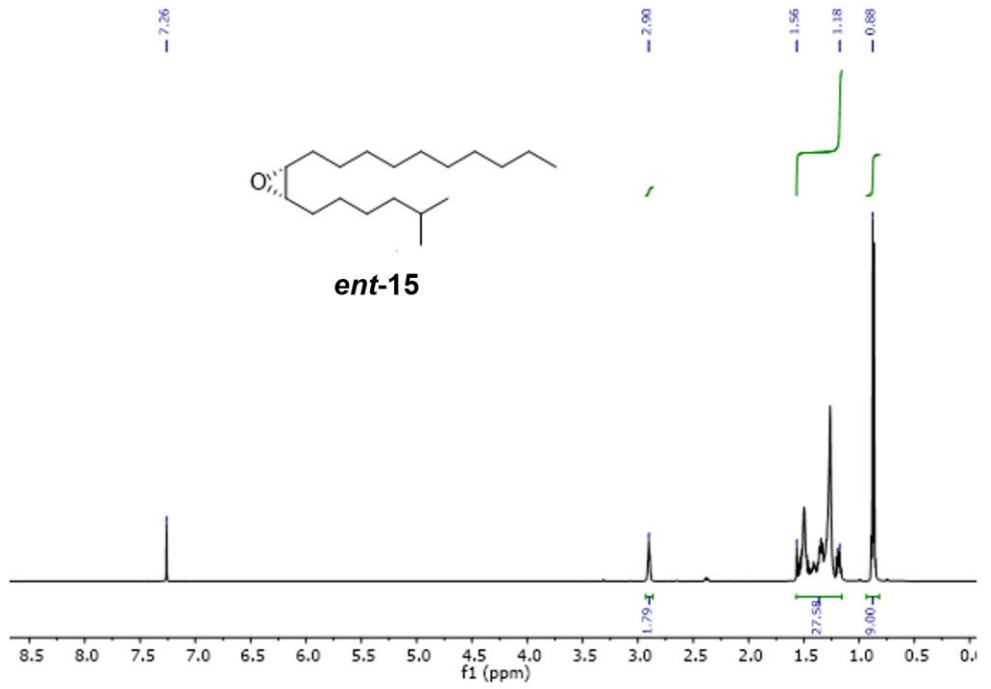
7.26
2.90
1.56
1.18
0.88
1.79
27.58
9.00
f1 (ppm)

***ent*-15**

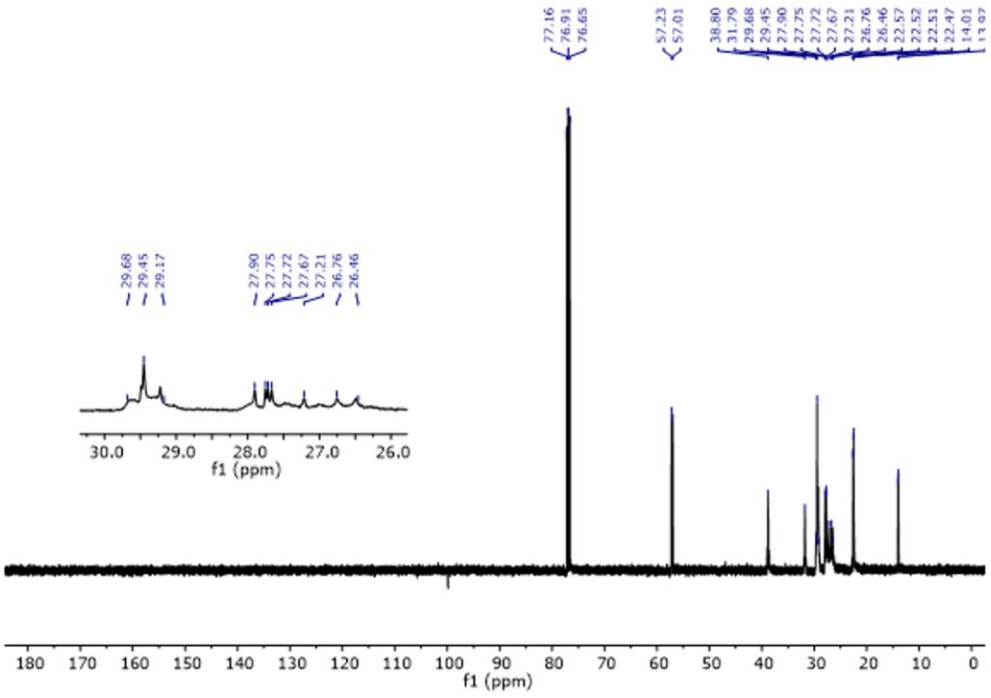
77.16
76.91
76.65
57.23
57.01
38.80
31.79
29.68
29.45
27.90
27.75
27.72
27.67
27.21
26.76
26.46
22.57
22.52
22.51
22.47
14.01
29.68
29.45
29.17
27.90
27.75
27.72
27.67
27.21
26.76
26.46
f1 (ppm)
f1 (ppm)

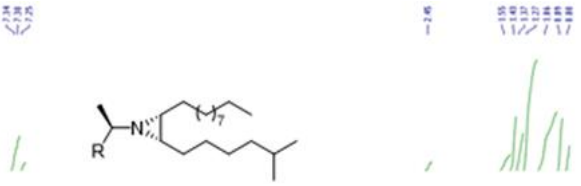

139

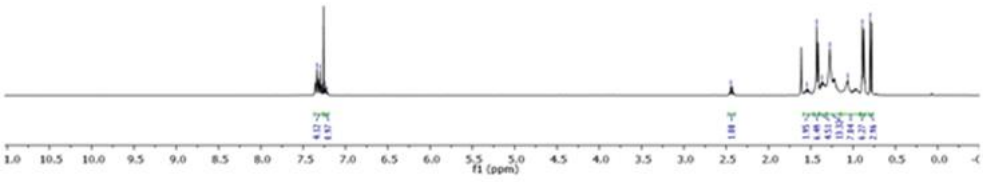

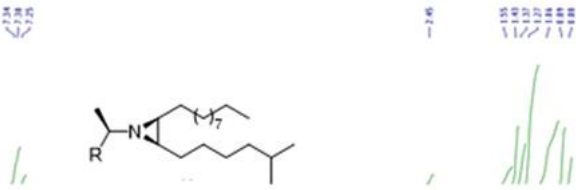

140

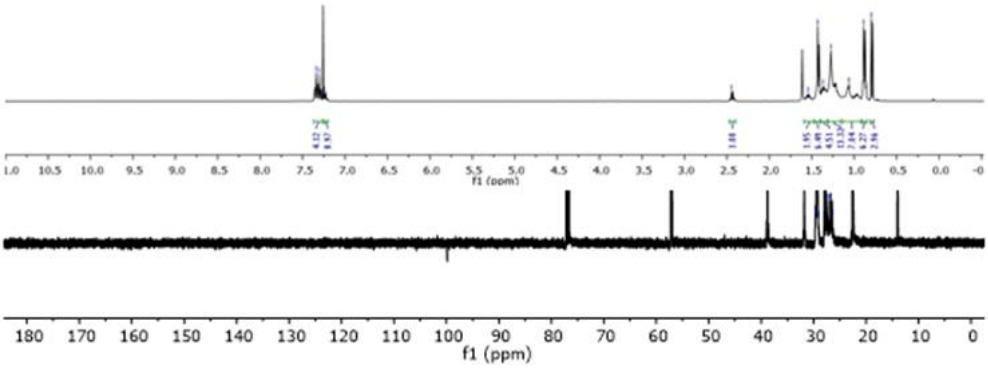

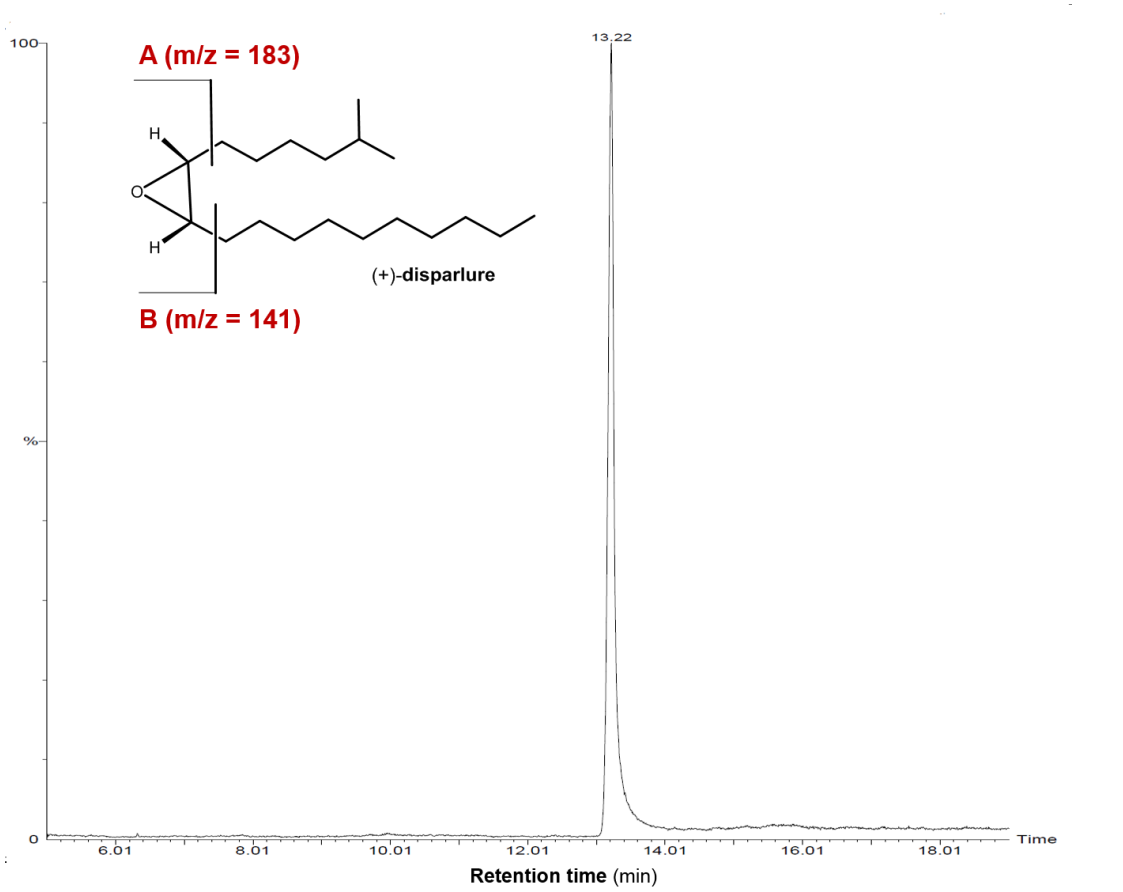
A (m/z = 183)
B (m/z = 141)
(+)-disparlure
13.22
100
%
0
6.01
8.01
10.01
12.01
14.01
16.01
18.01
Time
Retention time (min)

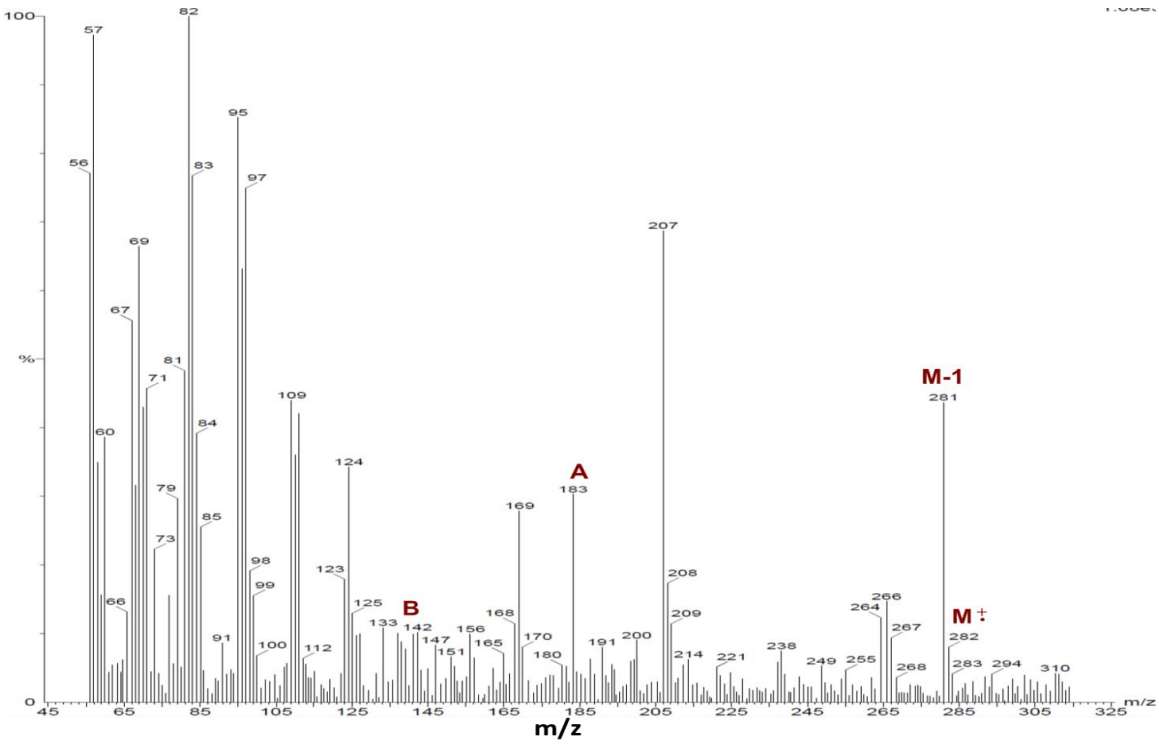
100
%
0
A
B
M-1
M+
m/z
45
65
85
105
125
145
165
185
205
225
245
265
285
305
325

APPENDIX B. Chapter 3 supporting information

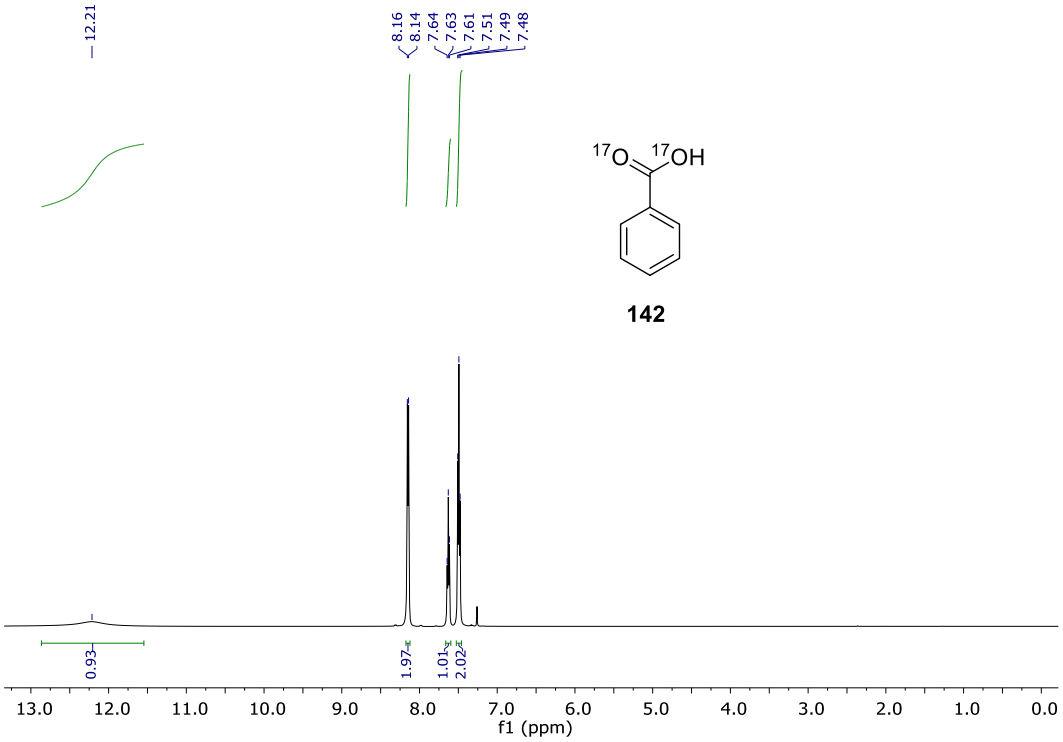

142

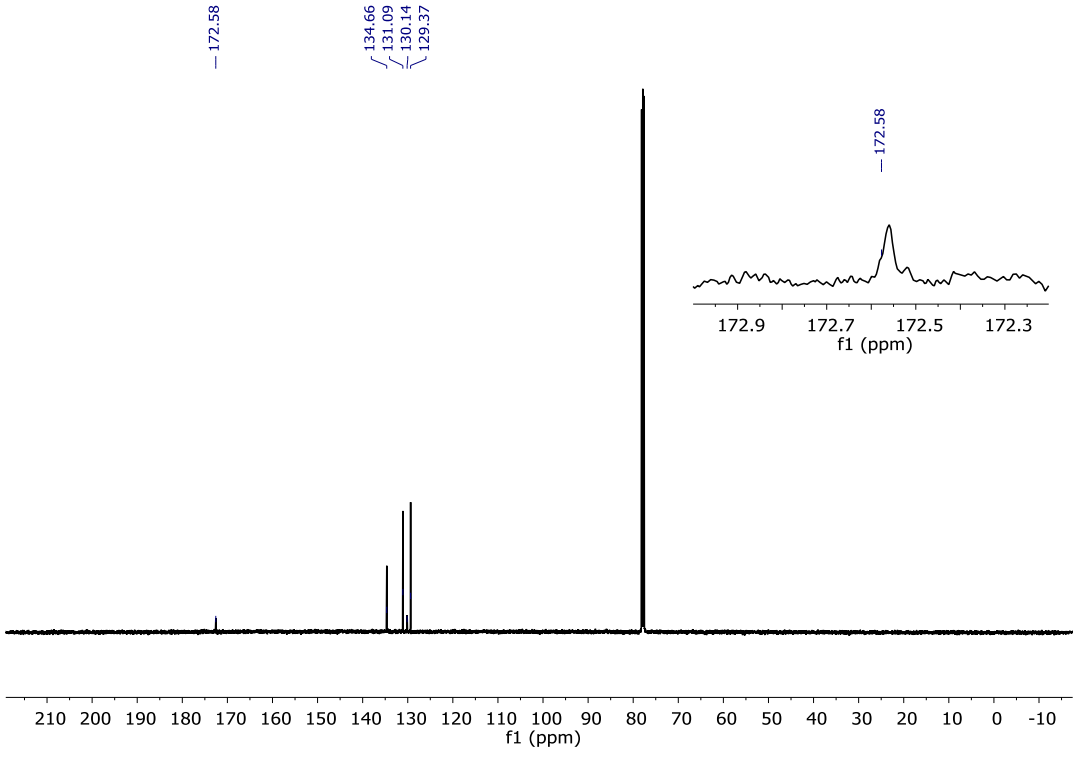

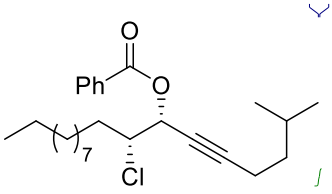
O
Ph
O
7
Cl

144: O = ^{17}O

8.09
8.08
7.60
7.58
7.57
7.47
7.44
7.26
5.75
5.74
4.12
4.08
2.26
2.22
2.07
2.00
1.88
1.80
1.70
1.65
1.26
0.89
0.87
2.31
1.18
2.40
1.00
1.12
2.39
1.08
1.19
0.99
19.63
11.24
f1 (ppm)

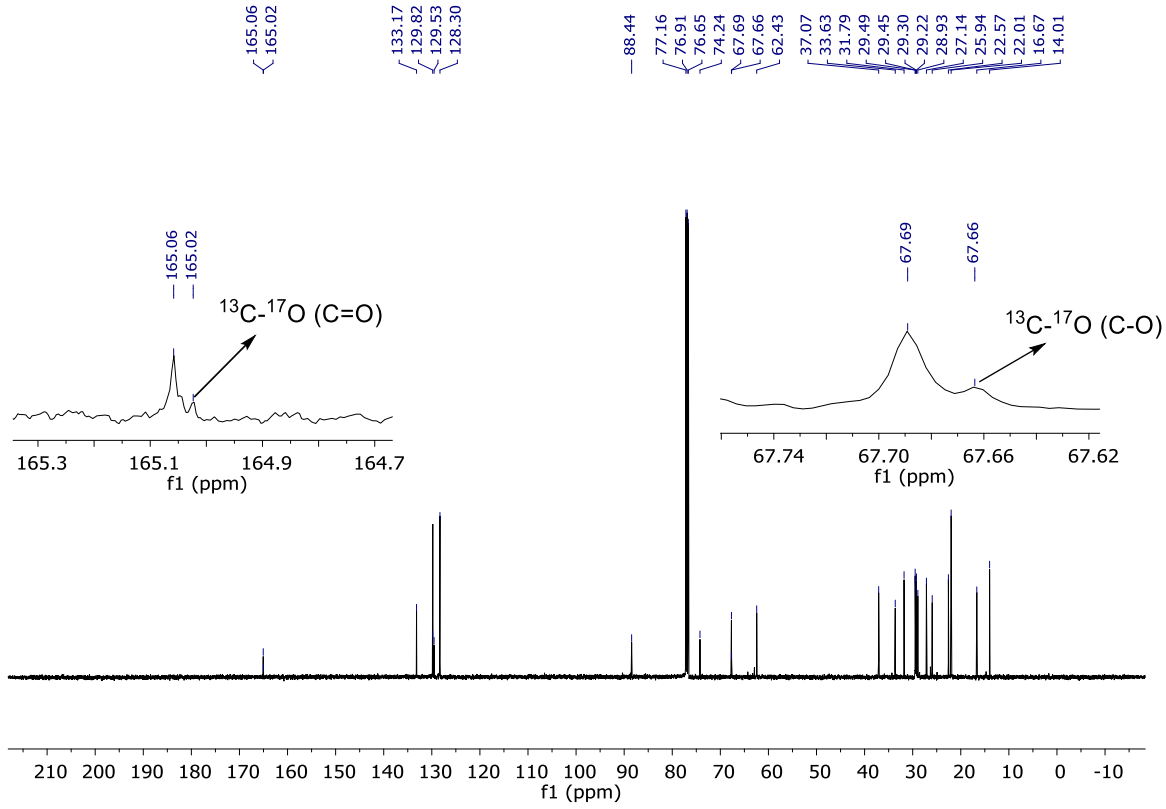
165.06
165.02
133.17
129.82
129.53
128.30
88.44
77.16
76.91
76.65
74.24
67.69
67.66
62.43
37.07
33.63
31.79
29.49
29.45
29.30
29.22
28.93
27.14
25.94
22.57
22.01
16.67
14.01
^{13}C-^{17}O (C=O)
^{13}C-^{17}O (C-O)
f1 (ppm)

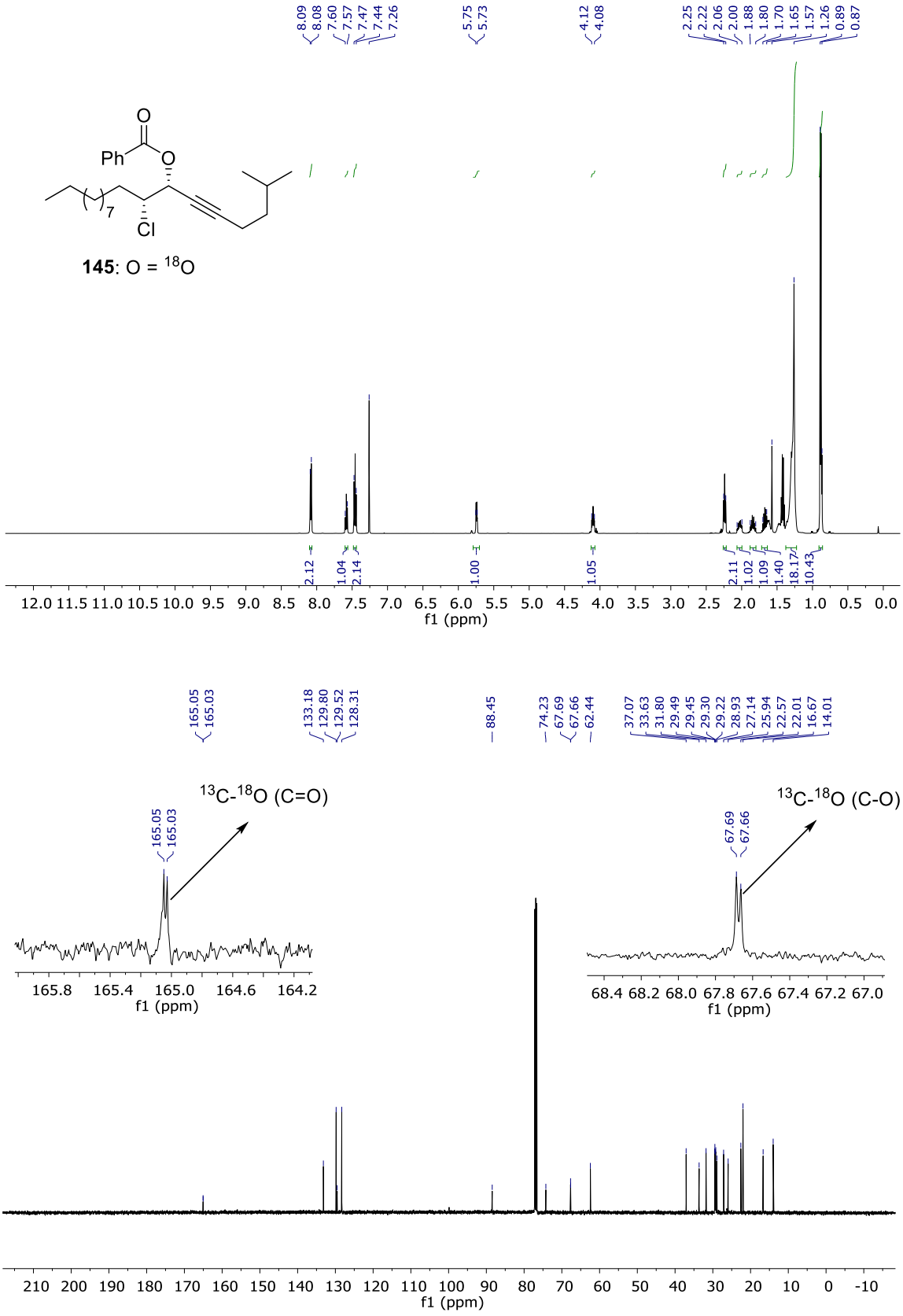
8.09
8.08
7.60
7.57
7.47
7.44
7.26
5.75
5.73
4.12
4.08
2.25
2.22
2.06
2.00
1.88
1.80
1.70
1.65
1.57
1.26
0.89
0.87
O
Ph
O
7
Cl
145: O = 18O
2.12
1.04
2.14
1.00
1.05
2.11
1.02
1.09
1.40
18.17
10.43
f1 (ppm)
165.05
165.03
133.18
129.80
129.52
128.31
88.45
74.23
67.69
67.66
62.44
37.07
33.63
31.80
29.49
29.45
29.30
29.22
28.93
27.14
25.94
22.57
22.01
16.67
14.01
13C-18O (C=O)
13C-18O (C-O)
f1 (ppm)
f1 (ppm)

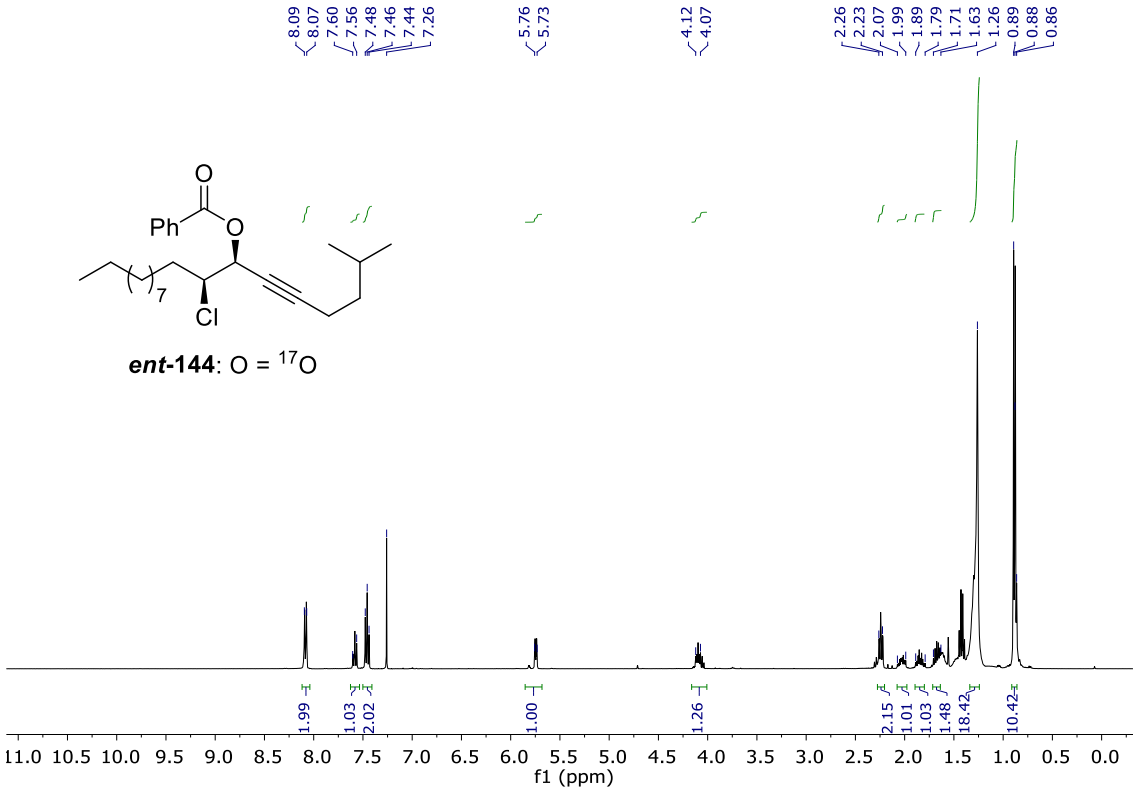
8.09
8.07
7.60
7.56
7.48
7.46
7.44
7.26
5.76
5.73
4.12
4.07
2.26
2.23
2.07
1.99
1.89
1.79
1.71
1.63
1.26
0.89
0.88
0.86
O
Ph
O
7
Cl
1.99
1.03
2.02
1.00
1.26
2.15
1.01
1.03
1.48
18.42
10.42
11.0 10.5 10.0 9.5 9.0 8.5 8.0 7.5 7.0 6.5 6.0 5.5 5.0 4.5 4.0 3.5 3.0 2.5 2.0 1.5 1.0 0.5 0.0
f1 (ppm)

***ent*-144**: O = ^{17}O

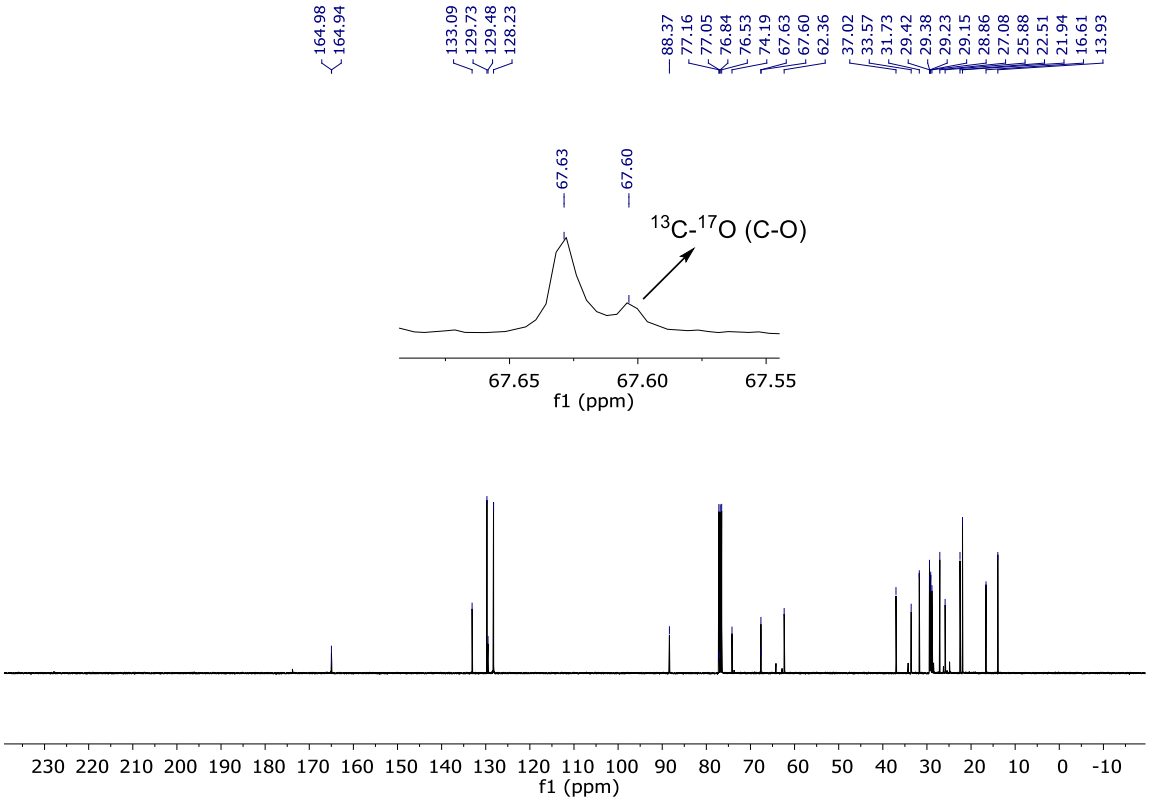
164.98
164.94
133.09
129.73
129.48
128.23
88.37
77.16
77.05
76.84
76.53
74.19
67.63
67.60
62.36
37.02
33.57
31.73
29.42
29.38
29.23
29.15
28.86
27.08
25.88
22.51
21.94
16.61
13.93
67.63
67.60
^{13}C-^{17}O (C-O)
67.65
67.60
67.55
f1 (ppm)
230 220 210 200 190 180 170 160 150 140 130 120 110 100 90 80 70 60 50 40 30 20 10 0 -10
f1 (ppm)

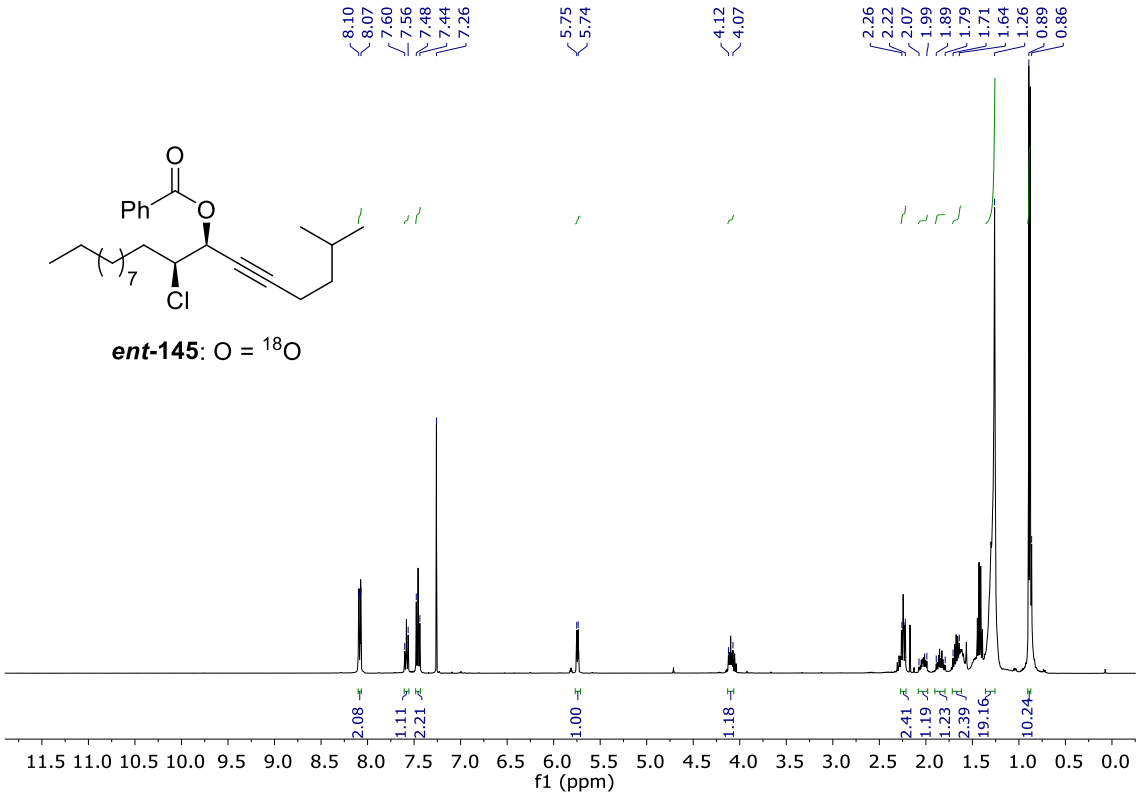
8.10
8.07
7.60
7.56
7.48
7.44
7.26
5.75
5.74
4.12
4.07
2.26
2.22
2.07
1.99
1.89
1.79
1.71
1.64
1.26
0.89
0.86
O
Ph
O
7
Cl
2.08
1.11
2.21
1.00
1.18
2.41
1.19
1.23
2.39
19.16
10.24
11.5 11.0 10.5 10.0 9.5 9.0 8.5 8.0 7.5 7.0 6.5 6.0 5.5 5.0 4.5 4.0 3.5 3.0 2.5 2.0 1.5 1.0 0.5 0.0
f1 (ppm)

***ent*-145**: O = ^{18}O

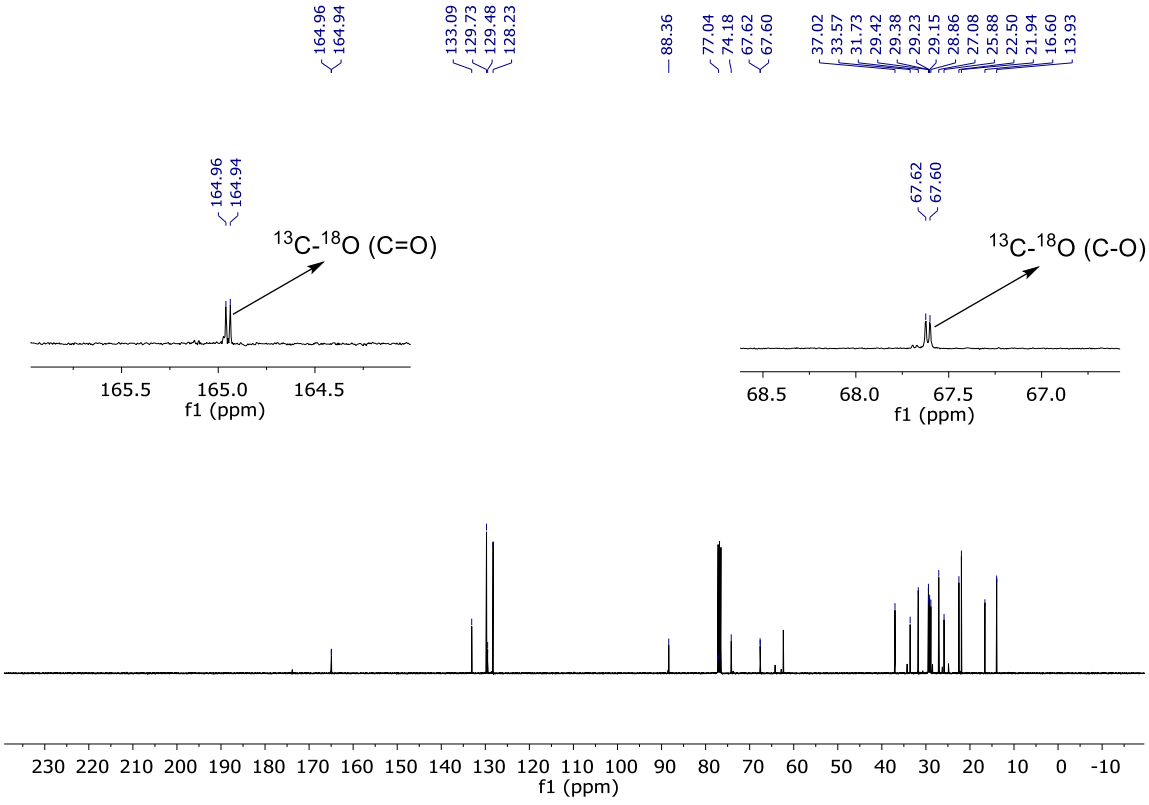
164.96
164.94
133.09
129.73
129.48
128.23
88.36
77.04
74.18
67.62
67.60
37.02
33.57
31.73
29.42
29.38
29.23
29.15
28.86
27.08
25.88
22.50
21.94
16.60
13.93
^{13}C-^{18}O (C=O)
165.5
165.0
164.5
f1 (ppm)
^{13}C-^{18}O (C-O)
68.5
68.0
67.5
67.0
f1 (ppm)
230 220 210 200 190 180 170 160 150 140 130 120 110 100 90 80 70 60 50 40 30 20 10 0 -10
f1 (ppm)

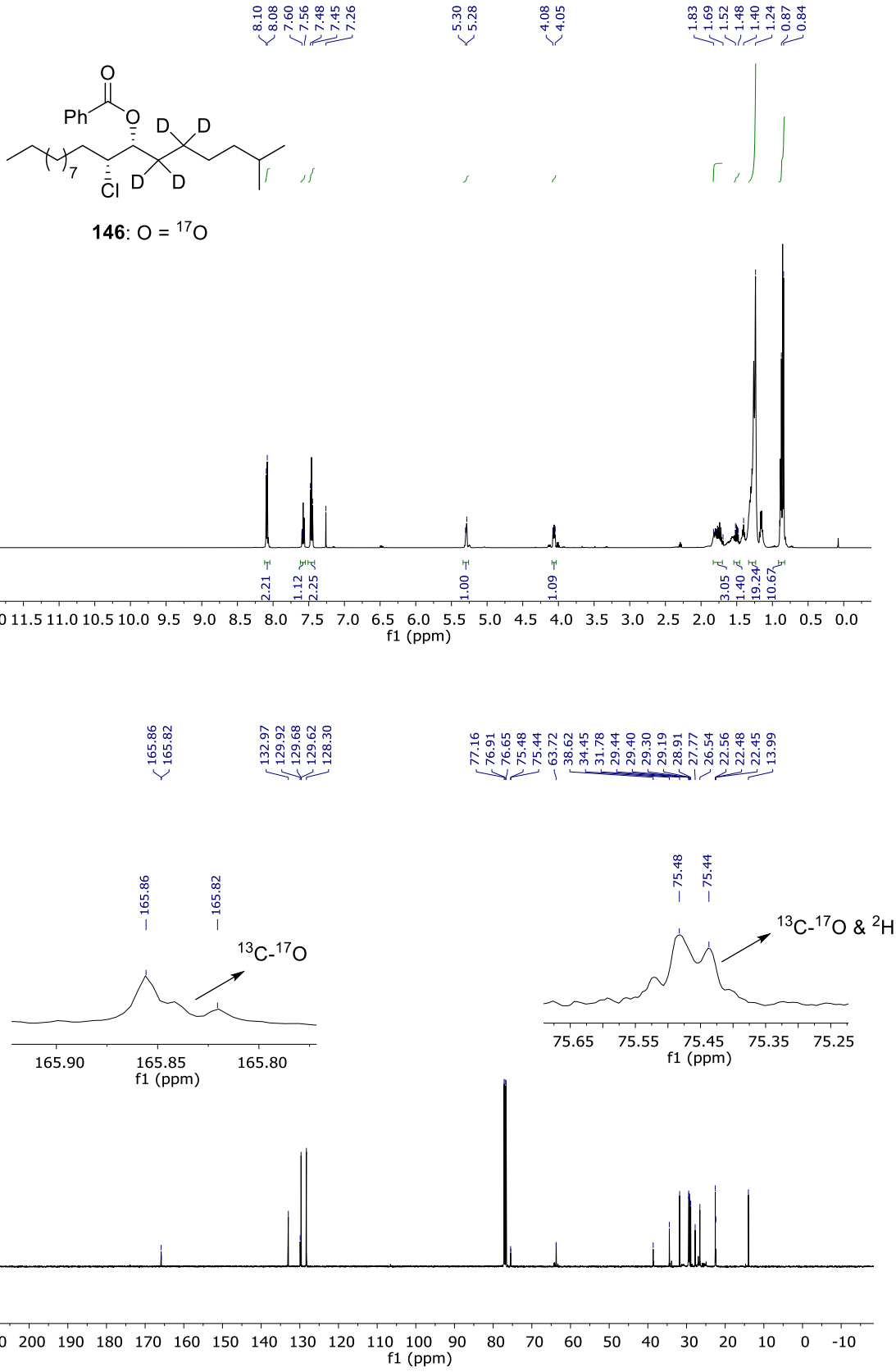
8.10
8.08
7.60
7.56
7.48
7.45
7.26
5.30
5.28
4.08
4.05
1.83
1.69
1.52
1.48
1.40
1.24
0.87
0.84
O
Ph
O
D
D
7
D
D
Cl
146: O = 17O
2.21
1.12
2.25
1.00
1.09
3.05
1.40
19.24
10.67
12.0 11.5 11.0 10.5 10.0 9.5 9.0 8.5 8.0 7.5 7.0 6.5 6.0 5.5 5.0 4.5 4.0 3.5 3.0 2.5 2.0 1.5 1.0 0.5 0.0
f1 (ppm)
165.86
165.82
132.97
129.92
129.68
129.62
128.30
77.16
76.91
76.65
75.48
75.44
63.72
38.62
34.45
31.78
29.44
29.40
29.30
29.19
28.91
27.77
26.54
22.56
22.48
22.45
13.99
165.86
165.82
13C-17O
165.90
165.85
165.80
f1 (ppm)
75.48
75.44
13C-17O & 2H
75.65
75.55
75.45
75.35
75.25
f1 (ppm)
210 200 190 180 170 160 150 140 130 120 110 100 90 80 70 60 50 40 30 20 10 0 -10
f1 (ppm)

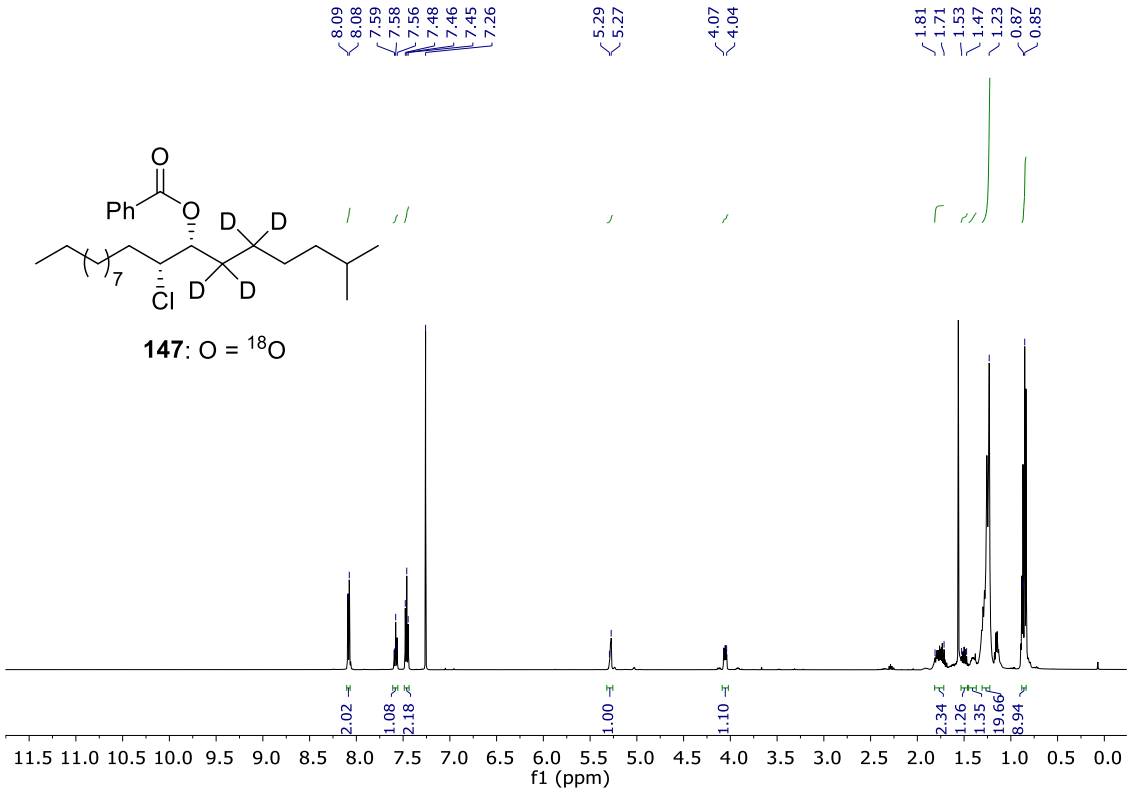
8.09
8.08
7.59
7.58
7.56
7.48
7.46
7.45
7.26
5.29
5.27
4.07
4.04
1.81
1.71
1.53
1.47
1.23
0.87
0.85
O
Ph
O
D
D
7
D
D
Cl
147: O = 18O
2.02
1.08
2.18
1.00
1.10
2.34
1.26
1.35
19.66
8.94
11.5 11.0 10.5 10.0 9.5 9.0 8.5 8.0 7.5 7.0 6.5 6.0 5.5 5.0 4.5 4.0 3.5 3.0 2.5 2.0 1.5 1.0 0.5 0.0
f1 (ppm)

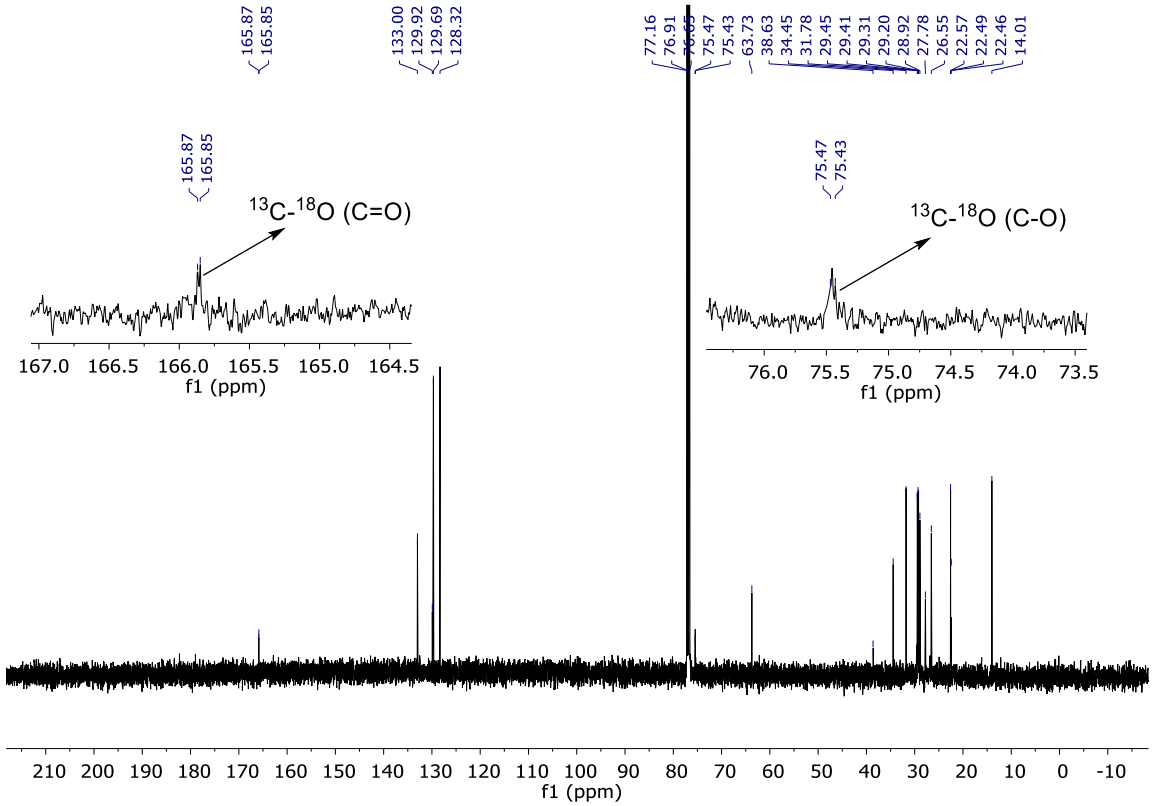
165.87
165.85
133.00
129.92
129.69
128.32
77.16
76.91
75.47
75.43
63.73
38.63
34.45
31.78
29.45
29.41
29.31
29.20
28.92
27.78
26.55
22.57
22.49
22.46
14.01
165.87
165.85
13C-18O (C=O)
167.0 166.5 166.0 165.5 165.0 164.5
f1 (ppm)
75.47
75.43
13C-18O (C-O)
76.0 75.5 75.0 74.5 74.0 73.5
f1 (ppm)
210 200 190 180 170 160 150 140 130 120 110 100 90 80 70 60 50 40 30 20 10 0 -10
f1 (ppm)

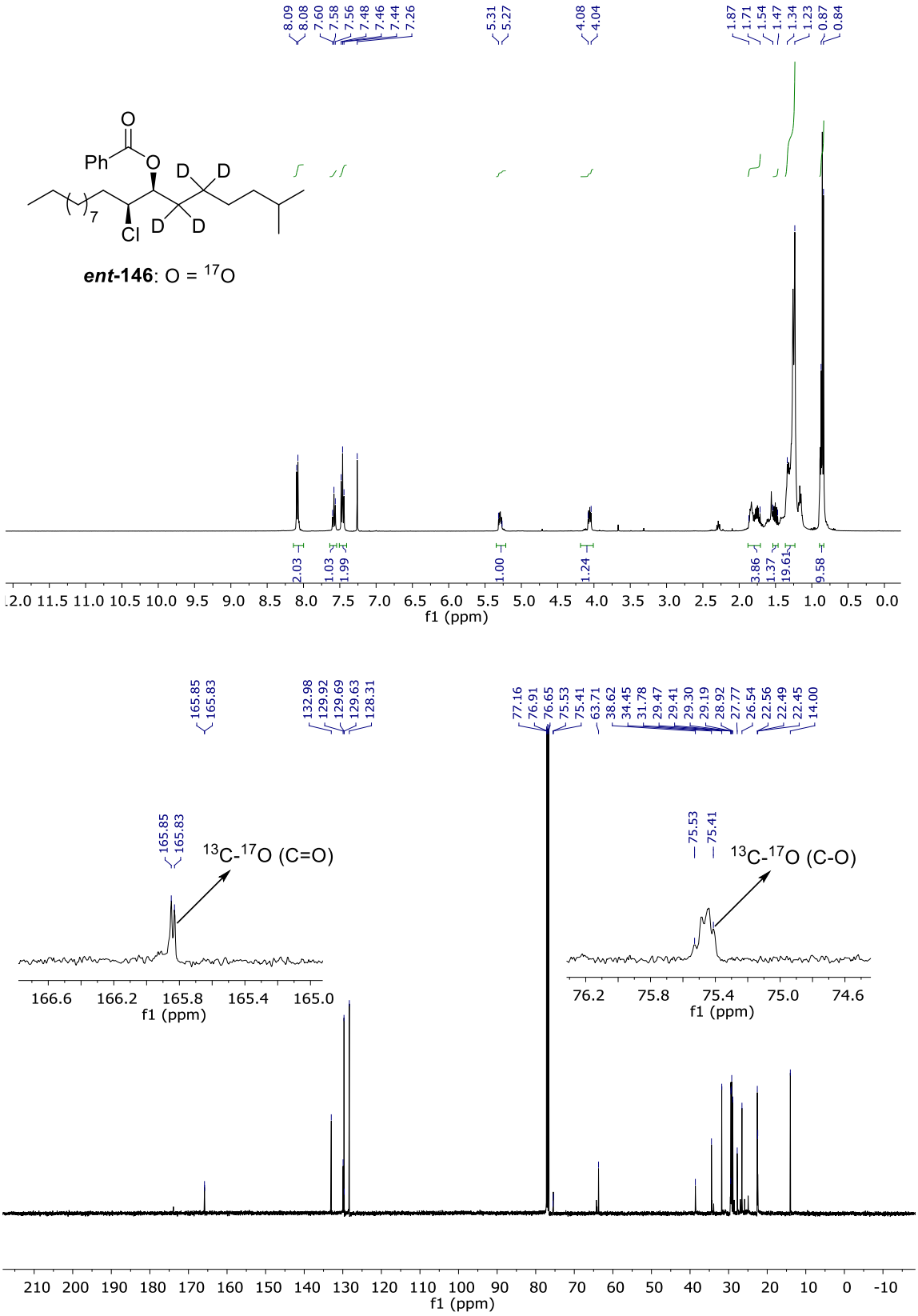
8.09
8.08
7.60
7.58
7.56
7.48
7.46
7.44
7.26
5.31
5.27
4.08
4.04
1.87
1.71
1.54
1.47
1.34
1.23
0.87
0.84
O
Ph
O
D
D
7
D
D
Cl
2.03
1.03
1.99
1.00
1.24
3.86
1.37
19.61
9.58
f1 (ppm)
165.85
165.83
132.98
129.92
129.69
129.63
128.31
77.16
76.91
76.65
75.53
75.41
63.71
38.62
34.45
31.78
29.47
29.41
29.30
29.19
28.92
27.77
26.54
22.56
22.49
22.45
14.00
13C-17O (C=O)
13C-17O (C-O)
f1 (ppm)

***ent*-146**: O = ^{17}O

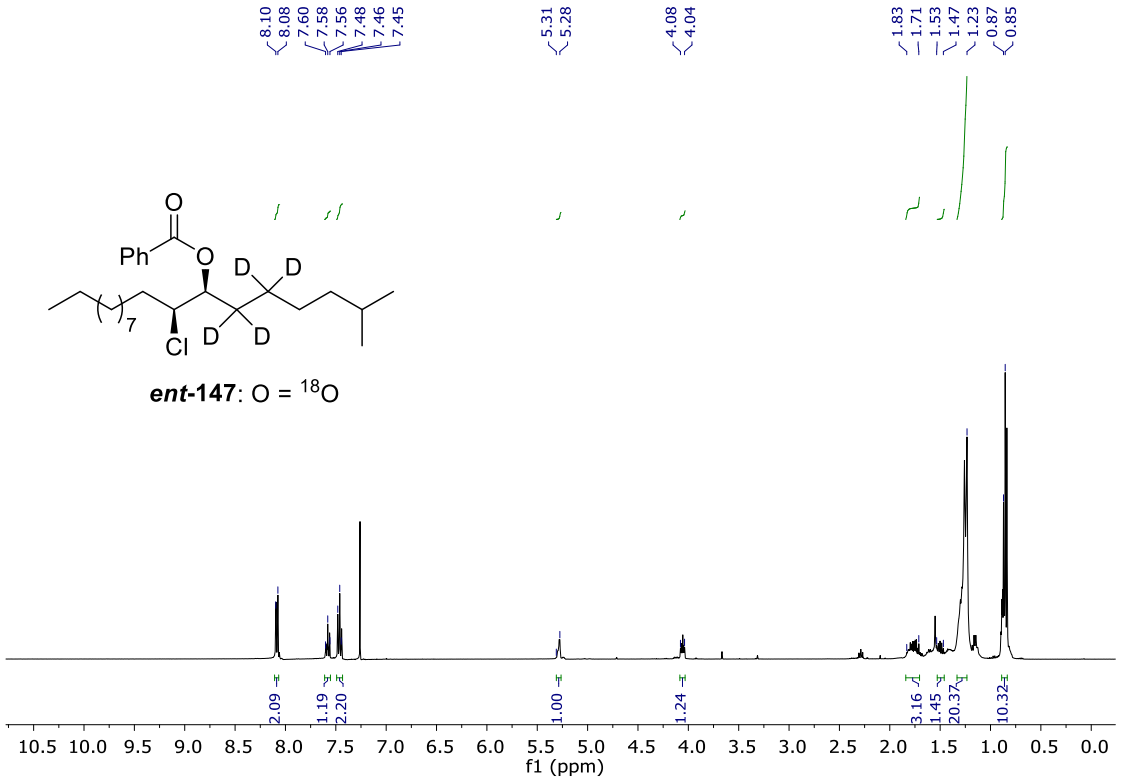
8.10
8.08
7.60
7.58
7.56
7.48
7.46
7.45
5.31
5.28
4.08
4.04
1.83
1.71
1.53
1.47
1.23
0.87
0.85
O
Ph
O
D
D
7
D
D
Cl
2.09
1.19
2.20
1.00
1.24
3.16
1.45
20.37
10.32
10.5 10.0 9.5 9.0 8.5 8.0 7.5 7.0 6.5 6.0 5.5 5.0 4.5 4.0 3.5 3.0 2.5 2.0 1.5 1.0 0.5 0.0
f1 (ppm)

***ent*-147**: O = ^{18}O

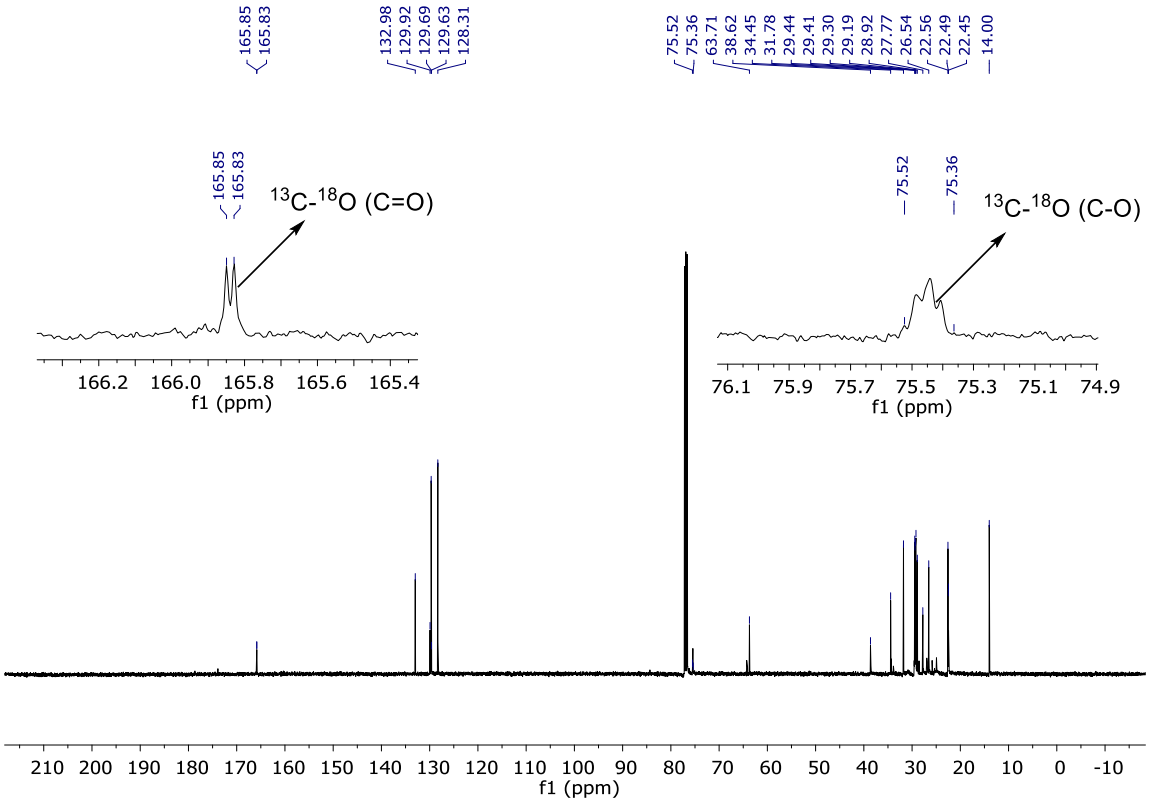
165.85
165.83
132.98
129.92
129.69
129.63
128.31
75.52
75.36
63.71
38.62
34.45
31.78
29.44
29.41
29.30
29.19
28.92
27.77
26.54
22.56
22.49
22.45
14.00
^{13}C-^{18}O (C=O)
166.2 166.0 165.8 165.6 165.4
f1 (ppm)
^{13}C-^{18}O (C-O)
76.1 75.9 75.7 75.5 75.3 75.1 74.9
f1 (ppm)
210 200 190 180 170 160 150 140 130 120 110 100 90 80 70 60 50 40 30 20 10 0 -10
f1 (ppm)

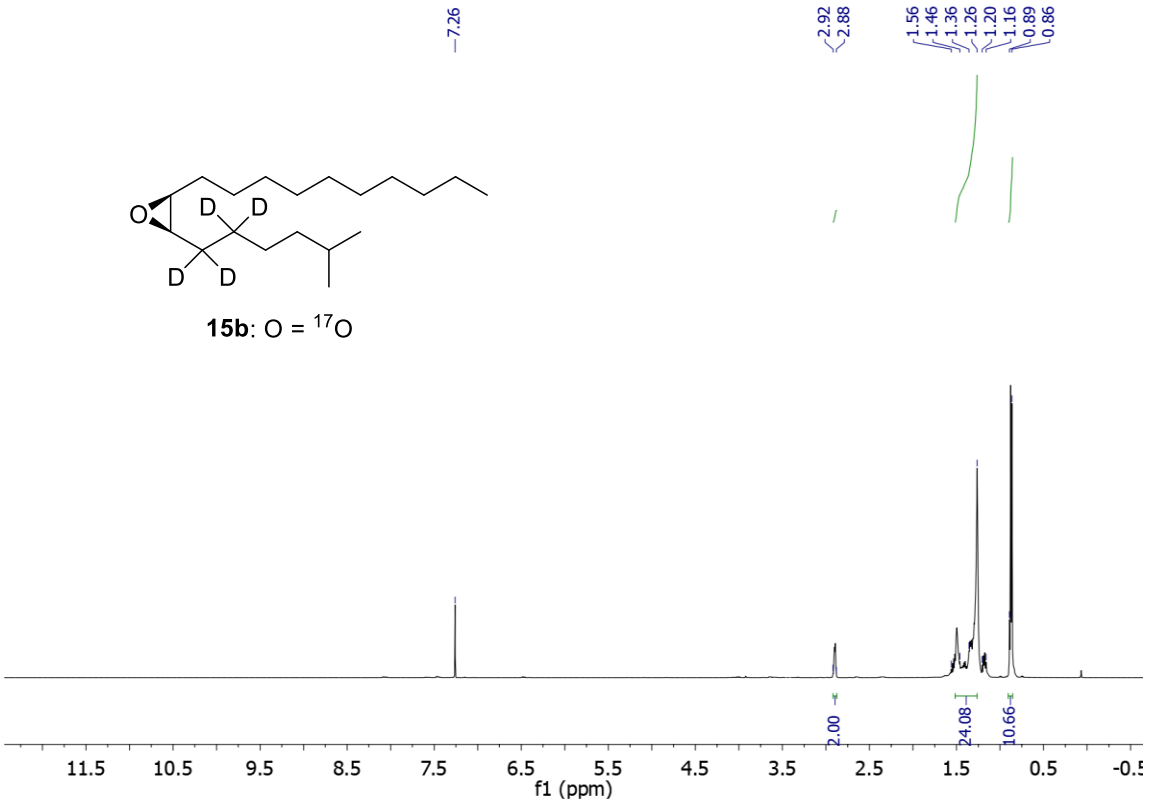
7.26
2.92
2.88
1.56
1.46
1.36
1.26
1.20
1.16
0.89
0.86
O
D
D
D
D
2.00
24.08
10.66
11.5
10.5
9.5
8.5
7.5
6.5
5.5
4.5
3.5
2.5
1.5
0.5
f1 (ppm)

15b: O = ^{17}O

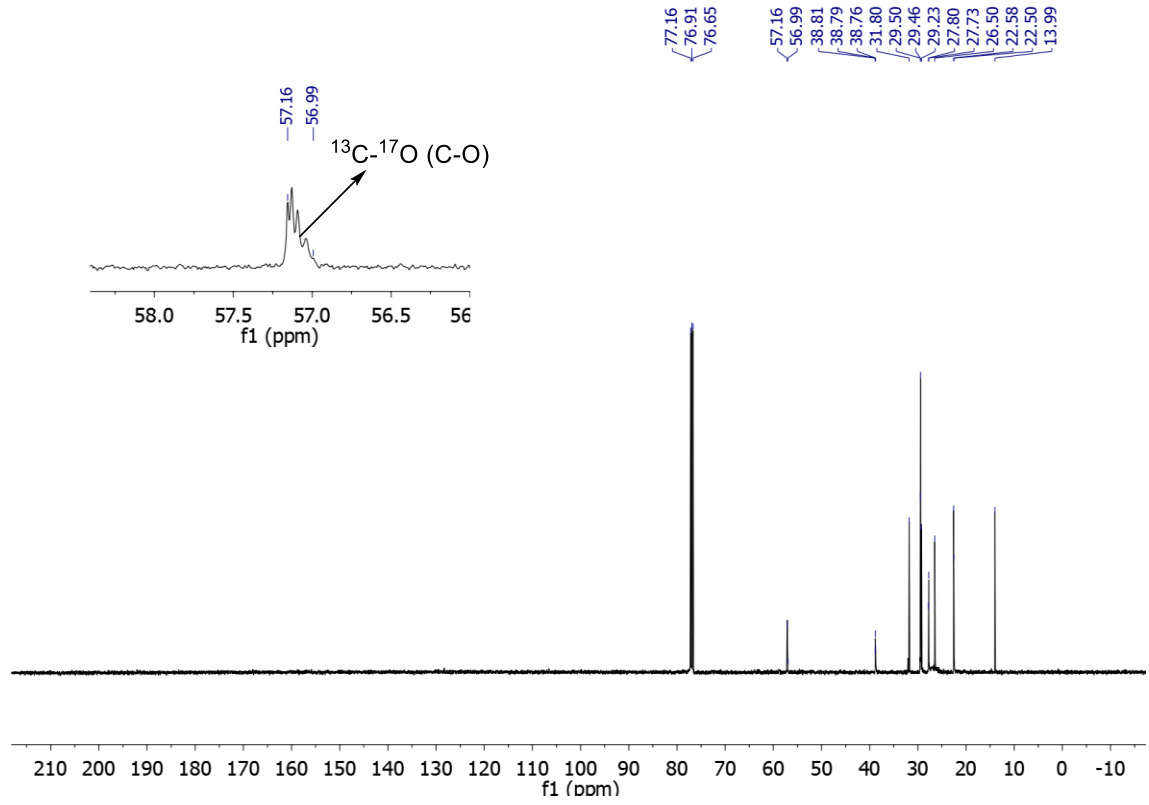
77.16
76.91
76.65
57.16
56.99
38.81
38.79
38.76
31.80
29.50
29.46
29.23
27.80
27.73
26.50
22.58
22.50
13.99
57.16
56.99
^{13}C-^{17}O (C-O)
58.0
57.5
57.0
56.5
f1 (ppm)
210 200 190 180 170 160 150 140 130 120 110 100 90 80 70 60 50 40 30 20 10 0 -10
f1 (ppm)

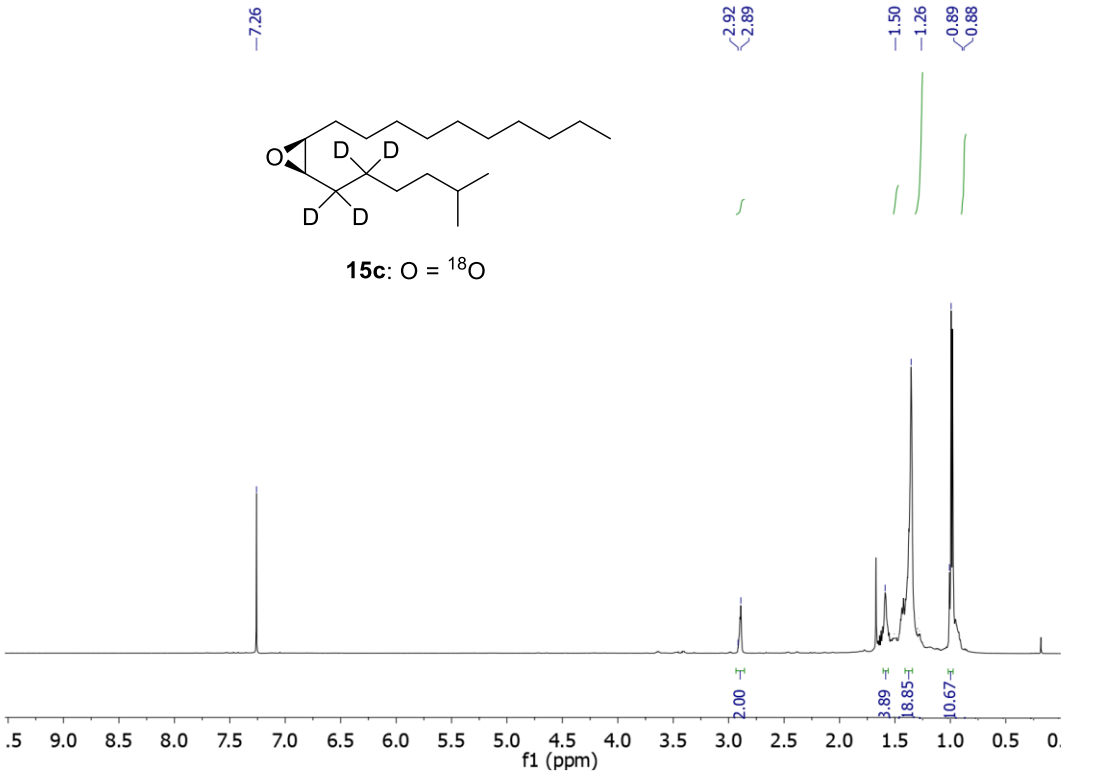
7.26
2.92
2.89
1.50
1.26
0.89
0.88
O
D
D
D
D
2.00
3.89
18.85
10.67
f1 (ppm)

15c: O = ^{18}O

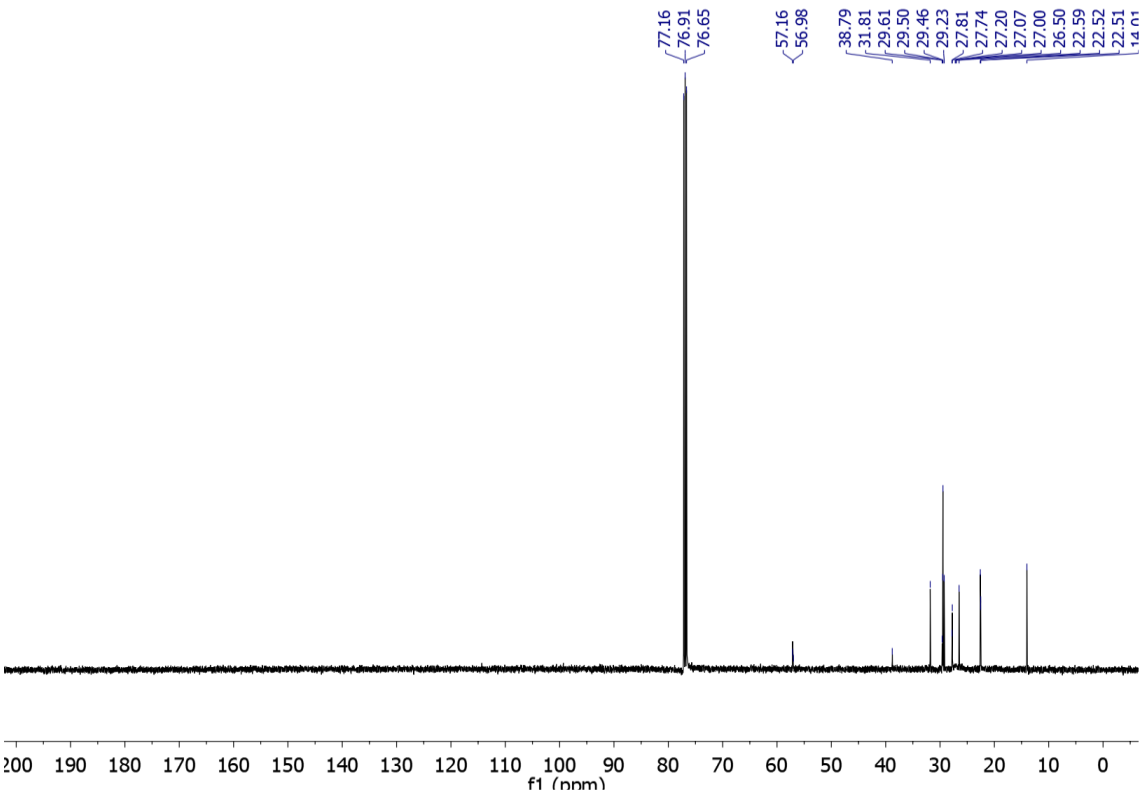
77.16
76.91
76.65
57.16
56.98
38.79
31.81
29.61
29.50
29.46
29.23
27.81
27.74
27.20
27.07
27.00
26.50
22.59
22.52
22.51
f1 (ppm)

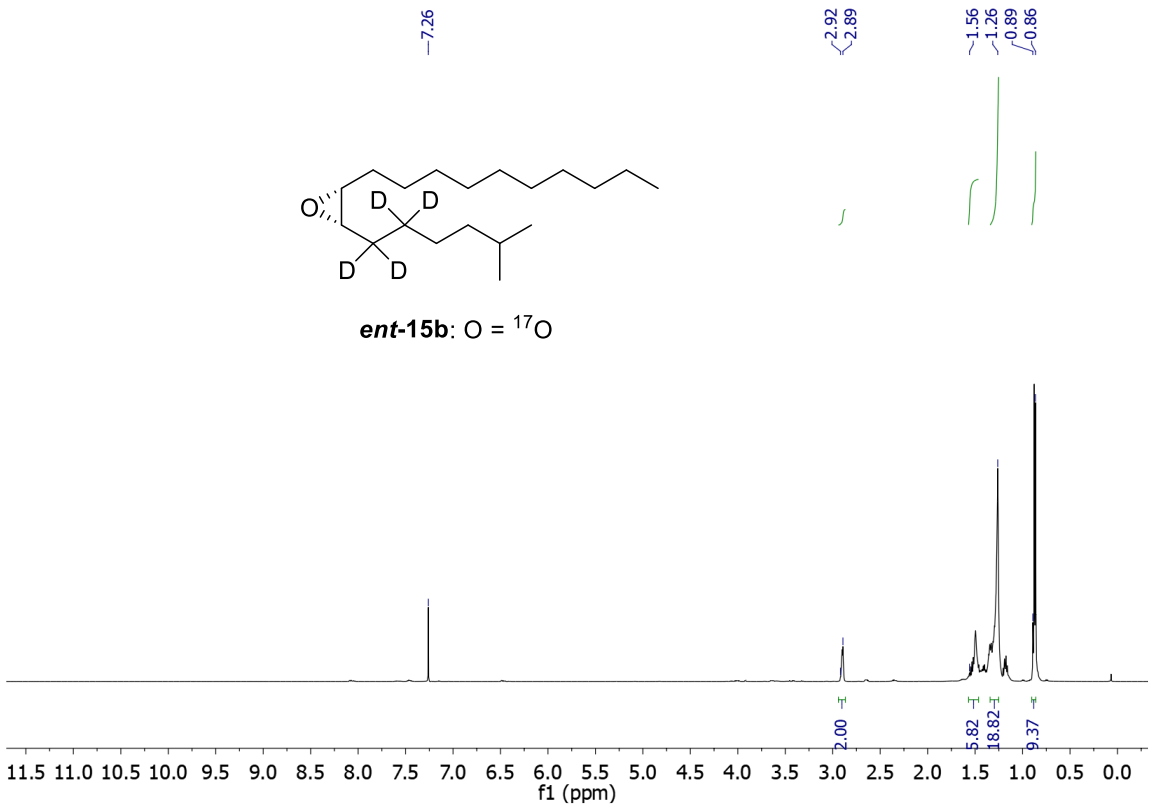
7.26
2.92
2.89
1.56
1.26
0.89
0.86
O
D
D
D
D
2.00
5.82
18.82
9.37
11.5 11.0 10.5 10.0 9.5 9.0 8.5 8.0 7.5 7.0 6.5 6.0 5.5 5.0 4.5 4.0 3.5 3.0 2.5 2.0 1.5 1.0 0.5 0.0
f1 (ppm)

***ent*-15b**: O = ^{17}O

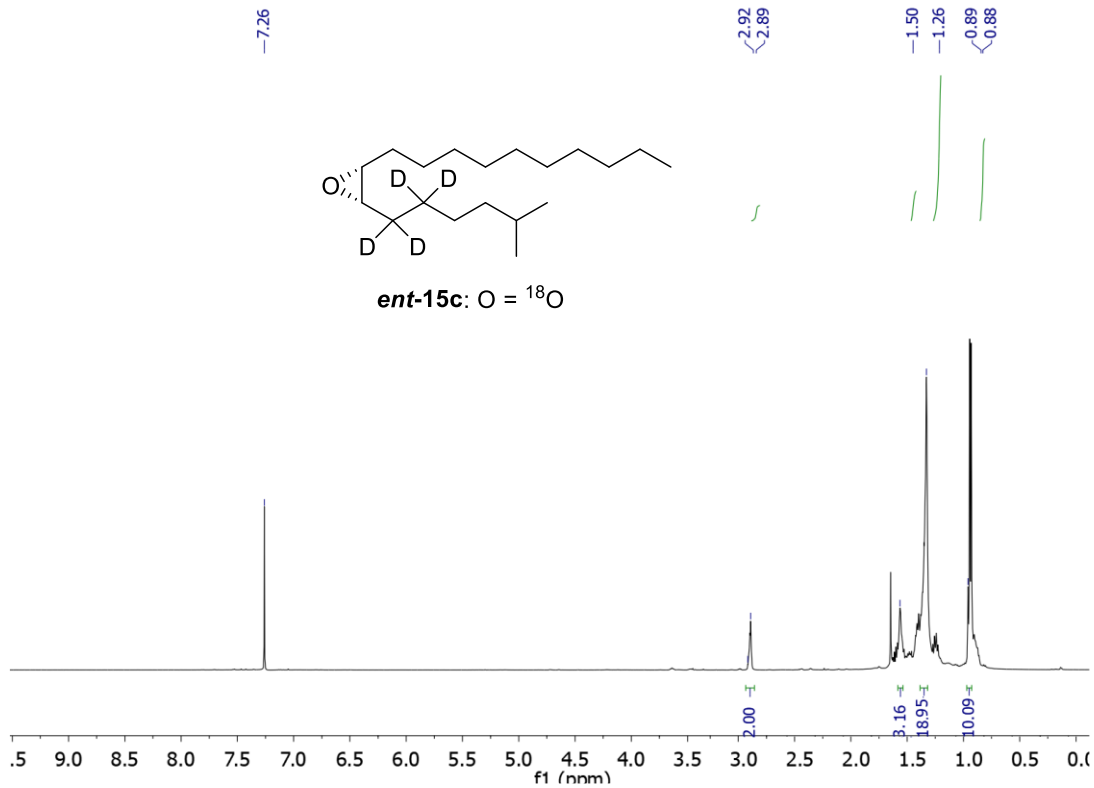
7.26
2.92
2.89
1.50
1.26
0.89
0.88
O
D
D
D
D
2.00
3.16
18.95
10.09
f1 (ppm)

***ent*-15c**: O = ^{18}O

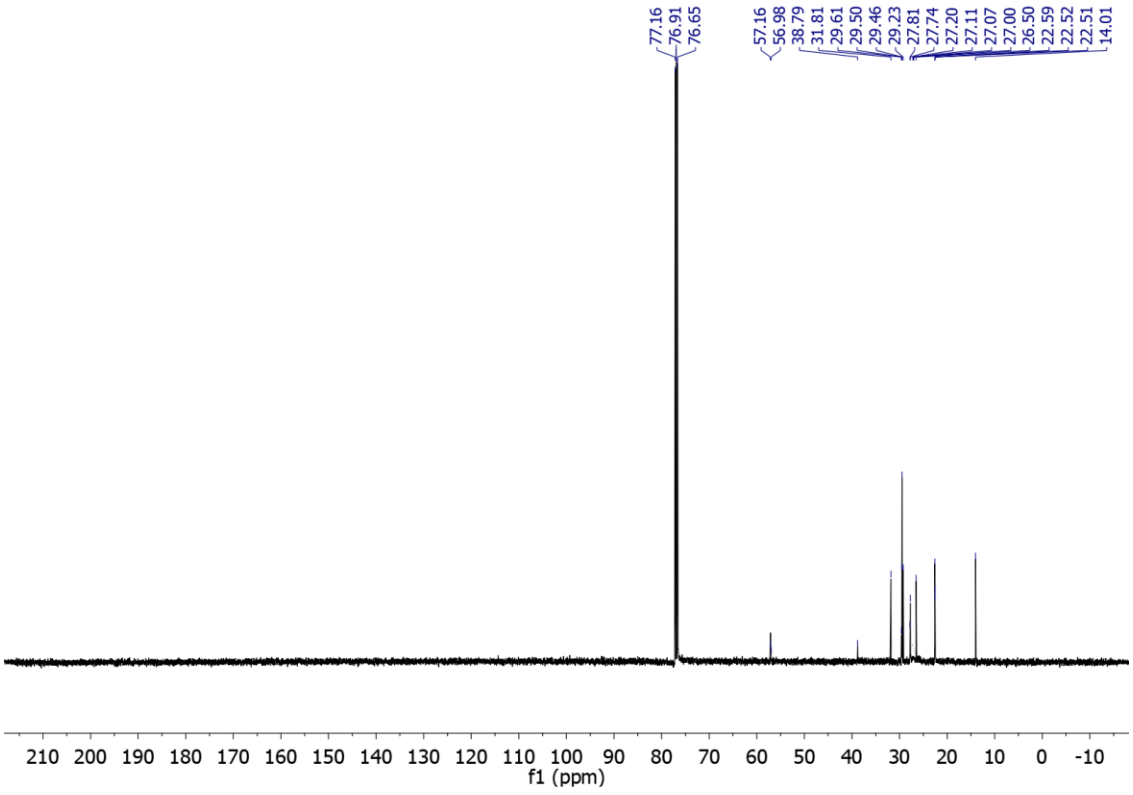
77.16
76.91
76.65
57.16
56.98
38.79
31.81
29.61
29.50
29.46
29.23
27.81
27.74
27.20
27.11
27.07
27.00
26.50
22.59
22.52
22.51
14.01
f1 (ppm)

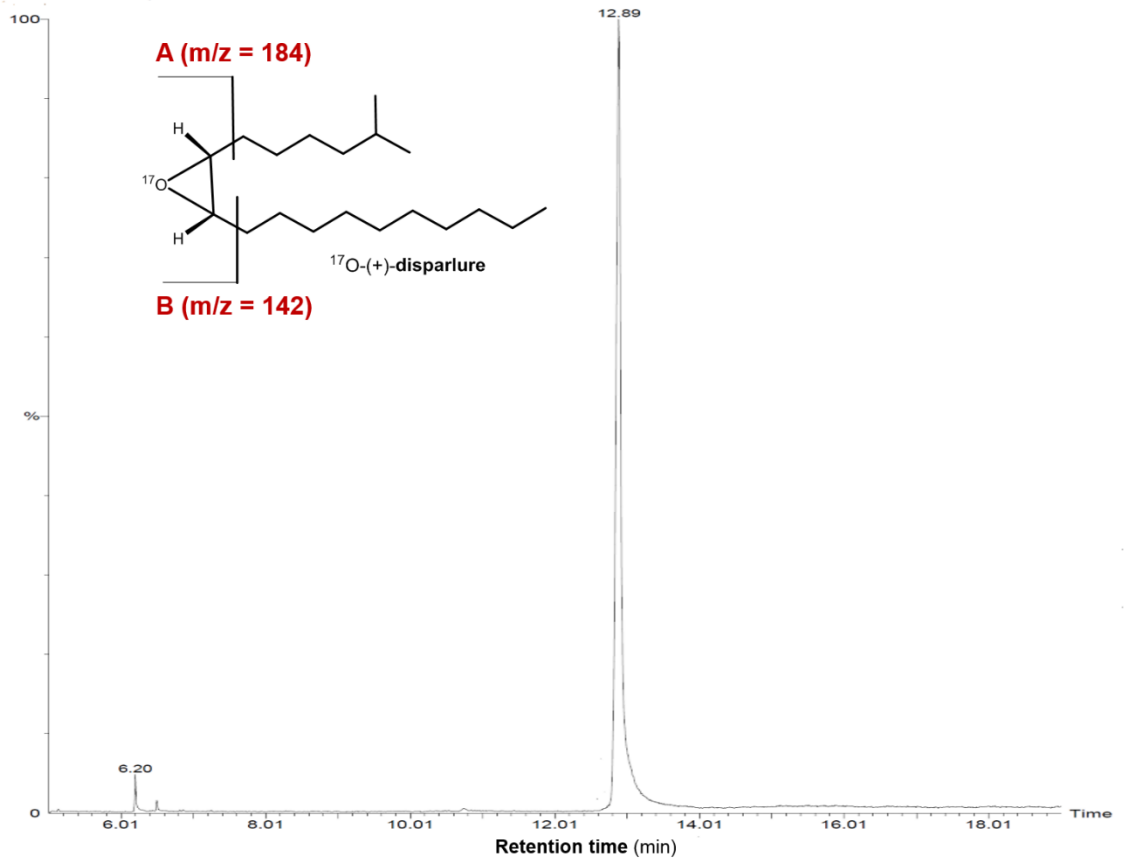
A (m/z = 184)
H
17O
H
17O-(+)-disparlure
B (m/z = 142)
100
%
0
12.89
6.20
6.01
8.01
10.01
12.01
14.01
16.01
18.01
Time
Retention time (min)

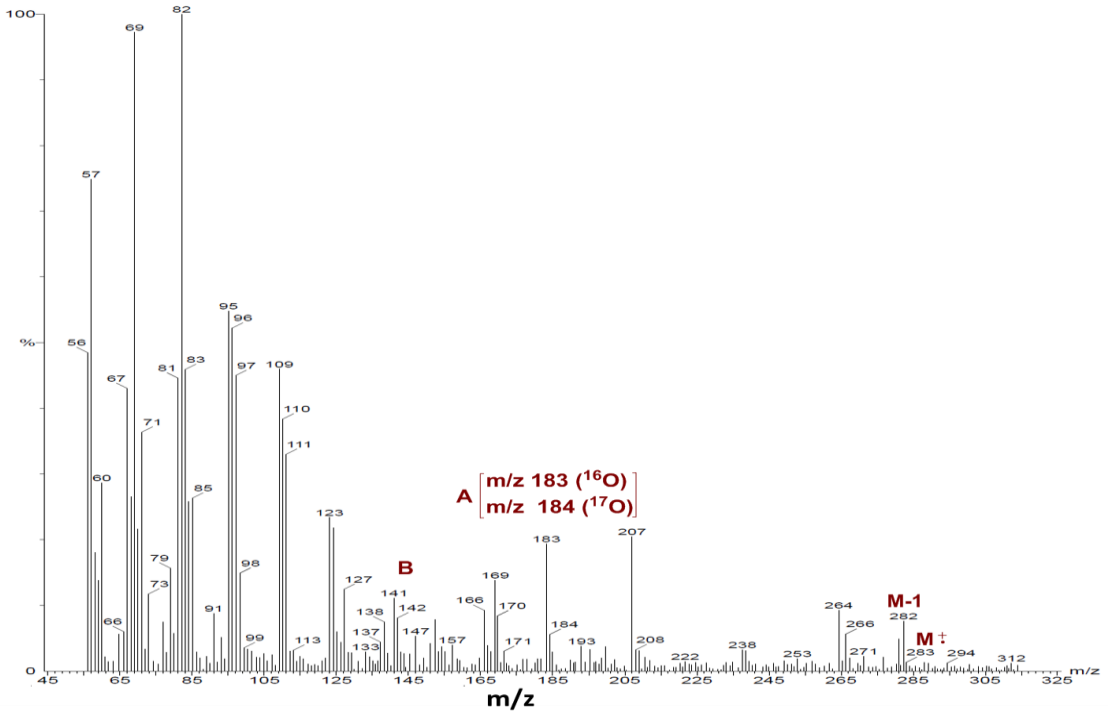
100
%
0
A [m/z 183 (16O) m/z 184 (17O)]
B
M-1
M+
45
65
85
105
125
145
165
185
205
225
245
265
285
305
325
m/z
m/z

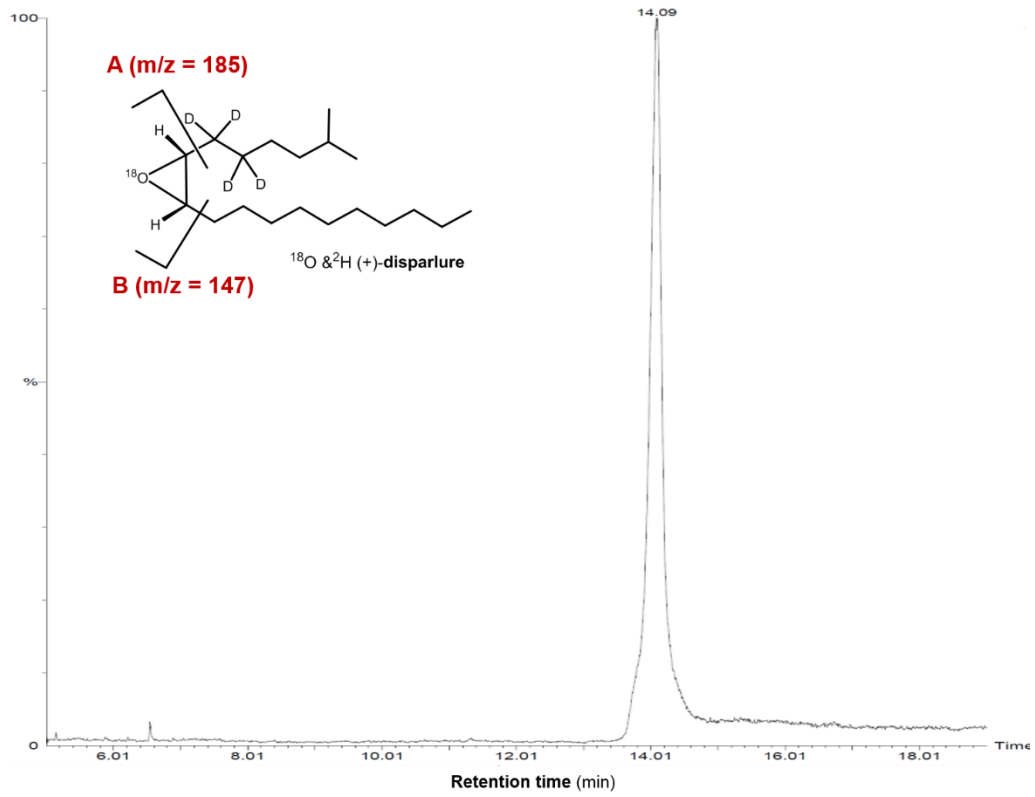
A (m/z = 185)
B (m/z = 147)
^{18}O &^{2}H (+)-disparlure
14.09
100
%
0
6.01
8.01
10.01
12.01
14.01
16.01
18.01
Time
Retention time (min)

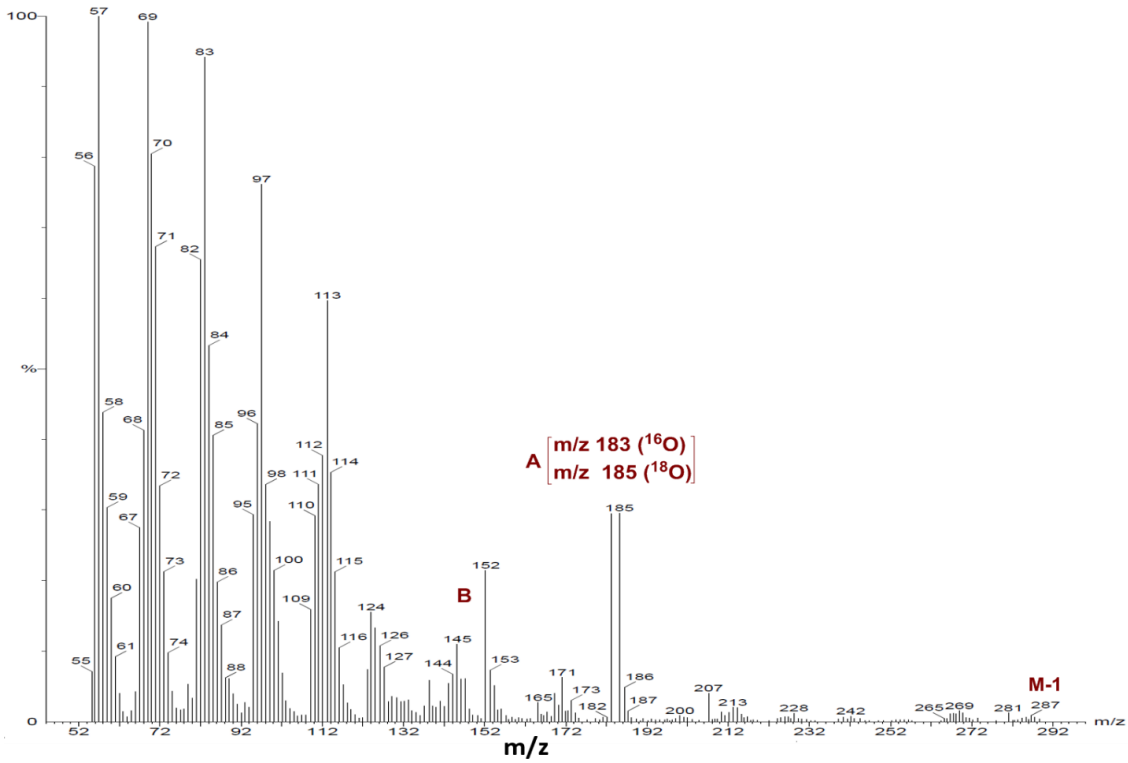
A [m/z 183 (^{16}O) m/z 185 (^{18}O)]
B
M-1
100
%
0
52
72
92
112
132
152
172
192
212
232
252
272
292
m/z

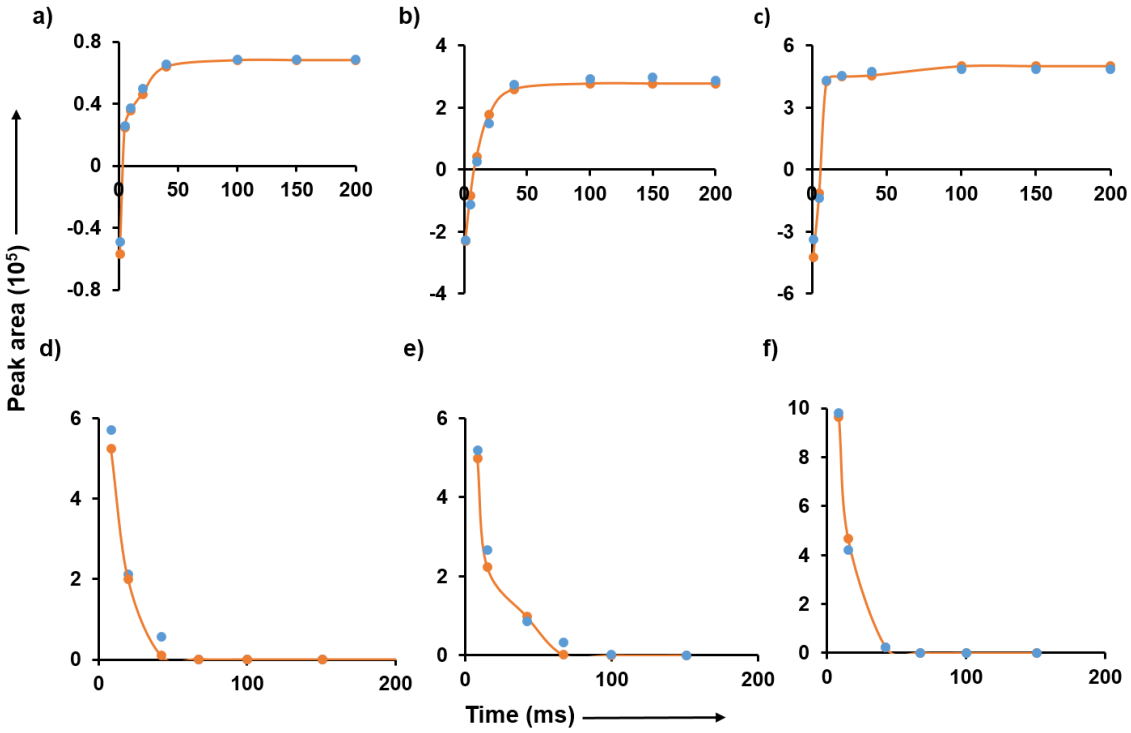

Appendix B1. The plots of T1 and T_2 relaxation curve fit data for deuterium atoms of *ent*-15c in phosphate buffer (pH 8). a) 5-Da (T1 = 11.5 ± 0.13) b) 5-Db (T1 = 11.66 ± 0.50) c) 6-Dab (T1 = 12.85 ± 1.0) d) 5-Da (T2 = 10.34 ± 0.50) e) 5-Db (T2 = 9.10 ± 0.23) f) 6-Dab (T2 = 11.72 ± 0.90). The data points (blue) represent the experimental data, and the solid line (orange) is the fitted curve obtained by the equation 1 and 2 of this thesis (Chapter 3)

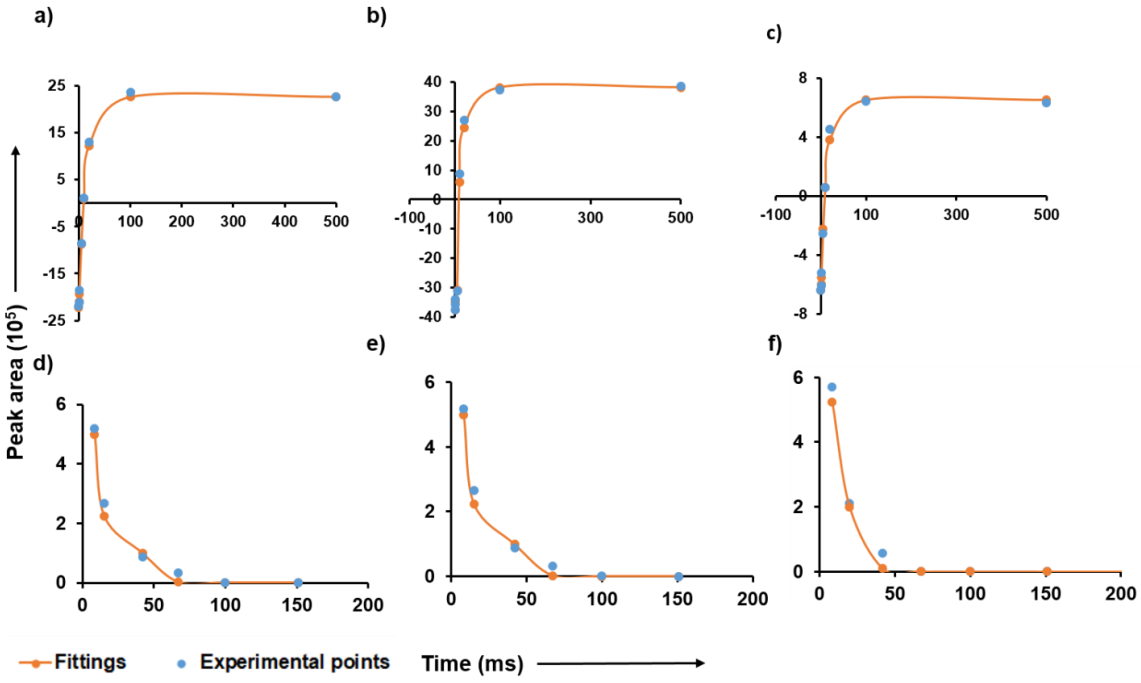

Appendix B2. The plots of T1 and T_2 relaxation curve fit data for deuterium atoms of *ent*-15c in $CDCl_3$. a) 5-Da (T1 = 13.6 ± 2.6) b) 5-Db (T1 = 12.7 ± 0.7 c) 6-Dab (T1 = 11.6 ± 1.5) d) 5-Da (T2 = 12.0 ± 0.1) e) 5-Db (T2 = 11.4 ± 0.6 f) 6-Dab (T2 = 10.2 ± 0.1). The data points (blue) represent the experimental data, and the solid line (orange) is the fitted curve obtained by the equation 1 and 2 of this thesis (Chapter 3).

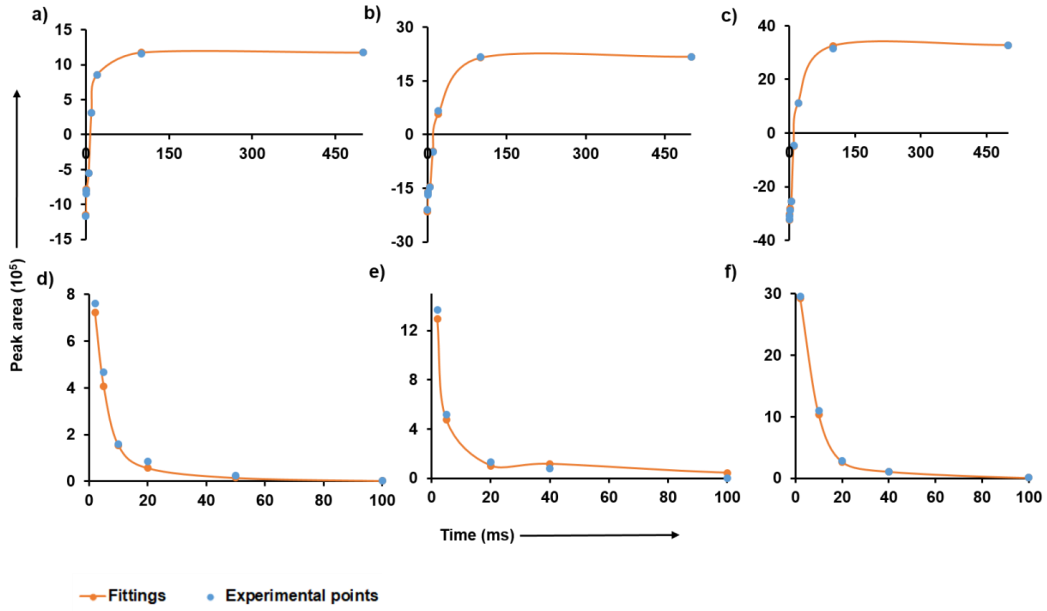

Appendix B3. The plots of T1 and T2 relaxation curve fit data for deuterium atoms of *ent*-15c in the *Ldis*PBP1 (pH 8). a) 5-Da (T1 = 10.0 ± 0.22) b) 5-Db (T1 = 20.05 ± 1.42) c) 6-Dab (T1 = 18.0 ± 2.12) d) 5-Da (T2 = 6.50 ± 0.80) e) 5-Db (T2 = 5.24 ± 1.30) f) 6-Dab (T2 = 7.20 ± 0.90). The data points (blue) represent the experimental data, and the solid line (orange) is the fitted curve obtained by the equation 1 and 2 of this thesis (Chapter 3).

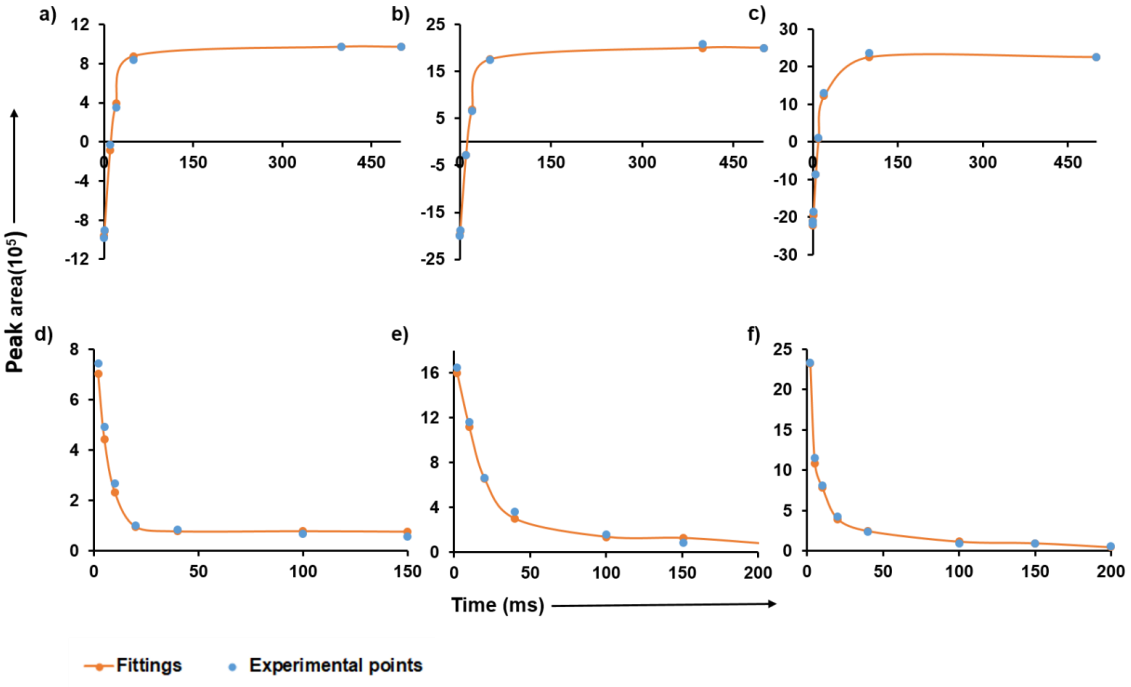

Appendix B4. The plots of T1 and T2 relaxation curve fit data for deuterium atoms of 15c in the *Ldis*PBP1 (pH 8). a) 5-Da (T1 = 16.5 ± 0.70) b) 5-Db (T1 = 17.90 ± 0.90) c) 6-Dab (T1 = 13.60 ± 2.44) d) 5-Da (T2 = 8.30 ± 0.90) e) 5-Db (T2 = 6.54 ± 0..55) f) 6-Dab (T2 = 4.60 ± 1.14). The data points (blue) represent the experimental data, and the solid line (orange) is the fitted curve obtained by the equation 1 and 2 of this thesis (Chapter 3).

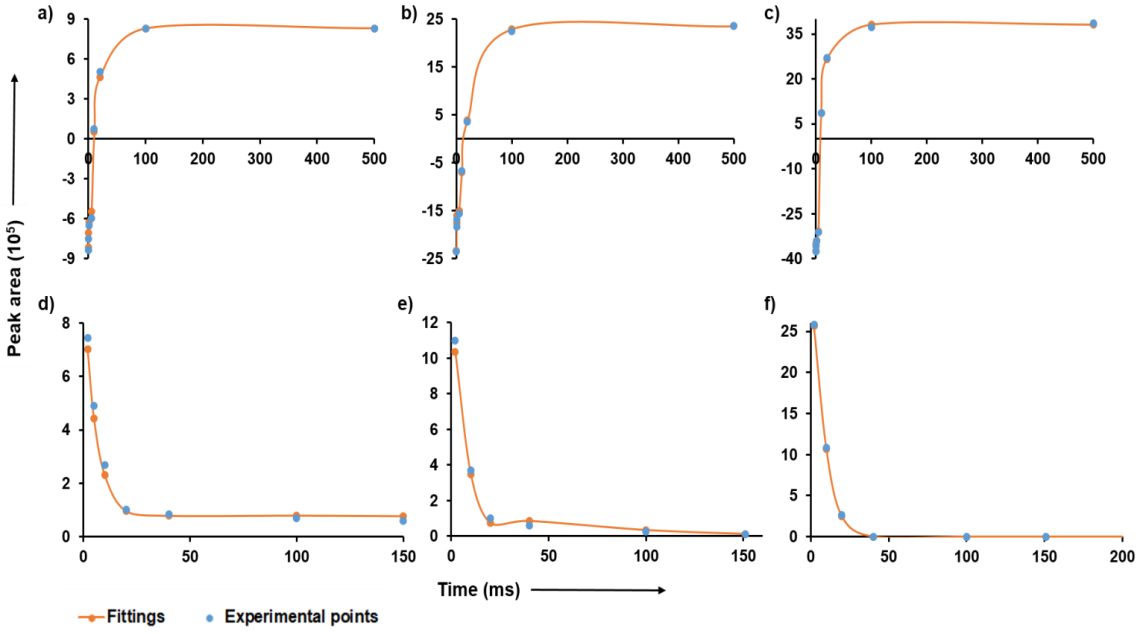

Appendix B5. The plots of T1 and T2 relaxation curve fit data for deuterium atoms of *ent*-15c in the *Ldis*PBP2 (pH 8). a) 5-Da (T1 = 13.2 ± 0.66) b) 5-Db (T1 = 23.0 ± 1.94) c) 6-Dab (T1 = 10.55 ± 1.90) d) 5-Da (T2 = 7.20 ± 0.53 e) 5-Db (T2 = 7.80 ± 0..51) f) 6-Dab (T2 = 3.15 ± 0.10). The data points (blue) represent the experimental data, and the solid line (orange) is the fitted curve obtained by the equation 1 and 2 of this thesis (Chapter 3).

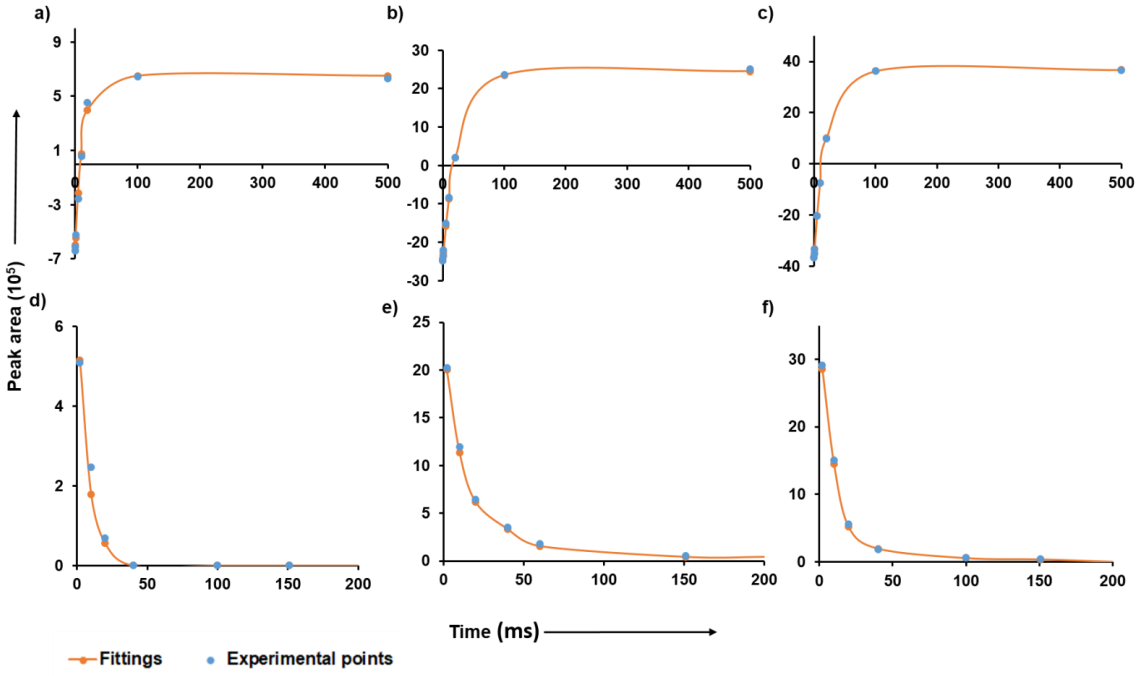

Appendix B6. The plots of T1 and T2 relaxation curve fit data for deuterium atoms of 15c in the *Ldis*PBP2 (pH 8). a) 5-Da (T1 = 12.23 ± 0.66) b) 5-Db (T1 = 25.54 ± 1.63) c) 6-Dab (T1 = 19.80 ± 0.50) d) 5-Da (T2 = 3.64 ± 0.50 e) 5-Db (T2 = 9.90 ± 0.62) f) 6-Dab (T2 = 7.52 ± 0.62). The data points (blue) represent the experimental data, and the solid line (orange) is the fitted curve obtained by the equation 1 and 2 of this thesis (Chapter 3).

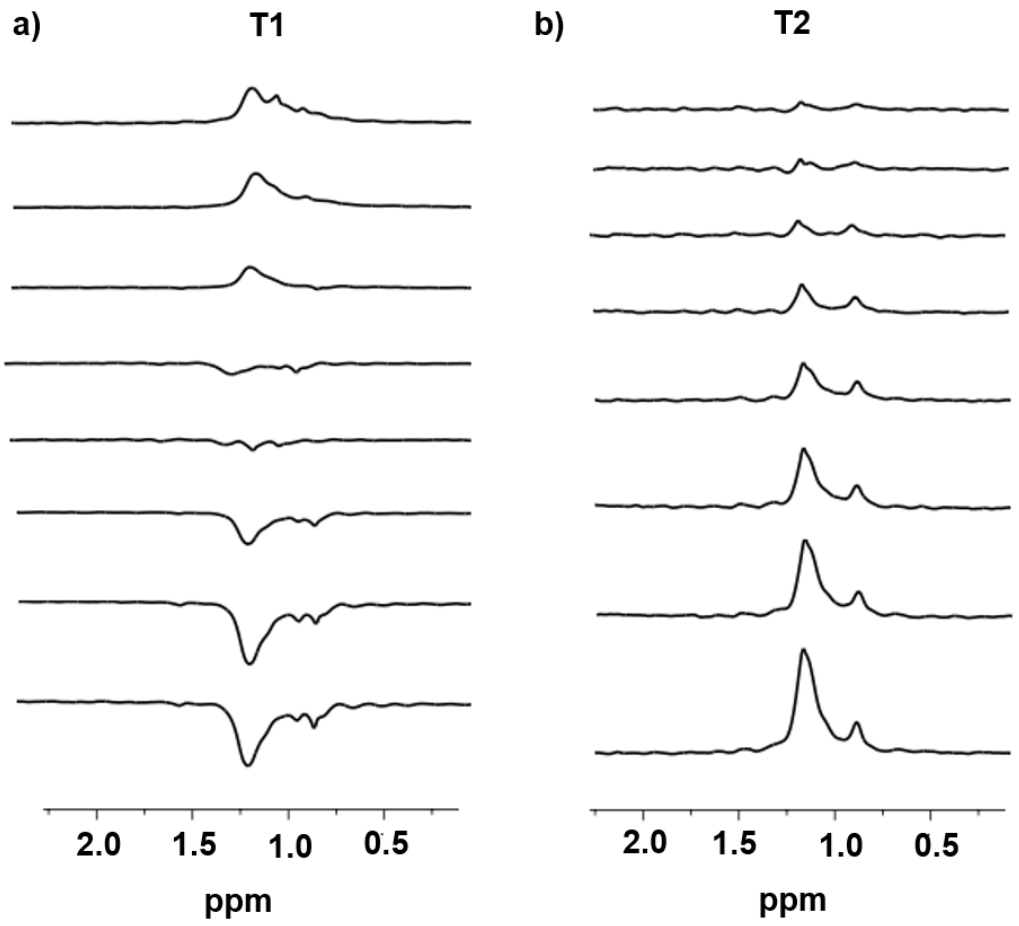

Appendix B7. a) Decay of signal intensity after a 180^o pulse, for determination of T_2. b) Re-establishment of magnetization after a 90^o pulse, for the determination of the spin-lattice relaxation time, T1

APPENDIX C. Chapter 4 supporting information

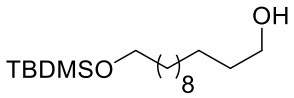

158

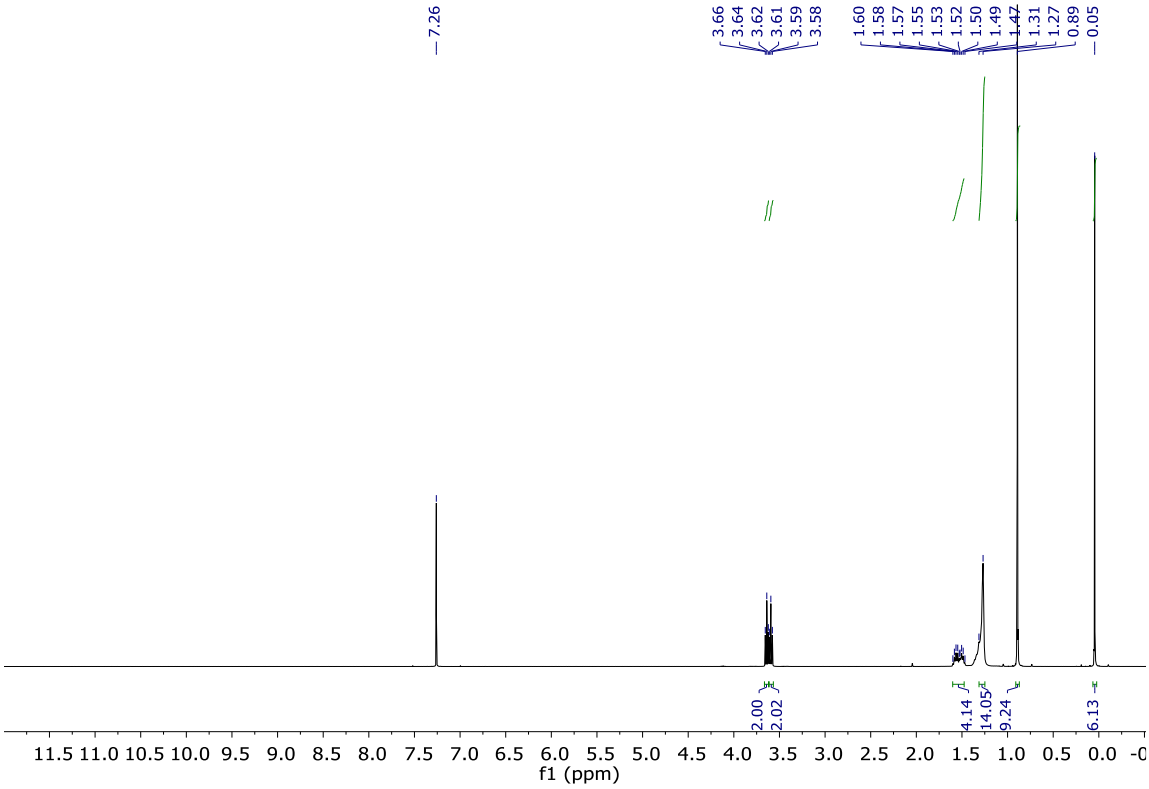

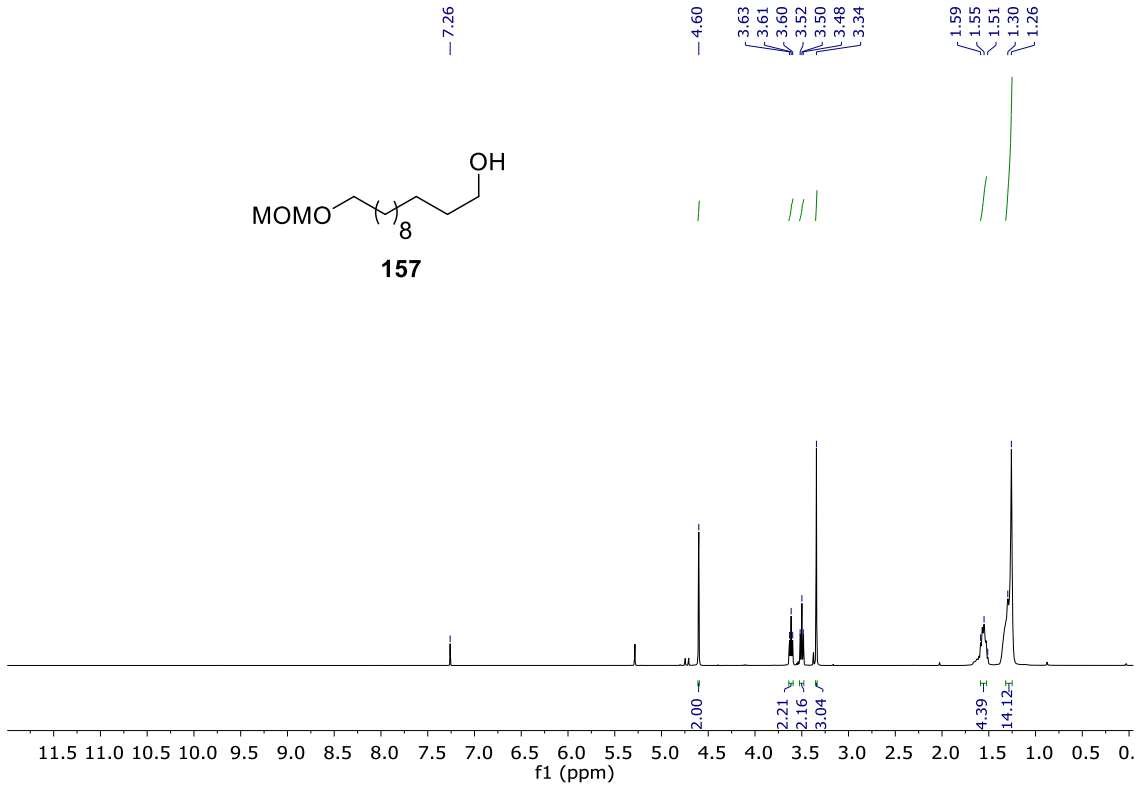
7.26
4.60
3.63
3.61
3.60
3.52
3.50
3.48
3.34
1.59
1.55
1.51
1.30
1.26
OH
MOMO
8
2.00
2.21
2.16
3.04
4.39
14.12
11.5 11.0 10.5 10.0 9.5 9.0 8.5 8.0 7.5 7.0 6.5 6.0 5.5 5.0 4.5 4.0 3.5 3.0 2.5 2.0 1.5 1.0 0.5 0.
f1 (ppm)

157

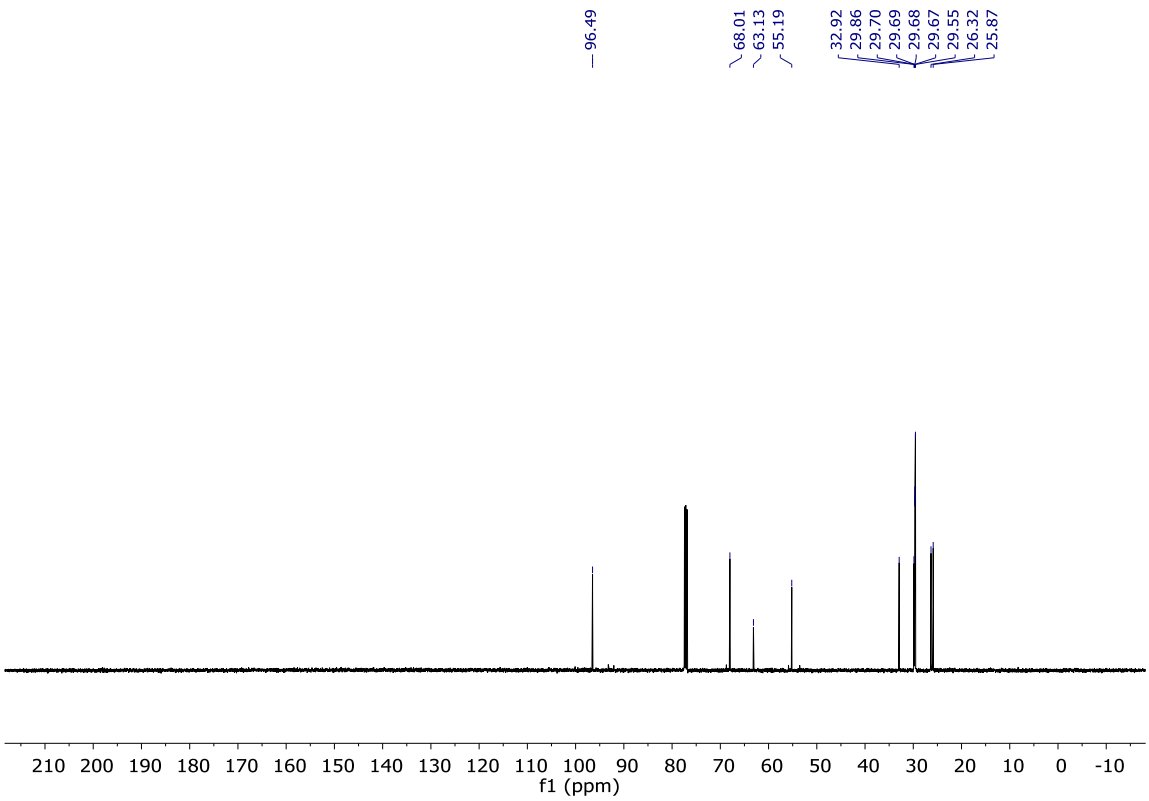
96.49
68.01
63.13
55.19
32.92
29.86
29.70
29.69
29.68
29.67
29.55
26.32
25.87
210 200 190 180 170 160 150 140 130 120 110 100 90 80 70 60 50 40 30 20 10 0 -10
f1 (ppm)

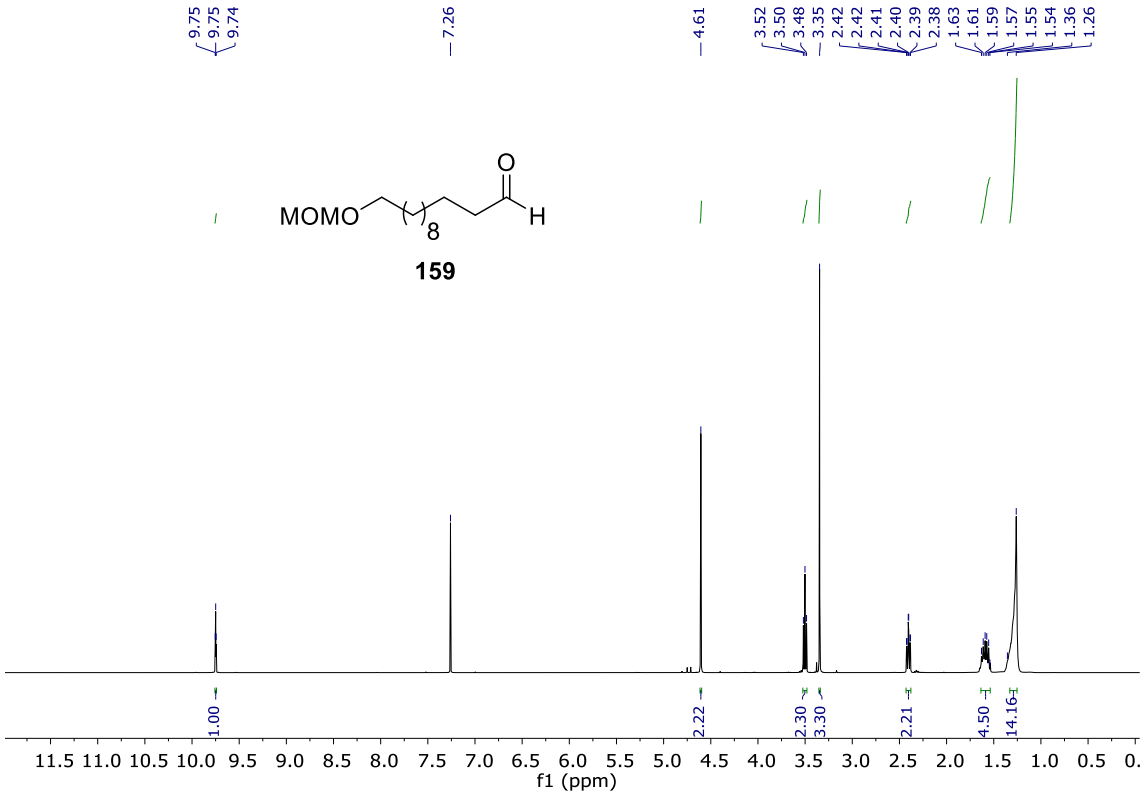
9.75
9.75
9.74
7.26
4.61
3.52
3.50
3.48
3.35
2.42
2.42
2.41
2.40
2.39
2.38
1.63
1.61
1.59
1.57
1.55
1.54
1.36
1.26
O
MOMO
8
H
1.00
2.22
2.30
3.30
2.21
4.50
14.16
11.5 11.0 10.5 10.0 9.5 9.0 8.5 8.0 7.5 7.0 6.5 6.0 5.5 5.0 4.5 4.0 3.5 3.0 2.5 2.0 1.5 1.0 0.5 0.
f1 (ppm)

159

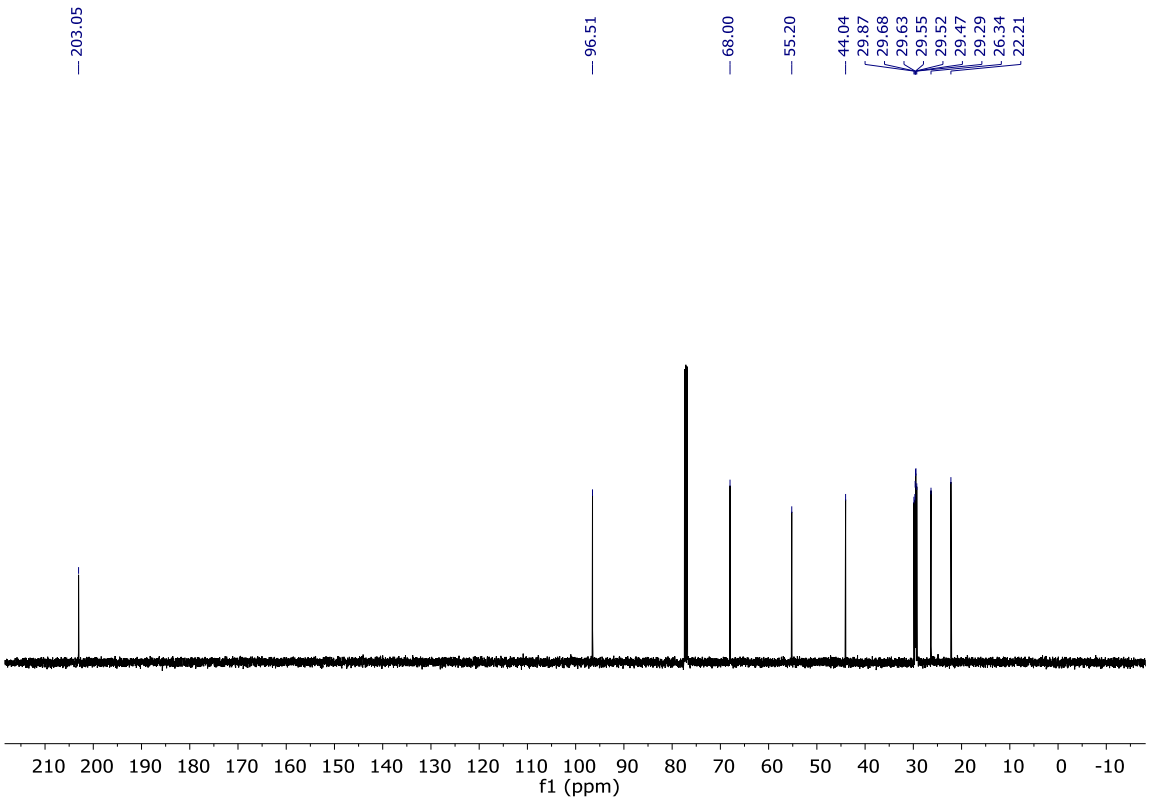
203.05
96.51
68.00
55.20
44.04
29.87
29.68
29.63
29.55
29.52
29.47
29.29
26.34
22.21
210 200 190 180 170 160 150 140 130 120 110 100 90 80 70 60 50 40 30 20 10 0 -10
f1 (ppm)

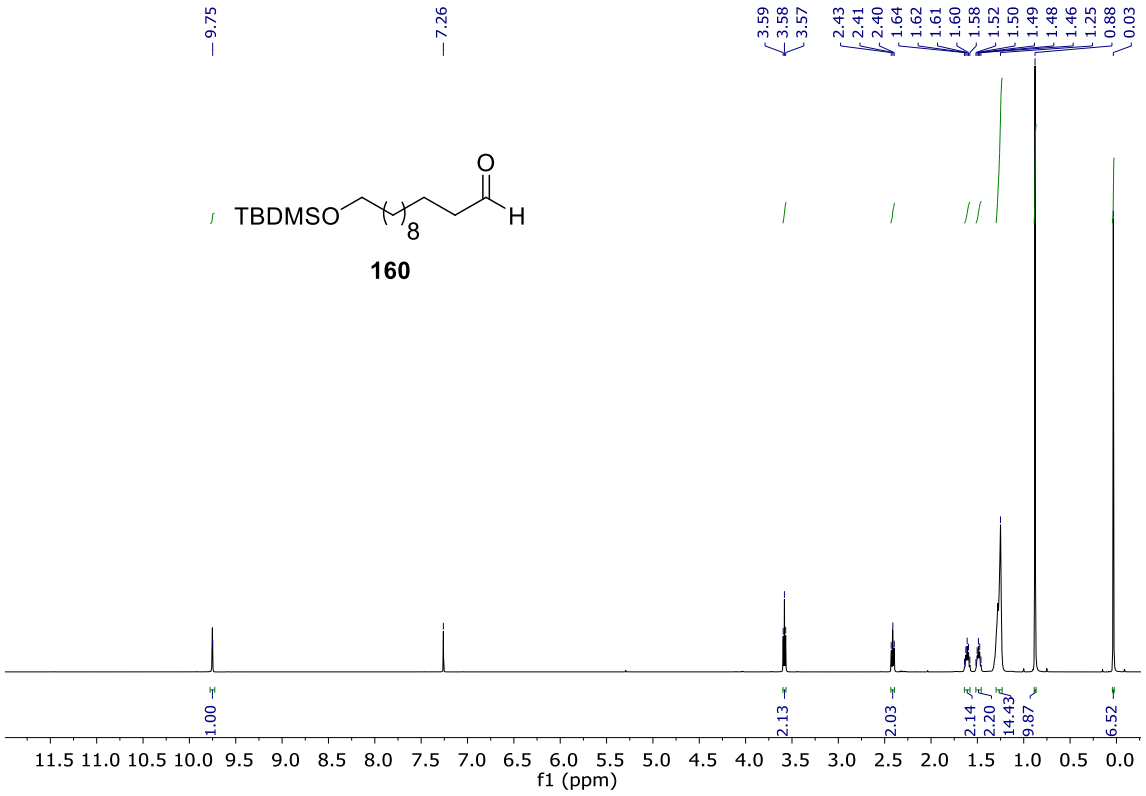
9.75
7.26
3.59
3.58
3.57
2.43
2.41
2.40
1.64
1.62
1.61
1.60
1.58
1.52
1.50
1.49
1.48
1.46
1.25
0.88
0.03
TBDMSO
8
O
H
160
1.00
2.13
2.03
2.14
2.20
14.43
9.87
6.52
11.5 11.0 10.5 10.0 9.5 9.0 8.5 8.0 7.5 7.0 6.5 6.0 5.5 5.0 4.5 4.0 3.5 3.0 2.5 2.0 1.5 1.0 0.5 0.0
f1 (ppm)

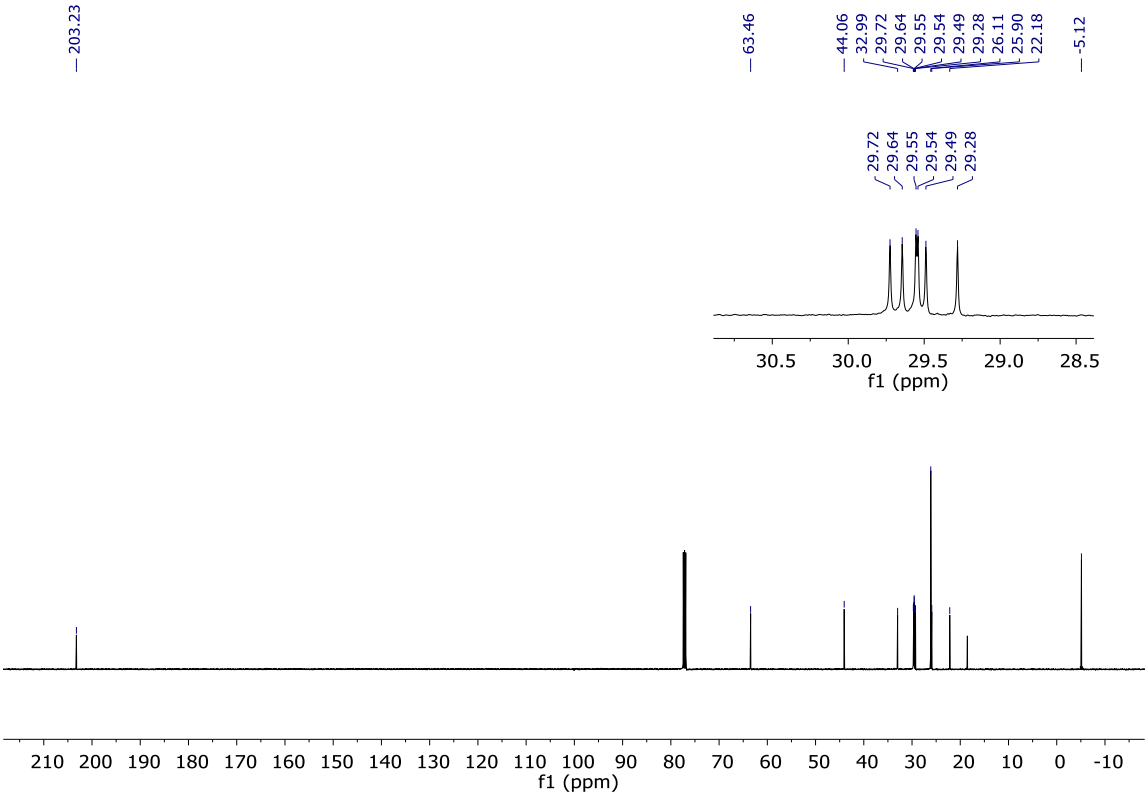
203.23
63.46
44.06
32.99
29.72
29.64
29.55
29.54
29.49
29.28
26.11
25.90
22.18
-5.12
30.5 30.0 29.5 29.0 28.5
f1 (ppm)
210 200 190 180 170 160 150 140 130 120 110 100 90 80 70 60 50 40 30 20 10 0 -10
f1 (ppm)

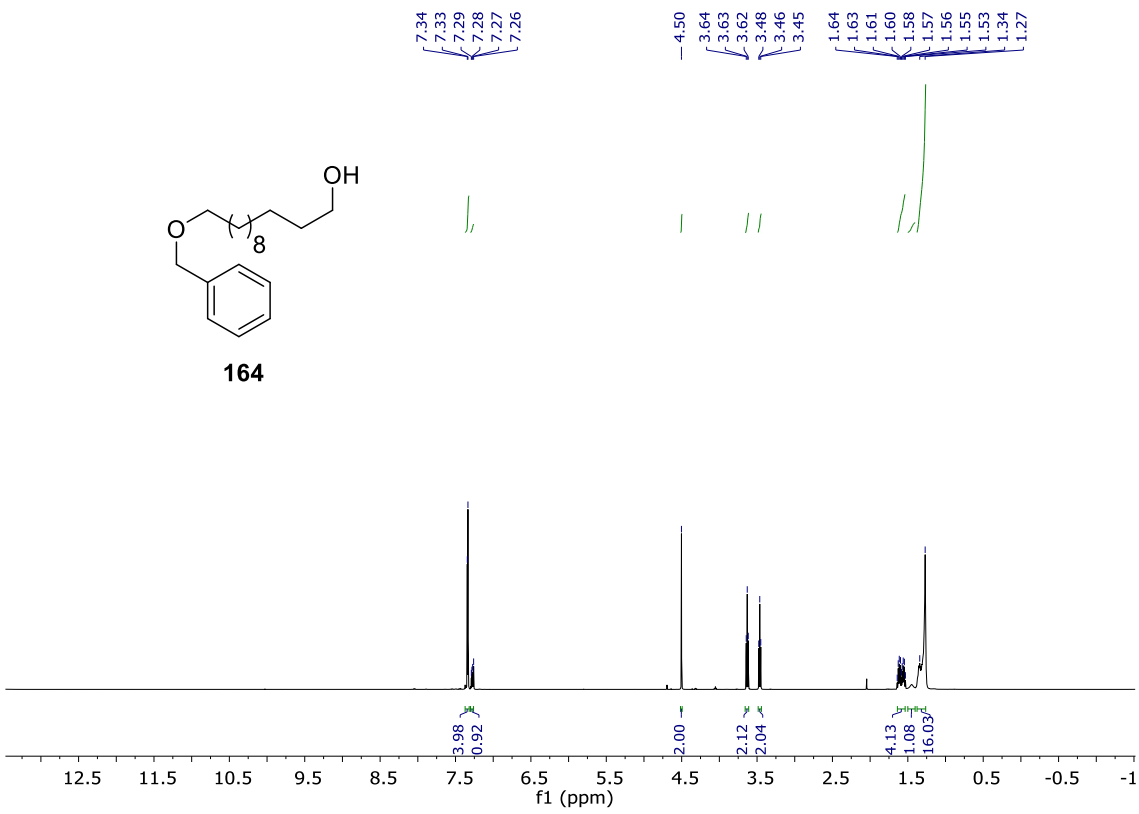
7.34
7.33
7.29
7.28
7.27
7.26
4.50
3.64
3.63
3.62
3.48
3.46
3.45
1.64
1.63
1.61
1.60
1.58
1.57
1.56
1.55
1.53
1.34
1.27
OH
O
8
3.98
0.92
2.00
2.12
2.04
4.13
1.08
16.03
12.5
11.5
10.5
9.5
8.5
7.5
6.5
5.5
4.5
3.5
2.5
1.5
0.5
-0.5
-1
f1 (ppm)

164

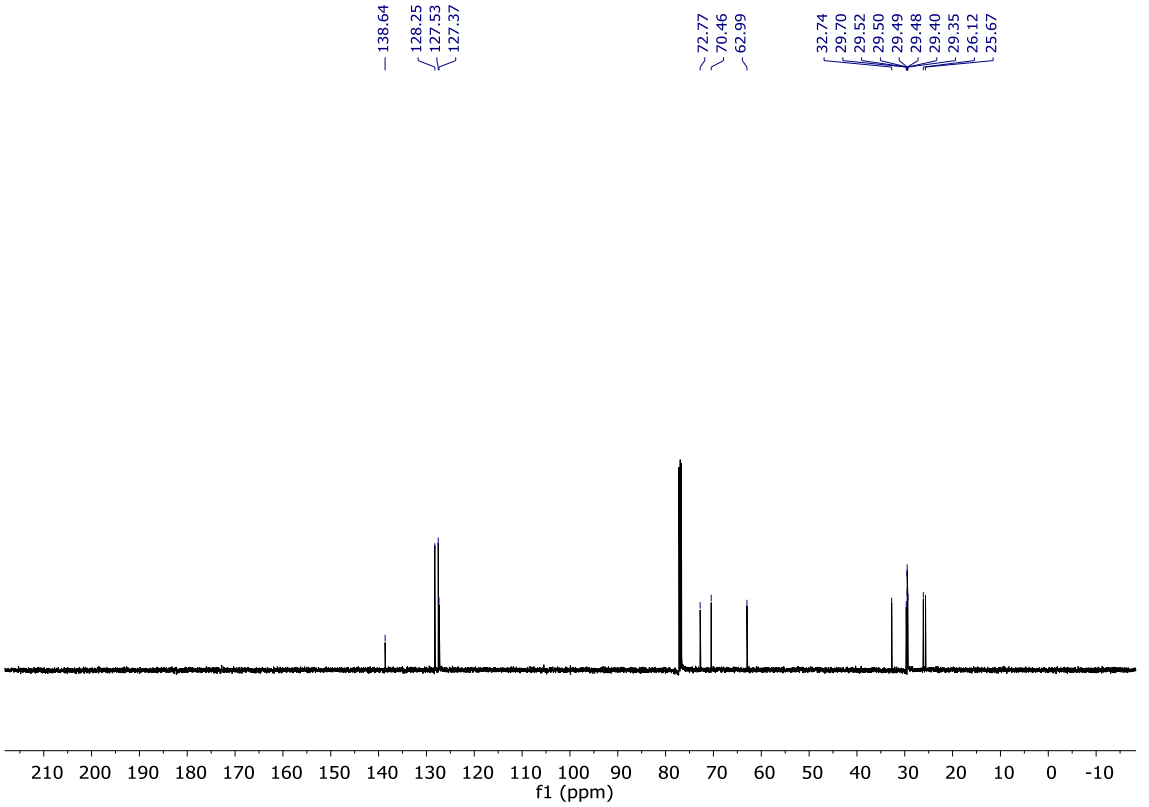
138.64
128.25
127.53
127.37
72.77
70.46
62.99
32.74
29.70
29.52
29.50
29.49
29.48
29.40
29.35
26.12
25.67
210
200
190
180
170
160
150
140
130
120
110
100
90
80
70
60
50
40
30
20
10
0
-10
f1 (ppm)

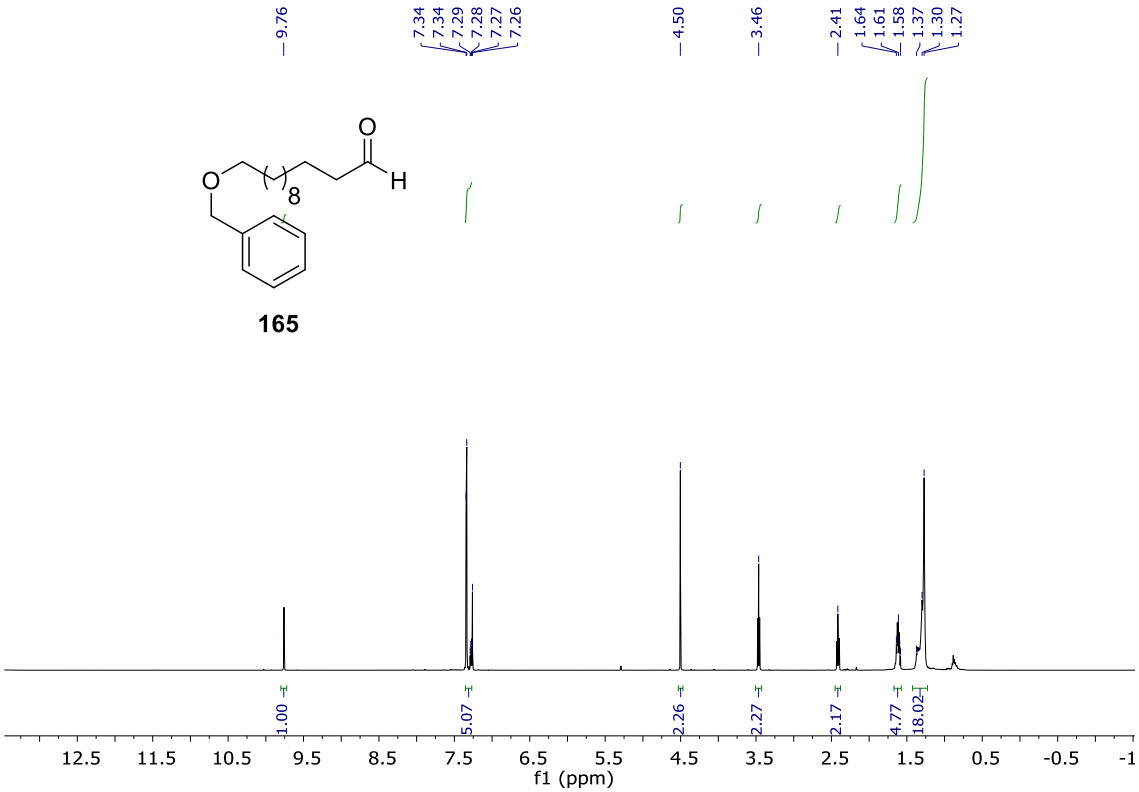
9.76
7.34
7.34
7.29
7.28
7.27
7.26
4.50
3.46
2.41
1.64
1.61
1.58
1.37
1.30
1.27
O
O
H
8
1.00
5.07
2.26
2.27
2.17
4.77
18.02
12.5 11.5 10.5 9.5 8.5 7.5 6.5 5.5 4.5 3.5 2.5 1.5 0.5 -0.5 -1
f1 (ppm)

165

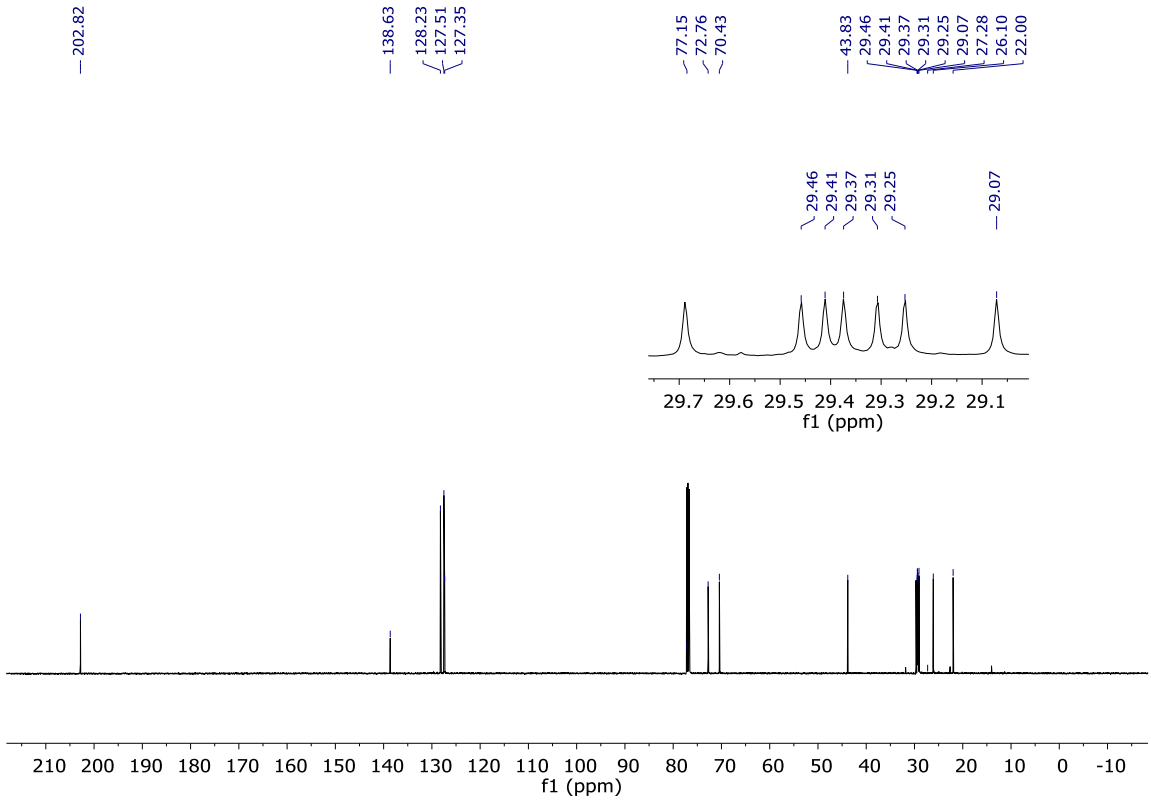
202.82
138.63
128.23
127.51
127.35
77.15
72.76
70.43
43.83
29.46
29.41
29.37
29.31
29.25
29.07
27.28
26.10
22.00
29.46
29.41
29.37
29.31
29.25
29.07
29.7 29.6 29.5 29.4 29.3 29.2 29.1
f1 (ppm)
210 200 190 180 170 160 150 140 130 120 110 100 90 80 70 60 50 40 30 20 10 0 -10
f1 (ppm)

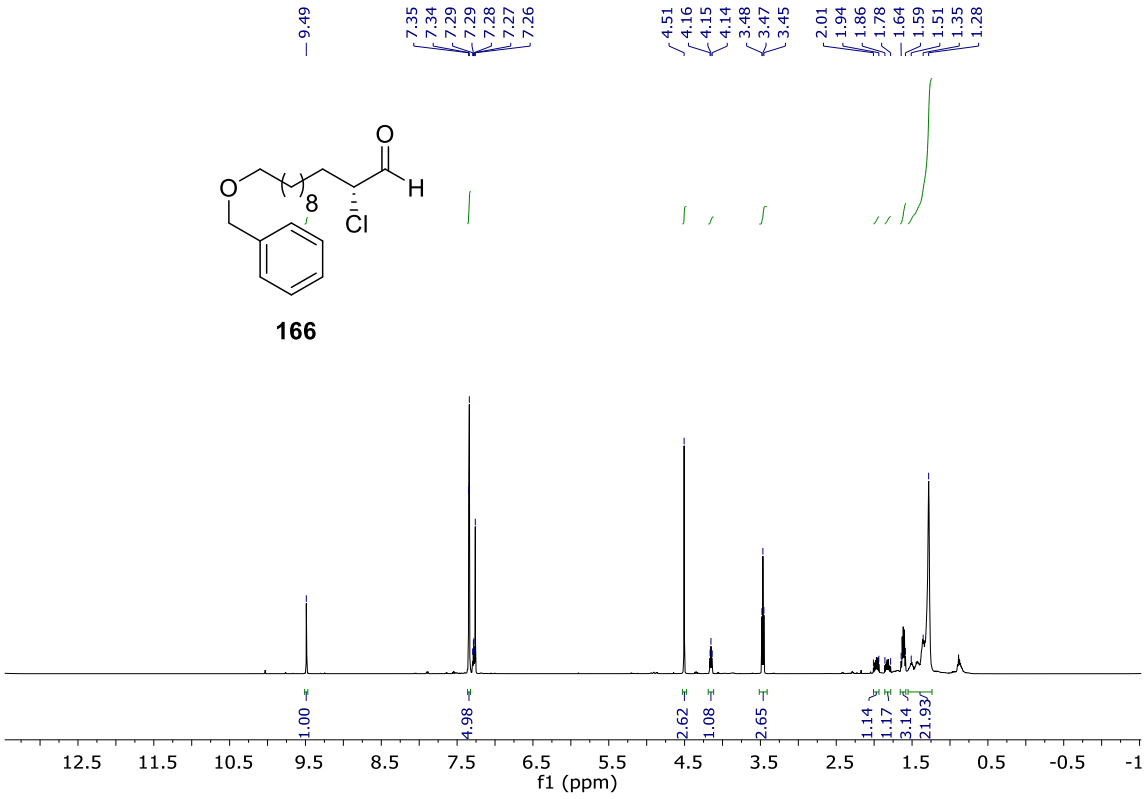
9.49
7.35
7.34
7.29
7.29
7.28
7.27
7.26
4.51
4.16
4.15
4.14
3.48
3.47
3.45
2.01
1.94
1.86
1.78
1.64
1.59
1.51
1.35
1.28
O
O
H
8
Cl
1.00
4.98
2.62
1.08
2.65
1.14
1.17
3.14
21.93
12.5 11.5 10.5 9.5 8.5 7.5 6.5 5.5 4.5 3.5 2.5 1.5 0.5 -0.5 -1
f1 (ppm)

166

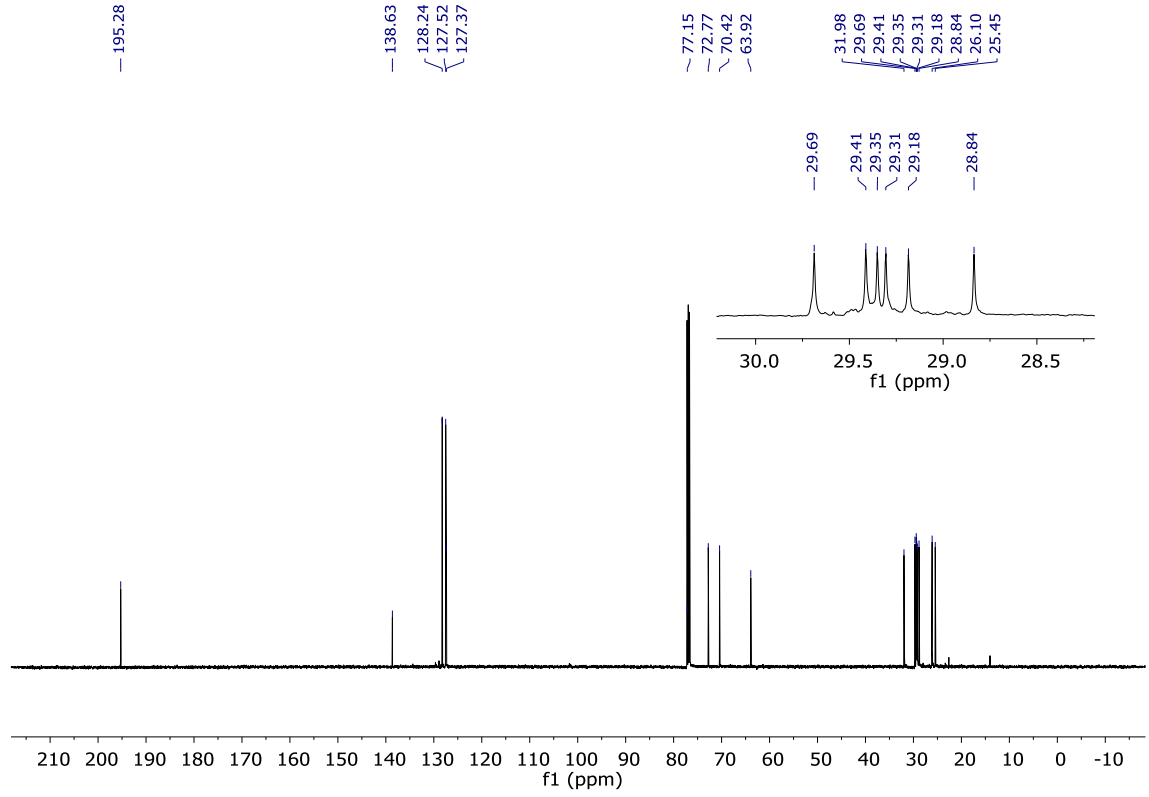
195.28
138.63
128.24
127.52
127.37
77.15
72.77
70.42
63.92
31.98
29.69
29.41
29.35
29.31
29.18
28.84
26.10
25.45
29.69
29.41
29.35
29.31
29.18
28.84
30.0 29.5 29.0 28.5
f1 (ppm)
210 200 190 180 170 160 150 140 130 120 110 100 90 80 70 60 50 40 30 20 10 0 -10
f1 (ppm)

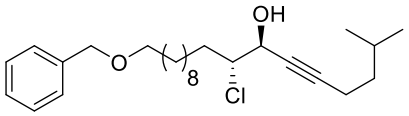
OH
O
8
Cl

167

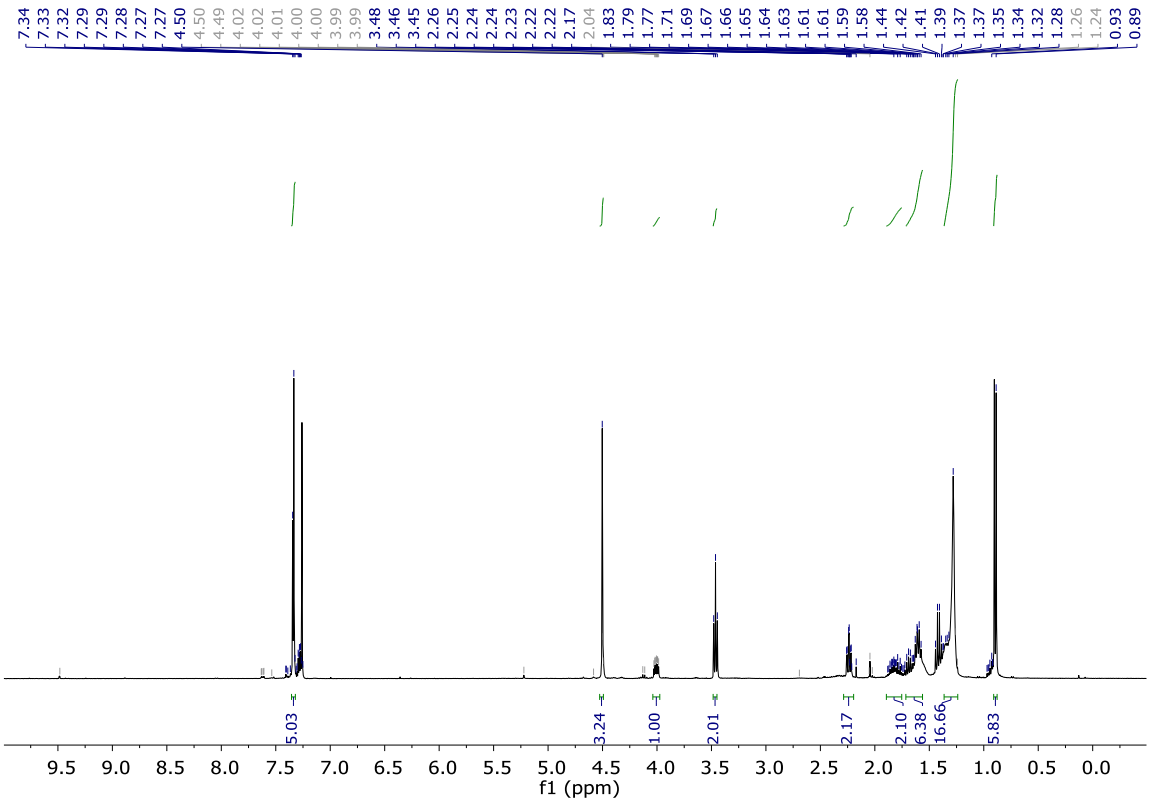
7.34 7.33 7.32 7.29 7.29 7.28 7.27 7.27 4.50 4.50 4.49 4.02 4.02 4.01 4.00 4.00 3.99 3.99 3.48 3.46 3.45 2.26 2.25 2.24 2.24 2.23 2.22 2.22 2.17 2.04 1.83 1.79 1.77 1.71 1.69 1.67 1.66 1.65 1.64 1.63 1.61 1.61 1.59 1.58 1.44 1.42 1.41 1.39 1.37 1.37 1.35 1.34 1.32 1.28 1.26 1.24 0.93 0.89
5.03
3.24
1.00
2.01
2.17
2.10
6.38
16.66
5.83
9.5 9.0 8.5 8.0 7.5 7.0 6.5 6.0 5.5 5.0 4.5 4.0 3.5 3.0 2.5 2.0 1.5 1.0 0.5 0.0
f1 (ppm)

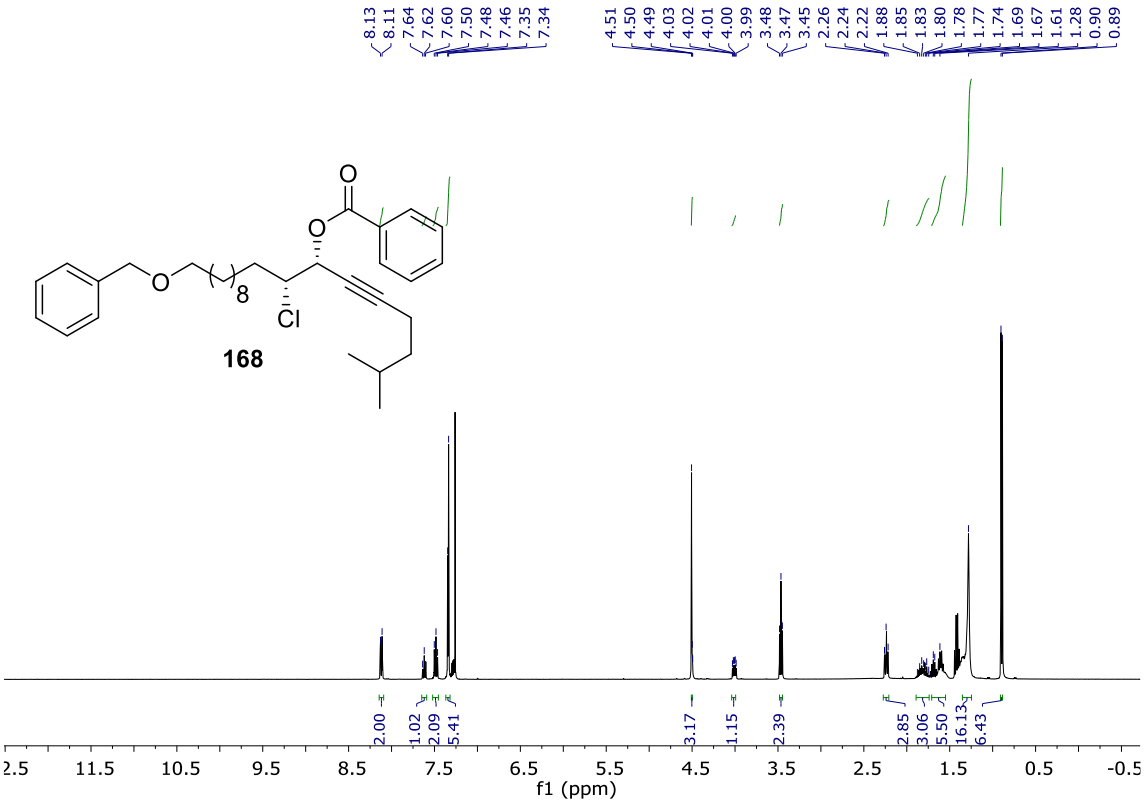
8.13
8.11
7.64
7.62
7.60
7.50
7.48
7.46
7.35
7.34
4.51
4.50
4.49
4.03
4.02
4.01
4.00
3.99
3.48
3.47
3.45
2.26
2.24
2.22
1.88
1.85
1.83
1.80
1.78
1.77
1.74
1.69
1.67
1.61
1.28
0.90
0.89
O
O
O
8
Cl
168
2.00
1.02
2.09
5.41
3.17
1.15
2.39
2.85
3.06
5.50
16.13
6.43
f1 (ppm)

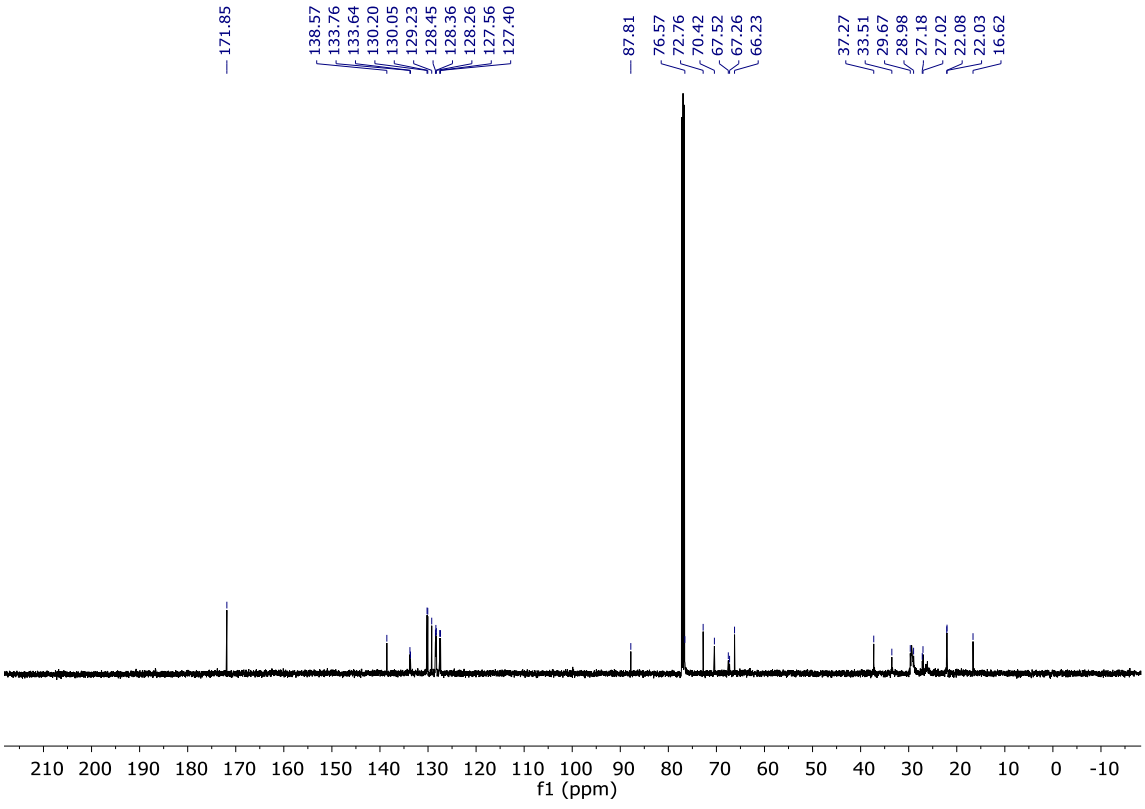
171.85
138.57
133.76
133.64
130.20
130.05
129.23
128.45
128.36
128.26
127.56
127.40
87.81
76.57
72.76
70.42
67.52
67.26
66.23
37.27
33.51
29.67
28.98
27.18
27.02
22.08
22.03
16.62
f1 (ppm)

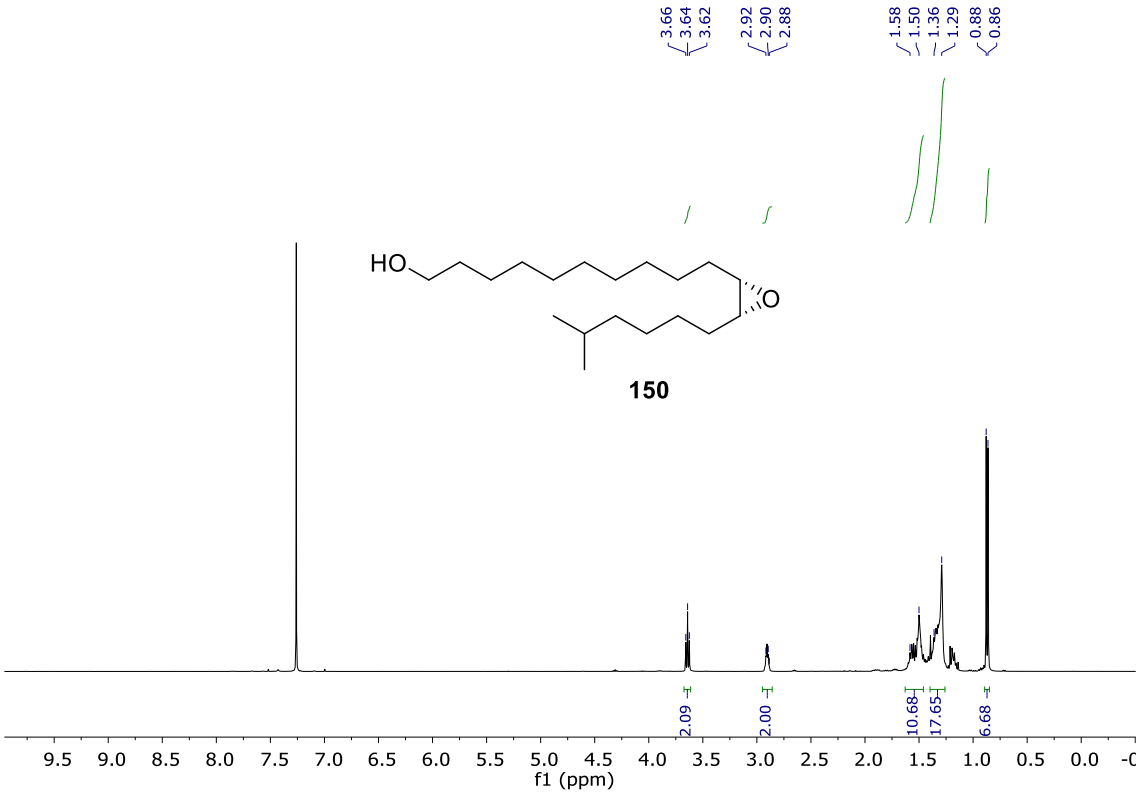
3.66
3.64
3.62
2.92
2.90
2.88
1.58
1.50
1.36
1.29
0.88
0.86
HO
O
150
2.09
2.00
10.68
17.65
6.68
f1 (ppm)

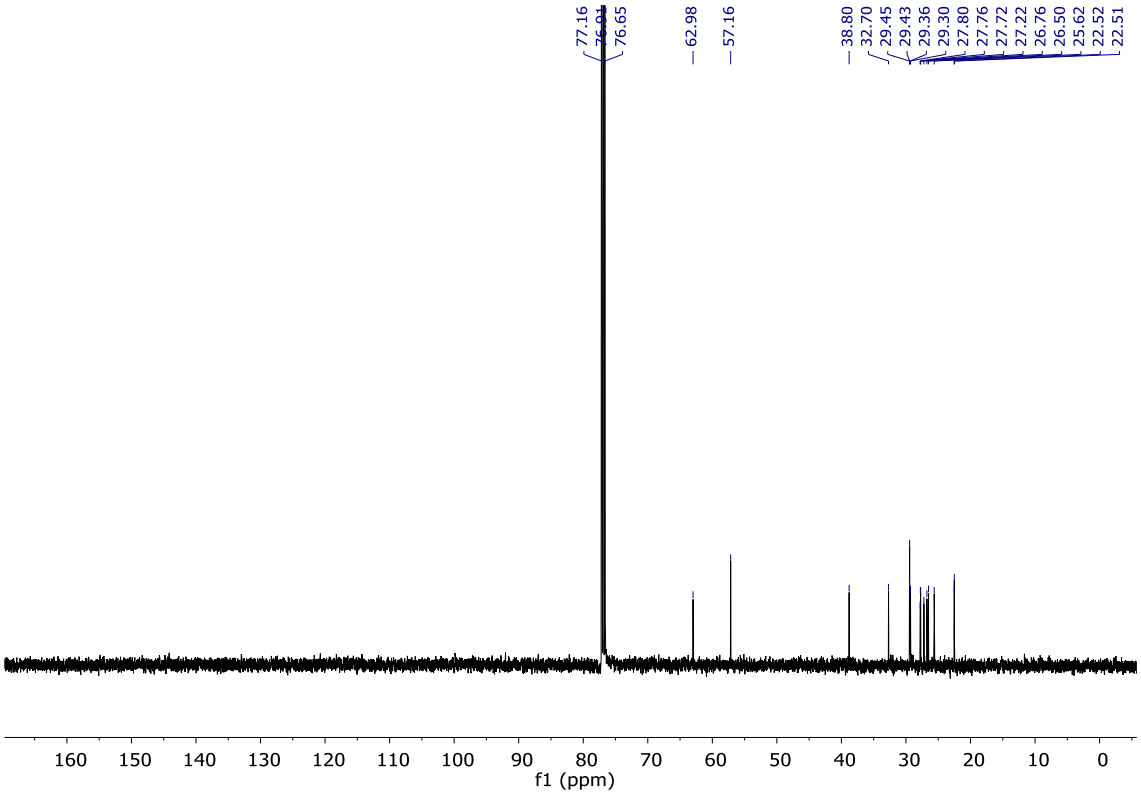
77.16
76.91
76.65
62.98
57.16
38.80
32.70
29.45
29.43
29.36
29.30
27.80
27.76
27.72
27.22
26.76
26.50
25.62
22.52
22.51
f1 (ppm)

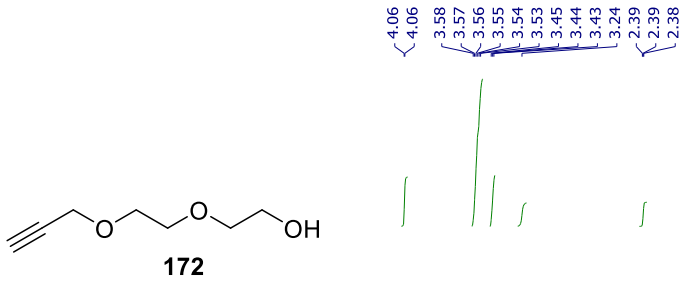
7.26
4.06
4.06
3.58
3.57
3.56
3.55
3.54
3.53
3.45
3.44
3.43
3.24
2.39
2.39
2.38
O
O
OH

172

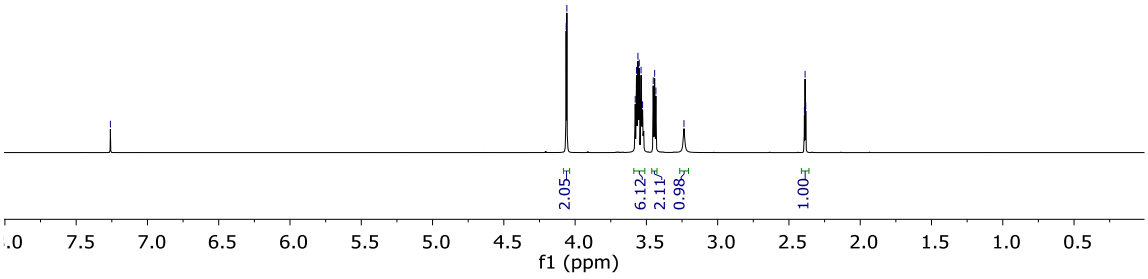
2.05
6.12
2.11
0.98
1.00
f1 (ppm)

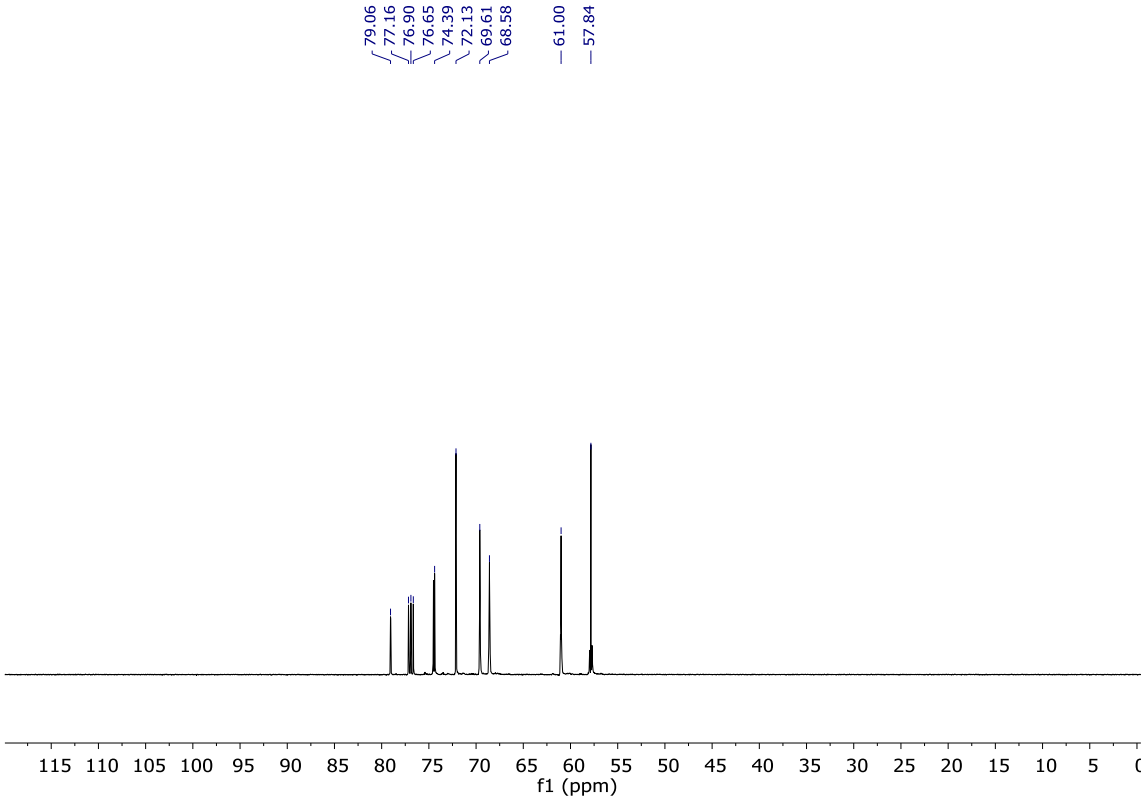
79.06
77.16
76.90
76.65
74.39
72.13
69.61
68.58
61.00
57.84
f1 (ppm)

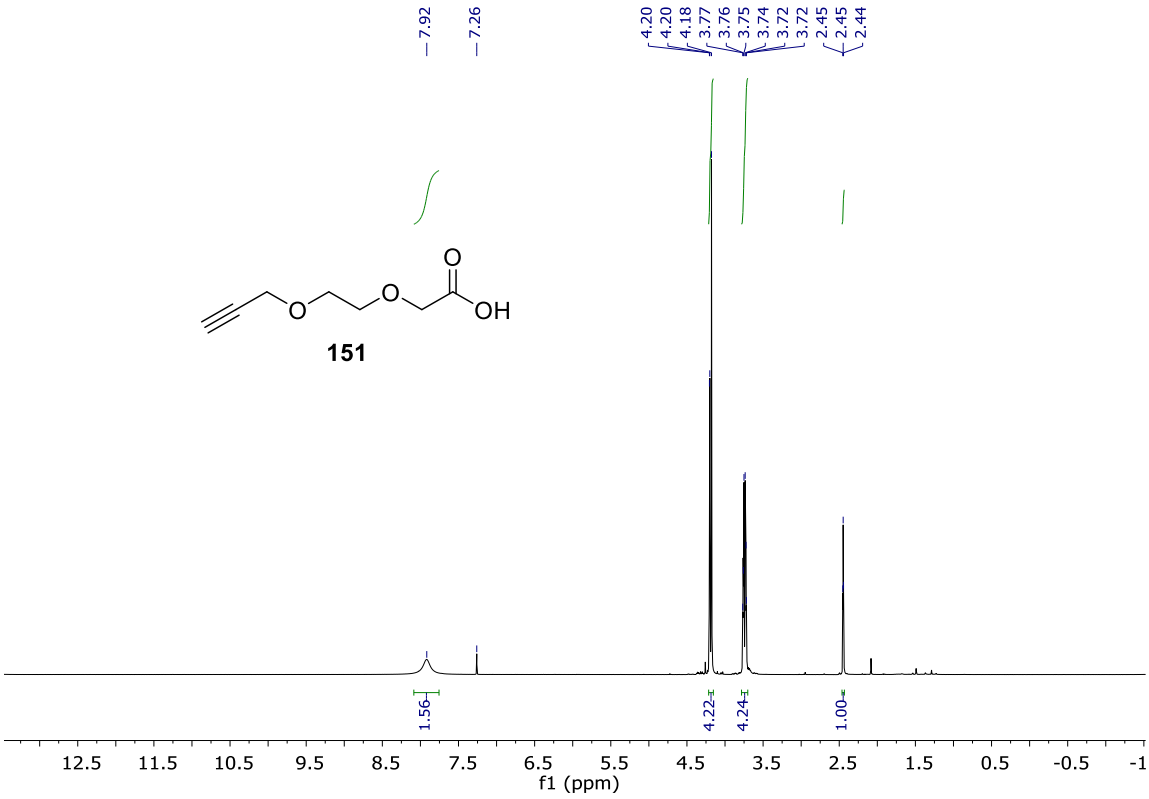
7.92
7.26
4.20
4.20
4.18
3.77
3.76
3.75
3.74
3.72
3.72
2.45
2.45
2.44
O
O
O
OH
151
1.56
4.22
4.24
1.00
12.5 11.5 10.5 9.5 8.5 7.5 6.5 5.5 4.5 3.5 2.5 1.5 0.5 -0.5 -1
f1 (ppm)

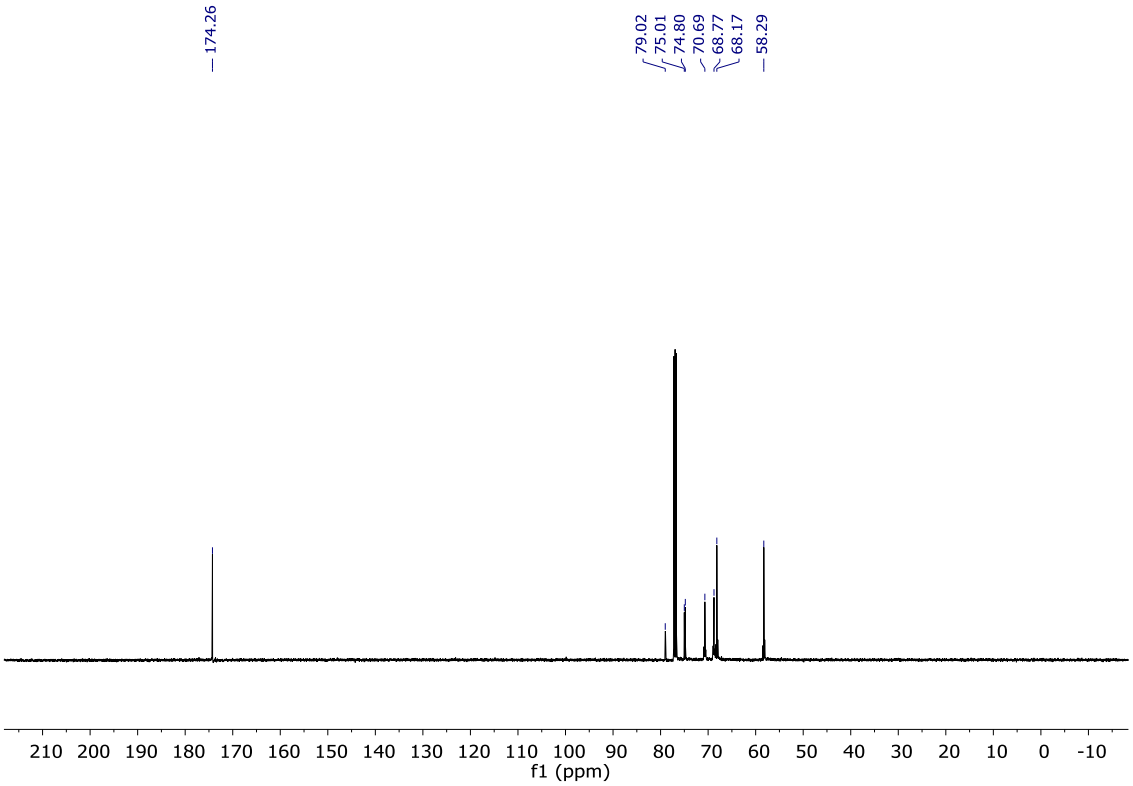
174.26
79.02
75.01
74.80
70.69
68.77
68.17
58.29
210 200 190 180 170 160 150 140 130 120 110 100 90 80 70 60 50 40 30 20 10 0 -10
f1 (ppm)

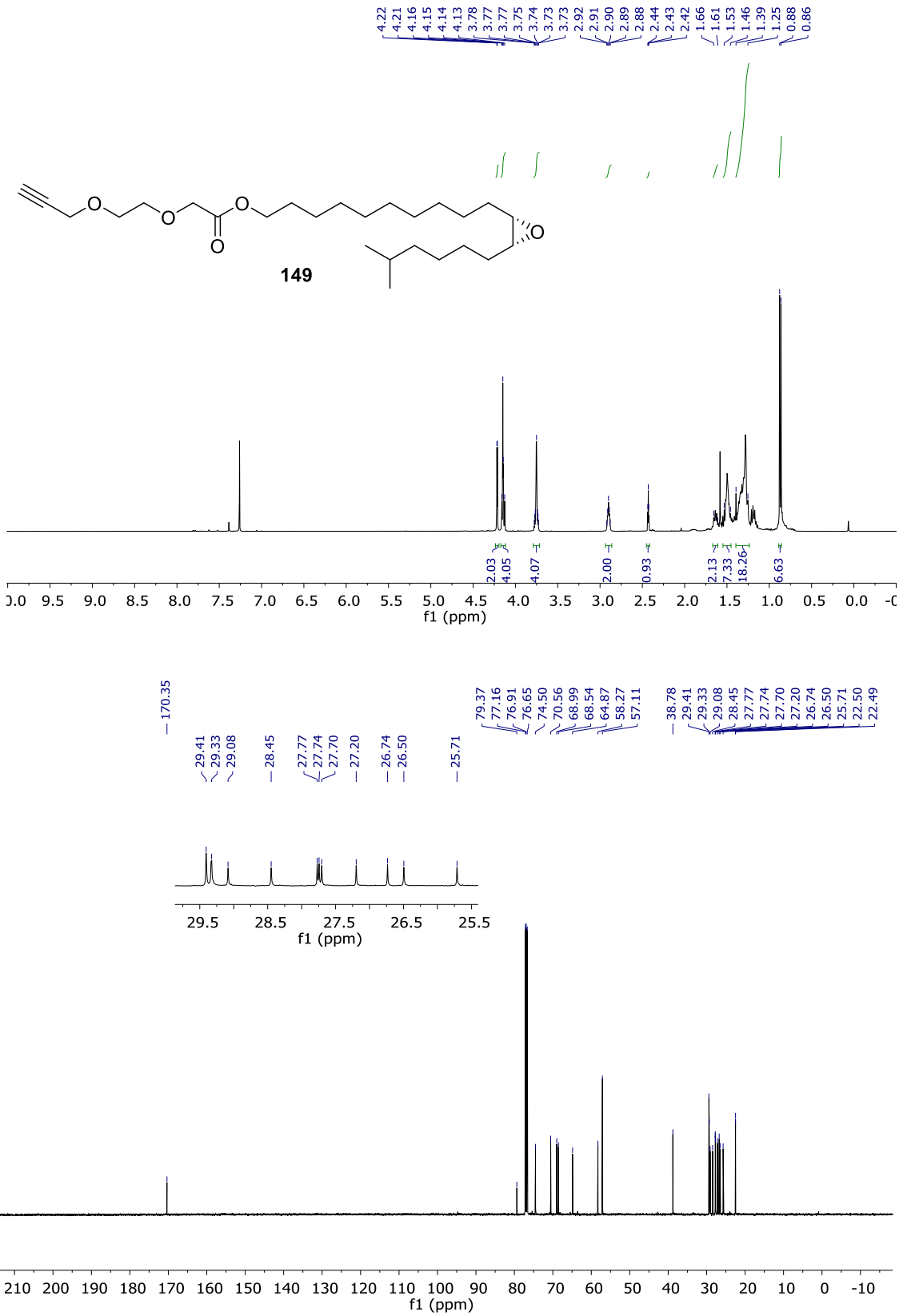
149
f1 (ppm)
f1 (ppm)
f1 (ppm)

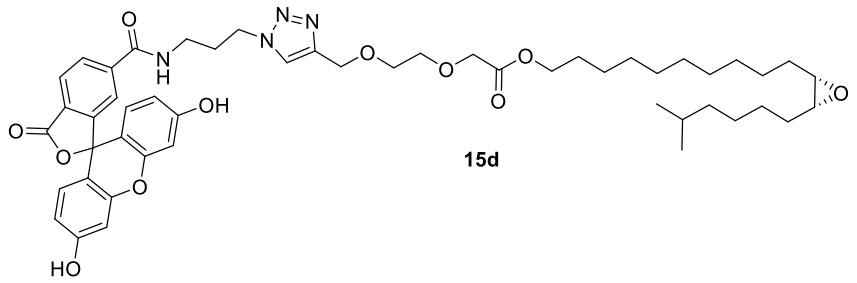

15d

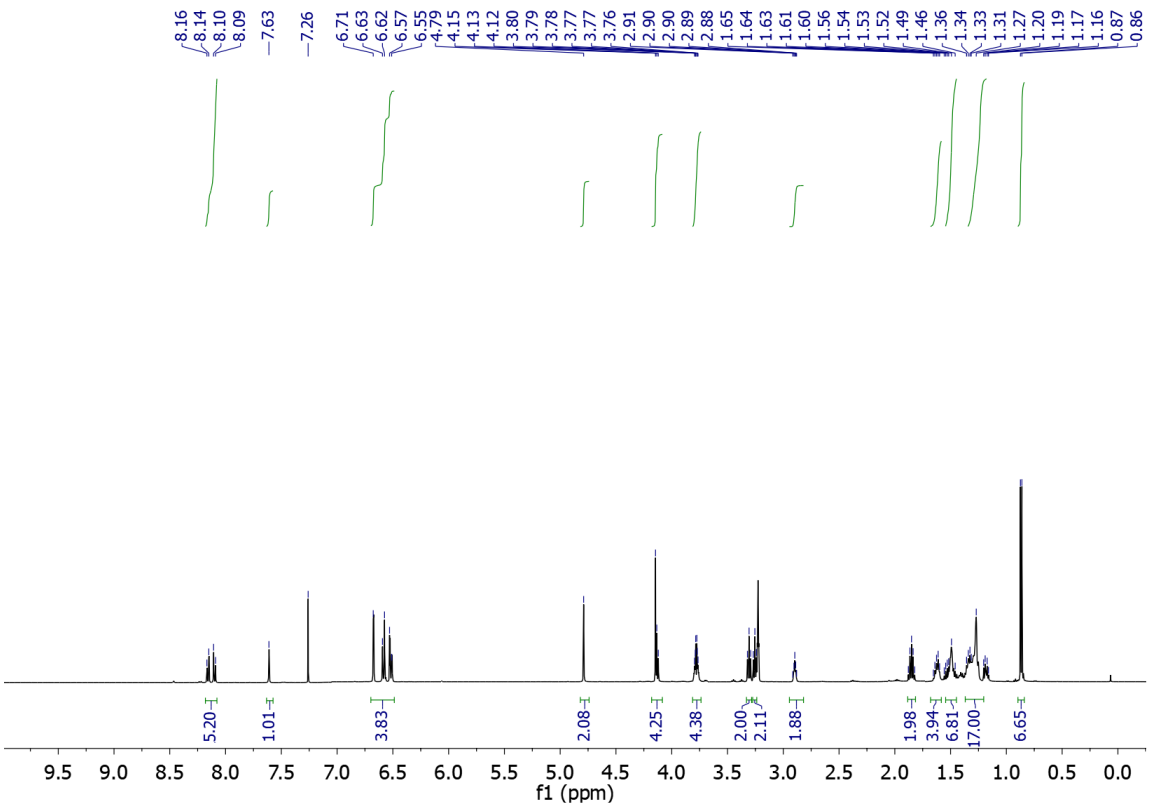
8.16
8.14
8.10
8.09
7.63
7.26
6.71
6.63
6.62
6.57
6.55
4.79
4.15
4.13
4.12
3.80
3.79
3.78
3.77
3.77
3.76
2.91
2.90
2.90
2.89
2.88
1.65
1.64
1.63
1.61
1.60
1.56
1.54
1.53
1.52
1.49
1.46
1.36
1.34
1.33
1.31
1.27
1.20
1.19
1.17
1.16
0.87
0.86
5.20
1.01
3.83
2.08
4.25
4.38
2.00
2.11
1.88
1.98
3.94
6.81
17.00
6.65
9.5 9.0 8.5 8.0 7.5 7.0 6.5 6.0 5.5 5.0 4.5 4.0 3.5 3.0 2.5 2.0 1.5 1.0 0.5 0.0
f1 (ppm)

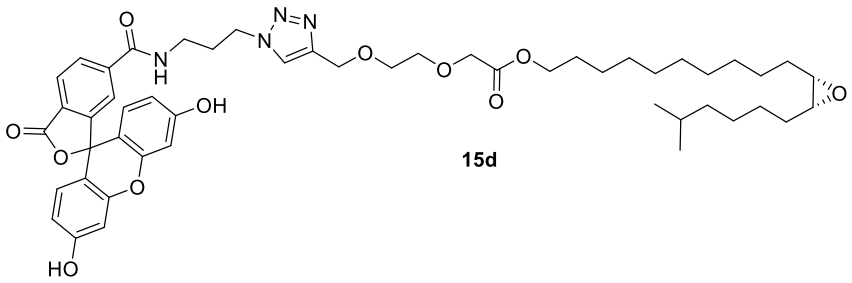

15d

Chromatogram and Spectrum

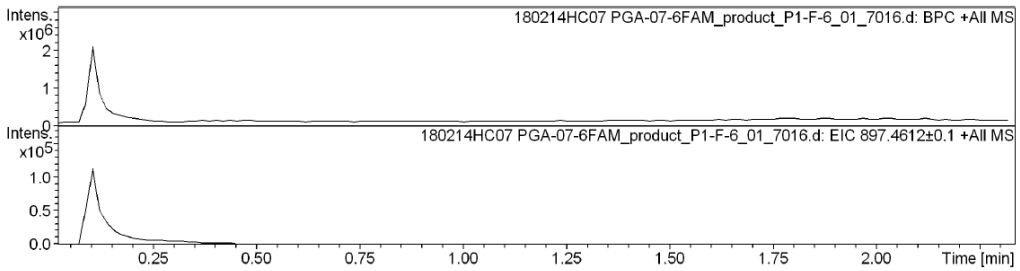

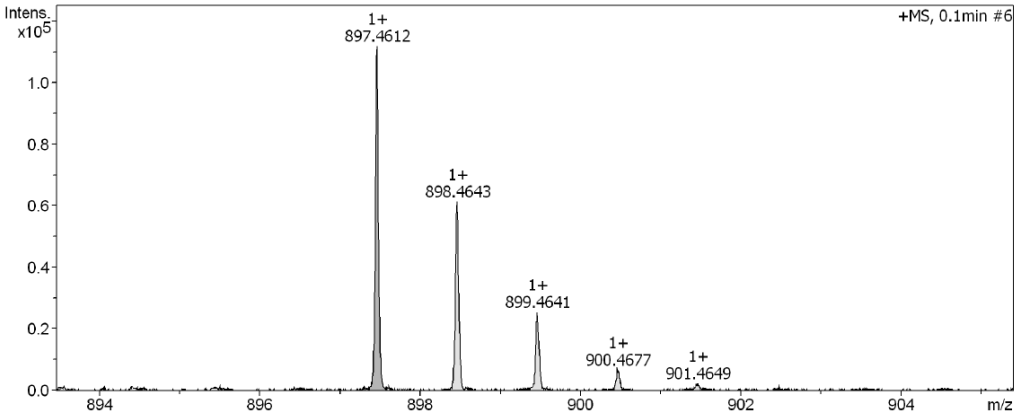

Formula Confirmation

Meas. m/z	#	Ion Formula	Score	m/z	err [mDa]	err [ppm]	mSigma	rdb	e⁻ Conf	N-Rule	Adduct
897.461236	1	C50H65N4O11	100.00	897.464435	-3.2	-3.6	25.1	20.5	even	ok	M+H

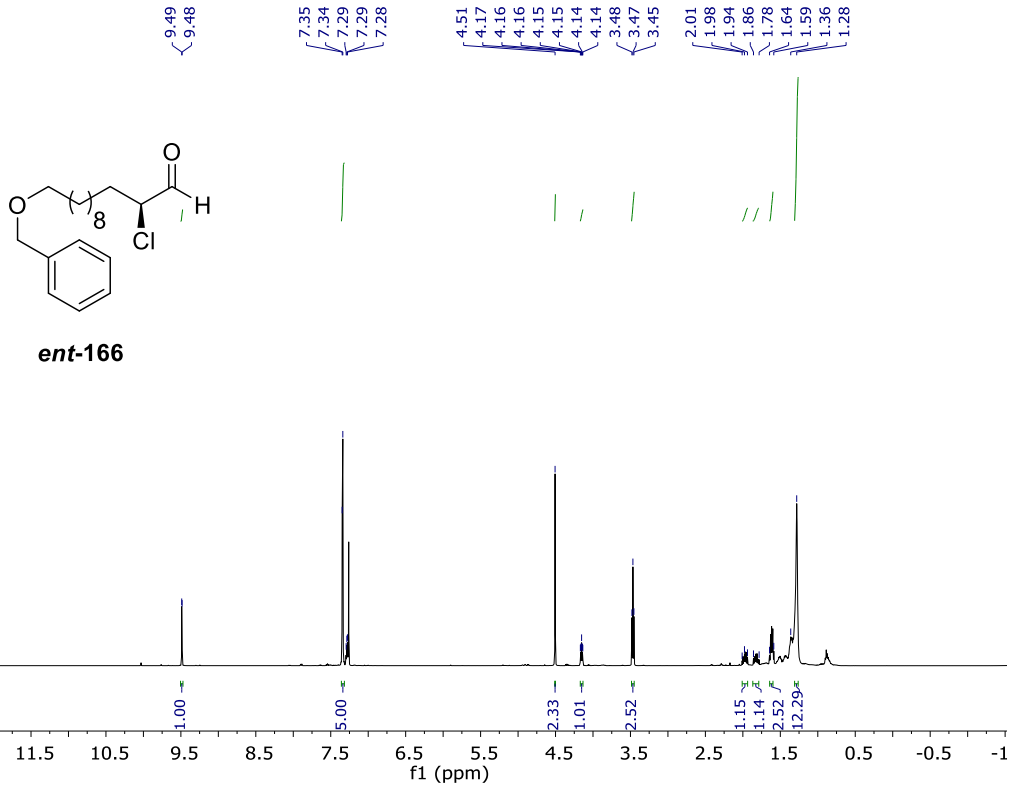
9.49
9.48
7.35
7.34
7.29
7.29
7.28
4.51
4.17
4.16
4.16
4.15
4.15
4.14
4.14
3.48
3.47
3.45
2.01
1.98
1.94
1.86
1.78
1.64
1.59
1.36
1.28
O
O
8
Cl
H
1.00
5.00
2.33
1.01
2.52
1.15
1.14
2.52
12.29
12.5
11.5
10.5
9.5
8.5
7.5
6.5
5.5
4.5
3.5
2.5
1.5
0.5
-0.5
-1
f1 (ppm)

***ent*-166**

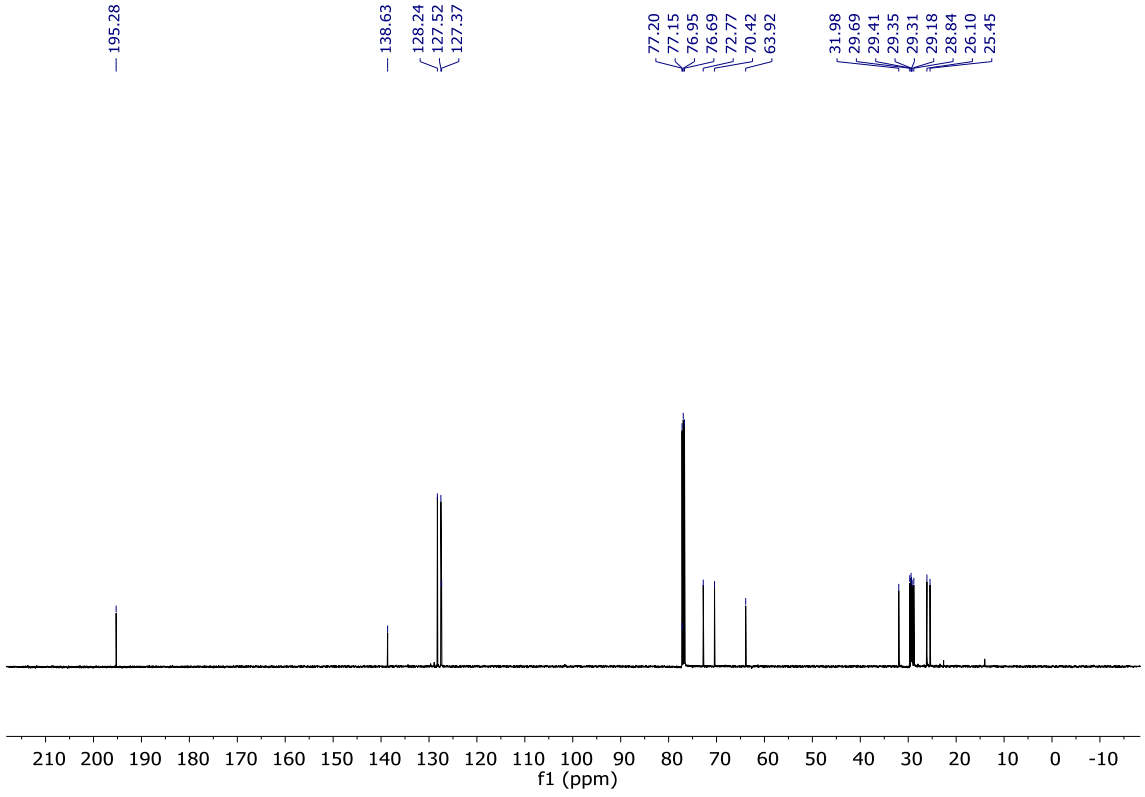
195.28
138.63
128.24
127.52
127.37
77.20
77.15
76.95
76.69
72.77
70.42
63.92
31.98
29.69
29.41
29.35
29.31
29.18
28.84
26.10
25.45
210
200
190
180
170
160
150
140
130
120
110
100
90
80
70
60
50
40
30
20
10
0
-10
f1 (ppm)

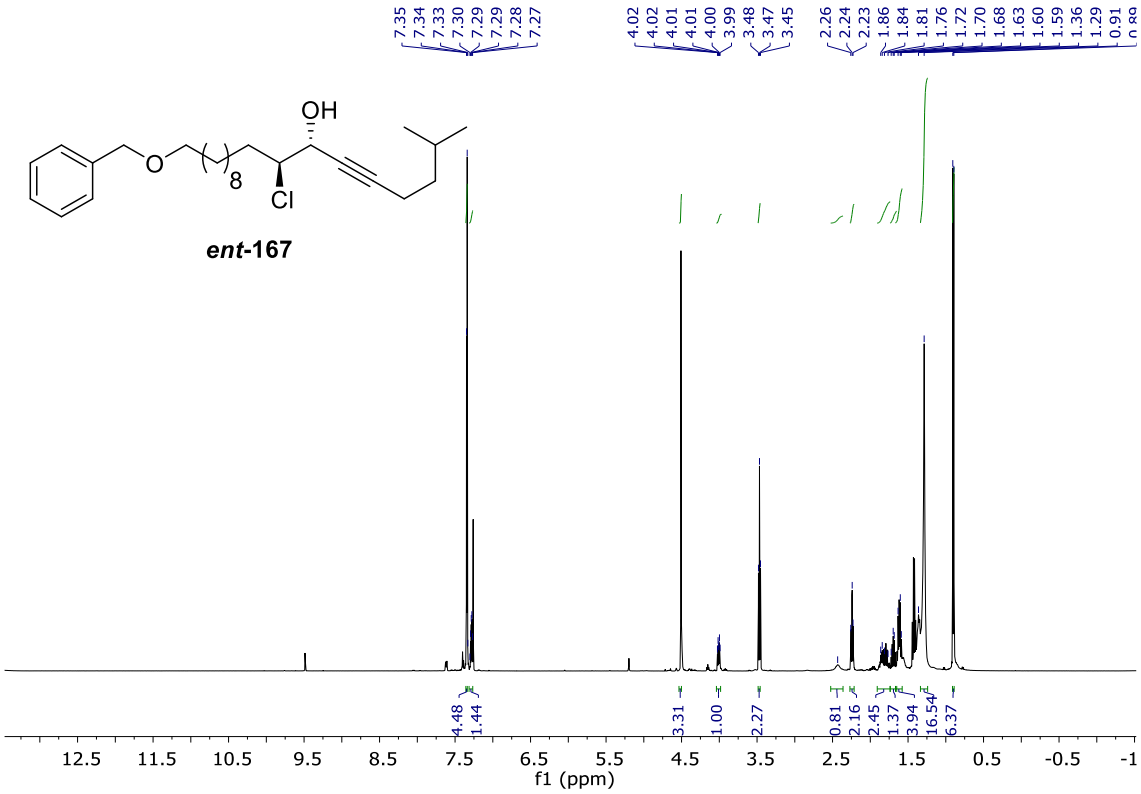
OH
O
8
Cl
ent-167
f1 (ppm)

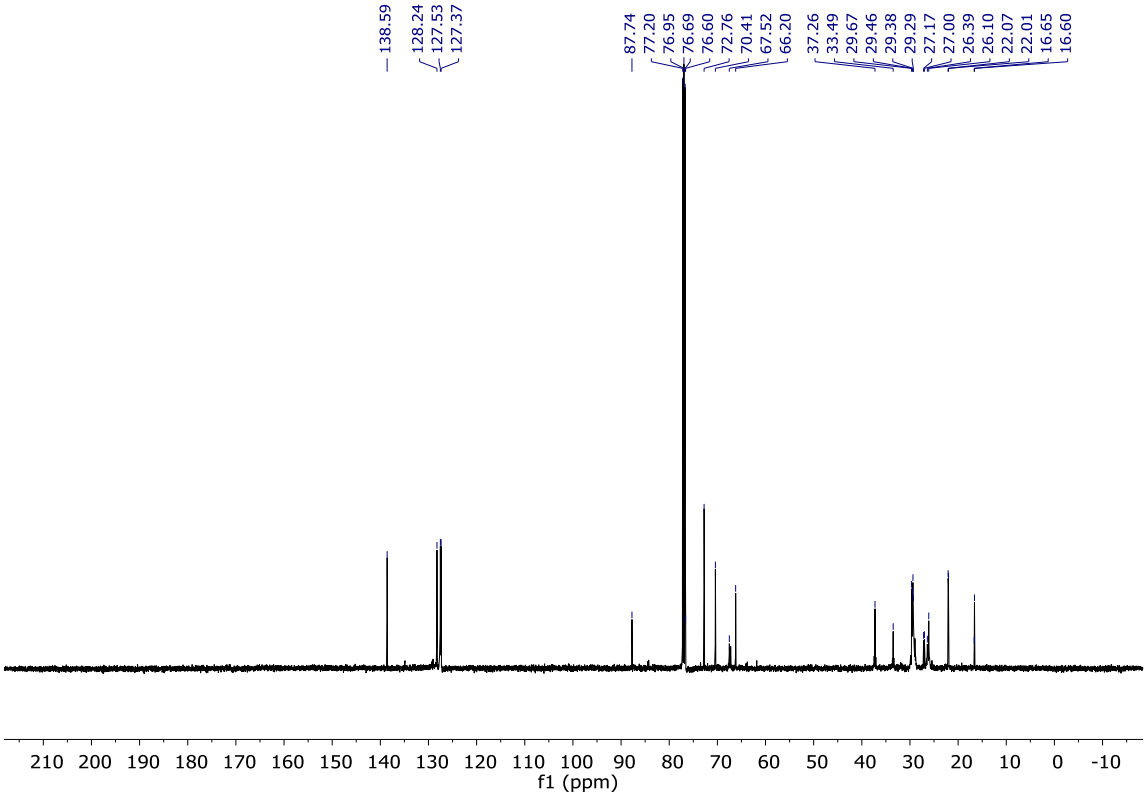
f1 (ppm)

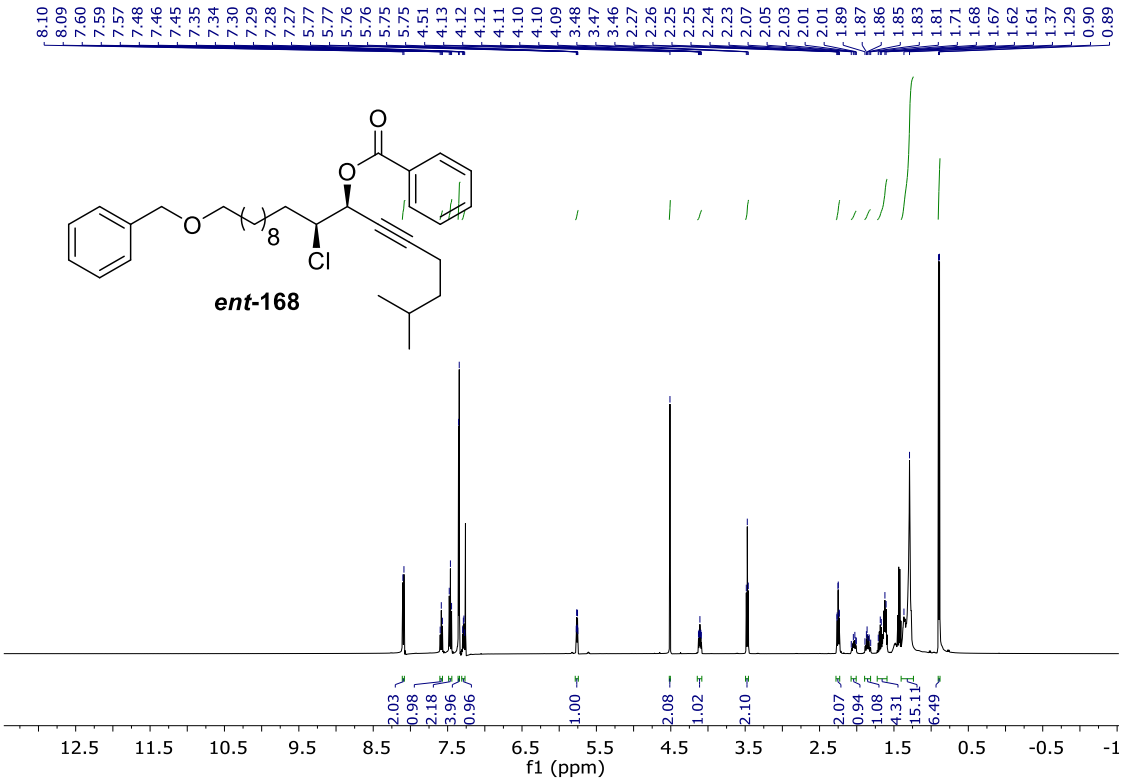
8.10 8.09 7.60 7.59 7.57 7.48 7.46 7.45 7.35 7.34 7.30 7.29 7.28 7.27 7.77 5.76 5.76 5.75 5.75 4.51 4.13 4.12 4.12 4.11 4.10 4.10 4.09 3.48 3.47 3.46 2.27 2.26 2.25 2.25 2.24 2.23 2.07 2.05 2.03 2.01 2.01 1.89 1.87 1.86 1.85 1.83 1.81 1.71 1.68 1.67 1.62 1.61 1.37 1.29 0.90 0.89
O
O
O
8
Cl
ent-168
2.03 0.98 2.18 3.96 0.96 1.00 2.08 1.02 2.10 2.07 0.94 1.08 4.31 15.11 6.49
12.5 11.5 10.5 9.5 8.5 7.5 6.5 5.5 4.5 3.5 2.5 1.5 0.5 -0.5 -1
f1 (ppm)

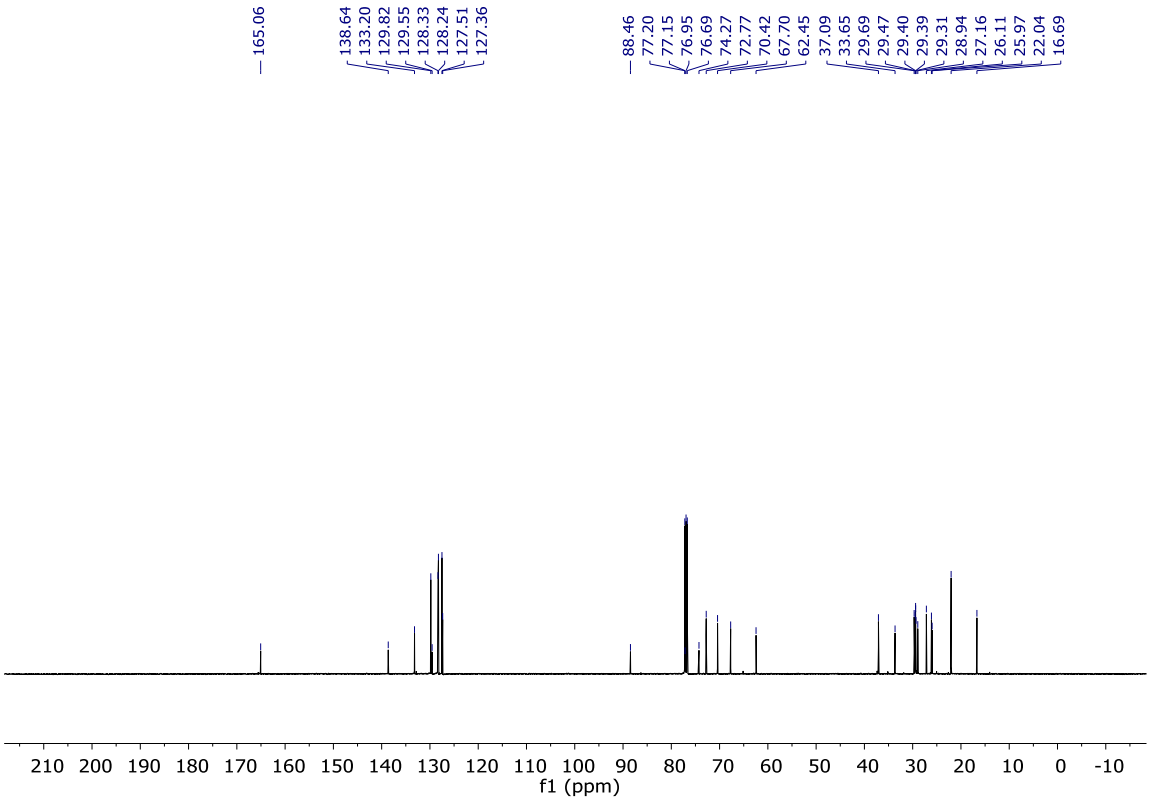
165.06
138.64 133.20 129.82 129.55 128.33 128.24 127.51 127.36
88.46 77.20 77.15 76.95 76.69 74.27 72.77 70.42 67.70 62.45 37.09 33.65 29.69 29.47 29.40 29.39 29.31 28.94 27.16 26.11 25.97 22.04 16.69
210 200 190 180 170 160 150 140 130 120 110 100 90 80 70 60 50 40 30 20 10 0 -10
f1 (ppm)

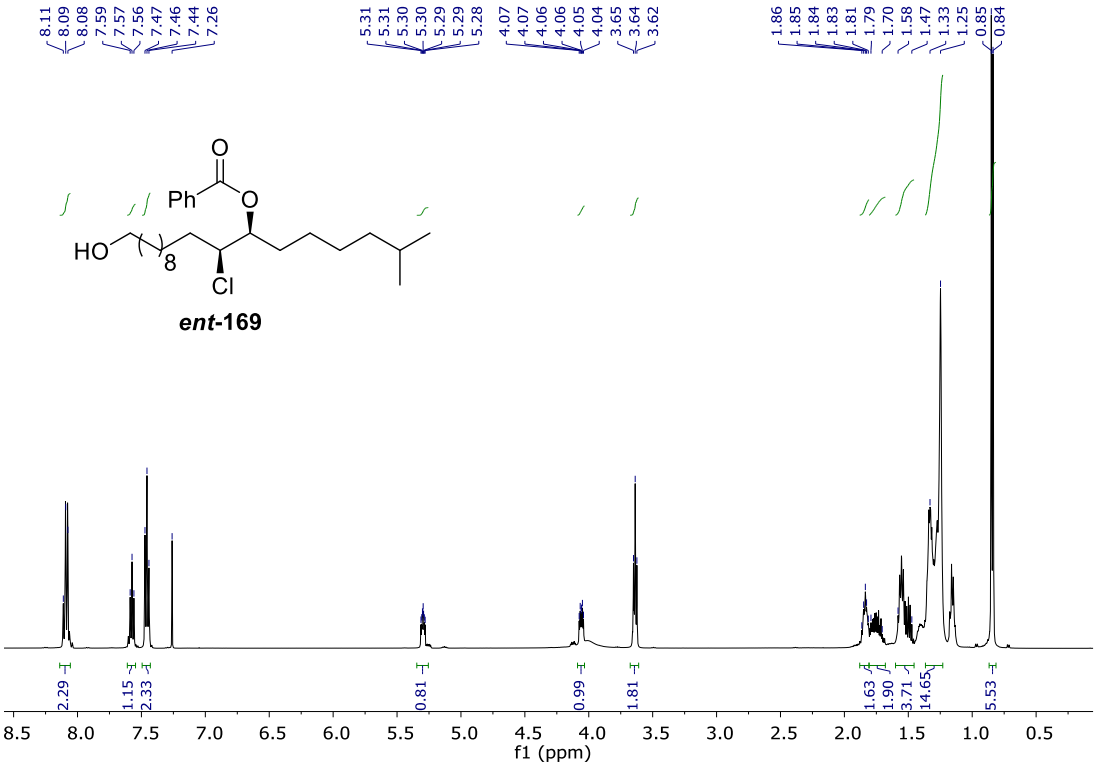
8.11
8.09
8.08
7.59
7.57
7.56
7.47
7.46
7.44
7.26
5.31
5.31
5.30
5.30
5.29
5.29
5.28
4.07
4.07
4.06
4.06
4.05
4.04
3.65
3.64
3.62
1.86
1.85
1.84
1.83
1.81
1.79
1.70
1.58
1.47
1.33
1.25
0.85
0.84
O
Ph
O
HO
8
Cl
2.29
1.15
2.33
0.81
0.99
1.81
1.63
1.90
3.71
14.65
5.53
8.5
8.0
7.5
7.0
6.5
6.0
5.5
5.0
4.5
4.0
3.5
3.0
2.5
2.0
1.5
1.0
0.5
f1 (ppm)

***ent*-169**

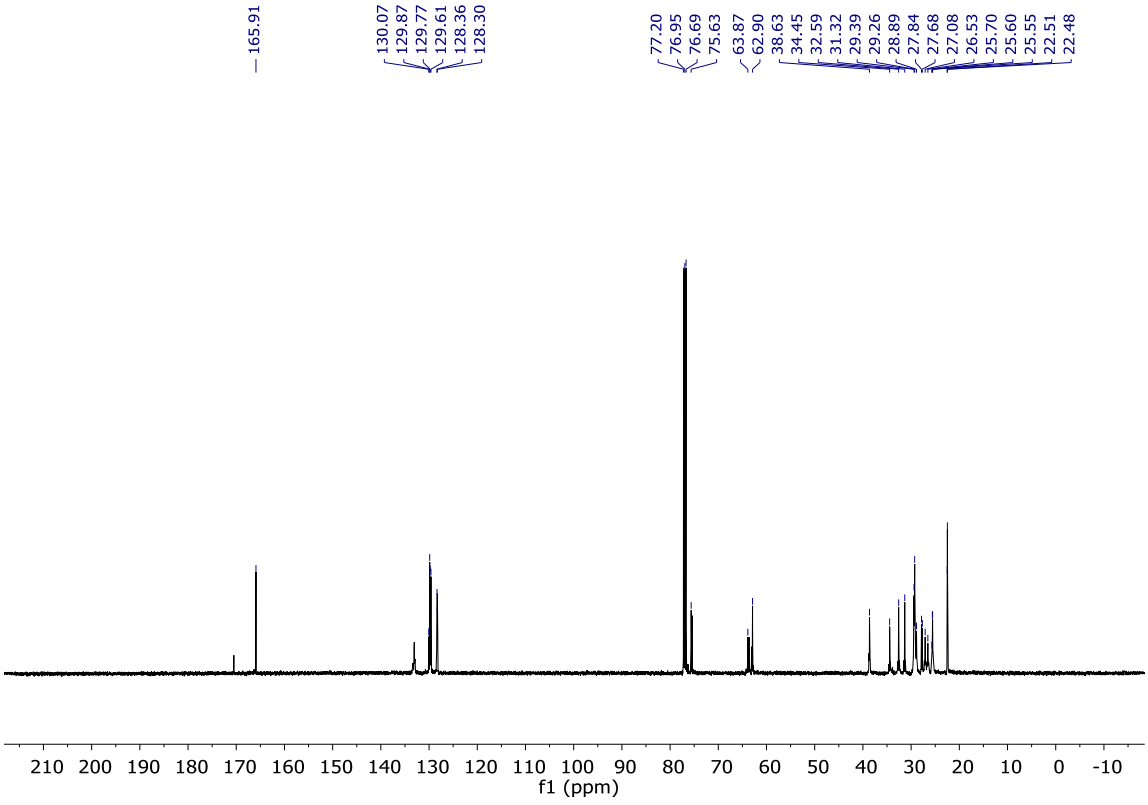
165.91
130.07
129.87
129.77
129.61
128.36
128.30
77.20
76.95
76.69
75.63
63.87
62.90
38.63
34.45
32.59
31.32
29.39
29.26
28.89
27.84
27.68
27.08
26.53
25.70
25.60
25.55
22.51
22.48
210
200
190
180
170
160
150
140
130
120
110
100
90
80
70
60
50
40
30
20
10
0
-10
f1 (ppm)

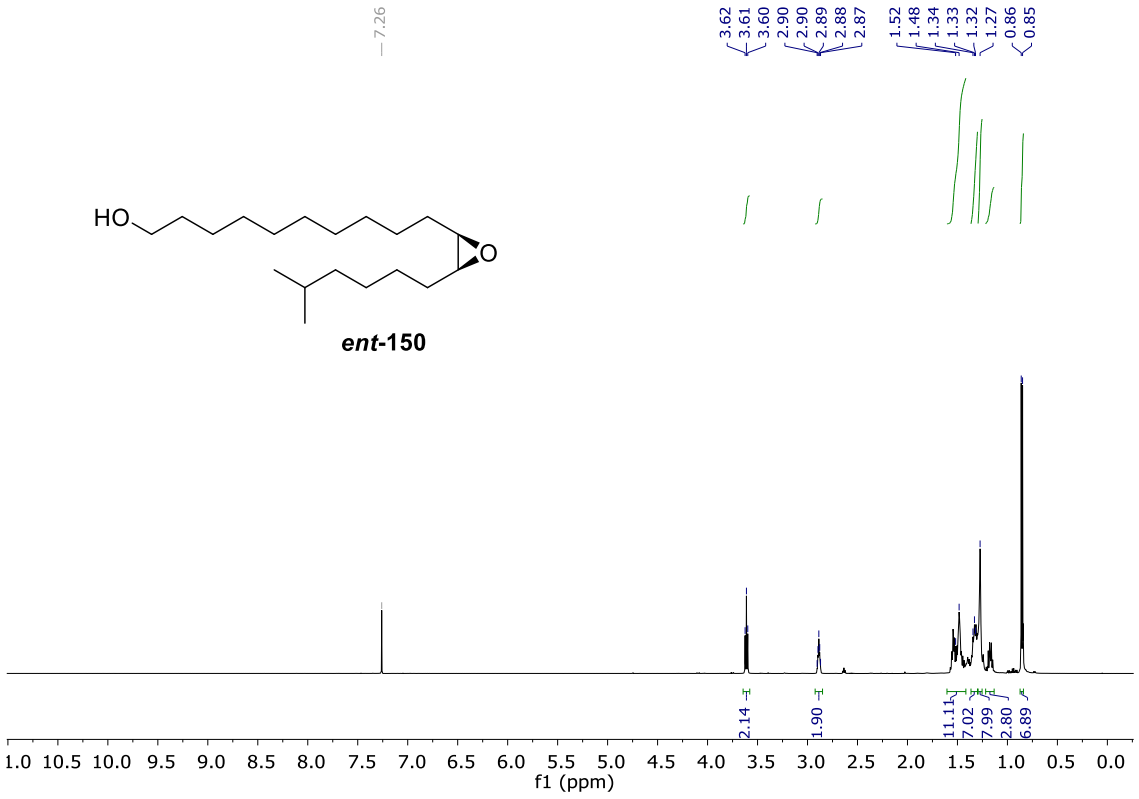
7.26
3.62
3.61
3.60
2.90
2.90
2.89
2.88
2.87
1.52
1.48
1.34
1.33
1.32
1.27
0.86
0.85
HO
O
2.14
1.90
11.11
7.02
7.99
2.80
6.89
1.0 10.5 10.0 9.5 9.0 8.5 8.0 7.5 7.0 6.5 6.0 5.5 5.0 4.5 4.0 3.5 3.0 2.5 2.0 1.5 1.0 0.5 0.0
f1 (ppm)

***ent*-150**

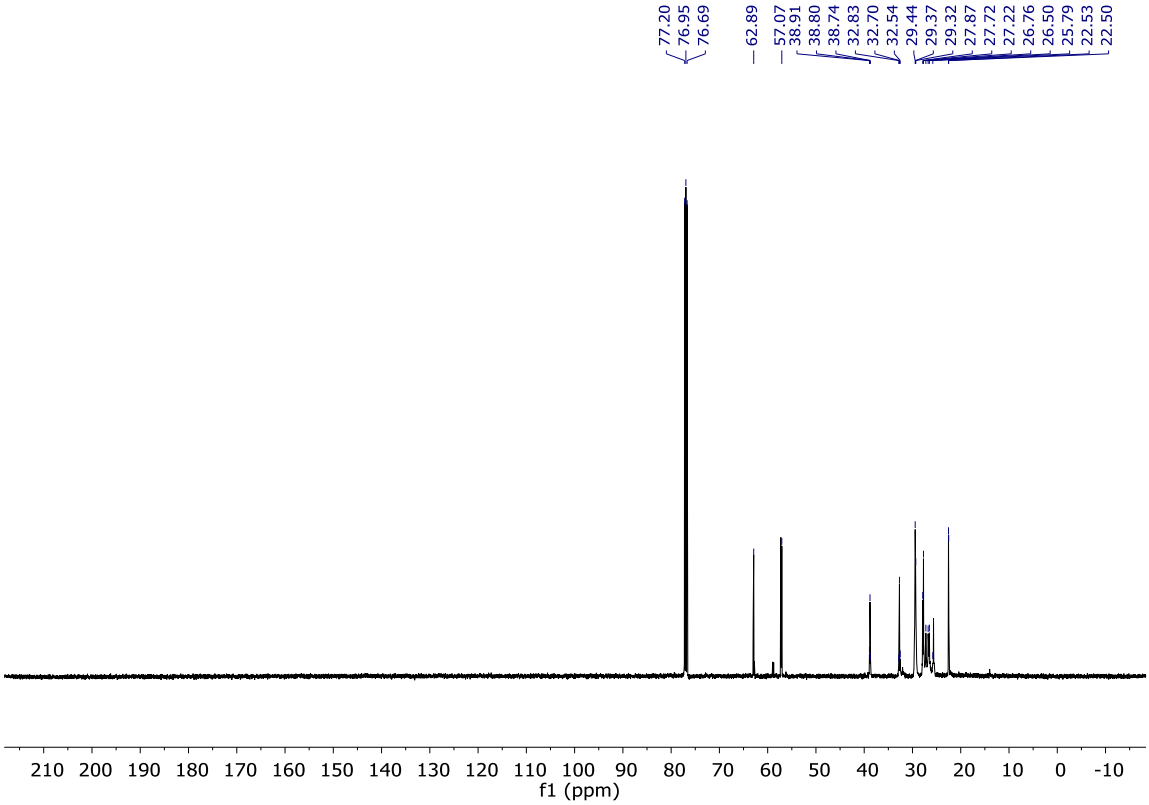
77.20
76.95
76.69
62.89
57.07
38.91
38.80
38.74
32.83
32.70
32.54
29.44
29.37
29.32
27.87
27.72
27.22
26.76
26.50
25.79
22.53
22.50
210 200 190 180 170 160 150 140 130 120 110 100 90 80 70 60 50 40 30 20 10 0 -10
f1 (ppm)

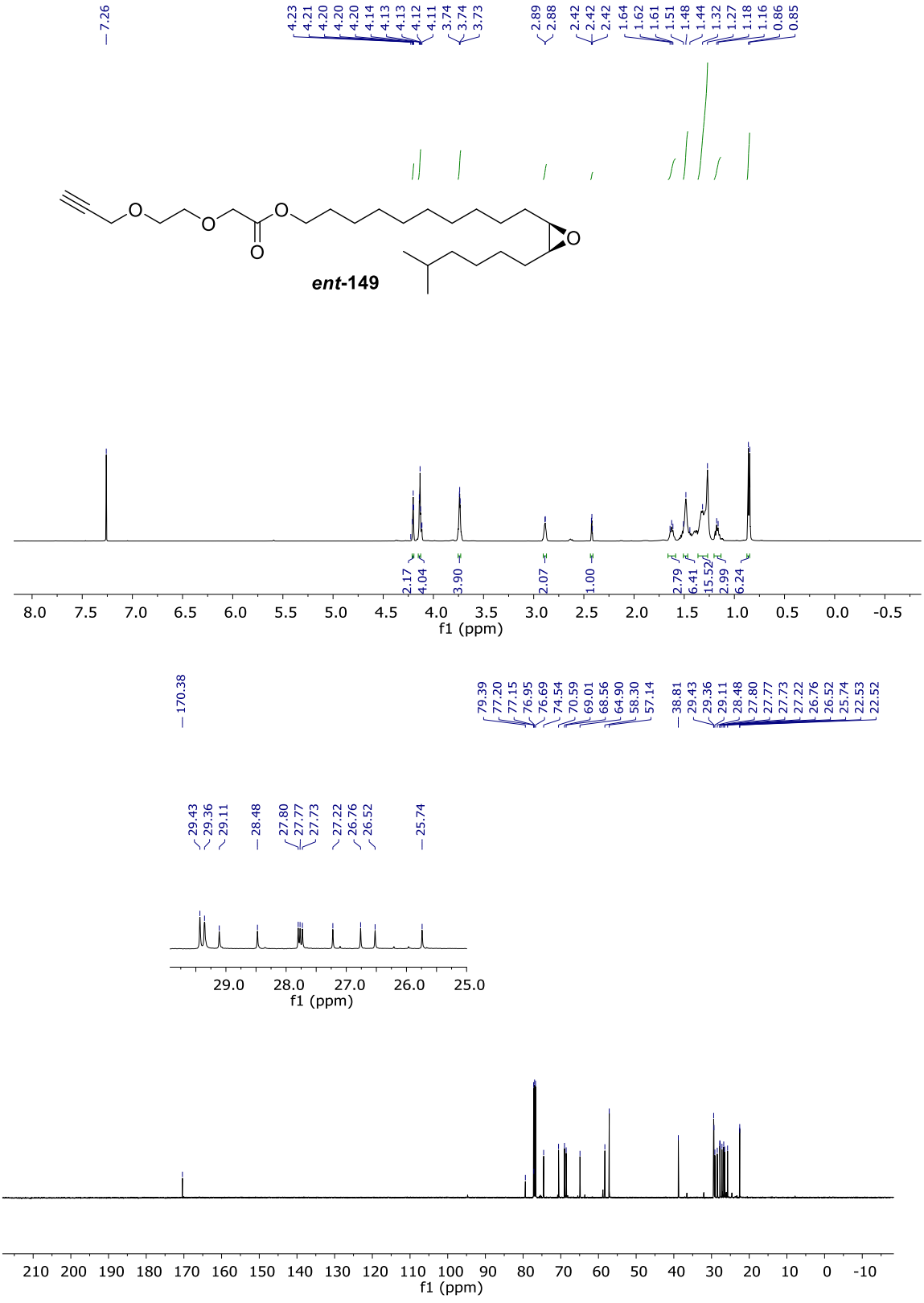
7.26
4.23
4.21
4.20
4.20
4.20
4.14
4.13
4.13
4.12
4.11
3.74
3.74
3.73
2.89
2.88
2.42
2.42
2.42
1.64
1.62
1.61
1.51
1.48
1.44
1.32
1.27
1.18
1.16
0.86
0.85
O
O
O
O
O
ent-149
2.17
4.04
3.90
2.07
1.00
2.79
6.41
15.52
2.99
6.24
8.0 7.5 7.0 6.5 6.0 5.5 5.0 4.5 4.0 3.5 3.0 2.5 2.0 1.5 1.0 0.5 0.0 -0.5
f1 (ppm)
170.38
79.39
77.20
77.15
76.95
76.69
74.54
70.59
69.01
68.56
64.90
58.30
57.14
38.81
29.43
29.36
29.11
28.48
27.80
27.77
27.73
27.22
26.76
26.52
25.74
22.53
22.52
29.43
29.36
29.11
28.48
27.80
27.77
27.73
27.22
26.76
26.52
25.74
29.0 28.0 27.0 26.0 25.0
f1 (ppm)
210 200 190 180 170 160 150 140 130 120 110 100 90 80 70 60 50 40 30 20 10 0 -10
f1 (ppm)

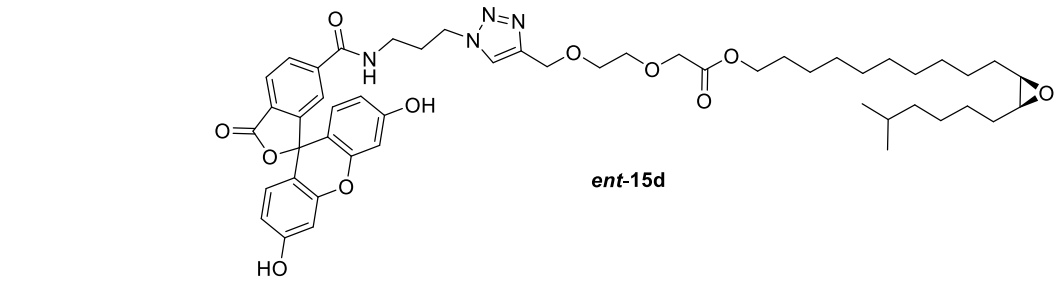

***ent*-15d**

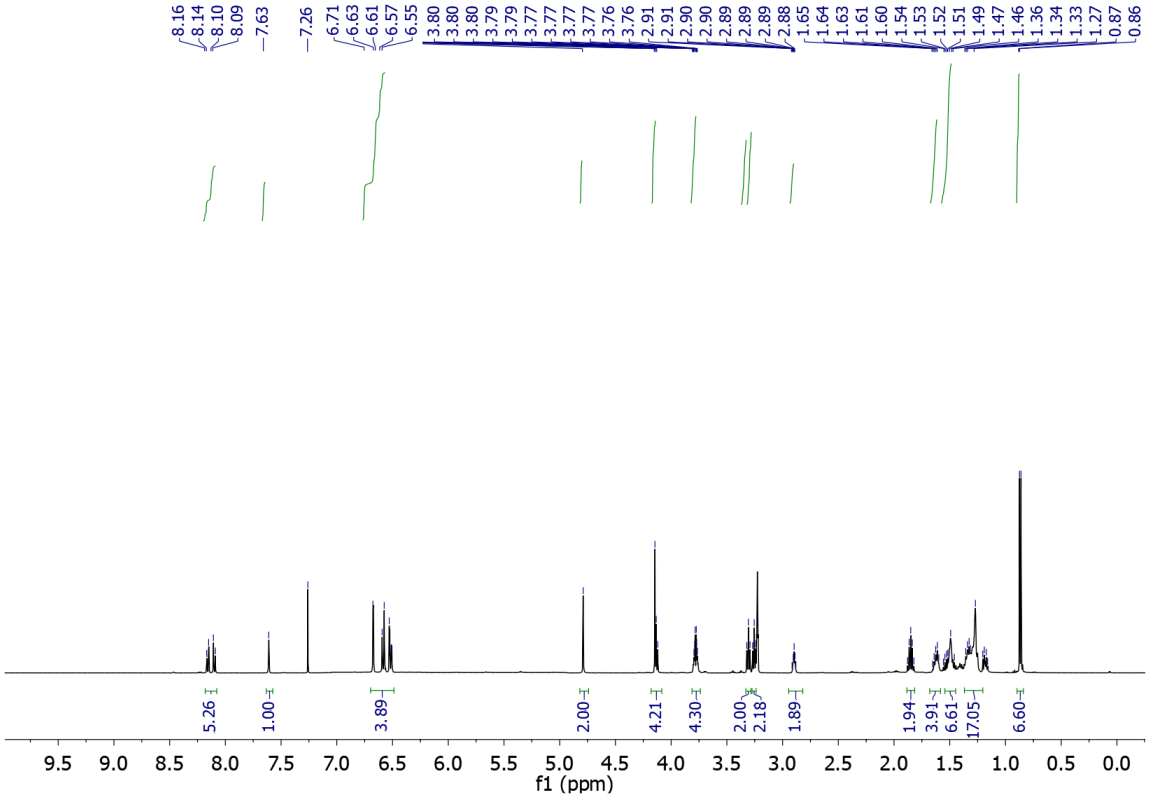
8.16
8.14
8.10
8.09
7.63
7.26
6.71
6.63
6.61
6.57
6.55
3.80
3.80
3.80
3.79
3.79
3.77
3.77
3.77
3.77
3.76
3.76
2.91
2.91
2.90
2.90
2.89
2.89
2.89
2.88
1.65
1.64
1.63
1.61
1.60
1.54
1.53
1.52
1.51
1.49
1.47
1.46
1.36
1.34
1.33
1.27
0.87
0.86
5.26
1.00
3.89
2.00
4.21
4.30
2.00
2.18
1.89
1.94
3.91
6.61
17.05
6.60
9.5 9.0 8.5 8.0 7.5 7.0 6.5 6.0 5.5 5.0 4.5 4.0 3.5 3.0 2.5 2.0 1.5 1.0 0.5 0.0
f1 (ppm)

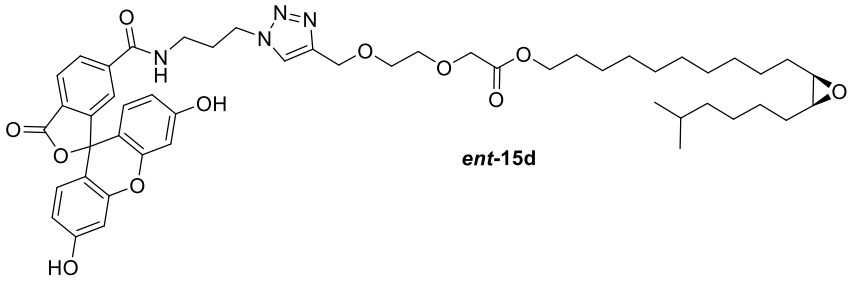

***ent*-15d**

Chromatogram and Spectrum

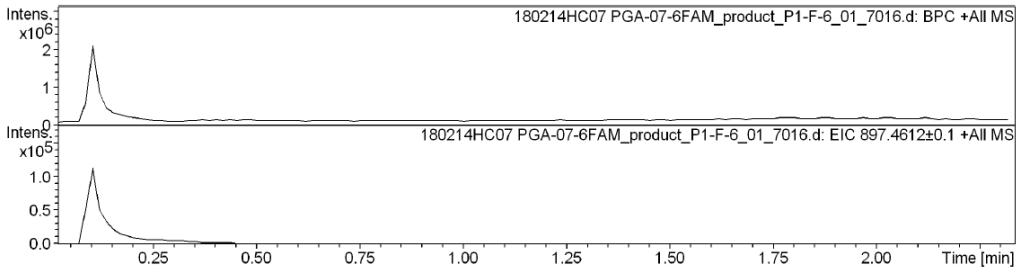

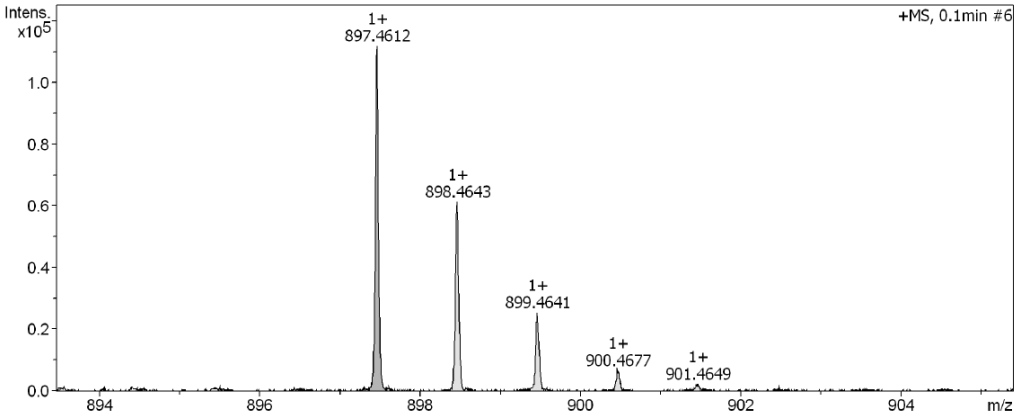

Formula Confirmation

Meas. m/z	#	Ion Formula	Score	m/z	err [mDa]	err [ppm]	mSigma	rdb	e⁻ Conf	N-Rule	Adduct
897.461236	1	C50H65N4O11	100.00	897.464435	-3.2	-3.6	25.1	20.5	even	ok	M+H

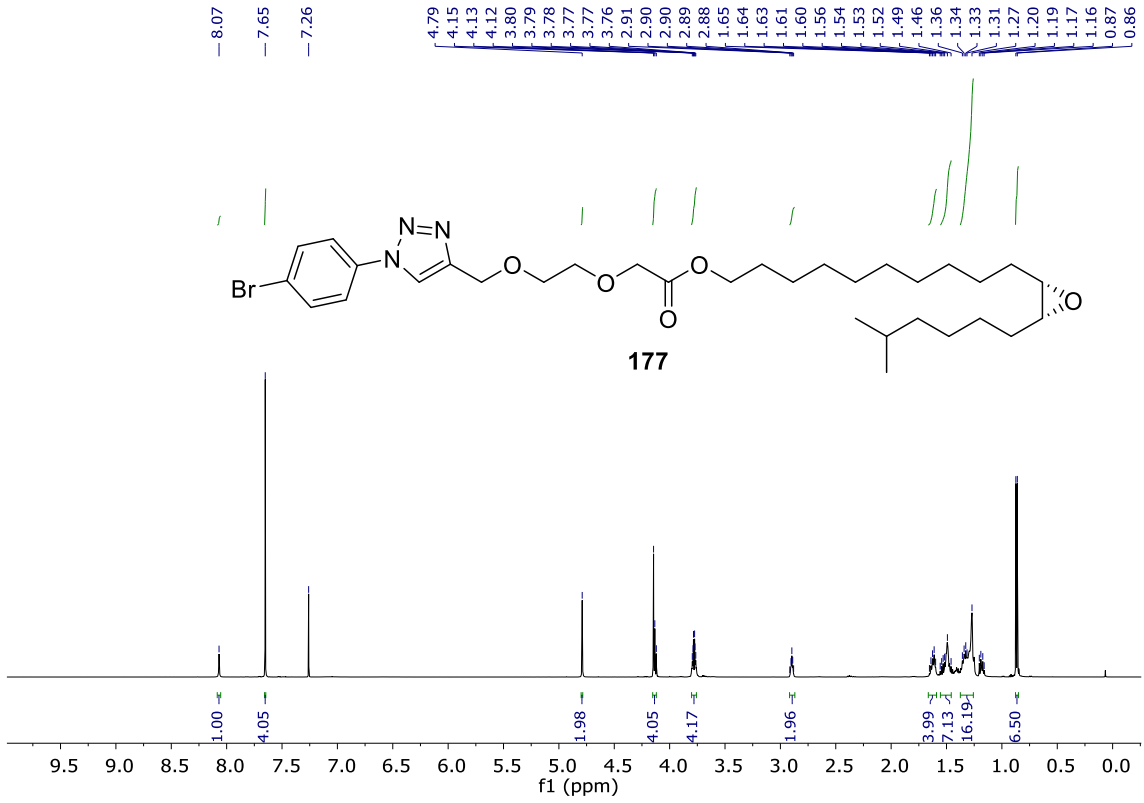
8.07
7.65
7.26
4.79
4.15
4.13
4.12
3.80
3.79
3.78
3.77
3.77
3.76
2.91
2.90
2.90
2.89
2.88
1.65
1.64
1.63
1.61
1.60
1.56
1.54
1.53
1.52
1.49
1.46
1.36
1.34
1.33
1.31
1.27
1.20
1.19
1.17
1.16
0.87
0.86
N=N
N
Br
O
O
O
O
O
1.00
4.05
1.98
4.05
4.17
1.96
3.99
7.13
16.19
6.50
f1 (ppm)

177

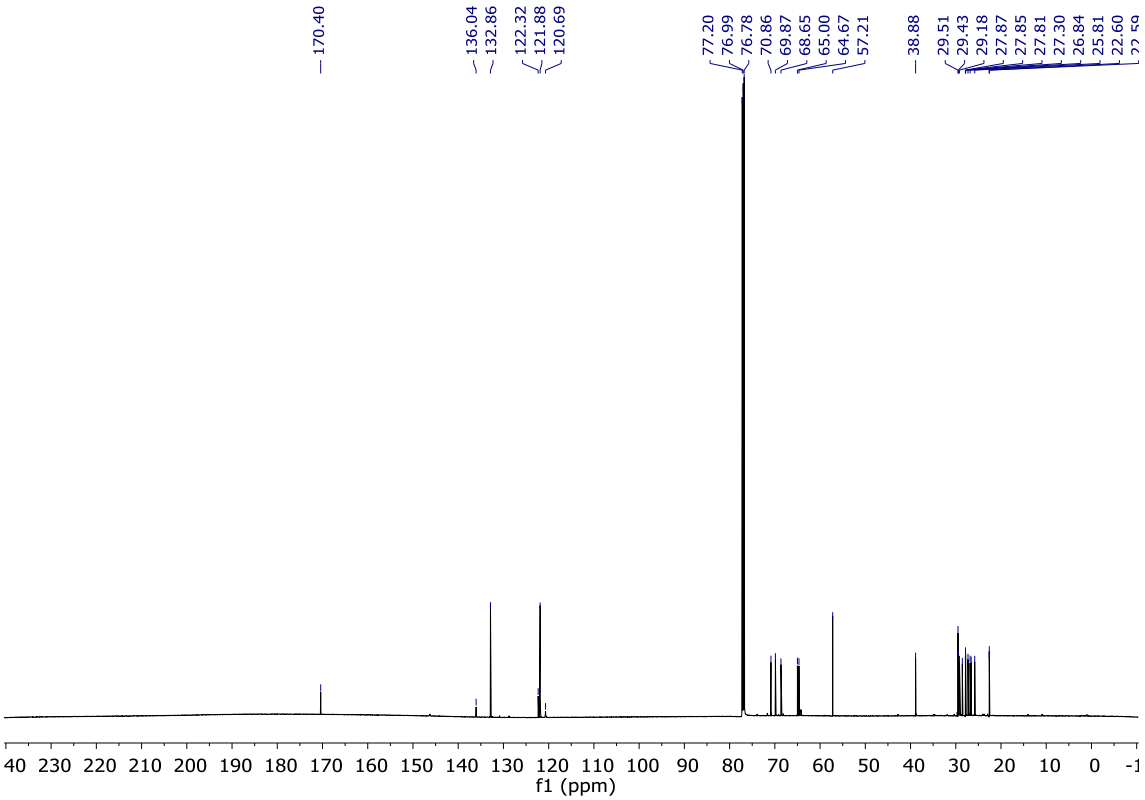
170.40
136.04
132.86
122.32
121.88
120.69
77.20
76.99
76.78
70.86
69.87
68.65
65.00
64.67
57.21
38.88
29.51
29.43
29.18
27.87
27.85
27.81
27.30
26.84
25.81
22.60
f1 (ppm)

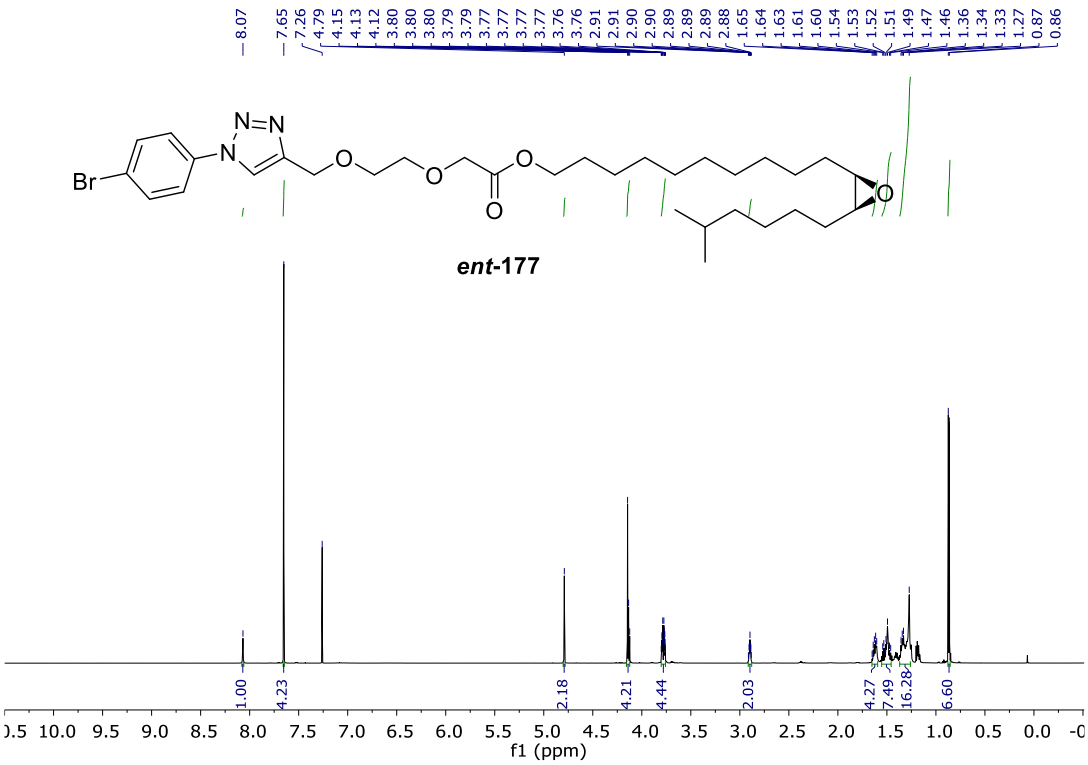
8.07
7.65
7.26
4.79
4.15
4.13
4.12
3.80
3.80
3.80
3.79
3.79
3.77
3.77
3.77
3.77
3.76
3.76
2.91
2.91
2.90
2.90
2.89
2.89
2.89
2.88
1.65
1.64
1.63
1.61
1.60
1.54
1.53
1.52
1.51
1.49
1.47
1.46
1.36
1.34
1.33
1.27
0.87
0.86
N=N
N
Br
O
O
O
O
O
1.00
4.23
2.18
4.21
4.44
2.03
4.27
7.49
16.28
6.60
f1 (ppm)

***ent*-177**

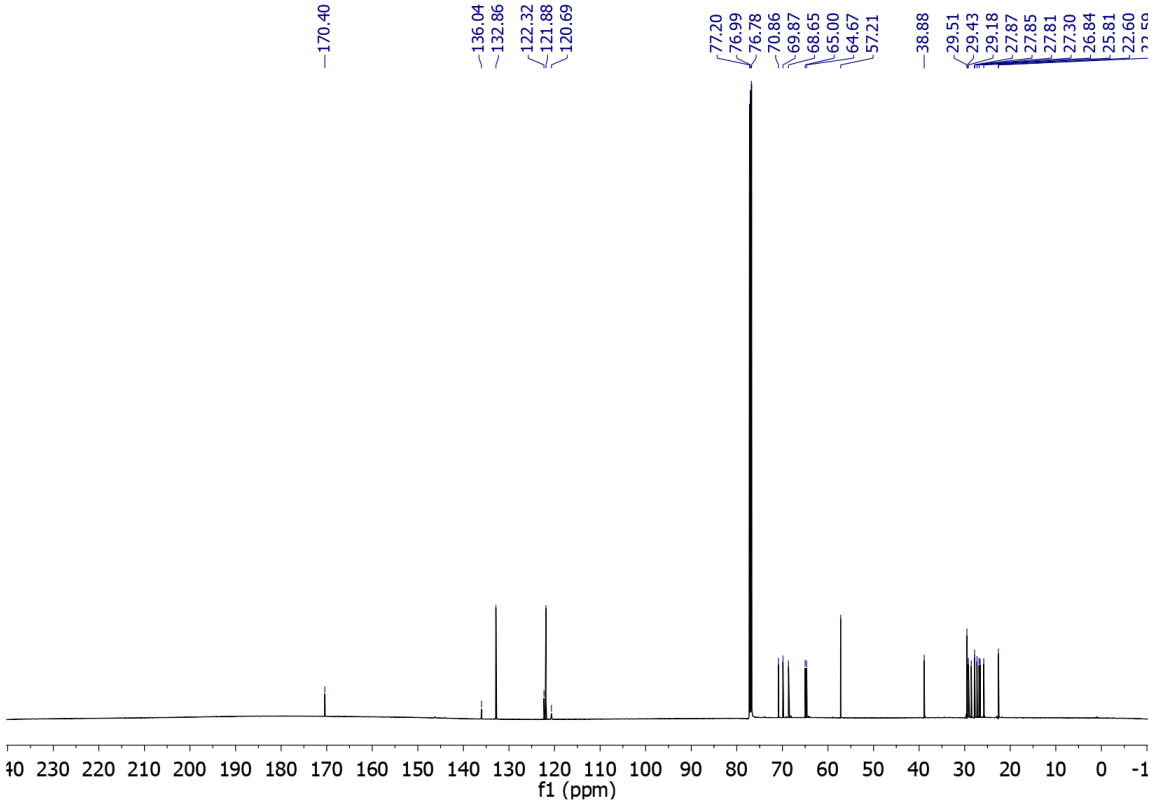
170.40
136.04
132.86
122.32
121.88
120.69
77.20
76.99
76.78
70.86
69.87
68.65
65.00
64.67
57.21
38.88
29.51
29.43
29.18
27.87
27.85
27.81
27.30
26.84
25.81
22.60
f1 (ppm)

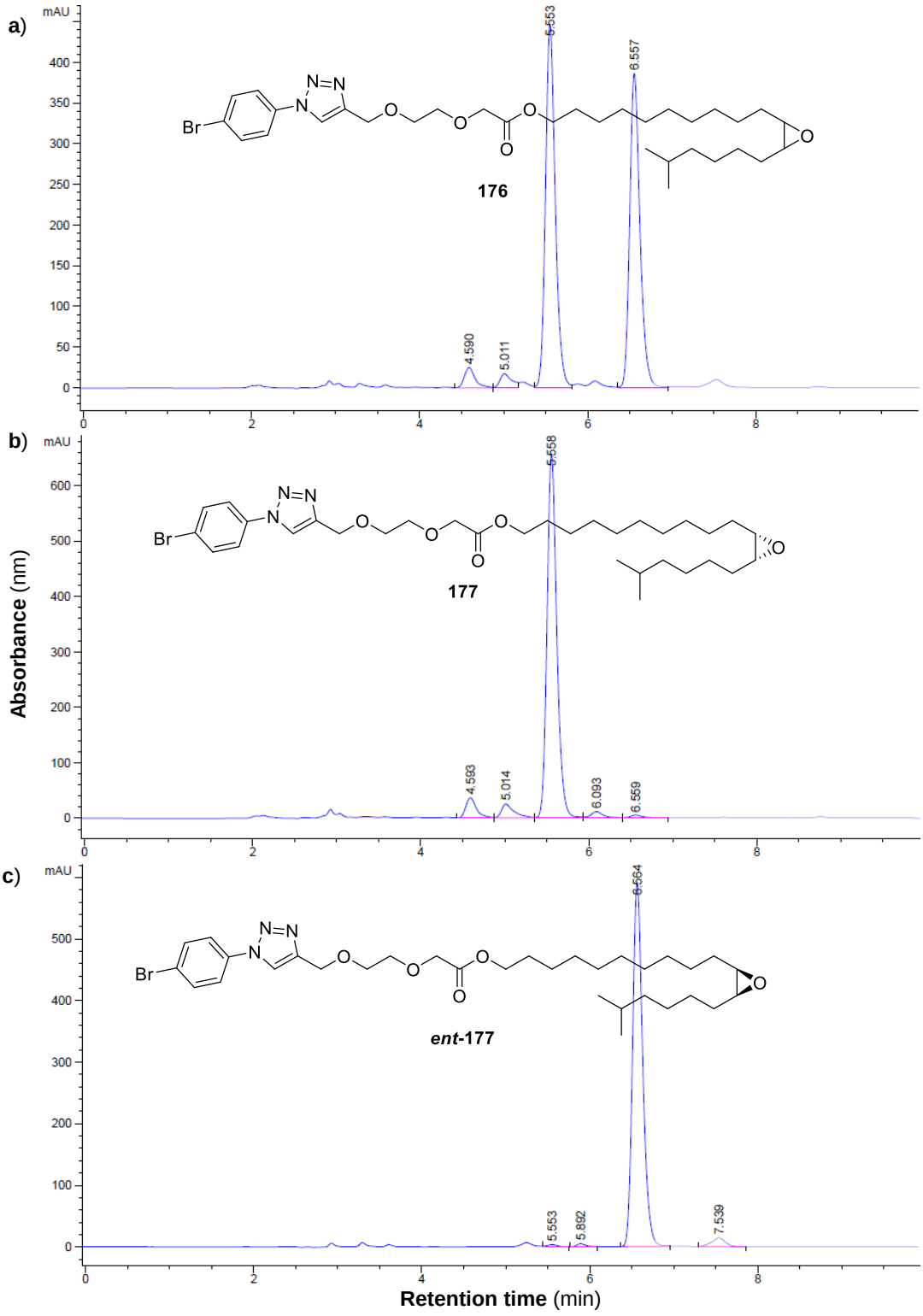

Appendix C1.HPLC chromatogram showing separation of a) nearly racemic cis epoxy triazole b) (*R*, *S*)-enantiomer 177 c) (*S*, *R*)-enantiomer *ent*-177 using CHIRALPAK-D chiral HPLC column

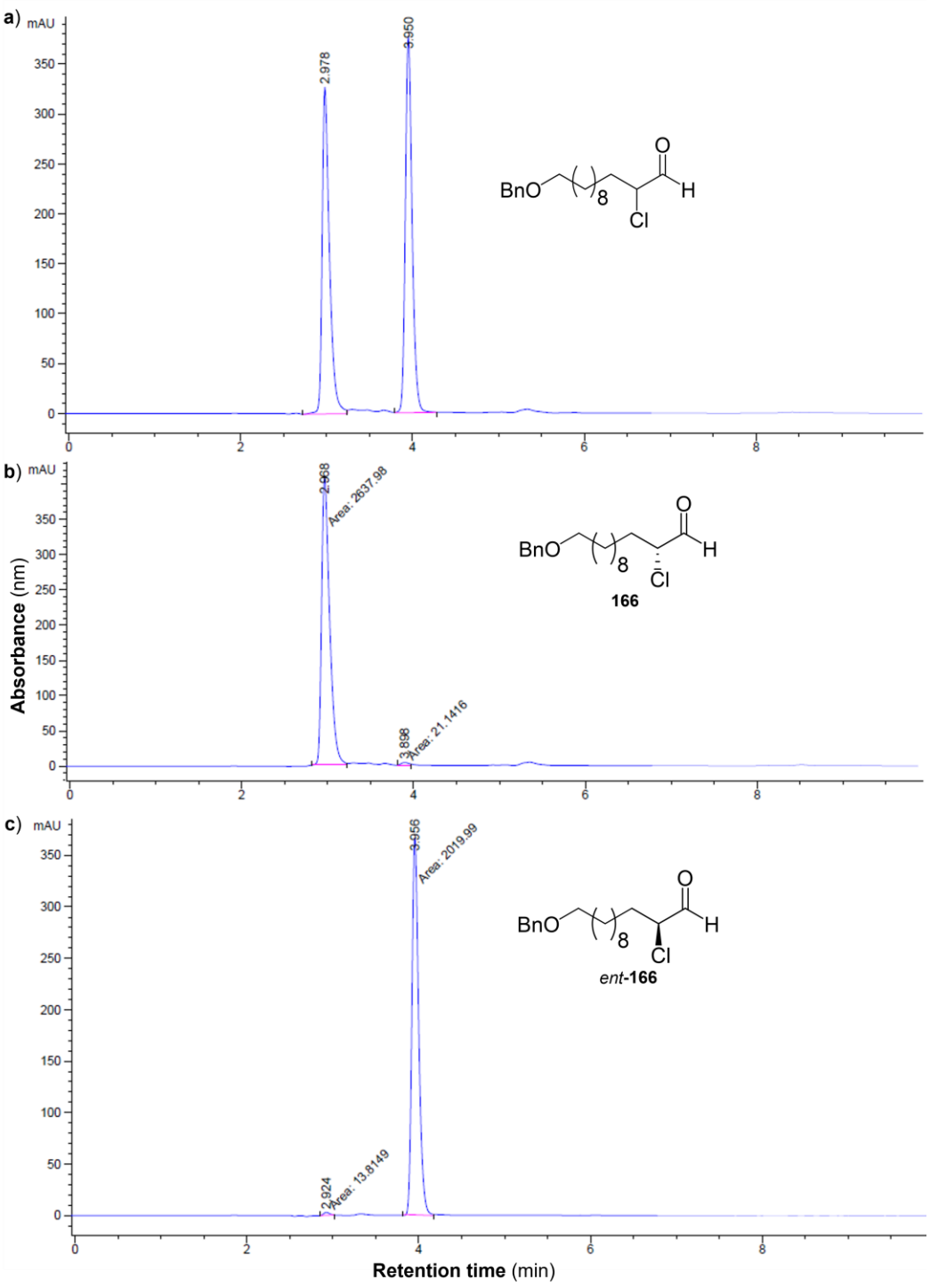

Appendix C2.High-performance liquid chromatograph a) Separation of nearly racemic α-chloroaldehyde by chiral HPLC column. b) & c) Elution of (*R*) and (*S*)-enantiomers at 2.668 min and 3.956 min respectively

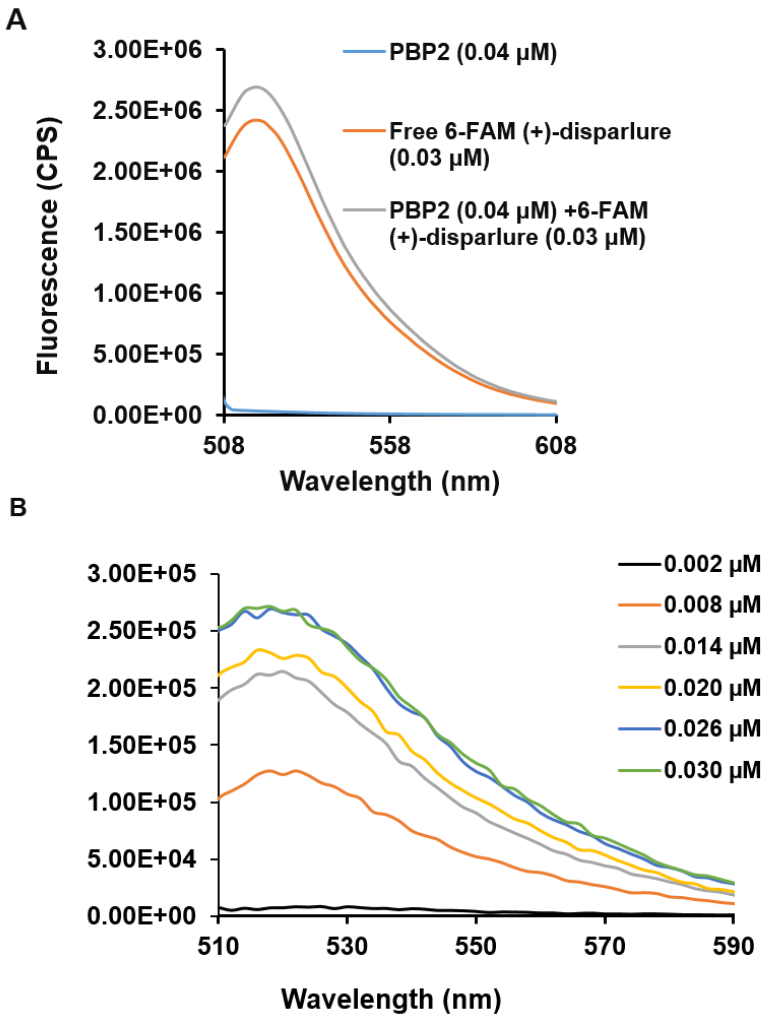

Appendix C3. A) 6-FAM (+)-disparlure 15d emission spectra. 15d bound to *Ldis*PBP2 was excited at 494 nm and its emission spectra (grey trace) was recorded. B) Fluorescence emission spectra were recorded with increasing doses of 6-FAM (+)-disparlure 15d

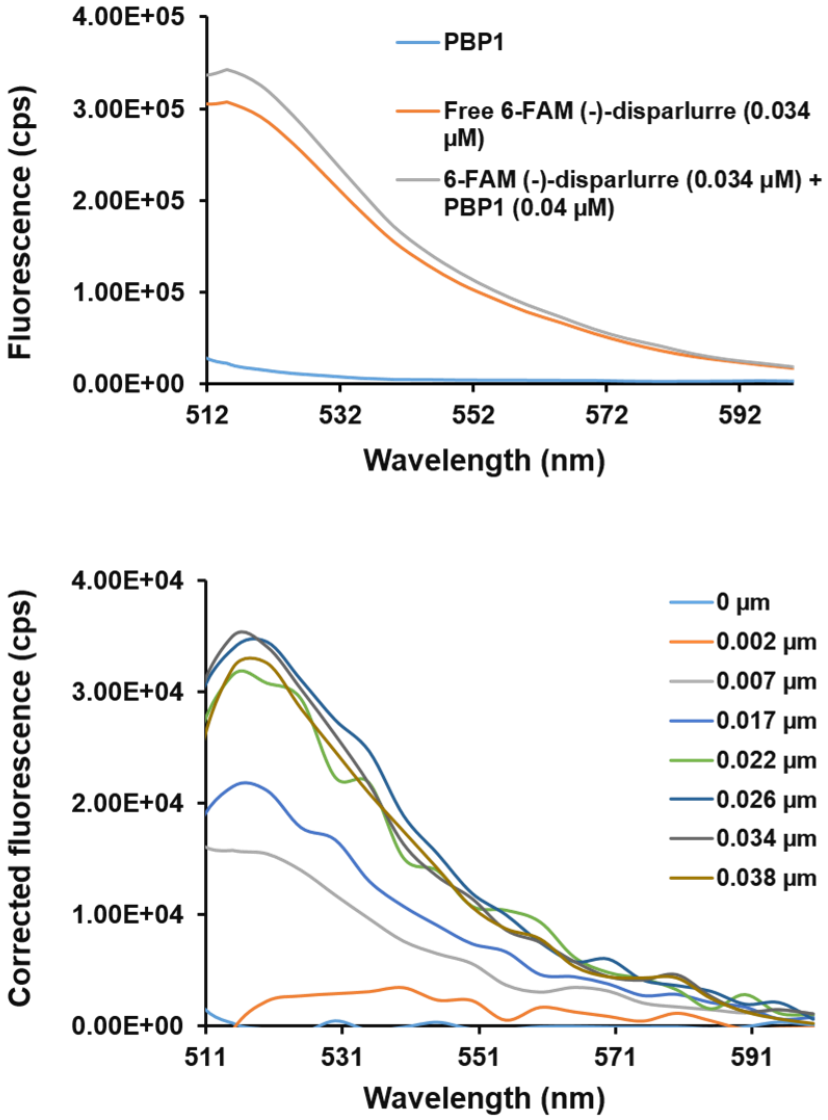

Appendix C4. A) 6-FAM (-)-disparlure *ent*-15d emission spectra. *ent*-15d bound to *Ldis*PBP1 was excited at 494 nm and its emission spectra (gray trace) was recorded. B) Fluorescence emission spectra were recorded with increasing doses of 6-FAM (-)-disparlure *ent*-15d

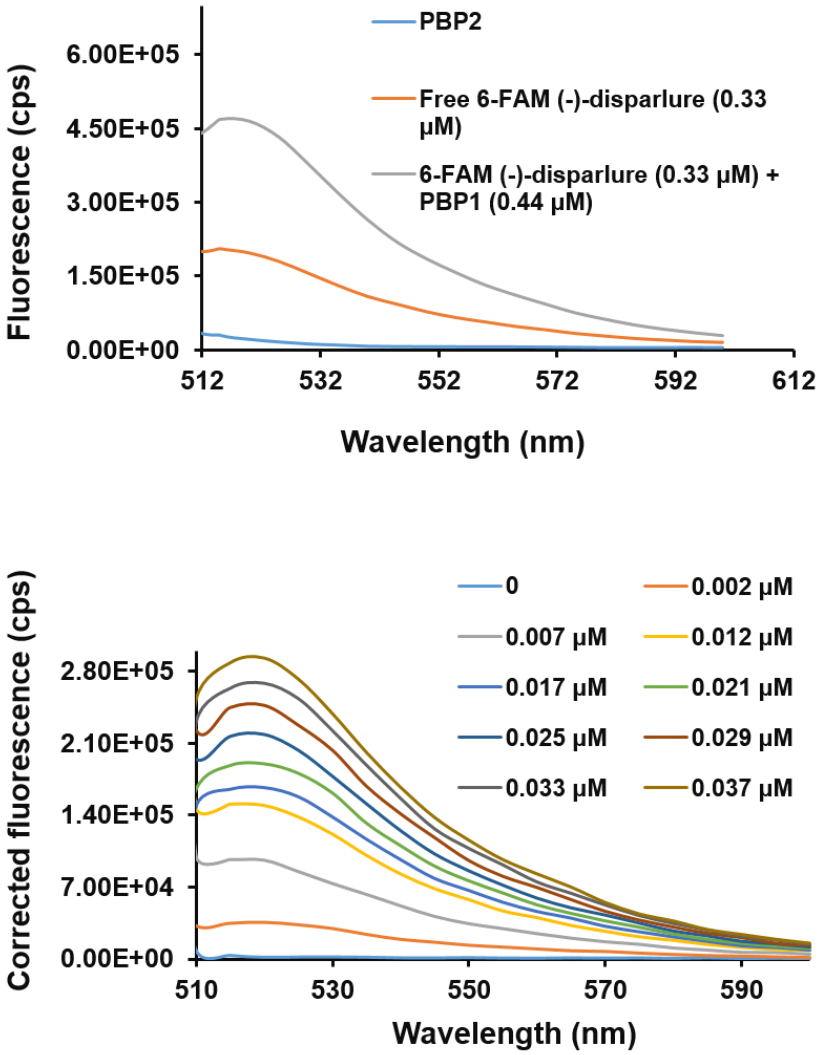

Appendix C5. A) 6-FAM (-)-disparlure *ent*-15d emission spectra. *ent*-15d bound to *Ldis*PBP2 was excited at 494 nm and its emission spectra (gray trace) was recorded. B) Fluorescence emission spectra were recorded with increasing doses of 6-FAM (-)-disparlure *ent*-15d

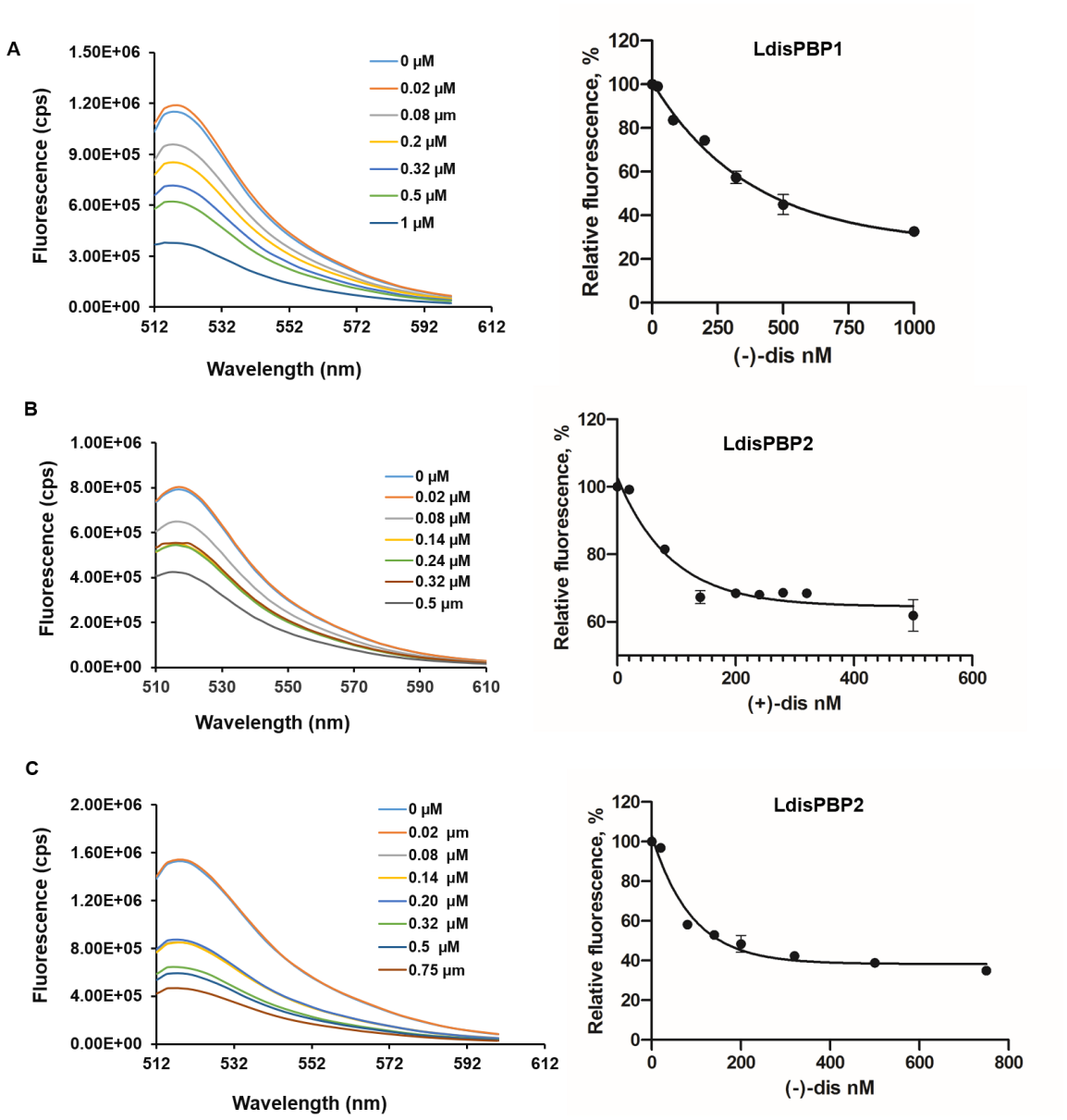

Appendix C6. Competition of fluorescent disparlure enantiomers binding to *Ldis*PBP1 and *Ldis*PBP2 by disparlure enantiomers. A) The decrease of 6-FAM (-)-disparlure/*Ldis*PBP1 fluorescence emission intensity at maximum (520 nm) at increasing concentrations of competitor (-)-disparlure. B) &C) The decrease of 6-FAM (+)-disparlure/*Ldis*PBP2 and 6-FAM (-)-disparlure/*Ldis*PBP2 fluorescene intensity at increasing concentrations of (+)-disparlure and (-)-disparlure, respectively

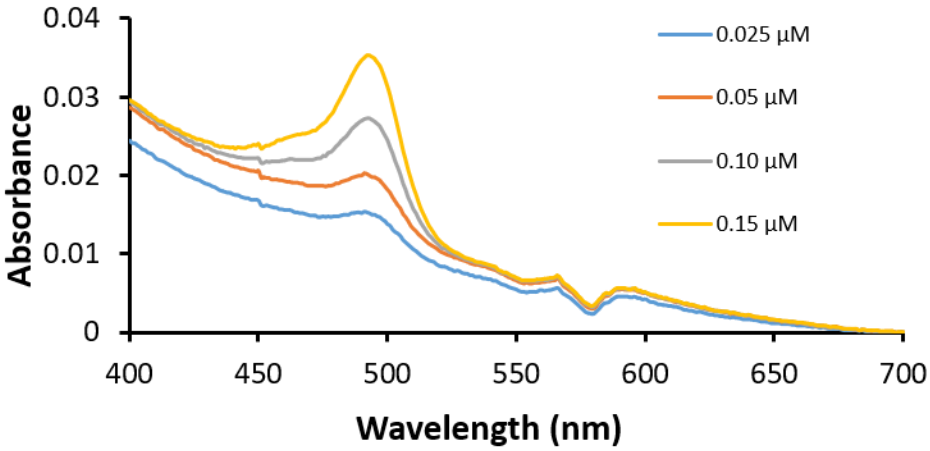

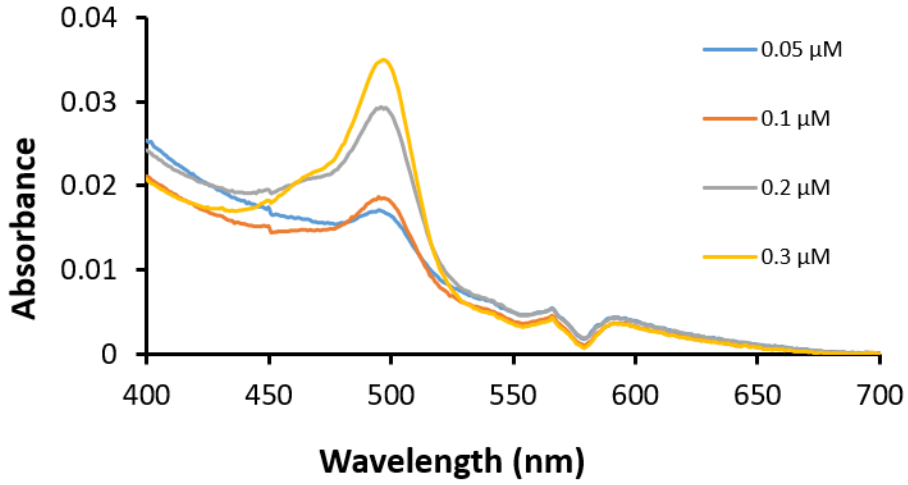

Appendix C7. Absorbance specta of 6-FAM azide (top) and 6-FAM (+)-disparlure 15d (bottom) samples with varying concentartions.

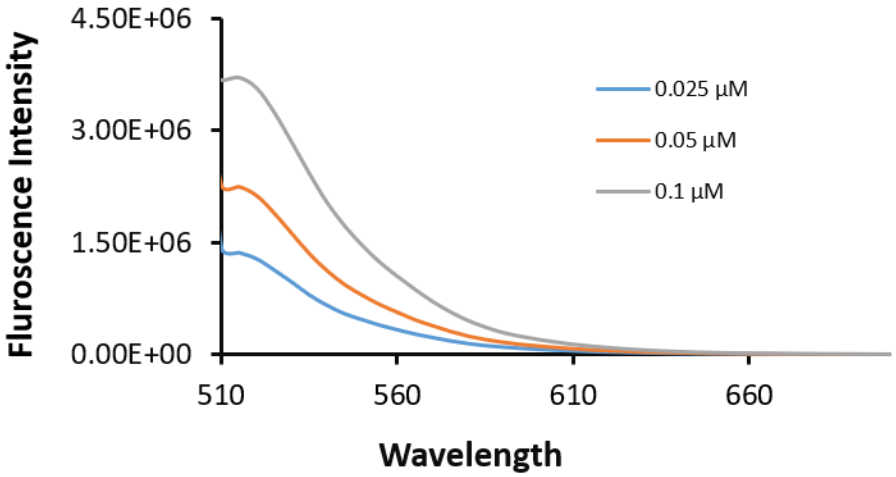

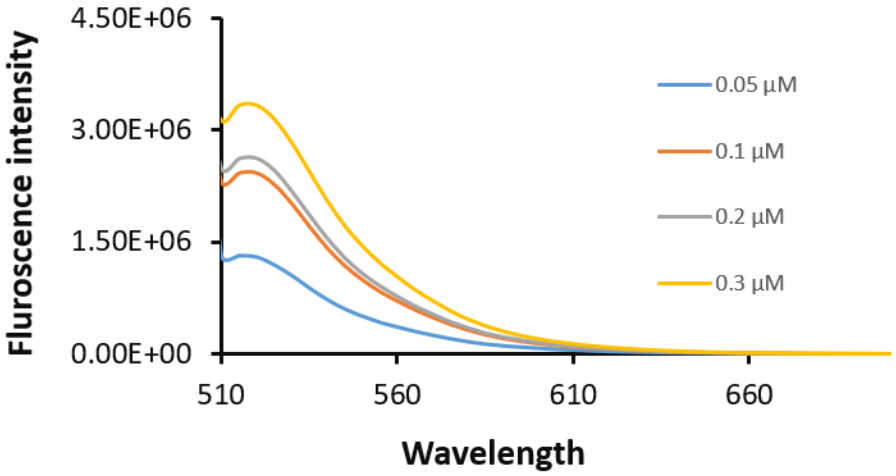

Appendix C8. Fluorescence emission specta of 6-FAM azide (top) and 6-FAM (+)-disparlure 15d (bottom) samples with varying concentartions.

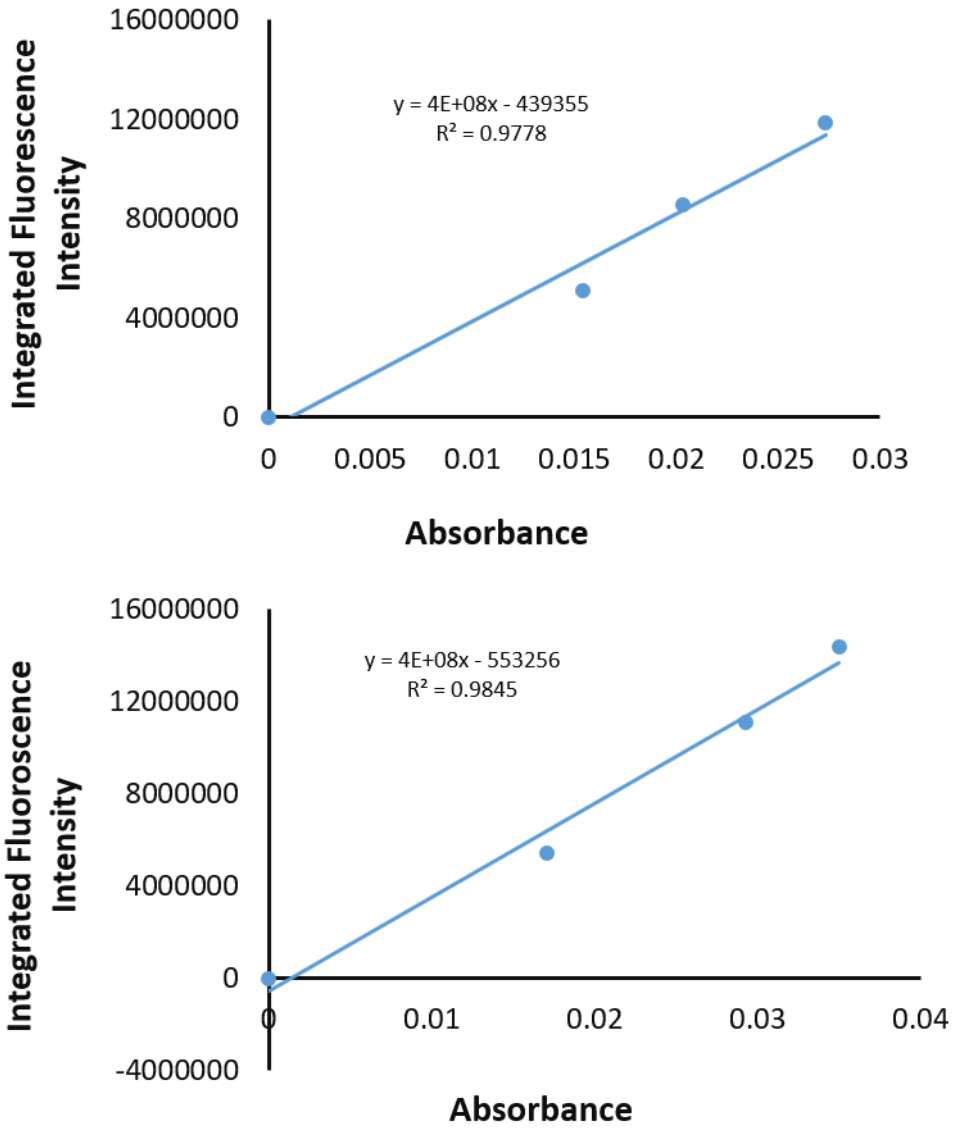

Appendix C9. Plots of integrated fluorescence intensity (area) vs absorbance for 6-FAM azide (top) and 6-FAM (+)-disparlure 15d (bottom).

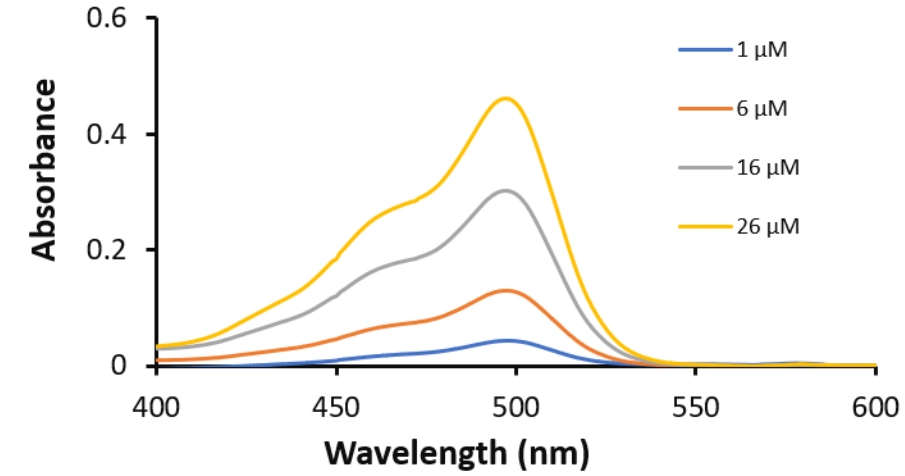

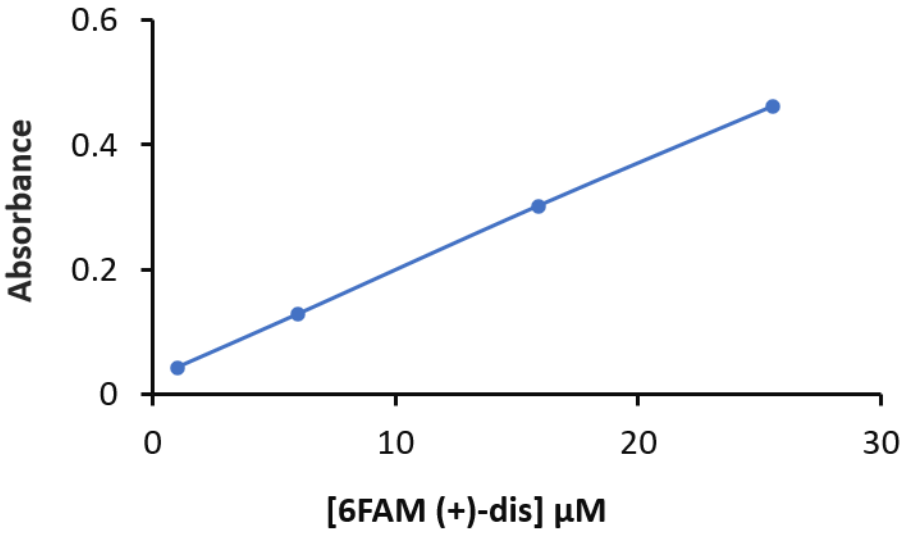

Appendix C10. Absorbance specta of 6-FAM (+)-disparlure 15d with varying concentartions (top) plot of absorbance against concentartion of 6-FAM (+)-disparlure 15d.

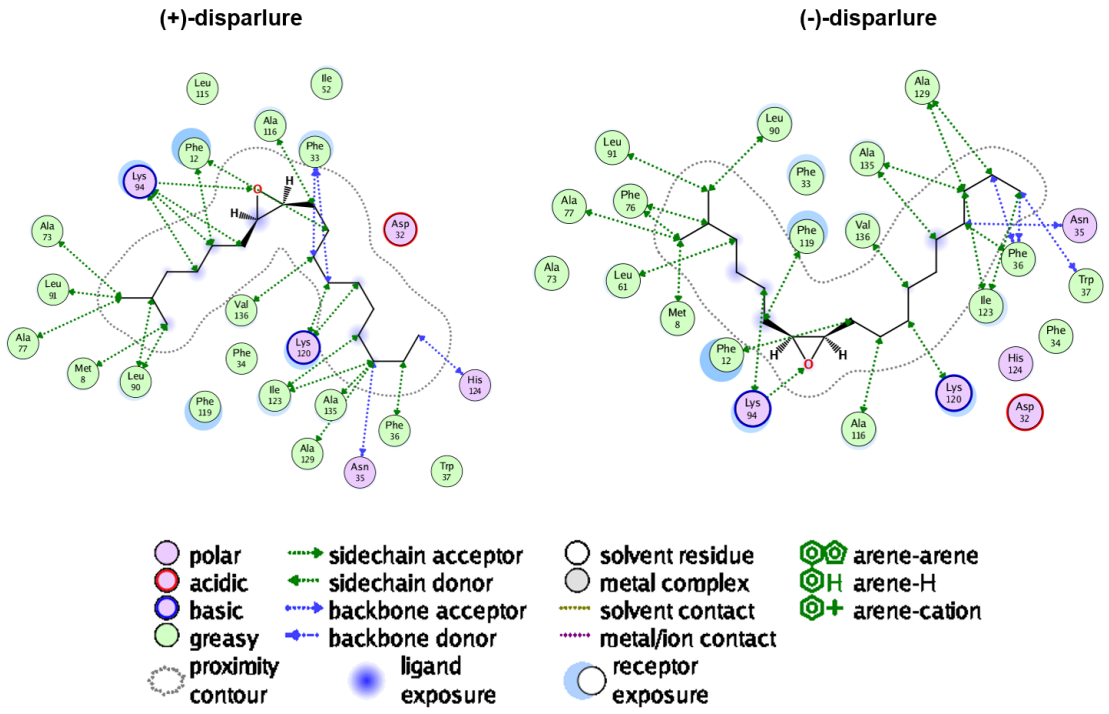

Appendix C11. *Ldis*PBP1-(+)-disparlure and (-)-disparlure interactions map

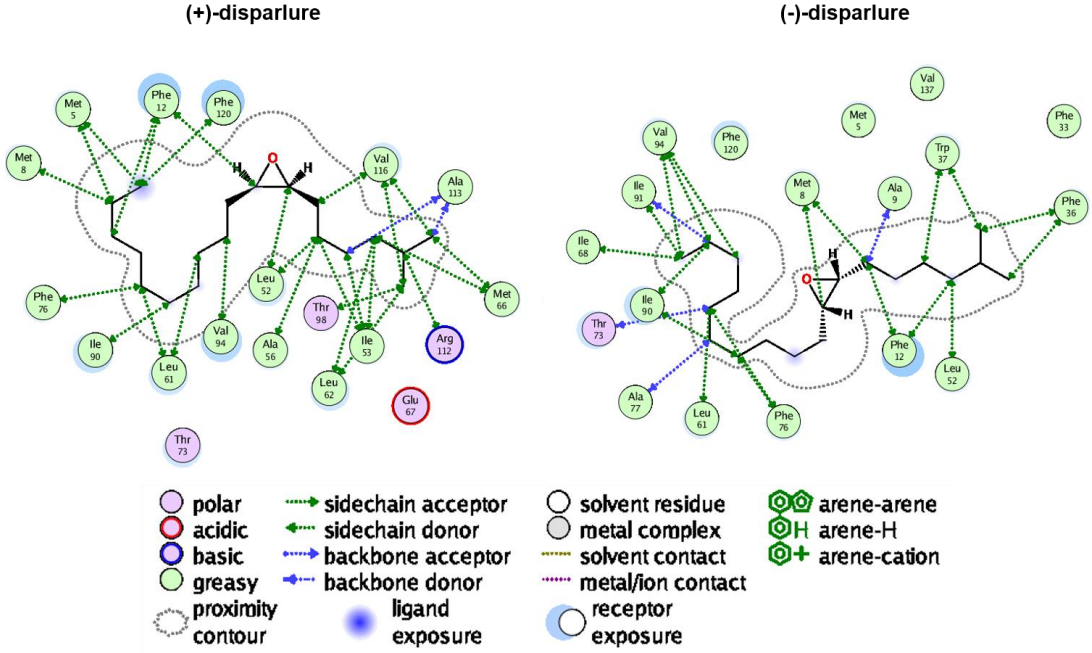

Appendix C12. *Ldis*PBP2-(+)-disparlure and (-)-disparlure ligand interactions map

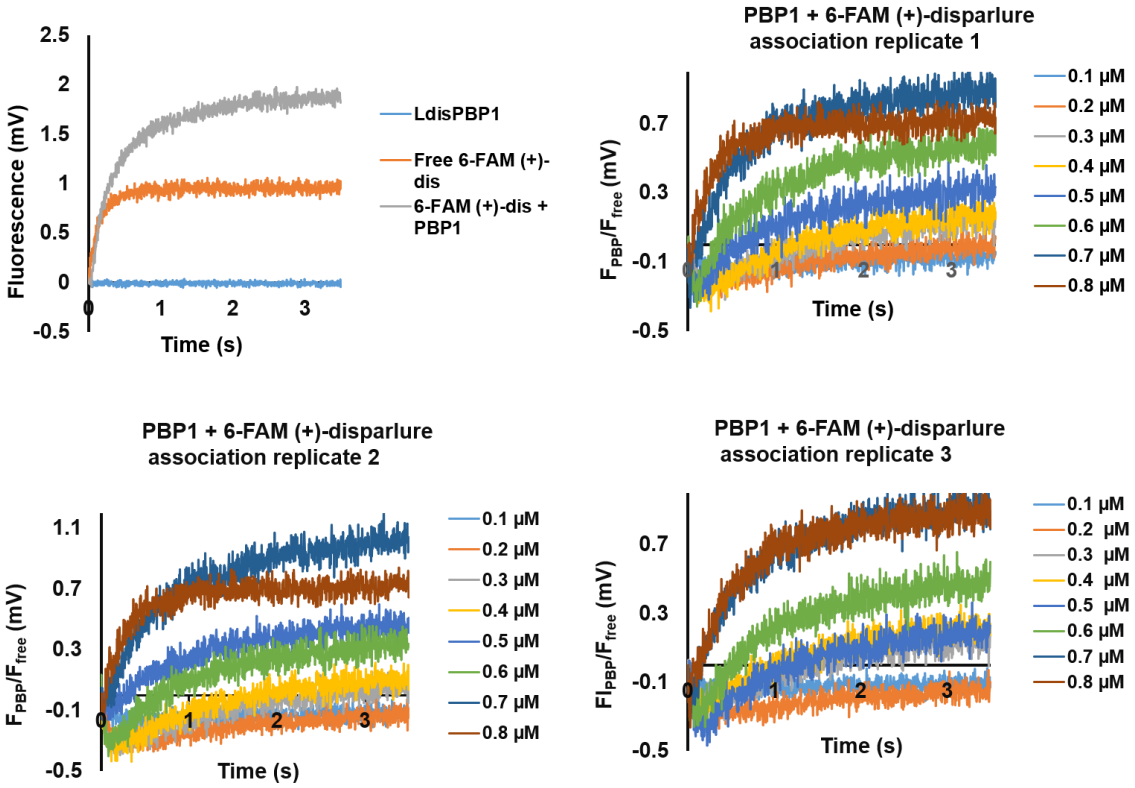

Appendix C13. Fluorescent traces of 6-FAM (+)-disparlure 15d association kinetics with *Ldis*PBP1

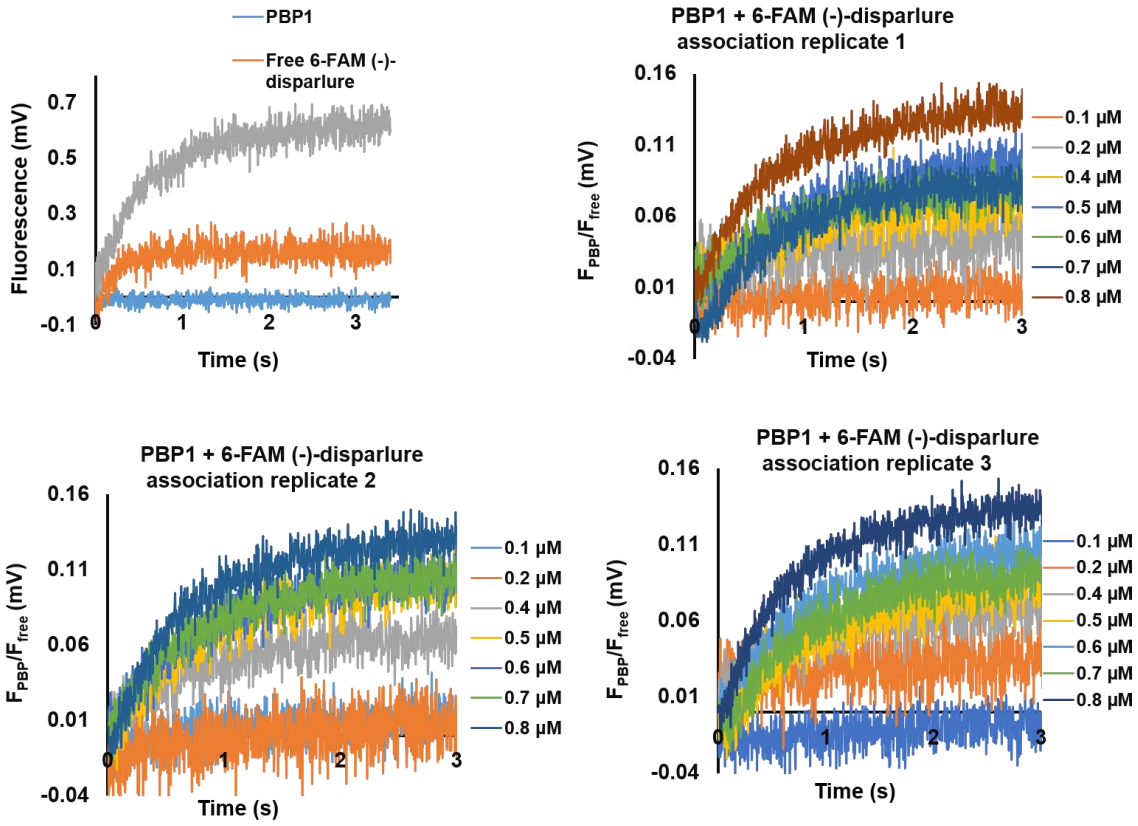

Appendix C14. Fluorescent traces of 6-FAM (-)-disparlure *ent*-15d association kinetics with *Ldis*PBP1

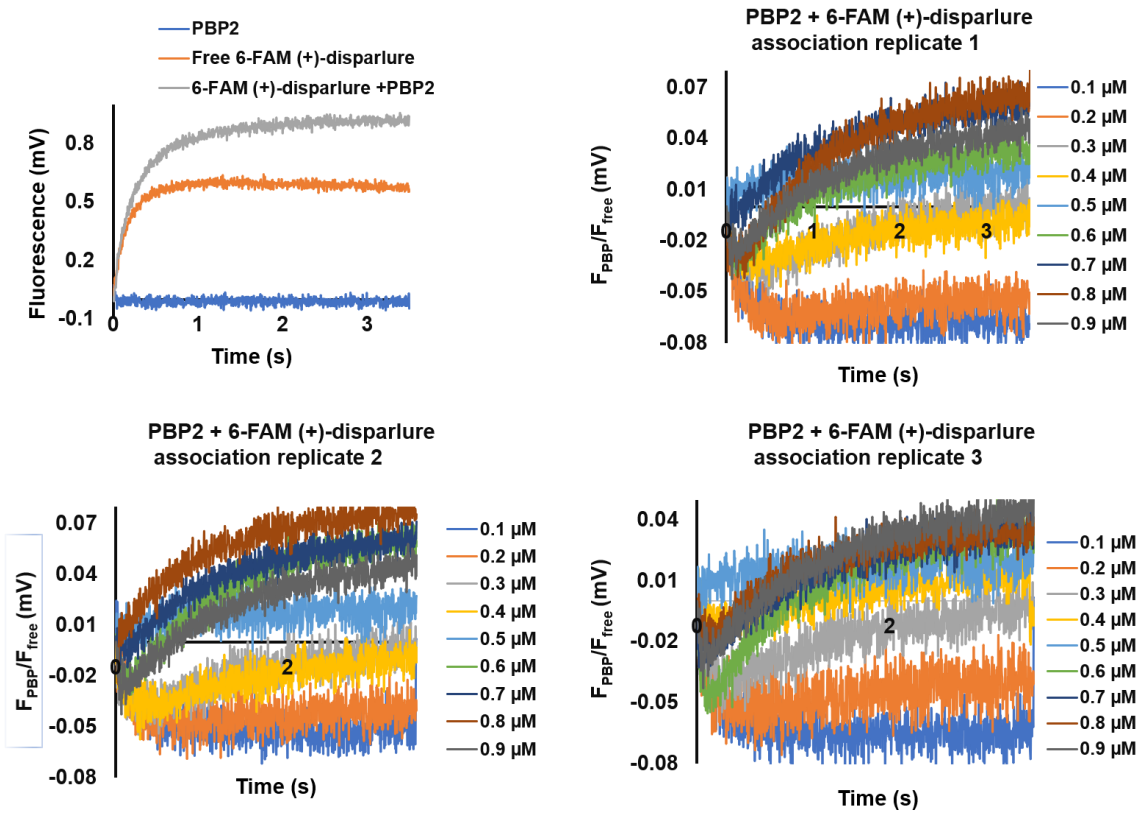

Appendix C15. Fluorescent traces of 6-FAM (+)-disparlure 15d association kinetics with *Ldis*PBP2

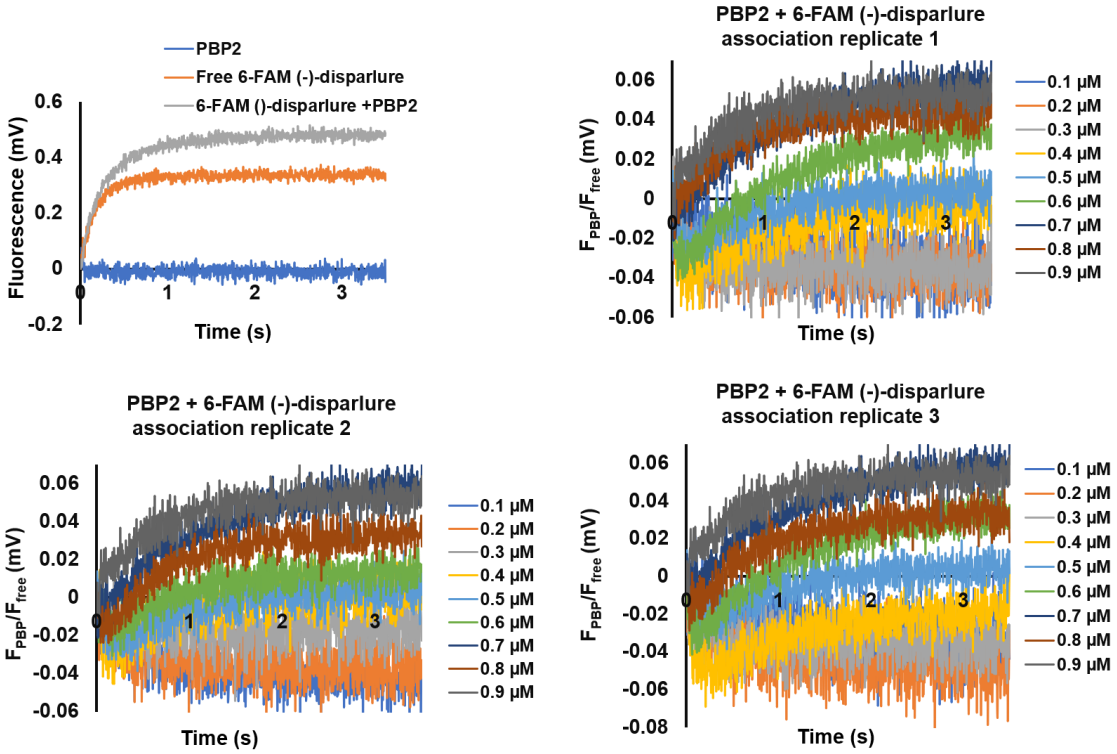

Appendix C16 Fluorescent traces of 6-FAM (-)-disparlure *ent*-15d association kinetics with *Ldis*PBP2.

[PBP1] = 0.6 µM
[6-FAM (+)-dis = 0.1-0.8 µM

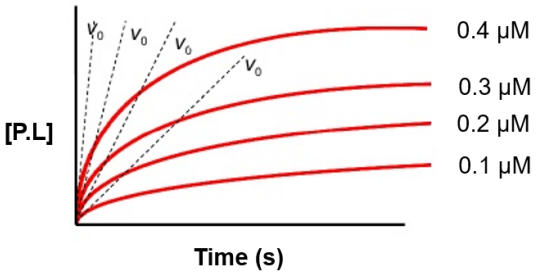

$V_0 = K_{on}[P]^n[L]^m$ n = order of the protein
m = order of the ligand

$[P.L] = F_A / F_c$

$F_A = F_{obs}/F_{blank}$

F_c = fluorescence constant, which is derived from saturation binding experiment (K_d data)

Appendix C17. Example of initial velocity (V_0) determination for 6-FAM disparlure/*Ldis*PBPs

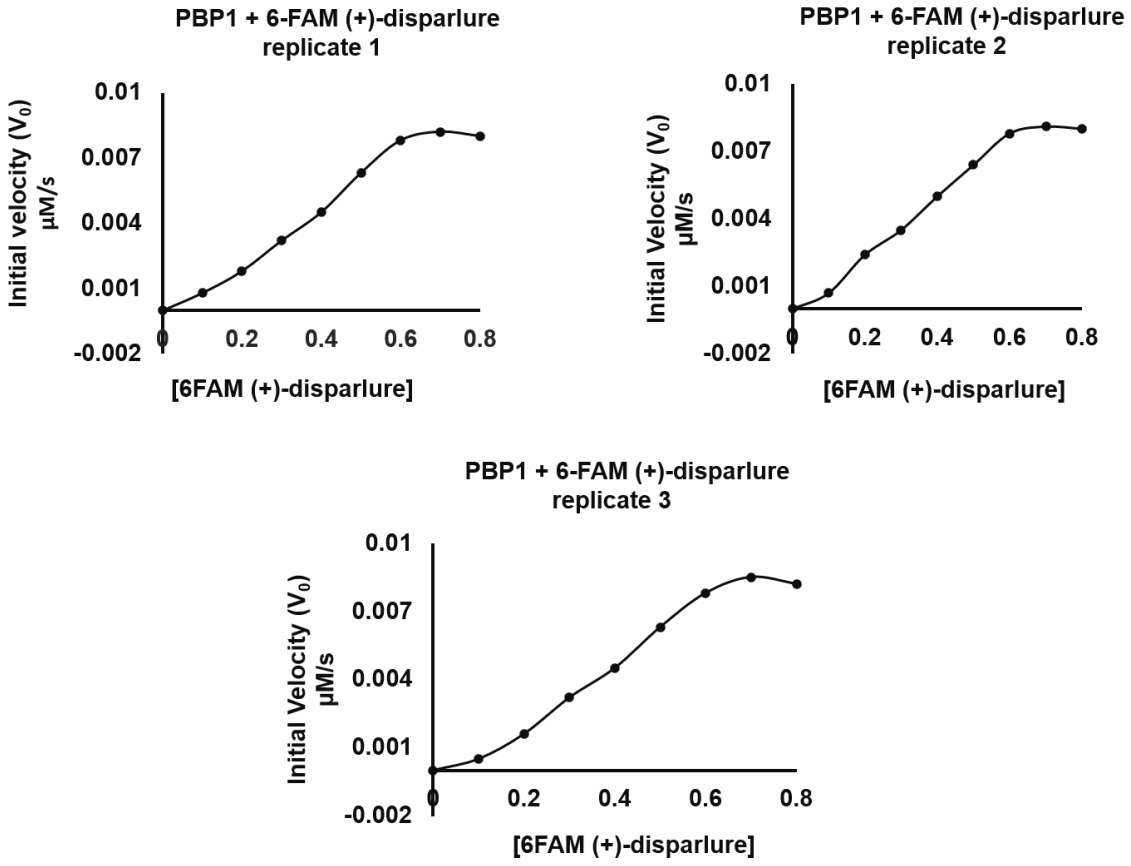

Appendix C18. Initial velocity (V_0) plots for *Ldis*PBP1 and 6-FAM (+)-disparlure 15d

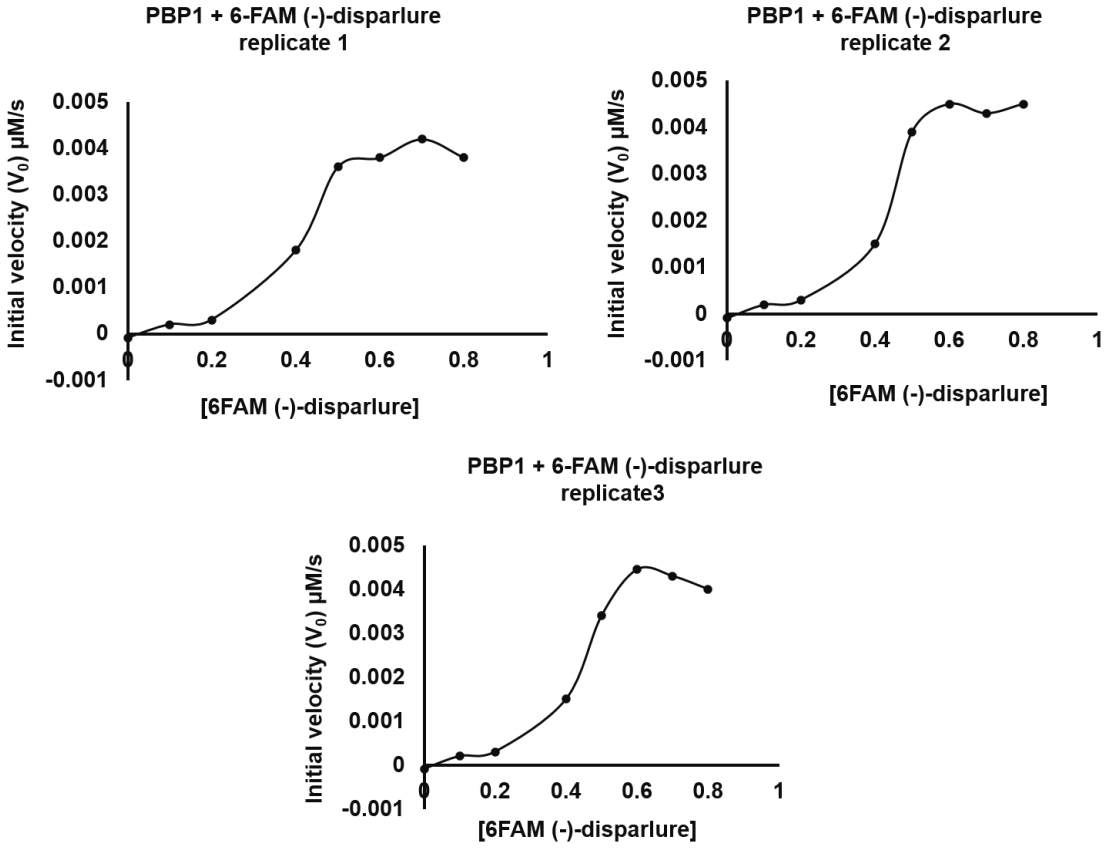

Appendix C19. Initial velocity (V_0) plots for *Ldis*PBP1 and 6-FAM (-)-disparlure *ent*-15d

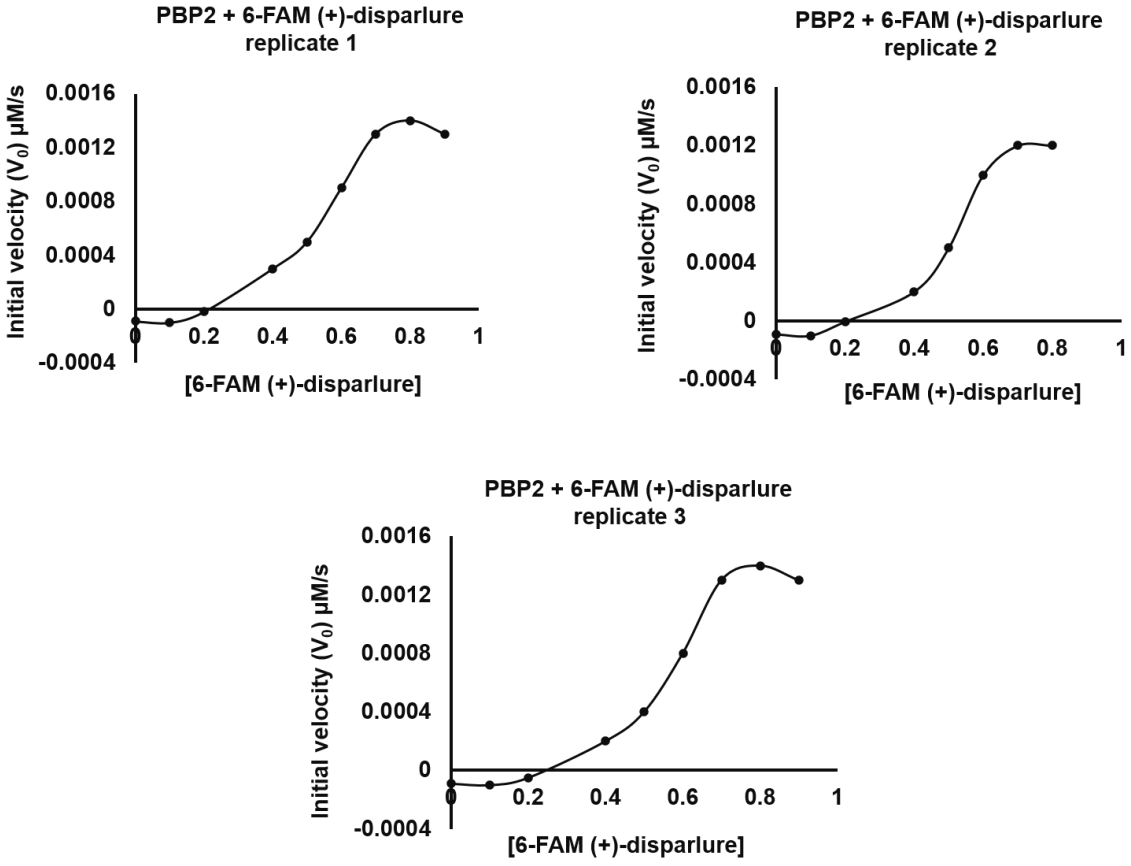

Appendix C20. Initial velocity (V_0) plots for *Ldis*PBP2 and 6-FAM (+)-disparlure 15d

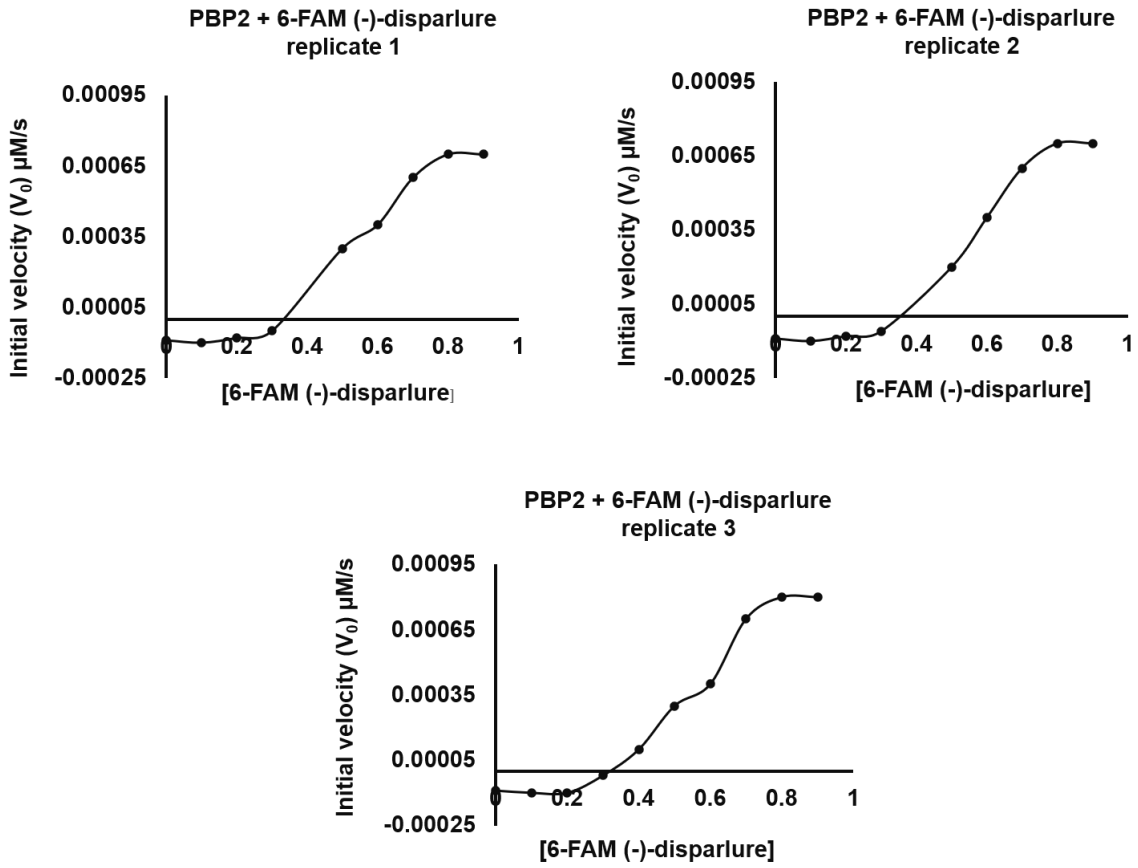

Appendix C21. Initial velocity (V_0) plots for *Ldis*PBP2 and 6-FAM (-)-disparlure *ent*-15d

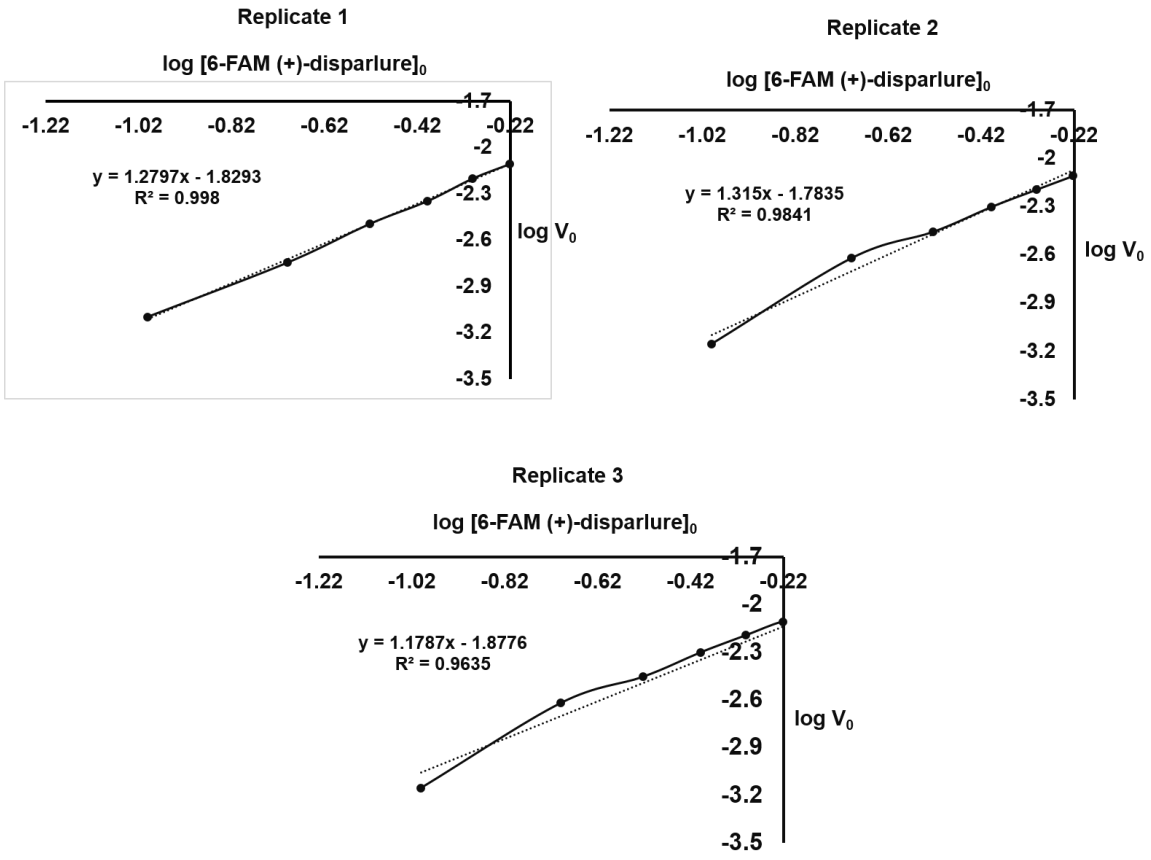

Appendix C22. The association order for 6-FAM (+)-disparlure with *Ldis*PBP1

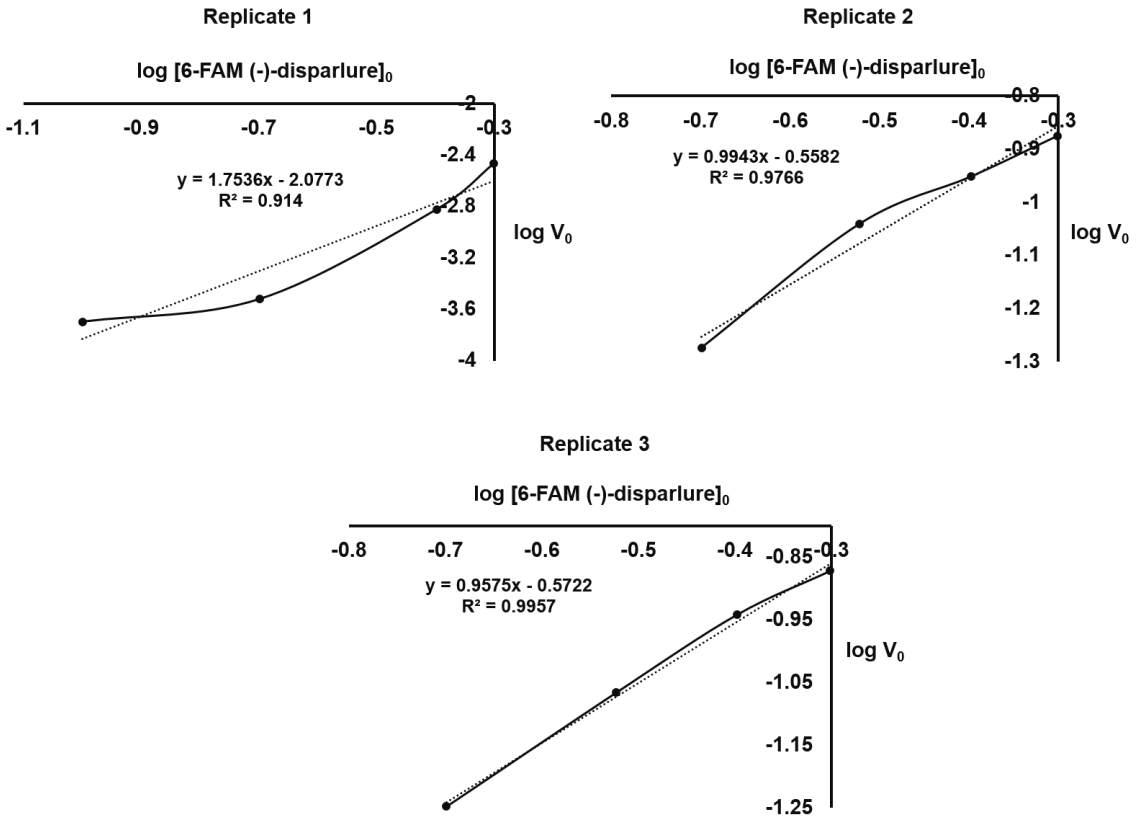

Appendix C23. The association order for 6-FAM (-)-disparlure with *Ldis*PBP1

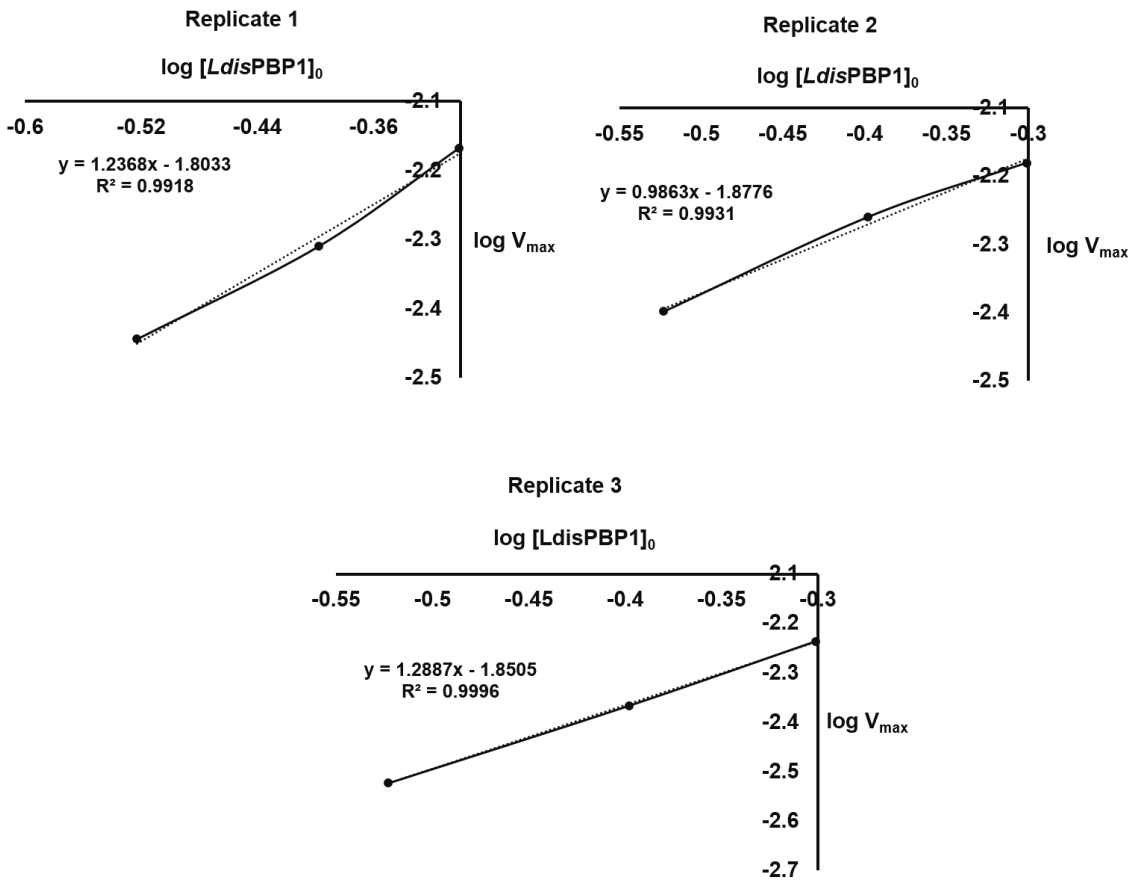

Appendix C24. The association order for *Ldis*PBP1 with 6-FAM (+)-disparlure

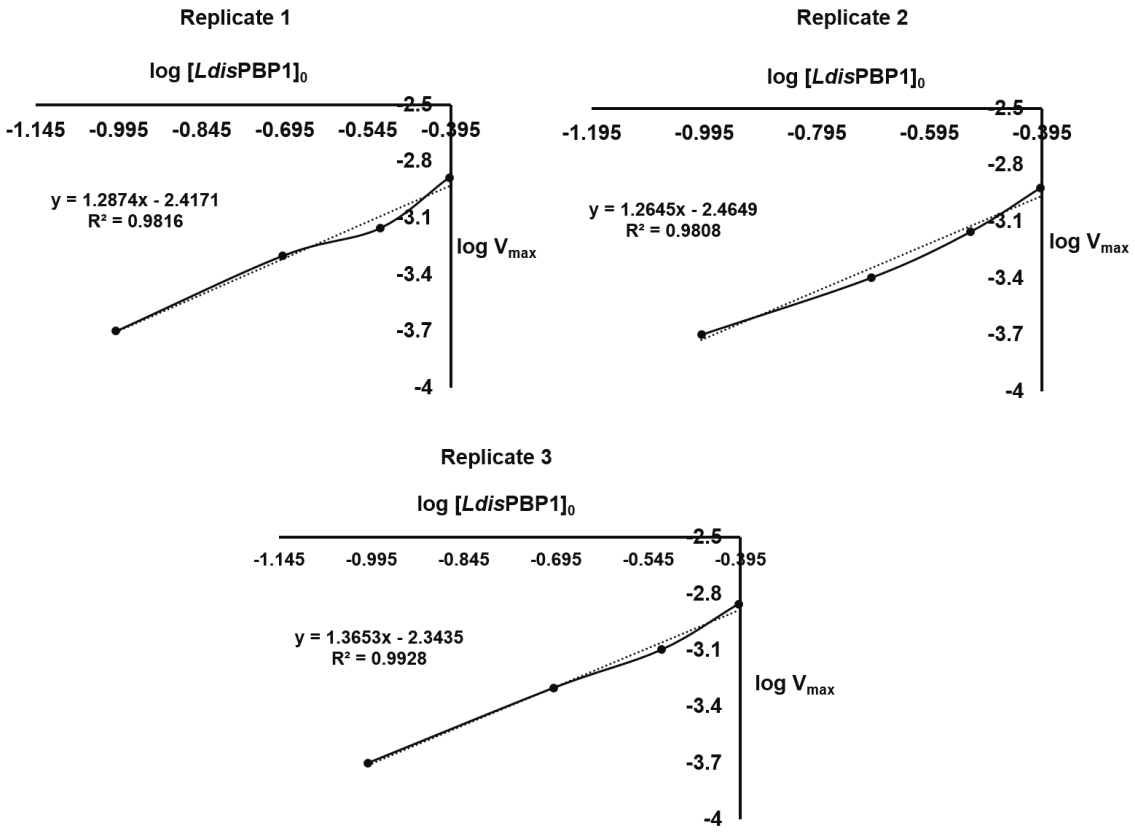

Appendix C25. The association order for *Ldis*PBP1 with 6-FAM (-)-disparlure

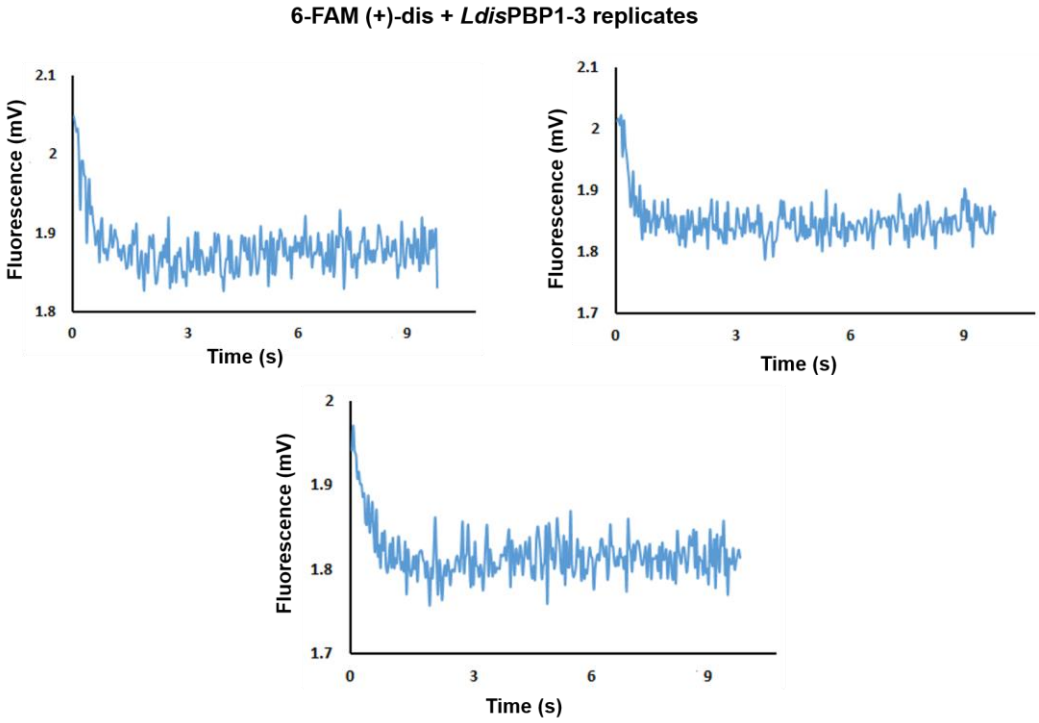

Appendix C26. Fluorescence traces of 6-FAM (+)-disparlure 15d dissociation kinetics with *Ldis*PBP1.

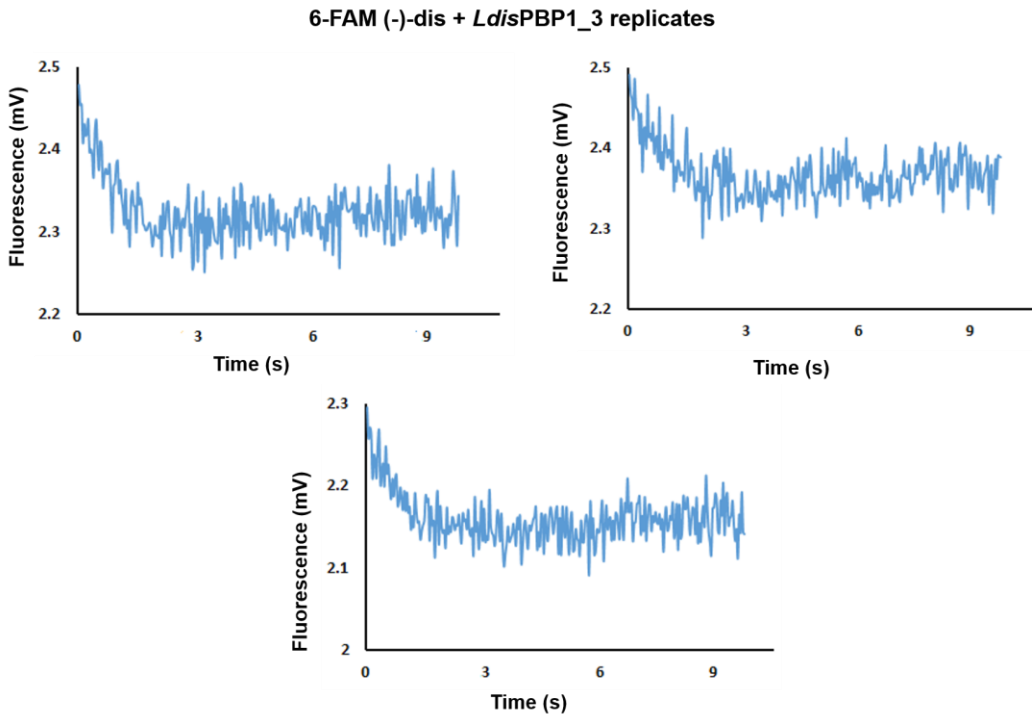

Appendix C27. Fluorescence traces of 6-FAM (-)-disparlure *ent*-15d dissociation kinetics with *Ldis*PBP1

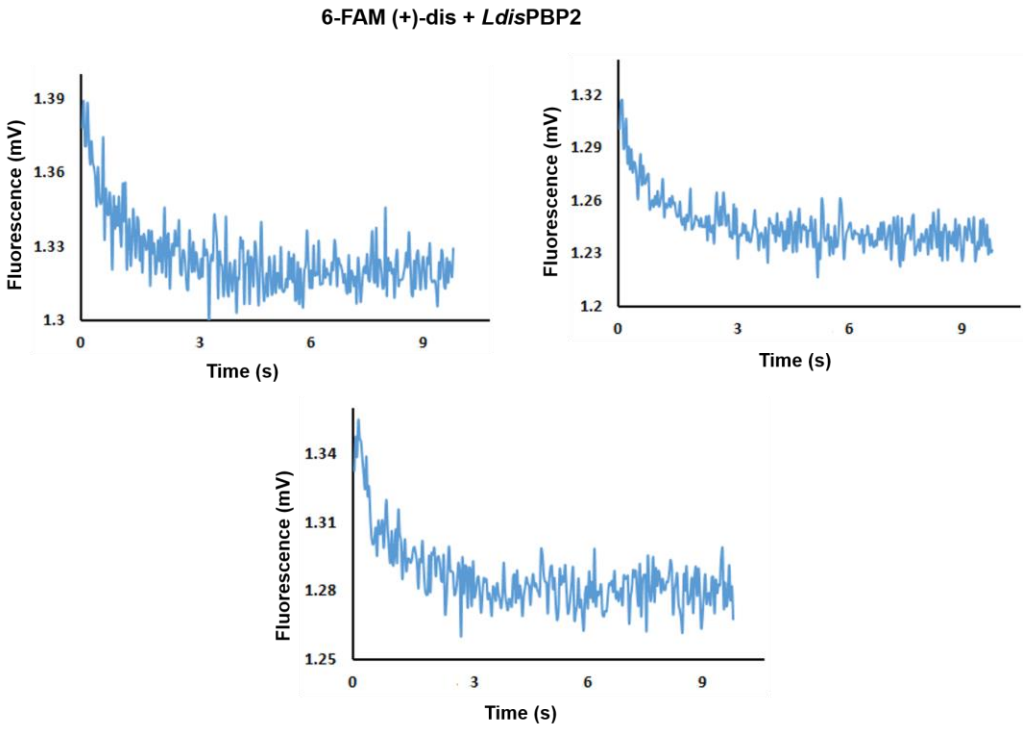

Appendix C28. Fluorescence traces of 6-FAM (+)-disparlure 15d dissociation kinetics with *Ldis*PBP2.

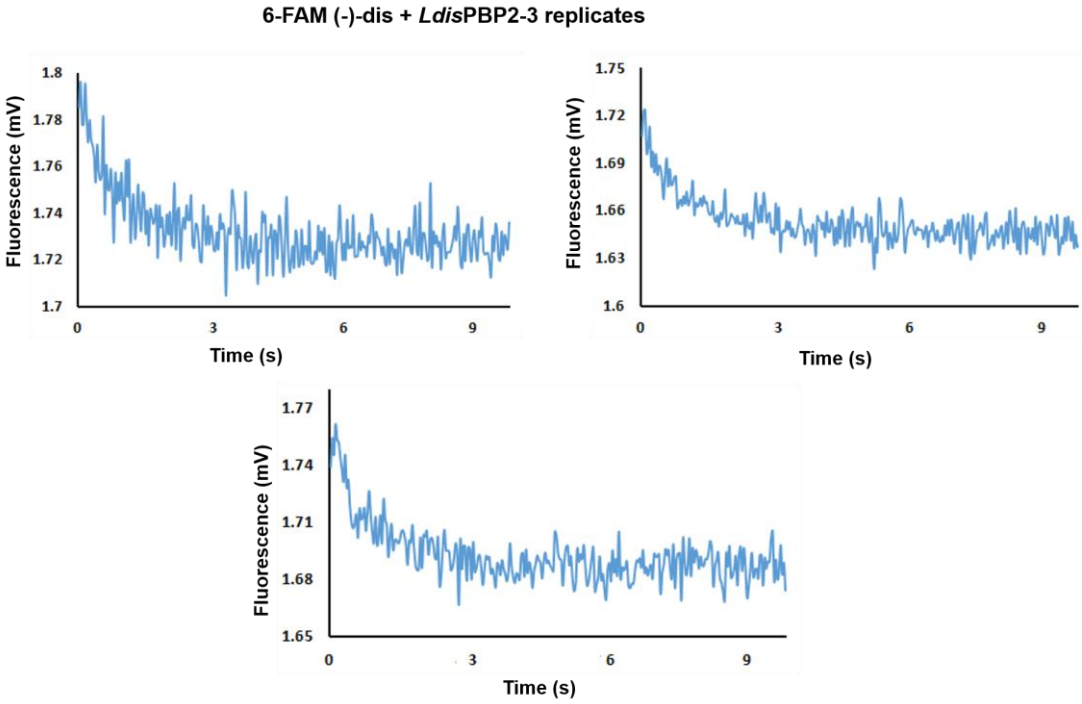

Appendix C29. Fluorescence traces of 6-FAM (-)-disparlure *ent*-15d dissociation kinetics with *Ldis*PBP2